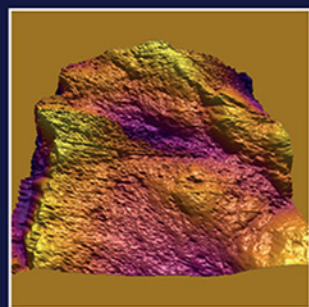
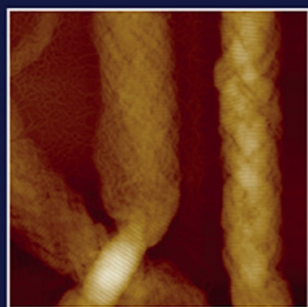


# FUNDAMENTALS AND APPLICATION OF ATOMIC FORCE MICROSCOPY FOR FOOD RESEARCH



Edited by  
Jian Zhong, Hongshun Yang and Claire Gaiani



# Fundamentals and Application of Atomic Force Microscopy for Food Research

This page intentionally left blank

# Fundamentals and Application of Atomic Force Microscopy for Food Research

Edited by

**JIAN ZHONG**

Xinhua Hospital, Shanghai Institute for Pediatric Research, Shanghai Key Laboratory of Pediatric Gastroenterology and Nutrition, Shanghai Jiao Tong University School of Medicine, Shanghai, China

**HONGSHUN YANG**

Department of Food Science and Technology, National University of Singapore, Singapore, Singapore

**CLAIRE GAIANI**

LIBio (Laboratoire d'Ingénierie des Biomolécules), Université de Lorraine, Vandoeuvre-lès-Nancy Cedex, France



**ACADEMIC PRESS**

An imprint of Elsevier

Academic Press is an imprint of Elsevier  
125 London Wall, London EC2Y 5AS, United Kingdom  
525 B Street, Suite 1650, San Diego, CA 92101, United States  
50 Hampshire Street, 5th Floor, Cambridge, MA 02139, United States  
The Boulevard, Langford Lane, Kidlington, Oxford OX5 1GB, United Kingdom

Copyright © 2023 Elsevier Inc. All rights reserved.

No part of this publication may be reproduced or transmitted in any form or by any means, electronic or mechanical, including photocopying, recording, or any information storage and retrieval system, without permission in writing from the publisher. Details on how to seek permission, further information about the Publisher's permissions policies and our arrangements with organizations such as the Copyright Clearance Center and the Copyright Licensing Agency, can be found at our website: [www.elsevier.com/permissions](http://www.elsevier.com/permissions).

This book and the individual contributions contained in it are protected under copyright by the Publisher (other than as may be noted herein).

### Notices

Knowledge and best practice in this field are constantly changing. As new research and experience broaden our understanding, changes in research methods, professional practices, or medical treatment may become necessary.

Practitioners and researchers must always rely on their own experience and knowledge in evaluating and using any information, methods, compounds, or experiments described herein. In using such information or methods they should be mindful of their own safety and the safety of others, including parties for whom they have a professional responsibility.

To the fullest extent of the law, neither the Publisher nor the authors, contributors, or editors, assume any liability for any injury and/or damage to persons or property as a matter of products liability, negligence or otherwise, or from any use or operation of any methods, products, instructions, or ideas contained in the material herein.

ISBN: 978-0-12-823985-8

For Information on all Academic Press publications  
visit our website at <https://www.elsevier.com/books-and-journals>

*Publisher:* Nikki P. Levy  
*Acquisitions Editor:* Nina Bandeira  
*Editorial Project Manager:* Lena Sparks  
*Production Project Manager:* Bharatwaj Varatharajan  
*Cover Designer:* Miles Hitchen

Typeset by MPS Limited, Chennai, India



# Contents

*List of contributors*

*xiii*

## **Section 1 Introduction of AFM for food research**

<b>1. An introduction</b>	<b>3</b>
Jian Zhong, Hongshun Yang and Claire Gaiani	
Acknowledgements	7
References	7

## **Section 2 Fundamentals of AFM**

<b>2. Atomic force microscopy: from theory to application in food science</b>	<b>15</b>
Sofiane El-Kirat-Chatel, Jennifer Burgain, Claire Gaiani and Grégory Francius	
2.1 History of atomic force microscopy	15
2.2 Basic principles of atomic force microscopy	16
2.2.1 Basic components	17
2.2.2 Working conditions, basic functions, and theory	20
2.3 Force measurements and nanomanipulation	23
2.4 New imaging modes	27
2.5 Measurement items	29
2.6 Atomic force microscopy integration with other instruments	30
2.7 Research ways and applications	30
2.7.1 Research type	30
2.7.2 Quick overview of applications in food sciences	34
2.8 Conclusion	37
References	38
<b>3. Operation procedures of atomic force microscopy for food and biological samples</b>	<b>45</b>
Lili Yang, Ting Zhang, Yao Liu, Rui Sun, Xichang Wang and Jian Zhong	
3.1 Introduction	45
3.2 Atomic force microscopy requirements for food samples	45
3.3 Substrates	46

3.3.1	Mica	49
3.3.2	Glass	49
3.3.3	Graphite	50
3.4	Sample preparation for food samples	50
3.4.1	Individual biomolecules	51
3.4.2	Artificially supported lipid layers	51
3.4.3	Cells	52
3.4.4	Food powder	53
3.4.5	Bulk solid sample	53
3.5	Cantilever selection	53
3.5.1	Spring constant	54
3.5.2	Tip geometry	55
3.5.3	Resonance frequency and quality factor	56
3.5.4	Tip functionalization	56
3.6	Common imaging procedure by atomic force microscopy	57
3.6.1	Power on system	57
3.6.2	Mount sample	57
3.6.3	Mount probe	59
3.6.4	Enable software	59
3.6.5	Align laser	59
3.6.6	Adjust photodiode signal	60
3.6.7	Cantilever tune (tapping mode only)	60
3.6.8	Set Initial scan parameters	60
3.6.9	Engage atomic force microscopy probe	60
3.6.10	Optimize scan parameters	61
3.6.11	Acquire and save the image	61
3.6.12	Withdraw atomic force microscopy probe	61
3.6.13	Unmount atomic force microscopy probe and sample	61
3.6.14	Shutdown system	61
3.6.15	Clean workspace	62
3.7	Common force measurement procedure by atomic force microscopy	62
3.7.1	Measure deflection sensitivity	63
3.7.2	Calculate spring constant	64
3.7.3	Force measurement	66
3.8	Common nanomanipulation procedure by atomic force microscopy	66
3.9	Data optimization	67
3.9.1	Real-time optimization	67
3.9.2	Offline optimization	68

3.10	Data analysis	69
3.10.1	Typical image artifacts	69
3.10.2	Image analysis	75
3.11	Conclusion	76
	Acknowledgments	76
	Conflict of interest	76
	References	76

## **Section 3 Application of AFM for food research**

### **4. Application of atomic force microscopy for food proteins 83**

Yangyi Zhang, Jiamin Xu, Ting Zhang, Shudan Huang, Xichang Wang and Jian Zhong

4.1	Introduction	83
4.2	Food protein extraction and sample preparation	85
4.2.1	Food protein extraction	85
4.2.2	Sample preparation	87
4.3	Grain proteins	88
4.3.1	Rice proteins	88
4.3.2	Wheat proteins	89
4.3.3	Maize proteins	91
4.3.4	Sorghum proteins	91
4.4	Bean proteins	92
4.4.1	Soy proteins	92
4.4.2	Pea proteins	93
4.5	Peanut proteins	95
4.6	Milk proteins	96
4.6.1	Caseins	97
4.6.2	Whey proteins	99
4.7	Meat proteins	102
4.8	Seafood proteins	104
4.9	Collagen and gelatin	106
4.9.1	Collagen	106
4.9.2	Gelatin	109
4.10	Egg proteins	110
4.11	Summary and outlook	112
	Acknowledgment	112
	Conflict of interest	112
	References	112



<b>5. Application of atomic force microscopy for food polysaccharides</b>	<b>121</b>
Lifen Zhang, Xiaoyang Sun, Shaojuan Lai, Fusheng Chen and Hongshun Yang	
5.1 Introduction	121
5.2 Plant polysaccharide	122
5.2.1 Starch	122
5.2.2 Pectin	126
5.2.3 Cellulose	142
5.2.4 Others	143
5.3 Measurement of molecule interactions of polysaccharides and food components	147
5.3.1 Polysaccharides-polysaccharides	147
5.3.2 Polysaccharides-protein	148
5.4 Conclusions	149
Acknowledgment	150
Declaration of competing interest	150
References	150
Further reading	159
<b>6. Application of atomic force microscopy in food microorganism research</b>	<b>161</b>
Lin Zhao and Hongshun Yang	
6.1 Introduction	161
6.2 Single microbial cell studies	162
6.2.1 Morphological change evaluation	162
6.2.2 Antimicrobial mechanism evaluation	165
6.3 Microbial biofilm studies	169
6.3.1 Biofilm morphological imaging	169
6.3.2 Biofilm adhesive property study	170
6.3.3 Biofilm dynamic process study	171
6.4 Microbial macromolecule studies	173
6.4.1 Surface layer protein study	173
6.4.2 Surface molecular interaction study	175
6.5 Representatively reported atomic force microscopy studies about different types of microorganisms	176
6.5.1 Prokaryotic microorganisms	176
6.5.2 Eukaryotic microorganisms	177
6.5.3 Viruses	178

6.6	Combined use of atomic force microscopy with other techniques	179
6.6.1	Atomic force microscopy and infrared combination	179
6.6.2	Atomic force microscopy and Raman spectroscopy combination	181
6.7	Conclusion and future trends	181
	Acknowledgements	182
	Declaration of competing interest	182
	References	182
<b>7.</b>	<b>Application of atomic force microscopy for food foams and emulsions</b>	<b>189</b>
	Christelle Lopez	
7.1	Introduction	189
7.2	Atomic force microscopy applied to food foams and emulsions: fundamentals, operating modes, imaging for topography and force–distance curves for nanomechanics	192
7.2.1	Fundamentals of atomic force microscopy: investigation of surfaces	192
7.2.2	Atomic force microscope	193
7.2.3	Operating modes for imaging	193
7.2.4	Force–distance curves for determining surface material properties	195
7.2.5	Probing air bubbles, lipid droplets, and interfaces	195
7.3	Application of atomic force microscopy for food foams	197
7.3.1	Components involved in the air/water interface	197
7.3.2	Components adsorbed at planar Langmuir films	198
7.3.3	Air bubbles under the atomic force microscope	201
7.4	Application of atomic force microscopy for food emulsions and nanoemulsions	202
7.4.1	Morphology of components used to stabilize oil-in-water emulsions	203
7.4.2	Morphology of components adsorbed at planar Langmuir films	207
7.4.3	Nanoemulsions and emulsions: lipid droplets under the atomic force microscopy tip	210
7.5	Application of atomic force microscopy to dairy lipid systems: membranes, liposomes, and emulsions	215
7.5.1	Milk: from natural to processed oil-in-water emulsions	215
7.5.2	Topography of lipid monolayers and membranes in air	217
7.5.3	Topography and mechanical properties of hydrated lipid bilayers	217
7.5.4	Surface topography and roughness of milk fat globules	222
7.5.5	Probing specific interactions and adhesion forces involved at the surface of milk fat globules	223

7.6	Conclusions	228
	Acknowledgments	229
	References	229
<b>8.</b>	<b>Application of atomic force microscopy for food powders and contact materials</b>	<b>233</b>
	Regis Badin, Jennifer Burgain and Claire Gaiani	
8.1	Introduction	233
8.2	Atomic force microscopy: a powerful tool during formulation and processing of food powders	234
8.2.1	Carbohydrate-based powders	235
8.2.2	Fat-based powders	240
8.2.3	Proteins powders	241
8.3	A better understanding and control of powder functional properties with atomic force microscopy	242
8.3.1	Reconstitution ability of food powders	242
8.3.2	Powder caking	246
8.3.3	Powder cohesion and flowability	248
8.3.4	Food powders as a vehicle of bioactive molecules	248
8.4	Contact materials related to food	250
8.4.1	Morphological studies of food material surfaces	251
8.4.2	Quantitative studies of food material surfaces	251
8.5	Prospects and advanced atomic force microscopy techniques to characterize food powders	253
8.6	Conclusion	255
	References	256
<b>9.</b>	<b>Advances in food material nanomechanics by means of atomic force microscopy</b>	<b>263</b>
	Benjamin Arredondo-Tamayo, Stefany Cárdenas-Pérez, Juan V. Méndez-Méndez, Israel Arzate-Vázquez, Héctor H. Torres-Ventura and José J. Chanona-Pérez	
9.1	Introduction	263
9.2	Operation modes in atomic force microscopy	264
9.3	Proteins stretching	274
9.4	Suppliers, sample preparation, fixation, and tip selection	276
9.5	Probe selection	283
9.6	Approaches in food science research with atomic force microscopy	285
9.7	Recent research on nanomechanical properties of food materials	286

9.8 Conclusion	300
References	300
<b>10. Current and potential combination of atomic force microscopy with other techniques for food science</b>	<b>307</b>
Xin Wang, Yang Liu, Xin Guo, Yaolun Liu and Hao Sun	
10.1 Introduction	307
10.2 Atomic force microscopy combined with infrared technique for food science	308
10.2.1 Principle and apparatus	310
10.2.2 Current atomic force microscopy-infrared applications in food science	312
10.2.3 Prospect of atomic force microscopy-infrared applications in food science	318
10.3 Atomic force microscopy combined with Raman technique for food science	320
10.3.1 Principle and apparatus	320
10.3.2 Current atomic force microscopy-Raman applications in food science	321
10.3.3 Prospect of atomic force microscopy-Raman applications in food science	326
10.4 Other atomic force microscopy-combined techniques and their potential applications in food science	327
10.4.1 Atomic force microscopy combined with mass spectrometry	327
10.4.2 Atomic force microscopy combined with optical microscopy	329
10.4.3 Atomic force microscopy combined with X-ray techniques	332
10.4.4 Atomic force microscopy combined with nanodynamic mechanical analysis	334
10.4.5 Atomic force microscopy combined with nuclear magnetic resonance	335
10.4.6 Atomic force microscopy combined with force-loading stage	337
10.4.7 Atomic force microscopy combined with fluidic force microscopy	340
10.4.8 Atomic force microscopy combined with optical tweezer	342
10.5 Summary	345
References	345
<i>Index</i>	363

This page intentionally left blank

## List of contributors

### **Benjamin Arredondo-Tamayo**

Departamento de Ingeniería Bioquímica, Escuela Nacional de Ciencias Biológicas, Instituto Politécnico Nacional, Mexico City, Mexico

### **Israel Arzate-Vázquez**

Centro de Nanociencias y Micro y Nanotecnologías, Instituto Politécnico Nacional, Mexico City, Mexico

### **Regis Badin**

LIBio (Laboratoire d'Ingénierie des Biomolécules), Université de Lorraine, Vandoeuvre-lès-Nancy Cedex, France

### **Jennifer Burgain**

LIBio (Laboratoire d'Ingénierie des Biomolécules), Université de Lorraine, Vandoeuvre-lès-Nancy Cedex, France

### **Stefany Cárdenas-Pérez**

Geobotany and Landscape Planning, Faculty of Biological and Veterinary Sciences, Nicolaus Copernicus University, Toruń, Poland

### **José J. Chanona-Pérez**

Departamento de Ingeniería Bioquímica, Escuela Nacional de Ciencias Biológicas, Instituto Politécnico Nacional, Mexico City, Mexico

### **Fusheng Chen**

College of Food Science and Technology, Henan University of Technology, Zhengzhou, P. R. China

### **Sofiane El-Kirat-Chatel**

Université de Lorraine, CNRS, LCPME, UMR 7564, Nancy, France

### **Grégory Francius**

Université de Lorraine, CNRS, LCPME, UMR 7564, Nancy, France

### **Claire Gaiani**

LIBio (Laboratoire d'Ingénierie des Biomolécules), Université de Lorraine, Vandoeuvre-lès-Nancy Cedex, France; Ministry of Higher Education, Research and Innovation, IUF (Institut Universitaire de France), Paris, France

### **Xin Guo**

Bruker (Beijing) Scientific Technology Co., Ltd., Beijing, P. R. China

### **Shudan Huang**

National R&D Branch Center for Freshwater Aquatic Products Processing Technology (Shanghai), Integrated Scientific Research Base on Comprehensive Utilization Technology for By-Products of Aquatic Product Processing, Ministry of Agriculture and Rural Affairs of the People's Republic of China, Shanghai Engineering Research Center of Aquatic-Product Processing and Preservation, College of Food Science & Technology, Shanghai Ocean University, Shanghai, P. R. China

**Shaojuan Lai**

College of Food Science and Technology, Henan University of Technology, Zhengzhou, P. R. China

**Yang Liu**

Bruker (Beijing) Scientific Technology Co., Ltd., Beijing, P. R. China

**Yao Liu**

Instrumental Analysis Center, Shanghai Jiao Tong University, Shanghai, P. R. China

**Yaolun Liu**

Bruker (Beijing) Scientific Technology Co., Ltd., Beijing, P. R. China

**Christelle Lopez**

INRAE, BIA, Nantes, France

**Juan V. Méndez-Méndez**

Centro de Nanociencias y Micro y Nanotecnologías, Instituto Politécnico Nacional, Mexico City, Mexico

**Hao Sun**

Bruker (Beijing) Scientific Technology Co., Ltd., Beijing, P. R. China

**Rui Sun**

National R&D Branch Center for Freshwater Aquatic Products Processing Technology (Shanghai), Integrated Scientific Research Base on Comprehensive Utilization Technology for By-Products of Aquatic Product Processing, Ministry of Agriculture and Rural Affairs of the People's Republic of China, Shanghai Engineering Research Center of Aquatic-Product Processing and Preservation, College of Food Science & Technology, Shanghai Ocean University, Shanghai, P. R. China

**Xiaoyang Sun**

College of Food and Biological Engineering, Henan University of Animal Husbandry and Economy, Zhengzhou, P. R. China

**Héctor H. Torres-Ventura**

Departamento de Ingeniería Bioquímica, Escuela Nacional de Ciencias Biológicas, Instituto Politécnico Nacional, Mexico City, Mexico

**Xichang Wang**

National R&D Branch Center for Freshwater Aquatic Products Processing Technology (Shanghai), Integrated Scientific Research Base on Comprehensive Utilization Technology for By-Products of Aquatic Product Processing, Ministry of Agriculture and Rural Affairs of the People's Republic of China, Shanghai Engineering Research Center of Aquatic-Product Processing and Preservation, College of Food Science & Technology, Shanghai Ocean University, Shanghai, P. R. China

**Xin Wang**

Bruker (Beijing) Scientific Technology Co., Ltd., Beijing, P. R. China

**Jiamin Xu**

National R&D Branch Center for Freshwater Aquatic Products Processing Technology (Shanghai), Integrated Scientific Research Base on Comprehensive Utilization Technology for By-Products of Aquatic Product Processing, Ministry of Agriculture and Rural Affairs of the People's Republic of China, Shanghai Engineering Research Center of Aquatic-Product Processing and Preservation, College of Food Science & Technology, Shanghai Ocean University, Shanghai, P. R. China

**Hongshun Yang**

Department of Food Science and Technology, National University of Singapore, Singapore, Singapore; National University of Singapore (Suzhou) Research Institute, Suzhou Industrial Park, Suzhou, Jiangsu, P. R. China

**Lili Yang**

Xinhua Hospital, Shanghai Institute for Pediatric Research, Shanghai Key Laboratory of Pediatric Gastroenterology and Nutrition, Shanghai Jiao Tong University School of Medicine, Shanghai, P. R. China; National R&D Branch Center for Freshwater Aquatic Products Processing Technology (Shanghai), Integrated Scientific Research Base on Comprehensive Utilization Technology for By-Products of Aquatic Product Processing, Ministry of Agriculture and Rural Affairs of the People's Republic of China, Shanghai Engineering Research Center of Aquatic-Product Processing and Preservation, College of Food Science & Technology, Shanghai Ocean University, Shanghai, P. R. China

**Lifen Zhang**

College of Food Science and Technology, Henan University of Technology, Zhengzhou, P. R. China

**Ting Zhang**

National R&D Branch Center for Freshwater Aquatic Products Processing Technology (Shanghai), Integrated Scientific Research Base on Comprehensive Utilization Technology for By-Products of Aquatic Product Processing, Ministry of Agriculture and Rural Affairs of the People's Republic of China, Shanghai Engineering Research Center of Aquatic-Product Processing and Preservation, College of Food Science & Technology, Shanghai Ocean University, Shanghai, P. R. China

**Yangyi Zhang**

Xinhua Hospital, Shanghai Institute for Pediatric Research, Shanghai Key Laboratory of Pediatric Gastroenterology and Nutrition, Shanghai Jiao Tong University School of Medicine, Shanghai, P. R. China; National R&D Branch Center for Freshwater Aquatic Products Processing Technology (Shanghai), Integrated Scientific Research Base on Comprehensive Utilization Technology for By-Products of Aquatic Product Processing, Ministry of Agriculture and Rural Affairs of the People's Republic of China, Shanghai Engineering Research Center of Aquatic-Product Processing and Preservation, College of Food Science & Technology, Shanghai Ocean University, Shanghai, P. R. China

**Lin Zhao**

Department of Food Science and Technology, National University of Singapore, Singapore, Singapore; National University of Singapore (Suzhou) Research Institute, Suzhou Industrial Park, Suzhou, Jiangsu, P. R. China

**Jian Zhong**

Xinhua Hospital, Shanghai Institute for Pediatric Research, Shanghai Key Laboratory of Pediatric Gastroenterology and Nutrition, Shanghai Jiao Tong University School of Medicine, Shanghai, P. R. China; National R&D Branch Center for Freshwater Aquatic Products Processing Technology (Shanghai), Integrated Scientific Research Base on Comprehensive Utilization Technology for By-Products of Aquatic Product Processing, Ministry of Agriculture and Rural Affairs of the People's Republic of China, Shanghai Engineering Research Center of Aquatic-Product Processing and Preservation, College of Food Science & Technology, Shanghai Ocean University, Shanghai, P. R. China



This page intentionally left blank

## **SECTION 1**

# **Introduction of AFM for food research**

This page intentionally left blank

# CHAPTER 1

## An introduction

**Jian Zhong<sup>1,2</sup>, Hongshun Yang<sup>3</sup> and Claire Gaiani<sup>4,5</sup>**

<sup>1</sup>Xinhua Hospital, Shanghai Institute for Pediatric Research, Shanghai Key Laboratory of Pediatric Gastroenterology and Nutrition, Shanghai Jiao Tong University School of Medicine, Shanghai, P. R. China

<sup>2</sup>National R&D Branch Center for Freshwater Aquatic Products Processing Technology (Shanghai), Integrated Scientific Research Base on Comprehensive Utilization Technology for By-Products of Aquatic Product Processing, Ministry of Agriculture and Rural Affairs of the People's Republic of China, Shanghai Engineering Research Center of Aquatic-Product Processing and Preservation, College of Food Science & Technology, Shanghai Ocean University, Shanghai, P. R. China

<sup>3</sup>Department of Food Science and Technology, National University of Singapore, Singapore, Singapore

<sup>4</sup>LIBio (Laboratoire d'Ingénierie des Biomolécules), Université de Lorraine, Vandoeuvre-lès-Nancy Cedex, France

<sup>5</sup>Ministry of Higher Education, Research and Innovation, IUF (Institut Universitaire de France), Paris, France

Atomic force microscope (AFM) was developed in 1985 by Binnig and Quate at IBM San Jose Research Laboratory, Stanford and Gerber (Binnig, Quate, & Gerber, 1986). It is a member of the family of scanning probe microscopes, which analyze the surface characteristics based on a variety of tip–sample interactions. Generally, AFM uses a sharp nanoscale tip to sense the surface characteristics (topographical, mechanical, electrical, and magnetic information) or to manipulate surface substances of a sample of interest at nanoscale (Collins, Liu, Ovchinnikova, & Proksch, 2019; Dufrière et al., 2017; Gross et al., 2018; Krieg et al., 2019; Pavliček & Gross, 2017). AFM has been widely applied in the field of materials, energy, biology, chemistry, physics, medicine, etc. (Bellon, 2020; Chen & Xu, 2020; Efremov, Okajima, & Raman, 2020; Kiio & Park, 2020; Li, Liu, Yuan, & Huang, 2021; Li, Xi, Wang, & Liu, 2021; Liu & Vancso, 2020; Nandi & Ainarapu, 2021; Si et al., 2020; Yadavalli & Ehrhardt, 2021). Moreover, with the boom in nanotechnology, AFM will attract more and more attention in the scientific and engineering fields due to its advantages such as multifunction and high resolution.

In the field of biology, AFM has been widely applied to image biomolecule structures (Kuchuk & Sivan, 2018; Main et al., 2021) and the morphologies of biological aggregates (Ma et al., 2013; Nievergelt, Banterle, Andany, Gönczy, & Fantner, 2018; Zhong & He, 2012) to analyze the effects of processing conditions on biological substances (Zhong et al., 2015; Zhong, Ma, et al., 2014), to observe biological dynamic process in liquid (Uchihashi & Scheuring, 2018; Zhong et al., 2007, 2009;

Zhong, 2011), to measure the force of biomolecular interaction (Martines et al., 2012; Sapra, Spoerri, Engel, Alsteens, & Müller, 2019), to manipulate biomolecules (Fukui et al., 2018; Zhao, Liu, & Gao, 2018), to analyze cell nanomechanics (Kilpatrick, Revenko, & Rodriguez, 2015; Zhou, Zhang, Tang, Yu, & Galluzzi, 2021), and to mechanically fabricate 3D bionanostructures (Zhong et al., 2013; Zhong, Sun, & He, 2014). Thus, AFM has proven to be a powerful technique for the studies of biological processes and biological nanomaterials.

AFM has been successfully and broadly explored in the field of food science and technology (Gunning & Morris, 2018; Jones, 2016; Obeid & Guyomarc'h, 2020; Wen, Xu, Liu, Corke, & Sui, 2020; Zhong, Finglas, Wang, & Wang, 2019). Foods and their production processes can be considered as typical biological nanomaterials and biological processes. With more research going into food science, the use of AFM has been expanded to analyzing different food samples ranging from the smallest biomolecules such as food proteins (Shi, He, Ding, Wang, & Zhong, 2019a,b), food carbohydrates (Wang & Nie, 2019), and food toxins (Alexander Reese & Xu, 2019) to food-related microorganisms and pathogens (Kuda, Shibata, Takahashi, & Kimura, 2015; Liu & Yang, 2019) and food cell wall structures (Posé et al., 2019) to all the way up to food materials (Cárdenas-Pérez et al., 2019), food packaging materials (Marinello, La Storia, Mauriello, & Passeri, 2019), and food emulsion (Ho, Abik, & Mikkonen, 2022). Hence, AFM has also proven to be a powerful technique for the studies of food production processes and food analyses.

As an increasingly popular nanotechnological tool, AFM has many advantages for food research. (1) AFM has many primary (e.g., contact, noncontact, and tapping) and secondary (e.g., phase imaging and deflection) imaging modes for sample surface analysis (Zhong & Yan, 2016), which are useful for analyzing many properties of food substances. (2) Compared with optical imaging techniques (e.g., general optical microscopy and fluorescence microscopy), AFM has higher spatial resolution (Z direction: subnanometer scale; X–Y direction: nanometer scale), and so the substructures of food substances can be observed (Fukuma, 2020). (3) Compared with electron imaging techniques (e.g., scanning electron microscopy and transmission electron microscopy), the sample preparation of AFM does not require complicated preparations or chemical modifications, which might result in possible artifacts. (4) Compared with other imaging techniques, AFM images the samples in a true three-dimensional

surface profile way, which can be applied to measure the height of the food substances and the surface roughness of food tissues and materials. (5) The samples can be analyzed in atmosphere and liquid environments (no need of dehydration like other electron microscopy imaging techniques), which is useful for analyzing the behaviors of food substances in simulated working and physiological conditions. (6) The samples can be analyzed in some special environments (e.g., vacuum, cryo, and controlled humidity and temperature), which is useful for analyzing the behaviors of food substances in simulated food processing and storage conditions (Zhao, Kristi, & Ye, 2021). (7) The samples can be in situ observed by normal and high-speed AFM, which is useful for obtaining a nanoscale topographic “movie” of the nanomaterial-related food processing and preservation processes. (8) AFM can be combined with other techniques such as optical microscopy (Gómez-Varela et al., 2020; Miranda et al., 2021), infrared spectroscopy (Dazzi & Prater, 2017), Raman (Fernandes, Mareau, & Gonon, 2018; Prats-Mateu & Gierlinger, 2017), mass spectrometry (Thiruvallur Eachambadi et al., 2021), and X-ray technique (Slobodskyy et al., 2015) to simultaneously analyze the different samples of interests. (9) AFM can be applied to measure the force–distance curves when AFM tip approaches to and retracts from the sample surfaces, which is useful for analyzing single-molecule interaction and nanomechanical properties of food materials (Alexander Reese & Xu, 2019; Cárdenas-Pérez et al., 2019). (10) AFM can be used as a mechanical nanomachining tool to manipulate and fabricate biological samples (Pavliček & Gross, 2017; Zhao et al., 2018), which is useful for analyze the behaviors of food substances during mechanical processing. Due to these specific advantages, AFM will undoubtedly attract the attention of food scientists and engineers in the future.

It should be noted that the application of AFM for food research has several disadvantages: (1) The poor temporal resolution (in minute range) of normal AFM greatly limits their application in biological research. To overcome these limitations, scientists have tried to develop high-speed AFM (Feuillie et al., 2020; Jiao, Cannon, Lin, Gladfelter, & Scheuring, 2020) and large-scan area high-speed AFM (Marchesi et al., 2021), which increases the temporal resolution to milliseconds. In addition, commercial high-speed AFMs have been developed recently. (2) Sample height compression effect may occur because of the elastic deformation of biological samples (Zhong & Yan, 2016) and the measured heights are lower than the real heights of biological samples. (3) Tip-broadening effect may occur

because of the tip–sample convolution (Yuan, Liang, Liang, Pang, & Jia, 2021), and the measured widths are larger than the real widths of biological samples. (4) Under liquid, the possible electrostatic repulsion between AFM tip and the sample surface may affect the AFM tip approach and retract process, which, in turn, may affect the measurement of the real morphology of biological samples (Müller & Engel, 1997; Zhong et al., 2010). We should be careful in eliminating the possible electrostatic repulsion by optimizing the liquid conditions such as the ionic strength. (5) It results in many possible image artifacts during the AFM operation process, which should be minimized to obtain reliable data.

We suggest food scientists and engineers to master the basic knowledge of AFM prior to using it. AFM is a very professional instrument and the operators should be very careful during the AFM work process. Thorough learning and training are imperative for new users. There is a steep learning curve for new users who hope to master AFM application. There are several books published on AFM application for biologists such as *Atomic force microscopy in cell biology* (Wilson, Matsudaira, Jena, & Horber, 2002), *Atomic force microscopy for biologists* (Morris, Kirby, & Gunning, 2009), *Atomic force microscopy in biomedical research: methods and protocols (methods in molecular biology)* (Braga & Ricci, 2011), *Atomic force microscopy in nanobiology* (Takeyasu, 2014), *Cellular analysis by atomic force microscopy* (Lekka, 2017), and *Atomic force microscopy in molecular and cell biology* (Cai, 2018). The interested readers could read these books for more detail. However, until now, no such book has systematically described the application of AFM for food research.

The purpose of this book is to introduce the reader to the fundamentals of application of AFM for food research. The book consists of three parts: Part I: Introduction of AFM for food research (Chapter 1); Part II: Fundamentals of AFM for food research (Chapters 2–3); and Part III: Application of AFM for food research (Chapters 4–10). Chapter 1 mainly discusses why this book is indispensable for the food community. Chapter 2 introduces the basic principles of AFM. Chapter 3 describes the operation procedure of AFM. Chapters 4–8 present the application of AFM for food proteins, food polysaccharides, food microorganisms, food foams and emulsions, and food powders and contact materials, respectively. Chapter 9 introduces AFM nanomechanics for food research. Chapter 10 discusses current and potential integration of AFM with other techniques for food science. This book does not discuss AFM application for food cells and tissues because very few studies have been published on

these two topics so far. The interested readers could read the books mentioned in the above paragraph or reviews on AFM application for biological cells (Bitler, Dover, & Shai, 2018; Chtcheglova & Hinterdorfer, 2018; Guillaume-Gentil et al., 2014; Kasas, Stupar, & Dietler, 2018; Sokolov, Dokukin, & Guz, 2013) and tissues (Han et al., 2017; Stylianou, Lekka, & Stylianopoulos, 2018). In summary, this book serves as a guide for understanding the application of AFM for food research. It can facilitate in understanding AFM application easily and thus shortening the learning time for new hands.

The target audience of this book is broad. This book is ideal for professional food scientists and engineers who are interested in food formulation and structuration. It is also ideal for AFM operators in instrumental analysis centers who are required to measure and analyze food samples. In addition, it is ideal for students pursuing undergraduate and postgraduate courses on food structures. It may also prove useful for AFM developers and application experts who want to develop and popularize AFM in the field of food science and technology.

## Acknowledgements

As the editors of this book, we thank Elsevier Publisher for giving us the opportunity to edit this book, and in particular Lena Sparks, Indhumathi Mani, Devlin Person, Nina Bandeira, and Bharatwaj Varatharajan on the editorial staff for their almost limitless patience. We also wish to acknowledge all the contributors who provided such grand writing. We wish to acknowledge the kind support of those publishers who provided copyrights of beautiful figures, and individual accreditations are given to the relevant figure captions. Finally, Jian Zhong wishes to acknowledge the research support from the National Key R&D Program of China (No. 2019YFD0902003).

## References

- Alexander Reese, R., & Xu, B. (2019). Single-molecule detection of proteins and toxins in food using atomic force microscopy. *Trends in Food Science & Technology*, 87, 26–34.
- Bellon, L. (2020). Atomic force microscopy. *Physics Today*, 73, 57–58.
- Binnig, G., Quate, C. F., & Gerber, C. (1986). Atomic force microscope. *Physical Review Letters*, 56, 930–933.
- Bitler, A., Dover, R. S., & Shai, Y. (2018). Fractal properties of cell surface structures: A view from AFM. *Seminars in Cell & Developmental Biology*, 73, 64–70.
- Braga, P. C., & Ricci, D. (2011). *Atomic force microscopy in biomedical research: Methods and protocols*. Springer.
- Cai, J. (2018). *Atomic force microscopy in molecular and cell biology*. Springer.



- Chen, J., & Xu, K. (2020). Applications of atomic force microscopy in materials, semiconductors, polymers, and medicine: A minireview. *Instrumentation Science & Technology*, *48*, 667–681.
- Chitchevlova, L. A., & Hinterdorfer, P. (2018). Simultaneous AFM topography and recognition imaging at the plasma membrane of mammalian cells. *Seminars in Cell & Developmental Biology*, *73*, 45–56.
- Collins, L., Liu, Y., Ovchinnikova, O. S., & Proksch, R. (2019). Quantitative electromechanical atomic force microscopy. *ACS Nano*, *13*, 8055–8066.
- Cárdenas-Pérez, S., Chanona-Pérez, J. J., Méndez-Méndez, J. V., Arzate-Vázquez, I., Hernández-Varela, J. D., & Vera, N. G. (2019). Recent advances in atomic force microscopy for assessing the nanomechanical properties of food materials. *Trends in Food Science & Technology*, *87*, 59–72.
- Dazzi, A., & Prater, C. B. (2017). AFM-IR: Technology and applications in nanoscale infrared spectroscopy and chemical imaging. *Chemical Reviews*, *117*, 5146–5173.
- Dufrière, Y. F., Ando, T., García, R., Alsteens, D., Martínez-Martin, D., Engel, A., ... Müller, D. J. (2017). Imaging modes of atomic force microscopy for application in molecular and cell biology. *Nature Nanotechnology*, *12*, 295–307.
- Efremov, Y. M., Okajima, T., & Raman, A. (2020). Measuring viscoelasticity of soft biological samples using atomic force microscopy. *Soft Matter*, *16*, 64–81.
- Fernandes, J. P. C., Mareau, V. H., & Gonon, L. (2018). AFM-Raman colocalization setup: Advanced characterization technique for polymers. *International Journal of Polymer Analysis and Characterization*, *23*, 113–119.
- Feuillie, C., Lambert, E., Ewald, M., Azouz, M., Henry, S., Marsaudon, S., ... Molinari, M. (2020). High speed afm and nano-infrared spectroscopy investigation of A $\beta$ 1–42 peptide variants and their interaction with POPC/SM/Chol/GM1 model membranes. *Frontiers in Molecular Biosciences*, *7*, 571696.
- Fukui, T., Uchihashi, T., Sasaki, N., Watanabe, H., Takeuchi, M., & Sugiyasu, K. (2018). Direct observation and manipulation of supramolecular polymerization by high-speed atomic force microscopy. *Angewandte Chemie International Edition*, *57*, 15465–15470.
- Fukuma, T. (2020). Subnanometer-scale imaging of nanobio-interfaces by frequency modulation atomic force microscopy. *Biochemical Society Transactions*, *48*, 1675–1682.
- Gross, L., Schuler, B., Pavliček, N., Fatayer, S., Majzik, Z., Moll, N., ... Meyer, G. (2018). Atomic force microscopy for molecular structure elucidation. *Angewandte Chemie International Edition*, *57*, 3888–3908.
- Guillaume-Gentil, O., Potthoff, E., Ossola, D., Franz, C. M., Zambelli, T., & Vorholt, J. A. (2014). Force-controlled manipulation of single cells: From AFM to FluidFM. *Trends in Biotechnology*, *32*, 381–388.
- Gunning, A. P., & Morris, V. J. (2018). Getting the feel of food structure with atomic force microscopy. *Food Hydrocolloids*, *78*, 62–76.
- Gómez-Varela, A. I., Stamov, D. R., Miranda, A., Alves, R., Barata-Antunes, C., Damboumet, D., ... De Beule, P. A. A. (2020). Simultaneous co-localized super-resolution fluorescence microscopy and atomic force microscopy: Combined SIM and AFM platform for the life sciences. *Scientific Reports*, *10*, 1122.
- Han, B., Nia, H. T., Wang, C., Chandrasekaran, P., Li, Q., Chery, D. R., ... Han, L. (2017). AFM-nanomechanical test: An interdisciplinary tool that links the understanding of cartilage and meniscus biomechanics, osteoarthritis degeneration, and tissue engineering. *ACS Biomaterials Science & Engineering*, *3*, 2033–2049.
- Ho, T. M., Abik, F., & Mikkonen, K. S. (2022). An overview of nanoemulsion characterization via atomic force microscopy. *Critical Reviews in Food Science and Nutrition*, *62*, 4908–4928.
- Jiao, F., Cannon, K. S., Lin, Y.-C., Gladfelter, A. S., & Scheuring, S. (2020). The hierarchical assembly of septins revealed by high-speed AFM. *Nature Communications*, *11*, 5062.

- Jones, O. G. (2016). Developments in dynamic atomic force microscopy techniques to characterize viscoelastic behaviors of food materials at the nanometer-scale. *Current Opinion in Food Science*, 9, 77–83.
- Kasas, S., Stupar, P., & Dietler, G. (2018). AFM contribution to unveil pro- and eukaryotic cell mechanical properties. *Seminars in Cell & Developmental Biology*, 73, 177–187.
- Kiio, T. M., & Park, S. (2020). Nano-scientific application of atomic force microscopy in pathology: From molecules to tissues. *International Journal of Medical Sciences*, 17, 844–858.
- Kilpatrick, J. I., Revenko, I., & Rodriguez, B. J. (2015). Nanomechanics of cells and biomaterials studied by atomic force microscopy. *Advanced Healthcare Materials*, 4, 2456–2474.
- Krieg, M., Fläschner, G., Alsteens, D., Gaub, B. M., Roos, W. H., Wuite, G. J. L., ... Müller, D. J. (2019). Atomic force microscopy-based mechanobiology. *Nature Reviews Physics*, 1, 41–57.
- Kuchuk, K., & Sivan, U. (2018). Hydration structure of a single DNA molecule revealed by frequency-modulation atomic force microscopy. *Nano Letters*, 18, 2733–2737.
- Kuda, T., Shibata, G., Takahashi, H., & Kimura, B. (2015). Effect of quantity of food residues on resistance to desiccation of food-related pathogens adhered to a stainless steel surface. *Food Microbiology*, 46, 234–238.
- Lekka, M. (2017). *Cellular analysis by atomic force microscopy*. CRC Press.
- Li, J., Liu, Y., Yuan, Y., & Huang, B. (2021). Applications of atomic force microscopy in immunology. *Frontiers of Medicine*, 15, 43–52.
- Li, M., Xi, N., Wang, Y.-c., & Liu, L.-q. (2021). Atomic force microscopy for revealing micro/nanoscale mechanics in tumor metastasis: From single cells to microenvironmental cues. *Acta Pharmacologica Sinica*, 42, 323–339.
- Liu, Q., & Yang, H. (2019). Application of atomic force microscopy in food microorganisms. *Trends in Food Science & Technology*, 87, 73–83.
- Liu, Y., & Vancso, G. J. (2020). Polymer single chain imaging, molecular forces, and nanoscale processes by Atomic Force Microscopy: The ultimate proof of the macromolecular hypothesis. *Progress in Polymer Science*, 104, 101232.
- Ma, M., Zhong, J., Li, W., Zhou, J., Yan, Z., Ding, J., & He, D. (2013). Comparison of four synthetic model peptides to understand the role of modular motifs in the self-assembly of silk fibroin. *Soft Matter*, 9, 11325–11333.
- Main, K. H. S., Provan, J. I., Haynes, P. J., Wells, G., Hartley, J. A., & Pyne, A. L. B. (2021). Atomic force microscopy—A tool for structural and translational DNA research. *APL Bioengineering*, 5, 031504.
- Marchesi, A., Umeda, K., Komekawa, T., Matsubara, T., Flechsig, H., Ando, T., ... Franz, C. M. (2021). An ultra-wide scanner for large-area high-speed atomic force microscopy with megapixel resolution. *Scientific Reports*, 11, 13003.
- Marinello, F., La Storia, A., Mauriello, G., & Passeri, D. (2019). Atomic force microscopy techniques to investigate activated food packaging materials. *Trends in Food Science & Technology*, 87, 84–93.
- Martines, E., Zhong, J., Muzard, J., Lee, A. C., Akhremitchev, B. B., Suter, D. M., & Lee, G. U. (2012). Single-molecule force spectroscopy of the *Aplysia* cell adhesion molecule reveals two homophilic bonds. *Biophysical Journal*, 103, 649–657.
- Miranda, A., Gómez-Varela, A. I., Stylianou, A., Hirvonen, L. M., Sánchez, H., & DeBeule, P. A. A. (2021). How did correlative atomic force microscopy and super-resolution microscopy evolve in the quest for unravelling enigmas in biology? *Nanoscale*, 13, 2082–2099.
- Morris, V. J., Kirby, A. R., & Gunning, P. A. (2009). *Atomic force microscopy for biologists*. World Scientific.
- Müller, D. J., & Engel, A. (1997). The height of biomolecules measured with the atomic force microscope depends on electrostatic interactions. *Biophysical Journal*, 73, 1633–1644.

- Nandi, T., & Ainaravapu, S. R. K. (2021). Applications of atomic force microscopy in modern biology. *Emerging Topics in Life Sciences*, 5, 103–111.
- Nievergelt, A. P., Banterle, N., Andany, S. H., Gönczy, P., & Fantner, G. E. (2018). High-speed photothermal off-resonance atomic force microscopy reveals assembly routes of centriolar scaffold protein SAS-6. *Nature Nanotechnology*, 13, 696–701.
- Obeid, S., & Guyomarc'h, F. (2020). Atomic force microscopy of food assembly: Structural and mechanical insights at the nanoscale and potential opportunities from other fields. *Food Bioscience*, 36, 100654.
- Pavliček, N., & Gross, L. (2017). Generation, manipulation and characterization of molecules by atomic force microscopy. *Nature Reviews Chemistry*, 1, 0005.
- Posé, S., Paniagua, C., Matas, A. J., Gunning, A. P., Morris, V. J., Quesada, M. A., & Mercado, J. A. (2019). A nanostructural view of the cell wall disassembly process during fruit ripening and postharvest storage by atomic force microscopy. *Trends in Food Science & Technology*, 87, 47–58.
- Prats-Mateu, B., & Gierlinger, N. (2017). Tip in–light on: Advantages, challenges, and applications of combining AFM and Raman microscopy on biological samples. *Microscopy Research and Technique*, 80, 30–40.
- Sapra, K. T., Spoerri, P. M., Engel, A., Alsteens, D., & Müller, D. J. (2019). Seeing and sensing single G protein-coupled receptors by atomic force microscopy. *Current Opinion in Cell Biology*, 57, 25–32.
- Shi, C., He, Y., Ding, M., Wang, Y., & Zhong, J. (2019a). Nanoimaging of food proteins by atomic force microscopy. Part I: Components, imaging modes, observation ways, and research types. *Trends in Food Science & Technology*, 87, 3–13.
- Shi, C., He, Y., Ding, M., Wang, Y., & Zhong, J. (2019b). Nanoimaging of food proteins by atomic force microscopy. Part II: Application for food proteins from different sources. *Trends in Food Science & Technology*, 87, 14–25.
- Si, H., Zhang, S., Ma, S., Xiong, Z., Kausar, A., Liao, Q., ... Zhang, Y. (2020). Emerging conductive atomic force microscopy for metal halide perovskite materials and solar cells. *Advanced Energy Materials*, 10, 1903922.
- Slobodskyy, T., Zozulya, A. V., Tholapi, R., Liefeth, L., Fester, M., Sprung, M., & Hansen, W. (2015). Versatile atomic force microscopy setup combined with micro-focused X-ray beam. *Review of Scientific Instruments*, 86, 065104.
- Sokolov, I., Dokukin, M. E., & Guz, N. V. (2013). Method for quantitative measurements of the elastic modulus of biological cells in AFM indentation experiments. *Methods (San Diego, Calif.)*, 60, 202–213.
- Stylianou, A., Lekka, M., & Stylianopoulos, T. (2018). AFM assessing of nanomechanical fingerprints for cancer early diagnosis and classification: From single cell to tissue level. *Nanoscale*, 10, 20930–20945.
- Takeyasu, K. (2014). *Atomic force microscopy in nanobiology*. CRC Press.
- Thiruvallur Eachambadi, R., Boschker, H. T. S., Franquet, A., Spampinato, V., Hidalgo-Martinez, S., Valcke, R., ... Manca, J. V. (2021). Enhanced laterally resolved ToF-SIMS and AFM imaging of the electrically conductive structures in cable bacteria. *Analytical Chemistry*, 93, 7226–7234.
- Uchihashi, T., & Scheuring, S. (2018). Applications of high-speed atomic force microscopy to real-time visualization of dynamic biomolecular processes. *Biochimica et Biophysica Acta (BBA) - General Subjects*, 1862, 229–240.
- Wang, J., & Nie, S. (2019). Application of atomic force microscopy in microscopic analysis of polysaccharide. *Trends in Food Science & Technology*, 87, 35–46.
- Wen, Y., Xu, Z., Liu, Y., Corke, H., & Sui, Z. (2020). Investigation of food microstructure and texture using atomic force microscopy: A review. *Comprehensive Reviews in Food Science and Food Safety*, 19, 2357–2379.

- Wilson, L., Matsudaira, P. T., Jena, B. P., & Horber, J. H. (2002). *Atomic force microscopy in cell biology*. Academic Press.
- Yadavalli, V. K., & Ehrhardt, C. J. (2021). Atomic force microscopy as a biophysical tool for nanoscale forensic investigations. *Science & Justice*, *61*, 1–12.
- Yuan, G., Liang, T., Liang, Y., Pang, X., & Jia, Z. (2021). The controlled growth of conjugated polymer–quantum dot nanocomposites via a unimolecular templating strategy. *Chemical Communications*, *57*, 1250–1253.
- Zhao, D., Liu, S., & Gao, Y. (2018). Single-molecule manipulation and detection. *Acta Biochimica et Biophysica Sinica*, *50*, 231–237.
- Zhao, L., Kristi, N., & Ye, Z. (2021). Atomic force microscopy in food preservation research: New insights to overcome spoilage issues. *Food Research International*, *140*, 110043.
- Zhong, J. (2011). From simple to complex: Investigating the effects of lipid composition and phase on the membrane interactions of biomolecules using in situ atomic force microscopy. *Integrative Biology*, *3*, 632–644.
- Zhong, J., Finglas, P., Wang, Y., & Wang, X. (2019). Application of atomic force microscopy in food science. *Trends in Food Science & Technology*, *87*, 1–2.
- Zhong, J., & He, D. (2012). Recent progress in the application of atomic force microscopy for supported lipid bilayers. *Chemistry—A European Journal*, *18*, 4148–4155.
- Zhong, J., Liu, X., Wei, D., Yan, J., Wang, P., Sun, G., & He, D. (2015). Effect of incubation temperature on the self-assembly of regenerated silk fibroin: A study using AFM. *International Journal of Biological Macromolecules*, *76*, 195–202.
- Zhong, J., Ma, M., Li, W., Zhou, J., Yan, Z., Ding, J., & He, D. (2014). Self-assembly of regenerated silk fibroin from random coil nanostructures to antiparallel  $\beta$ -sheet nanostructures. *Biopolymers*, *101*, 1181–1192.
- Zhong, J., Ma, M., Zhou, J., Wei, D., Yan, Z., & He, D. (2013). Tip-induced micropatterning of silk fibroin protein using in situ solution atomic force microscopy. *ACS Applied Materials & Interfaces*, *5*, 737–746.
- Zhong, J., Sun, G., & He, D. (2014). Classic, liquid, and matrix-assisted dip-pen nanolithography for materials research. *Nanoscale*, *6*, 12217–12228.
- Zhong, J., & Yan, J. (2016). Seeing is believing: Atomic force microscopy imaging for nanomaterial research. *RSC Advances*, *6*, 1103–1121.
- Zhong, J., Yang, C., Zheng, W., Huang, L., Hong, Y., Wang, L., & Sha, Y. (2009). Effects of lipid composition and phase on the membrane interaction of the prion peptide 106–126 amide. *Biophysical Journal*, *96*, 4610–4621.
- Zhong, J., Yang, C., Zheng, W., Huang, L., Hong, Y., Wang, L., & Sha, Y. (2010). The role of calcium ions in the interactions of PrP106–126 amide with model membranes. *Colloids and Surfaces B: Biointerfaces*, *77*, 40–46.
- Zhong, J., Zheng, W., Huang, L., Hong, Y., Wang, L., Qiu, Y., & Sha, Y. (2007). PrP106–126 amide causes the semi-penetrated poration in the supported lipid bilayers. *BBA - Biomembranes*, *1768*, 1420–1429.
- Zhou, G., Zhang, B., Tang, G., Yu, X.-F., & Galluzzi, M. (2021). Cells nanomechanics by atomic force microscopy: Focus on interactions at nanoscale. *Advances in Physics: X*, *6*, 1866668.

This page intentionally left blank

## SECTION 2

# Fundamentals of AFM

This page intentionally left blank

## CHAPTER 2

# Atomic force microscopy: from theory to application in food science

Sofiane El-Kirat-Chatel<sup>1</sup>, Jennifer Burgain<sup>2</sup>, Claire Gaiani<sup>2,3</sup> and Grégoiry Francius<sup>1</sup>

<sup>1</sup>Université de Lorraine, CNRS, LCPME, UMR 7564, Nancy, France

<sup>2</sup>LIBio (Laboratoire d'Ingénierie des Biomolécules), Université de Lorraine, Vandoeuvre-lès-Nancy Cedex, France

<sup>3</sup>Ministry of Higher Education, Research and Innovation, IUF (Institut Universitaire de France), Paris, France

## 2.1 History of atomic force microscopy

Atomic force microscopy (AFM) was developed in 1986 by the researchers Gerd Binnig, Christoph Gerber, and Calvin Quate (Binnig, Quate, & Gerber, 1986). It was developed based on the principles of the scanning tunneling microscope (STM), which was developed earlier in 1982 at the International Business Machines Corporation (IBM) in Zurich (Binnig, Rohrer, Gerber, & Weibel, 1982). AFM is based on the integration of the “tunnel current” (quantum effect of crossing a potential barrier by particles of energy lower than this barrier) with a scanning of the surface to produce images, initially based on semiconductor materials. This important breakthrough allowing the imaging of atomic structure on a sample surface earned them the Nobel Prize in Physics. However, STM could only be used to analyze conductive or semi-conductive samples, thus limiting its scope of application. To broaden and extend this type of microscopy to the study of nonconductive materials, AFM was developed via a collaboration between IBM and Stanford University, allowing the imaging of sample surfaces according to operating modes (contact, intermittent, and noncontact modes).

First, AFM was operated in contact mode where samples could be examined in air, liquid, or vacuum (Binnig et al., 1986, 1982; Rugar & Hansma, 1990). However, the investigation of biological samples in contact mode remained tricky because their softness and weak immobilization on to a substrate often resulted in surface damages. To improve the



performance of AFM for soft biological samples, a noncontact mode was first introduced in 1987 (Martin, Williams, & Wickramasinghe, 1987; Meyer & Amer, 1988; J. Yang, Tamm, Somlyo, & Shao, 1993). Later, the first microfabricated AFM probes were developed in 1991, enhancing the performance of AFM in terms of imaging accuracy and resolution (Prater, Hansma, Tortonese, & Quate, 1991). Furthermore, the use of AFM boomed with mass production of microfabricated AFM probes and the development of the optical beam deflection method, allowing more accurate detection of cantilever deflection (Meyer & Amer, 1988). Tapping mode in air was first developed in 1993 and then extended to the fluid environment in 1994 by Hansma's Lab (Hansma et al., 1994; Zhong, Inniss, Kjoller, & Elings, 1993). Such operating modes for the first time allowed the imaging of soft and biological samples in an aqueous medium with high resolution while limiting and/or avoiding sample surface alteration. However, AFM was severely limited by its image acquisition time irrespective of its operating mode, although tapping mode is slightly faster. Monitoring the dynamics of fast processes (i.e., occurring in less than a few minutes) on sample surfaces was not possible. This limitation was overcome with the introduction of high-speed AFMs (HS-AFM) in 2001 by Ando's group (Ando et al., 2001). Such an improvement for the first time allowed real-time monitoring of biomolecules in action (Ando, 2017; Ando, Uchihashi, & Kodera, 2013; Casuso et al., 2012; Kodera, Yamamoto, Ishikawa, & Ando, 2010).

AFM was first used to image sample surfaces, but it also allows probing physicochemical properties according to the measurement of interactions between the AFM probe and the surface. New operating modes combining imaging and force measurements have been under development since 2010 to simultaneously provide imaging and force characterization in a quantitative manner. Such modes allow access to spatially resolved images in correlation with mechanical, chemical, and electrical data in only one acquisition (Fischer, Stadler, & Erina, 2013; Krieg et al., 2019; Last, Russell, Nealey, & Murphy, 2010; "Product News," 2020; Xu et al., 2018).

## 2.2 Basic principles of atomic force microscopy

Microscopy is a commonly used technique in the food industry mainly because it allows examination at high magnification of food materials (cereals, meat, creams, beverages, fruits, vegetables, dairy products, etc.)

(Kaláb, Allan-Wojtas, & Miller, 1995). Such a technique is very important for investigating morphology, texture, microstructures, and possible biological and inorganic contaminants in food materials (Fazaeli, Tahmasebi, & Emam-Djomeh, 2012). A wide variety of microscopy instruments have been developed and used in food science and technology research. Among these instruments, optical and electron microscopes (including scanning and transmission ones [SEM/TEM]) are currently the most used in the examination of food samples (Caillet, Cogné, Andrieu, Laurent, & Rivoire, 2003; He, Feng, Yang, Wu, & Li, 2004). SEM and TEM facilitate collecting insightful information about the food structure at the macromolecular scale; however, there are some drawbacks associated with these techniques that limit the accuracy and interpretation of the observations. Indeed, samples need to be pretreated by staining, freezing, and drying and are generally examined under high vacuum. Such pretreatment can alter or modify microstructures and sample surface particularly for the ones containing water.

Recently, AFM has been adapted in food science and technology research to overcome these drawbacks (Kirby, Gunning, & Morris, 1995; Liu & Wang, 2011; Obeid & Guyomarc'h, 2020; Yang et al., 2007). Basically, AFM is a commonly used technique in materials and life sciences (Chang, Chiang, Yang, & Liou, 2012; Min, 2015; Parot et al., 2007), which allows nanoscale examination of samples' morphology, and physicochemical and surface properties (Jandt, 2001; Variola, 2015) (electrostatic charge density, hydrophobicity, nanomechanics, etc.) under different conditions, including aqueous media, organic solvents, air, vacuum, and controlled temperature (Broekmaat, Brinkman, Blank, & Rijnders, 2008; Gaponenko, Gamperle, Herberg, Muller, & Paruch, 2016; Han, Mou, Sheng, Yang, & Shao, 1995; Stukalov, Murray, Jacina, & Dutcher, 2006). Despite having these advantages compared to classic optical and electron microscopies, AFM technologies and their application to food sciences remain underexplored.

### 2.2.1 Basic components

AFM microscopes are generally constructed with components similar to those found in a stylus profiler and an STM. The main difference is that in AFM, the probe forces on the sample surface are much smaller than those in a stylus profiler. Basically, AFM operation is based on the measurement of interactions between a probe (usually a sharp and thin

pyramidal tip associated with a reflective cantilever of fixed spring constant) and the sample surface, as illustrated in Fig. 2.1. The cantilever is mounted on the AFM device, which controls its vertical displacement (along the  $z$  axis, perpendicular to the surface) using a piezoelectric transducer (ceramic). Lateral motions (along the  $x$  and  $y$  axes, parallel to the plane of the surface) are controlled by the deformation of piezoelectric ceramics. These piezoelectric transducers therefore make it possible to manage the relative position of the AFM-tip and the surface, for example, to perform a scan ( $x, y$ ) or to maintain the AFM-tip at a constant altitude ( $z$ ).

Most AFMs have two types of configuration. In the first one, the cantilever is integrated with the piezoelectric scanner, while in the second configuration, it is the sample that is fixed on the scanner and mobile. Transducers or piezoelectric ceramics are materials that could be mechanically deformed under the effect of an electric voltage. Briefly, it is possible to control the displacement, elongation, and/or torsion of a piezoelectric ceramic by applying an electrical signal, with less than a nanometer precision. It is particularly this property that has made it possible to achieve sub-nanometric spatial resolution.

The interaction forces exerted on the AFM-tip are measured by means of a laser spot always focused at the end of the cantilever (above the tip).

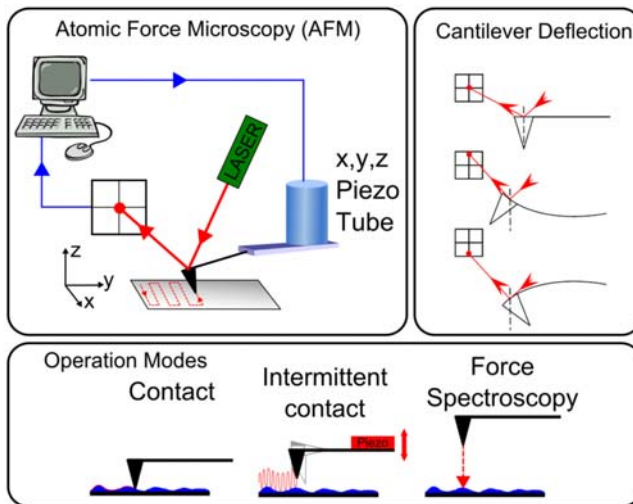


**Figure 2.1** Basics and principles of atomic force microscopy. Modified from <http://bio-mechanicalregulation-lab.org/afm>.

The laser reflection is then collected on a quadrant photodetector consisting of four photodiodes. It is the position of the spot reflected on the photodetector that makes it possible to quantify the motion of the AFM-tip (deflection) with a resolution of the order of a tenth of a nanometer. Indeed, when the laser is not deflected, it strikes at the center of the quadrants, and therefore illuminates the four photodiodes in the same way with the same intensity. If the laser beam is deflected upwards, the two top photodiodes will receive more light than the bottom ones, and a voltage difference will appear at the photodetector. It is this voltage difference that is used for the feedback loop.

In practice, it is necessary to calibrate the AFM before taking measurements. To do this, the reflected spot must first be aligned at the center of the four photodiodes. This position will then be used as a reference to detect either attractive forces (negative values with respect to this reference) or repulsive forces (positive values) or even friction forces through the lateral displacements of the spot on the photodiodes, as illustrated in Fig. 2.1.

Commercial cantilevers used in AFM are based on microelectronics (e.g., by etching, photo-lithography, or chemical attack) (Caballero et al., 2010; Pan et al., 2020; Ximen & Russell, 1992). The AFM-tips attached to the end of the cantilevers as well as the cantilevers themselves are usually made of silicon or silicon nitride, the main materials found in microelectronics. Commercial cantilevers can have a rectangular or triangular geometry (Fig. 2.2). The latter geometry has the advantage of being much more resistant to torsional stresses. Typical dimensions of a cantilever vary from 5 to 300  $\mu\text{m}$  in length, from 3 to 200  $\mu\text{m}$  in width, and from 0.3 to 1  $\mu\text{m}$  in thickness.

The spring constant  $k$  of the cantilevers ranges from 0.01 to 300 N/m, depending largely on their shape and geometry. The thicker and shorter cantilevers are the stiffest. However, too rigid cantilevers can exert too high forces, which can damage both AFM-tip and sample. The minimum forces required to produce images are of the order of 1–10 nN, except for biological samples where they are less than 0.1 nN. The resonance frequencies of the cantilevers generally lie between 10 and 5000 kHz depending again on their shape and geometry. The thicker and shorter levers are those with the highest resonance frequency.

Typically, AFM-tips should be as sharp as possible because the resolution of images depends on the radius of curvature of the apex of the tips. Microfabrication methods make it possible to design AFM-tips with a

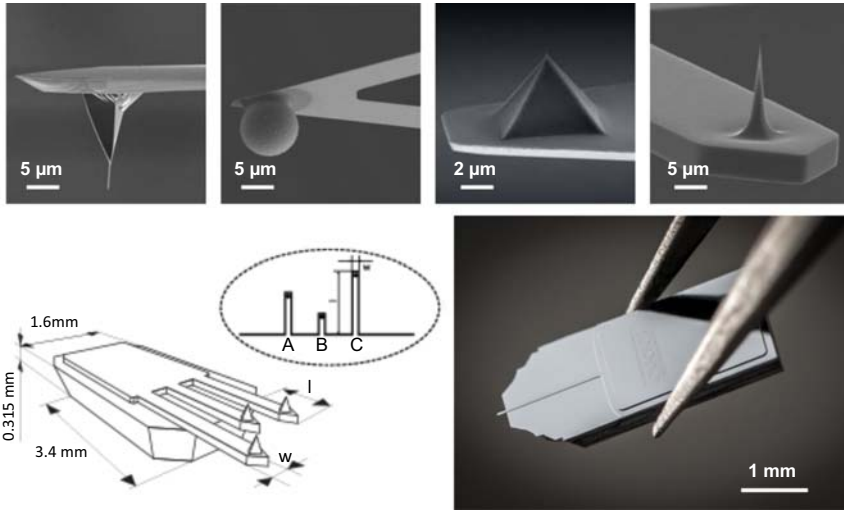


**Figure 2.2** SEM images of atomic force microscopy (AFM) cantilever differing in their respective geometry and representative schemes of AFM technical data. Adapted from <https://www.nanoandmore.com/> and <https://www.spmtips.com/>.

radius of curvature ranging from about only 1 nm to several tens of nm. AFM-tips can be conical or pyramidal with a square, diamond, or triangular base (Fig. 2.2). The thinnest and sharpest ones allow high-resolution (molecular) imaging, commonly denoted as “high-aspect-ratio” AFM-tips. However, they are extremely fragile and very easily break because they are silicon-based. The other AFM-tips are generally made of silicon nitride and are less sharp with a larger radius of curvature, denoted as “low-aspect-ratio” AFM-tips. These are the most commonly used tips for imaging and force measurements.

Both AFM-tips and cantilevers can be coated with a thin metallic layer (chrome, silver, gold) or any specific coating depending on their application in materials and life sciences. The thickness of these layers varies from 2 to 50 nm, and does not significantly alter the sharpness of the AFM-tip. Moreover, the tips can be replaced with colloidal particles (gold, borosilicate, polystyrene) whose diameter can vary from 50 to 50  $\mu\text{m}$ , for example, colloidal probes.

## 2.2.2 Working conditions, basic functions, and theory

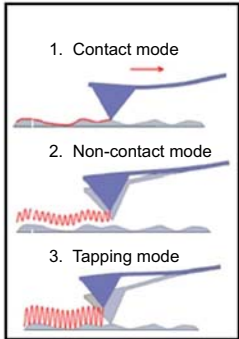
The versatility and advantages of AFM microscopes over conventional electron microscopes mainly originate from the fact that they allow

in-depth investigation of the sample surfaces under different conditions (Broekmaat et al., 2008; Gaponenko et al., 2016; Han et al., 1995; He et al., 2004; Stukalov et al., 2006) (air, vacuum, controlled humidity, controlled pressure and temperature, etc.) and especially in aqueous media without any preparation and pretreatment of the sample, thus allowing the study in real time of living biological systems (Berquand et al., 2010; Shi, Zhang, Xia, & Fang, 2012; You & Yu, 1999) but also of organic/inorganic ones under real/environmental conditions.

However, the only condition required for forming images and carrying out force measurements in AFM is the immobilization of the samples. To this end, simple preparation methods such as direct sample adsorption onto a classic or specific/coated substrate can be applied (immobilization is obtained by capillary, van der Waals or electrostatic interactions) (Allison, Sullivan, Mortensen, Retterer, & Doktycz, 2011; Sahai et al., 2016; J. Wang & Wang, 2010). Moreover, samples can be mechanically entrapped or immobilized onto membranes, polydimethylsiloxane stamps, cells arrays, or silicon traps (Formosa-Dague et al., 2015; Peric, Hannebelle, Adams, & Fantner, 2017). Glue or wax can also be used for food powder immobilization as well detailing in several works (Burgain, El Zein, et al., 2016; Morgan, Raghunathan, Thomasy, Murphy, & Russell, 2014; Starostina et al., 2008). All these preparation or sample immobilization methods are valid irrespective of whether measurements are performed in an aqueous medium or under air conditions.

AFM has three main imaging operating modes, including contact, intermittent contact, and noncontact ones; the noncontact mode is seldom used and can be considered under certain working conditions as belonging to the intermittent contact mode (Fig. 2.3). Only contact (non-vibrating) and intermittent (vibrating) modes are frequently used in AFM imaging. All these modes have been developed with time based on experiments and applications. The simplest or easiest imaging mode in AFM is the contact mode, so-called “static mode.” The others imaging modes belong to the so-called “dynamic mode,” which is further categorized into noncontact and intermittent contact modes. These different operating modes make it possible to acquire three-dimensional images of the sample surface with high resolution.

Static mode consists of scanning the sample surface with continuous “contact” between AFM probe and the sample surface. Here, the forces involved in the “contact” are repulsive, both long- and short-range forces adding up to the imaging signal. The AFM-tip is dragged over the



AFM Modes of Operation	Working Principle	Advantage	Disadvantage
Contact Mode	<ul style="list-style-type: none"> <li>Physical contact between the tip and the surface</li> </ul>	<ul style="list-style-type: none"> <li>High scan speeds</li> <li>High resolution</li> </ul>	<ul style="list-style-type: none"> <li>Damage to soft sample</li> <li>Lateral forces may produce image artefacts</li> </ul>
Non-contact Mode	<ul style="list-style-type: none"> <li>No contact between the tip and the sample</li> </ul>	<ul style="list-style-type: none"> <li>Low resolution</li> <li>No damage to sample</li> </ul>	<ul style="list-style-type: none"> <li>Slower scan speed if compared with both contact and tapping mode</li> </ul>
Tapping Mode	<ul style="list-style-type: none"> <li>Intermittent and short contact between the sample and the tip</li> </ul>	<ul style="list-style-type: none"> <li>High resolution</li> <li>Minimal damage to sample</li> </ul>	<ul style="list-style-type: none"> <li>Slower scan speed if compared with contact mode</li> </ul>

**Figure 2.3** Atomic force microscopy operation modes. Contact mode: The tip is moved over the surface by the scanning system. A value of the cantilever deflection, for example, is selected and then the feedback system adjusts the height of the cantilever base to keep this deflection constant as the tip moves over the surface. Noncontact mode: The cantilever oscillates close to the sample surface but without making contact with the surface. The capillary force makes this particularly difficult to control under ambient conditions. Very stiff cantilevers are needed. Tapping mode: The cantilever oscillates and the tip makes repulsive contact with the surface of the sample at the lowest point of the oscillation. Tapping mode is useful for imaging soft samples such as biology or polymers. Adapted from <http://slideplayer.com/slide/9702681/>.

substrate, maintaining the cantilever deflection at a constant position. The applied force can be estimated from the detected variations of the cantilever bending according to Hooke’s law:

$$F = k \times \Delta z \tag{2.1}$$

Both AFM-tip and sample can be subjected to deformation provided by the applied or pushing force, which can lead to collision/hitting risks distorting roughness and morphology of the sample. So, cantilevers supporting the AFM-tips require as small spring constant as possible to generate lateral strains weaker than forces allowing sample sorption onto substrate. The sample surface is iso-force scanned line by line according to the (x, y) plane depicting the topographic view of the sample.

The “dynamic mode” is based on the cantilever oscillations (resonance and off-resonance frequencies) obtained by external excitation coming from an actuator. The vibrating energy stored by the cantilever can be tuned to reach close to the cantilever resonance characterized by specific amplitude, phase, and frequency often of the order of 100 kHz. When the oscillating cantilever is brought close to or in intermittent contact to the sample surface, these three parameters are modified due to the

interaction forces acting between the AFM-tip and the sample. Here, the AFM-tip periodically interacts with the surface, and when it is close or comes in contact with the surface, the amplitude decreases with shift in resonance frequency. So, a control loop is then applied to maintain the amplitude at a constant value during the scanning of the sample surface along the  $(x, y)$  plane. This feedback makes it possible to reconstruct the surface topography according to the theoretical formalism described elsewhere (García, 2002; Nalwa & Magonov, 2001). It should be noticed that this imaging allows analysis of fragile samples without damaging them (nondestructive method).

Noncontact mode is a rarely used one based on the attractive forces occurring between the tip and the surface under study. This mode is very rarely used because attractive forces are very weak and their accurate detection requires an extremely low noise environment. In addition, the surface of the samples is generally covered with a thin layer (few nanometers thick) consisting mainly of water vapor and various pollutants. These adsorbates have a significant impact on the measurements. Hence, noncontact-mode imaging usually needs to be done in vacuum to limit pollutant layer formation and to achieve sufficient resolution. A lift from the sample surface of several nanometer is always maintained with the AFM-tips oscillating at their resonance frequency. Here, the feedback is exerted either on the deflection (attraction) of the cantilever or on the amplitude of the oscillations during the scanning of the sample surface along the  $(x, y)$  plane. This feedback allows reconstruction of the surface topography.

### 2.3 Force measurements and nanomanipulation

There are two main families of forces existing in nature, those acting over distances ranging from nanometers to kilometers and those acting only at very short distances. The latter family of forces includes the intermolecular ones responsible for a large number of physicochemical properties and phenomena. Among the four fundamental forces (strong, weak, gravitational, and electromagnetic), only electrostatic interactions (belonging to the family of electromagnetic forces) are considered when studying intermolecular interactions.

AFM allows measurements of surface forces that are the sum of intermolecular forces that differ in the distance at which they are exerted. At a very short distance to the surface ( $<0.2$  nm), the best known forces are



Born interactions corresponding to the repulsive forces in Lennard–Jones potential. van der Waals' forces generally occur when distances to the surface are less than 10 nm irrespective of the system and the medium considered. For greater distances to the sample surface, electrostatic and hydrophobic forces may be present with, in the case of electrostatic ones, singularities, which vary according to the medium (pH, ionic strength). Steric forces or interactions are often invoked in the case of polymers or macromolecules. They refer to the repulsive forces due to the presence and/or compression of these polymers. Fig. 2.4 summarizes several types of forces commonly measured in AFM. These interactions between AFM-tip and sample surface are involved in the contrast obtained in AFM images. It can be noticed that other forces described in Fig. 2.5 (mechanical, molecular stretching) are special cases allowing stiffness and adhesion measurements but also conformational analysis in the case where the samples consist of macromolecules. All these physicochemical parameters are generally determined by the analysis of the force curves.

The force curves are obtained from the variations in the magnitude of interactions between the AFM-tip and the sample surface with variation in distance between them. Two configurations should be considered during force measurements, as reported in Fig. 2.5. In the first configuration, the AFM-tip is approached until contact to the sample surface corresponding to the approach curve. The approach curve can be divided into three domains:

- The first domain, so-called baseline, corresponds to a distance range where no interaction is detected because the cantilever is not close enough to the sample surface. This region is used to normalize the force curves by setting this value as the zero force.
- In the second domain the AFM-tip is very close to the sample surface where negative or positive (attractive or repulsive) interactions can be detected. These interactions generally originate from electrostatic or van der Waals' interactions. It can be noticed that at this position the AFM-tip is not in contact with the sample.
- In the last domain, the AFM-tip is physically in contact with the sample surface with increasing measured forces, and the sample can be deformed or indented. For nondeformable samples, the applied or pushing force increases linearly with the deformation/deflection of the cantilever. On the other hand, for deformable samples, the compression and/or indentation of these samples generally leads to nonlinear behaviors.

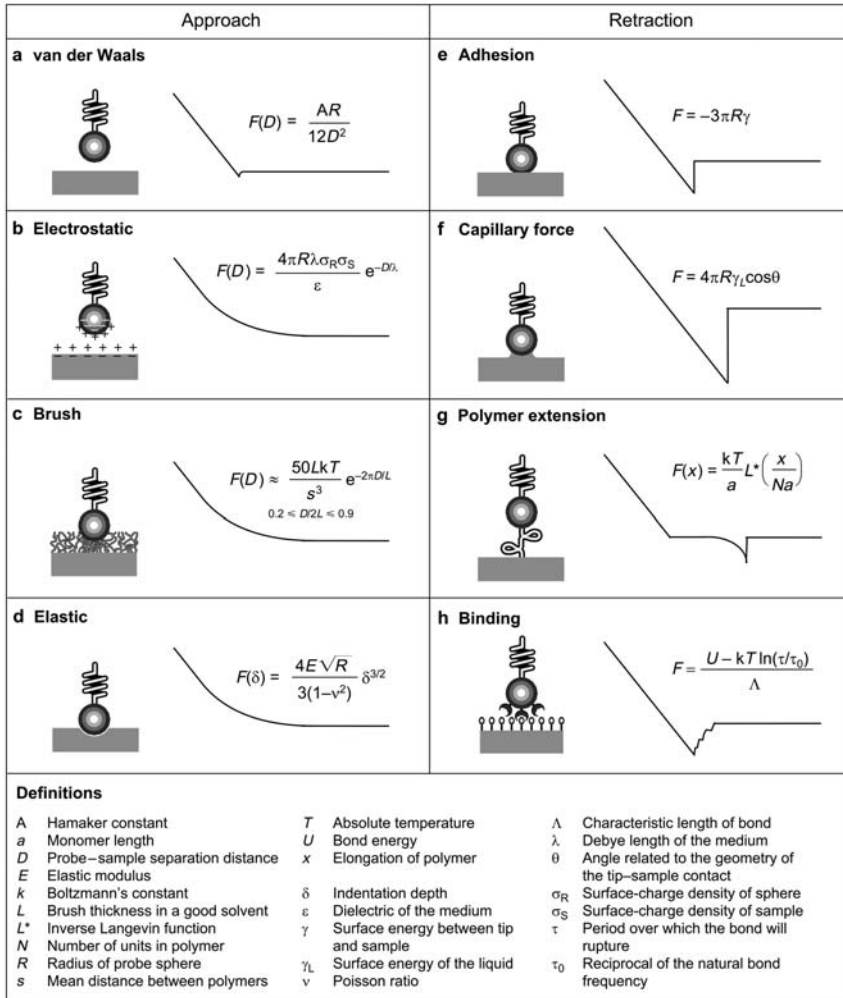


**Figure 2.4** Panorama of forces measurable with atomic force microscopy. Data from Heinz, W. F., & Hoh, J. H. (1999). *Spatially resolved force spectroscopy of biological surfaces using the atomic force microscope*. Trends in Biotechnology, 17(4), 143–150.

- The second configuration is obtained when the AFM-tip is withdrawn from the sample surface and corresponds to the retract curve. This curve can be divided into two domains:
- In the first one, the applied force decreasing with AFM-tip withdrawal while always remaining in contact with the sample. A hysteresis between the approach and retract curves can occur, reflecting the

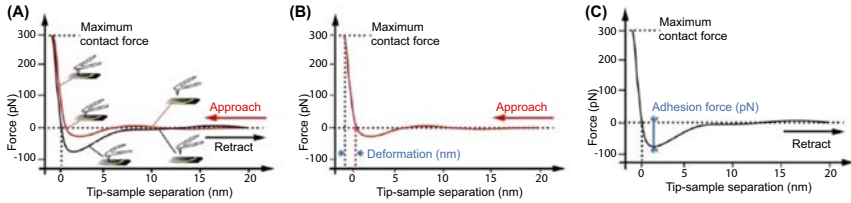


**Figure 2.5** Description and decomposition of the different regions in approach and retraction force–distance curves. Adapted from Wegmann, S., Medalsy, I., Mandelkow, E., & Müller, D. (2012). *Proceedings of the National Academy of Sciences of the United States of America*, 110.

viscoelastic properties of the sample. For nondeformable samples, this hysteresis is zero.

- In the second domain, the curve can exhibit linear and/or nonlinear negative peaks corresponding to adhesive interactions between AFM-tips and the sample surface. These adhesive forces generally depend on the contact area, contact time, sample–AFM-tip surface energy, and also on intermolecular interactions if some molecules are sorbed onto both interacting surfaces.

Consequently, force mode has been developed in AFM for a better force control and detection, particularly in physics, chemistry, and biology applications. Force–volume or force–mapping mode is one of most interesting AFM applications to biophysics. This operating mode allows spatially resolved maps of the force curves, and therefore to visualize and measure point by point the variations in the interaction forces between AFM-tip and samples. In this case, sample morphology can be correlated to the force map. Indeed, the sample surface to be studied is divided into a grid (e.g., a grid of  $32 \times 32$  pixels) perfectly defined and located in space ( $x$ ,  $y$ , and  $z$  coordinates). Furthermore, the possibility of functionalizing AFM-tips with molecules (alkanethiols, lectins, proteins or antibodies) makes it possible to obtain adhesion maps of specific interactions. In the case of an AFM-tip modified with  $\text{CH}_3$ -terminated alkanethiols, hydrophobicity mappings (Alsteens, Dague, Rouxhet, Baulard, & Dufrene, 2007; Beaussart et al., 2012; Dague et al., 2007) can be done, while for lectins or antibodies, it is rather biomolecularly recognizing ones related to receptor–ligand interactions (Beaussart et al., 2012; Dupres, Alsteens, Andre, Verbelen, & Dufrière, 2009; Francius et al., 2008; Francius et al., 2009; Verbelen et al., 2009). Besides, mechanical properties as well as elasticity or stiffness mappings (Heinisch, Dupres, Alsteens, & Dufrene, 2010; Krieg et al., 2019; Tripathi et al., 2013) can be determined

according to the data processing of the force curves with adequate theory (Polyakov et al., 2011).

For almost two decades, nanomanipulations using AFM were under development and now they provide the ability to automatically assemble and build nanostructures from nanoscale objects such as particles, nanorods, nanotubes, polymers, and organic and inorganic molecules (Kim, Ratchford, & Li, 2009; A. Requicha, 2010; Rubio-Sierra, Heckl, & Stark, 2005). In this case, AFM is used and programmed as a robot equipped with a mechanical arm—the AFM-tip—allowing direct manipulation of nanoscale objects and/or micrometric samples (Chacko, Harke, Canale, & Diaspro, 2014; Requicha, Arbuckle, Mokaberi, & Yun, 2009; Wang et al., 2013). Indeed, AFM-tip can be modified and adapted to entrap and then unfold or displace specific molecules or nanoscale objects such as DNA, fullerene nanoparticles, or protein assemblies. These nanomanipulations are also used to decipher second structures and conformational properties of proteins and organic molecules assemblies (oligomers) or to evaluate their nanomechanical properties at the molecular scale (A. Requicha, 2010; Xie, Onal, Régnier, & Sitti, 2012). Besides, nanomanipulations allow investigating single molecules and single cells in the field of biophysics and biology applications (Aprikian et al., 2011; Funami, 2010; Ott, Jobst, Schoeler, Gaub, & Nash, 2017; Scholl, Li, & Marszalek, 2014). AFM can be also programmed for automated biomechanical testing of several biological cells in parallel to their morphology (Chacko et al., 2014).

## 2.4 New imaging modes

Among all developments in AFM techniques that have happened over the last decade, imaging modes have emerged as the most notable one. In particular, PeakForce Tapping, PeakForce QNM, and ScanAsyst imaging modes developed by Bruker in 2010 are extensively used for studying biomolecules, polymers, viruses, living cells, and nanoparticles. Indeed, PeakForce Tapping has emerged as one of the most significant scientific breakthroughs in AFM techniques since the introduction of TappingMode in the early 1990s. It allows unprecedented high-resolution imaging for a range of samples, which was not possible previously. Besides, it facilitates simultaneous nanoscale surface property mapping and morphology with more accurate and direct force control with significant time savings in image acquisition.

Basically, PeakForce Tapping mode is based on the tip-sample distance modulation by a sinusoidal motion at amplitudes in the range of

2–400 nm for frequencies up to 8.0 kHz. Moreover, when the AFM-tip is brought into contact with the sample surface, the interactions between tip and sample are controlled by maintaining the maximum force between the tip and the sample constant (peak force), as described in Fig. 2.6. Thus, a force curve is performed at every pixel position on the sample surface with respect to the  $z$  position of the AFM-tip. The peak force interaction of each of these force curves is then used as the imaging feedback signal. Analysis of whole force curve data is done on the fly, providing a map of multiple properties (e.g., elastic modulus, energy dissipation, adhesion, etc.) that have the same resolution as the topography image (up to 1 million pixels per image) in a few minutes. Such performances in terms of acquisition time and resolution are possible because this mode can be operated at very high frequencies (e.g., between 1.0 and 2.0 kHz). Furthermore, the introduction of self-optimizing ScanAsyst mode has enabled significant improvement in terms of both resolution and quality in PeakForce Tapping imaging. ScanAsyst technology is based on “intelligent” algorithms that allow considerable decrease and control on the set-point drift that normally occurs in other AFM operating modes. Besides, this optional mode also allows automated and continuous monitoring of image quality by auto-optimization and adjustment of the imaging force at the point of each tip–sample interaction.

Additionally, PeakForce Tapping technology makes it possible to produce quantitative data helping researchers to address the critical question of what physicochemical properties of samples they should be investigating in relation to their topography. To this end, several derivative modes have been introduced such as PeakForce QNM, which is one of the most used. It allows us to establish a correlation between AFM imaging and quantitative mapping of

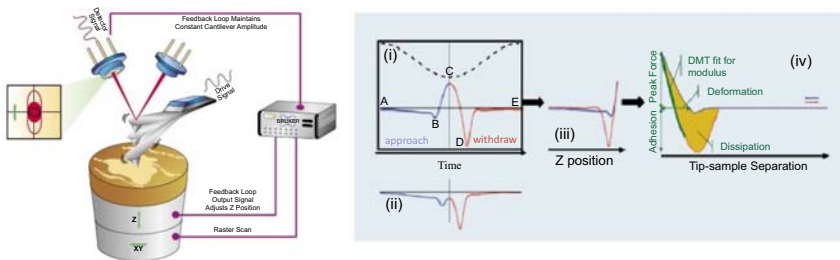


**Figure 2.6** Principles and description of PeakForce Tapping™ mode. Adapted from <https://www.bruker.com/products/surface-and-dimensional-analysis/atomic-force-microscopes/modes/modes/peakforce-modes.html>.

mechanical, chemical, and physicochemical interactions. Indeed, these quantitative data produced can help identify components and their mixing at interfaces, as well as map mechanical properties at previously unattainable resolution. It can be inferred that PeakForce technology enables several derivative modes, including PeakForce TUNA, PeakForce KPFM (Kelvin Probe Force Microscopy), PeakForce SECM (Scanning ElectroChemical Microscopy), and PeakForce sMIM (scanning Microwave Impedance Microscopy), which are used for full nanoelectrical, electrochemical, and mechanical characterization of materials, including biological ones.

## 2.5 Measurement items

There are many suppliers who manufacture AFM devices, including Bruker, Agilent Technologies, Angstrom Advanced, NanoScience Technologies, Oxford Instruments, NanoSurf, and Park Systems. Depending on where the scanner is located, AFM devices can be classified into three different types, as illustrated by Fig. 2.7: (1) tip-scanning devices where the cantilever moves while the sample is fixed on the sample stage; (2) sample-scanning devices where the scanner is placed under the sample and the latter is placed onto a piezo stage that moves while the cantilever is held at a fixed position; and (3) AFM devices that employ decoupled  $xy$  and  $z$  scanners, i.e. the sample is mounted onto the  $xy$  scanner while the cantilever is fixed to the  $z$  scanner to reduce the cross-talk between the two scanners.

Notice that AFM can be also integrated with non and inverted optical microscopes, X-ray photoelectron spectroscopy (XPS), or infrared/Raman microscopes. Prior to such integrations, samples analyses were often not collocated between the different techniques, limiting the accuracy and interpretation of the results. Now the integrated systems allow in situ and collocated,

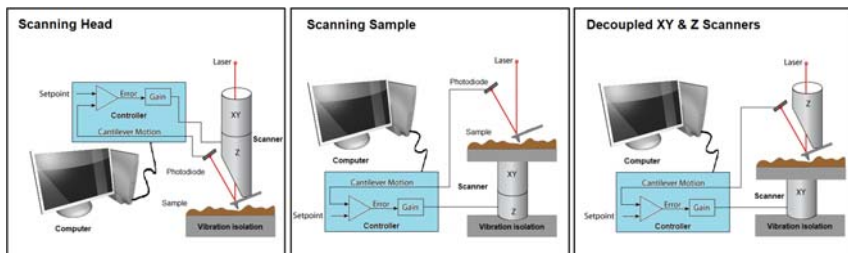


**Figure 2.7** Classification of atomic force microscopy devices according to their technical configuration.

multiparametric and simultaneous measurements combining imaging with elemental (XPS) or biochemical (infrared, Raman) analyses. For more details about AFM integrated systems, see Chapter 11.

AFM integrated with optical microscopes are the most sold and used devices, particularly in the fields of biology and chemistry, because it allows direct observation and additional optical monitoring of microscale samples. Besides, integration with optical microscopy opens up new possibilities, particularly in epifluorescence microscopy or confocal laser scanning microscopy. Such supplementary techniques are very useful in biology for in situ and real-time investigation of biological processes involving living cells or microorganisms as well as chemical or physical phenomena involving nanoparticles and macromolecules.

## **2.6 Atomic force microscopy integration with other instruments**

AFM has made it possible to quantify and explore the surface, electrical, mechanical, and other physical properties of various samples with nanoscale resolution in many environments. However, it remains limited in certain scientific fields, for example, it does not give information about chemical specificity. Thus, new developments have been initiated in recent years to provide new functionality to AFM equipment and or combine/integrating it with other scientific devices. Concerning the surface chemistry of samples, AFM has been integrated with laser spectroscopy (including Raman spectroscopy, luminescence, and fluorescence) to overcome their fundamental limitation in terms of spatial resolution and offer complete collocated surface chemistry analysis and AFM characterization. Some developments have also allowed combining AFM with scanning electron microscopy and X-ray photoelectron spectroscopy to enhance spatial resolution for elemental analysis mapping for example. Nowadays, manufacturers offer many options for AFM, which are detailed in Chapter 11.

## **2.7 Research ways and applications**

### **2.7.1 Research type**

AFM has become the reference characterization and observation technique for nanosciences as well as for materials/food science and engineering. This tool has also taken a prominent place in industrial research and development centers. The latest developments make it a major asset in understanding

physical, chemical, and biological phenomena from the micro- to the nano-scales. The scope of combination of high-resolution imaging and the measurement of physical quantities (forces, adhesion, stiffness, etc.) to characterize samples is a major advantage of this approach compared to other techniques available in the laboratories. The application of AFM in food science and engineering allows three types of observation (direct, ex situ and in situ) of the sample according to the condition under which an investigation is done. Direct observation is the most commonly used or applied method. Indeed, most basic food research primarily requires imaging, for example, the structure and topography of proteins and polysaccharides (Kirby et al., 1995; Liu & Wang, 2011). Ex situ observation is generally carried out by imaging the surface of the sample before and then after the treatment of the latter (Alsteens et al., 2007; Burgain, El Zein, et al., 2016). In situ observation is usually achieved by continuously imaging the same area during the sample processing process (Burgain, El Zein, et al., 2016). In situ observation also makes it possible to follow the dynamic evolution of the surface or the surface properties of the sample, whereas ex situ observation simply accounts for the modifications resulting from this evolution. Since the advent of high-speed AFMs, in situ observations by AFM have made it possible to study dynamic phenomena over very short times (a few minutes), whereas conventional AFMs allowed the study of slower phenomena over time ranging from a few tens of minutes to several days (Ando, 2017; Ando et al., 2001; Casuso et al., 2012).

Recent works highlighted that specific interactions between bacteria (*Lactobacillus rhamnosus* GG) and dairy proteins can be deciphered. The authors clearly identified these specific interactions and evidenced that many factors influence the bacterial interaction with the dairy matrix, including the nature of the proteins, the nature of the strains, and the pH of the media. Indeed, they investigated the molecular organization at the outer surface of *L. rhamnosus* GG by single cell force spectroscopy at various pH. Such investigations have revealed that bacterial-pili interactions with whey proteins could be screened to an extent depending on the pH-mediated embedment of the pili within the exopolysaccharide layer that decorates the bacterial cell wall (J. Burgain et al., 2015; Guerin et al., 2016). AFM-based studies related to food science and engineering as well as biology and materials science have been on the rise since the evolution this technique providing relevant information from direct observations, as summarized in Table 2.1. Notice that all important references and works cited in this chapter are reported in this table.



**Table 2.1** Summary of research ways reported herein. Typical examples of different research types of atomic force microscopy imaging and force spectroscopy measurements related to biology, food, and biomaterials science and engineering.

No.	AFM modes	Research types	Observation	Purpose of the study	References
1	Imaging and force	Topography and stiffness	Direct	Bacteria, lipid membranes, polysaccharides	<a href="#">Obeid and Guyomarc'h (2020)</a>
2	Imaging	Topography	Direct	Gelatin, casein, amylopectin, carrageenan	<a href="#">Liu and Wang (2011)</a>
3	Imaging and force	Topography and adhesion	Direct	Pectic polysaccharides	<a href="#">Kirby et al. (1995)</a>
4	Imaging and force	Topography and adhesion	Direct	Eukaryotic cells, yeast, bacteria, membranes, DNA	<a href="#">Variola (2015)</a>
5	Imaging	Topography	Direct	Myosin V, bacteriorhodopsin, immunoglobulin	<a href="#">Ando et al. (2001)</a>
6	Video	Topography	Direct	Myosin V, actin filament	<a href="#">Kodera et al. (2010)</a>
7	Time lapse imaging	Topography	Direct	Membrane proteins	<a href="#">Casuso et al. (2012)</a>
8	Imaging and force	Topography, stiffness, adhesion	Direct	Mammalian cells, bacteria, viruses, proteins	<a href="#">Krieg et al. (2019)</a>
9	Imaging and force	Topography and stiffness	Direct	Mammalian cells, worm cells, antibodies, proteins	<a href="#">Xu et al. (2018)</a>
10	Imaging and force	Topography and stiffness	Direct	Mammalian cells	<a href="#">Berquand et al. (2010)</a>
11	Imaging and force	Stiffness and adhesion	Direct	Mammalian cells	<a href="#">Shi et al. (2012)</a>
12	Force	Stiffness	Direct	Human Wharton's jelly, mammalian cells	<a href="#">Sahai et al. (2016)</a>

13	Imaging	Topography	Direct	Bacteria immobilization	Allison et al. (2011)
14	Imaging and force	Topography and adhesion	Direct	Yeast and cell wall proteins	Beaussart et al. (2012)
15	Imaging and force	Topography, stiffness, adhesion	Direct	Bacteria, exopolysaccharides	Francius et al. (2008)
16	Imaging and force	Topography and adhesion	Direct	Protein isolate powders	Burgain, Scher, Petit, Francius, and Gaiani, (2016)
17	Force	Stiffness	Direct	Nanomechanical properties of food materials	Cárdenas-Pérez et al. (2019)
18	Imaging and force	Topography and adhesion	Direct	Lactic bacteria, lactoglobulin	Gomand et al. (2019)

## 2.7.2 Quick overview of applications in food sciences

Over the past decade or so, AFM has gained considerable attention for its use in food industry mainly because it allows deciphering fine structures of food and its component at a micrometer to nanometer scale and under different environmental conditions. In this way, AFM applications to food sciences enable us to reveal novel clues for elucidating mechanisms of food-related phenomena, including correlations between classic imaging and surface properties at the local or nanoscale level. In the following paragraph, we discuss representative examples of AFM applications in food sciences and technology.

AFM is a very useful tool for conducting morphological and rheological investigations of food components at the nanoscale. Such studies allow unraveling molecular structures of molecules (polysaccharides and polypeptides) and biophysical processes involved in their aggregation and/or (self) organization, as illustrated in Fig. 2.8.

For example, molecular interactions involved in gelation of gellan gums and impact of salt in the resulting rheological properties have been elucidated by AFM (Funami, 2010; Liu & Wang, 2011). These investigations revealed the impact of potassium and sodium cation concentration on the structuration of the fiber network constituting the gel as well as on the resulting rheological properties (Fig. 2.7). Characterization of macromolecules and colloids (polysaccharides, polypeptides, glycopeptides, etc.) by AFM are currently used in food science. AFM is also used for the elucidation of interfacial phenomena (e.g., foam and emulsion formations) and complex processes (e.g., digestion, fermentation, etc.) to understand and improve processes in food industry (Gunning & Morris, 2018; Gunning et al., 2004). The development of force mode in AFM (force spectroscopy) has enabled development of numerous methodologies and techniques. Force spectroscopy is also gaining interest in food research since it allows both quantification and location of surface physicochemical features (e.g., hydrophobicity, adhesion, capillary, elasticity, etc.) of food products. Furthermore, nanoindentation by AFM is a novel and emerging technique that allows the determination of several nanomechanical properties such as stiffness, elasticity, deformation as well as sample morphology, providing important insight into the complex processes associated with food materials. Some studies have reported that AFM can be used to monitor the quality of food materials (e.g., milk, gelatin, pectins, casein or proteins, etc.) during processing and

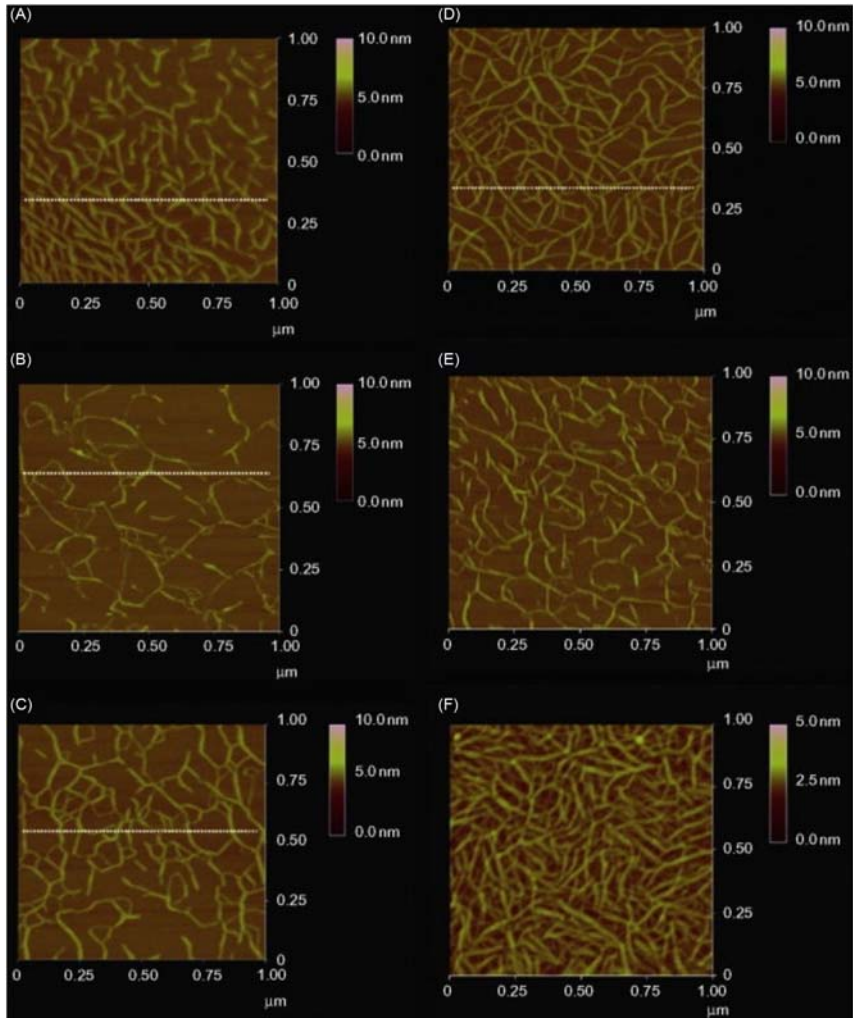


**Figure 2.8** Topographical atomic force microscopy images of molecular assemblies of gellan gum with different acyl contents in the absence of added cations (A, B) or in the presence of sodium (E, F) cations. Adapted from Liu, S., Wang, Y. (2011). A review of the application of atomic force microscopy (AFM) in food science and technology. *Advances in Food and Nutrition Research*, 62, 201–240.

storage (Burgain, El Zein, et al., 2016; Burgain, Scher, et al., 2016). AFM is also used to monitor nanomechanical and physicochemical properties of dairy products such as whey protein powders, as reported in Fig. 2.9 (Burgain, El Zein, et al., 2016; Cárdenas-Pérez et al., 2019).

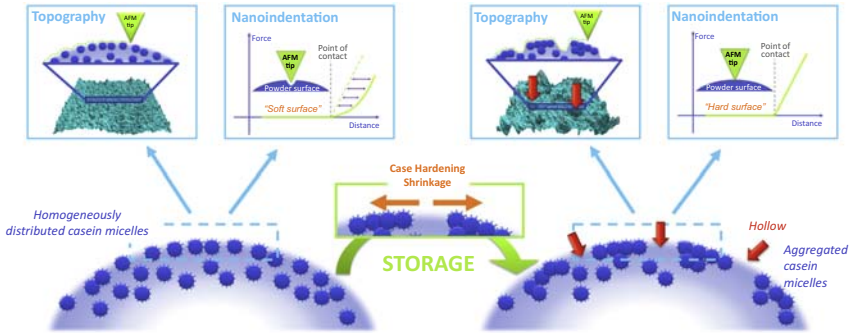


**Figure 2.9** Proposed underlying mechanism in play during storage of casein powders: hollow zone formation and surface stiffening. *Modified from Burgain, J., Scher, J., Petit, J., Francius, & G., Gaiani, C. (2016). Links between particle surface hardening and rehydration impairment during micellar casein powder storage. Food Hydrocolloids, 61, 277–285.*

These methodologies are relevant for following and quantifying at the local scale the occurrence of Maillard reactions and the degree of denaturation of the dairy products. Some authors used chemical force microscopy, a derivative AFM mode force spectroscopy where the AFM-tip is decorated with chemical groups (methyl, hydroxyl, etc.) to demonstrate a correlation between macroscopic observations in whey powders (through the browning index) and local modifications at the nanoscale (through the surface hydrophobicity). It was found that a high browning index was related to an increase in surface hydrophobicity when whey powders were stored at high temperatures. It was revealed that Maillard reaction is the main phenomenon responsible for powder alteration during storage, as illustrated in Fig. 2.10.

An understanding of the microbial environment and especially the bacterial interactions occurring within fresh or manufactured food is of great interest for food industry to further explore potential applications and to bring in improvement/control of some processing steps, such as fermentation of ripening. Microbial interactions are one of the underlying mechanisms of interfacial phenomena such as bacterial adhesion. Identifying, locating, and quantifying molecular interactions at the surface of food products is a challenge, which could be most possibly overcome using AFM methodologies (Burgain et al., 2014; Gomand et al., 2019; J. Guerin et al., 2018; J. Guerin et al., 2016).

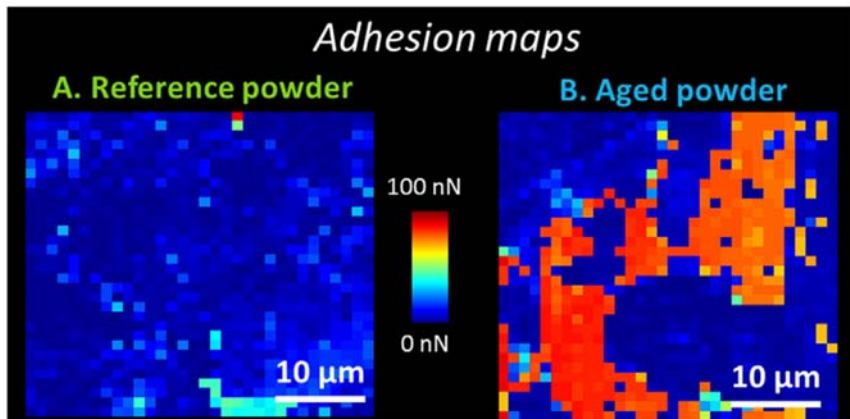
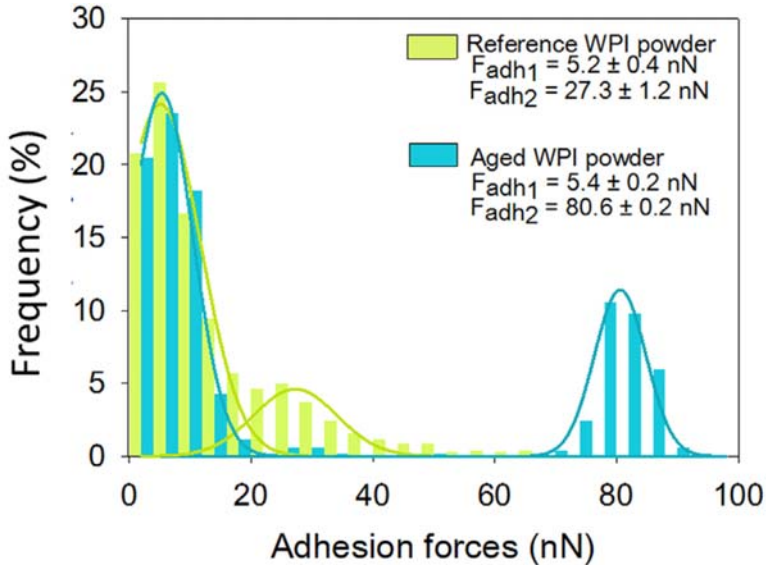


**Figure 2.10** Evolution of surface hydrophobic features of whey protein isolate (WPI) powders upon storage at 60°C for a period of 1 month. From Burgain, J., El Zein, R., Scher, J., Petit, J., Norwood, E.-A., Francius, G., & Gaiani, C. (2016). Local modifications of whey protein isolate powder surface during high temperature storage. *Journal of Food Engineering*, 178, 39–46.

## 2.8 Conclusion

AFM has emerged as one of the most relevant tools for investigating surface and mechanical features in food, providing unique spatially resolved insights into structures and functional behaviors at the nanoscale. Furthermore, high-resolution images from small molecules (lipids,

proteins, carbohydrate polymers) to bigger structures (gels, starch, gum, chocolate, and milk micelles) can be addressed under various conditions (pressure, temperature, humidity, medium environment, etc.), allowing studies of phase transition and other interfacial phenomena. AFM was first used in fundamental research of basic food components. In food science, understanding the structure of foods and evaluating their functionality are paramount in improving food quality, formulation, and processing. Besides, AFM derivative modes have been developed and adapted to study rheological and physicochemical properties and functional mechanisms of foods products under conditions close to their original status.

AFM enables gaining insights into deciphering many interfacial and functional processes from the macro- to the nanoscale to improve industrial processing and storage techniques. Studies related to further development of AFM and its derivative modes in combination with other complementary analysis techniques such as spectroscopy (X-photoelectron spectroscopy, infrared and Raman spectroscopy, etc.) are in progress, which may help derive more information (e.g., biochemical signature and composition) on food materials and also establish correlations between imaging and surface and mechanical features with chemical composition of food materials.

## References

- Allison, D. P., Sullivan, C. J., Mortensen, N. P., Retterer, S. T., & Doktycz, M. (2011). Bacterial immobilization for imaging by atomic force microscopy. *Journal of Visualized Experiments : JoVE*, 54, 2880. Available from <https://doi.org/10.3791/2880>.
- Alsteens, D., Dague, E., Rouxhet, P. G., Baulard, A. R., & Dufrene, Y. F. (2007). Direct measurement of hydrophobic forces on cell surfaces using AFM. *Langmuir: The ACS Journal of Surfaces and Colloids*, 23(24), 11977–11979. Available from <https://doi.org/10.1021/la702765c>.
- Ando, T. (2017). Directly watching biomolecules in action by high-speed atomic force microscopy. *Biophysical Reviews*, 9(4), 421–429. Available from <https://doi.org/10.1007/s12551-017-0281-7>.
- Ando, T., Kodera, N., Takai, E., Maruyama, D., Saito, K., & Toda, A. (2001). A high-speed atomic force microscope for studying biological macromolecules. *Proceedings of the National Academy of Sciences*, 98(22), 12468–12472. Available from <https://doi.org/10.1073/pnas.211400898>.
- Ando, T., Uchihashi, T., & Kodera, N. (2013). High-speed AFM and applications to biomolecular systems. *Annual Review of Biophysics*, 42(1), 393–414. Available from <https://doi.org/10.1146/annurev-biophys-083012-130324>.
- Aprikian, P., Interlandi, G., Kidd, B. A., Le Trong, I., Tchesnokova, V., Yakovenko, O., ... Sokurenko, E. V. (2011). The bacterial fimbrial tip acts as a mechanical force sensor. *PLoS Biology*, 9(5), e1000617. Available from <https://doi.org/10.1371/journal.pbio.1000617>.

- Beaussart, A., Alsteens, D., El-Kirat-Chatel, S., Lipke, P. N., Kucharikova, S., Van Dijck, P., & Dufrene, Y. F. (2012). Single-molecule imaging and functional analysis of Als adhesins and mannans during *Candida albicans* morphogenesis. *ACS Nano*, *6*(12), 10950–10964. Available from <https://doi.org/10.1021/nm304505s>.
- Berquand, A., Roduit, C., Kasas, S., Holloschi, A., Ponce, L., & Hafner, M. (2010). Atomic force microscopy imaging of living cells. *Microscopy Today*, *18*(6), 8–14. Available from <https://doi.org/10.1017/S1551929510000957>.
- Binnig, G., Quate, C. F., & Gerber, C. (1986). Atomic force microscope. *Physical Review Letters*, *56*(9), 930–933. Available from <https://doi.org/10.1103/PhysRevLett.56.930>.
- Binnig, G., Rohrer, H., Gerber, C., & Weibel, E. (1982). Surface studies by scanning tunneling microscopy. *Physical Review Letters*, *49*, 57–61.
- Broekmaat, J., Brinkman, A., Blank, D. H. A., & Rijnders, G. (2008). High temperature surface imaging using atomic force microscopy. *Applied Physics Letters*, *92*(4), 043102. Available from <https://doi.org/10.1063/1.2836943>.
- Burgain, J., El Zein, R., Scher, J., Petit, J., Norwood, E.-A., Francius, G., & Gaiani, C. (2016). Local modifications of whey protein isolate powder surface during high temperature storage. *Journal of Food Engineering*, *178*, 39–46. Available from <https://doi.org/10.1016/j.jfoodeng.2016.01.005>.
- Burgain, J., Scher, J., Francius, G., Borges, F., Corgneau, M., Revol-Junelles, A. M., ... Gaiani, C. (2014). Lactic acid bacteria in dairy food: Surface characterization and interactions with food matrix components. *Advances in Colloid and Interface Science*, *213*, 21–35. Available from <https://doi.org/10.1016/j.cis.2014.09.005>.
- Burgain, J., Scher, J., Lebeer, S., Vanderleyden, J., Corgneau, M., Guerin, J., ... Gaiani, C. (2015). Impacts of pH-mediated EPS structure on probiotic bacterial pili-whey proteins interactions. *Colloids and Surfaces. B, Biointerfaces*, *134*, 332–338. Available from <https://doi.org/10.1016/j.colsurfb.2015.06.068>.
- Burgain, J., Scher, J., Petit, J., Francius, G., & Gaiani, C. (2016). Links between particle surface hardening and rehydration impairment during micellar casein powder storage. *Food Hydrocolloids*, *61*, 277–285. Available from <https://doi.org/10.1016/j.foodhyd.2016.05.021>.
- Caballero, D., Villanueva, G., Plaza, J. A., Mills, C. A., Samitier, J., & Errachid, A. (2010). Sharp high-aspect-ratio AFM tips fabricated by a combination of deep reactive ion etching and focused ion beam techniques. *Journal of Nanoscience and Nanotechnology*, *10* (1), 497–501. Available from <https://doi.org/10.1166/jnn.2010.1737>.
- Caillet, A., Cogné, C., Andrieu, J., Laurent, P., & Rivoire, A. (2003). Characterization of ice cream structure by direct optical microscopy. Influence of freezing parameters. *LWT - Food Science and Technology*, *36*(8), 743–749. Available from [https://doi.org/10.1016/S0023-6438\(03\)00094-X](https://doi.org/10.1016/S0023-6438(03)00094-X).
- Casuso, I., Khao, J., Chami, M., Paul-Gilloteaux, P., Husain, M., Duneau, J.-P., ... Scheuring, S. (2012). Characterization of the motion of membrane proteins using high-speed atomic force microscopy. *Nature Nanotechnology*, *7*(8), 525–529. Available from <https://doi.org/10.1038/nnano.2012.109>.
- Chacko, J. V., Harke, B., Canale, C., & Diaspro, A. (2014). Cellular level nanomanipulation using atomic force microscope aided with superresolution imaging. *Journal of Biomedical Optics*, *19*(10), 105003. Available from <https://doi.org/10.1117/1.JBO.19.10.105003>.
- Chang, K.-C., Chiang, Y.-W., Yang, C.-H., & Liou, J.-W. (2012). Atomic force microscopy in biology and biomedicine. *Tzu Chi Medical Journal*, *24*(4), 162–169. Available from <https://doi.org/10.1016/j.tcmj.2012.08.002>.
- Cárdenas-Pérez, S., Chanona-Pérez, J. J., Méndez-Méndez, J. V., Arzate-Vázquez, I., Hernández-Varela, J. D., & Vera, N. G. (2019). Recent advances in atomic force microscopy for assessing the nanomechanical properties of food materials. *Trends in*



- Food Science and Technology*, 87, 59–72. Available from <https://doi.org/10.1016/j.tifs.2018.04.011>.
- Dague, E., Alsteens, D., Latge, J. P., Verbelen, C., Raze, D., Baulard, A. R., & Dufrene, Y. F. (2007). Chemical force microscopy of single live cells. *Nano Letters*, 7(10), 3026–3030. Available from <https://doi.org/10.1021/nl071476k>.
- Dupres, V., Alsteens, D., Andre, G., Verbelen, C., & Dufrene, Y. F. (2009). Fishing single molecules on live cells. *Nano Today*, 4(3), 262–268. Available from <https://doi.org/10.1016/j.nantod.2009.04.011>.
- Fazaeli, M., Tahmasebi, M., & Emam-Djomeh, Z. (2012). *Characterization of Food Texture: Application of Microscopic Technology*, 855–871.
- Fischer, H., Stadler, H., & Erina, N. (2013). Quantitative temperature-depending mapping of mechanical properties of bitumen at the nanoscale using the AFM operated with PeakForce Tapping (TM) mode. *Journal of Microscopy*, 250(3), 210–217. Available from <https://doi.org/10.1111/jmi.12036>.
- Formosa-Dague, C., Pillet, F., Schiavone, M., Duval, R., Ressler, L., & Dague, E. (2015). Generation of living cell arrays for atomic force microscopy studies. *Nature Protocols*, 10, 199–204. Available from <https://doi.org/10.1038/nprot.2015.004>.
- Francius, G., Alsteens, D., Dupres, V., Lebeer, S., De Keersmaecker, S., Vanderleyden, J., ... Dufrene, Y. F. (2009). Stretching polysaccharides on live cells using single molecule force spectroscopy. *Nature Protocols*, 4(6), 939–946. Available from <https://doi.org/10.1038/nprot.2009.65>.
- Francius, G., Lebeer, S., Alsteens, D., Wildling, L., Gruber, H. J., Hols, P., ... Dufrene, Y. F. (2008). Detection, localization, and conformational analysis of single polysaccharide molecules on live bacteria. *ACS Nano*, 2(9), 1921–1929. Available from <https://doi.org/10.1021/nn800341b>.
- Funami, T. (2010). Atomic force microscopy imaging of food polysaccharides. *Food Science and Technology Research*, 16(1), 1–12. Available from <https://doi.org/10.3136/fstr.16.1>.
- Gaponenko, I., Gamperle, L., Herberg, K., Muller, S. C., & Paruch, P. (2016). Low-noise humidity controller for imaging water mediated processes in atomic force microscopy. *Review of Scientific Instruments*, 87(6), 063709. Available from <https://doi.org/10.1063/1.4954285>.
- García, Á. (2002). Unifying theory of tapping-mode atomic-force microscopy. *Physical Review B*, 66. Available from <https://doi.org/10.1103/PhysRevB.66.041406>.
- Gomand, F., Borges, F., Guerin, J., El-Kirat-Chatel, S., Francius, G., Dumas, D., ... Gaiani, C. (2019). Adhesive interactions between lactic acid bacteria and beta-lactoglobulin: Specificity and impact on bacterial location in whey protein isolate. *Frontiers in Microbiology*, 10, 1512. Available from <https://doi.org/10.3389/fmicb.2019.01512>.
- Guerin, J., Bacharouche, J., Burgain, J., Lebeer, S., Francius, G., Borges, F., ... Gaiani, C. (2016). Pili of *Lactobacillus rhamnosus* GG mediate interaction with  $\beta$ -lactoglobulin. *Food Hydrocolloids*, 58, 35–41. Available from <https://doi.org/10.1016/j.foodhyd.2016.02.016>.
- Guerin, J., Soligot, C., Burgain, J., Hugué, M., Francius, G., El-Kirat-Chatel, S., ... Gaiani, C. (2018). Adhesive interactions between milk fat globule membrane and *Lactobacillus rhamnosus* GG inhibit bacterial attachment to Caco-2 TC7 intestinal cell. *Colloids and Surfaces, B, Biointerfaces*, 167, 44–53. Available from <https://doi.org/10.1016/j.colsurfb.2018.03.044>.
- Gunning, A. P., Kirby, A. R., Mackie, A. R., Kroon, P., Williamson, G., & Morris, V. J. (2004). Watching molecular processes with the atomic force microscope: Dynamics of polymer adsorption and desorption at the single molecule level. *Journal of Microscopy-Oxford*, 216, 52–56. Available from <http://<GotoISI>://000223875400007>.
- Gunning, A. P., & Morris, V. J. (2018). Getting the feel of food structure with atomic force microscopy. *Food Hydrocolloids*, 78, 62–76. Available from <https://doi.org/10.1016/j.foodhyd.2017.05.017>.

- Han, W., Mou, J., Sheng, J., Yang, J., & Shao, Z. (1995). Cryo atomic force microscopy: A new approach for biological imaging at high resolution. *Biochemistry*, *34*(26), 8215–8220. Available from <https://doi.org/10.1021/bi00026a001>.
- Hansma, P. K., Cleveland, J. P., Radmacher, M., Walters, D. A., Hillner, P. E., Bezanilla, M., . . . Elings, V. (1994). Tapping mode atomic-force microscopy in liquids. *Applied Physics Letters*, *64*(13), 1738–1740. Available from <https://doi.org/10.1063/1.111795>.
- He, S. Y., Feng, G. P., Yang, H. S., Wu, Y., & Li, Y. F. (2004). Effects of pressure reduction rate on quality and ultrastructure of iceberg lettuce after vacuum cooling and storage. *Postharvest Biology and Technology*, *33*(3), 263–273. Available from <https://doi.org/10.1016/j.postharvbio.2004.03.006>.
- Heinisch, J. J., Dupres, V., Alsteens, D., & Dufrene, Y. F. (2010). Measurement of the mechanical behavior of yeast membrane sensors using single-molecule atomic force microscopy. *Nature Protocols*, *5*(4), 670–677. Available from <https://doi.org/10.1038/nprot.2010.19>.
- Jandt, K. (2001). Atomic force microscopy of biomaterials surfaces and interfaces. *Surface Science*, *491*, 303–332. Available from [https://doi.org/10.1016/S0039-6028\(01\)01296-1](https://doi.org/10.1016/S0039-6028(01)01296-1).
- Kaláb, M., Allan-Wojtas, P., & Miller, S. S. (1995). Microscopy and other imaging techniques in food structure analysis. *Trends in Food Science and Technology*, *6*(6), 177–186. Available from [https://doi.org/10.1016/S0924-2244\(00\)89052-4](https://doi.org/10.1016/S0924-2244(00)89052-4).
- Kim, S., Ratchford, D. C., & Li, X. (2009). Atomic force microscope nanomanipulation with simultaneous visual guidance. *ACS Nano*, *3*(10), 2989–2994. Available from <https://doi.org/10.1021/nn900606s>.
- Kirby, A. R., Gunning, A. P., & Morris, V. J. (1995). Atomic force microscopy in food research: A new technique comes of age. *Trends in Food Science and Technology*, *6*(11), 359–365. Available from [https://doi.org/10.1016/S0924-2244\(00\)89191-8](https://doi.org/10.1016/S0924-2244(00)89191-8).
- Kodera, N., Yamamoto, D., Ishikawa, R., & Ando, T. (2010). Video imaging of walking myosin V by high-speed atomic force microscopy. *Nature*, *468*(7320), 72–76. Available from <https://doi.org/10.1038/nature09450>.
- Krieg, M., Fläschner, G., Alsteens, D., Gaub, B. M., Roos, W. H., Wuite, G. J. L., . . . Müller, D. J. (2019). Atomic force microscopy-based mechanobiology. *Nature Reviews Physics*, *1*(1), 41–57. Available from <https://doi.org/10.1038/s42254-018-0001-7>.
- Last, J. A., Russell, P., Nealey, P. F., & Murphy, C. J. (2010). The applications of atomic force microscopy to vision science. *Investigative Ophthalmology and Visual Science*, *51*(12), 6083–6094. Available from <https://doi.org/10.1167/iovs.10-5470>.
- Liu, S., & Wang, Y. (2011). A review of the application of atomic force microscopy (AFM) in food science and technology. *Advances in Food and Nutrition Research*, *62*, 201–240. Available from <https://doi.org/10.1016/B978-0-12-385989-1.00006-5>.
- Martin, Y., Williams, C. C., & Wickramasinghe, H. K. (1987). Atomic force microscope-force mapping and profiling on a sub 100-Å scale. *Journal of Applied Physics*, *61*(10), 4723–4729. Available from <https://doi.org/10.1063/1.338807>.
- Meyer, G., & Amer, N. M. (1988). Novel optical approach to atomic force microscopy. *Applied Physics Letters*, *53*(12), 1045–1047. Available from <https://doi.org/10.1063/1.100061>.
- Min, H. (2015). The applications of atomic force microscopy in materials science research. *Chemical Sciences Journal*, *6*. Available from <https://doi.org/10.4172/2150-3494.1000e107>.
- Morgan, J. T., Raghunathan, V. K., Thomasy, S. M., Murphy, C. J., & Russell, P. (2014). Robust and artifact-free mounting of tissue samples for atomic force microscopy. *Biotechniques*, *56*(1), 40–42. Available from <https://doi.org/10.2144/000114126>.
- Nalwa, H. S., & Magonov, S. (2001). *Chapter 10 – Visualization of polymers at surfaces and interfaces with atomic force microscopy. Handbook of Surfaces and Interfaces of Materials* (pp. 393–430). Academic Press. Available from <https://doi.org/10.1016/B978-012513910-6/50029-3>.

- Obeid, S., & Guyomarc'h, F. (2020). Atomic force microscopy of food assembly: Structural and mechanical insights at the nanoscale and potential opportunities from other fields. *Food Bioscience*, 36. Available from <https://doi.org/10.1016/j.fbio.2020.100654>.
- Ott, W., Jobst, M. A., Schoeler, C., Gaub, H. E., & Nash, M. A. (2017). Single-molecule force spectroscopy on polyproteins and receptor-ligand complexes: The current toolbox. *Journal of Structural Biology*, 197(1), 3–12. Available from <https://doi.org/10.1016/j.jsb.2016.02.011>.
- Pan, D., Liu, S., Ji, S., Cai, Z., Li, J., Hou, Y., . . . Chu, J. (2020). Efficient fabrication of a high-aspect-ratio AFM tip by one-step exposure of a long focal depth holographic femtosecond axilens beam. *Optics Letters*, 45(4), 897–900. Available from <https://doi.org/10.1364/OL.384249>.
- Parot, P., Dufrière, Y. F., Hinterdorfer, P., Le Grimellec, C., Navajas, D., Pellequer, J.-L., & Scheuring, S. (2007). Past, present and future of atomic force microscopy in life sciences and medicine. *Journal of Molecular Recognition*, 20(6), 418–431. Available from <https://doi.org/10.1002/jmr.857>.
- Peric, O., Hannebelle, M., Adams, J. D., & Fantner, G. E. (2017). Microfluidic bacterial traps for simultaneous fluorescence and atomic force microscopy. *Nano Research*, 10(11), 3896–3908. Available from <https://doi.org/10.1007/s12274-017-1604-5>.
- Polyakov, P., Soussen, C., Duan, J., Duval, J. F. L., Brie, D., & Francius, G. (2011). Automated force volume image processing for biological samples. *PLoS One*, 6(4), e18887. Available from <https://doi.org/10.1371/journal.pone.0018887>.
- Prater, C. B., Hansma, P. K., Tortonese, M., & Quate, C. F. (1991). Improved scanning ion-conductance microscope using microfabricated probes. *Review of Scientific Instruments*, 62(11), 2634–2638. Available from <https://doi.org/10.1063/1.1142244>.
- Product News. (2020). *Journal of Failure Analysis and Prevention*, 20(1), 58–60. Available from <https://doi.org/10.1007/s11668-020-00820-1>.
- Requicha, A. (2010). Nanomanipulation with the atomic force microscope. *Nanotechnology*, 239–273. Available from <https://doi.org/10.1002/9783527628155.nanotech027>.
- Requicha, A. A. G., Arbuckle, D. J., Mokaberi, B., & Yun, J. (2009). Algorithms and software for nanomanipulation with atomic force microscopes. *The International Journal of Robotics Research*, 28(4), 512–522. Available from <https://doi.org/10.1177/0278364908100926>.
- Rubio-Sierra, F. J., Heckl, W. M., & Stark, R. W. (2005). Nanomanipulation by atomic force microscopy. *Advanced Engineering Materials*, 7(4), 193–196. Available from <https://doi.org/10.1002/adem.200400174>.
- Rugar, D., & Hansma, P. (1990). Atomic force microscopy. *Physics Today*, 43(10), 23–30. Available from <https://doi.org/10.1063/1.881238>.
- Sahai, S., Wilkerson, M., Zaske, A. M., Olson, S. D., Jr., Cox, C. S., & Triolo, F. (2016). A cost-effective method to immobilize hydrated soft-tissue samples for atomic force microscopy. *Biotechniques*, 61(4), 206–209. Available from <https://doi.org/10.2144/000114461>.
- Scholl, Z. N., Li, Q., & Marszalek, P. E. (2014). Single molecule mechanical manipulation for studying biological properties of proteins, DNA, and sugars. *Wiley Interdiscip Rev Nanomed Nanobiotechnol*, 6(3), 211–229. Available from <https://doi.org/10.1002/wnan.1253>.
- Shi, X., Zhang, X., Xia, T., & Fang, X. (2012). Living cell study at the single-molecule and single-cell levels by atomic force microscopy. *Nanomedicine: Nanotechnology, Biology, and Medicine*, 7(10), 1625–1637. Available from <https://doi.org/10.2217/nmm.12.130>.

- Starostina, N., Brodsky, M., Prikhodko, S., Hoo, C. M., Mecartney, M. L., & West, P. (2008). AFM capabilities in characterization of particles and surfaces: From angstroms to microns. *Journal of Cosmetic Science*, 59(3), 225–232. Available from <http://<GotoISI>://WOS:000256552200004>.
- Stukalov, O., Murray, C. A., Jacina, A., & Dutcher, J. R. (2006). Relative humidity control for atomic force microscopes. *Review of Scientific Instruments*, 77(3), 033704. Available from <https://doi.org/10.1063/1.2182625>.
- Tripathi, P., Beaussart, A., Alsteens, D., Dupres, V., Claes, I., von Ossowski, I., ... Dufrene, Y. F. (2013). Adhesion and nanomechanics of pili from the probiotic *Lactobacillus rhamnosus* GG. *ACS Nano*, 7(4), 3685–3697. Available from <https://doi.org/10.1021/nn400705u>.
- Variola, F. (2015). Atomic force microscopy in biomaterials surface science. *Physical Chemistry Chemical Physics*, 17(5), 2950–2959. Available from <https://doi.org/10.1039/c4cp04427d>.
- Verbelen, C., Christiaens, N., Alsteens, D., Dupres, V., Baulard, A. R., & Dufrene, Y. F. (2009). Molecular mapping of lipoarabinomannans on mycobacteria. *Langmuir: The ACS Journal of Surfaces and Colloids*, 25(8), 4324–4327. Available from <https://doi.org/10.1021/la900302a>.
- Wang, J., & Wang, C. (2010). Study on methods of protein immobilization for AFM. In *2010 4th International Conference on Bioinformatics and Biomedical Engineering*, iCBBE 2010, pp. 1–4. <https://doi.org/10.1109/ICBBE.2010.5514974>.
- Wang, Z., Liu, L., Wang, Y., Wang, Z., Xi, N., Hou, J., ... Yuan, S. (2013). Stable nanomanipulation using atomic force microscopy: A virtual nanohand for a robotic nanomanipulation system. *IEEE Nanotechnology Magazine*, 7(4), 6–11. Available from <https://doi.org/10.1109/MNANO.2013.2289693>.
- Xie, H., Onal, C., Régnier, S., & Sitti, M. (2012). Nanomechanics of AFM based nanomanipulation. In *atomic force microscopy based nanorobotics: Modelling, simulation, setup building and experiments*. Springer Berlin Heidelberg. Available from [https://doi.org/10.1007/978-3-642-20329-9\\_4](https://doi.org/10.1007/978-3-642-20329-9_4).
- Ximen, H., & Russell, P. E. (1992). Microfabrication of AFM tips using focused ion and electron beam techniques. *Ultramicroscopy*, 42–44, 1526–1532. Available from [https://doi.org/10.1016/0304-3991\(92\)90477-2](https://doi.org/10.1016/0304-3991(92)90477-2).
- Xu, K., Sun, W., Shao, Y., Wei, F., Zhang, X., Wang, W., & Li, P. (2018). Recent development of PeakForce tapping mode atomic force microscopy and its applications on nanoscience. *Nanotechnology Reviews*, 7(6), 605. Available from <https://doi.org/10.1515/ntrev-2018-0086>.
- Yang, H., Wang, Y., Lai, S., An, H., Li, Y., & Chen, F. (2007). Application of atomic force microscopy as a nanotechnology tool in food science. *Journal of Food Science*, 72(4), R65–R75. Available from <https://doi.org/10.1111/j.1750-3841.2007.00346.x>.
- Yang, J., Tamm, L. K., Somlyo, A. P., & Shao, Z. (1993). Promises and problems of biological atomic force microscopy. *Journal of Microscopy*, 171(3), 183–198. Available from <https://doi.org/10.1111/j.1365-2818.1993.tb03375.x>.
- You, H. X., & Yu, L. (1999). Atomic force microscopy imaging of living cells: Progress, problems and prospects. *Methods in Cell Science*, 21(1), 1–17. Available from <https://doi.org/10.1023/A:1009876320336>.
- Zhong, Q., Inniss, D., Kjoller, K., & Elings, V. B. (1993). Fractured polymer/silica fiber surface studied by tapping mode atomic force microscopy. *Surface Science Letters*, 290(1), L688–L692. Available from [https://doi.org/10.1016/0167-2584\(93\)90906-Y](https://doi.org/10.1016/0167-2584(93)90906-Y).

This page intentionally left blank

## CHAPTER 3

# Operation procedures of atomic force microscopy for food and biological samples

Lili Yang<sup>1,2</sup>, Ting Zhang<sup>2</sup>, Yao Liu<sup>3</sup>, Rui Sun<sup>2</sup>, Xichang Wang<sup>2</sup> and Jian Zhong<sup>1,2</sup>

<sup>1</sup>Xinhua Hospital, Shanghai Institute for Pediatric Research, Shanghai Key Laboratory of Pediatric Gastroenterology and Nutrition, Shanghai Jiao Tong University School of Medicine, Shanghai, P. R. China

<sup>2</sup>National R&D Branch Center for Freshwater Aquatic Products Processing Technology (Shanghai), Integrated Scientific Research Base on Comprehensive Utilization Technology for By-Products of Aquatic Product Processing, Ministry of Agriculture and Rural Affairs of the People's Republic of China, Shanghai Engineering Research Center of Aquatic-Product Processing and Preservation, College of Food Science & Technology, Shanghai Ocean University, Shanghai, P. R. China

<sup>3</sup>Instrumental Analysis Center, Shanghai Jiao Tong University, Shanghai, P. R. China

### 3.1 Introduction

With the development of science and technology, life science began to welcome the arrival of micro- and nanocharacterization techniques and to study the multiscale structures of biological samples. Atomic force microscopy (AFM) is a useful tool to analyze the multiscale structures of biological samples. AFM can be used to analyze biological samples in air, cryo state, or liquid. The application of AFM mainly includes three aspects: surface morphology observation, force measurement, and nanomanipulation (Fukui et al., 2018; Nandi & Ainavarapu, 2021; Qiao et al., 2017; Zhang, Zhu, Chu, Xiao, & Chen, 2021). Correct and careful operation procedures are necessary to obtain accurate results from AFM. This chapter describes the basic operation procedures of AFM for food and biological samples.

### 3.2 Atomic force microscopy requirements for food samples

Atomic force microscopy has many types of operation modes for its imaging, force measurement, and nanomanipulation functions. Furthermore, AFM has many types of imaging modes, such as height imaging, deflection imaging, phase imaging, lateral force imaging, magnetic force gradient imaging, torsional resonance imaging, conductive imaging, electric

field gradient distribution imaging, surface potential imaging, electrical carrier concentration imaging, scanning spreading resistance imaging, force modulation imaging, and surface thermal imaging (Zhong & Yan, 2016). AFM has three types of force measurement functions: single-molecule force spectroscopy (Alexander Reese & Xu, 2019), nanoindentation (Cárdenas-Pérez et al., 2019), and molecular pulling techniques (Bujalowski & Oberhauser, 2013; Fernandez & Li, 2004). AFM has two types of nanomanipulation tools to manipulate samples: nanomechanical machining (Yan et al., 2010) and dip-pen nanolithography (Zhong, Sun, & He, 2014).

In the field of food science, AFM has already been applied to analyze protein (Shi, Bi, et al., 2019; Shi, He, Ding, Wang, & Zhong, 2019a, 2019b), polysaccharides (Wang & Nie, 2019), food microorganisms (Liu & Yang, 2019), fruit cell walls (Posé et al., 2019), and food packaging materials (Marinello, La Storia, Mauriello, & Passeri, 2019). Especially, AFM has been applied to perform single-molecule analyses and nanomechanical measurements of food samples (Alexander Reese & Xu, 2019; Cárdenas-Pérez et al., 2019; Ding, Shi, & Zhong, 2019).

According to different analytical requirements, different AFM machines and different AFM operation modes are required to analyze food samples. Height imaging is the basic function and can be performed by three primary operation modes, including contact mode, noncontact mode (also known as the frequency modulation mode), and tapping mode (also known as the amplitude modulation mode or intermittent contact mode). Almost all the commercial AFM instruments have at least one mode to finish height imaging. Phase imaging is derived from the tapping or noncontact mode. Some special analytical requirements, such as surface potential imaging and nanomechanical machining, may require special AFM modules. Table 3.1 summarizes the basic function type, function description, operation mode, and characteristics of AFM. According to Table 3.1, the readers can choose the appropriate operation mode for their research purposes. Interested food scientists can also discuss what they want to analyze by AFM with application scientists in instrumental analysis centers of universities or commercial AFM companies such as Bruker and Agilent.

### 3.3 Substrates

AFM has become a useful and well-established nanotool to study a wide range of food and biological samples from molecules (e.g., protein, DNA,

**Table 3.1** Functions and characteristics of atomic force microscopy operation modes.

Function type	Function description	Operation mode	Characteristics
Imaging	To observe the surface morphology of a sample	Contact mode for height imaging	High scan speeds Good for rough samples
	To observe the surface morphology of a sample	Tapping mode for height imaging	High resolution Almost eliminated lateral forces High lateral resolution Less damage to soft samples and tips Good for biological samples
	To observe the surface morphology of a sample	Noncontact mode for height imaging	Both normal and lateral forces are minimized Good for biological samples Atomic resolution
	To observe the surface morphology of a sample	ScanAsyst mode	Self-optimization of parameters for high-resolution imaging Based on the tapping mode
	To observe the surface properties of a very flat sample	Deflection imaging	Performed in the contact mode
	To observe the surface properties, such as composition, elasticity, adhesion, friction, electrical properties, and magnetism	Phase mode	Performed in the tapping or noncontact mode
	To map the relative differences in the friction force between the tip and the sample surface	Lateral force imaging	Performed by lateral force microscopy (simultaneous height imaging)
	To map the magnetic response of a sample	Magnetic force gradient imaging	Performed by magnetic force microscopy (simultaneous height imaging)
	To examine the in-plane mechanical properties of a sample	Torsional resonance imaging	Performed by torsional resonance microscopy (simultaneous height imaging)
	To map the current distribution of a sample	Conductive imaging	Performed by conductive microscopy (simultaneous height imaging)
	To map the surface electrical properties of a sample	Electric field gradient distribution imaging	Performed by electric force microscopy (simultaneous height imaging) Derived from the tapping mode
	To map the electrostatic potential of a sample	Surface potential imaging	Performed by scanning surface potential microscopy (also named scanning Kelvin probe microscopy) Derived from the tapping mode

(Continued)



**Table 3.1 (Continued)**

Function type	Function description	Operation mode	Characteristics
Force measurement	To map the surface capacitance of a sample	Electrical carrier concentration imaging	Performed by scanning capacitance microscopy (simultaneous height imaging) Derived from the contact mode
	To map the local spreading resistance of a sample	Scanning spreading resistance imaging	Performed by scanning spreading resistance microscopy (simultaneous height imaging) Derived from the contact mode
	To map the differences in the surface stiffness or elasticity of a sample	Force modulation imaging	Performed by force modulation microscopy (simultaneous height imaging) Derived from the contact mode
	To map the surface-temperature-related properties of a sample	Surface thermal imaging	Performed by scanning thermal microscopy (simultaneous height imaging) Derived from the contact mode
	To analyze the spectroscopy data (interaction affinity and kinetics) of biological molecules with substrates (e.g., functionalized molecules, lipid layer, and cell membranes) in aqueous solution	Single-molecule force spectroscopy	Performed by (1) topography and recognition imaging or (2) single-molecule dynamic force spectroscopy Biological molecule can be functionalized to AFM tip by some chemistry methods, such as silanization chemistry or gold–thiol chemistry
	To quantitatively analyze the nanomechanical properties (e.g., stiffness, elasticity, and deformation) of biological materials	Nanoindentation	Performed by nanoindentation module in AFM No special sample preparation is needed for biological materials
	To track unfolding and refolding reactions of single biomolecules (e.g., polyprotein)	Molecular pulling technique	Classified into length clamp and force clamp techniques Biomolecule of interest is immobilized on a substrate and then is attached to the tip prior to pulling
Nanomanipulation	To nanomechanically machine biological substances (e.g., single biomolecule and biological materials)	Nanomechanical machining	Performed by special or custom-designed module
	To fabricate stable, precisely controlled and reproducible micro- and nanopattern of biological substances	Dip-pen nanolithography	Performed by dip-pen nanolithography Classified into classic, liquid, and matrix-assisted methods

and RNA) to subcellular structures (e.g., artificial and native membranes), to food nanoemulsion, all the way up to living cells and tissues (Ho, Abik, & Mikkonen, 2021; Li, Liu, Yuan, & Huang, 2021; Li, Xi, & Liu, 2021; Main et al., 2021; Nandi & Ainarapu, 2021; Zhong & He, 2012). These biological samples are required to be deposited and secured onto a rigid and flat substrate. The most common types of substrates (e.g., mica, glass, and graphite) used for biological samples are described below. There are also some common substrates for inorganic and organic samples, such as silicon wafer and sapphire (Zhou et al., 2015). In addition, many functionalized substrates have been developed using some functionalization methods. Typical functionalized substrates include silanized substrates, poly-L-lysine-coated substrates, and hydrophobic/hydrophilic substrates. Interested readers can search and read some articles for details.

### 3.3.1 Mica

Mica is the most popular AFM substrate, particularly for studying biological molecules and artificially supported lipid bilayers. It is composed of a series of thin and flat crystalline plates. The plates can be easily cleaved by inserting a pin at their edge or pulling the adhesive tape on the mica. The obtained surface is atomically flat, clean, and large (typically micron  $\times$  micron level), which is especially suitable for molecular and atomic level observation of samples. Depending on the present metal ions in mica, mica can be classified into many different types. The most common type is muscovite mica  $[(\text{KAl}_2(\text{OH})_2\text{AlSi}_3\text{O}_{10})]$ , which can be easily obtained at low cost (Ma et al., 2013). The minimum step size on the surface is the thickness of an individual layer (1 nm). There are hexagonal lattices within the layers with a constant of 0.52 nm. The root-mean-square roughness is about 0.06 nm. The mica surface is generally negatively charged in aqueous solutions at neutral pH due to the dissolution of metal ions from the mica surface into the solution.

### 3.3.2 Glass

Glass, usually in the form of a polished coverslip, has a higher surface roughness (a few nanometer levels) than mica. It is an ideal and cheap substrate for AFM work of large biological samples such as tubulin molecules, chromosomes, cell organelles, and cells, where molecular and atomic resolutions are often unnecessary. The glass coverslip is often cleaned by air plasma treatment and chemical cleaning methods (e.g.,

piranha solution or isopropanol) to remove possible contaminants prior to biological sample preparation. Cells and bacteria can be directly cultured onto the clean glass coverslips. The possible sample debris in the culture solution may disturb AFM observation. Therefore appropriate washing is necessary for the cultured cells and bacteria prior to AFM observation to make sure that the imaging solution is clean enough. The glass surface is also generally negatively charged in aqueous solutions at neutral pH. Glass is suitable for sample observation using a combination of AFM and optical microscopy because visible light can be transmitted across the glass.

### 3.3.3 Graphite

Graphite (highly oriented pyrolytic graphite) is mainly used for scanning tunneling microscopy, which requires the substrate conductive. Graphite is generally cleaved by pulling the adhesive tape on the graphite. It needs some practice to avoid removing thick layers and producing graphite debris on the surface. Graphite is extremely hydrophobic and recently not thought as the prime substrate candidate for biological AFM studies. However, it could be used as substrates for AFM studies to observe protein (Marchin & Berrie, 2003), individual peptides (Wang et al., 2003), and DNA (Jiang & Lin, 2004). These works suggested biological molecules showed different conformation on mica and graphite. Therefore mica/graphite can be used as substrates to analyze whether the biomolecular conformation is affected by the interaction of molecule with the substrate surface with different hydrophilic/hydrophobic properties or not.

## 3.4 Sample preparation for food samples

Food samples are typical biological samples. The sample preparation process of food samples is similar to that of biological samples. The biological samples can be analyzed in different states such as high vacuum state, ambient condition, cryo state, or liquid state. The choice of biological preparation methods is dependent on the biological samples and the sample states (El Kirat, Burton, Dupres, & Dufrene, 2005). The sample preparation methods for high vacuum and cryo AFM are similar to those for AFM at ambient condition except for high vacuum and cryo treatments. The sample preparation methods for liquid AFM remain a challenging work in biology due to the requirements of sample immobilization and clean liquid. The biological samples should be immobilized on a substrate to make sure they “stick” on the substrate after immersion in liquid and

the AFM tip can examine these biological samples on the substrate. After adding the liquid, the biological samples should not float into the solution to form sample debris, which may disturb the AFM examination or produce wrong results. Tissues are generally cut into thin slices, which are stuck to a substrate for AFM studies. AFM studies of tissues are also challenging because it is really difficult to prepare flat tissue surfaces with nanometer-level roughness. The exploration of sample preparation conditions may be painful, especially for new hands in this field. Therefore AFM users should be patient and try their best.

### 3.4.1 Individual biomolecules

A biomolecule of interest can be imaged in both air and liquid. If it is imaged in air, a drop of clean biomolecule solution with an appropriate concentration is cast on a clean substrate (e.g., freshly cleaved muscovite mica) that is stuck to the sample support, such as iron disk and glass slides, and is allowed to dry in ambient air at room temperature and low relative humidity of 30%–40% for 10 min–30 min (Zhong, Ma et al., 2014). Typical protein/peptide concentrations are from 1 to 100  $\mu\text{g}/\text{mL}$ . Typical DNA concentrations are from 1 to 10  $\mu\text{g}/\text{mL}$ .

For liquid imaging, there are two types of immobilization methods to make sure that biomolecules are immobilized onto a substrate in liquid. (1) Electrostatic adsorption methods: For some polyelectrolytes (e.g., proteins and peptides), the solution pH is adjusted to be lower than the polyelectrolyte isoelectric point, and therefore polyelectrolyte molecules are positively charged and can be attached to negatively charged substrates (e.g., mica and glass). For some negatively charged biomolecules (e.g., DNA), divalent cations such as  $\text{Ni}^{2+}$  and  $\text{Mg}^{2+}$  are added to the solution to bridge the negative charges of the biomolecule and the substrate. (2) Covalent immobilization methods: The biomolecule of interest can be attached to silicon and silicon nitride tip/substrate via silanization chemistry (Koehler et al., 2017) or to a gold tip/substrate via gold–thiol chemistry (Martines et al., 2012).

### 3.4.2 Artificially supported lipid layers

Artificially supported lipid layers can be prepared using the Langmuir–Blodgett technique or the liposome fusion method. A lipid film often spontaneously adsorbs on a substrate and can be imaged in the air or liquid. Sometimes a submolecular structure of lipid can be obtained

(Zhong & He, 2012). The obtained supported lipid layer can be stored in water at 4°C and be examined by AFM for no more than several days.

The Langmuir–Blodgett technique can be applied to prepare lipid monolayers and bilayers (Girard-Egrot & Blum, 2007; Hollars & Dunn, 1998). In this technique, a lipid mixture is dispersed onto a water phase in a Langmuir–Blodgett trough and the surface pressure is adjusted to an appropriate value (e.g., 20 mN/m) to form a lipid monolayer at the water/air interface. After that, a lipid monolayer and a bilayer can be formed by pulling and dipping/pulling, respectively, a hydrophilic substrate into the water phase. In order to prepare a lipid monolayer, a hydrophilic substrate in the water phase is vertically pulled out through the air/water interface to transfer a monolayer to the hydrophilic substrate (lipid headgroup down). In order to prepare a lipid bilayer, a hydrophilic substrate in the water is vertically dipped through the air/water interface to transfer a monolayer to the substrate surface and then vertically pulled out through the air/water interface to transfer a second monolayer to the substrate surface.

The liposome fusion method is mainly applied to prepare a lipid bilayer (Zhong, 2011; Zhong et al., 2007). In this method, the liposome is first prepared by sonication or extrusion methods. Then, the formed liposome solutions are added onto a clean hydrophilic substrate and incubated at a high temperature (>lipid phase transition temperature) for a period (e.g., 2–10 h). Then, the sample is cooled down and carefully and slowly rinsed with aqueous solution to obtain a clean and stable lipid bilayer.

Biomolecule-inserted artificially supported lipid bilayers can also be obtained for AFM studies. Biomolecules can be inserted into artificially supported lipid bilayers by the proteoliposome fusion method (Koehler et al., 2017) or the reconstituted liposome fusion method (Abdulreda, Bhalla, Chapman, & Moy, 2008).

### 3.4.3 Cells

Fixed and living cells can be studied by AFM (Braet, Rotsch, Wisse, & Radmacher, 1998). Generally, cells are cultured on Petri dishes. When the cells are about 70%–80% confluent, the cells are gently rinsed about three times. The living cells can be treated with glutaraldehyde for fixation. Finally, the cells are gently rinsed about three times prior to AFM analysis. The cells should be attached to the bottom glass surface of the

petri dish. If cells are not firmly attached to the glass surface, AFM users may use some adhesives to assist the cell attachment. Common cell adhesives include poly-L-lysine, collagen, laminin, entactin, polyethylene glycol derivatives, and CellTak.

Contact and tapping modes of AFM can be applied to observe the fixed and living cells. Due to the force difference between the AFM tip and the cell membrane, contact and tapping modes show different information about cells. In the contact mode, the obtained images mainly show the cytoskeleton beneath the cell membrane. In the tapping mode, the obtained images may show more cellular details, such as the membrane, the nucleus, and vesicles beneath/on the cell membrane.

### 3.4.4 Food powder

Generally, food powders such as starch granules are directly spread on adhesive tape on sample supports such as iron disk and glass slides (Fornal et al., 2012). After excessive food powders are removed, a single layer of food powders is formed on the adhesive tape. Therefore the fine surface structures of food powders can be analyzed by AFM under an ambient environment.

### 3.4.5 Bulk solid sample

Due to the sample space constraints of AFM, the bulk solid sample should be cut into small samples. Different commercial AFM instruments have different sample space constraints. A typical example is that the sample should be less than 12 mm in diameter and less than 8 mm in thickness. The bulk solid sample is stuck to the sample support, such as iron disk and glass slides, and then analyzed by an AFM.

## 3.5 Cantilever selection

The probe is one of the most important components of AFM. It can directly “feel” the force between the tip and the sample surface. A probe consists of a probe base, a cantilever, and a sharp tip. A cantilever is protruding from the probe base. The sharp tip has a height of less than 5  $\mu\text{m}$  and an apex diameter of less than 10 nm. The sharp tip is located at the end of a microscale cantilever with a length of 100–500  $\mu\text{m}$ . An appropriate AFM cantilever is important for the optimal quality of AFM results. The cantilevers are usually made of silicon or silicon nitride.

Two common types of artifacts can be produced when an AFM tip scans on the sample surface: the sample height compression effect and the tip-broadening effect (Zhong & Yan, 2016). The former generally results from the elastic deformation of the sample. The latter generally results from the tip–sample convolution. There are generally three ways to minimize the effects of these artifacts. The first way is to minimize the force between the AFM tip and the sample surface, which will minimize the elastic deformation of the sample. The second way is to apply surface/tip deconvolution algorithms to analyze the surface information for possibly subtracting the effect of tip–sample convolution. The third way is to choose and try many types of commercial cantilevers to obtain the best AFM results. When selecting the commercial cantilevers, one should consider the following key parameters of cantilevers.

### 3.5.1 Spring constant

Cantilevers can be thought of as springs. The force between the AFM tip and the sample surface can make the cantilever work like a spring. Springs can be described by Hooke's law, and the spring constant is the most important parameter. The spring constant of a cantilever is mainly dependent on the cantilever shape and the cantilever material. Thicker and shorter cantilevers tend to be stiffer and have higher spring constants. The silicon cantilever has a higher spring constant than the silicon nitride cantilever. The spring constants of the commercially available cantilevers vary over several orders of magnitude, from 0.005 to 200 N/m. Typical cantilevers for biomolecule imaging in the air include the RTESP phosphorous (n)-doped silicon cantilever with a spring constant of 40 N/m (Ma et al., 2013) and the SNL silicon cantilever with a spring constant of 0.35 N/m (Shi, Bi, et al., 2019). Typical cantilevers for biomolecule imaging under liquid include the OTR8 cantilever with a spring constant of 0.15 N/m (Zhong et al., 2007), NP-series silicon nitride cantilevers with a nominal spring constant of 0.58 N/m (Zhong et al., 2013), and SNL-series silicon cantilevers with a nominal spring constant of 0.32 N/m (Zhong et al., 2013).

If the hardness of the sample is significantly less than that of the cantilever, a downward movement of the cantilever will penetrate the sample and the cantilever may not bend. If the hardness of the sample is significantly greater than that of the cantilever, a downward movement of the cantilever will cause the cantilever to bend at the same deflection distance.

This is an ideal condition for the contact mode of AFM. In the nanoindentation experiment, the sample should produce a certain deformation (nanoindentation) and the cantilever should produce a certain deflection distance for measuring the force. Therefore an AFM tip with an appropriate spring constant should be used for nanoindentation. Silicon cantilevers are often chosen for the tapping mode because they often have a higher and enough resonant frequency. Silicon nitride cantilevers are often chosen for the contact mode because they are often soft and may not produce excessive force to destroy the sample surface.

### 3.5.2 Tip geometry

AFM tip geometry (e.g., tip shape, tip height, and tip apex radius) is an important parameter concerning the effect of tip–sample convolution. The selection of the tip geometry is closely linked to the properties of the sample under study. There are many different tip geometries available commercially. According to the tip shape, the tips can be classified into the following five important categories: traditional pyramid-shaped, fine traditional pyramid-shaped, truncated pyramid-shaped, fine parabolic, and wide parabolic tips. According to the tip height, the tips can be classified into two important categories: low (traditional and common) and high aspect ratio tips. The tip apex is generally thought of as a sphere, and the tip apex radius is typically less than 10 nm.

If the height of a sample (e.g., individual biomolecules) is less than the tip apex radius such as 10 nm, the tip apex radius is an important parameter that AFM users should consider. Tip shape and tip height can be neglected. The large tip apex radius had a large tip-broadening effect. The tip apex radius determines the horizontal resolution of AFM. However, the tip apex radius has no obvious effect on the vertical resolution of AFM. It should be considered when we analyze the widths of individual biomolecules according to the AFM images. Generally, the measured width is larger than the real width of individual biomolecules due to the tip-broadening effect. If the individual biomolecules form round-line-like nanostructures, we generally use the thickness of the nanostructure as the real height/width of the individual biomolecule.

If the height of a sample is higher than 10 nm, the tip shape and the tip height are important parameters that AFM users should consider. The tip apex radius can be neglected. The tip height should be at least double the sample height to prevent contact between the cantilever and the



sample, which may disturb the AFM scanning and produce wrong results. Different tip shapes produce different tip-broadening effects. AFM users should remember the potential effect of the tip shape of the applied commercial cantilever when they use AFM to analyze the sample. A high aspect ratio tip is required for a very rough sample (Morris, Kirby, & Gunning, 2010). A typical commercial high aspect ratio cantilever has a tip height of 10–15  $\mu\text{m}$ , a spike height of 1–2  $\mu\text{m}$ , and a tip apex radius of 10 nm. In addition, the carbon-nanotube-modified tip is also a good high aspect ratio cantilever for AFM studies (Cheng, Yang, Woldu, Shafique, & Wang, 2020). However, these high aspect ratio tips are more expensive than traditional low aspect ratio tips.

### 3.5.3 Resonance frequency and quality factor

The resonance frequency and quality factor are important parameters of an AFM cantilever for the tapping mode. In the tapping mode, the cantilever oscillates near its resonance frequency with an amplitude of up to 100 nm. The quality factor is defined as the ratio of the stored energy in a resonator to the energy loss. A cantilever with a high resonance frequency is preferable because it allows for a faster scan rate. Cantilevers with a high resonance frequency of  $>300$  kHz can provide fast scan rates. The tapping mode generally uses silicon cantilevers, which have a high resonant frequency. A cantilever with a high quality factor is desirable in the tapping mode to optimize the sensitivity. For a cantilever with a given resonance frequency and spring constant, a rectangular cantilever generally has a higher quality factor than a triangular cantilever.

### 3.5.4 Tip functionalization

Tip functionalization is a significant advance in AFM. Generally, tip functionalization means coating the tip with certain materials for special AFM operation requirements. It can be classified into the following three types: inorganic coating, organic functionalization, and biological functionalization. A typical inorganic coating includes conductive (e.g., 10–50 nm Pt coating) and magnetic (e.g., ferromagnetic layer coating consisting of Co or Fe) material coatings. The obtained conductive and magnetic cantilevers can be applied in conductive AFM and magnetic AFM, respectively. Typical organic substances for organic functionalization include small organic molecules (e.g., alkyl-thiols, C60 molecules, and carbon nanotubes) and polymers (e.g., polyethylene glycol (PEG)). The obtained

functionalized cantilevers can be applied in chemical force microscopy to control and analyze the chemical interactions between the tip and the sample (Ito, Ibrahim, & Grabowska, 2010). Biological coating tips have special advantages for the application of AFM to biology. The biological molecules, such as antibodies, antigens, ligands, and receptors, are attached to the tips using some modification methods (Ebner, Wildling, & Gruber, 2019). Now, it is possible to purchase functionalized tips from some specialist labs, which can significantly promote the application of AFM in biology.

### 3.6 Common imaging procedure by atomic force microscopy

The imaging procedure is generally dependent on the sample characteristics, AFM machine, imaging modes, imaging environments, etc. The detailed imaging procedures are generally in the instrument manuals provided by the commercial instrument companies. Herein, we summarized the common imaging procedure by AFM (Fig. 3.1):

#### 3.6.1 Power on system

1. Make sure that the actual voltage matches the required operating voltage.
2. Make sure that all the cables are properly connected.
3. Make sure the antivibration platform is in a working state.
4. Make sure the operating environment meets the requirements.
5. Turn on the computer, screen, and laser light source.
6. Turn on the controller.

#### 3.6.2 Mount sample

Sample mounting varies a great deal depending on the machine, the sample, and the experiment. The general mounting procedure is provided below.

##### 3.6.2.1 Prepare the sample

For individual biomolecules, artificially supported lipid layers, and cells, a substrate is stuck to a sample support (e.g., a metal disk or a glass slide) with a double-sided adhesive tape. For food powders and bulk solid samples, adhesive tape is stuck to a sample support. Then, the sample is prepared according to machine requirements and sample characteristics. Some sample preparation methods are described in Section 3.4. If you are

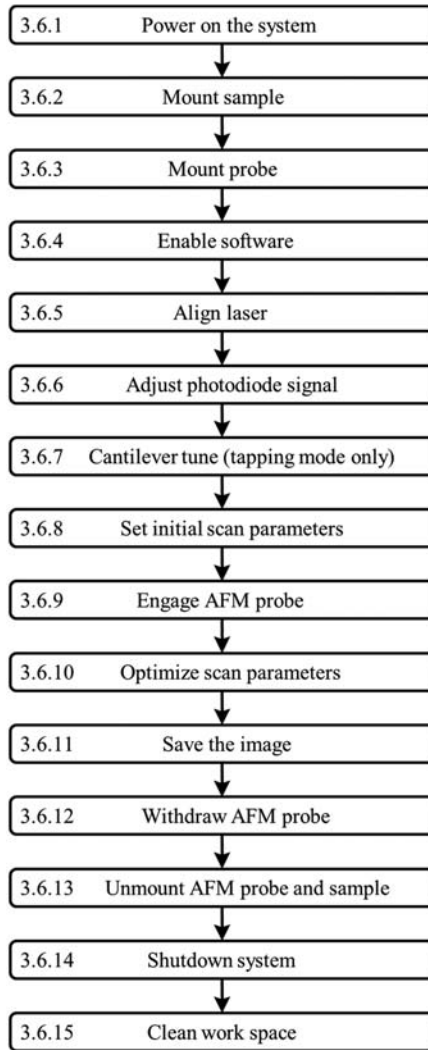


**Figure 3.1** Common imaging procedure by atomic force microscopy.

a user to operating the microscope, we recommend that you use the calibration sample from the commercial company (usually a 10  $\mu\text{m}$ -pitch grid of 200 nm step height).

### **3.6.2.2 Load the sample**

The AFM head is removed, the sample is gently loaded, and then the AFM head is put back. During this period, keep your eyes on the AFM

head and sample. The probe holder in the AFM head should not touch the sample surface. If you estimate the probe holder may crush the sample surface (or liquid surface if the sample is in liquid), AFM users should lift the probe holder until they feel it is safe.

### 3.6.3 Mount probe

1. Make sure no dust is present in the probe holder prior to probe mounting.
2. Mount a probe into the probe holder.

The probe should be in firm contact with the end and bottom of the groove. No dust should be present between the probe and the probe holder. Generally, silicon, silicon nitride, and silicon nitride probes are used for tapping, contact, and ScanAsyst modes, respectively.

#### ***3.6.3.1 Mount the probe holder to the atomic force microscopy head***

The probe holder should be correctly and securely mounted. The probe holder should be on the top of the sample of interest and should not touch the sample surface (or liquid surface if the sample is in liquid).

### 3.6.4 Enable software

1. Click the software icon on the computer desktop.
2. Select an appropriate operation mode for your experiment.

### 3.6.5 Align laser

#### ***3.6.5.1 Align the laser spot on the front end of the cantilever***

The laser spot is carefully aligned using the laser positioning knobs and mirrors in the AFM head. Generally, there are two methods for aligning the laser: the magnifier method (also known as paper method) and the optical viewing microscope method. AFM users should not stare at the laser beam, which can result in eye damage.

#### ***3.6.5.2 Maximize the laser SUM signal***

In order to obtain the best sensitivity, the laser SUM signal should be maximized. The maximizing process involves the adjusting of the mirrors and the laser positioning knobs. The adjusting of the mirror may significantly increase the laser SUM signal. The adjusting of the laser positioning knobs is to finely maximize the laser SUM signal.

### 3.6.6 Adjust photodiode signal

According to the requirements of operation modes, the photodiode signal is adjusted to an appropriate value using photodetector positioning knobs. Typical photodiode signals for common operation modes are as follows.

1. Tapping mode: horizontal difference value of zero, vertical difference value of zero.
2. Contact mode: horizontal difference value of zero, vertical difference value of about  $-2.0$  V.
3. ScanAsyst mode: horizontal difference value of zero, vertical difference value of zero.

### 3.6.7 Cantilever tune (tapping mode only)

This step is to find the resonance peak of the cantilever and adjust the oscillation voltage so the cantilever will vibrate at an appropriate amplitude. The cantilever tune can be performed in an autotune way (in air) or a manual tune way (in liquid). A range of vibration frequencies will be applied to the cantilever to determine the frequency that produces the largest response (the resonance frequency). The resonance peak has a sharp Gaussian distribution in air and is ragged in liquid. If the resonance peak is not correct, possible reasons should be checked, such as incorrect probe mounting and a destroyed tip.

### 3.6.8 Set Initial scan parameters

1. Set the scan size, scan angle, X offset, and Y offset to zero.
2. Set the integral gain and proportional gain according to the machine manual.

Typically, the proportional gain is 20%–100% higher than the integral gain.

3. Set the scan rate to about 1.0 Hz.
4. Set the number of samples to 256.

If you are familiar with your sample, you can set this value to fewer values (64 or 128 for rougher samples) or higher values (512 for flat samples).

### 3.6.9 Engage atomic force microscopy probe

#### 3.6.9.1 Manually engage the atomic force microscopy probe

The AFM probe is manually engaged to be close to the sample surface using Probe Z-positioning knobs. During this period, keep your eyes on the decreased distance between the probe and the sample.

### **3.6.9.2 Automatically engage the atomic force microscopy probe**

The AFM probe is automatically engaged by clicking the engage menu in the AFM software. As long as the AFM tip contacts the sample surface, AFM scanning will start, and you can see the imaging process via the real-time imaging.

### **3.6.10 Optimize scan parameters**

The trace and retrace lines are checked to see if they are tracking each other well. By adjusting the scan size, scan rate, integral gain, proportional gain, and number of samples, the lines are adjusted to be the same. It is not necessary to overlap each other, either horizontally or vertically. Then, the scan parameters are further optimized according to the image quality.

### **3.6.11 Acquire and save the image**

The sample surface is acquired and saved according to the machine manual. It is necessary to image several different positions to see whether the obtained images can represent the sample surface.

### **3.6.12 Withdraw atomic force microscopy probe**

After the experiment, the AFM probe is automatically withdrawn by clicking the “Withdraw” menu in the software. Then, the AFM probe is manually withdrawn to be far away from the sample surface using Probe Z-positioning knobs. During this period, keep your eyes on the increased distances between probe and sample.

### **3.6.13 Unmount atomic force microscopy probe and sample**

The AFM probe and sample are carefully unmounted. During the process, one should be careful not to scratch and destroy the AFM probe holder and the sample holder. If the sample is in liquid, the liquid should not to be leaked to electronic devices and scanner that are below the liquid sample.

### **3.6.14 Shutdown system**

1. Turn off software.
2. Turn off controller.
3. Turn off laser light source, computer, and screen.

### 3.6.15 Clean workspace

1. Clean and store the sample support and other AFM-related stuff.
2. Clean the AFM table and the experiment table.

## 3.7 Common force measurement procedure by atomic force microscopy

Atomic force microscopy force measurements are generally operated in the contact mode of AFM. The force measurement procedure is generally dependent on the sample characteristics, AFM machine, operational modes, operational environments, etc. The detailed procedures are generally in the instrument manuals provided by the commercial instrument companies. The common force measurement procedure also includes some similar procedures to AFM imaging (contact mode, see [Section 3.6](#) and [Fig. 3.1](#)), such as “power on system,” “Mount sample,” “Mount probe,” “Enable software,” “Align laser,” “Adjust photodiode signal,” “Set initial scan parameters,” “Engage AFM probe,” “Withdraw AFM probe,” “Unmount AFM probe and sample,” “Shutdown system,” and “Clean workspace.” In this section, we only list the common force measurement procedures ([Fig. 3.2](#)) after the step of “Adjust photodiode signal” and before “Withdraw AFM probe.”

The main function of the AFM force measurement is to analyze the force between the AFM tip and the sample surface. Therefore AFM force measurement can be applied to analyze the mechanical properties of the sample and analyze single-molecule force spectroscopy. The manufacturers often specify the spring constant in a wide range that may span values up

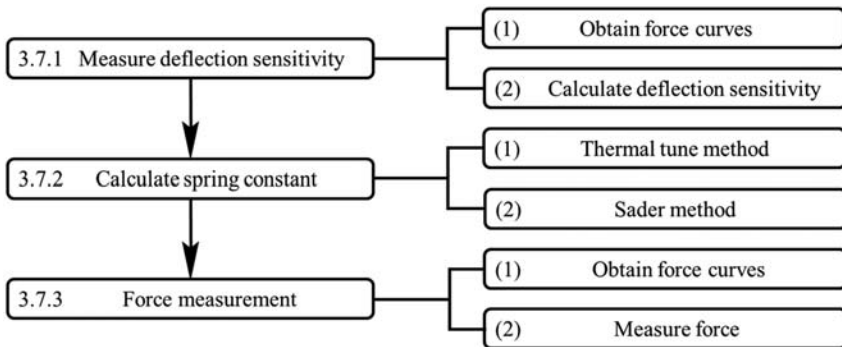


**Figure 3.2** Common force measurement procedure by atomic force microscopy.

to four times smaller and four times larger than the nominal value. This is because the fabrication techniques can result in substantially different cantilever dimensions, especially thickness, from wafer to wafer and smaller variations within a single wafer. Moreover, tip functionalization can also change the spring constant of the cantilever. In order to accurately measure the interaction between the AFM tip and the sample surface, it is necessary to measure the spring constant of the applied cantilever. Therefore the operation procedure of AFM force measurements contains three steps: “Step 1: Measure deflection sensitivity,” “Step 2: Calibrate spring constant,” and “Step 3: Force measurement,” which is the common commercial operation procedure. This procedure is good for the analysis of nanomechanical properties of a sample (the tip is generally not functionalized). However, if the AFM tip is commonly functionalized by biological molecules, such as proteins, the single-molecule force spectroscopy process may damage biological molecules. In order to decrease the potential damage risk to biological molecules, we suggest AFM users first perform “Force measurement,” and then perform “Measure deflection sensitivity” and “Calibrate spring constant.” In this case, the force is obtained by multiplying the force by the ratio of the measured spring constant and the nominal spring constant. The force calculation can be performed using commercial calculation software. Of course, it can also be performed by modifying AFM software or developing custom-designed software.

### 3.7.1 Measure deflection sensitivity

Deflection sensitivity is defined as the ratio between the deflection of the cantilever (nm) and the applied Z-piezo voltage. It depends upon several factors such as the back surface of the cantilever and the position of the AFM light beam spot on the cantilever, so it needs to be calibrated each time you change the cantilever or adjust the laser spot. Generally, there are the following two steps to measure the deflection sensitivity of a cantilever.

1. Obtain force curves on a hard and stiff substrate (e.g., sapphire, silicon wafer, glass) in the contact mode.

Triggering is used to limit the total amount of force exerted by the tip upon the sample. Depending on which trigger you use and how it is set, you may operate the trigger independent of drift (Relative) or at some arbitrarily fixed point (Absolute) or at an off state (Off).



## 2. Calculate deflection sensitivity using the commercial software.

Deflection sensitivity is the slope of the deflection versus Z-piezo voltage curve when the AFM tip is in contact with the hard substrate surface. Therefore the deflection sensitivity can be measured by using commercial software to analyze the obtained force curve in step (1). In order to obtain reliable deflection sensitivity, multiple values should be measured at different positions on the hard substrate. A standard deviation of <5% suggests the results are reliable.

### 3.7.2 Calculate spring constant

When cantilever deflection is sufficiently small, the relationship of the tip-sample force ( $F$ ) and cantilever deflection ( $d$ ) can be described by Hooke's law

$$F = -kd \quad (3.1)$$

where  $k$  is the proportionality constant, known as the spring constant, in N/m (or equivalently, and more typically in nanoscale work, in pN/pm).

After obtaining the deflection sensitivity of a cantilever, the cantilever deflection can be measured with great accuracy and sub-Angstrom sensitivity. However, converting these cantilever deflection values to forces requires the spring constant of each cantilever.

There are several methods to analyze the spring constant of a cantilever. Among these methods, thermal tune and Sader methods are two kinds of relatively simple and reliable calibration methods.

#### 3.7.2.1 Thermal tune method

The thermal tune method is an algorithm to analyze the spring constant of a cantilever by analyzing the thermal vibration energy of the cantilever and fitting the curve (Ohler, 2007). Generally, this algorithm is implemented in the commercial AFM software, which allows the cantilever spring constant to be calibrated in either air or in fluid. After obtaining the deflection sensitivity, the thermal tune method becomes a simple measurement in the Thermal Tune window. The thermal tune technique is suitable for cantilevers with a spring constant of <5 N/m (e.g., FESP) all the way down to the very softest silicon nitride cantilevers (e.g., MLCT). The thermal tune method consists of four steps: (1) open thermal tune window and input some basic parameters, such as thermal tune range, deflection sensitivity correction, and temperature; (2) acquire

thermal tune curve; (3) fit the thermal tune curve; (4) calculate spring constant.

### 3.7.2.2 Sader method

The Sader method is based on the general theory of a cantilever that is immersed in a fluid (typically in air) and is excited by an external driving force. There are two different forces that act on the cantilever: the hydrodynamic force from the motion of the fluid around the cantilever and the driving force from the piezoelectric system. Therefore a hydrodynamic function [ $\Gamma(\omega)$ ] was introduced, which was later used as a correction factor, to estimate the spring constant (Sader, Chon, & Mulvaney, 1999). This Sader method is generally used for the spring constant calibration of the rectangular cantilever based on the following equation (Kim, Choi, Kim, & Park, 2010):

$$k = 0.1906\rho_f b^2 L Q \Gamma_i(\omega_f) \omega_f^2 \quad (3.2)$$

where  $\rho_f$  is the density of the fluid ( $\text{kg/m}^3$ ),  $b$  is the width of the cantilever ( $\mu\text{m}$ ),  $L$  is the length of the cantilever ( $\mu\text{m}$ ),  $Q$  is the quality factor,  $\omega_f$  is the angular resonance frequency (kHz),  $\Gamma_i$  is the imaginary component of the hydrodynamic function,  $\Gamma$ , which depends on the Reynolds number  $\text{Re} = \rho_f b^2 \omega_f / 4\eta_f$  only, with  $\eta_f$  being the viscosity of the fluid ( $\text{kg/m/s}$ ).

According to (3.2), the spring constant calibration requires measuring the width of the cantilever, the length of the cantilever, the quality factor, the resonance frequency, the density of the fluid, and the viscosity of the fluid. Generally, the density and viscosity of the fluid can be obtained from previous handbooks or references. Therefore you only need to get the four former parameters. The Sader method includes the following five steps: (1) measure the length and width of the cantilever using optical microscopy. Standard grid with micrometer scales is used as control; (2) open Thermal Tune window in the AFM commercial software and input some basic parameters, such as thermal tune range, deflection sensitivity correction, and temperature; (3) acquire thermal tune curve; (4) fit the thermal tune curve to get the quality factor and the resonance frequency; (5) calculate the spring constant using the equation or online calculation interface (<http://www.ampc.Ms.unimelb.edu.au/afm/calibration.html>). The Sader method can only be valid for rectangular cantilevers with length-to-width ratios in the range of 3–14 and with a quality factor of

>> 1. The obtained spring constant value generally has an accuracy of the order of 15%–20% (Clifford & Seah, 2005).

### 3.7.3 Force measurement

#### 1. Obtain force curves

After obtaining deflection sensitivity and spring constant, AFM users can execute force curves as much as they need.

#### 2. Measure force

Force–distance curves are displayed, and the forces between the tip and the sample surface can be measured.

## 3.8 Common nanomanipulation procedure by atomic force microscopy

Nanomanipulation is a useful function of AFM for biological research. It can be performed by custom-designed software and electronics in some biophysical laboratories. Recently, it can also be achieved in some commercial AFM instruments. Both immediate and programmed commands are available to manipulate a sample. By controlling the force applied through the cantilever and the position of the cantilever, AFM nanomanipulation can achieve a variety of basic operations: cut molecules, push objects, create a pattern, and etch suitable surfaces. The nanomanipulation procedure is generally dependent on the sample characteristics, AFM machine, nanomanipulation modes, operational environments, etc. The detailed imaging procedures are generally in the instrument manuals provided by the commercial instrument companies. The general nanomanipulation operation procedure includes the following seven steps.

1. Image the sample to find the appropriate nanomanipulation position.
2. Locate the AFM tip at the desired start point of the sample of interest.
3. Lower AFM tip and start to manipulate the sample of interest.
4. Optimize the nanomanipulation parameters.
5. Manipulate the sample of interest.
6. End this nanomanipulation operation.
7. Image the sample to check the results.

According to the different purposes, the operation procedure may be a little bit different. The detailed information can be found in the AFM manuals provided by the commercial company.

## 3.9 Data optimization

Data optimization can be performed in both real-time and offline ways.

### 3.9.1 Real-time optimization

There are mainly four real-time operations to adjust and optimize the AFM results, that is scan size, scan rate, setpoint, integral gain, and proportional gain.

#### 3.9.1.1 Scan size

Scan size is the size of the scan area. The scan size should be carefully set in order to image the surface characteristics with as many as possible and as clear as possible. Too large and too small scan sizes will induce inadequate and excessive, respectively, data points on the surface, and therefore incomplete and overcontacted, respectively, surface information are obtained.

#### 3.9.1.2 Scan rate

The scan rate is the number of trace and retrace scan lines performed per second (Hz). It is generally set to 0.5–1.5 Hz for tapping and ScanAsyst modes and 1.0–3.0 Hz for contact mode. A high scan rate may result in poor tracking of the sample surface. A low scan rate can result in low working efficiency.

#### 3.9.1.3 Setpoint

Setpoint is used to set the force in the imaging modes and force measurement modes. The setpoint should be appropriately set in order to apply the smallest amount of force to maintain a stable engagement on the sample surface. The higher the force is set, the better the tip will track the sample topography. However, if the force is set too high, the sample surface may be disturbed. If the force is set too low, the AFM tip may not track on the sample surface.

#### 3.9.1.4 Integral gain

Integral gain controls the amount of the integrated error signal in the feedback system. The higher the integral gain is set, the better the tip will track the sample topography. However, if the integral gain is set too high, noise will be introduced into the results due to the appearance of feedback oscillation. The critical integral gain as high as possible should be

carefully found by increasing the integral gain until noise is seen and then reducing the integral gain just lower than the value where the noise disappears.

### **3.9.1.5 Proportional gain**

Proportional gain controls the amount of proportional error signal in the feedback system. Typically, it is set 20%–100% higher than the integral gain.

## **3.9.2 Offline optimization**

After AFM experiments, the obtained results can also be offline optimized to show the exact state of the sample. There are mainly three offline operations to adjust and optimize the AFM results: planefit, flatten, and erase scan line.

### **3.9.2.1 Planefit**

Planefit is used to remove the tilt or bow of the obtained images. It calculates a single polynomial fit for the entire image and then subtracts the polynomial fit from the image. It can be executed by applying a zeroth-, first-, second-, or third-order polynomial fit to the image in the *X* or *Y* directions. There are three types of planefit functions: full, offset, and none. Full planefit is to apply a first-order planefit to the *X* and *Y* directions of the image and remove the *Z* offset. The offset planefit is to remove the *Z* offset. None planefit means no treatment to the image.

### **3.9.2.2 Flatten**

Flatten is used to remove image artifacts due to vertical scanner drift, image bow, skips, and anything else that may have resulted in a vertical offset between scan lines. It modifies an image on a line-by-line basis in the fast scan direction by calculating a least-square fit polynomial for a scan line and subtracting the polynomial fit from the original scan line. Flatten can be executed by applying a zeroth-, first-, second-, or third-order polynomial fit to the image. For an image that consists of a flat plane with “bumps” or “pits,” it can be executed by drawing boxes around the raised or depressed features with the cursor to exclude the features prior to the flattening operation.

### 3.9.2.3 Erase scan line

Erase scan line is a function to remove abnormal scan lines (too high or too low) due to skips, noise, etc. By drawing a line to cover the abnormal scan line with the cursor and then erasing the line, the abnormal scan line will be replaced with the average of the two scan lines adjacent to it.

## 3.10 Data analysis

During and after the process of AFM experiments, the data can be viewed and measured with online and offline commercial software. It is exciting to obtain useful information from the AFM data for research and development. However, it is really important to see if the data are correct or not prior to data acquirement and analysis.

### 3.10.1 Typical image artifacts

A serious disadvantage of AFM is that many artifacts can appear in AFM images, which are difficult to recognize by new users, even by experienced users. Artifacts can originate for a variety of reasons, such as AFM tip–sample convolution, contaminated tip, scanner, optical interference, high-frequency operation, friction, inappropriate imaging parameters, electronic noise, and vibration (Canale, Torre, Ricci, & Braga, 2011; Digital Instruments, 2000; Eaton & Batziou, 2019; Gołek, Mazur, Ryszka, & Zuber, 2014; Ricci & Braga, 2004; Ukraintsev, Kromka, Kozak, Remeš, & Rezek, 2012; Velegol, Pardi, Li, Velegol, & Logan, 2003; West & Starostina, 2003). The interested readers are suggested to carefully learn these references prior to AFM operation and analysis. This section mainly describes common AFM image artifacts and potential solutions to eliminate or minimize them (Table 3.2).

#### 3.10.1.1 Artifacts caused by tip–sample convolution

When AFM images are analyzed, tip–sample convolution should be considered due to the tip-broadening effect (see Section 3.5). The tip-broadening effect may induce a broadened and trapezoidal feature (Fig. 3.3), which may cover the real morphology of the sample surface. In this case, an appropriate AFM tip should be used, such as a high aspect ratio tip, to minimize the possible tip-broadening effect on the sample surface. It should be noted that the tip–sample convolution cannot be eliminated by using a high aspect ratio tip. In order to understand the effect of the tip-broadening effect on the sample, it is important to know

**Table 3.2** Typical image artifacts.

Possible source	Possible reason	Artifact appearance	Possible solution
Tip-sample convolution	Tip-broadening effect	Broadened and trapezoidal feature	Use an appropriate AFM tip
Tip	Tip contamination	Two, multiple, or even all the same shapes	Use new tip
Scanner	Large scan size	Loss of resolution	Perform second- or third-order plane fit
	Scanner hysteresis	Arch-shaped or S-shaped bow	Decrease scan rate
	Thermal drift of scanner	Edge overshoot (narrow hills and valleys at the edges)	Rescan without changing the operation
	Cross-talk between the x- and y-motion signals	Image distortion	Perform AFM calibration
Laser	Cross-talk between the z-motion signal and the x-y motion signals	x-direction and y-direction are not orthogonal	Repair the scanner
	Optical interference	Recognize it by combining the sample structures from other techniques	Adjust the laser alignment
		Sinusoidal pattern	Modulate the laser current at a high frequency
Tapping mode	Operated on the high-frequency side of the resonance peak	Ring-like artifact	Decrease the drive frequency
Friction	Friction force	Some domains are different in different scan directions	Use other operation modes
Operation	Inappropriate imaging parameters	Tail-like artifact	Adjust scan rate, gains, and setpoint
Electronics	Electronic noise	Surface-disturbed artifact	Check the ground connection
Building, people talking, etc.	Floor vibrations and acoustic vibrations	Periodic oscillation or repeating pattern	Set a quiet and vibration-free environment
		Spurious periodic structures	
		Short-time abnormal structures	

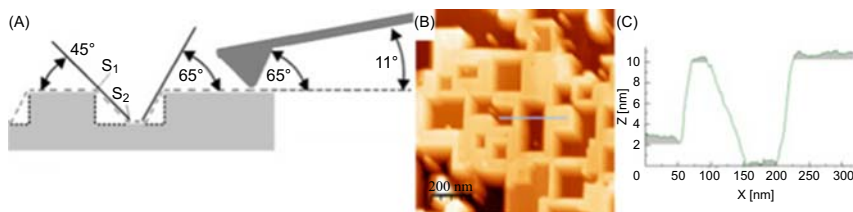


**Figure 3.3** Artifacts caused by the tip–sample convolution on the rectangular-shaped LiF fences grown on the NaCl (001) surface. (A) Drawing explaining the image artifact generation when the tip is from right to left. Dotted and dashed lines indicate the sample surface profile and the obtained sample surface profile, respectively. (B) AFM height image of the sample. (C) Height profile along the line drawn in (B). Reprinted with permission from Golek, F., Mazur, P., Ryszka, Z., & Zuber, S. (2014). *AFM image artifacts*. *Applied Surface Science*, 304, 11–19.

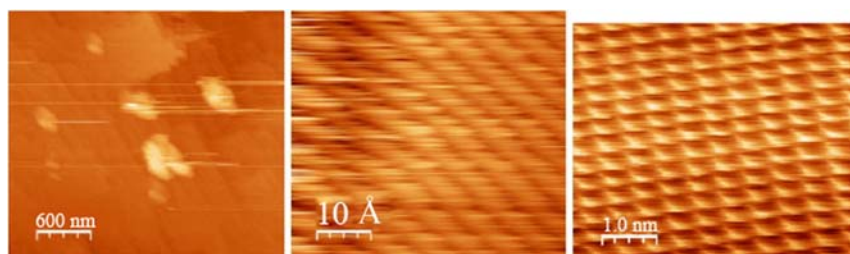


**Figure 3.4** Artifacts caused by contaminated tips on the LiF crystal surfaces under UHV conditions. Left panel: two atomic force microscopy height images exemplifying tip-contamination-induced noise. Right panel: atomic force microscopy height image with tip-contamination-induced noise significantly reduced. Reprinted with permission from Golek, F., Mazur, P., Ryszka, Z., & Zuber, S. (2014). *AFM image artifacts*. *Applied Surface Science*, 304, 11–19.

some dimension information of the sample by other techniques, such as transmission electron microscopy.

### 3.10.1.2 Artifacts caused by the contaminated tip

If debris attaches itself to the end of the tip, the features in the image may show repeat features (two, multiple, or even all the same shapes) or loss of resolution in some areas (Fig. 3.4). In these cases, a new AFM tip should be used to obtain correct AFM images.

### 3.10.1.3 Artifacts caused by the scanner

Atomic force microscopy uses a ceramic piezoelectric scanner to control the movement of the AFM tip or sample in three dimensions ( $x$ ,  $y$ , and



$z$ ). The relationship between the applied voltage to the piezo and the amount of movement is generally nonlinear. In addition, self-heating of the piezo may cause hysteresis in the scanner motion. According to the company's suggestion, the three-dimensional calibration of AFM should be performed at least every 3 months during the first year of operation and every six months thereafter. However, nonlinearity and hysteresis of the scanner may occasionally introduce errors in both positioning and scanning.

At large scan sizes, an arch-shaped or S-shaped bow may appear in the images. It can be removed by performing second- and third-order plane-fits, respectively, in  $X$ - and  $Y$ -directions.

Edge overshoot can occur at the edges of a sample due to piezoelectric scanner hysteresis (Golek et al., 2014). It can be seen as artificial, narrow hills and valleys at the edges of surface terraces, such as patterned silicon wafers and compact disks (Fig. 3.5). To minimize it, AFM users should consider the decrease in the scan rate.

Distortion of AFM images can occur due to thermal drift of piezo. The most common type of drift occurs at the start area of an image after the operation of “scan from top to bottom,” “scan from bottom to top,” or “zoomed in.” Rescanning without changing the operation will usually remove drift distortion.

Distortion of AFM images can also occur due to cross-talk between the  $x$ - and  $y$ -motion signals. It can be seen as the  $x$ -direction and  $y$ -direction are not orthogonal. This error can be checked and confirmed by imaging a square assay standard test. If the horizontal and vertical rows are

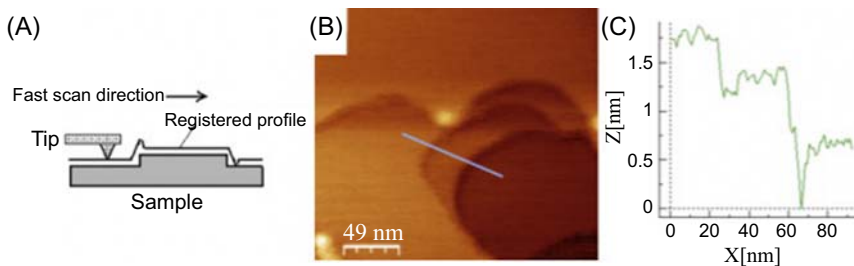


**Figure 3.5** Edge overshoots caused by the scanner. (A). Scheme showing the edge overshoots. (B). AFM height image of the LiF crystal surface. (C) Height profile along the line drawn in (B). Reprinted with permission from Golek, F., Mazur, P., Ryszka, Z., & Zuber, S. (2014). *AFM image artifacts*. *Applied Surface Science*, 304, 11–19.

not exactly perpendicular, AFM calibration should be performed to solve this error.

Distortion of AFM images can also occur due to cross-talk between the z-motion signal and the x–y motion signals. This error is really hard to recognize according to the AFM images. Experienced users will recognize it by combining the sample structures from other techniques. This error can be checked and confirmed by imaging a repeating triangular test sample with known dimensions. This may have resulted from a damaged or improperly designed scanner.

### 3.10.1.4 Artifacts caused by optical interference

Optical interference may occur between the incident and reflected light from the sample surface. It can be seen as a sinusoidal pattern in the AFM image with a period typically ranging from dozens of nanometers to micrometers. It is most often seen on a highly reflective surface (Fig. 3.6). This error can usually be reduced or eliminated by adjusting the laser alignment to decrease the light on the sample surface. Another possible way is to modulate the laser current at a high frequency. The light interference effect can also be removed by the flattening function of the WSxM program (Golek et al., 2014).

### 3.10.1.5 Artifacts caused by high-frequency operation

If the tapping mode is operated on the high-frequency side of the resonance peak, ring-like artifacts may appear around raised features. This

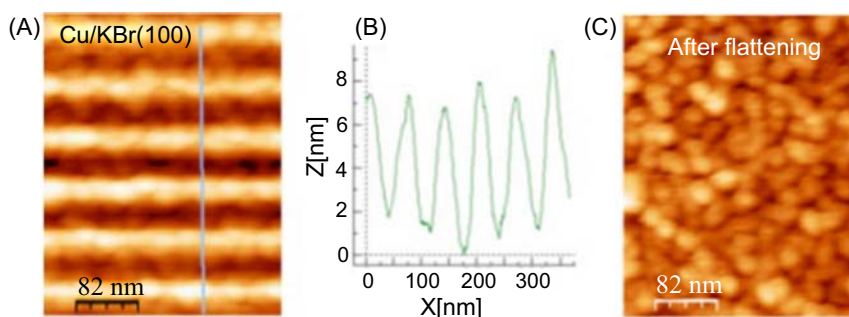


**Figure 3.6** Artifacts caused by optical interference. (A) Atomic force microscopy (AFM) height image with the optical interference effect. (B) Height profile along the line drawn in (A). (C) AFM height image without the optical interference effect, which was removed by the flattening function of the WSxM program. Reprinted with permission from Golek, F., Mazur, P., Ryszka, Z., & Zuber, S. (2014). AFM image artifacts. *Applied Surface Science*, 304, 11–19.

error can be eliminated by decreasing the drive frequency to the low-frequency side of the resonance peak. It should be noted that the setpoint should be also reduced to obtain the best quality.

### 3.10.1.6 Artifacts caused by friction

The friction forces tend to induce some torsion of the cantilever. Friction-related artifacts may occur for the samples with different friction property distributions. The friction force depends on many factors such as force load, sample surface, applied AFM tip, scan rate, and scan direction. If some domains in the image are seen as valleys when scanned in the forward direction and as hills when scanned in the backward direction, typical friction-related artifacts are formed in these images (Fig. 3.7). The best way to solve it is to use other operation modes (e.g., tapping or noncontact modes) to image the sample surface.

### 3.10.1.7 Artifacts caused by inappropriate imaging parameters

During the imaging process, the feedback parameters (e.g., setpoint and gains) should be carefully set. Tail-like artifacts and surface-disturbed artifacts may occur when the tip does not trace down the side of features and when the tip tracks too much on the features, respectively. They can be solved by adjusting the scan rate, gains, and setpoint. For example, tail-like artifacts may be removed with a slower scan rate, increased gains, and a lower setpoint voltage.

### 3.10.1.8 Artifacts caused by electronic noise

Electronic noise may be introduced into AFM images, which is commonly seen as periodic oscillations or repeating patterns in the images.

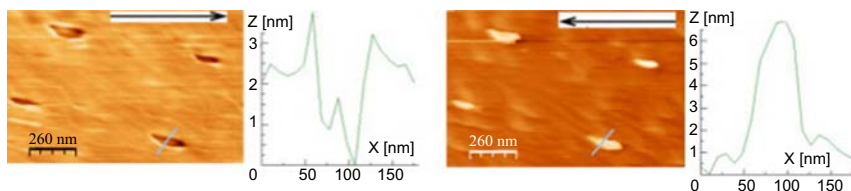


**Figure 3.7** Artifacts caused by friction on a contaminated (1 0 0) surface of the NaCl crystal. Left and right panel: atomic force microscopy height image and the height profile (along the line drawn in the height image) obtained for the forward (right) and backward (left) scan directions, respectively. Valleys in the forward scan image occur as hills in the backward scan image. Reprinted with permission from Golek, F., Mazur, P., Ryszka, Z., & Zuber, S. (2014). *AFM image artifacts*. Applied Surface Science, 304, 11–19.

The common sources are ground loop currents due to improper electrical grounding of the stage or defective electronic devices. The possible way to solve it is to make sure all the ground connections are tight and free of corrosion or insulating films.

### **3.10.1.9 Artifacts caused by vibration**

Both floor vibrations and acoustic vibrations may cause artifacts in AFM images. Floor vibrations can cause spurious periodic structures, and acoustic vibrations can cause short-time abnormal structures in AFM images. Typical floor vibrations include an elevator, a train going by, or even people passing by. Typical acoustic vibrations include airplanes passing overhead and loud talking. A quiet and vibration-free environment should be set up to obtain clean and noise-free images.

## **3.10.2 Image analysis**

There are several analytical functions in the real-time and offline commercial software to analyze the sample surface features in AFM images. The most common analysis functions are section, roughness, and bearing.

### **3.10.2.1 Section**

Section function can be used to measure the depth, height, width, or angular in the sample. By drawing a cross-sectional line across any part of the AFM image, the vertical profile along the line is shown. Then, mouse cursors may be placed on the line at any point to make the measurements.

### **3.10.2.2 Roughness**

Roughness is an important characteristic of a surface. Roughness measurement can be executed using the roughness function on an entire AFM image or on a selected area. The most common roughness results include root-mean-square roughness and mean roughness.

### **3.10.2.3 Bearing**

The bearing function is a useful way to measure bearing ratio and depth histogram. The bearing ratio of a surface is the percentage of the surface at a specific depth with respect to the analyzed area. A depth histogram plots depth versus percentage of occurrence of data at different depths, which can be applied to measure relative depth.

### 3.11 Conclusion

AFM is a powerful nanotool for food research and has mainly three types of functions, that is imaging, force measurement, and nanomanipulation. Correct and careful operation procedures are necessary to ensure accurate results from AFM. In this chapter, the basic operation procedures of AFM were introduced. AFM requirements, substrates, sample preparation, cantilever selection, common imaging procedure, common force measurement procedure, common nanomanipulation procedure, data optimization, and data analysis were comprehensively reviewed and discussed. These procedures discussed the basic information and some key considerations for the AFM choice, preparatory work, AFM procedures, data optimization, and data analysis. Further information can be obtained from the commercial manuals and discussions with AFM experts. What is learned from books is superficial after all. It is crucial to have it personally tested somehow. Therefore practice is an important part of AFM application.

### Acknowledgments

This research has been supported by research grants from the National Key R & D Program of China (No. 2018YFD0901006).

### Conflict of interest

The authors declare no conflict of interest.

### References

- Abdulreda, M. H., Bhalla, A., Chapman, E. R., & Moy, V. T. (2008). Atomic force microscope spectroscopy reveals a hemifusion intermediate during soluble N-ethylmaleimide-sensitive factor-attachment protein receptors-mediated membrane fusion. *Biophysical Journal*, *94*, 648–655.
- Alexander Reese, R., & Xu, B. (2019). Single-molecule detection of proteins and toxins in food using atomic force microscopy. *Trends in Food Science & Technology*, *87*, 26–34.
- Braet, F., Rotsch, C., Wisse, E., & Radmacher, M. (1998). Comparison of fixed and living liver endothelial cells by atomic force microscopy. *Applied Physics A*, *66*, S575–S578.
- Bujalowski, P. J., & Oberhauser, A. F. (2013). Tracking unfolding and refolding reactions of single proteins using atomic force microscopy methods. *Methods (San Diego, Calif.)*, *60*, 151–160.
- Canale, C., Torre, B., Ricci, D., & Braga, P. C. (2011). Recognizing and avoiding artifacts in atomic force microscopy imaging. In P. C. Braga, & D. Ricci (Eds.), *Atomic*

- force microscopy in biomedical research: Methods and protocols* (pp. 31–43). Totowa, NJ: Humana Press.
- Cárdenas-Pérez, S., Chanona-Pérez, J. J., Méndez-Méndez, J. V., Arzate-Vázquez, I., Hernández-Varela, J. D., & Vera, N. G. (2019). Recent advances in atomic force microscopy for assessing the nanomechanical properties of food materials. *Trends in Food Science & Technology*, *87*, 59–72.
- Cheng, B., Yang, S., Woldu, Y. T., Shafique, S., & Wang, F. (2020). A study on the mechanical properties of a carbon nanotube probe with a high aspect ratio. *Nanotechnology*, *31*, 145707.
- Clifford, C. A., & Seah, M. P. (2005). The determination of atomic force microscope cantilever spring constants via dimensional methods for nanomechanical analysis. *Nanotechnology*, *16*, 1666–1680.
- Digital Instruments, V.M.G. (2000). Scanning Probe Microscopy Training Notebook. [https://www.nanophys.kth.se/nanolab/afm/dim3100/Trng\\_Ntb\\_v3.0.pdf](https://www.nanophys.kth.se/nanolab/afm/dim3100/Trng_Ntb_v3.0.pdf).
- Ding, M., Shi, C., & Zhong, J. (2019). 28 - Atomic force microscopy for food quality evaluation. In J. Zhong, & X. Wang (Eds.), *Evaluation Technologies for Food Quality* (pp. 715–741). Woodhead Publishing.
- Eaton, P., & Batziou, K. (2019). Artifacts and practical issues in atomic force microscopy. In N. C. Santos, & F. A. Carvalho (Eds.), *Atomic Force Microscopy: Methods and Protocols* (pp. 3–28). New York, NY: Springer New York.
- Ebner, A., Wildling, L., & Gruber, H. J. (2019). Functionalization of AFM Tips and Supports for Molecular Recognition Force Spectroscopy and Recognition Imaging. In N. C. Santos, & F. A. Carvalho (Eds.), *Atomic Force Microscopy: Methods and Protocols* (pp. 117–151). New York, NY: Springer New York.
- El Kirat, K., Burton, I., Dupres, V., & Dufrene, Y. F. (2005). Sample preparation procedures for biological atomic force microscopy. *Journal of Microscopy*, *218*, 199–207.
- Fernandez, J. M., & Li, H. (2004). Force-clamp spectroscopy monitors the folding trajectory of a single protein. *Science (New York, N.Y.)*, *303*, 1674–1678.
- Fornal, J., Sadowska, J., Błaszczak, W., Jeliński, T., Stasiak, M., Molenda, M., & Hajnos, M. (2012). Influence of some chemical modifications on the characteristics of potato starch powders. *Journal of Food Engineering*, *108*, 515–522.
- Fukui, T., Uchihashi, T., Sasaki, N., Watanabe, H., Takeuchi, M., & Sugiyasu, K. (2018). Direct observation and manipulation of supramolecular polymerization by high-speed atomic force microscopy. *Angewandte Chemie International Edition*, *57*, 15465–15470.
- Girard-Egrot, A. P., & Blum, L. J. (2007). Langmuir-Blodgett technique for synthesis of biomimetic lipid membranes. In D. K. Martin (Ed.), *Nanobiotechnology of biomimetic membranes* (pp. 23–74). Boston, MA: Springer US.
- Golek, F., Mazur, P., Ryszka, Z., & Zuber, S. (2014). AFM image artifacts. *Applied Surface Science*, *304*, 11–19.
- Ho, T. M., Abik, F., & Mikkonen, K. S. (2021). An overview of nanoemulsion characterization via atomic force microscopy. *Critical Reviews in Food Science and Nutrition*. Available from <https://doi.org/10.1080/10408398.2021.1879727>.
- Hollars, C. W., & Dunn, R. C. (1998). Submicron structure in l- $\alpha$ -dipalmitoylphosphatidylcholine monolayers and bilayers probed with confocal, atomic force, and near-field microscopy. *Biophysical Journal*, *75*, 342–353.
- Ito, T., Ibrahim, S., & Grabowska, I. (2010). Chemical-force microscopy for materials characterization. *TrAC Trends in Analytical Chemistry*, *29*, 225–233.
- Jiang, X., & Lin, X. (2004). Atomic force microscopy of DNA self-assembled on a highly oriented pyrolytic graphite electrode surface. *Electrochemistry Communications*, *6*, 873–879.
- Kim, M.-S., Choi, J.-H., Kim, J.-H., & Park, Y.-K. (2010). Accurate determination of spring constant of atomic force microscope cantilevers and comparison with other methods. *Measurement*, *43*, 520–526.

- Koehler, M., Macher, G., Rupprecht, A., Zhu, R., Gruber, H. J., Pohl, E. E., & Hinterdorfer, P. (2017). Combined recognition imaging and force spectroscopy: A new mode for mapping and studying interaction sites at low lateral density. *Science of Advanced Materials*, 9, 128–134.
- Li, J., Liu, Y., Yuan, Y., & Huang, B. (2021). Applications of atomic force microscopy in immunology. *Frontiers of Medicine*, 15, 43–52.
- Li, M., Xi, N., & Liu, L. (2021). Peak force tapping atomic force microscopy for advancing cell and molecular biology. *Nanoscale*, 13, 8358–8375.
- Liu, Q., & Yang, H. (2019). Application of atomic force microscopy in food microorganisms. *Trends in Food Science & Technology*, 87, 73–83.
- Ma, M., Zhong, J., Li, W., Zhou, J., Yan, Z., Ding, J., & He, D. (2013). Comparison of four synthetic model peptides to understand the role of modular motifs in the self-assembly of silk fibroin. *Soft Matter*, 9, 11325–11333.
- Main, K. H. S., Provan, J. I., Haynes, P. J., Wells, G., Hartley, J. A., & Pyne, A. L. B. (2021). Atomic force microscopy—A tool for structural and translational DNA research. *APL Bioengineering*, 5, 031504.
- Marchin, K. L., & Berrie, C. L. (2003). Conformational changes in the plasma protein fibrinogen upon adsorption to graphite and mica investigated by atomic force microscopy. *Langmuir: the ACS Journal of Surfaces and Colloids*, 19, 9883–9888.
- Marinello, F., La Storia, A., Mauriello, G., & Passeri, D. (2019). Atomic force microscopy techniques to investigate activated food packaging materials. *Trends in Food Science & Technology*, 87, 84–93.
- Martins, E., Zhong, J., Muzard, J., Lee, A. C., Akhremitchev, B. B., Suter, D. M., & Lee, G. U. (2012). Single-molecule force spectroscopy of the *Aplysia* cell adhesion molecule reveals two homophilic bonds. *Biophysical Journal*, 103, 649–657.
- Morris, V. J., Kirby, A. R., & Gunning, A. P. (2010). *Atomic Force Microscopy for Biologists* (Second ed.). London, UK: Imperial College Press.
- Nandi, T., & Ainaravaru, S. R. K. (2021). Applications of atomic force microscopy in modern biology. *Emerging Topics in Life Sciences*, 5, 103–111.
- Ohler, B. (2007). Cantilever spring constant calibration using laser Doppler vibrometry. *Review of Scientific Instruments*, 78, 063701.
- Posé, S., Paniagua, C., Matas, A. J., Gunning, A. P., Morris, V. J., Quesada, M. A., & Mercado, J. A. (2019). A nanostructural view of the cell wall disassembly process during fruit ripening and postharvest storage by atomic force microscopy. *Trends in Food Science & Technology*, 87, 47–58.
- Qiao, Y., Qiao, R., He, Y., Shi, C., Liu, Y., Hao, H., . . . Zhong, J. (2017). Instrumental analytical techniques for the characterization of crystals in pharmaceuticals and foods. *Crystal Growth & Design*, 17, 2138–2148.
- Ricci, D., & Braga, P. C. (2004). Recognizing and avoiding artifacts in AFM imaging. In P. C. Braga, & D. Ricci (Eds.), *Atomic Force Microscopy: Biomedical Methods and Applications* (pp. 25–37). Totowa, NJ: Humana Press.
- Sader, J. E., Chon, J. W. M., & Mulvaney, P. (1999). Calibration of rectangular atomic force microscope cantilevers. *Review of Scientific Instruments*, 70, 3967–3969.
- Shi, C., Bi, C., Ding, M., Xie, J., Xu, C., Qiao, R., . . . Zhong, J. (2019). Polymorphism and stability of nanostructures of three types of collagens from bovine flexor tendon, rat tail, and tilapia skin. *Food Hydrocolloids*, 93, 253–260.
- Shi, C., He, Y., Ding, M., Wang, Y., & Zhong, J. (2019a). Nanoimaging of food proteins by atomic force microscopy. Part I: Components, imaging modes, observation ways, and research types. *Trends in Food Science & Technology*, 87, 3–13.
- Shi, C., He, Y., Ding, M., Wang, Y., & Zhong, J. (2019b). Nanoimaging of food proteins by atomic force microscopy. Part II: Application for food proteins from different sources. *Trends in Food Science & Technology*, 87, 14–25.

- Ukraitsev, E., Kromka, A., Kozak, H., Remeš, Z., & Rezek, B. (2012). Artifacts in atomic force microscopy of biological samples. In F. Christopher (Ed.), *Force Microscopy Investigations Into Biology—From Cell to Protein* (pp. 29–54). *InTech*.
- Velegol, S. B., Pardi, S., Li, X., Velegol, D., & Logan, B. E. (2003). AFM imaging artifacts due to bacterial cell height and AFM tip geometry. *Langmuir: the ACS Journal of Surfaces and Colloids*, *19*, 851–857.
- Wang, J., & Nie, S. (2019). Application of atomic force microscopy in microscopic analysis of polysaccharide. *Trends in Food Science & Technology*, *87*, 35–46.
- Wang, Z., Wan, L., Zhou, C., Fang, X., Wang, C., & Bai, C. (2003). Study of  $\beta$ -amyloid adsorption and aggregation on graphite by STM and AFM. *Chinese Science Bulletin*, *48*, 437–440.
- West, P., & Starostina, N. (2003). How to recognize and avoid AFM image artifacts. *Microscopy Today*, *11*, 20–27.
- Yan, Y., Hu, Z., Zhao, X., Sun, T., Dong, S., & Li, X. (2010). Top-down nanomechanical machining of three-dimensional nanostructures by atomic force microscopy. *Small (Weinheim an der Bergstrasse, Germany)*, *6*, 724–728.
- Zhang, Y., Zhu, X., Chu, C., Xiao, X., & Chen, B. (2021). Applications of atomic force microscopy-based imaging and force spectroscopy in assessing environmental interfacial processes. *Critical Reviews in Environmental Science and Technology*.
- Zhong, J. (2011). From simple to complex: investigating the effects of lipid composition and phase on the membrane interactions of biomolecules using in situ atomic force microscopy. *Integrative Biology*, *3*, 632–644.
- Zhong, J., & He, D. (2012). Recent progress in the application of atomic force microscopy for supported lipid bilayers. *Chemistry – A European Journal*, *18*, 4148–4155.
- Zhong, J., Ma, M., Li, W., Zhou, J., Yan, Z., & He, D. (2014). Self-assembly of regenerated silk fibroin from random coil nanostructures to antiparallel  $\beta$ -sheet nanostructures. *Biopolymers*, *101*, 1181–1192.
- Zhong, J., Ma, M., Zhou, J., Wei, D., Yan, Z., & He, D. (2013). Tip-induced micropatterning of silk fibroin protein using in situ solution atomic force microscopy. *ACS Applied Materials & Interfaces*, *5*, 737–746.
- Zhong, J., Sun, G., & He, D. (2014). Classic, liquid, and matrix-assisted dip-pen nanolithography for materials research. *Nanoscale*, *6*, 12217–12228.
- Zhong, J., & Yan, J. (2016). Seeing is believing: atomic force microscopy imaging for nanomaterial research. *RSC Advances*, *6*, 1103–1121.
- Zhong, J., Zheng, W., Huang, L., Hong, Y., Wang, L., Qiu, Y., & Sha, Y. (2007). PrP106–126 amide causes the semi-penetrated poration in the supported lipid bilayers. *Biochimica et Biophysica Acta (BBA) – Biomembranes*, *1768*, 1420–1429.
- Zhou, H., Xu, Q., Li, S., Zheng, Y., Wu, X., Gu, C., ... Zhong, J. (2015). Dynamic enhancement in adhesion forces of truncated and nanosphere tips on substrates. *RSC Advances*, *5*, 91633–91639.



This page intentionally left blank

## **SECTION 3**

# **Application of AFM for food research**

This page intentionally left blank

## CHAPTER 4

# Application of atomic force microscopy for food proteins

Yangyi Zhang<sup>1,2</sup>, Jiamin Xu<sup>2</sup>, Ting Zhang<sup>2</sup>, Shudan Huang<sup>2</sup>, Xichang Wang<sup>2</sup> and Jian Zhong<sup>1,2</sup>

<sup>1</sup>Xinhua Hospital, Shanghai Institute for Pediatric Research, Shanghai Key Laboratory of Pediatric Gastroenterology and Nutrition, Shanghai Jiao Tong University School of Medicine, Shanghai, P. R. China  
<sup>2</sup>National R&D Branch Center for Freshwater Aquatic Products Processing Technology (Shanghai), Integrated Scientific Research Base on Comprehensive Utilization Technology for By-Products of Aquatic Product Processing, Ministry of Agriculture and Rural Affairs of the People's Republic of China, Shanghai Engineering Research Center of Aquatic-Product Processing and Preservation, College of Food Science & Technology, Shanghai Ocean University, Shanghai, P. R. China

### 4.1 Introduction

Proteins are important macromolecules that are made of one or more polypeptide chains. They are essential structural and functional substances for many biological units, ranging from subcellular structures (native membrane, organelles, etc.) to living cells, all the way up to tissues and organisms. As an important nontoxic and nutritional diet for human health, food proteins are intake by humans every day (Phillips, 2013). Food processing and preservation may affect the structures of food proteins or disrupt food proteins, which may further affect their flavor, digestion, in vivo bioavailability, absorption, distribution, metabolism, excretion, and nutrition values (Deleu, Wilderjans, Van Haesendonck, Brijs, & Delcour, 2016; Sun-Waterhouse, Zhao, & Waterhouse, 2014). In addition, to improve the functions of food proteins, protein structure may be modified by physical, chemical, enzymatic, and complex modification methods (Huang et al., 2019). Considering that protein structure determines its function, it is important to analyze the structural characteristics of food proteins and their changes after structural modifications.

Food proteins are readily available and agriculturally sustainable proteins. According to the source difference, food proteins can be classified into four types (Phillips & Williams, 2011): (1) food proteins from animal sources such as meat, seafood, blood, milk, and egg. Animal proteins are the main food proteins in the world. (2) Food proteins from botanical sources such as cereals, legumes, pulses, vegetables, tubers, and oil seeds.

(3) Food proteins from macro-algae sources such as green and blue-green seaweeds. These proteins include *Spirulina*, *Anabaena*, *Nostoc*, *Ulva*, *Enteromorpha*, etc. (4) Food proteins from microorganisms such as Fungi. A typical protein from microorganisms is also called mycoproteins. Different food proteins have different structures and different nutritional values.

In the field of protein research, atomic force microscopy (AFM) has been successfully and broadly applied to image individual protein (Czajkowsky, Li, Sun, Hu, & Shao, 2011), to image self-assembled protein structures (Ma et al., 2013; Zhong & He, 2012), to analyze the effects of processing and preservation conditions on proteins (Zhong, Liu, et al., 2015; Zhong, Ma, et al., 2014), to observe dynamic protein interactions (Ando, 2019; Zhong, 2011), to measure the molecular force spectroscopy of protein interaction (Martines et al., 2012; Walder, Van Patten, Adhikari, & Perkins, 2018), to analyze the unfolding and folding kinetics of protein conformation by stretching individual protein (Lei et al., 2017; Manibog, Yen, & Sivasankar, 2017), to characterize nanomechanical properties of protein-based materials (Bahri, Martin, Gergely, Marchesseau, & Chevalier-Lucia, 2018), to manipulate protein/peptides (Zhang et al., 2010), to analyze protein interaction in living cells (Yang et al., 2007), and to mechanically fabricate three-dimensional (3D) bio nanostructures (Zhong et al., 2013; Zhong, Sun, & He, 2014).

AFM has also been successfully applied to study food substances (Ding, Shi, & Zhong, 2019; Gunning & Morris, 2017; Jones, 2016), which range from the smallest biomolecules such as food proteins (Alexander Reese & Xu, 2019; Shi, He, Ding, Wang, & Zhong, 2019b; Shi, He, Ding, Wang, & Zhong, 2019a) and food carbohydrates (Wang & Nie, 2019), to food-related microorganisms and pathogens (Kuda, Shibata, Takahashi, & Kimura, 2015; Liu & Yang, 2019), all the way up to food-based materials (Cárdenas-Pérez et al., 2019), and food packaging materials (Marinello, La Storia, Mauriello, & Passeri, 2019).

As a relatively simple food sample, food protein has been examined by AFM over the past three decades. Among the application methods (nanoimaging, force measurement, manipulation, etc.) of AFM, nanoimaging is the most popular method to understand the structures, functions, and the relationships of food proteins. Force measurement is also used to analyze food proteins and interested readers can read Chapter 9 in this book and some previous references (Cárdenas-Pérez et al., 2019). Nanomanipulation has almost not been applied to food protein research and interested readers can read some previous references (Ikai, Afrin, Saito, & Watanabe-Nakayama, 2018;

Pavliček & Gross, 2017). Considering that almost all food scientists only focus on one type of food protein such as cereal proteins or meat proteins, the summary and discussion of AFM application for food proteins from different sources can save the precious time and energy of food scientists. In this chapter, food protein extraction and sample preparation are first introduced. Then, the application of AFM in food protein research is mainly introduced according to different protein sources.

## 4.2 Food protein extraction and sample preparation

Some food proteins such as whey protein concentrate and caseins can be obtained from commercial companies. In this case, the protein samples were directly prepared for AFM studies. However, if the authors want to study some commercialized food proteins or to study the effect of preparation factors on the food proteins, they have to obtain pure food proteins in the laboratory. In this case, food protein preparation is an important step prior to AFM studies.

There are two types of common methods to obtain pure proteins: protein expression (Hunt, 2005) and protein extraction (Sari, Mulder, Sanders, & Bruins, 2015). Protein expression is a mature way to synthesize and purify reconstituted protein in protein expression systems such as mammalian, insect, yeast, bacteria, algae, and acellular systems. Protein extraction is a common method to extract and purify basic protein from tissues. Compared with the protein expression method, the protein extraction method is the most popular method to prepare pure food proteins because proteins can be easily extracted from food protein-based raw materials. The obtained food proteins are then often deposited on flat substrates such as mica and analyzed by AFM. Therefore, in this section, we mainly introduce food protein extraction and sample preparation.

### 4.2.1 Food protein extraction

The food protein extraction process mainly consists of five stages (Bi et al., 2019): (1) cleaning of raw materials to remove adhering unwanted tissues by cutting, scraping, and washing; (2) removal of nonprotein substances in raw materials such as fats by sodium hydroxide solution; (3) pretreatment of the raw materials to convert insoluble proteins into soluble proteins by sodium chloride, acids, alkalis, or enzymes; (4) extraction of the soluble gelatin from the raw material into hot water (e.g., incubation at 55°C for 6 h); and (5) purification (e.g., centrifugation and filtration)

and freeze-drying of the protein. According to the used solvents in stage 3, the food protein extraction methods can be classified into sodium chloride, acidic, alkali, hot water, and enzymatic pretreatment methods. It should be noted that not all the steps were necessary for food protein extraction. Removal of fat in tissue (stage 2) and conversion of insoluble proteins into soluble proteins (stage 3) can be merged in some methods such as the hot water method (Zhang, Sun, Ding, Tao, et al., 2020). The hot water pretreatment method can be applied to extract soluble or less covalently cross-linked food proteins. The properties of the extracted food proteins depend on the raw materials and the extraction conditions such as the solvent type, solvent concentration, enzyme type, enzyme activity, reaction time, and reaction temperature.

Enzymatic pretreatment extraction can be divided into protease pretreatment extraction method and nonprotease pretreatment extraction method. The protease pretreatment extraction method is to degrade and modify proteins by using proteases to convert insoluble proteins into soluble proteins. Common proteases include pepsin, trypsin, papain, neutrase, bromelain, proctase, and crude protease. The nonprotease pretreatment extraction method is to separate proteins from the polysaccharide structure. Common nonproteases include cellulase, hemicellulase, pectinase, and xylanase. These nonproteases can hydrolyze the high-molecular-weight cell wall components of rice bran to improve the extraction rate of proteins from plant sources such as rice bran (Ansharullah, Hourigan, & Chesterman, 1997).

Some physical pretreatments such as microwaving, ultrasonication, freeze-thaw cycles, milling, and high-speed homogenization can be applied to speed the extraction process or improve the properties of food proteins. For example, microwaving and ultrasonication can be applied to assist in gelatin extraction. Short-term (5–30 min) microwaving assistance could make the extracted gelatin have higher gel strength and lower yield than hot water-extracted rabbit skin gelatin. Moreover, longer microwave-assisted time increased yield and decreased gel strength (Liu et al., 2019). Ultrasonication assistance could make the extracted Asian bullfrog skin gelatin with improved gelatin yield and recovery than acetic acid-pretreated gelatin. Moreover, different ultrasonication modes and times determined the gelatin characteristics (Karnjanapratum & Benjakul, 2020). Ultrasonication-assisted common carp by-products (scales and fins) gelatins had higher gel strengths, viscosities, melting points, and gelling points than microwave-assisted gelatins (Mirzapour-Kouhdasht, Sabzipour, Taghizadeh, & Moosavi-Nasab, 2019).

### 4.2.2 Sample preparation

The sample preparation process is mainly dependent on the AFM imaging environments such as the common air or liquid. The sample preparation process for AFM imaging in the air mainly contains three steps: (1) preparation of protein molecule solution; (2) protein solution deposition on a flat substrate; and (3) protein drying on the substrate at room temperature. The sample preparation process for AFM imaging in liquid mainly contains two steps: (1) preparation of protein molecule solution and (2) protein solution injection into the liquid sample chamber. The sample preparation process for AFM imaging under cryo mainly contains four steps (Zhang, Sheng, & Shao, 1996): (1) preparation of protein molecule solution; (2) protein solution deposition on a flat substrate in a clean nitrogen environment; (3) buffer washing and water washing; and (4) sample cleaning by pressurized nitrogen.

Protein solution preparation is the most important step to make sure that protein molecules are dissolved, not aggregated, in the solution. According to Osborne's classification (Osborne & Thomas, 1924), proteins can be divided into four classes based on their solubility: albumin (water-soluble), globulin (salt-soluble), glutelin (alkali/acid-soluble), and prolamin (alcohol-soluble, also named as gliadin). Albumin can be easily dissolved in water. Globulin can be dissolved in a dilute salt solution. Gliadin can be dissolved in 50%–90% ethanol. Glutenin can be dissolved in dilute acids or bases. Therefore, protein solution preparation should choose an appropriate solvent to dissolve the objective proteins. Especially, food proteins are commonly a mixture of these four classes of proteins. For example, milled rice or rice endosperm proteins contain 3.8%–8.8% albumin, 9.6%–10.8% globulin, 2.6%–3.3% prolamin, and 66%–78% glutelin (Van Der Borght et al., 2006). Due to different solubility of food protein components, AFM users should carefully consider what kinds of solvents should be used to dissolve the objective proteins. After imaging, the data analysis should also recheck the applied solvents to understand what kinds of proteins they are imaging.

The subsequent sample preparation can be seen in Section 3.3 (Substrates) and Section 3.4 (Sample preparation). Typically, a drop of protein solution is cast on a flat substrate such as freshly cleaved muscovite mica that was stuck to an iron disk. It is dried in ambient air at room temperature for 20 min. Then, this sample is examined by AFM. It should be a coffee stain effect (a very inhomogeneous distribution of the protein on



a substrate) that may occur during the solution drying process (Zhong, Liu, et al., 2015). Therefore, the possible coffee stain effect should be carefully evaluated by examining three center and three peripheral positions of three independent samples.

### 4.3 Grain proteins

Grains generally contain 6%–8% protein. Moreover, grains generally do not contain all the essential amino acids. However, the nutritional and health properties of grain proteins have been widely recognized today and grain protein-containing products have become commercially available in recent years (Amagliani, O'Regan, Kelly, & O'Mahony, 2017). Therefore, the relationship between the structure and function of grain proteins has attracted much attention. Typical grains include rice, wheat, maize, and sorghum. Grain proteins contain all four classes of protein with different solubility: albumin, globulin, prolamin, and glutenin (Amagliani et al., 2017; De Mesa-Stonestreet, Alavi, & Bean, 2010; Juhász, Békés, & Wrigley, 2014; Rodriguez-Nogales, Garcia, & Marina, 2006). AFM has been widely applied to analyze grain proteins.

#### 4.3.1 Rice proteins

AFM nanoimaging has been used to characterize the morphology of rice protein. Tapping mode AFM found that rice bran protein was nanofibrils after heat treatment. The rice bran protein nanofibrils had a periodicity between 20 and 30 nm, which suggested they might be in a helical structure (Zhang & Huang, 2014). The morphology and size change of rice glutenin before and after heat treatment were studied by AFM nanoimaging (Zhao, Xiong, Chen, Zhu, & Wang, 2020). Untreated glutenin at pH 12 showed a wide range of protein aggregates. After heating treatment, the size of rice glutenin aggregates significantly reduced. Moreover, the size was dependent on heating temperature.

AFM nanoimaging can be used to observe the interaction of rice protein with other substances. The interaction between rice bran protein hydrolysate and gelatinized rice starch was studied by AFM nanoimaging (Niu, Wu, & Xiao, 2017). As shown in Fig. 4.1, rice bran protein hydrolysates were nanoparticles and rice starch showed irregular structures with a height of a few nanometers. After mixing, the rice bran protein hydrolysate nanoparticles are scattered on the surface of the rice starch. This

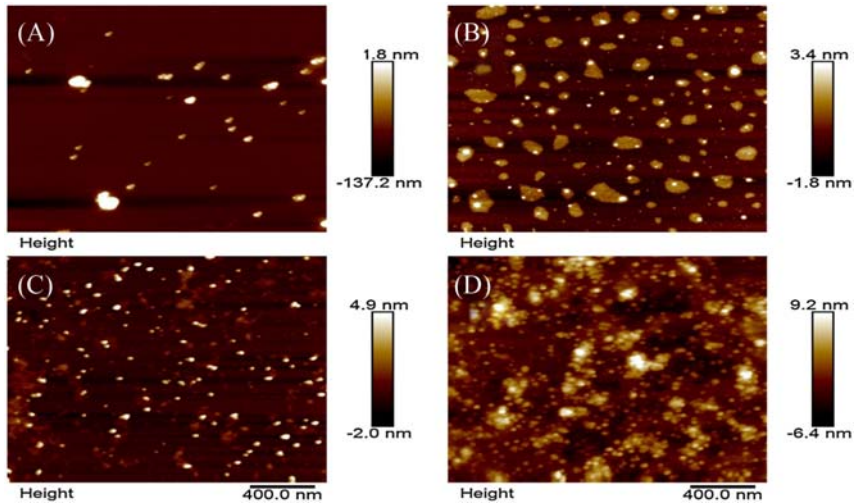


**Figure 4.1** Atomic force microscopy height images of the (A) protamex-hydrolyzed rice bran protein at 1 h and its mixtures with rice starch at mass ratios of (B) 0:100, (C) 6:100, and (D) 12:100. Reprinted with permission from reference Niu, L., Wu, L., & Xiao, J. (2017). *Inhibition of gelatinized rice starch retrogradation by rice bran protein hydrolysates*. *Carbohydrate Polymers*, 175, 311–319.

AFM work directly proved that rice bran protein hydrolysate could react with gelatinized rice starch.

### 4.3.2 Wheat proteins

AFM nanoimaging has been applied to observe the real-time interaction of wheat proteins with different substrates. In situ AFM was applied to real-time observe the deposition process of wheat proteins ( $\omega$ -gliadin and  $\gamma$ -gliadin) on hydrophilic mica and hydrophobic graphite (Haward, Shewry, Miles, & McMaster, 2010). The liquid cell was examined to obtain the AFM height image of the substrates and then wheat protein solutions were injected into the liquid cell prior to subsequent imaging.  $\omega$ -gliadin could form near-monolayers on mica and  $\gamma$ -gliadin could form near-monolayers on graphite. These results suggested that  $\omega$ -gliadin was more hydrophilic and  $\gamma$ -gliadin was more hydrophobic. The sequential pairwise adsorption experiments by in situ AFM showed the deposition process was not commutative since  $\gamma$ -gliadin could partly displace the pre-adsorbed  $\omega$ -gliadin on mica. These in situ AFM results provided useful information to understand the inter- and intramolecular interactions between wheat proteins and the substrates.

AFM nanoimaging has been applied to study the interaction of the wheat protein with other substances. The interactions between wheat gluten proteins and soy protein isolates were studied by AFM (He, Wang, Feng, Chen, & Wang, 2020). With moderate addition of soy bean isolates (wheat protein/soy protein isolate ratios = 1:0.1–1:1.5), the composites were uniformly dispersed nanoparticles with diameters around 100 nm and thicknesses of several nanometers (insets at the right of figure). With the high addition of soy bean isolate (wheat protein/soy protein isolate ratio = 1:2), the nanoparticles aggregated into clusters. These results provided basic structural information to understand the formation of the coassembled food protein nanostructures. This work suggested that AFM was a useful work to analyze food protein interaction at the nanoscale.

AFM nanoimaging has been applied to investigate the effects of processing and preservation on wheat proteins. AFM nanoimaging was applied to observe the morphologies of native and succinic acid-deamidated wheat gluten after freeze- and spray-drying (Liao, Wang, & Zhao, 2013). These results demonstrated that native wheat gluten was a bulk network complicated by island-like and strip aggregates. After succinic acid-deamidation under hydrothermal treatment, the modified wheat gluten was a porous network with flat and striped aggregates. After dehydration by freeze-drying, the wheat gluten was an unnetworkable and individual island-like aggregate. After dehydration by spray-drying, the wheat gluten was linked-island-like aggregates. The AFM results provided basic morphological changes of wheat proteins after processing, which was helpful to understand the structural and functional behaviors of wheat proteins. During the frozen storage process (0, 30, 60, 90, and 120 days), the morphologies of wheat gluten were observed by AFM (Zhang et al., 2016). The AFM results showed wheat gluten chains aggregated from 60 to 120 days, which provided direct visual evidence to show the protein structure changes during the frozen storage process.

AFM nanomanipulation (scratching) function has also been applied to compare the surfaces of tablets made of wheat gluten (Chichti, George, Delenne, Radjai, & Lullien-Pellerin, 2013). The morphological changes after scratching were estimated by AFM imaging and the shear forces were measured by keeping a constant normal force. AFM results together with a simple tribological model provided clear evidence that wheat gluten had a lower hardness and shear strength than starch. Moreover, the mechanical properties of wheat gluten were close to that of soft materials. This work confirmed that gluten might have similar mechanical properties to soft materials, whereas starch had higher hardness.

### 4.3.3 Maize proteins

AFM has been applied to study the effect of processing and preservation conditions on maize proteins. The effects of environmental parameters on self-assembly behaviors of  $\alpha$ -zein in aqueous ethanol solution were studied by AFM (Sun, Xiong, Zhang, & Fang, 2020). The AFM results showed that  $\alpha$ -zein concentration, pH, and heating time affected the morphology and size of  $\alpha$ -zein assemblies. A variety of structures such as large/small spheres, worm-like strings, irregular aggregates, and ordered fibrils were observed in AFM images. The synergistic effect between heat treatment and high-pressure homogenization on zein proteins was explored by AFM (Sun et al., 2016). Native zein showed typical nanospheres with a diameter of 137–544 nm. Heating might induce zein protein to form oval-like, dumbbell-like, and irregular structures. High-pressure homogenization changed zein proteins from sphericity to oval, dumbbell-like, and random geometrical shapes after high-pressure homogenization. The synergistic effect between heat treatment (95°C) and high-pressure homogenization (75 MPa) resulted in the size reduction of zein nanoparticles. The AFM results provided direct evidence of the synergistic effect between heat treatment and high-pressure homogenization to zein nanoparticles.

AFM has been applied to characterize the surface topography and adhesion property of maize protein-based films. The effects of different fractions ( $\alpha$ -zein-riched,  $\beta$ -zein-riched, and unpurified) of zein on the mechanical and roughness properties of zein films were studied by AFM (Panchapakesan, Sozer, Dogan, Huang, & Kokini, 2012). Adhesion forces measured by the AFM force curves increased with increasing water activity. The film processing technologies (solvent casting, drop deposition, and spin casting) had obvious effects on the surface roughness and surface morphologies of zein films. In addition, the  $\alpha$ -zein-riched films were found to have the highest roughness values. This work provided processing and composition guides for the fabrication of zein-based biomaterials.

### 4.3.4 Sorghum proteins

AFM nanoimaging has been applied to study the nanostructures of sorghum proteins. The morphologies of kafirin, a sorghum prolamin protein, at different concentrations were studied by AFM (Xiao, Li, et al., 2015). Kafirin protein assemblies were uniform nanoparticles at low concentrations and disk- or rod-like nanostructures at high concentrations. Further, the assembly of kafirin/carboxymethyl chitosan nanoparticles was studied

by the same group (Xiao, Si, & Huang, 2015). AFM height and phase images demonstrated both curcumin/kafirin mixtures and curcumin/kafirin/carboxymethyl chitosan mixtures were spherical nanoparticles. The latter nanoparticles were a little larger (average particle size of 225 nm) than the former nanoparticles (average particle size of 193 nm). Based on the AFM results and other results, the formation mechanisms of these particles were proposed. These works proved AFM nanoimaging was a useful tool to analyze the self-assembly mechanisms of food proteins.

## 4.4 Bean proteins

Beans generally contain about 40% proteins. Peptides from common bean proteins have potential anti-inflammatory, antihypertensive, antioxidant, metal-chelating, and antifungal activities. Therefore, bean protein-based foods such as tofu and soy flour have been widely used for dieting in the world (Fukushima, 2011). In addition, some novel bean protein-based foods have also been explored in the field of food science and technology. Typical bean proteins include soy and pea proteins.

### 4.4.1 Soy proteins

AFM nanoimaging has been applied to observe the interaction between soy proteins and other substances. The interaction of soy protein isolate with curcumin was observed by AFM (Chen, Zhang, & Tang, 2016). AFM results showed they formed nanocomplexes, which had similar particle morphology to soy protein isolate. Therefore, curcumin binding did not have an obvious effect on the particle aggregation and formation of soy protein isolate. The interaction of soy protein isolate with betalain was also studied by AFM (Zhao, Ma, & Jing, 2020). AFM results showed that the soy protein isolate/betalain nanocomplex was a small and amorphous aggregate. These works demonstrated that AFM was a good tool to directly show the formed nanocomplexes between soy proteins and other substances, which is helpful to understand their interactions.

AFM has been applied to characterize the surface topography of soy protein-based films. Soy protein isolate/cellulose films and soy protein isolate/TiO<sub>2</sub> films were examined by AFM height imaging and phase imaging (Jensen, Lim, Barbut, & Marcone, 2015). Glycerol plasticized soy protein-based materials were examined by AFM (Tian, Guo, Xiang, & Zhong, 2018). The results showed that the morphologies were heterogeneous at the nanoscale and there were two important phases (protein-rich

domain and glycerol-rich domain). The protein-rich domain was composed of compact aggregations of pan-like protein while the glycerol-rich domain possessed a loose chain-like structure. These works proved that AFM could directly observe the surface morphologies of soy protein-based films, which will be helpful for biomaterial development.

AFM nanoimaging has been applied to investigate the effect of processing and preservation on soy proteins. The influence of heat treatment and storage on acid-tolerant emulsions prepared from acid-soluble soy protein and soy soluble polysaccharide complexes was studied by AFM (Liu et al., 2016). The emulsion droplets produced from complexes with or without heat treatment showed spherical shapes with a homogeneous appearance. After long-time storage (90 days), the droplets aggregated together. The effects of different processing methods (radio frequency, microwaving, and high hydrostatic pressure) on black soy proteins were studied by AFM (Zhong, Wang, & Zhao, 2015). After processing of radio frequency, microwaving, and high hydrostatic pressure, the black soy protein nanoparticles aggregated with sizes of 45–135, 50–190, and 20–100 nm, respectively. The effects of different freeze-thaw cycles on soy protein isolate films were studied by AFM (Zhao, Sun, Li, Liu, & Kong, 2016). As shown in Fig. 4.2, the film topography became smoother and the surface roughness decreased with the increase of freeze-thaw cycles. The effect of ultrasonication on soy protein isolate hydrolysate was studied by AFM (Tian et al., 2020). The AFM results demonstrated that the hydrolysate aggregates were dependent on hydrolysis time and ultrasonication. It demonstrated protein solubility increase after ultrasonication was due to the structural disruption of tightly formed peptide aggregates. These AFM works provided direct morphological comparisons of soy proteins after different processing methods, which will be helpful in comprehensively understanding the underlying mechanisms by combining other technologies.

#### 4.4.2 Pea proteins

Pea proteins are commercially available and have been widely applied in the food industry. AFM can be used to analyze the effects of processing and storage on pea proteins. Pea protein isolates before and after microfluidization at different protein concentrations were characterized by AFM (Liang & Tang, 2014). Pea protein isolates were mainly undissociated nanoparticles. Microfluidization decreased the height or contour size of pea protein isolates. Higher concentrations increased the height or

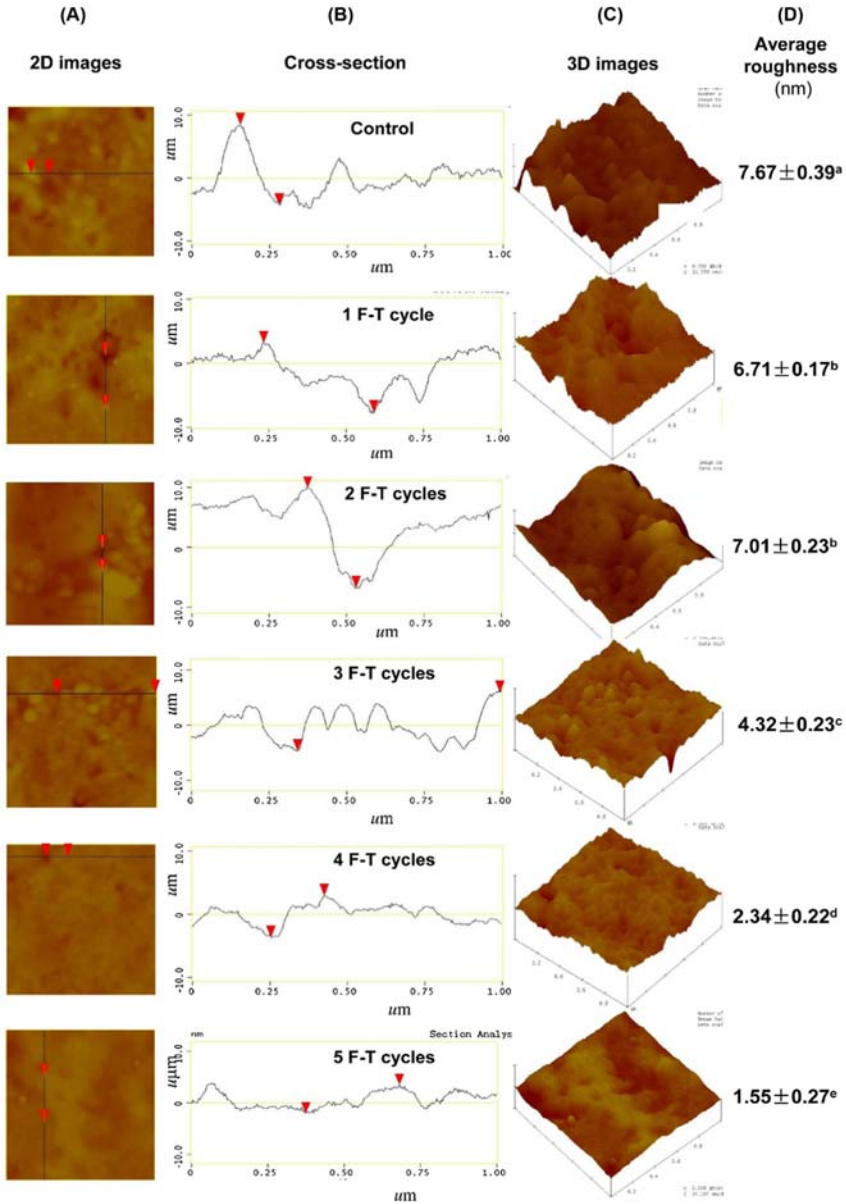


**Figure 4.2** Effect of different freeze-thaw (F-T) cycles on the surface morphology of soy protein isolate gel by atomic force microscopy 2D (A) and 3D (C) images. The middle cross-section image (B) corresponded to the straight line on the left image. The right values in (D) with different letters (a–e) indicated the average roughness as mean value ± standard deviation. Scan sizes were 1.0 × 1.0 μm. *Reprinted with permission from Zhao, J., Sun, F., Li, Y., Liu, Q., & Kong, B. (2016). Modification of gel properties of soy protein isolate by freeze-thaw cycles are associated with changes of molecular force involved in the gelation. Process Biochemistry, 52, 200–208.*

contour size of the proteins. These results provided useful information for understanding the structure of pea protein isolates at the oil/water interface in microfluidized emulsions. In order to understand the effect of protein oxidation on the emulsion during the storage process, the structural heterogeneity of dried Langmuir-Blodgett films prepared at the air-water interface with soluble pea protein after different incubation times in oxidative conditions was examined by AFM (Hinderink, Kaade, Sagis, Schroën, & Berton-Carabin, 2020). Compared with the fresh pea protein film, the film after 3-h oxidization showed larger aggregates and the film after 24-h oxidization showed a more structurally homogenous interface with only a few small protein clusters present. These results suggested oxidized pea proteins might aggregate and then desorb from the monolayer. Therefore, it is important to inhibit protein oxidation for long-term emulsion storage. These results provided useful information to understand underlying mechanisms of the effect of protein oxidation level on the coalescence susceptibility of pea protein-stabilized emulsions.

AFM has been applied to characterize pea protein-based biomaterials. In order to observe pea protein-based nanocarriers for protecting resveratrol from degradation, the interaction of pea protein isolates with resveratrol was observed by AFM (Fan, Zeng, Yi, & Zhang, 2020). AFM results showed that resveratrol-loaded pea protein isolate nanoparticles in the presence of  $\text{Ca}^{2+}$  had higher sizes than those in the absence of  $\text{Ca}^{2+}$ . The AFM results confirmed that pea protein isolate could be aggregated due to calcium-induced salt bridge. Moreover, AFM results showed no resveratrol crystals around the pea protein-based nanocarriers (nanocomplexes and nanoparticles), which suggested that resveratrol was successfully buried into the soy protein isolate matrix. This work confirmed that AFM can be efficiently applied to characterize and analyze pea protein-based nanocarriers.

## 4.5 Peanut proteins

Peanuts generally contain about 10%–30% proteins. Peanut protein is one of the most important food proteins in the world. Due to their good nutritional value and potential health effects, peanut proteins have been widely applied in many food formulations in the past decades. Peanut protein isolate is a commercially available peanut protein product and it mainly consisted of arachin and conarachin.

AFM has been applied to study the effect of processing and extraction conditions on peanut proteins. The influence of ionic strength on the



morphology of peanut proteins was observed by AFM (Ning et al., 2020). With the increase of  $\text{Na}^+$  ionic strength, the size of the peanut protein nanoparticles increased, which is consistent with dynamic light scattering data. The effect of extraction methods on the nanoclusters of arachin and conarachin was observed by AFM (Sun, Zhang, Zhang, Tian, & Chen, 2020). As shown in Fig. 4.3, AFM height images and size distribution showed the averaged diameters of arachin and conarachin from ultrasound-assisted extraction were lower than those from alkali-soluble and acid precipitation. This provided basic information to understand that the peanut protein from ultrasound-assisted extraction had the highest emulsifying property. Therefore, AFM could provide important structural information on peanut proteins to understand their functional properties.

## 4.6 Milk proteins

Milk contains hundreds of types of proteins. These proteins can be classified into caseins, whey proteins, and other minor fractions. Milk proteins

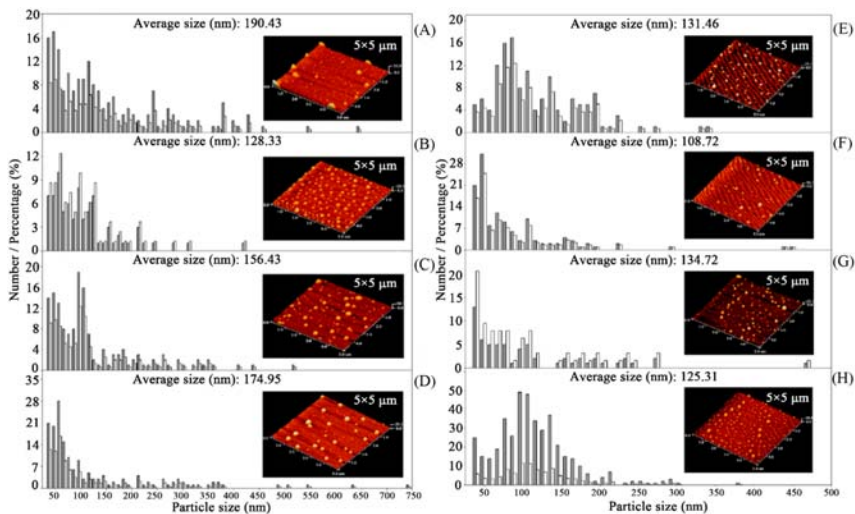


**Figure 4.3** Effects of ultrasonication-assisted extraction time on arachin and conarachin: (A and E) alkali-soluble and acid precipitation, (B and F) ultrasonication time of 10 min, (C and G) ultrasonication time of 30 min, (D and H) ultrasonication time of 50 min, (A, B, C, and D): arachin, (E, F, G, and H): images of conarachin. Revised with permission from Sun, X., Zhang, W., Zhang, L., Tian, S., & Chen, F. (2020). *Molecular and emulsifying properties of arachin and conarachin of peanut protein isolate from ultrasound-assisted extraction*. LWT, 109790.

are known for their high nutritional values and diverse functional properties. Milk proteins are precursors of many different biologically active peptides. Therefore, it is important to characterize milk protein structures to understand the relationships between the structures and functions of milk proteins.

#### 4.6.1 Caseins

Caseins are a family of phosphoproteins that are synthesized in the mammary gland and are secreted as large colloidal aggregates. They can be classified into four subgroups:  $\alpha$ S1,  $\alpha$ L1,  $\beta$ , and  $\kappa$ . They have been widely used in food industry such as nutritional fortifiers, thickening agents, emulsifying stabilizers, binders, fillers, and carrier.

AFM nanoimaging has been applied to characterize casein-based films. The surface morphologies of casein multilayers built step-by-step were examined by AFM (Nagy, Váró, & Szalontai, 2012). The results confirmed that  $\alpha$ -casein, CaP nanostructure,  $\alpha$ -casein, and  $\kappa$ -casein were step-by-step deposited onto polyelectrolyte film. Therefore, AFM is an efficient way to characterize casein-based films and confirmed achievements of layer-by-layer adsorption. Casein films prepared by the size-fractionation method were characterized by AFM (Gebhardt, Vendrely, & Kulozik, 2011). Both the untreated and size-fractionated casein films were inhomogeneous on a microscale. Moreover, the untreated films consisted of casein micelles with a broad spectrum of sizes, whereas the size-fractionated films consisted of casein micelles with similar sizes. These AFM results proved that size fractionation was an efficient pretreatment way to prepare casein films with uniform nanoparticle.

AFM nanoimaging has also been applied to characterize casein micelles (Qi, 2007). Casein micelles were immobilized via carbodiimide to a self-assembled monolayer on gold-coated slides and then AFM was applied to analyze error signal surface topography and elastic properties (Uricanu, Duits, & Mellema, 2004). The results suggested that higher temperatures and lower serum casein concentrations resulted in stiffer micelles. Moreover, pH below 5.0 could induce the formation of particulate gels and multilayers from micelles. Ex situ AFM experiments showed that high pressure could disintegrate native casein micelles with substructure on a 20 nm scale into small fragments and even into monomeric constituents (Gebhardt, Doster, Friedrich, & Kulozik, 2006). In situ liquid AFM experiments showed heterogeneous raspberry-like milk casein micelles

decreased in size and lost their surface heterogeneities under acidic conditions of pH 5 (Ouanazar, Guyomarc'h, & Bouchoux, 2012), which suggested the surface topography was highly sensitive to variations in mineral content and caseins net charge. These works proved AFM is a powerful tool to analyze the surface topography of protein particles such as casein micelles.

AFM nanoimaging and force measurements have been applied to observe the interaction of casein with other substances. The interaction between casein and modified starch in a simulation yogurt system was studied by AFM (Cui, Tan, Lu, Liu, & Li, 2014). The decrease in pH promoted the aggregation of pure casein micelles. The starch granule surface was smooth at any pH. Casein particles appeared on the surface of the starch granule in the AFM images, which suggested that some casein particles adsorbed on the surface of the starch granule in the mixed solutions. In order to understand the effect of chymosin on the casein micelle, AFM nanoimaging was applied to observe the morphologies of milk casein micelles after incubation with chymosin (Freitas et al., 2019). AFM clearly showed the milk casein micelle aggregated and the sizes increased with the increased incubation time (0, 15, 30, 45, and 60 min), which confirmed the casein micelle aggregation was induced by chymosin. The interfacial composition and structure of milk fat globules and their interaction with casein micelles have been explored by AFM nanoimaging and adhesion force measurements (Obeid, Guyomarc'h, Francius, Guillemin, & Lopez, 2019). Homogenized milk fat globules appeared smaller than native milk fat globules. The adhesion forces were measured between the casein micelles-modified probes and the immobilized milk fat globules. The measurements demonstrated that homogenized milk fat globules required more force, more energy, and longer pulling distance to detach casein micelles than native milk fat globules. This work provided useful mechanical information to understand the interaction between casein with fat globules.

AFM nanoimaging has been applied to investigate the effects of processing and preservation conditions on caseins. The effect of ultrasonication treatment on the morphology of casein was observed by AFM (Lin et al., 2014). According to the particle size distribution, ultrasonication time had an obvious effect on the size of casein particles. The morphology of casein micelles during storage was also examined by AFM (Burgain, Scher, Petit, Francius, & Gaiani, 2016). AFM results showed the casein micelle surface became rougher during storage. After storage for

10 months at 40°C, casein micelle showed many hollow zones (around 500 nm) on the surface. These AFM results showed the disrupting process and provided useful information to understand the micelle disrupting mechanism during storage.

### 4.6.2 Whey proteins

Whey protein is isolated from milk and is one of the high-quality proteins given its amino acid content. It is a mixture of globular proteins and mainly contains  $\beta$ -lactoglobulin and  $\alpha$ -lactalbumin. It typically comes in four major forms: whey protein concentrate, whey protein isolate, whey protein hydrolysate, and native whey proteins. They have been widely applied in the food industry as dietary supplements, food additives, and food packaging material.

AFM nanoimaging has been applied to characterize the morphology of whey proteins. Whey protein isolates were observed by AFM (Mohammadian & Madadlou, 2016b). After heating at pH 2, whey protein isolates showed nanofibrils in AFM images. These nanofibrils were stable at pH 2.0–7.5. Further, whey protein hydrolysates and whey protein isolates formed at pH 2.0 followed by heating at 85°C for 5 h were examined by AFM (Mohammadian & Madadlou, 2016a). Both of them formed nanofibrils with similar heights. However, whey protein hydrolysates formed less nanofibrils compared to whey protein isolates. The AFM results demonstrated the two kinds of whey proteins had obvious structural differences, which suggested that they had obvious chemical differences. This work proved that AFM was a direct tool to compare different morphologies of two kinds of food proteins and an indirect tool to distinguish the chemical difference between the two kinds of food proteins.

AFM nanoimaging has been applied to investigate the effects of processing and preservation on whey proteins. In order to understand the effect of fibrillization on the foaming capacity of whey proteins, the effects of protein concentration, thermal treatment, pH, and whipping time on whey protein isolates were observed by AFM height imaging (Oboroceanu, Wang, Magner, & Mae, 2014). The whey protein isolates after heating at 80°C for 20 h and pH 7 showed globular aggregates, while those after heating at 80°C for 20 h and pH 2 showed nanofibrils with a height of 2–3 nm and a length of up to 15  $\mu$ m. The whipping had no obvious effects on globular aggregates, but decreased the height of the nanofibrils to 0.5–1.2 nm. Further, both microfluidization treatment and shear mixing Ultra-Turrax treatment could decrease the length of

nanofibrils. These AFM results provided basic structural information to understand the underlying mechanisms of the foaming capacity of whey proteins. The effect of extrusion moisture content on the shape and distribution of whey protein isolates was observed by AFM (Qi & Onwulata, 2011). The fine differences of the whey protein particles at different moisture contents and temperatures were consistent with the results obtained by other techniques. This work proved that AFM could provide a convenient and direct imaging tool to study the effects of processing conditions on the properties of proteins. In order to explore the structural changes during storage, the aged (60°C for 1 month) and reference (4°C for 1 month) whey protein isolate powders were observed by AFM height imaging and adhesion force imaging (Burgain, Zein, et al., 2016). The reference powder showed smooth microparticles with large dents, whereas the aged powder showed broken dents with cracks. This work proved AFM was an efficient tool to compare and analyze the structural and mechanical changes of food proteins during storage. Recently, AFM nanoimaging was applied to image Langmuir-Blodgett films made from native whey protein isolate, aggregate- and bead-stabilized interfaces (Yang, Thielen, Berton-Carabin, van der Linden, & Sagis, 2020). The native whey protein isolate and aggregate films showed highly heterogeneous structures in which the proteins form dense clustered networks. The beads were randomly distributed throughout the film, separated by large areas, where smaller proteinaceous material was present. These AFM results provided useful structural information to understand the physico-chemical properties of whey protein isolate and potential application mechanisms in emulsion stabilization.

AFM has been applied to investigate the structural and mechanical information of cell growth on whey protein-based biomaterials. In order to develop and prove whey protein microbeads as potential matrices for probiotic protection, probiotic strain *Lactobacillus rhamnosus* GG viability in denatured whey protein isolate as a function of pH was observed by AFM (Doherty et al., 2011), which suggested that micro-bead extrusion at pH 4.6 fueled strong cohesive interactions within protein-probiotic amalgams. Recently, the AFM force spectroscopy function was applied to study the adhesion interactions of *L. rhamnosus* GG to different pure milk proteins: casein micelles,  $\beta$ -lactoglobulin, and  $\alpha$ -lactalbumin (Guerin et al., 2018). Mica was coated by *L. rhamnosus* GG (ATCC 53103) (LGGWT) or three of its surface mutants. AFM probes were functionalized by different pure milk proteins. As shown in Fig. 4.4, the adhesion force spectroscopy between

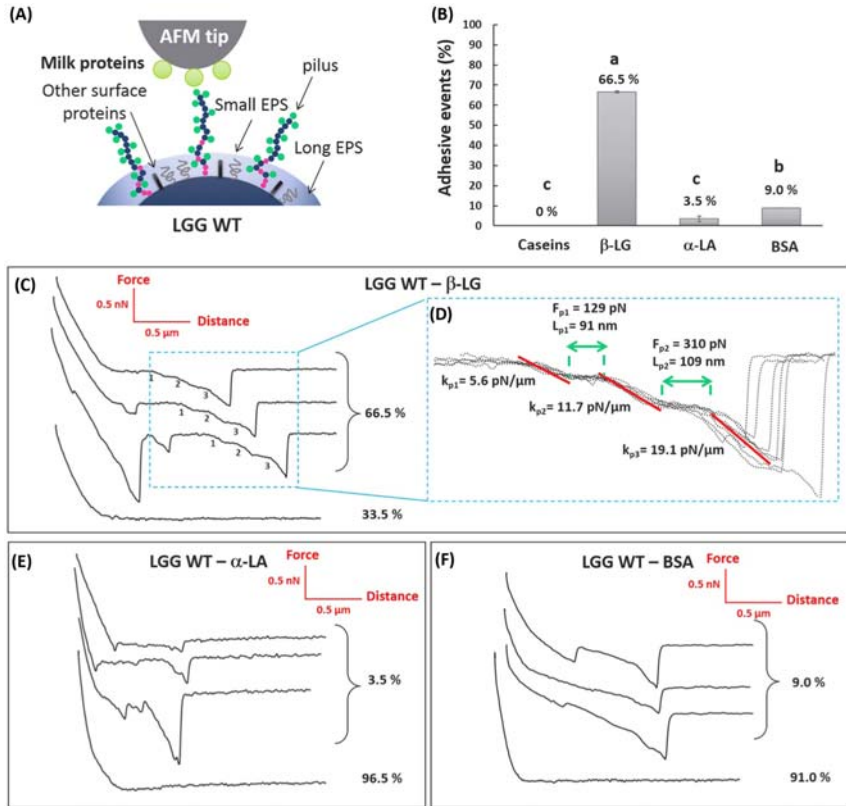


**Figure 4.4** Adhesive interactions between *Lactobacillus rhamnosus* GG (LGG WT) and milk proteins: casein micelles,  $\beta$ -lactoglobulin ( $\beta$ -LG),  $\alpha$ -lactalbumin ( $\alpha$ -LA), and bovine serum albumin (BSA). (A) Schematic of the principle of AFM-based force spectroscopy to measure the interaction between milk protein-coated probes and the surface of LGG WT. (B) Frequency of adhesive events between LGG WT and individual milk proteins. (C, E, F) Representative retraction curves recorded between LGG and  $\beta$ -LG (C),  $\alpha$ -LA (E), or BSA (F), respectively. (D) Superimposition of retraction curves and determination of spring-like properties of pili SpaCBA. Reprinted with permission from Guerin, J., Burgain, J., Francius, G., El-Kirat-Chatel, S., Beaussart, A., Scher, J., & Gaiani, C. (2018). Adhesion of *Lactobacillus rhamnosus* GG surface biomolecules to milk proteins. *Food Hydrocolloids*, 82, 296–303.

*L. rhamnosus* GG and milk proteins demonstrated that the adhesion interactions were dependent on milk protein components. Further force spectroscopy work using different bacteria-coated mica demonstrated the adhesion interactions were also dependent on the surface biomolecules composition of *L. rhamnosus* GG. These results provided useful information to understand the location of bacteria in the dairy matrix.

## 4.7 Meat proteins

The meat proteins are derived from meats, which is defined as “the edible postmortem component originating from live animals.” Meat proteins can be classified into three types: myofibrils (also named muscle fibrils), sarcoplasmic proteins, and connective tissue proteins (Tornberg, 2005). Myofibrils are the main components of meat proteins and are composed of long proteins including actin, myosin, titin, and other proteins that hold them together. Connective tissue proteins mainly include collagen and elastin. AFM has been widely used to analyze the morphology and mechanical properties of myofibrils for understanding the structure and tenderness/toughness of meat (Soltanizadeh & Kadivar, 2014).

AFM nanoimaging has been applied to study the structures of meat proteins. The myosin spacing in relaxed sarcomeres was studied by AFM (Li, Lang, & Linke, 2016). The 3D height image of rabbit psoas half-sarcomere showed irregularly spaced peaks. These peaks were myosin filaments. In addition, AFM image showed clear sarcomeric Z-disk, I-bands, A-bands, and the filamentous structures along the A-bands. The measured interfilament (peak-to-peak) distances agreed well with the expected values according to previous works. Further, an algorithm was developed to detect the elevated longitudinal structures in each line scan and to calculate all nearest peak-to-peak (=interfilament) distances. It quantitatively gave the interfilament distances. The AFM results and quantitative analyses demonstrated the normal interfilament lattice spacing was maintained in single isolated myofibrils. It provided useful information to understand the relationship between the structure and function of myofibrils.

AFM nanoimaging has been applied to observe the interaction between meat proteins and other substances. The interaction between drebrin A and F-actin was studied by AFM at subnanometer resolution (Sharma, Grintsevich, Phillips, Reisler, & Gimzewski, 2011). AFM images clearly showed the bound of drebrin with F-actin. Subsequently, the self-assembly of inverted formin-2 (regulatory protein) and its complexes with F-actin was studied by the same group using AFM (Sharma et al., 2014). The inverted formin-2 is organized into ring-like structures around single actin filaments. These AFM works provided important structural information on meat protein interactions.

AFM nanoimaging has been applied to investigate the effects of processing conditions on meat proteins. The effects of ultrasonication, CaCl<sub>2</sub>, and sodium tripolyphosphate on the ultrastructure of the milk goat

longissimus muscle fiber were studied by AFM (Gao et al., 2016). AFM results showed the sarcomere length was dependent on these processing conditions. Among these processing conditions, ultrasonication was the preferred tenderization method. This work proved AFM was useful to analyze the effect of processing methods on food proteins at the nano-scale. The effects of various high-pressure homogenization pressures on chicken breast myofibrillar protein aqueous suspensions were studied by AFM (Chen, Xu, & Zhou, 2016). Highly ordered structured myofibrils were completely disrupted and changed to some filaments, oligomers, and myosin monomers with submicron/nm range after high-pressure treatment. Moreover, the higher the pressure was, the more nanoparticles were produced. Based on these AFM results, this work proposed a mechanism to explain solubilization of myofibrils in water after high-pressure homogenization. In order to illustrate the influence of extreme alkaline pH on pale, soft, and exudative-like chicken proteins, AFM was used to observe the microstructure of the control and pH 11.0, 11.5, and 12.0-treated chicken proteins (Zhao, Xing, Xu, & Zhou, 2020). As shown in Fig. 4.5, the control sample showed a loose structure and the alkaline

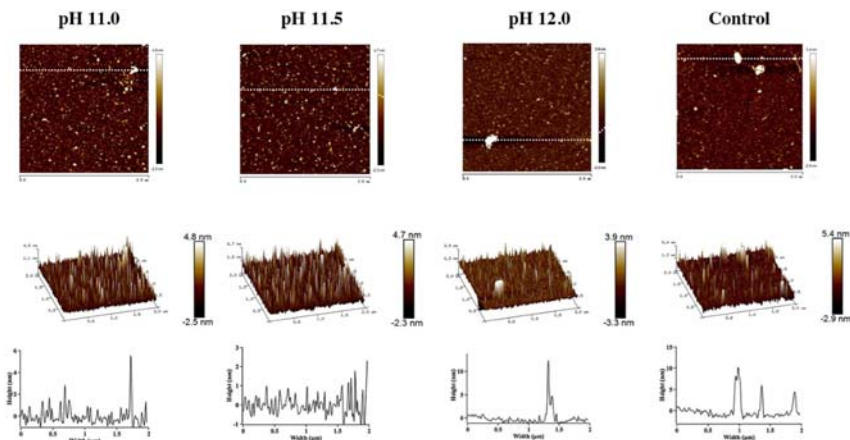


**Figure 4.5** Atomic force microscopy 2D and 3D images of the pale, soft, and exudative-like meat protein at extreme alkaline pH (11.0, 11.5, and 12.0) conditions. The protein solubilized in 0.6 M PBS is treated as the control. The scale displayed the above ranges from 0 to 200 nm. The sectional images at the bottom correspond to the straight line on the 2D images at the top. *Reprinted with permission from Zhao, X., Xing, T., Xu, X., & Zhou, G. (2020). Influence of extreme alkaline pH induced unfolding and aggregation on PSE-like chicken protein edible film formation. Food Chemistry, 319, 126574.*



pH-treated samples mainly showed scattered uniform spherical nanoparticles (height less than 6 nm). Among the pH-treated samples, the pH 11.5 group showed the greatest uniformity. The pH 12.0 group showed protein aggregates with a height of >10 nm. No myofibril structures were found in the AFM images, which suggested that alkaline pH treatment disrupted the ordered structure of myofibrils. Combined with the results from other technologies, this work elucidated the effects of chicken meat protein unfolding and aggregation on edible film properties under extreme alkaline pH treatments. These works proved AFM could provide structural information on food protein to elucidate its functional properties.

## 4.8 Seafood proteins

Seafoods are important sources of high-quality proteins. Seafood proteins contain sufficient amounts of essential amino acids required for human health. Moreover, seafood proteins are highly digestible and absorbable in the human gastrointestinal tract. Therefore, seafoods are important protein source for human beings. In addition, seafoods have been used to prepare many protein-based seafood products such as surimi seafoods (Park & Reed, 2014). Similar to meat proteins, seafood proteins are also classified into three types: myofibrils, sarcoplasmic proteins, and connective tissue proteins.

AFM nanoimaging has been applied to study the effects of processing and preservation conditions on seafood food proteins. In order to study the effect of boiling and gelatin addition on the nanostructures of myofibrils in golden pomfret fish balls, AFM was applied to observe myofibrils extracted from fish balls (Feng, Fu, & Yang, 2017). As shown in Fig. 4.6, the AFM results demonstrated that boiling significantly decreased the width of rod-like myofibrils, which suggested the degradation and aggregation of myofibrils due to the thermal process and heat-activated proteases. In addition, gelatin addition had no obvious effect on the nanostructures of myofibrils. The same group used AFM to study the combined effect of fish gelatin with chitosan coating on myofibrils in golden pomfret fillet during cold storage (Feng, Bansal, & Yang, 2016). AFM results showed the chitosan coating could preserve the length of myofibrils during cold storage, which suggested that the chitosan coating could inhibit myofibril degradation. Using AFM, the same group also confirmed fish gelatin and tea polyphenol coating could maintain the nanostructure of myofibrils in

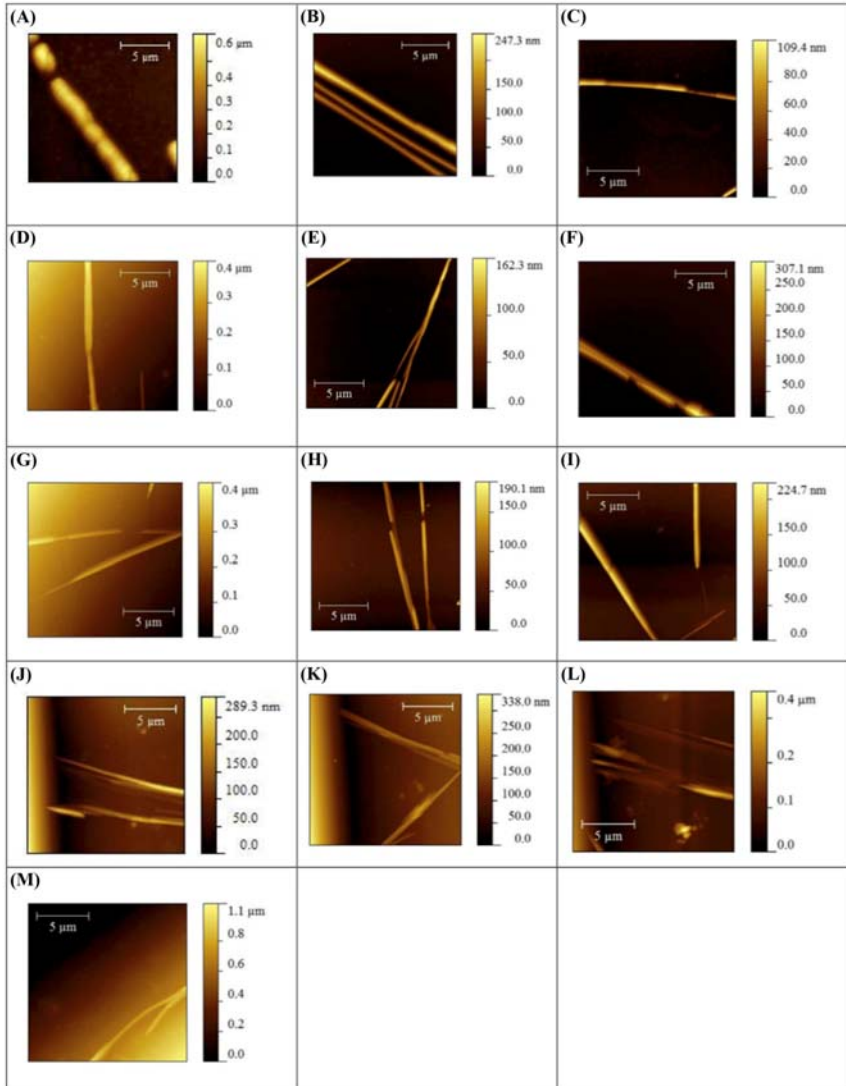


**Figure 4.6** Atomic force microscopy height images of myofibrils extracted from fish balls. (A) Sample before boiling. (B–E) Samples boiled for 10 min with 0, 0.75, 1.5, and 3 g of gelatin in 100 g of fish. (F–I) Samples boiled for 20 min with 0, 0.75, 1.5, and 3 g of gelatin in 100 g of fish. (J–M) Samples boiled for 30 min with 0, 0.75, 1.5, and 3 g of gelatin in 100 g of fish. *Reprinted with permission from Feng, X., Fu, C., & Yang, H. (2017). Gelatin addition improves the nutrient retention, texture and mass transfer of fish balls without altering their nanostructure during boiling. LWT – Food Science and Technology, 77, 142–151.*

fish fillets during cold storage (Feng, Ng, Mikš-Krajnik, & Yang, 2017). Vacuum impregnation of fish gelatin combined with grape seed extract on myofibrillar protein in chilled *Tilapia* fillets was studied by AFM (Zhao et al., 2019). AFM further showed that the fish gelatin-grape seed extract coating could significantly prevent the degradation of myofibrillar proteins during refrigeration by quantitatively analyzing the length, width, and height of the myofibrillar proteins. These AFM works demonstrated AFM nanoimaging can be applied to observe the nanostructures of myofibrils in seafood products.

## 4.9 Collagen and gelatin

Collagen is the most prominent insoluble fibrous protein in the connective tissues of mammalian and aquatic animals. It plays pivotal role in the distinctive physiological functions of tissues in bones, skin, tendons, and cartilage (Yousefi, Ariffin, & Huda, 2017). Gelatins are derived from the controlled hydrolysis of native collagens. Due to their excellent properties, collagen and gelatin have been widely used and explored in food, pharmaceuticals, leather, cosmetics, tissue engineering, etc. In order to understand their functional properties, AFM has been widely applied to analyze the nanostructures of collagen and gelatin. In addition, mammalian and aquatic collagens have similar chemical composition and structures. Therefore, AFM application for collagen and gelatin is discussed in this section rather than Sections 4.7 and 4.8.

### 4.9.1 Collagen

AFM nanoimaging has been applied to study the nanostructures of collagen. In order to explore the surface topography of collagen thin films, the nanostructures of collagen nanofibers on different substrates (glass, mica, and polystyrene latex particle surfaces) by different preparation methods (spin coating and hydrodynamic flow) were examined by AFM (Stylianou & Yova, 2013). Collagen nanofibers with kinks were observed. AFM results demonstrated that collagen film consisting of natural fibrils could be achieved by adjusting the working parameters. These results demonstrated that the AFM nanoimaging method was an efficient observation tool to analyze the nanostructures of food proteins after different processing methods. Acid-soluble collagen and pepsin soluble collagen from the scales of northern pike were characterized by AFM (Kozłowska, Sionkowska, Skopinska-Wisniewska, & Piechowicz, 2015). AFM results

showed acid-soluble collagen was composed of banded nanofibrils and pepsin soluble collagen was not composed of nanofibrils. Subsequently, high-speed AFM was applied to observe the fibril formation processes of *Tilapia* and porcine collagen (Matsumoto et al., 2015). The results showed that *Tilapia* collagen had faster and denser collagen nanofiber formation than porcine collagen, which suggested *Tilapia* collagen might be better for osteoblastic differentiation of human mesenchymal stem cells. Therefore, AFM nanoimaging is a useful tool to decide if the food protein layers are suitable for cell culture.

AFM has been applied to study the effect of preservation on the nanostructures of collagen. The polymorphism and stability of nanostructures of bovine flexor tendon, rat tail, and *Tilapia* skin of three types of collagen were studied by AFM (Shi, Bi, et al., 2019). AFM results showed three types of collagens had a variety of nanostructures: nanofibers, nanofilaments, protofibrils, protofilaments, and nanoparticles. Moreover, as shown in Fig. 4.7, these collagen nanostructures were changed during the storage process at room temperature. Therefore, AFM nanoimaging was a useful tool to observe the structural polymorphism of food proteins and their structural changes during the storage process.

AFM has been applied to explore the interactions of collagen with other substances. AFM nanoimaging was applied to observe collagen nanostructures in the presence of protocathechualdehyde (Wan et al., 2019). The results demonstrated protocathechualdehyde significantly suppressed collagen fibrillogenesis, which suggested protocathechualdehyde inhibited intramolecular cross-links in collagen. By exploring the dewetting patterns of collagen layers from AFM images, another work demonstrated that collagen nanofiber formation was strongly impacted by the presence of TiO<sub>2</sub> nanoparticles (Beauvais et al., 2019). AFM force spectroscopy was applied to study collagen–collagen interactions mediated by plant-derived proanthocyanidins (Vidal et al., 2016). The force histograms between collagen-coated AFM tip and collagen-coated substrate in the presence of proanthocyanidins showed an increased number of interactions in the force range of 500–1000 pN, which suggested the cross-linking between collagen fibrils due to the presence of proanthocyanidins. Therefore, AFM force spectroscopy was an efficient way to study molecular interactions of food proteins. Piezoresponse force microscopy has been applied to study the piezoelectricity of collagen and the effects of chemical cross-linking on it (Beauvais et al., 2019). Among three chemically distinct treatments used to form structurally and mechanically stable scaffolds

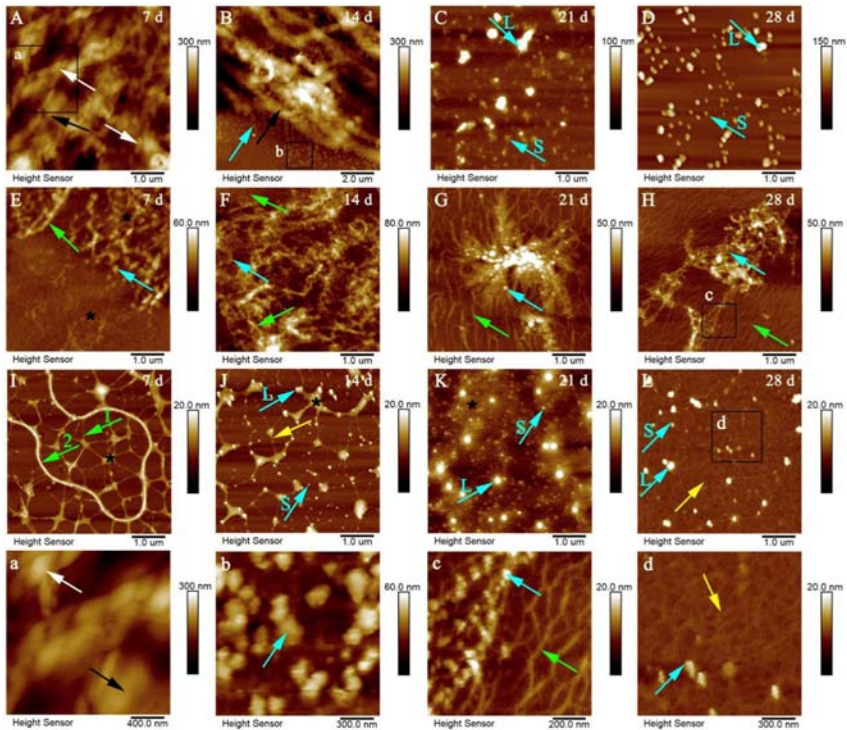


**Figure 4.7** Atomic force microscopy height images of three types of collagens (A–D: bovine flexor tendon collagen; E–H: rat tail collagen; I–L: *Tilapia* skin collagen) after different incubation times (upper right corner of each image) at a concentration of 0.4 mg/mL. (a–d) Zoomed-in height images from the corresponding regions shown in (A, B, H, and L). White, black, green, yellow, and cyan arrows indicate left-handed helix periodic collagen nanofibers, nonperiodic collagen nanofibers, collagen protofibrils, collagen protofilaments, and collagen nanoparticles (“L” means large nanoparticles and “S” means small nanoparticles), respectively. Black asterisks indicate disordered collagen aggregates. Z scales are shown at the right of the height images. Reprinted with permission from Shi, C., Bi, C., Ding, M., Xie, J., Xu, C., Qiao, R., . . . Zhong, J. (2019). Polymorphism and stability of nanostructures of three types of collagens from bovine flexor tendon, rat tail, and tilapia skin. *Food Hydrocolloids*, 93, 253–260.

(EDC-NHS, genipin, and tissue transglutaminase), only cross-linking with EDC-NHS produced distinct self-assembly of collagen fibers into bundles roughly 300 nm in width regardless of the collagen origin. According to the AFM results, the cross-linking mechanisms on the molecular structure of collagen were proposed. It demonstrated AFM could be applied to analyze the electromechanical properties of collagen using chemical cross-linking methods.

### 4.9.2 Gelatin

AFM nanoimaging has been applied to study the nanostructures of gelatin. To explore the emulsion stabilization ability of gelatin nanoparticles, the gelatin and custom-made gelatin nanoparticles were characterized by our group using AFM (Ding et al., 2020). AFM height images showed gelatin-formed film-like structures and confirmed the successful preparation of gelatin nanoparticles prepared by a two-step desolvation method. Subsequent emulsion stabilization studies demonstrated that these gelatin molecular structures affected the behaviors of fish oil-loaded traditional and Pickering emulsions. Commercial cold-water fish skin gelatin and bovine bone gelatin were characterized by AFM (Zhang, Sun, Ding, Li, et al., 2020). According to AFM results, both the gelatins were mainly dispersed film-like nanostructures with different heights: fish skin gelatin (1.0–2.0 nm) < bovine bone gelatin (2.8–3.2 nm). Therefore, the thickness of the gelatin interfacial layer of the droplets in gelatin-stabilized emulsions could be assumed to be: fish skin gelatin < bovine bone gelatin. According to emulsion theory, the creaming velocity of gelatin-stabilized emulsions could be proposed: fish skin gelatin < bovine bone gelatin. Further emulsion stabilization experiments also confirmed this proposal. Later, our group also used AFM to characterize *Tilapia* skin gelatin extracted by three different methods: acetic acid, hot water, and pepsin enzyme methods (Zhang, Sun, Ding, Tao, et al., 2020), which also explained the emulsion stabilization differences of these gelatins. These results demonstrated that AFM was an efficient way to characterize the nanostructures of food proteins, which would be useful for understanding their food application.

AFM nanoimaging has been applied to study the interaction of gelatin with other substances. The nanostructures of *Tilapia* fish gelatin affected by gellan and calcium chloride addition were analyzed by AFM (Sow et al., 2017). AFM results showed gellan and calcium chloride had obvious effects on the nanostructures in gelatin gels, which explained the textural modification induced by these chemicals. The interaction of fish gelatin with sodium alginate was also studied by AFM (Sow, Toh, Wong, & Yang, 2019). The fish gelatin-sodium alginate complex coacervates, sodium alginate fibrous network, and fish gelatin-sodium alginate complex network were confirmed by AFM. It provided solid structural evidence to propose the schematic model of the interactions between fish gelatin and sodium alginate depending on the relative concentrations.

AFM nanoimaging has been applied to characterize gelatin-based films. Fish gelatin/chitosan nanoparticles and essential oil-blended fish gelatin/chitosan nanoparticles composite films were characterized by AFM (Hosseini, Rezaei, Zandi, & Farahmandghavi, 2015; Hosseini, Rezaei, Zandi, & Farahmandghavi, 2016). AFM results provided nanostructural information of these films for understanding their physicochemical properties. Gelatin/zein composite films fabricated by the solvent casting method were characterized by AFM (Ahmed, Liu, Khin, Yokoyama, & Zhong, 2020). Gelatin/zein films showed a smooth surface, which suggested a strong interaction between gelatin and zein molecules. These works demonstrated AFM was useful to characterize food protein-based films to understand their physicochemical properties.

#### 4.10 Egg proteins

An egg is produced from poultry and is a high-quality protein resource. It is mainly used as both a main dish and an ingredient for processed foods such as baked foods. Egg proteins can be classified into egg white proteins and egg yolk proteins (Strixner & Kulozik, 2011). Egg white protein is attracting considerable attention due to its excellent nutritional and functional properties. Egg yolk protein is also an important food resource due to its important nutritional values.

AFM has been applied to study the effect of processing conditions on egg proteins. Heat-induced aggregation of a globular egg white protein ovalbumin was studied by AFM height imaging, electrical double layer mode imaging, and surface force mapping (Najbar, And, & Drummond, 2003). At a relatively low concentration (0.5  $\mu\text{g}/\text{mL}$ ), heat treatment caused the aggregation of globular structures to form large globular structures. At a relatively high concentration (20  $\mu\text{g}/\text{mL}$ ), heat treatment caused the protein film formation and electrical double layer imaging revealed that the heat-induced globular structures were more heterogeneous than the native protein. Surface force mapping showed heat induced the reduction of the internal cohesiveness of the protein molecular structures. AFM was applied to characterize the egg white protein particles prepared by heating at 90°C for 45 min and then homogenization under low pressure (Chang et al., 2016). At pH 3.8, egg white protein mainly formed granular particles and at pH 3.0, egg white protein mainly formed from fibrous structure to granular structure with the increase of protein concentration or salt addition. The granular particles showed

higher surface loading of protein and viscoelastic moduli in the integrated Pickering emulsions. Therefore, this structural information from AFM nanoimaging provided useful information to understand the functional properties of food proteins.

AFM has been applied to characterize the interaction of egg protein with other substances. Recently, AFM nanoimaging was used to characterize two heat-induced (85°C, 5 min, formed at pH 11.35 or 7.50) ovalbumin nanoparticles and ovalbumin nanoparticle–polyunsaturated fatty acid inclusion nanocomplexes (Visentini, Perez, & Santiago, 2019). AFM results showed the nanoparticles and nanocomplexes showed a rounded shape and an increase in dimensions of the nanocomplexes. The size increase was attributed to linoleic acid and conjugated linoleic acid binding. In order to study the effect of yolk granule (interface adsorbing protein particles) with lecithin on their emulsifying properties, the interaction of yolk granule with lecithin was analyzed by AFM nanoimaging (Shen et al., 2020). As shown in Fig. 4.8, AFM results showed the aggregated

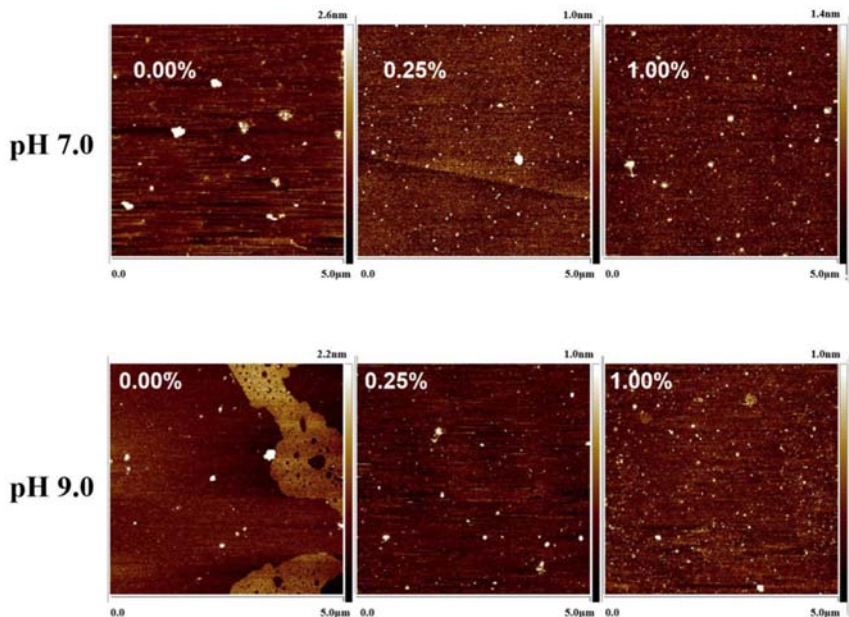


**Figure 4.8** Atomic force microscopy height images of the gee yolk granule (pH 7.0 and pH 9.0) with different concentrations of lecithin (0.00%, 0.25%, and 1.00%). Reprinted with permission from Shen, Y., Chang, C., Shi, M., Su, Y., Gu, L., Li, J., & Yang, Y. (2020). *Interactions between lecithin and yolk granule and their influence on the emulsifying properties*. Food Hydrocolloids, 101, 105510.



structure of the egg yolk granule could be destroyed by the increase of solution pH and the addition of lecithin. The disrupted granule exhibited better emulsion stability than that of the native granule. Therefore, the structural information from AFM results provided a possible explanation for the better emulsion stability due to the lower particle size.

#### 4.11 Summary and outlook

This chapter summarized and discussed the application of AFM technology in food proteins from different sources. First, food protein extraction and sample preparation of food proteins for AFM examination were introduced. Then, the application of AFM for food proteins was mainly introduced according to different protein sources: grain, bean, peanut, milk, meat, sea-food, and egg. Considering collagens/gelatins have been widely studied by AFM and both mammalian and aquatic collagens have similar chemical composition and structures, this chapter also discussed the application of AFM in collagen and gelatin research in a section. All these discussions demonstrated that AFM was a powerful and versatile nanotechnology tool for food protein research and could significantly promote food protein-related research. Though AFM has not been applied in some food proteins such as blood proteins, Algal proteins, and mycoproteins, AFM has a wide application prospective in food protein research. More and more food protein scientists will use the AFM technique for their food protein research in the future.

#### Acknowledgment

This research has been supported by research grant from the National Key R. & D Program of China (No. 2019YFD0902003).

#### Conflict of interest

The authors declare no conflict of interest.

#### References

- Ahamed, S., Liu, F., Khin, M. N., Yokoyama, W. H., & Zhong, F. (2020). Improvement of the water resistance and ductility of gelatin film by zein. *Food Hydrocolloids*, 105, 105804.
- Alexander Reese, R., & Xu, B. (2019). Single-molecule detection of proteins and toxins in food using atomic force microscopy. *Trends in Food Science & Technology*, 87, 26–34.

- Amagliani, L., O'Regan, J., Kelly, A. L., & O'Mahony, J. A. (2017). The composition, extraction, functionality and applications of rice proteins: A review. *Trends in Food Science & Technology*, *64*, 1–12.
- Ando, T. (2019). High-speed atomic force microscopy. *Current Opinion in Chemical Biology*, *51*, 105–112.
- Ansharullah, Hourigan, J. A., & Chesterman, C. F. (1997). Application of carbohydrases in extracting protein from rice bran. *Journal of the Science of Food and Agriculture*, *74*, 141–146.
- Bahri, A., Martin, M., Gergely, C., Marchesseau, S., & Chevalier-Lucia, D. (2018). Topographical and nanomechanical characterization of casein nanogel particles using atomic force microscopy. *Food Hydrocolloids*, *83*, 53–60.
- Beauvais, M., Degabriel, T., Aissaoui, N., Dupres, V., Colaço, E., El Kirat, K., ... Landoulsi, J. (2019). Supramolecular self-assembly and organization of collagen at solid/liquid interface: Effect of spheroid- and rod-shaped TiO<sub>2</sub> nanocrystals. *Advanced Materials Interfaces*, *6*, 1900195.
- Bi, C., Li, X., Xin, Q., Han, W., Shi, C., Guo, R., ... Zhong, J. (2019). Effect of extraction methods on the preparation of electrospun/electrosprayed microstructures of tilapia skin collagen. *Journal of Bioscience and Bioengineering*, *128*, 234–240.
- Burgain, J., Scher, J., Petit, J., Francius, G., & Gaiani, C. (2016). Links between particle surface hardening and rehydration impairment during micellar casein powder storage. *Food Hydrocolloids*, *61*, 277–285.
- Burgain, J., Zein, R. E., Scher, J., Petit, J., Norwood, E. A., Francius, G., & Gaiani, C. (2016). Local modifications of whey protein isolate powder surface during high temperature storage. *Journal of Food Engineering*, *178*, 39–46.
- Cárdenas-Pérez, S., Chanona-Pérez, J. J., Méndez-Méndez, J. V., Arzate-Vázquez, I., Hernández-Varela, J. D., & Vera, N. G. (2019). Recent advances in atomic force microscopy for assessing the nanomechanical properties of food materials. *Trends in Food Science & Technology*, *87*, 59–72.
- Chang, C., Niu, F., Gu, L., Li, X., Yang, H., Zhou, B., ... Yang, Y. (2016). Formation of fibrous or granular egg white protein microparticles and properties of the integrated emulsions. *Food Hydrocolloids*, *61*, 477–486.
- Chen, S., Zhang, N., & Tang, C. H. (2016). Influence of nanocomplexation with curcumin on emulsifying properties and emulsion oxidative stability of soy protein isolate at pH 3.0 and 7.0. *Food Hydrocolloids*, *61*, 102–112.
- Chen, X., Xu, X., & Zhou, G. (2016). Potential of high pressure homogenization to solubilize chicken breast myofibrillar proteins in water. *Innovative Food Science & Emerging Technologies*, *33*, 170–179.
- Chichti, E., George, M., Delenne, J. Y., Radjai, F., & Lullien-Pellerin, V. (2013). Nanomechanical properties of starch and gluten biopolymers from atomic force microscopy. *European Polymer Journal*, *49*, 3788–3795.
- Cui, B., Tan, C., Lu, Y., Liu, X., & Li, G. (2014). The interaction between casein and hydroxypropyl distarch phosphate (HPDSP) in yoghurt system. *Food Hydrocolloids*, *37*, 111–115.
- Czajkowsky, D. M., Li, L., Sun, J., Hu, J., & Shao, Z. (2011). Heteroepitaxial streptavidin nanocrystals reveal critical role of proton “fingers” and subsurface atoms in determining adsorbed protein orientation. *ACS Nano*, *6*, 190–198.
- De Mesa-Stonestreet, N. J., Alavi, S., & Bean, S. R. (2010). Sorghum proteins: The concentration, isolation, modification, and food applications of kafirins. *Journal of Food Science*, *75*, R90–R104.
- Deleu, L. J., Wilderjans, E., Van Haesendonck, I., Brijs, K., & Delcour, J. A. (2016). Protein network formation during pound cake making: The role of egg white proteins and wheat flour gliadins. *Food Hydrocolloids*, *61*, 409–414.

- Ding, M., Shi, C., & Zhong, J. (2019). 28 - Atomic force microscopy for food quality evaluation. In J. Zhong, & X. Wang (Eds.), *Evaluation technologies for food quality* (pp. 715–741). Woodhead Publishing.
- Ding, M., Zhang, T., Zhang, H., Tao, N., Wang, X., & Zhong, J. (2020). Gelatin molecular structures affect behaviors of fish oil-loaded traditional and Pickering emulsions. *Food Chemistry*, *309*, 125642.
- Doherty, S. B., Gee, V. L., Ross, R. P., Stanton, C., Fitzgerald, G. F., & Brodtkorb, A. (2011). Development and characterisation of whey protein micro-beads as potential matrices for probiotic protection. *Food Hydrocolloids*, *25*, 1604–1617.
- Fan, Y., Zeng, X., Yi, J., & Zhang, Y. (2020). Fabrication of pea protein nanoparticles with calcium-induced cross-linking for the stabilization and delivery of antioxidative resveratrol. *International Journal of Biological Macromolecules*, *152*, 189–198.
- Feng, X., Bansal, N., & Yang, H. (2016). Fish gelatin combined with chitosan coating inhibits myofibril degradation of golden pomfret (*Trachinotus blochii*) fillet during cold storage. *Food Chemistry*, *200*, 283–292.
- Feng, X., Fu, C., & Yang, H. (2017). Gelatin addition improves the nutrient retention, texture and mass transfer of fish balls without altering their nanostructure during boiling. *LWT - Food Science and Technology*, *77*, 142–151.
- Feng, X., Ng, V. K., Mikš-Krajnc, M., & Yang, H. (2017). Effects of fish gelatin and tea polyphenol coating on the spoilage and degradation of myofibril in fish fillet during cold storage. *Food and Bioprocess Technology*, *10*, 89–102.
- Freitas, C. D. T., Silva, M. Z. R., Oliveira, J. P. B., Silva, A. F. B., Ramos, M. V., & de Sousa, J. S. (2019). Study of milk coagulation induced by chymosin using atomic force microscopy. *Food Bioscience*, *29*, 81–85.
- Fukushima, D. (2011). Soy proteins. In G. O. Phillips, & P. A. Williams (Eds.), *Handbook of food proteins* (pp. 210–232). Woodhead Publishing.
- Gao, J., Wang, Y., Liu, L., Li, K., Zhang, S., & Zhu, J. (2016). Effects of ultrasound, CaCl<sub>2</sub> and STPP on the ultrastructure of the milk goat longissimus muscle fiber observed with atomic force microscopy. *Scanning*, *38*, 545–553.
- Gebhardt, R., Doster, W., Friedrich, J., & Kulozik, U. (2006). Size distribution of pressure-decomposed casein micelles studied by dynamic light scattering and AFM. *European Biophysics Journal*, *35*, 503–509.
- Gebhardt, R., Vendrely, C., & Kulozik, U. (2011). Structural characterization of casein micelles: Shape changes during film formation. *Journal of Physics Condensed Matter*, *23*, 444201.
- Guerin, J., Burgain, J., Francius, G., El-Kirat-Chatel, S., Beaussart, A., Scher, J., & Gaiani, C. (2018). Adhesion of *Lactobacillus rhamnosus* GG surface biomolecules to milk proteins. *Food Hydrocolloids*, *82*, 296–303.
- Gunning, A. P., & Morris, V. J. (2017). Getting the feel of food structure with atomic force microscopy. *Food Hydrocolloids*. Available from <https://doi.org/10.1016/j.foodhyd.2017.050.017>.
- Haward, S. J., Shewry, P. R., Miles, M. J., & McMaster, T. J. (2010). Direct real-time imaging of protein adsorption onto hydrophilic and hydrophobic surfaces. *Biopolymers*, *93*, 74–84.
- He, J., Wang, R., Feng, W., Chen, Z., & Wang, T. (2020). Design of novel edible hydrocolloids by structural interplays between wheat gluten proteins and soy protein isolates. *Food Hydrocolloids*, *100*, 105395.
- Hinderink, E. B. A., Kaade, W., Sagis, L., Schroën, K., & Berton-Carabin, C. C. (2020). Microfluidic investigation of the coalescence susceptibility of pea protein-stabilised emulsions: Effect of protein oxidation level. *Food Hydrocolloids*, *102*, 105610.
- Hosseini, S. F., Rezaei, M., Zandi, M., & Farahmandghavi, F. (2015). Fabrication of bio-nanocomposite films based on fish gelatin reinforced with chitosan nanoparticles. *Food Hydrocolloids*, *44*, 172–182.

- Hosseini, S. F., Rezaei, M., Zandi, M., & Farahmandghavi, F. (2016). Development of bioactive fish gelatin/chitosan nanoparticles composite films with antimicrobial properties. *Food Chemistry*, *194*, 1266–1274.
- Huang, T., Tu, Z.-c., Shangguan, X., Sha, X., Wang, H., Zhang, L., & Bansal, N. (2019). Fish gelatin modifications: A comprehensive review. *Trends in Food Science & Technology*, *86*, 260–269.
- Hunt, I. (2005). From gene to protein: A review of new and enabling technologies for multi-parallel protein expression. *Protein Expression and Purification*, *40*, 1–22.
- Ikai, A., Afrin, R., Saito, M., & Watanabe-Nakayama, T. (2018). Atomic force microscope as a nano- and micrometer scale biological manipulator: A short review. *Seminars in Cell & Developmental Biology*, *73*, 132–144.
- Jensen, A., Lim, L. T., Barbut, S., & Marcone, M. (2015). Development and characterization of soy protein films incorporated with cellulose fibers using a hot surface casting technique. *LWT - Food Science and Technology*, *60*, 162–170.
- Jones, O. G. (2016). Developments in dynamic atomic force microscopy techniques to characterize viscoelastic behaviors of food materials at the nanometer-scale. *Current Opinion in Food Science*, *9*, 77–83.
- Juhász, A., Békés, F., & Wrigley, C. W. (2014). Wheat proteins. In Z. Ustunol (Ed.), *Applied food protein chemistry* (pp. 219–303). West Sussex, UK: John Wiley & Sons, Ltd.
- Karnjanapratum, S., & Benjakul, S. (2020). Asian bullfrog (*Rana tigerina*) skin gelatin extracted by ultrasound-assisted process: Characteristics and in-vitro cytotoxicity. *International Journal of Biological Macromolecules*, *148*, 391–400.
- Kozłowska, J., Sionkowska, A., Skopinska-Wisniewska, J., & Piechowicz, K. (2015). Northern pike (*Esox lucius*) collagen: Extraction, characterization and potential application. *International Journal of Biological Macromolecules*, *81*, 220–227.
- Kuda, T., Shibata, G., Takahashi, H., & Kimura, B. (2015). Effect of quantity of food residues on resistance to desiccation of food-related pathogens adhered to a stainless steel surface. *Food Microbiology*, *46*, 234–238.
- Lei, H., Guo, Y., Hu, X., Hu, C., Hu, X., & Li, H. (2017). Reversible unfolding and folding of the metalloprotein ferredoxin revealed by single-molecule atomic force microscopy. *Journal of the American Chemical Society*, *139*, 1538–1544.
- Li, Y., Lang, P., & Linke, W. A. (2016). Titin stiffness modifies the force-generating region of muscle sarcomeres. *Scientific Reports*, *6*, 24492.
- Liang, H. N., & Tang, C. H. (2014). Pea protein exhibits a novel Pickering stabilization for oil-in-water emulsions at pH 3.0. *Lebensmittel-Wissenschaft und-Technologie*, *58*, 463–469.
- Liao, L., Wang, Q., & Zhao, M. M. (2013). Functional, conformational and topographical changes of succinic acid deamidated wheat gluten upon freeze- and spray-drying: A comparative study. *LWT - Food Science and Technology*, *50*, 177–184.
- Lin, L., Cui, H., He, R., Lei, L., Zhou, C., Mamdough, W., & Ma, H. (2014). Effect of ultrasonic treatment on the morphology of casein particles. *Ultrasonics Sonochemistry*, *21*, 513.
- Liu, Q., & Yang, H. (2019). Application of atomic force microscopy in food microorganisms. *Trends in Food Science & Technology*, *87*, 73–83.
- Liu, Q. R., Qi, J. R., Yin, S. W., Wang, J. M., Guo, J., Feng, J. L., ... Yang, X. Q. (2016). The influence of heat treatment on acid-tolerant emulsions prepared from acid soluble soy protein and soy soluble polysaccharide complexes. *Food Research International*, *89*, 211–218.
- Liu, T., Dai, H., Ma, L., Yu, Y., Tang, M., Li, Y., ... Zhang, Y. (2019). Structure of Hyla rabbit skin gelatin as affected by microwave-assisted extraction. *International Journal of Food Properties*, *22*, 1594–1607.

- Ma, M., Zhong, J., Li, W., Zhou, J., Yan, Z., Ding, J., & He, D. (2013). Comparison of four synthetic model peptides to understand the role of modular motifs in the self-assembly of silk fibroin. *Soft Matter*, *9*, 11325–11333.
- Manibog, K., Yen, C. F., & Sivasankar, S. (2017). Chapter twelve - measuring force-induced dissociation kinetics of protein complexes using single-molecule atomic force microscopy. In Maria Spies, & Yann R. Chemla (Eds.), *Methods in enzymology* (Vol. 582, pp. 297–320). Academic Press.
- Marinello, F., La Stora, A., Mauriello, G., & Passeri, D. (2019). Atomic force microscopy techniques to investigate activated food packaging materials. *Trends in Food Science & Technology*, *87*, 84–93.
- Martines, E., Zhong, J., Muzard, J., Lee, A. C., Akhremitchev, B. B., Suter, D. M., & Lee, G. U. (2012). Single-molecule force spectroscopy of the *Aplysia* cell adhesion molecule reveals two homophilic bonds. *Biophysical Journal*, *103*, 649–657.
- Matsumoto, R., Uemura, T., Xu, Z., Yamaguchi, I., Ikoma, T., & Tanaka, J. (2015). Rapid oriented fibril formation of fish scale collagen facilitates early osteoblastic differentiation of human mesenchymal stem cells. *Journal of Biomedical Materials Research. Part A*, *103*, 2531–2539.
- Mirzapour-Kouhdasht, A., Sabzipour, F., Taghizadeh, M. S., & Moosavi-Nasab, M. (2019). Physicochemical, rheological, and molecular characterization of colloidal gelatin produced from Common carp by-products using microwave and ultrasound-assisted extraction. *Journal of Texture Studies*, *50*, 416–425.
- Mohammadian, M., & Madadlou, A. (2016a). Characterization of fibrillated antioxidant whey protein hydrolysate and comparison with fibrillated protein solution. *Food Hydrocolloids*, *52*, 221–230.
- Mohammadian, M., & Madadlou, A. (2016b). Cold-set hydrogels made of whey protein nanofibrils with different divalent cations. *International Journal of Biological Macromolecules*, *89*, 499–506.
- Nagy, K., Váró, G., & Szalontai, B. (2012).  $\kappa$ -Casein terminates casein micelle build-up by its “soft” secondary structure. *European Biophysics Journal*, *41*, 959–968.
- Najbar, L. V., And, R. F. C., & Drummond, C. J. (2003). Heat-induced aggregation of a globular egg-white protein in aqueous solution: I investigation by atomic force microscope imaging and surface force mapping modalities. *Langmuir: The ACS Journal of Surfaces and Colloids*, *19*, 2880–2887.
- Ning, F., Ge, Z., Qiu, L., Wang, X., Luo, L., Xiong, H., & Huang, Q. (2020). Double-induced se-enriched peanut protein nanoparticles preparation, characterization and stabilized food-grade pickering emulsions. *Food Hydrocolloids*, *99*, 105308.
- Niu, L., Wu, L., & Xiao, J. (2017). Inhibition of gelatinized rice starch retrogradation by rice bran protein hydrolysates. *Carbohydrate Polymers*, *175*, 311–319.
- Obeid, S., Guyomarc’h, F., Francius, G., Guillemin, H., & Lopez, C. (2019). The surface properties of milk fat globules govern their interactions with the caseins: Role of homogenization and pH probed by AFM force spectroscopy. *Colloids and Surfaces B: Biointerfaces*, *182*, 110363.
- Oborocanu, D., Wang, L., Magner, E., & Mae, A. (2014). Fibrillization of whey proteins improves foaming capacity and foam stability at low protein concentrations. *Journal of Food Engineering*, *121*, 102–111.
- Osborne., & Thomas, B. (1924). *The vegetable proteins*. Longmans: Green and Co.
- Ouanezar, M., Guyomarc’h, F., & Bouchoux, A. (2012). AFM imaging of milk casein micelles: Evidence for structural rearrangement upon acidification. *Langmuir: The ACS Journal of Surfaces and Colloids*, *28*, 4915–4919.
- Panchapakesan, C., Sozer, N., Dogan, H., Huang, Q., & Kokini, J. L. (2012). Effect of different fractions of zein on the mechanical and phase properties of zein films at nano-scale. *Journal of Cereal Science*, *55*, 174–182.

- Park, J. W., & Reed, Z. H. (2014). Seafood proteins and surimi. In Zeynep Ustunol (Ed.), *Applied food protein chemistry* (pp. 323–359). West Sussex, UK: John Wiley & Sons, Ltd.
- Pavliček, N., & Gross, L. (2017). Generation, manipulation and characterization of molecules by atomic force microscopy. *Nature Reviews Chemistry*, 1, 0005.
- Phillips, G. O., & Williams, P. A. (2011). Introduction to food proteins. In G. O. Phillips, & P. A. Williams (Eds.), *Handbook of food proteins* (pp. 1–12). Woodhead Publishing.
- Phillips, L. G. (2013). *Structure-function properties of food proteins*. Academic Press.
- Qi, P. X. (2007). Studies of casein micelle structure: The past and the present. *Le Lait*, 87, 363–383.
- Qi, P. X., & Onwulata, C. I. (2011). Physical properties, molecular structures, and protein quality of texturized whey protein isolate: Effect of extrusion temperature. *Journal of Agricultural & Food Chemistry*, 59, 4668–4675.
- Rodriguez-Nogales, J. M., Garcia, M. C., & Marina, M. L. (2006). High-performance liquid chromatography and capillary electrophoresis for the analysis of maize proteins. *Journal of Separation Science*, 29, 197–210.
- Sari, Y. W., Mulder, W. J., Sanders, J. P. M., & Bruins, M. E. (2015). Towards plant protein refinery: Review on protein extraction using alkali and potential enzymatic assistance. *Biotechnology Journal*, 10, 1138–1157.
- Sharma, S., Grintsevich, E. E., Phillips, M. L., Reisler, E., & Gimzewski, J. K. (2011). Atomic force microscopy reveals drebrin induced remodeling of F-actin with subnanometer resolution. *Nano Letters*, 11, 825–827.
- Sharma, S., Grintsevich, E. E., Woo, J., Gurel, P. S., Higgs, H. N., Reisler, E., & Gimzewski, J. K. (2014). Nanostructured self-assembly of inverted formin 2 (INF2) and F-actin-INF2 complexes revealed by atomic force microscopy. *Langmuir: The ACS Journal of Surfaces and Colloids*, 30, 7533–7539.
- Shen, Y., Chang, C., Shi, M., Su, Y., Gu, L., Li, J., & Yang, Y. (2020). Interactions between lecithin and yolk granule and their influence on the emulsifying properties. *Food Hydrocolloids*, 101, 105510.
- Shi, C., Bi, C., Ding, M., Xie, J., Xu, C., Qiao, R., ... Zhong, J. (2019). Polymorphism and stability of nanostructures of three types of collagens from bovine flexor tendon, rat tail, and tilapia skin. *Food Hydrocolloids*, 93, 253–260.
- Shi, C., He, Y., Ding, M., Wang, Y., & Zhong, J. (2019a). Nanoimaging of food proteins by atomic force microscopy. Part I: Components, imaging modes, observation ways, and research types. *Trends in Food Science & Technology*, 87, 3–13.
- Shi, C., He, Y., Ding, M., Wang, Y., & Zhong, J. (2019b). Nanoimaging of food proteins by atomic force microscopy. Part II: Application for food proteins from different sources. *Trends in Food Science & Technology*, 87, 14–25.
- Soltanzadeh, N., & Kadivar, M. (2014). Nanomechanical characteristics of meat and its constituents postmortem: A review. *Critical Reviews in Food Science and Nutrition*, 54, 1117–1139.
- Sow, L. C., Peh, Y. R., Pekerti, B. N., Fu, C., Bansal, N., & Yang, H. (2017). Nanostructural analysis and textural modification of tilapia fish gelatin affected by gelatin and calcium chloride addition. *LWT - Food Science and Technology*, 85, 137–145.
- Sow, L. C., Toh, N. Z. Y., Wong, C. W., & Yang, H. (2019). Combination of sodium alginate with tilapia fish gelatin for improved texture properties and nanostructure modification. *Food Hydrocolloids*, 94, 459–467.
- Strixner, T., & Kulozik, U. (2011). *Egg proteins*. *Handbook of food proteins* (pp. 150–209). Woodhead Publishing.
- Stylianou, A., & Yova, D. (2013). Surface nanoscale imaging of collagen thin films by atomic force microscopy. *Materials Science & Engineering C*, 33, 2947.
- Sun, C., Dai, L., He, X., Liu, F., Yuan, F., & Gao, Y. (2016). Effect of heat treatment on physical, structural, thermal and morphological characteristics of zein in ethanol-water solution. *Food Hydrocolloids*, 58, 11–19.

- Sun, C., Xiong, Z., Zhang, J., & Fang, Y. (2020). Environmental parameters-dependent self-assembling behaviors of  $\alpha$ -zein in aqueous ethanol solution studied by atomic force microscopy. *Food Chemistry*, 331, 127349.
- Sun, X., Zhang, W., Zhang, L., Tian, S., & Chen, F. (2020). Molecular and emulsifying properties of arachin and conarachin of peanut protein isolate from ultrasound-assisted extraction. *LWT*, 109790.
- Sun-Waterhouse, D., Zhao, M., & Waterhouse, G. I. N. (2014). Protein modification during ingredient preparation and food processing: Approaches to improve food processability and nutrition. *Food and Bioprocess Technology*, 7, 1853–1893.
- Tian, H., Guo, G., Xiang, A., & Zhong, W.-H. (2018). Intermolecular interactions and microstructure of glycerol-plasticized soy protein materials at molecular and nanometer levels. *Polymer Testing*, 67, 197–204.
- Tian, R., Feng, J., Huang, G., Tian, B., Zhang, Y., Jiang, L., & Sui, X. (2020). Ultrasound driven conformational and physicochemical changes of soy protein hydrolysates. *Ultrasonics Sonochemistry*, 68, 105202.
- Tornberg, E. (2005). Effects of heat on meat proteins – Implications on structure and quality of meat products. *Meat Science*, 70, 493–508.
- Uricanu, V. I., Duits, M. H. G., & Mellema, J. (2004). Hierarchical networks of casein proteins: An elasticity study based on atomic force microscopy. *Langmuir: The ACS Journal of Surfaces and Colloids*, 20, 5079–5090.
- Van Der Borgh, A., Vandeputte, G. E., Derycke, V., Brijs, K., Daenen, G., & Delcour, J. A. (2006). Extractability and chromatographic separation of rice endosperm proteins. *Journal of Cereal Science*, 44, 68–74.
- Vidal, C. M. P., Zhu, W., Manohar, S., Aydin, B., Keiderling, T. A., Messersmith, P. B., & Bedran-Russo, A. K. (2016). Collagen-collagen interactions mediated by plant-derived proanthocyanidins: A spectroscopic and atomic force microscopy study. *Acta Biomaterialia*, 41, 110–118.
- Visentini, F. F., Perez, A. A., & Santiago, L. G. (2019). Self-assembled nanoparticles from heat treated ovalbumin as nanocarriers for polyunsaturated fatty acids. *Food Hydrocolloids*, 93, 242–252.
- Walder, R., Van Patten, W. J., Adhikari, A., & Perkins, T. T. (2018). Going vertical to improve the accuracy of atomic force microscopy based single-molecule force spectroscopy. *ACS Nano*, 12, 198–207.
- Wan, Y.-J., Guo, Q., Liu, D., Jiang, Y., Zeng, K.-W., & Tu, P.-F. (2019). Protocatechualdehyde reduces myocardial fibrosis by directly targeting conformational dynamics of collagen. *European Journal of Pharmacology*, 855, 183–191.
- Wang, J., & Nie, S. (2019). Application of atomic force microscopy in microscopic analysis of polysaccharide. *Trends in Food Science & Technology*, 87, 35–46.
- Xiao, J., Li, Y., Li, J., Gonzalez, A. P., Xia, Q., & Huang, Q. (2015). Structure, morphology, and assembly behavior of kafirin. *Journal of Agricultural and Food Chemistry*, 63, 216–224.
- Xiao, J., Si, N., & Huang, Q. (2015). Assembly of kafirin/carboxymethyl chitosan nanoparticles to enhance the cellular uptake of curcumin. *Food Hydrocolloids*, 51, 166–175.
- Yang, H., Yu, J., Fu, G., Shi, X., Xiao, L., Chen, Y., . . . He, C. (2007). Interaction between single molecules of Mac-1 and ICAM-1 in living cells: An atomic force microscopy study. *Experimental Cell Research*, 313, 3497–3504.
- Yang, J., Thielens, I., Berton-Carabin, C. C., van der Linden, E., & Sagis, L. M. C. (2020). Nonlinear interfacial rheology and atomic force microscopy of air-water interfaces stabilized by whey protein beads and their constituents. *Food Hydrocolloids*, 101, 105466.
- Yousefi, M., Ariffin, F., & Huda, N. (2017). An alternative source of type I collagen based on by-product with higher thermal stability. *Food Hydrocolloids*, 63, 372–382.

- Zhang, F.-C., Zhang, F., Su, H.-N., Li, H., Zhang, Y., & Hu, J. (2010). Mechanical manipulation assisted self-assembly to achieve defect repair and guided epitaxial growth of individual peptide nanofilaments. *ACS Nano*, 4, 5791–5796.
- Zhang, T., Sun, R., Ding, M., Li, L., Tao, N., Wang, X., & Zhong, J. (2020). Commercial cold-water fish skin gelatin and bovine bone gelatin: Structural, functional, and emulsion stability differences. *LWT*, 125, 109207.
- Zhang, T., Sun, R., Ding, M., Tao, L., Liu, L., Tao, N., ... Zhong, J. (2020). Effect of extraction methods on the structural characteristics, functional properties, and emulsion stabilization ability of Tilapia skin gelatins. *Food Chemistry*, 328, 127114.
- Zhang, Y., Sheng, S., & Shao, Z. (1996). Imaging biological structures with the cryo atomic force microscope. *Biophysical Journal*, 71, 2168–2176.
- Zhang, Y., Wang, B., Zhou, C., Atungulu, G. G., Xu, K., Ma, H., ... Abdulrahman, M. A. (2016). Surface topography, nano-mechanics and secondary structure of wheat gluten pretreated by alternate dual-frequency ultrasound and the correlation to enzymolysis. *Ultrasonics Sonochemistry*, 31, 267.
- Zhang, Y.-H., & Huang, L.-H. (2014). Effect of heat-induced formation of rice bran protein fibrils on morphological structure and physicochemical properties in solutions and gels. *Food Science and Biotechnology*, 23, 1417–1423.
- Zhao, H.-S., Ma, Z., & Jing, P. (2020). Interaction of soy protein isolate fibrils with beta-lain from red beetroots: Morphology, spectroscopic characteristics and thermal stability. *Food Research International*, 135, 109289.
- Zhao, J., Sun, F., Li, Y., Liu, Q., & Kong, B. (2016). Modification of gel properties of soy protein isolate by freeze-thaw cycles are associated with changes of molecular force involved in the gelation. *Process Biochemistry*, 52, 200–208.
- Zhao, M., Xiong, W., Chen, B., Zhu, J., & Wang, L. (2020). Enhancing the solubility and foam ability of rice glutelin by heat treatment at pH12: Insight into protein structure. *Food Hydrocolloids*, 103, 105626.
- Zhao, X., Xing, T., Xu, X., & Zhou, G. (2020). Influence of extreme alkaline pH induced unfolding and aggregation on PSE-like chicken protein edible film formation. *Food Chemistry*, 319, 126574.
- Zhao, X., Zhou, Y., Zhao, L., Chen, L., He, Y., & Yang, H. (2019). Vacuum impregnation of fish gelatin combined with grape seed extract inhibits protein oxidation and degradation of chilled tilapia filets. *Food Chemistry*, 294, 316–325.
- Zhong, J. (2011). From simple to complex: Investigating the effects of lipid composition and phase on the membrane interactions of biomolecules using in situ atomic force microscopy. *Integrative Biology*, 3, 632–644.
- Zhong, J., & He, D. (2012). Recent progress in the application of atomic force microscopy for supported lipid bilayers. *Chemistry—A European Journal*, 18, 4148–4155.
- Zhong, J., Liu, X., Wei, D., Yan, J., Wang, P., Sun, G., & He, D. (2015). Effect of incubation temperature on the self-assembly of regenerated silk fibroin: A study using AFM. *International Journal of Biological Macromolecules*, 76, 195–202.
- Zhong, J., Ma, M., Li, W., Zhou, J., Yan, Z., Ding, J., & He, D. (2014). Self-assembly of regenerated silk fibroin from random coil nanostructures to antiparallel  $\beta$ -sheet nanostructures. *Biopolymers*, 101, 1181–1192.
- Zhong, J., Ma, M., Zhou, J., Wei, D., Yan, Z., & He, D. (2013). Tip-induced micropatterning of silk fibroin protein using in situ solution atomic force microscopy. *ACS Applied Materials & Interfaces*, 5, 737–746.
- Zhong, J., Sun, G., & He, D. (2014). Classic, liquid, and matrix-assisted dip-pen nanolithography for materials research. *Nanoscale*, 6, 12217–12228.
- Zhong, Y., Wang, Z., & Zhao, Y. (2015). Impact of radio frequency, microwaving, and high hydrostatic pressure at elevated temperature on the nutritional and antinutritional components in black soybeans. *Journal of Food Science*, 80, C2732–C2739.



This page intentionally left blank

## CHAPTER 5

# Application of atomic force microscopy for food polysaccharides

Lifen Zhang<sup>1</sup>, Xiaoyang Sun<sup>2</sup>, Shaojuan Lai<sup>1</sup>, Fusheng Chen<sup>1</sup> and Hongshun Yang<sup>3,4</sup>

<sup>1</sup>College of Food Science and Technology, Henan University of Technology, Zhengzhou, P. R. China

<sup>2</sup>College of Food and Biological Engineering, Henan University of Animal Husbandry and Economy, Zhengzhou, P. R. China

<sup>3</sup>Department of Food Science and Technology, National University of Singapore, Singapore, Singapore

<sup>4</sup>National University of Singapore (Suzhou) Research Institute, Suzhou Industrial Park., Suzhou, P. R. China

### 5.1 Introduction

Binnig and Quate developed atomic force microscopy (AFM) in 1986 (Funami, 2010). As a scanning probe microscopy, AFM then opens a new vision in imaging and force measurements. AFM can be used to visualize dispersed or isolated molecules, assemble molecules, supermolecular structures, gel precursors, microgels, and network structures of bulk gels, and determine the polymer chain length distribution and chain flexibility (Sletmoen, Maurstad, Sikorski, Paulsen, & Stokke, 2003). Additionally, AFM can be used to stretch single polysaccharide chains to determine the mechanical fingerprints for reflecting the chemical composition, linkage geometry, and higher order structure of polysaccharides. This single-molecule probe technique can also be used to determine the molecular interactions among polysaccharides (Sletmoen et al., 2003). It has been widely used in polysaccharides research; for example, pectin, cellulose, hemicellulose, carrageenan, gellan gum, xanthan gum, xyloglucan (XG), and so on. AFM has the advantage of offering both air and aqueous environments, which make the samples' behaviors similar to those in actual systems (Funami, 2010). It provides the capacity to detect real-time morphology and reactions of samples at an atomic level. Meanwhile, AFM can be used to directly observe and quantify the heterogeneity of polysaccharides (Funami, 2010).

## 5.2 Plant polysaccharide

### 5.2.1 Starch

#### 5.2.1.1 Analysis of morphology and structure properties of starch

Starch, one of the most common natural carbohydrate polymers, is a major component of various crops, and an energy provider in our daily diet. As a raw material, starch has been widely used in the chemical and food industries. The major components of starch are amylose and amylopectin composed of glucose units. Amylose is almost linearly, while amylopectin is highly branched. The diameter of starch granules from different sources varies from 1 to 200  $\mu\text{m}$ , and its gelatinization and retrogradation are critical for its use, particularly in food. These properties depend on the modification of starch, and the interactions between starch and other components. It is necessary to understand the structural changes of starch during processing, which could explain the relationship between the structural and functional properties of starch. Thus, AFM is a strong tool to provide structural perspectives of starch. AFM could be used to obtain topography, frictional force, and phase imaging of starch. The AFM images of cornstarch nanocrystals showed that particle size of 10–150 nm could be achieved in the shape of round-edge platelet-like particles (Javidi, Razavi, & Mohammad Amini, 2019). The sizes of hot distilled water isolated amylose-lipid nanomaterials obtained from pasted native (un-irradiated) high amylose maize starch (HAMS) with 0%, 1.5%, and 5% stearic acid were 5–80, 5–100, and 5–110 nm, respectively (Ocloo, Ray, & Emmambux, 2019).

Starch granule has a relationship with the physicochemical properties of starch. Investigation of structure characteristics of starch granules could benefit understanding the functionality of starch. AFM was used to observe the internal structure and surface morphology of starch granules at the molecular level (Yang et al., 2019). For instance, the differences in the internal structure of banana starch granules with different mature stages indicated that the start of enzymatic hydrolysis of starch varied (Peroni-Okita et al., 2015). The observed surface morphology of starch granules in potato, wheat, rice, and corn was different (Baldwin, Davies, & Melia, 1997; Funami, 2010). The functional properties of starch are closely related to the surface structural characteristics of the granules. Chen et al. (2019) applied AMF to investigate the surface features of fractionated potato starch granules, and the results showed that the surfaces of fractionated granules had “blocklet” structures of different nanoscales.

This indicated that the self-assembly behaviors of amylopectin side chains were different.

AFM also could provide the important roughness parameters [average roughness values ( $R_q$ ) and root mean square roughness ( $R_a$ )] of starch granules surfaces. Higher values of  $R_q$  and  $R_a$  corresponded to more unevenness of the surface (Fig. 5.1) (Chen et al., 2019). Larger granules

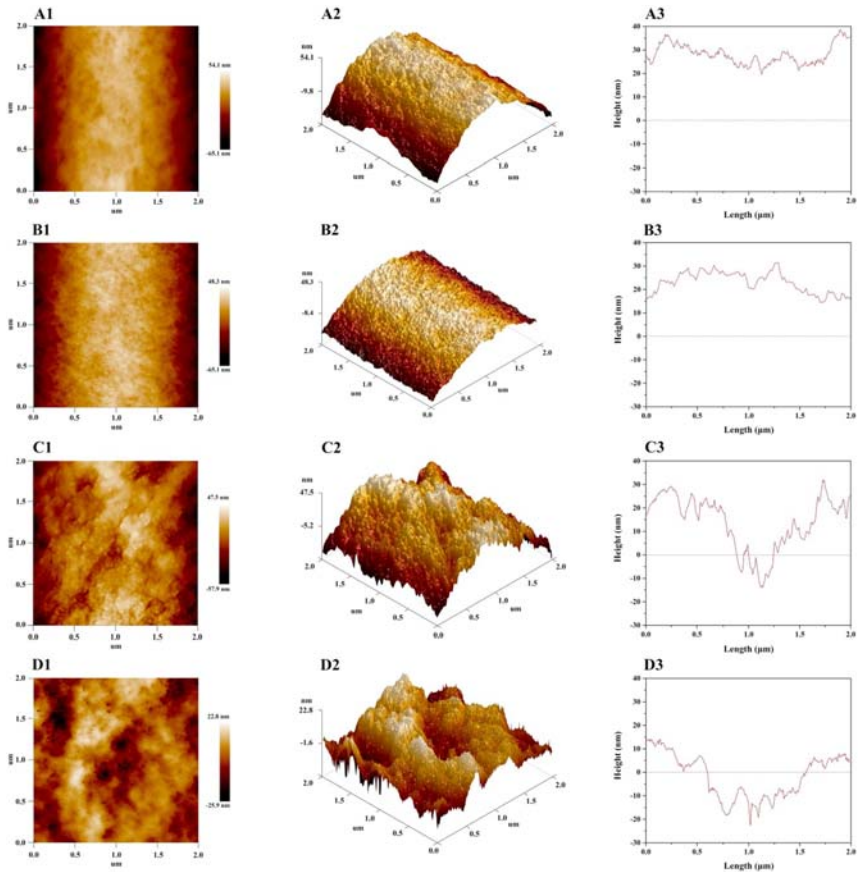


**Figure 5.1** Atomic force microscopy scanning of the surface of fractionated potato starch granules. Note: (A1), (B1), (C1) and (D1) topographic images; (A2), (B2), (C2) and (D2) phase images; (A3), (B3), (C3) and (D3) cross section images; (A1, A2, A3) PS-VS; (B1, B2, B3) PS-S; (C1, C2, C3) PS-M; (D1, D2, D3) PS-L. From Chen, L., Ma, R., Zhang, Z., Huang, M., Cai, C., Zhang, R., McClements, D. J., Tian, Y., & Jin, Z. (2019). *Comprehensive investigation and comparison of surface microstructure of fractionated potato starches*. *Food Hydrocolloids*, 89, 11–19. <https://doi.org/10.1016/j.foodhyd.2018.10.017>.

with rougher surfaces could easily absorb water and swell. AFM also provides an approach to investigate the starch modification and processing (Wen, Xu, Liu, Corke, & Sui, 2020). AFM imaged the surface of hydrolyzed starches of wheat, corn, and potato, and the results showed that potato and corn starch had similar patterns, while it had different surficial morphology for wheat starch (Tavallaie, Khomeiri, Mousivand, Maghsoudlou, & Hashemi, 2019). Hedayati, Shahidi, Majzoobi, Koocheki, and Farahnaky (2020) investigated the effects of  $\text{CaCl}_2$  and  $\text{NaCl}$  on the surface properties of cold water swelling maize starch, and the AFM results showed that  $\text{NaCl}$  increased the surface wrinkles of starch granules, while  $\text{CaCl}_2$  reduced the roughness of starch granule surface (Hedayati et al., 2020).

AFM was also applied to investigate the internal structure and biopolymer chains of starch and modified starch. Researchers studied the internal structures of potato, banana, and maize starch granules. The images of maize starch showed a central hole and a radial crack. Globular structures existed within or across the growth rings. The central region of the starch granule of the banana was made up of different materials with different viscoelasticities. Blocklet structures of the size of about 80–200 nm mainly consisted of the central region. Meanwhile, there also existed a few blocklet structures with the size of 15–50 nm in the central region (Chakraborty, Pallen, Shetty, Roy, & Mazumder, 2020; Peroni-Okita et al., 2015; Ridout, Parker, Hedley, Bogracheva, & Morris, 2003).

### **5.2.1.2 Atomic force microscopy study of starch films**

Starch is one of the most biodegradable materials with affordable price, renewability, and wide availability. Starch can be used to produce biodegradable films, and has been widely used in food packaging. The surface properties of films are very important to their mechanical and gas permeability properties. Smooth surfaces can provide a barrier for diffusion of gases and moisture. AFM analysis revealed that ultraviolet (UV)–irradiation method could produce stable bio-thermoplastic films with low surface roughness and high barrier properties. Thus, surface roughness is closely related to film quality (Chandra Mohan, Harini, Karthikeyan, Sudharsan, & Sukumar, 2018). What's more, differences in the microstructure of starches from different sources caused the intermolecular interactions of different intensities during the film formation process, which may lead to the different surface roughness of films. For instance, the surface of cassava, sweet potato, and potato starch films was

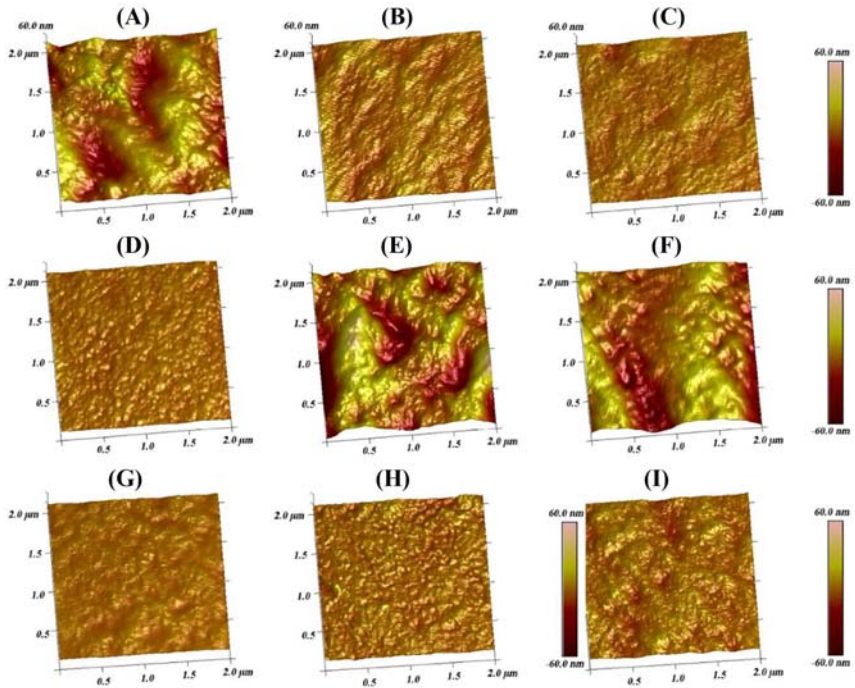


**Figure 5.2** Atomic force microscopy topographic images of native starch films (A–F), modified cassava starch films (G–I). Note: (A) WCS film, (B) CAS film, (C) SPS film, (D) PS film, (E) WS film, (F) CS film, (G) ECS film, (H) CCS film, and (I) OCS film. Scan size is  $2 \times 2 \mu\text{m}$  and all figures (A–I) have the same 3D height coordinate scale. Results are expressed as mean  $\pm$  SD (standard deviation) of three determinations. From Dai, L., Zhang, J., & Cheng, F. (2019). *Effects of starches from different botanical sources and modification methods on physicochemical properties of starch-based edible films*. *International Journal of Biological Macromolecules*, 132, 897–905. <https://doi.org/10.1016/j.ijbiomac.2019.03.197>.

homogeneous except for waxy corn, wheat, and corn starch films (Fig. 5.2) (Dai, Zhang, & Cheng, 2019).

The morphologies of starch films also can be investigated by AFM. Research works applied AFM studied the morphologies of potato starch-olive oil edible films containing zein nanoparticles. The results indicated that  $R_q$  of the pure starch film was 30.2, and 34 nm for starch/olive oil film. The addition of zein could increase the smoothness of the film surface. The decrease in surface roughness corresponded to the decrease in water permeability of the film (Farajpour, Emam Djomeh, Moieni, Tavahkolipour, & Safayan, 2020). The microstructure of films prepared using corn/octenylsuccinated starch incorporated with soybean oil in

different concentrations exhibited an irregular and coarse surface, while a smooth and uniform surface was observed in the control film (Gao et al., 2020). According to AFM results, a more compact surface structure of the morphology of bentonite powder modified starch film than that of control was observed. Meanwhile, the average surface roughness of the bentonite-starch film was  $21.4 \pm 7$ , and of the control film was  $33.4 \pm 10$  nm (Aguilar-Sánchez et al., 2019).

AFM, as a tool to study the food hydrocolloids, can visualize the gel precursors, microgels, and network structures of bulk gels, and obtain the structural information of food hydrocolloids, such as amylose and starch (Funami, 2010; McIntire & Brant, 1999; Ridout, Gunning, Parker, Wilson, & Morris, 2002). The tapping mode is most suitable for food hydrocolloid analysis. Cai et al. investigated the effects of NaCl on the nanostructure of carboxymethyl starch/xanthan gum combinations stabilized emulsions, and the results confirmed that NaCl caused the extension of the molecular chain of carboxymethyl starch, while the double helix structure of xanthan gum was intertwined with carboxymethyl starch, forming a stable network structure (Cai, Du, Zhu, & Cao, 2020).

## 5.2.2 Pectin

As a complex anionic polysaccharide, pectin consists of several different *monosaccharides* in various plants (Vincken et al., 2003), and the three polymers of pectin are homogalacturonan (HG), rhamnogalacturonan I (RG I), and rhamnogalacturonan II (RG II). HG and RG I are called “smooth region” and “hairy region,” respectively. HG consists of (1,4)-linked  $\alpha$ -D-GalA residues. Groups of HG can be methyl esterified or acetylated. The methyl-esterified of HG has great value to the binding capacity, gelation, and rheological behaviors of pectin (Willats, Knox, & Mikkelsen, 2006). This may be covalently cross-linked with RG I through rhamnose (Rha) units. The main bone of RG I consists of alternating GalA and Rha units. RG I also contains side chains including of galactose (Gal) and arabinose (Ara) (Kozioł, Cybulska, Pieczywek, & Zdunek, 2017; Willats, McCartney, Mackie, & Knox, 2001). RG II is a complex compound that is highly branched (Ishii et al., 1999).

AFM was used to investigate the morphology, degradation, surface manipulation, biomolecular interactions, and mechanical properties of polymers. It also could be used to directly observe the three-dimensional structure of polymers (Magonov & Reneker, 1997). AFM was widely

used to study the nanostructure of pectin. For example, the structural properties of alkali-soluble *Canna edulis* Ker pectin were evaluated by AFM (Zhang, Cui, Xiao, & Wang, 2014). Meanwhile, pectin degradation of fruits and vegetables during storage also could be investigated by AFM (Yang, Chen, An, & Lai, 2009).

AFM could be used to image the molecules in a liquid, and directly provide information about the height of the molecular chain. It also could be applied to provide information on the contour and branch length, and distribution of the pectin backbone, and be used to observe branch (br), short chain (sc), long chain (lc), the linear single fraction (ls), mutibranch (mbr), and polymer (p) morphologies of pectin chains. Meanwhile, AFM could be useful to determine the single molecules and distinguishing branches of the molecule backbone of overlapping molecules. AFM could provide information about the properties of aggregated structures (Paniagua et al., 2017).

#### **5.2.2.1 Analysis of pectin degradation during cell wall disassembly**

As the structural unit of fresh cells and the junction between cells, pectin widely exists in almost all fruit and vegetables (Guo et al., 2014), and accounts up to 60% of cell wall mass. The length, diameter, and branching of pectin play an important role in the texture of fruits. The lengths of pectin polymer and the number of aggregates decreased along with the maturation of fruits (Paniagua et al., 2014). RGII, as the branched structure of pectin, is also important to the cell wall structure (Mohnen, 2008). For the degradation of cell wall polysaccharides, pectin has an obvious effect on the texture change of fruits.

Pectin degradation was due to the change of pectin content and was significantly influenced by the alteration of its nanostructure. Pectin structures affect the stiffness, diffusivity, intercellular cell wall properties, and the macroproperties. Covalently linked pectin is critical to cell walls stiffness during fruit softening. Degradation of pectin in the middle lamella cell wall leads to the decrease of cell-to-cell adhesion, and the stiffening of primary cell walls. During fruit maturation, self-assembly behaviors of the sodium-carbonate soluble pectin (SSP) degraded to a regular gel-like network, which was responsible for the stiffening of primary cell walls (Zdunek, Koziół, Cybulska, Lekka, & Pieczywek, 2016).

During the ripeness of fruits, softening is mainly related to the dissociation of the middle lamella. The disassembly process of the cell wall has a close relationship to the depolymerization of matrix glycans, the



depolymerization and dissolution of pectin, and the loss of neutral sugars in pectin side chains. Pectin solubilization during fruit ripening may cause the content of acid-water pectin to increase, and the amount of covalently bound pectin to decrease. Thus, the pectin network may be disentangled, and the motility of wall enzymes in the cell wall matrix will be increased. Pectin solubilization could be directly involved in ripe fruits' texture, but its mechanism is unclear. AFM would reveal the changing process of cell wall polymers during softening (Posé et al., 2019).

AFM is a useful tool that was used to observe the structure of plant cell walls in recent years, especially for the changes of pectin during fruit softening. The insights on structural features of pectin and their changes during fruit ripening and postharvest were summarized, and Table 5.1 shows AFM analysis of quality, quantify, and morphology features of pectin during ripening and storage of fruits and vegetables.

Yang et al. introduced AFM to analyze the nanostructures of pectin in fruits for the first time (Yang et al., 2005). They did a series of research on the characterizations including morphology, length, height, and width of pectin nanostructure of peach, apricot, strawberry, cherry, tomato, loquat, red bayberry, winter jujube, and so on. ls, lc, sc, cp, br, mbr, and p morphologies of pectin chains were observed in these fresh fruits. Network also could be observed in calcium-treated fruits (Figs. 5.3 and 5.4).

Quantitative parameters of pectin were different according to the fruit variety and origin. Zhang et al. investigated the widths and lengths of SSP of crisp and soft cherries. The range of widths and lengths were 37–140 nm and 123–1404 nm, respectively. Compared to soft groups, the widths of SSP were larger in crisp groups, but the lengths of SSP in crisp groups were smaller. The relative percentage of wide SSP chains of crisp fruit was higher than that of soft fruit (Zhang et al., 2008). Yang et al. found that the differences in suppleness among three varieties of peaches may own to the different lengths of pectin chains (Yang et al., 2009). The widths and lengths of stone fruits (peach, jujube, and apricot) were also different from each other. The lengths of SSP chain of crisp fruit were mainly within the range of 50–900 nm, while it was 20–100 nm for soft peaches. The main widths of pectin in crisp and soft cultivars were 20–100 nm. Meanwhile, almost all the heights of pectin [chelate-soluble pectin (CSP), water-soluble pectin (WSP), and SSP] were from 1 to 5 nm in the two cultivars (Yang et al., 2009). The pectin chain widths of jujubes were smaller than that of peaches. For unripe jujubes, most of the pectin chain widths were in the range of 47–70 nm. Pectin

**Table 5.1** Atomic force microscopy analysis of quality, quantity, and morphology features of pectin from fruits and vegetables during ripening and storage.

Fruits and vegetables (species)	Ripening or storage	Pectin	Nanostructural properties	References
Peach (“Jinxiu,” <i>Prunus persicu</i> L. Batsch.)	Controlled atmosphere storage	WSP	Linear, branched, blocks, and polymers structures; chain widths were composed of four basic units: 11.719, 15.625, 19.531, and 35.156 nm.	Yang, An, Feng, Li, and Lai (2005)
		CSP	Linear segments, branch points, aggregates, single linear molecule, cleavage points, branch, polymers, linear single fractions, short and long chains, and releasing point structures; widths of chains were composed of four basic units: 17.578, 19.531, 23.438, and 29.297 nm.	Yang, Lai, An, and Li (2006)
		SSP	Linear, branched, blocks, polymers, and large aggregates; widths of chains were composed of four basic units: 11.719, 15.625, 19.531, and 17.578 nm.	Yang, Feng, An, and Li (2006)
Peach (crisp “Jinxiu,” and soft “Milu,” <i>Prunus persicu</i> L. Batsch.)	Cooled for 12 h at 4°C, and stored at 20°C for 6 days	WSP, CSP, and SSP	Aggregates, branched, short and long chains, multiple branched chains, and releasing point structures; widths: about 20–100 nm; heights: about 1–5 nm; lengths: firm peaches, WSP, about 0.3–4.0 μm; CSP, approximately from 0.1 to 3.0 μm; SSP, 249 ± 256 nm ( <i>n</i> = 138); soft peaches, WSP, 0.8–4.2 μm; CSP, approximately from 0.1 to 3.0 μm; SSP, 57 ± 27 nm ( <i>n</i> = 40).	Yang et al. (2009)

(Continued)

**Table 5.1** (Continued)

Fruits and vegetables (species)	Ripening or storage	Pectin	Nanostructural properties	References
Peach ("Cangfangzaosheng" and "Songsenzaosheng," <i>Prunus persicu</i> L. Batsch.)	Cold storage	WSP, CSP, and SSP	Polymers, blocks, and single linear chains structures; widths of peach pectin (WSP, CSP, and SSP) were composed of limited basic values.	Zhang et al. (2010, 2012)
Chinese cherry ( <i>Prunus pseudocerasus</i> L.)	Unripe and ripe	SSP	Linear single fraction, cleavage point, branched, and polymers structures; heights: 1.3–6.8 nm; widths: four basic units 37, 47, 55, and 61 nm; lengths: four basic units 123, 202, and 380 nm.	Zhang et al. (2008)
Apricots ("Jinhong," <i>P. armeniaca</i> L.)	Calcium treatment	CSP	Branched, linear single fraction, short and long chains, polymers, releasing point, and cleavage point structures; heights: 0.2–3.0 nm; lengths: 400–3600 nm.	Liu et al. (2009)
	Pectinase treatment	CSP	Branched, linear single fraction, short and long chain, cleavage point, releasing point, and polymer structures; lengths: untreated samples, 0.5–1 $\mu$ m; pectinase treated samples, 0–1 $\mu$ m; heights: 0.2–3.0 nm for both control and treated samples.	Chen et al. (2013)
Jujubes ("Huanghua" and "Zhanhua," <i>Zizyphus jujuba</i> )	Unripe and ripe	CSP, and SSP	Unripe: CSP widths, 35–60 nm for both cultivars; SSP widths, 35–157 nm for both cultivars; ripe: CSP widths, 15–35 nm for	Wang et al. (2012)

Strawberries ("Shijixiang," <i>Fragaria annanassa</i> Duch.)	Calcium treatment	WSP, CSP, and SSP	both cultivars; SSP widths, 15–80 nm for both cultivars. Long and single chains, and multibranched structures; widths: WSP, and CSP, 23–80 nm; SSP, 23–60 nm; lengths: WSP, and SSP mainly in 50–2000 nm.	Chen et al. (2011)
Tomatoes (crisp "Dongsheng" and soft "Geruisi" <i>Lycopersicon esculentum</i> Mill.)	Ripening	CSP	Polymers, long chains, linear single fraction, short chains, branched, cleavage points, and releasing point structures; widths: 15–118 nm; heights: 0.5–6 nm.	Xin et al. (2010)
Cherry tomatoes ("Mali," <i>Lycopersicon esculentum</i> Mill.)	Rice bran wax coating	CSP	Branched, linear strands, short and long chains, and polymer structures; widths: 15–250 nm; heights: 0.2–2 nm.	Zhang, Chen, Zhang, Lai, and Yang (2017)
Chinese red bayberries ("Lang dangzi," <i>Myrica rubra</i> Sieb. Et Zucc.)	Vacuum impregnation combined with calcium ascorbate treatment	CSP	Short and long chains, linear single fractions, branched, polymers, and aggregates structures; widths: fresh, 20–90 nm; lengths: fresh, 100–1200 nm; heights: fresh, 0.5–4.5 nm; larger frequency of CSP chain width and length of samples treated by the combination of vacuum impregnation and calcium ascorbate were observed.	Li, Zhang, Chen, Lai, and Yang (2018)
Winter jujubes ("Nongke I," <i>Zizyphus jujube</i> Miller.)	Calcium and pectin methylesterase treatment	WSP, CSP, and SSP	Long and short chains, branches, polymer structures; larger frequency of WSP, CSP, and SSP chain width and length were observed in calcium and pectin methylesterase treated samples.	Zhang et al. (2019)

(Continued)

**Table 5.1** (Continued)

Fruits and vegetables (species)	Ripening or storage	Pectin	Nanostructural properties	References
Fresh-cut honeydew melon ( <i>Cucumis melo L. var inodorus</i> )	Chitosan combined with calcium chloride treatment	SSP	Short and long chain, linear single fraction, branched, multiple branched chain, cleavage point, and aggregates structures; widths: untreated, 51–60 nm (44%); day 13, mainly in 21–30 nm; lengths: untreated, 401–500 nm (33%); day 13, 301–400 nm for treated samples.	Chong, Lai, and Yang (2015)
Grapes (“Kyoho,” <i>Vitis vinifera</i> × <i>V. labrusca</i> )	Vacuum impregnation combined with calcium lactate	WSP, CSP, and SSP	Long chains, linear single fractions, polymers, short chains, branched, releasing point, and cleavage points structures; widths: mainly within 40–60 nm; heights: CSP, 0.4–3.5 nm.	Mao et al. (2017)
Fresh-cut papayas (“Sekaki”)	Vacuum impregnation with calcium lactate and pectin methylesterase (PME) treatment	CSP	Linear single fractions, polymers, branched, and conglomerate structures; the percentage of chain widths greater than 45 nm had increased 35.0% in fresh-cut papayas vacuum impregnated with calcium lactate and PME at the end of storage.	Yang, Wu, Ng, and Wang (2017)

CSP, Chelate-soluble pectin; SSP, sodium carbonate-soluble pectin; WSP, water-soluble pectin.

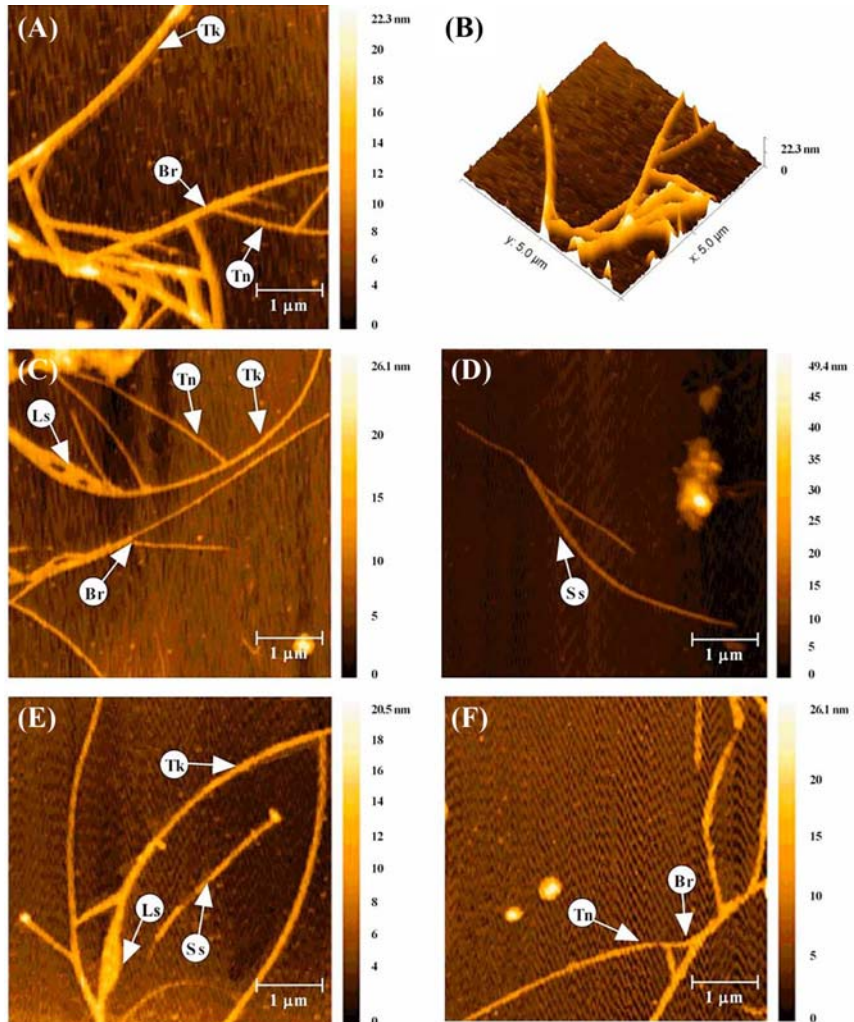


**Figure 5.3** Atomic force microscopy images of sodium carbonate-soluble pectin chains in mung bean sprouts. Note: (A): control group before treatment; (B): three-dimensional image of the control group before treatment; (C, D): control group at day 3; (E, F): ATP treatment group at day 3. *Br*, branched chain; *Tk*, thick chain; *Tn*, thin chain; *Ls*, loose structure; *Ss*, short straight chain. From Chen, L., Zhou, Y., He, Z., Liu, Q., Lai, S. & Yang, H. (2018). Effect of exogenous ATP on the postharvest properties and pectin degradation of mung bean sprouts (*Vigna radiata*). *Food Chemistry*, 251, 9–17. <https://doi.org/10.1016/j.foodchem.2018.01.061>.

chain widths of ripe jujubes were less than 40 nm (Wang et al., 2012). The widths and lengths of CSP of apricot were larger than that of fruits treated with 1%  $\text{CaCl}_2$ . The treated group maintained larger quantitative parameters of CSP, and this was probably due to the ionic cross-linking

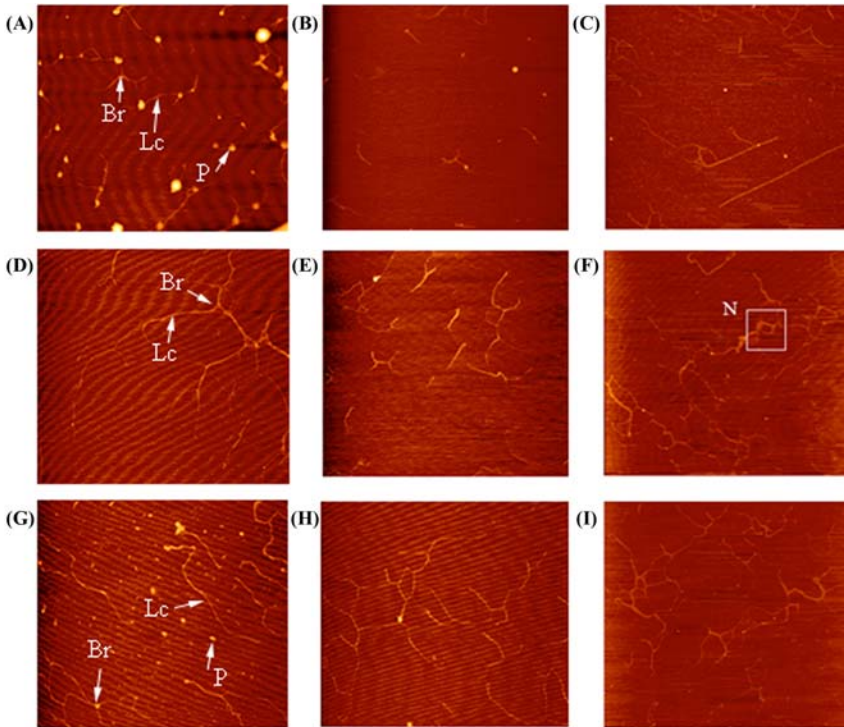


**Figure 5.4** Atomic force microscopy images of water-soluble pectin (images A–C), chelate-soluble pectin (images D–F), and sodium carbonate-soluble pectin (images G–I) chains in cherry tomatoes. Note: A, D, G, images from cherry tomatoes of fresh fruit; B, E, H, images from cherry tomatoes of the calcium lactate treated group (15 min, and 15°C); C, F, I, images from cherry tomatoes of the ultrasound combined with calcium lactate treated group (20 W/L, 15 min, and 15°C); Scan area,  $5.000 \times 5.000 \mu\text{m}$ . Lc, Long straight chains; Sc, short chains; Br, branched chains; P, polymer structure; N, net-like structure. From Zhang, L., Wang, P., Sun, X., Chen, F., Lai, S. & Yang, H. (2020). Calcium permeation property and firmness change of cherry tomatoes under ultrasound combined with calcium lactate treatment. *Ultrasonics Sonochemistry*, 60, 104784. <https://doi.org/10.1016/j.ultsonch.2019.104784>.

of HG s through calcium among pectin molecules. Meanwhile, the high calcium content in the cell wall could induce an increase in the cross-linking ability of HG s (Liu et al., 2009). The widths and lengths of pectin chain in berry fruits (strawberries, tomatoes, and Chinese red bayberry) were roughly equivalent to that of stone fruits (Chen et al., 2011; Li et al., 2018; Xin et al., 2010).

Pectin is in the middle lamella of plant tissues, and is the major component of cell wall. It may undergo structural changes during fruit

ripening, storage, and process. This resulted in decreasing firmness and facilitated infestation by pathogens. Therefore postharvest fruit decay increased and the quality of fresh fruits decreased (Lin et al., 2010). AFM has been extensively used to observe differences of pectin structures with different cultivars, ripening stage, and storage of peach (Zhang et al., 2012), jujubes (Wang et al., 2012), apricot (Liu et al., 2009), tomatoes (Xin et al., 2010), and Chinese cherry (Zhang et al., 2008). Liu et al. (2009) found that the firmness changed along with the changes in morphology of pectin molecules for apricot during storage (Liu et al., 2009). During the ripening, the widths of pectin chains of tomatoes decreased and a large of pectin polymers degraded with the decreased firmness (Xin et al., 2010). Zhang et al. (2010) observed that there was a relationship between the width of SSP chains of peaches and its firmness (Zhang et al., 2010). The self-assembled network of pectin in cell walls of carrots of different ripening stages was observed, and the results indicated that the network decomposed into individual molecules led to the softening of fruits and vegetables (Cybulska, Zdunek, & Kozioł, 2015).

In recent years, the extracellular materials impregnation in fruit and vegetables attracted great interest. Extracellular materials have a close relationship with fruit pectin. Preservation effects could be observed according to the AFM results, for example, AFM was used to observe the nanostructure of SSP of postharvest fresh-cut honeydew melon coated by calcium chloride, chitosan, and their combination, and these results indicated that there was a close relationship between the firmness and the nanostructure of SSP in fresh-cut honeydew melon. Meanwhile, the short and narrow SSP chains corresponded to less firmness (Chong et al., 2015). In addition, extracellular ATP could activate a specific recognition mechanism, and this could elevate the content of cytosolic free calcium ions ( $\text{Ca}^{2+}$ ). AFM images were used to observe effects of exogenous ATP on the degradation of pectin in mung bean sprouts (*Vigna radiata*), and the results indicated that the treatment of ATP could slow the degradation of pectin. Meanwhile, pectin backbone width (47.1%) and height were higher than the control (45.6%) (Chen et al., 2018).

As one of the impregnation solutions, calcium could enhance fruit cell walls. It could keep the functional and structural integrity of membranes through the formation of cross-links or bridges with uronic acid carboxyls (Tappi et al., 2016). During the processing and storage of fruit, calcium that existed in cell walls could prevent tissue softening. Calcium cross-linked with pectin chains plays an important role in maintaining the



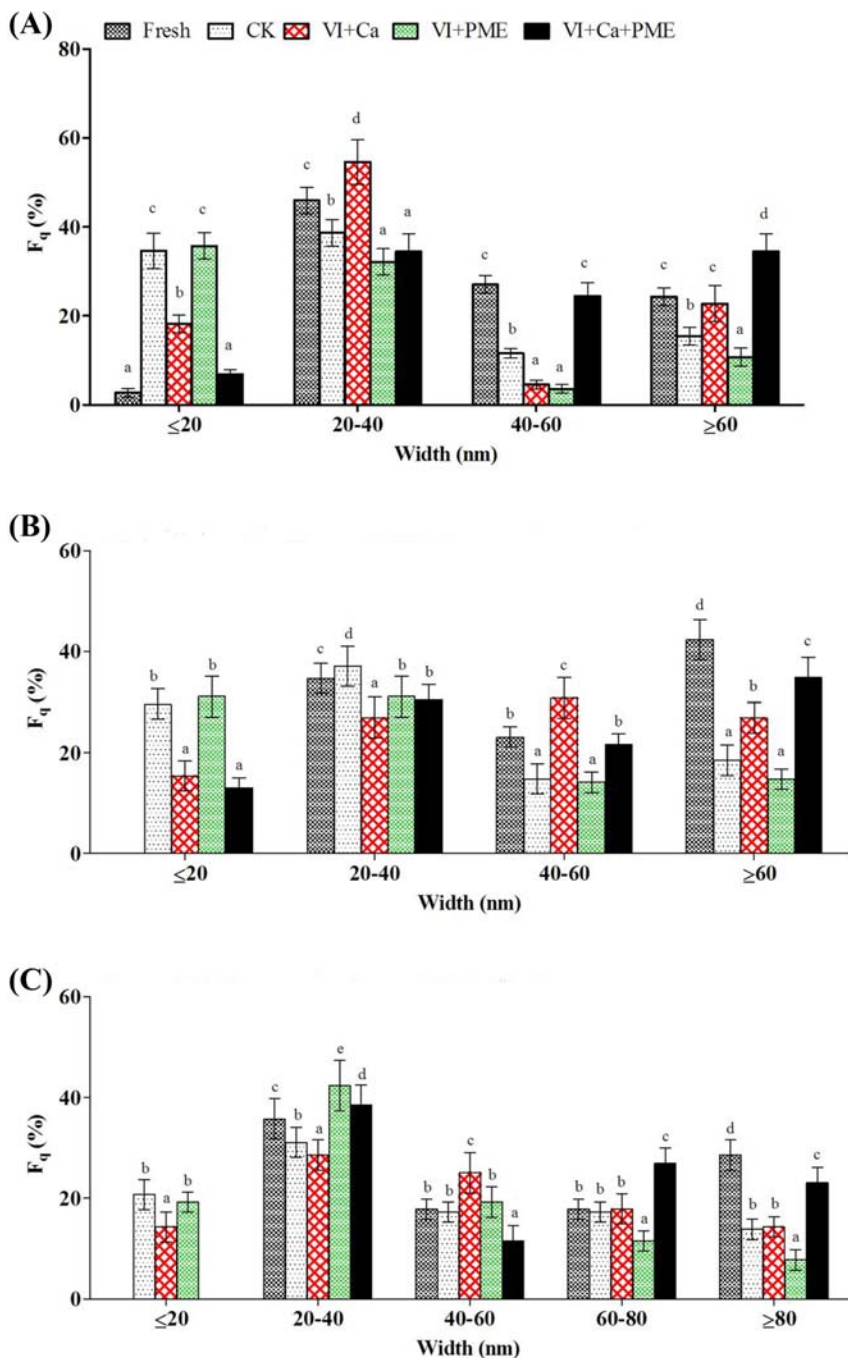


**Figure 5.5** Width of (A) water-soluble pectin, (B) chelate-soluble pectin, and (C) sodium carbonate-soluble pectin chains in jujubes. Note: Fresh, untreated fresh jujubes (0 day); CK, jujubes treated with vacuum impregnation (VI) with an isotonic

texture of fruit (Chen et al., 2011; Lai et al., 2013; Liu et al., 2017). The enhancement of calcium ions into the tissue of raw materials could improve the texture and limit softening (Radziejewska-Kubzdela, Biegańska-Marecik, & Kidoń, 2014). Thus, different types of physical technology combined with impregnation solutions were used to prevent fruit decay and maintain their quality.

Vacuum impregnation (VI) and ultrasound could efficiently enhance external solutions in the tissues of vegetable and fruit to improve their physicochemical, sensory, and nutritional properties (Radziejewska-Kubzdela et al., 2014; Yusof, Wadsö, Rasmusson, & Gómez Galindo, 2017; Zhi et al., 2017). The internal gas and external solution change during the VI process of porous products. Ultrasound could enhance the penetration of compounds from extracellular to intracellular environment. What's more, the firmness of fruit was affected by the intense pressure generated during the cavitation process of ultrasound (Duarte et al., 2018).

Effects of VI on the nanostructures of CSP and SSP were investigated by AFM, and the results showed that calcium inhibited CSP and SSP degraded into short branches during the VI process (Mao et al., 2017). Li et al. studied the nanostructure properties of CSP of VI-treated Chinese red bayberries, and the results showed that CSP had large widths and lengths in calcium ascorbate impregnated group. Meanwhile, vacuum impregnated with 2% calcium ascorbate could prevent the dissociation and degradation of CSP (Li et al., 2018). Zhang et al. observed effects of pectin methylesterase (PME) and calcium chloride on the quality of jujubes under VI, and the frequencies of molecules in WSP, CSP, and SSP with a width  $\geq 60$  nm were the highest in the VI + Ca + PME group at the end of storage. VI + Ca + PME treatment could delay the degradation of CSP, WSP, and SSP (Fig. 5.5) (Zhang et al., 2019). The

- 
- ◀ sucrose solution (56 days); VI + Ca, jujubes treated with vacuum impregnation (VI) combined with calcium chloride (56 days); VI + PME, jujubes treated with vacuum impregnation (VI) with an isotonic sucrose solution (56 days); VI + Ca, jujubes treated with vacuum impregnation (VI) combined with calcium chloride (56 days); VI + PME, jujubes treated with VI combined with pectin methylesterase (56 days); VI + Ca + PME, jujubes treated with VI combined with calcium chloride and pectin methylesterase (56 days); *Fq*, the percentage of pectin chains of particular width among all the chains observed. Error bars represent the standard deviation of the mean of three replicates. Different small case letters indicate a significant difference at  $P < .05$  among different treatment methods. From Zhang, L., Wang, P., Chen, F., Lai, S., Yu, H., & Yang, H. (2019). Effects of calcium and pectin methylesterase on quality attributes and pectin morphology of jujube fruit under vacuum impregnation during storage. *Food Chemistry*, 289, 40–48. <https://doi.org/10.1016/j.foodchem.2019.03.008>.

proportion of chain widths greater than 45 nm increased 35.0% in fresh-cut papayas at the end of storage, which were impregnated with calcium lactate and PME (Yang et al., 2017). Zhang et al. also used ultrasound to increase the permeation of calcium, and investigated the effects of ultrasound on the nanostructure of pectin in strawberries and cherry tomatoes. The results indicated that the percentage of width  $\geq 90$  nm and length  $\geq 800$  nm CSP molecules was larger for strawberries treated by the combination of ultrasound and calcium. A similar phenomenon of CSP and SSP was observed in cherry tomatoes (Zhang et al., 2020; Zhang, Zhao, Lai, Chen, & Yang, 2018).

The edible coating used to prolong the shelf life of vegetables and fruits attracted great attention, especially for the biodegradable and environment-friendly materials. The main ingredients of edible coatings are polysaccharides, proteins, and lipids. Chitosan, protein, and their complexes have been used to preserve fruits and vegetables for their biodegradability, biocompatibility, nontoxicity, and antimicrobial activity. Effects of edible coating on the shelf life and cell wall polysaccharides of vegetables and fruits were investigated by AFM. Zhang et al. (2018) found that the SPI-chitosan coating could inhibit the degradation of pectin.  $F_q$  (the percentage of particular length or width of pectin chains among all chains investigated by AFM) of widths  $\geq 61$  nm and lengths  $\geq 3$   $\mu\text{m}$  of pectin molecules was larger in samples coated by SPI-chitosan (Zhang, Chen, Lai, Wang, & Yang, 2018). Xin, Jin, Chen, Lai, and Yang (2020) reported that more linked, branched, and long SSP chains existed in chitosan-coated sweet cherries. Widths of the pectin backbone in sweet cherries also could be maintained by chitosan coating (Xin et al., 2020). Meanwhile, the structural analysis by AFM showed that CSP degradation could be inhibited when coated by rice bran wax, the width of CSP molecules was in the range of 15–250 nm, and their vertical heights varied from 0.2 to 2.0 nm. Compared to the control, higher frequency ( $F_q$ ) of CSP molecules with large widths and lengths were observed in waxed fruits (Zhang et al., 2017).

Cell wall stiffness is important to elucidate the mechanism of fruit softening, and cell walls become loosen and weaker during fruit ripening. Meanwhile, it is difficult to measure the cell wall elastic properties at micrometer scale. AFM can image the surface morphology of nanometer resolution and sense the nanomechanical properties. Thereby, AFM has been used to analyze the mechanical properties of plant cells. Changes in cell wall stiffness during pear ripening could be evaluated by AFM, which

could be used to investigate the cell wall components affecting cell wall mechanics, including neutral sugars, hemicelluloses, and related enzymes (Zdunek et al., 2016). Yang et al. used AMF to analyze the root mean square roughness ( $R_q$ ) and arithmetic roughness ( $R_a$ ) of “Jinxiu” yellow peach skin (*Prunus persicu* L. Batsch.) during storage. The  $R_a$  and  $R_q$  increased for both the controlled atmosphere (CA) and regular air (RA) group, while the values of CA group were smaller than that of RA group. AFM also could observe the three-dimensional profiles of the skin (Fig. 5.6) (Yang, An, Feng, & Li, 2005).

Pieczywek et al. investigated the cell wall stiffness of ultrasonically (US) treated apple by AFM. There was a significant linear decrease in cell wall stiffness along with the US treatment time. US caused the pronounced disassembly of the polysaccharide network according to AFM results (Pieczywek, Koziół, Konopacka, Cybulska, & Zdunek, 2017). The nanomechanical properties of fruit cells observed could provide insights on the internal fruit properties and the changes of these properties over time, which affected the quality of fruits. Cárdenas-Pérez et al. obtained Young’s modulus (YM) of apple tissue at cellular level using AFM. Meanwhile, the relationship between apple tissue and other macroscopic physical parameters was utilized to evaluate the ripeness during the storage of apples (Cárdenas-Pérez et al., 2017).

### 5.2.2.2 Nanostructural analysis of pectin

AFM is a valuable tool to investigate the nanostructure and nanomechanical properties of single biomolecules and assemblies, including pectin, and is appropriate to observe single molecules on a nanometer scale. It needs minimal sample and simple preparation, and can distinguish overlapping molecules from true branching points through the height analysis. For example, peanut polysaccharide molecules exhibited interweaved or overlapped chains morphology (Ye et al., 2020). The length of molecules with a curved shape was difficult to estimate (Cybulska et al., 2015).

Researchers used AFM to investigate structures of pectin in an aqueous solution. Compared to high methoxyl pectin, low methoxyl pectin networks couldn’t be dissociated when dissolved in water with concentrations less than 6.6  $\mu\text{g}/\text{mL}$  (Fishman et al., 2015). Pea soluble polysaccharides possessed star-like structures with side chains according to the AFM images (Cheng et al., 2018). Guo et al. investigated the nanostructure of copper-precipitated pectin and copper-unprecipitated pectin from sugar beet by AFM. Pectin precipitated by copper had branched fibrous

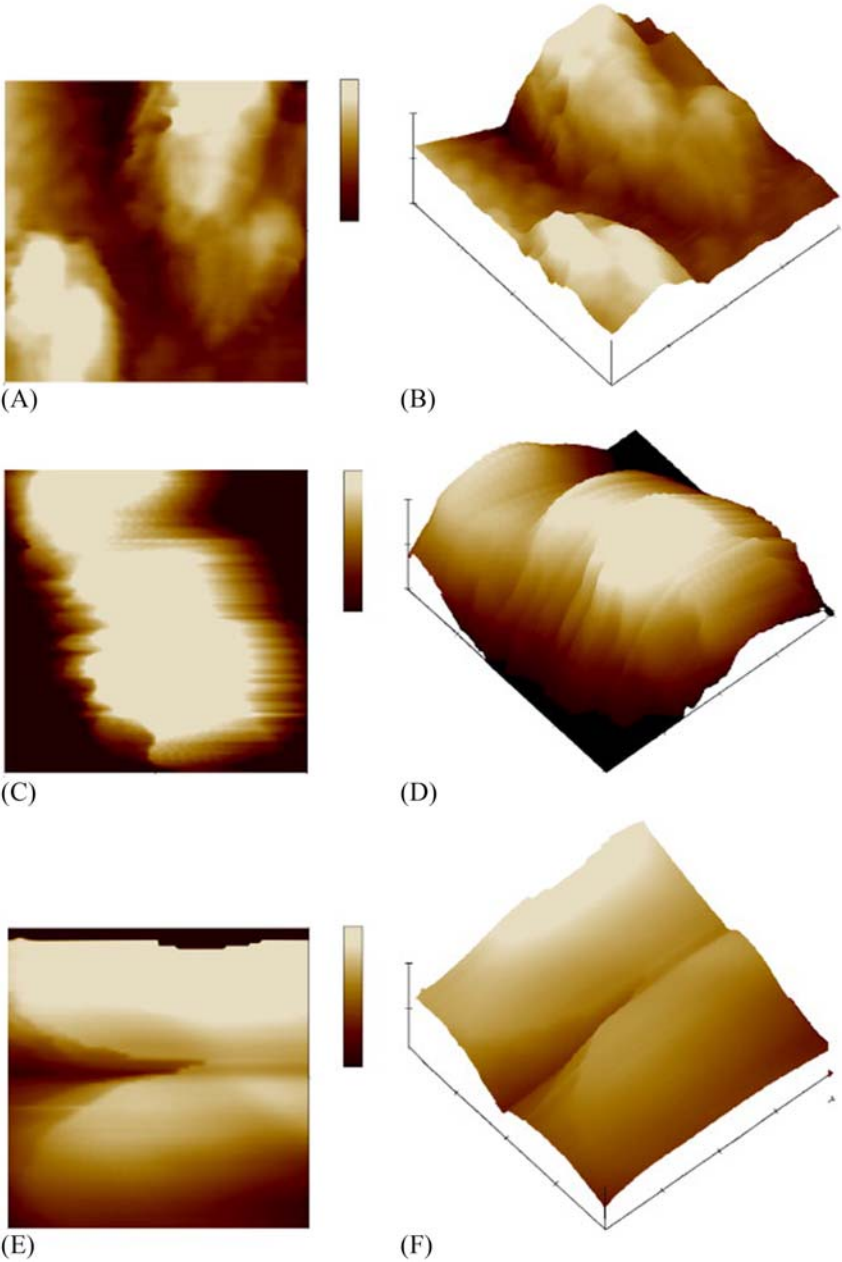


**Figure 5.6** Profiles of peach skin at different stage of controlled atmosphere storage by atomic force microscopy. Note: (A) and (B) plane and three-dimensional profiles after 15-day storage, respectively. Scan area = 2.003 mm, height bar = 50 nm. (C) and (D) plane and three-dimensional profiles after 30-day storage respectively. Scan

structures, while pectin unprecipitated by copper exhibited distinguishable granular-like shapes (Guo, Meng, Zhu, Zhang, & Yu, 2015).

Branched morphology and self-assembly properties of pectin also could be investigated by AFM. Branched-chain morphology of RG I enriched pectin of mandarin citrus peel was observed by AFM (Zhang et al., 2018). The percentage content of branched RG I of chelator-extractable pectin, water-soluble pectin, and sodium carbonate extractable pectin from black tomato pomace were 5.32%, 10.97%, and 29.08%, respectively (Zhang et al., 2020).

The AFM images revealed that sodium carbonate molecules from apple fruit structurally resembled rod-like objects, which consisted of relatively long linear sections separated by bend points or branches (Pieczywek, Kozioł, Płaziński, Cybulska, & Zdunek, 2020). AFM revealed the self-assembly of high- and low-methoxyl pectin of different concentrations. Pectin would link and aggregate with the raise of concentration. Lengths of high- and low-methoxyl pectin of 0.005 mg/mL were from 19.22 to 312.11 nm. AFM enabled research works on the model of “egg-box” of pectin-calcium ions from a new perspective (Wang, Fei, Wang, Zan, & Zhu, 2020). The morphology of ultrahigh methoxylated pectin aggregation presented a network structure and irregular clusters at 10 and 1  $\mu\text{g/mL}$  based on AFM (Liu et al., 2020). AFM research works indicated the self-organize on mica of chicory root pectin extracted by citric acid (CEP). These revealed that the random coil conformation was caused by the interaction of multiple branching. However, chicory root pectin extracted by alkaline (AEP) showed long linear filamentous structures (Zhang et al., 2020).

AFM could investigate the single-molecular behavior under applied force, and provide important kinetic parameters of pectin single-molecular (Zlatanova & van Holde, 2006). Cybulska et al. used AFM to stretch the galacturonic acid oligomers, and defined their mechanical properties (Cybulska, Brzyska, Zdunek, & Woliński, 2014).

- 
- ◀ area = 2.000 mm \* 2.000 mm, height bar = 50 nm. (C) and (D) plane and three-dimensional profiles after 30-day storage respectively. Scan area = 2.000 mm \* 2.000 mm, height bar = 100 nm. (E), (F) plane and three-dimensional profiles after 45-day storage, respectively. Scan area = 2.004 mm \* 2.004 mm, height bar = 100 nm. From Yang, H., An, H., Feng, G., & Li, Y. (2005). *Visualization and quantitative roughness analysis of peach skin by atomic force microscopy under storage*. *LWT – Food Science and Technology*, 38(6), 571–577. <https://doi.org/10.1016/j.lwt.2004.09.007>.

### 5.2.3 Cellulose

As an important biopolymer and the most abundant renewable resource, cellulose is widely applied due to its biocompatibility, availability, biodegradability, and sustainable production potential (Khorasani & Shojaosadati, 2017). Cellulose is composed of long chains with unbranched  $\beta$  (1  $\rightarrow$  4) linked D-glucopyranosyl units, while the lengths of  $\beta$  (1  $\rightarrow$  4) linked D-glucan rely on the species, maturity, and growth environment of the plant (Venkateshaiah et al., 2020). It usually contains 500–7500 D-glucose monomers.

Cellulose is the basic structural molecule of plant cell walls, and its structural arrangements affect the functional properties of fruits and vegetables. The relationship among cellulose microfibrils properties, diameter, crystallinity, and texture of fruits was investigated. Cybulska et al. reported that microfibrils of lower crystallinity of crisp apple cultivars were thicker than that of softer apple cultivars (Cybulska, Zdunek, Psonka-Antonczyk, & Stokke, 2013). However, cellulose microfibrils had similar diameters in different pear cultivars (Zdunek et al., 2016).

AFM could be used to evaluate the morphology and quantity parameter (diameter) of cellulose microfibrils. Liu et al., 2017 investigated the nanostructure of carboxymethylated polysaccharide (CMSERP) by AFM, and the results revealed that CMSERP could be dispersed in 0.05 M sodium sulfate and aggregated in water (Liu et al., 2017). The morphology of a coprocessed bio-based polymer observed by AFM showed that the polymers exhibited almost oval and spherical particles, and the surface of the particles had a loosely packed structure and was composed of irregular, globular structural elements (Singh, Nwabor, Ontong, Kaewnopparat, & Voravuthikunchai, 2020). Cheikh Rouhou, Abdelmoumen, Thomas, Attia, and Ghorbel (2018) reported that diameter of cactus rackets dietary fibers was 80 nm (Cheikh Rouhou et al., 2018). The diameter of cellulose from apple pomace, carrot pomace, tomato pomace, and cucumber pomace were analyzed by AFM, and the results showed that the distribution of microfibrils was similar. Furthermore, the largest diameter fraction was from 20 to 30 nm, while the average thickness of cellulose microfibrils from four pomaces varied (carrot pomace: 28.68 ( $\pm$  9.27) nm; cucumber pomace: 29.03 ( $\pm$  9.43) nm; apple pomace: 28.73 ( $\pm$  10.17) nm; and tomato pomace: 32.24 ( $\pm$  10.35) nm) (Szymańska-Chargot, Chylińska, Gdula, Koziół, & Zdunek, 2017). The diameters of cellulose microfibrils of onion and maize were 3–4 nm according to AFM analysis (Ding et al., 2012; Zhang, Zheng, & Cosgrove, 2016). Meanwhile, the diameter of ultrathin microfibril was 1–2 nm in peach and strawberry fruits (Niimura, Yokoyama, Kimura, Matsumoto, & Kuga, 2010).

AFM could efficiently evaluate the width, length, and aspect ratios of cellulose nanocrystal (Nagalakshmaiah, kissi, Mortha, & Dufresne, 2016).

### 5.2.4 Others

AFM could be used to observe the conformation of individual macromolecule, and analyze the quantitative parameters of xanthan. In pure water, xanthan existed a single helix structure, while double helix conformation was observed in KCl solution. The length of xanthan decreased from 1651 to 450 nm, and its number-average contour length decreased from 417 to about 150 nm (Camesano & Wilkinson, 2001; Yang & Zhang, 2009). Xanthan from different sources had different structural features according to AFM results. For example, xanthan of the wild-type strain *Xanthomonas campestris* B100 had branching and overlapping structures, while that of the strain JBL007 had no branching. The xanthan of acetate-free had single- and double-stranded areas with no branching, while xanthan of pyruvate-free had a branched and homogenous structure with single and double strands (Teckentrup et al., 2017; Venkateshaiah et al., 2020).

The nanostructure and self-assembly of XG in plants were observed by AFM. The mean height and mean length of was  $2.3 \pm 0.5$  nm and  $640 \pm 360$  nm, respectively. XG chains had a helical structure and could be aggregated as cross-like and a parallel-like assembly (Kozioł, Cybulska, Pieczywek, & Zdunek, 2015).

Polysaccharide hyaluronan (HA) exists in the extracellular, pericellular, and intracellular matrix. It consists of repeated disaccharide structure poly [(1/3)-b-DGlcNAc-(1/4)-b-D-GlcA-]. The conformations and specific binding interactions of HA have a close relationship to its biological functions. AFM could provide an alternative view of the conformation of HA with different sample preparation. An extended conformation could be observed when HA deposited on a prehydrated mica surface. However, HA favored relaxed, weakly helical, and coiled conformations when it was deposited on freshly cleaved mica. Necklace forms, thick rods, networks, and twisted fibers were also observed in intramolecularly condensed and intermolecular association of HA (Cowman et al., 2005).

Li et al. (2017) investigated the chain conformation of four sulfated polysaccharides from sea cucumbers by AFM. The chain conformation of fucosylated chondroitin sulfate (fCS) from *Isostichopus badiionotus* (fCS-Ib), fCS derived from *Pearsonothuria graeffei* (fCS-Pg), and fucoidan from fuc-Pg were random coil with polysaccharide chain outstretched, while fucoidan from fuc-Ib was spherical conformation in solution. fuc-Pg and fuc-Ib were linear polysaccharides without side branches, while fucose was the only monosaccharide. The lengths



of fCS-Pg, fCS-Ib, and fuc-Pg chain were from 100 to 1000 nm. Meanwhile, molecular aggregation took place among polysaccharide chains. Fuc-Ib formed a sphere with a diameter of about 100 nm, and had no linear chains on the surface of mica. Chain conformation could be used to determine the hypolipidemic activity of sulfated polysaccharides with regular structure (Li et al., 2017).

Lots of polysaccharides from seaweeds are hydrocolloids, and could be utilized to adjust rheological properties of food systems. *Eucheuma* is the red seaweed found in Southeast Asia. Yang et al. (2020) investigated the effect of extraction temperature on structures of extracted polysaccharides from *Eucheuma*. According to AFM results, the heights of polysaccharides decreased along with the increase in temperature. Polysaccharides of side-by-side association tended to be formed under relatively low temperature (Fig. 5.7) (Yang & Yang, 2020). Other polysaccharides such as  $\kappa$ -carrageenan (KC) and chitosan also could be observed by AFM. An interconnected porous fibrous network was observed in KC (Sow, Nicole Chong, Liao, & Yang, 2018). Yang and Yang (2020) also found that side-by-side association was observed in KC with lower temperatures extraction. The contour lengths and average height of single chitosan strands were 94–178 nm and  $0.45 \pm 0.04$  nm, respectively (Kocun, Grandbois, & Cuccia, 2011).

AFM data of nanostructural characters of polysaccharides are shown in Table 5.2.

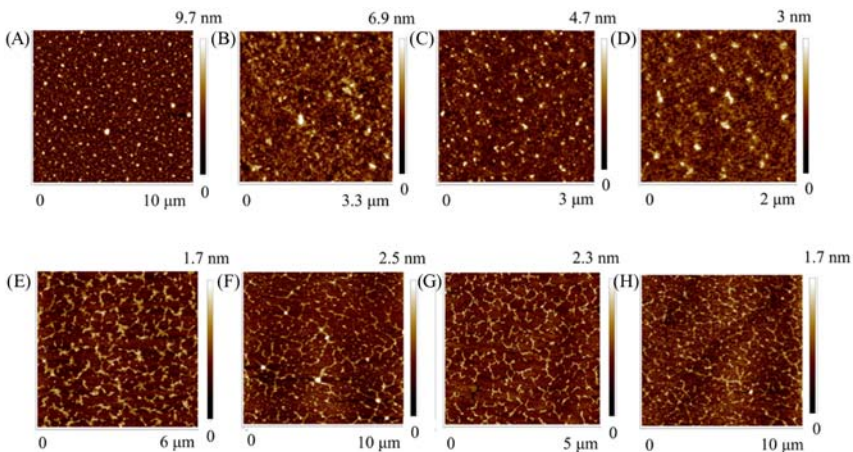


**Figure 5.7** Atomic force microscopy images of different extracts. AFM images of: (A) 0.02 mg/mL 60°C extract; (B) 0.02 mg/mL 70°C extract; (C) 0.02 mg/mL 80°C extract; (D) 0.02 mg/mL 90°C extract; (E) 0.002 mg/mL 60°C extract; (F) 0.002 mg/mL 70°C; (G) 0.002 mg/mL 80°C extract; (H) 0.002 mg/mL 90°C From Yang, D. & Yang, H. (2020). *The temperature dependent extraction of polysaccharides from eucheuma and the rheological synergistic effect in their mixtures with kappa carrageenan*. LWT – Food Science and Technology, 129, 109515. <https://doi.org/10.1016/j.lwt.2020.109515>.

**Table 5.2** Atomic force microscopy data of nanostructural characters of polysaccharides.

Polysaccharides	Sources	Nanostructural properties	References
Pectin	Citrus peel	Linear strands, singly branched, multiply branched, and polymer structures.	Zhang et al. (2013); Zhang, Zhang, Liu, Ding, and Ye (2015)
	Tomato pectin	Linear and branched structures, weight average ( $L_W$ ) and number average ( $L_N$ ) contour lengths were 174 and 132 nm, respectively; $L_W/L_N = 1.32$ .	Kirby, MacDougall, and Morris (2008)
	Sugar beet	Unaggregated molecules, and branched structures, weight average ( $L_W$ ) = 138 nm, number average ( $L_N$ ) = 108 nm, $L_W/L_N = 1.27$ .	Kirby et al. (2008)
	Apple peel	Network structure (pH 4 and 9), aggregates (pH11); height: $0.51 \pm 0.25$ nm (pH 3); length: $>5000$ nm (pH 4 and 9); $\leq 1000$ nm (pH 7 and 11).	Gawkowska, Cieřła, Zdunek, and Cybulska (2019)
Starch	Wheat	$R_a$ and $R_q$ vales: $14.2 \pm 2.7$ nm and $11.3 \pm 2.3$ nm for native starch; $58.2 \pm 8.0$ nm and $46.5 \pm 7.5$ nm for damaged starch.	Barrera et al. (2013)
	Potato	Rough and heterogeneous morphologies, “blocklets” structures; diameter, 10–100 nm; $R_q$ , 4.42–10.30 nm; $R_a$ , 3.58–8.16 nm.	(Chen et al., 2019)
Hemicellulose	Corn	Larger column arrangements and spherical particles.	Sujka, Jamroz (2009)
	Pear	Rod-like shape, tangled assemblies; length: 20–400 nm (“Conference”), and 80–400 nm (“Xenia”).	(Zdunek, Koziol, Pieczywek, & Cybulska, 2014)

(Continued)

**Table 5.2** (Continued)

Polysaccharides	Sources	Nanostructural properties	References
Cellulose	Apple pomace, carrot pomace, tomato pomace, cucumber pomace	The average cellulose microfibril thickness: 28.68 ( $\pm$ 9.27) nm for carrot pomace, 29.03 ( $\pm$ 9.43) nm for cucumber pomace, 28.73 ( $\pm$ 10.17) nm for apple pomace, and 32.24 ( $\pm$ 10.35) nm for tomato pomace; the cellulose microfibril diameter for carrot, cucumber, and apple pomaces with the largest diameter fraction (more than 45% of estimated microfibrils) between 20–30 nm, while cellulose microfibrils isolated from tomato, the distribution maximum (more than 45% of estimated microfibrils) is shifted to the thicker fractions of 25–35 nm.	Szymańska-Chargot et al. (2017)
Chitason	—	Contour lengths, 94–178 nm; average heights, $0.45 \pm 0.04$ nm.	Kocun et al. (2011)
Xanthan	<i>Xanthomonas campestris</i>	Double helix conformation, aggregates.	Wang, Xiang, Li, Zhang, and Bai (2021)
Xyloglucan	Tamarind seed	Rod-like structures, mean height of $2.3 \pm 0.5$ nm and mean length of $640 \pm 360$ nm; helical structure with a period of $115.8 \pm 29.2$ nm.	Koziol et al. (2015)
Fucosylated chondroitin sulfate	<i>Pearsonothuria graeffei</i> (fCS-Pg), <i>Isostichopus badionotus</i> (fCS-Ib)	fCS-Pg, fCS-Ib, random linear chains with a few spherical aggregations; lengths, 100–1000 nm.	Li et al. (2017)
$\kappa$ -carrageenan	SeaKem CM 611	Interconnected porous fibrous network	Sow et al. (2018)
<i>Eucheuma</i> polysaccharide	<i>Eucheuma</i>	side-by-side association	Yang and Yang (2020)
Peanut polysaccharide	Peanut	spheres; diameter, 15–50 nm; lengths, 100–300 nm.	Ye et al. (2020)

Note:  $R_a$ , roughness average;  $R_q$ , root mean square roughness.

## 5.3 Measurement of molecule interactions of polysaccharides and food components

Components could interact with each other and form complexes in food systems. For example, there are complex interactions among polysaccharides, proteins, lipids, and their modified products. Research on a single component is usually insufficient to understand the food framework. Thereby, research on interaction among components is needed. AFM could be applied to investigate the real structure of complexes of natural materials. Intra- and intermolecular interaction forces (50 pN to 1–2 nN) could be investigated by AFM (Zlatanova & Leuba, 2002).

### 5.3.1 Polysaccharides-polysaccharides

Nowadays, pectin is used as a biopolymer-based food packaging for its low cost and good film-forming property. However, the edible films prepared using pure pectin have a poor barrier, thermo mechanical, and water resistance properties. Crystalline nanocellulose (CNC) could strengthen the barrier and mechanical properties of final films. Thus, using nanoreinforcement of biopolymers to produce bionanocomposites attracted great interest. AFM images could provide the morphology and distribution of CNC in pectin-CNC composite films. CNC particles were dispersed uniformly on the surface of the pectin-CNC (2% and 5%) composite films without any aggregation. The presence of uneven plateaus on the AFM images increased with the increase of CNC level, and this was due to the agglomeration of CNC (Chaichi, Hashemi, Badii, & Mohammadi, 2017). Chaichi et al. reported that nanocellulose could enhance the properties of pectin films based on the structure and properties of films determined by AFM (Chaichi et al., 2017).

AFM also could be used to evaluate the effect of noncellulosic polysaccharides on the structure and arrangement of cellulose microfibrils (Szymańska-Chargot et al., 2017). Hiasa et al. investigated the effects of pectin on the aggregation of cellulose nanofibers (CNFs) by AFM. AFM images showed that the pectin covered the surfaces of the CNFs, and the CNFs obtained from mandarin peel were finer than those obtained from wood cellulose (Hiasa, Kumagai, Endo, & Edashige, 2016).

The surface morphology of the entrapment biocomposite (pectin-non-starch nanofibers) was analyzed in the air at ambient temperature, using the contact mode of AFM. The nanofibers were intercalated into a pectin matrix. A percolating NC (nanofibers of chitin) network developed

within the pec-NC biocomposite according to the uniform morphology and a homogenous distribution of the nanofibrillar network structure. The surface of the biocomposite was continuous without pores and cracks (Khorasani & Shojaosadati, 2017).

### 5.3.2 Polysaccharides-protein

The multilayer microcapsules prepared by high methoxyl pectin and soy protein isolate fibrils were determined by AFM, and the results showed that the thickness of the soy protein isolate fibrils varied from 1 to 10 nm, and their structures were highly branched (Ansarifar, Mohebbi, Shahidi, Koocheki, & Ramezani, 2017).

Pectin and MTGase could be used to improve the rheological behavior, gel, and thermal properties of fish scales gelatin. According to the results of AFM and scanning electron microscopy analysis, MTGase catalyzed the cross-links among soluble fish scales gelatin-pectin complexes, which affected the increase of gel strength, rheological behavior, and melting temperature of modified complex gels (Huang et al., 2017).

AFM images confirmed the spherical morphology and nanostructure of WPC-pectin complexes (Ghasemi, Jafari, Assadpour, & Khomeiri, 2017). A compact conformation of sugar beet pectin was observed to be covalently bridged with the amino groups of lysine residues of the proteinaceous moiety according to AFM analysis (Lin, Yu, Ai, Zhang, & Guo, 2020). Structural characteristics of polysaccharide-protein-based films, such as gelatin-pectin, fish gelatin/chitosan nanoparticle composites, hydroxypropyl methyl cellulose and zein nanoparticles, were also elucidated by AFM (Farris et al., 2011; Gilbert, Cheng, & Jones, 2018; Hosseini, Rezaei, Zandi, & Farahmandghavi, 2016).

Sow et al. (2018) evaluated the effect of the ratio of fish gelatin (FG) and KC on the interaction and structures of FG using AFM. With low amount of KC in FG, a few spherical and irregular aggregates were observed in FG. Complex coacervates were obvious with KC: FG of 2:98 and 4:96, while the bicontinuous structure was found when KC: FG was 10:90. Dense complex coacervates regions were also found with KC: FG at 10:90 (Fig. 5.8). The morphology of the tea water-insoluble protein/KC (TWIP/KC) mixtures was also assessed by AFM. The results illustrated the aggregation behavior of TWIP. The protein particles progressively clustered with the increase of KC addition (Ren et al., 2021).

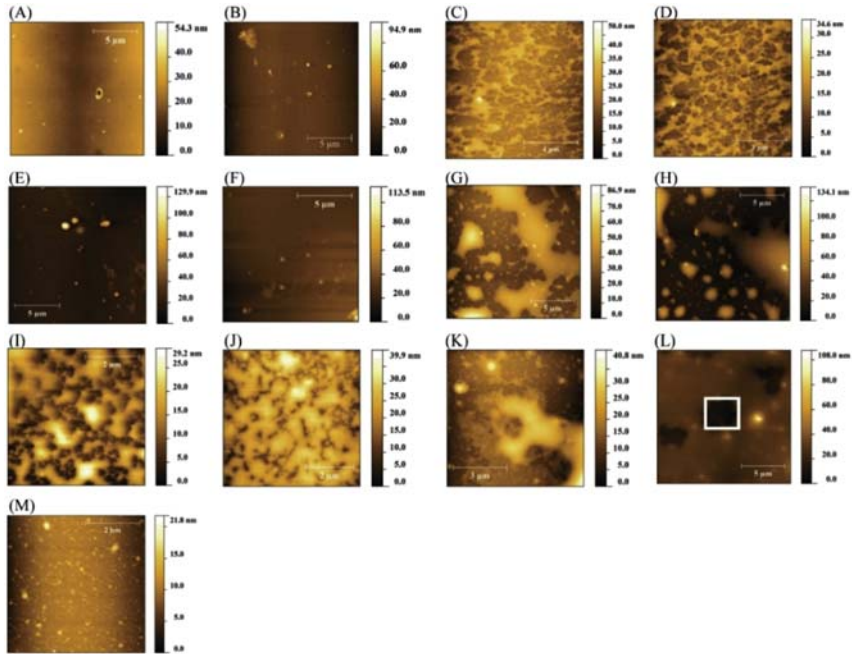


**Figure 5.8** Nanostructure. Note: (A, B) fish gelatin (FG); (C, D)  $\kappa$ -carrageenan (KC); and the FG-KC mixtures at different mixing ratios (KC:FG, w/w) of (E, F) 0.5:99.5 (FGC1); (G, H) 2:98 (FGC3) and (I, J) 4: 96 (FGC4); (K, L, M) 10:90 (FGC6) featuring bicontinuous phase comprising (K, L) a complex coacervates region and (M) thin fibril structure underneath the dense region (white square) of (M). \*The images were obtained from samples prepared at 0.01% (w/v) of KC-FG mixture. From Sow, L. C., Nicole Chong, J. M., Liao, Q. X., & Yang, H. (2018). Effects of  $\kappa$ -carrageenan on the structure and rheological properties of fish gelatin. *Journal of Food Engineering*, 239, 92–103. <https://doi.org/10.1016/j.jfoodeng.2018.05.035>.

## 5.4 Conclusions

AFM opened new horizons in imaging and force measurements of food polysaccharides. In this chapter, the applications of AFM in starch, pectin, cellulose, and other polysaccharides were discussed. AFM could provide the surface morphology, roughness parameters, internal structures of starch granules, and reveal the surface properties of starch films. Furthermore, AFM could be utilized to investigate morphology, qualitative, and quantitative characteristic of pectin, cellulose, and other polysaccharide molecules. AFM also could be used to observe the three-dimensional structure of pectin molecules, and stretch single pectin molecular chains. This

chapter was focused on introducing structure changes of pectin molecules of fruits and vegetables during storage by AFM. These observations could provide novel ideas for fruits and vegetables preservation. Moreover, AFM was significantly contributed to understand the intra and intermolecular interactions, which played a key role in understanding the food framework. AFM could provide more opportunities to improve food quality during processing and preservation.

## Acknowledgment

This study was funded by the Young-aged Backbone Teacher Funds of Henan Province of China (2020GGJS083), Applied Basic Research Project (Agricultural) Suzhou Science and Technology Planning Programme (SNG2020061), Natural Science Foundation of Jiangsu Province (BK20181184), Singapore Ministry of Education Academic Research Fund Tier 1 (R-160-000-A40-114), and an industry grant supported by Shenzhen Zhiyun Optoelectronics Co., Ltd. (R-143-000-A24-597).

## Declaration of competing interest

We declare that there was no commercial or associative interest that represents a conflict of interest in connection with this manuscript. We have no financial and personal relationships with other people or organizations that can inappropriately influence our work.

## References

- Aguilar-Sánchez, R., Munguía-Pérez, R., Reyes-Jurado, F., Navarro-Cruz, A. R., Cid-Pérez, T. S., Hernández-Carranza, P., . . . Avila-Sosa, R. (2019). Structural, physical, and antifungal characterization of starch edible films added with nanocomposites and Mexican Oregano (*Lippia berlandieri* Schauer) essential oil. *Molecules (Basel, Switzerland)*, 24(12), 2340. Available from <https://doi.org/10.3390/molecules24122340>.
- Ansarifar, E., Mohebbi, M., Shahidi, F., Koocheki, A., & Ramezani, N. (2017). Novel multilayer microcapsules based on soy protein isolate fibrils and high methoxyl pectin: Production, characterization and release modeling. *International Journal of Biological Macromolecules*, 97, 761–769. Available from <https://doi.org/10.1016/j.ijbiomac.2017.01.056>.
- Baldwin, P. M., Davies, M. C., & Melia, C. D. (1997). Starch granule surface imaging using low-voltage scanning electron microscopy and atomic force microscopy. *International Journal of Biological Macromolecules*, 21(1–2), 103–107. Available from [https://doi.org/10.1016/S0141-8130\(97\)00048-2](https://doi.org/10.1016/S0141-8130(97)00048-2).
- Barrera, G. N., Calderón-Domínguez, G., Chanona-Pérez, J., Gutiérrez-López, G. F., León, A. E., & Ribotta, P. D. (2013). Evaluation of the mechanical damage on wheat starch granules by SEM, ESEM, AFM and texture image analysis. *Carbohydrate*

- Polymers*, 98(2), 1449–1457. Available from <https://doi.org/10.1016/j.carbpol.2013.07.056>.
- Cai, X., Du, X., Zhu, G., & Cao, C. (2020). Induction effect of NaCl on the formation and stability of emulsions stabilized by carboxymethyl starch/xanthan gum combinations. *Food Hydrocolloids*, 105, 105776. Available from <https://doi.org/10.1016/j.foodhyd.2020.105776>.
- Camesano, T. A., & Wilkinson, K. J. (2001). Single molecule study of Xanthan conformation using atomic force microscopy. *Biomacromolecules*, 2(4), 1184–1191. Available from <https://doi.org/10.1021/bm015555g>.
- Chaichi, M., Hashemi, M., Badii, F., & Mohammadi, A. (2017). Preparation and characterization of a novel bionanocomposite edible film based on pectin and crystalline nanocellulose. *Carbohydrate Polymers*, 157, 167–175. Available from <https://doi.org/10.1016/j.carbpol.2016.09.062>.
- Chakraborty, I., Pallen, S., Shetty, Y., Roy, N., & Mazumder, N. (2020). Advanced microscopy techniques for revealing molecular structure of starch granules. *Biophysical Reviews*, 12(1), 105–122. Available from <https://doi.org/10.1007/s12551-020-00614-7>.
- Chandra Mohan, C., Harini, K., Karthikeyan, S., Sudharsan, K., & Sukumar, M. (2018). Effect of film constituents and different processing conditions on the properties of starch based thermoplastic films. *International Journal of Biological Macromolecules*, 120, 2007–2016. Available from <https://doi.org/10.1016/j.ijbiomac.2018.09.161>.
- Cheikh Rouhou, M., Abdelmoumen, S., Thomas, S., Attia, H., & Ghorbel, D. (2018). Use of green chemistry methods in the extraction of dietary fibers from cactus rackets (*Opuntia ficus indica*): Structural and microstructural studies. *International Journal of Biological Macromolecules*, 116, 901–910. Available from <https://doi.org/10.1016/j.ijbiomac.2018.05.090>.
- Chen, F., Liu, H., Yang, H., Lai, S., Cheng, X., Xin, Y., ... Deng, Y. (2011). Quality attributes and cell wall properties of strawberries (*Fragaria annanassa* Duch.) under calcium chloride treatment. *Food Chemistry*, 126(2), 450–459. Available from <https://doi.org/10.1016/j.foodchem.2010.11.009>.
- Chen, L., Ma, R., Zhang, Z., Huang, M., Cai, C., Zhang, R., ... Jin, Z. (2019). Comprehensive investigation and comparison of surface microstructure of fractionated potato starches. *Food Hydrocolloids*, 89, 11–19. Available from <https://doi.org/10.1016/j.foodhyd.2018.10.017>.
- Chen, L., Zhou, Y., He, Z., Liu, Q., Lai, S., & Yang, H. (2018). Effect of exogenous ATP on the postharvest properties and pectin degradation of mung bean sprouts (*Vigna radiata*). *Food Chemistry*, 251, 9–17. Available from <https://doi.org/10.1016/j.foodchem.2018.01.061>.
- Chen, Y., Chen, F., Lai, S., Yang, H., Liu, H., Liu, K., ... Deng, Y. (2013). In vitro study of the interaction between pectinase and chelate-soluble pectin in postharvest apricot fruits. *European Food Research and Technology*, 237(6), 987–993. Available from <https://doi.org/10.1007/s00217-013-2071-1>.
- Cheng, M., Qi, J. R., Feng, J. L., Cao, J., Wang, J. M., & Yang, X. Q. (2018). Pea soluble polysaccharides obtained from two enzyme-assisted extraction methods and their application as acidified milk drinks stabilizers. *Food Research International*, 109, 544–551. Available from <https://doi.org/10.1016/j.foodres.2018.04.056>.
- Chong, J. X., Lai, S., & Yang, H. (2015). Chitosan combined with calcium chloride impacts fresh-cut honeydew melon by stabilising nanostructures of sodium-carbonate-soluble pectin. *Food Control*, 53, 195–205. Available from <https://doi.org/10.1016/j.foodcont.2014.12.035>.
- Cowman, M. K., Spagnoli, C., Kudasheva, D., Li, M., Dyal, A., Kanai, S., & Balazs, E. A. (2005). Extended, relaxed, and condensed conformations of hyaluronan observed by



- atomic force microscopy. *Biophysical Journal*, 88(1), 590–602. Available from <https://doi.org/10.1529/biophysj.104.049361>.
- Cybulska, J., Brzyska, A., Zdunek, A., & Woliński, K. (2014). Simulation of force spectroscopy experiments on galacturonic acid oligomers. *PLoS One*, 9(9). Available from <https://doi.org/10.1371/journal.pone.0107896>.
- Cybulska, J., Zdunek, A., & Koziół, A. (2015). The self-assembled network and physiological degradation of pectins in carrot cell walls. *Food Hydrocolloids*, 43, 41–50. Available from <https://doi.org/10.1016/j.foodhyd.2014.04.032>.
- Cybulska, J., Zdunek, A., Psonka-Antonczyk, K. M., & Stokke, B. T. (2013). The relation of apple texture with cell wall nanostructure studied using an atomic force microscope. *Carbohydrate Polymers*, 92(1), 128–137. Available from <https://doi.org/10.1016/j.carbpol.2012.08.103>.
- Cárdenas-Pérez, S., Méndez-Méndez, J. V., Chanona-Pérez, J. J., Zdunek, A., Güemes-Vera, N., Calderón-Domínguez, G., & Rodríguez-González, F. (2017). Prediction of the nanomechanical properties of apple tissue during its ripening process from its firmness, color and microstructural parameters. *Innovative Food Science and Emerging Technologies*, 39, 79–87. Available from <https://doi.org/10.1016/j.ifset.2016.11.004>.
- Dai, L., Zhang, J., & Cheng, F. (2019). Effects of starches from different botanical sources and modification methods on physicochemical properties of starch-based edible films. *International Journal of Biological Macromolecules*, 132, 897–905. Available from <https://doi.org/10.1016/j.ijbiomac.2019.03.197>.
- Ding, S. Y., Liu, Y. S., Zeng, Y., Himmel, M. E., Baker, J. O., & Bayer, E. A. (2012). How does plant cell wall nanoscale architecture correlate with enzymatic digestibility? *Science (New York, N.Y.)*, 338(6110), 1055–1060. Available from <https://doi.org/10.1126/science.1227491>.
- Duarte, A. L. A., do Rosário, D. K. A., Oliveira, S. B. S., de Souza, H. L. S., de Carvalho, R. V., Carneiro, J. C. S., ... Bernardes, P. C. (2018). Ultrasound improves antimicrobial effect of sodium dichloroisocyanurate to reduce Salmonella Typhimurium on purple cabbage. *International Journal of Food Microbiology*, 269, 12–18. Available from <https://doi.org/10.1016/j.ijfoodmicro.2018.01.007>.
- Farajpour, R., Emam Djomeh, Z., Moeini, S., Tavahkolipour, H., & Safayan, S. (2020). Structural and physico-mechanical properties of potato starch-olive oil edible films reinforced with zein nanoparticles. *International Journal of Biological Macromolecules*, 149, 941–950. Available from <https://doi.org/10.1016/j.ijbiomac.2020.01.175>.
- Farris, S., Schaich, K. M., Liu, L. S., Cooke, P. H., Piergiorganni, L., & Yam, K. L. (2011). Gelatin-pectin composite films from polyion-complex hydrogels. *Food Hydrocolloids*, 25(1), 61–70. Available from <https://doi.org/10.1016/j.foodhyd.2010.05.006>.
- Fishman, M. L., Chau, H. K., Qi, P. X., Hotchkiss, A. T., Garcia, R. A., & Cooke, P. H. (2015). Characterization of the global structure of low methoxyl pectin in solution. *Food Hydrocolloids*, 46, 153–159. Available from <https://doi.org/10.1016/j.foodhyd.2014.12.021>.
- Funami, T. (2010). Atomic force microscopy imaging of food polysaccharides. *Food Science and Technology Research*, 16(1), 1–12. Available from <https://doi.org/10.3136/str.16.1>.
- Gao, W., Wu, W., Liu, P., Hou, H., Li, X., & Cui, B. (2020). Preparation and evaluation of hydrophobic biodegradable films made from corn/octenylsuccinated starch incorporated with different concentrations of soybean oil. *International Journal of Biological Macromolecules*, 142, 376–383. Available from <https://doi.org/10.1016/j.ijbiomac.2019.09.108>.
- Gawkowska, D., Cieśla, J., Zdunek, A., & Cybulska, J. (2019). Cross-linking of diluted alkali-soluble pectin from apple (*Malus domestica* fruit) in different acid-base

- conditions. *Food Hydrocolloids*, 92, 285–292. Available from <https://doi.org/10.1016/j.foodhyd.2019.02.010>.
- Ghasemi, S., Jafari, S. M., Assadpour, E., & Khomeiri, M. (2017). Production of pectin-whey protein nano-complexes as carriers of orange peel oil. *Carbohydrate Polymers*, 177, 369–377. Available from <https://doi.org/10.1016/j.carbpol.2017.09.009>.
- Gilbert, J., Cheng, C. J., & Jones, O. G. (2018). Vapor barrier properties and mechanical behaviors of composite hydroxypropyl methylcellulose/zein nanoparticle films. *Food Biophysics*, 13(1), 25–36. Available from <https://doi.org/10.1007/s11483-017-9508-1>.
- Guo, X., Meng, H., Zhu, S., Zhang, T., & Yu, S. (2015). Purifying sugar beet pectins from non-pectic components by means of metal precipitation. *Food Hydrocolloids*, 51, 69–75. Available from <https://doi.org/10.1016/j.foodhyd.2015.05.009>.
- Guo, X., Zhao, W., Pang, X., Liao, X., Hu, X., & Wu, J. (2014). Emulsion stabilizing properties of pectins extracted by high hydrostatic pressure, high-speed shearing homogenization and traditional thermal methods: A comparative study. *Food Hydrocolloids*, 35, 217–225. Available from <https://doi.org/10.1016/j.foodhyd.2013.05.010>.
- Hedayati, S., Shahidi, F., Majzoobi, M., Koocheki, A., & Farahnaky, A. (2020). Structural, rheological, pasting and textural properties of granular cold water swelling maize starch: Effect of NaCl and CaCl<sub>2</sub>. *Carbohydrate Polymers*, 242, 116406. Available from <https://doi.org/10.1016/j.carbpol.2020.116406>.
- Hiasa, S., Kumagai, A., Endo, T., & Edashige, Y. (2016). Prevention of aggregation of pectin-containing cellulose nanofibers prepared from mandarin peel. *Journal of Fiber Science and Technology*, 17–26. Available from <https://doi.org/10.2115/fiberst.2016-0006>.
- Hosseini, S. F., Rezaei, M., Zandi, M., & Farahmandghavi, F. (2016). Development of bioactive fish gelatin/chitosan nanoparticles composite films with antimicrobial properties. *Food Chemistry*, 194, 1266–1274. Available from <https://doi.org/10.1016/j.foodchem.2015.09.004>.
- Huang, T., Tu, Z. c., Wang, H., Shangguan, X., Zhang, L., Zhang, Nh, & Bansal, N. (2017). Pectin and enzyme complex modified fish scales gelatin: Rheological behavior, gel properties and nanostructure. *Carbohydrate Polymers*, 156, 294–302. Available from <https://doi.org/10.1016/j.carbpol.2016.09.040>.
- Ishii, T., Matsunaga, T., Pellerin, P., O'Neill, M. A., Darvill, A., & Albersheim, P. (1999). The plant cell wall polysaccharide rhamnogalacturonan II self-assembles into a covalently cross-linked dimer. *Journal of Biological Chemistry*, 274(19), 13098–13104. Available from <https://doi.org/10.1074/jbc.274.19.13098>.
- Javidi, F., Razavi, S. M. A., & Mohammad Amini, A. (2019). Cornstarch nanocrystals as a potential fat replacer in reduced fat O/W emulsions: A rheological and physical study. *Food Hydrocolloids*, 90, 172–181. Available from <https://doi.org/10.1016/j.foodhyd.2018.12.003>.
- Khorasani, A. C., & Shojaosadati, S. A. (2017). Pectin-non-starch nanofibers biocomposites as novel gastrointestinal-resistant prebiotics. *International Journal of Biological Macromolecules*, 94, 131–144. Available from <https://doi.org/10.1016/j.ijbiomac.2016.10.011>.
- Kirby, A. R., MacDougall, A. J., & Morris, V. J. (2008). Atomic force microscopy of tomato and sugar beet pectin molecules. *Carbohydrate Polymers*, 71(4), 640–647. Available from <https://doi.org/10.1016/j.carbpol.2007.07.014>.
- Kocun, M., Grandbois, M., & Cuccia, L. A. (2011). Single molecule atomic force microscopy and force spectroscopy of chitosan. *Colloids and Surfaces B: Biointerfaces*, 82(2), 470–476. Available from <https://doi.org/10.1016/j.colsurfb.2010.10.004>.
- Kozioł, A., Cybulska, J., Pieczywek, P. M., & Zdunek, A. (2015). Evaluation of structure and assembly of xyloglucan from tamarind seed (*Tamarindus indica* L.) with atomic

- force microscopy. *Food Biophysics*, 10(4), 396–402. Available from <https://doi.org/10.1007/s11483-015-9395-2>.
- Koziół, A., Cybulska, J., Pieczywek, P. M., & Zdunek, A. (2017). Changes of pectin nanostructure and cell wall stiffness induced in vitro by pectinase. *Carbohydrate Polymers*, 161, 197–207. Available from <https://doi.org/10.1016/j.carbpol.2017.01.014>.
- Lai, S., Chen, F., Zhang, L., Yang, H., Deng, Y., & Yang, B. (2013). Nanostructural difference of water-soluble pectin and chelate-soluble pectin among ripening stages and cultivars of Chinese cherry. *Natural Product Research*, 27(4–5), 379–385. Available from <https://doi.org/10.1080/14786419.2012.696259>.
- Li, S., Li, J., Zhi, Z., Wei, C., Wang, W., Ding, T., . . . Chen, S. (2017). Macromolecular properties and hypolipidemic effects of four sulfated polysaccharides from sea cucumbers. *Carbohydrate Polymers*, 173, 330–337. Available from <https://doi.org/10.1016/j.carbpol.2017.05.063>.
- Li, Y., Zhang, L., Chen, F., Lai, S., & Yang, H. (2018). Effects of vacuum impregnation with calcium ascorbate and disodium stannous citrate on chinese red bayberry. *Food and Bioprocess Technology (Elmsford, N.Y.)*, 11(7), 1300–1316. Available from <https://doi.org/10.1007/s11947-018-2092-7>.
- Lin, J., Yu, S., Ai, C., Zhang, T., & Guo, X. (2020). Emulsion stability of sugar beet pectin increased by genipin crosslinking. *Food Hydrocolloids*, 101, 105459. Available from <https://doi.org/10.1016/j.foodhyd.2019.105459>.
- Lin, M., Deng, Y., Xiao, C., Liu, M., Zhu, L., Luo, W., & Yang, H. (2010). Influence of pure oxygen on nanostructure of water-soluble pectin in pear (*Pyrus bretschneideri* Rehd cv. Huangguan). *Philippine Agricultural Scientist*, 93(2), 190–197. Available from [http://www.pas-uplbcu.edu.ph/downloadPDF.php?file=008\\_Min.pdf](http://www.pas-uplbcu.edu.ph/downloadPDF.php?file=008_Min.pdf).
- Liu, H., Chen, F., Lai, S., Tao, J., Yang, H., & Jiao, Z. (2017). Effects of calcium treatment and low temperature storage on cell wall polysaccharide nanostructures and quality of postharvest apricot (*Prunus armeniaca*). *Food Chemistry*, 225, 87–97. Available from <https://doi.org/10.1016/j.foodchem.2017.01.008>.
- Liu, H., Chen, F., Yang, H., Yao, Y., Gong, X., Xin, Y., & Ding, C. (2009). Effect of calcium treatment on nanostructure of chelate-soluble pectin and physicochemical and textural properties of apricot fruits. *Food Research International*, 42(8), 1131–1140. Available from <https://doi.org/10.1016/j.foodres.2009.05.014>.
- Liu, J., Tan, J., Hua, X., Jiang, Z., Wang, M., Yang, R., & Cao, Y. (2020). Interfacial properties of ultrahigh methoxylated pectin. *International Journal of Biological Macromolecules*, 152, 403–410. Available from <https://doi.org/10.1016/j.ijbiomac.2020.02.264>.
- Liu, W., Hu, C., Liu, Y., Dai, S., Lu, W., lv, X., . . . Gao, X. (2017). Preparation, characterization, and  $\alpha$ -glycosidase inhibition activity of a carboxymethylated polysaccharide from the residue of *Sarcandra glabra* (Thunb.) Nakai. *International Journal of Biological Macromolecules*, 99, 454–464. Available from <https://doi.org/10.1016/j.ijbiomac.2017.02.065>.
- Magonov, S. N., & Reneker, D. H. (1997). Characterization of polymer surfaces with atomic force microscopy. *Annual Review of Materials Science*, 27(1), 175–222. Available from <https://doi.org/10.1146/annurev.matsci.27.1.175>.
- Mao, J., Zhang, L., Chen, F., Lai, S., Yang, B., & Yang, H. (2017). Effect of vacuum impregnation combined with calcium lactate on the firmness and polysaccharide morphology of kyoho grapes (*Vitis vinifera* x *V. labrusca*). *Food and Bioprocess Technology (Elmsford, N.Y.)*, 10(4), 699–709. Available from <https://doi.org/10.1007/s11947-016-1852-5>.
- McIntire, T. M., & Brant, D. A. (1999). Imaging of carrageenan macrocycles and amylose using noncontact atomic force microscopy. In *International Journal of Biological*

- Macromolecules*, 26(4), 303–310. Available from [https://doi.org/10.1016/S0141-8130\(99\)00097-5](https://doi.org/10.1016/S0141-8130(99)00097-5).
- Mohnen, D. (2008). Pectin structure and biosynthesis. *Current Opinion in Plant Biology*, 11(3), 266–277. Available from <https://doi.org/10.1016/j.pbi.2008.03.006>.
- Nagalakshmaiah, M., kissi, N. E., Mortha, G., & Dufresne, A. (2016). Structural investigation of cellulose nanocrystals extracted from chili leftover and their reinforcement in cariflex-IR rubber latex. *Carbohydrate Polymers*, 136, 945–954. Available from <https://doi.org/10.1016/j.carbpol.2015.09.096>.
- Niimura, H., Yokoyama, T., Kimura, S., Matsumoto, Y., & Kuga, S. (2010). AFM observation of ultrathin microfibrils in fruit tissues. *Cellulose*, 17(1), 13–18. Available from <https://doi.org/10.1007/s10570-009-9361-6>.
- Ocloo, F. C. K., Ray, S. S., & Emmambux, N. M. (2019). Effects of stearic acid and irradiation alone and in combination on properties of amylose-lipid nanomaterial from high amylose maize starch. *Carbohydrate Polymers*, 212, 352–360. Available from <https://doi.org/10.1016/j.carbpol.2019.02.065>.
- Paniagua, C., Kirby, A. R., Gunning, A. P., Morris, V. J., Matas, A. J., Quesada, M. A., & Mercado, J. A. (2017). Unravelling the nanostructure of strawberry fruit pectins by endo-polygalacturonase digestion and atomic force microscopy. *Food Chemistry*, 224, 270–279. Available from <https://doi.org/10.1016/j.foodchem.2016.12.049>.
- Paniagua, C., Posé, S., Morris, V. J., Kirby, A. R., Quesada, M. A., & Mercado, J. A. (2014). Fruit softening and pectin disassembly: An overview of nanostructural pectin modifications assessed by atomic force microscopy. *Annals of Botany*, 114(6), 1375–1383. Available from <https://doi.org/10.1093/aob/mcu149>.
- Peroni-Okita, F. H. G., Gunning, A. P., Kirby, A., Simão, R. A., Soares, C. A., & Cordenunsi, B. R. (2015). Visualization of internal structure of banana starch granule through AFM. *Carbohydrate Polymers*, 128, 32–40. Available from <https://doi.org/10.1016/j.carbpol.2015.04.019>.
- Pieczywek, P. M., Koziół, A., Konopacka, D., Cybulska, J., & Zdunek, A. (2017). Changes in cell wall stiffness and microstructure in ultrasonically treated apple. *Journal of Food Engineering*, 197, 1–8. Available from <https://doi.org/10.1016/j.jfoodeng.2016.10.028>.
- Pieczywek, P. M., Koziół, A., Płaziński, W., Cybulska, J., & Zdunek, A. (2020). Resolving the nanostructure of sodium carbonate extracted pectins (DASP) from apple cell walls with atomic force microscopy and molecular dynamics. *Food Hydrocolloids*, 104, 105726. Available from <https://doi.org/10.1016/j.foodhyd.2020.105726>.
- Posé, S., Paniagua, C., Matas, A. J., Gunning, A. P., Morris, V. J., Quesada, M. A., & Mercado, J. A. (2019). A nanostructural view of the cell wall disassembly process during fruit ripening and postharvest storage by atomic force microscopy. *Trends in Food Science and Technology*, 87, 47–58. Available from <https://doi.org/10.1016/j.tifs.2018.02.011>.
- Radziejewska-Kubzdela, E., Biegańska-Marecik, R., & Kidoń, M. (2014). Applicability of vacuum impregnation to modify physico-chemical, sensory and nutritive characteristics of plant origin products—A review. *International Journal of Molecular Sciences*, 15(9), 16577–16610. Available from <https://doi.org/10.3390/ijms150916577>.
- Ren, Z., Li, Z., Chen, Z., Zhang, Y., Lin, X., Wang, W., ... Li, B. (2021). Characteristics and application of fish oil-in-water pickering emulsions structured with tea water-insoluble proteins/ $\kappa$ -carrageenan complexes. *Food Hydrocolloids*, 114, 106562. Available from <https://doi.org/10.1016/j.foodhyd.2020.106562>.
- Ridout, M. J., Gunning, A. P., Parker, M. L., Wilson, R. H., & Morris, V. J. (2002). Using AFM to image the internal structure of starch granules. *Carbohydrate Polymers*, 50(2), 123–132. Available from [https://doi.org/10.1016/S0144-8617\(02\)00021-8](https://doi.org/10.1016/S0144-8617(02)00021-8).
- Ridout, M. J., Parker, M. L., Hedley, C. L., Bogracheva, T. Y., & Morris, V. J. (2003). Atomic force microscopy of pea starch granules: Granule architecture of wild-type

- parent, r and rb single mutants, and the rrb double mutant. *Carbohydrate Research*, 338 (20), 2135–2147. Available from [https://doi.org/10.1016/S0008-6215\(03\)00309-4](https://doi.org/10.1016/S0008-6215(03)00309-4).
- Singh, S., Nwabor, O. F., Ontong, J. C., Kaewnopparat, N., & Voravuthikunchai, S. P. (2020). Characterization of a novel, co-processed bio-based polymer, and its effect on mucoadhesive strength. *International Journal of Biological Macromolecules*, 145, 865–875. Available from <https://doi.org/10.1016/j.ijbiomac.2019.11.198>.
- Sletmoen, M., Maurstad, G., Sikorski, P., Paulsen, B. S., & Stokke, B. T. (2003). Characterisation of bacterial polysaccharides: Steps towards single-molecular studies. *Carbohydrate Research*, 338(23), 2459–2475. Available from <https://doi.org/10.1016/j.carres.2003.07.007>.
- Sow, L. C., Nicole Chong, J. M., Liao, Q. X., & Yang, H. (2018). Effects of  $\kappa$ -carrageenan on the structure and rheological properties of fish gelatin. *Journal of Food Engineering*, 239, 92–103. Available from <https://doi.org/10.1016/j.jfoodeng.2018.05.035>.
- Sujka, M., & Jamroz, J. (2009).  $\alpha$ -Amylolysis of native potato and corn starches – SEM, AFM, nitrogen and iodine sorption investigations. *LWT - Food Science and Technology*, 42(7), 1219–1224. Available from <https://doi.org/10.1016/j.lwt.2009.01.016>.
- Szymańska-Chargot, M., Chylińska, M., Cybulska, J., Koziol, A., Pieczywek, P. M., & Zdunek, A. (2017). Simultaneous influence of pectin and xyloglucan on structure and mechanical properties of bacterial cellulose composites. *Carbohydrate Polymers*, 174, 970–979. Available from <https://doi.org/10.1016/j.carbpol.2017.07.004>.
- Szymańska-Chargot, M., Chylińska, M., Gdula, K., Koziol, A., & Zdunek, A. (2017). Isolation and characterization of cellulose from different fruit and vegetable pomaces. *Polymers*, 9(10), 495. Available from <https://doi.org/10.3390/polym9100495>.
- Tappi, S., Tylewicz, U., Romani, S., Siroli, L., Patignani, F., Dalla Rosa, M., & Rocculi, P. (2016). Optimization of vacuum impregnation with calcium lactate of minimally processed melon and shelf-life study in real storage conditions. *Journal of Food Science*, 81(11), E2734–E2742. Available from <https://doi.org/10.1111/1750-3841.13513>.
- Tavallaie, S., Khomeiri, M., Mousivand, M., Maghsoudlou, Y., & Hashemi, M. (2019). Starches from different sources hydrolysis using a new thermo-tolerant amylase complex produced by *Bacillus subtilis* T41a: Characterization and efficiency evaluation. *LWT*, 112, 108218. Available from <https://doi.org/10.1016/j.lwt.2019.05.116>.
- Teckentrup, J., Al-Hammood, O., Steffens, T., Bednarz, H., Walhorn, V., Niehaus, K., & Anselmetti, D. (2017). Comparative analysis of different xanthan samples by atomic force microscopy. *Journal of Biotechnology*, 257, 2–8. Available from <https://doi.org/10.1016/j.jbiotec.2016.11.032>.
- Venkateshaiah, A., Padil, V. V. T., Nagalakshmaiah, M., Waclawek, S., Černík, M., & Varma, R. S. (2020). Microscopic techniques for the analysis of micro and nanostructures of biopolymers and their derivatives. *Polymers*, 12(3). Available from <https://doi.org/10.3390/polym12030512>.
- Vincken, J. P., Schols, H. A., Oomen, R. J. F. J., McCann, M. C., Ulvskov, P., Voragen, A. G. J., & Visser, R. G. F. (2003). If homogalacturonan were a side chain of rhamnogalacturonan I. Implications for cell wall architecture. *Plant Physiology*, 132(4), 1781–1789. Available from <https://doi.org/10.1104/pp.103.022350>.
- Wang, H., Chen, F., Yang, H., Chen, Y., Zhang, L., & An, H. (2012). Effects of ripening stage and cultivar on physicochemical properties and pectin nanostructures of jujubes. *Carbohydrate Polymers*, 89(4), 1180–1188. Available from <https://doi.org/10.1016/j.carbpol.2012.03.092>.
- Wang, H., Fei, S., Wang, Y., Zan, L., & Zhu, J. (2020). Comparative study on the self-assembly of pectin and alginate molecules regulated by calcium ions investigated by atomic force microscopy. *Carbohydrate Polymers*, 231, 115673. Available from <https://doi.org/10.1016/j.carbpol.2019.115673>.

- Wang, L., Xiang, D., Li, C., Zhang, W., & Bai, X. (2021). Effects of lyophilization and low-temperature treatment on the properties and conformation of xanthan gum. *Food Hydrocolloids*, *112*, 106352. Available from <https://doi.org/10.1016/j.foodhyd.2020.106352>.
- Wen, Y., Xu, Z., Liu, Y., Corke, H., & Sui, Z. (2020). Investigation of food microstructure and texture using atomic force microscopy: A review. *Comprehensive Reviews in Food Science and Food Safety*, *19*(5), 2357–2379. Available from <https://doi.org/10.1111/1541-4337.12605>.
- Willats, W. G. T., Knox, J. P., & Mikkelsen, J. D. (2006). Pectin: New insights into an old polymer are starting to gel. *Trends in Food Science and Technology*, *17*(3), 97–104. Available from <https://doi.org/10.1016/j.tifs.2005.10.008>.
- Willats, W. G. T., McCartney, L., Mackie, W., & Knox, J. P. (2001). Pectin: Cell biology and prospects for functional analysis. *Plant Molecular Biology*, *47*(1–2), 9–27. Available from <https://doi.org/10.1023/A:1010662911148>.
- Xin, Y., Chen, F., Yang, H., Zhang, P., Deng, Y., & Yang, B. (2010). Morphology, profile and role of chelate-soluble pectin on tomato properties during ripening. *Food Chemistry*, *121*(2), 372–380. Available from <https://doi.org/10.1016/j.foodchem.2009.12.038>.
- Xin, Y., Jin, Z., Chen, F., Lai, S., & Yang, H. (2020). Effect of chitosan coatings on the evolution of sodium carbonate-soluble pectin during sweet cherry softening under non-isothermal conditions. *International Journal of Biological Macromolecules*, *154*, 267–275. Available from <https://doi.org/10.1016/j.ijbiomac.2020.03.104>.
- Yang, D., & Yang, H. (2020). The temperature dependent extraction of polysaccharides from eucheuma and the rheological synergistic effect in their mixtures with kappa carrageenan. *LWT*, *129*, 109515. Available from <https://doi.org/10.1016/j.lwt.2020.109515>.
- Yang, H., An, H., Feng, G., & Li, Y. (2005). Visualization and quantitative roughness analysis of peach skin by atomic force microscopy under storage. *LWT – Food Science and Technology*, *38*(6), 571–577. Available from <https://doi.org/10.1016/j.lwt.2004.09.007>.
- Yang, H., An, H., Feng, G., Li, Y., & Lai, S. (2005). Atomic force microscopy of the water-soluble pectin of peaches during storage. *European Food Research and Technology*, *220*(5–6), 587–591. Available from <https://doi.org/10.1007/s00217-004-1102-3>.
- Yang, H., Chen, F., An, H., & Lai, S. (2009). Comparative studies on nanostructures of three kinds of pectins in two peach cultivars using atomic force microscopy. *Postharvest Biology and Technology*, *51*(3), 391–398. Available from <https://doi.org/10.1016/j.postharvbio.2008.08.009>.
- Yang, H., Lai, S., An, H., & Li, Y. (2006). Atomic force microscopy study of the ultrastructural changes of chelate-soluble pectin in peaches under controlled atmosphere storage. *Postharvest Biology and Technology*, *39*(1), 75–83. Available from <https://doi.org/10.1016/j.postharvbio.2005.08.001>.
- Yang, H., Wu, Q., Ng, L. Y., & Wang, S. (2017). Effects of vacuum impregnation with calcium lactate and pectin methyltransferase on quality attributes and chelate-soluble pectin morphology of fresh-cut papayas. *Food and Bioprocess Technology (Elmsford, N. Y.)*, *10*(5), 901–913. Available from <https://doi.org/10.1007/s11947-017-1874-7>.
- Yang, H. S., Feng, G. P., An, H. J., & Li, Y. F. (2006). Microstructure changes of sodium carbonate-soluble pectin of peach by AFM during controlled atmosphere storage. *Food Chemistry*, *94*(2), 179–192. Available from <https://doi.org/10.1016/j.foodchem.2004.11.003>.
- Yang, L., & Zhang, L. M. (2009). Chemical structural and chain conformational characterization of some bioactive polysaccharides isolated from natural sources. *Carbohydrate Polymers*, *76*(3), 349–361. Available from <https://doi.org/10.1016/j.carbpol.2008.12.015>.

- Yang, Z., Xu, X., Singh, R., de Campo, L., Gilbert, E. P., Wu, Z., & Hemar, Y. (2019). Effect of amyloglucosidase hydrolysis on the multi-scale supramolecular structure of corn starch. *Carbohydrate Polymers*, 212, 40–50. Available from <https://doi.org/10.1016/j.carbpol.2019.02.028>.
- Ye, J., Hua, X., Zhao, Q., Zhao, W., Chu, G., Zhang, W., & Yang, R. (2020). Chain conformation and rheological properties of an acid-extracted polysaccharide from peanut sediment of aqueous extraction process. *Carbohydrate Polymers*, 228, 115410. Available from <https://doi.org/10.1016/j.carbpol.2019.115410>.
- Yusof, N. L., Wadsö, L., Rasmusson, A. G., & Gómez Galindo, F. (2017). Influence of vacuum impregnation with different substances on the metabolic heat production and sugar metabolism of spinach leaves. *Food and Bioprocess Technology*, 10(10), 1907–1917. Available from <https://doi.org/10.1007/s11947-017-1959-3>.
- Zdunek, A., Koziół, A., Cybulska, J., Lekka, M., & Pieczywek, P. M. (2016). The stiffening of the cell walls observed during physiological softening of pears. *Planta*, 243(2), 519–529. Available from <https://doi.org/10.1007/s00425-015-2423-0>.
- Zdunek, A., Koziół, A., Pieczywek, P. M., & Cybulska, J. (2014). Evaluation of the nanostructure of pectin, hemicellulose and cellulose in the cell walls of pears of different texture and firmness. *Food and Bioprocess Technology (Elmsford, N.Y.)*, 7(12), 3525–3535. Available from <https://doi.org/10.1007/s11947-014-1365-z>.
- Zhang, H., Chen, J., Li, J., Yan, L., Li, S., Ye, X., ... Chen, S. (2018). Extraction and characterization of RG-I enriched pectic polysaccharides from mandarin citrus peel. *Food Hydrocolloids*, 79, 579–586. Available from <https://doi.org/10.1016/j.foodhyd.2017.12.002>.
- Zhang, J., Cui, J., Xiao, L., & Wang, Z. (2014). The combination of atomic force microscopy and sugar analysis to evaluate alkali-soluble *Canna edulis* Ker pectin. *Food Chemistry*, 156, 64–71. Available from <https://doi.org/10.1016/j.foodchem.2014.01.096>.
- Zhang, L., Chen, F., An, H., Yang, H., Sun, X., Guo, X., & Li, L. (2008). Physicochemical properties, firmness, and nanostructures of sodium carbonate-soluble pectin of 2 chinese cherry cultivars at 2 ripening stages. *Journal of Food Science*, 73(6), N17–N22. Available from <https://doi.org/10.1111/j.1750-3841.2008.00799.x>.
- Zhang, L., Chen, F., Lai, S., Wang, H., & Yang, H. (2018). Impact of soybean protein isolate-chitosan edible coating on the softening of apricot fruit during storage. *LWT*, 96, 604–611. Available from <https://doi.org/10.1016/j.lwt.2018.06.011>.
- Zhang, L., Chen, F., Yang, H., Sun, X., Liu, H., Gong, X., ... Ding, C. (2010). Changes in firmness, pectin content and nanostructure of two crisp peach cultivars after storage. *LWT - Food Science and Technology*, 43(1), 26–32. Available from <https://doi.org/10.1016/j.lwt.2009.06.015>.
- Zhang, L., Chen, F., Yang, H., Ye, X., Sun, X., Liu, D., ... Deng, Y. (2012). Effects of temperature and cultivar on nanostructural changes of water-soluble pectin and chelate-soluble pectin in peaches. *Carbohydrate Polymers*, 87(1), 816–821. Available from <https://doi.org/10.1016/j.carbpol.2011.08.074>.
- Zhang, L., Chen, F., Zhang, P., Lai, S., & Yang, H. (2017). Influence of rice bran wax coating on the physicochemical properties and pectin nanostructure of cherry tomatoes. *Food and Bioprocess Technology (Elmsford, N.Y.)*, 10(2), 349–357. Available from <https://doi.org/10.1007/s11947-016-1820-0>.
- Zhang, L., Wang, P., Chen, F., Lai, S., Yu, H., & Yang, H. (2019). Effects of calcium and pectin methylesterase on quality attributes and pectin morphology of jujube fruit under vacuum impregnation during storage. *Food Chemistry*, 289, 40–48. Available from <https://doi.org/10.1016/j.foodchem.2019.03.008>.
- Zhang, L., Wang, P., Sun, X., Chen, F., Lai, S., & Yang, H. (2020). Calcium permeation property and firmness change of cherry tomatoes under ultrasound combined with

- calcium lactate treatment. *Ultrasonics Sonochemistry*, 60, 104784. Available from <https://doi.org/10.1016/j.ultsonch.2019.104784>.
- Zhang, L., Ye, X., Xue, S. J., Zhang, X., Liu, D., Meng, R., & Chen, S. (2013). Effect of high-intensity ultrasound on the physicochemical properties and nanostructure of citrus pectin. *Journal of the Science of Food and Agriculture*, 93(8), 2028–2036. Available from <https://doi.org/10.1002/jsfa.6011>.
- Zhang, L., Zhang, X., Liu, D., Ding, T., & Ye, X. (2015). *Effect of degradation methods on the structural properties of citrus pectin*. *LWT - Food Science and Technology*, 61(2), 630–637. Available from <https://doi.org/10.1016/j.lwt.2014.11.002>.
- Zhang, L., Zhao, S., Lai, S., Chen, F., & Yang, H. (2018). Combined effects of ultrasound and calcium on the chelate-soluble pectin and quality of strawberries during storage. *Carbohydrate Polymers*, 200, 427–435. Available from <https://doi.org/10.1016/j.carbpol.2018.08.013>.
- Zhang, T., Zheng, Y., & Cosgrove, D. J. (2016). Spatial organization of cellulose microfibrils and matrix polysaccharides in primary plant cell walls as imaged by multichannel atomic force microscopy. *Plant Journal*, 85(2), 179–192. Available from <https://doi.org/10.1111/tpj.13102>.
- Zhang, W., Fan, X., Gu, X., Gong, S., Wu, J., Wang, Z., ... Wang, S. (2020). Emulsifying properties of pectic polysaccharides obtained by sequential extraction from black tomato pomace. *Food Hydrocolloids*, 100, 105454. Available from <https://doi.org/10.1016/j.foodhyd.2019.105454>.
- Zhang, X., Lin, J., Pi, F., Zhang, T., Ai, C., & Yu, S. (2020). Rheological characterization of RG-I chicory root pectin extracted by hot alkali and chelators. *International Journal of Biological Macromolecules*, 164, 759–770. Available from <https://doi.org/10.1016/j.ijbiomac.2020.07.020>.
- Zhi, H., Liu, Q., Xu, J., Dong, Y., Liu, M., & Zong, W. (2017). Ultrasound enhances calcium absorption of jujube fruit by regulating the cellular calcium distribution and metabolism of cell wall polysaccharides. *Journal of the Science of Food and Agriculture*, 97(15), 5202–5210. Available from <https://doi.org/10.1002/jsfa.8402>.
- Zlatanova, J., & van Holde, K. (2006). Single-molecule biology: What is it and how does it work? *Molecular Cell*, 24(3), 317–329. Available from <https://doi.org/10.1016/j.molcel.2006.10.017>.
- Zlatanova, J., & Leuba, S. H. (2002). Stretching and imaging single DNA molecules and chromatin. *Journal of Muscle Research and Cell Motility*, 23(5–6), 377–395. Available from <https://doi.org/10.1023/A:1023498120458>.

## Further reading

- Liu, D., & Cheng, F. (2011). Advances in research on structural characterisation of agricultural products using atomic force microscopy. *Journal of the Science of Food and Agriculture*, 91(5), 783–788. Available from <https://doi.org/10.1002/jsfa.4284>.



This page intentionally left blank

## CHAPTER 6

# Application of atomic force microscopy in food microorganism research

Lin Zhao<sup>1,2</sup> and Hongshun Yang<sup>1,2</sup>

<sup>1</sup>Department of Food Science and Technology, National University of Singapore, Singapore, Singapore

<sup>2</sup>National University of Singapore (Suzhou) Research Institute, Suzhou Industrial Park, Suzhou, Jiangsu, P. R. China

### 6.1 Introduction

Foodborne disease has become a major public health challenge worldwide, causing suffering to patients and bringing considerable financial burden to society. Many foods are vulnerable to be spoiled or contaminated by disease-causing microbes or pathogens, due to environmental contamination or improper handling occurring at any point in food production, processing, delivery, and consumption (Heaton & Jones, 2008). According to the 2017 annual report released by Centre for Disease Control and Prevention (CDC), 841 cases of foodborne disease outbreaks were reported in the US, most of which could be attributed to norovirus infection, followed by *Salmonella*, Shiga toxin-producing *Escherichia coli*, and *Clostridium perfringens* successively (“Surveillance for Foodborne Disease Outbreaks, 2019”). Therefore, understanding the characteristics of microorganisms in different species, states, and environmental conditions is of great significance for the prevention of foodborne disease outbreaks, among which the study of microbial surface properties could be one crucial part.

While microorganisms can alter their surface structure or cell profile as a survival mechanism under adverse environments, little is known about their cell surface dynamics with respect to the cellular interactions or the interactions with environment at the nanoscale, due to their small sizes (Araújo, Viana, Gómez, Pontes, & Frases, 2019). However, atomic force microscopy (AFM) can be used as an examination tool to monitor real-time microbiological systems, by providing high nanoscale resolution nondestructively in both air and fluid environments, which cannot be achieved by light microscopy (LM) or transmission/scanning electron microscopy (TEM/SEM) (Yang

et al., 2007). The disadvantages of LM, TEM, and SEM in the study of microbial systems (e.g., pretreatment needed, only 2D images obtained, samples in nonnative status, etc.) can be overcome by AFM, as the latter can provide different views of the sample and unique insights into the microbial surface structure by atomic-scale imaging after minimal sample preparation (Braga & Ricci, 2004). The advantages and disadvantages of AFM, LM, TEM, SEM, and CLSM are compared and summarized in Table 6.1. Moreover, AFM is not only a surface imaging tool, considering its force measurement capability offering further details on the interactions and mechanical properties of macromolecules at microbial surfaces, which can extend the AFM application in the characterization of microbial surface function.

Besides studying “bad” bacteria that can cause serious diseases and food poisoning, “good” bacteria with benefits to human body are also worth studying, and their surface protein layers are thought to play key roles in cell–host interactions (De Sa Peixoto et al., 2015). This chapter summarizes recent studies on the applications of AFM in food microorganisms at different scales: from single cells to the biofilms, from foodborne pathogens to beneficial bacteria, from prokaryotic microorganisms to eukaryotic microorganisms and viruses, characterizing their surface properties and illustrating the molecular interactions in relation to the microbial adhesion or aggregation by probing their surface structures and other physical properties. The current trend of combining AFM and other complementary techniques is also introduced briefly, exploring more possibilities of AFM application in the field of food microorganism.

## 6.2 Single microbial cell studies

### 6.2.1 Morphological change evaluation

Atomic force microscopy provides new opportunities to analyze single microorganism cells qualitatively and quantitatively after antimicrobial treatments, which was almost impossible before as conventional methods mainly focused on large numbers of cells. Some researchers used it to compare the nanostructures of *E. coli* and *Listeria innocua* to investigate the cell morphological and dimensional changes after acidic electrolysed water (AEW) and levulinic acid (LA) treatments, respectively (Fig. 6.1) (Zhao, Zhao, Phey, & Yang, 2019). AFM images indicated that the surfaces of both bacteria were wrinkled and became irregular after being treated by LA alone and LA combined with AEW, accompanied by the leakage of intracellular contents as some small substances were observed around the cells, which could be the aggregation of the cytoplasmic components due

**Table 6.1** Comparison of the advantages and disadvantages of different microscopy techniques.

Characteristics	Microscopy <sup>a</sup> AFM	LM	SEM	TEM	CLSM
Advantages	High resolution; nanoscale; minimal sample preparation; near-native status; 2D and 3D; in air/liquid; in-situ, continuous process; can be manipulated	Large scan area; fast scan speed; economical	High resolution; nanoscale; fast scan speed	High resolution; nanoscale; fast scan speed	Study dynamic process; fast scan speed; 2D and 3D; in situ
Disadvantages	Small scan size; slower scan speed; difficult for soft material	Only 2D; needs pretreatment; low resolution and magnification	Only 2D; needs pretreatment; nonnative status	Only 2D; needs pretreatment; nonnative status	Complicated operation; needs pretreatment

<sup>a</sup>AFM, atomic force microscopy; LM, light microscopy; SEM, scanning electron microscopy; TEM, transmission electron microscopy; CLSM, confocal light scanning microscopy; 2D, two dimensional; 3D, three dimensional.

Source: Reprinted with permission from John Wiley and Sons, Inc. (Yang, H., Wang, Y., Lai, S., An, H., Li, Y., & Chen, F. (2007). Application of atomic force microscopy as a nanotechnology tool in food science. *Journal of Food Science*, 72(4), R65–R75).

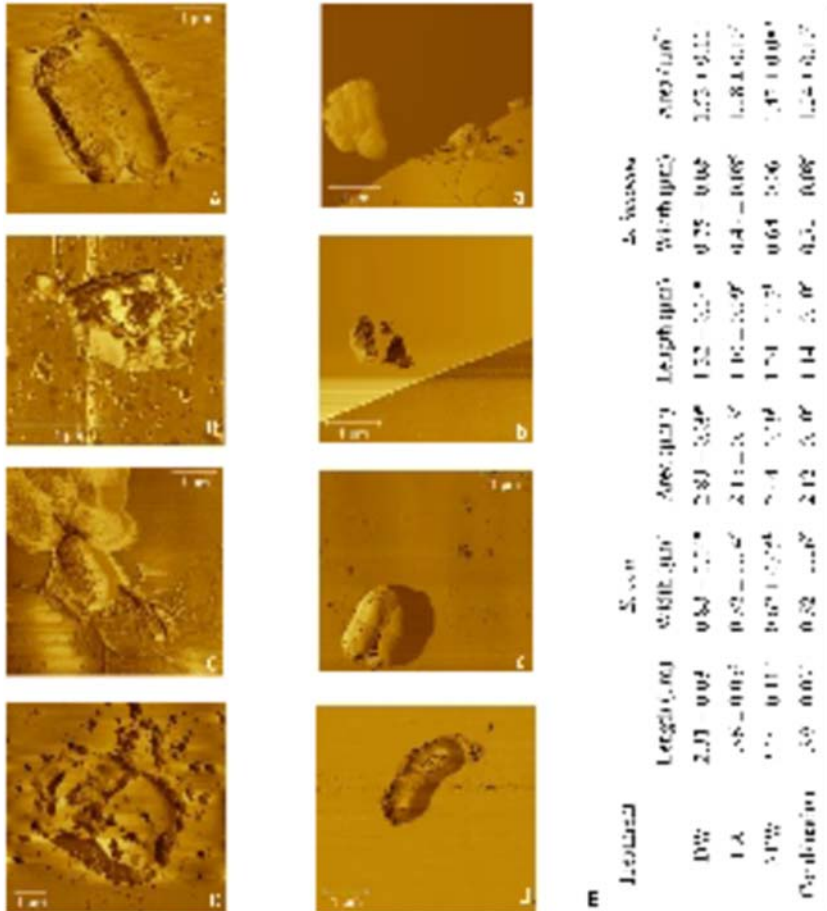


**Figure 6.1** Atomic force microscopy (AFM) images of *Escherichia coli* (A–D) and *Listeria innocua* (a–d) cells after DW (A, a), LA (B, b), AEW (C, c) and combination (D, d) treatments. Effects of different treatments on the quantification of their dimension (E). Note: DW, deionized water; LA, levulinic acid; AEW, acidic electrolysed water; Combination: AEW + LA. Different letters represent significant differences between different treatments with the same parameter ( $P < .05$ ). All subgraphs are reproduced with permission from Elsevier (From Zhao, L., Zhao, M. Y., Phey, C. P., & Yang, H. (2019). Efficacy of low concentration acidic electrolysed water and levulinic acid combination on fresh organic lettuce (*Lactuca sativa* Var. *Crispa* L.) and its antimicrobial mechanism. *Food Control*, 101, 241–250. <https://doi.org/10.1016/j.foodcont.2019.02.039>).

to the change of cell membrane permeability. Besides, the quantitative changes, including changes in length, width, and area of the cells obtained from hundreds of AFM parallel images, also supported the above analysis as the leakage of cytoplasm could cause smaller cellular sizes (Fig. 6.1E). Moreover, AFM could also be used to investigate the morphological

changes of *L. monocytogenes* after being treated by nisin and grape seed extract (Zhao, Chen, Zhao, He, & Yang, 2020). Coarse and irregular cell surface and deformed cell structure were observed in the samples under this combined treatment, following decreased width and height and increased surface roughness compared to the untreated cells. Another study revealed the morphological changes of pathogenic and nonpathogenic *E. coli* after mild heat and lactic acid treatment, respectively (Chen et al., 2022). Under AFM examination, although both types of *E. coli* became inflated and had smoother surface, pathogenic *E. coli* had higher cell surface roughness after being treated with lactic acid alone or combined with mild heat treatments compared to its counterpart, demonstrating less extent of membrane disruption of pathogenic strain.

### 6.2.2 Antimicrobial mechanism evaluation

Due to its high resolution and sensitivity, AFM is a promising approach to help unravel the bactericidal mechanisms of different antimicrobial agents on different microbial species. One study demonstrated that (-)-epigallocatechin-3-gallate (EGCG), a main component of tea catechins, inhibited the growth of Gram-positive and -negative bacteria in different modes: EGCG damaged the cell wall of Gram-positive cells by binding to their peptidoglycan layers, leading to the shrinkage of cell envelope and the rupture of cells. However, the profile changes of Gram-negative bacterial cell walls could be attributed to the H<sub>2</sub>O<sub>2</sub> generated by EGCG, which caused membrane degradation as pore-like lesions were observed in AFM images (Cui et al., 2012). Another study used *E. coli* (Gram-negative bacteria representative), *Staphylococcus xylosus* (Gram-positive bacteria representative), and *Zygosaccharomyces bailii* (food-spoilage yeast representative) as models to investigate the interactions between monocaprylate and cell membranes. The differences of membrane fluidity and phospholipid composition among different species of microorganisms played an important role in their susceptibility to monocaprylate, which only integrated into the liquid disordered lipid phase of the membrane as visualized by AFM imaging (Hyldgaard, Sutherland, Sundh, Mygind, & Meyer, 2012). Moreover, some researchers found that the *E. coli* surface was significantly remodeled after 2,4-dichlorophenoxyacetic acid (2,4-D) treatment under AFM examination, with increased surface roughness and altered envelope integrity, indicating 2,4-D cannot only enter the cell leading to oxidative damage but also interact with surface macromolecules directly (Bhat et al., 2015). The studies mentioned above and others related to the surface structure imaging are summarized in Table 6.2.

**Table 6.2** Atomic force microscopy imaging for different food microorganisms.

Food microorganism	Operation mode	Sample carrier and imaging environment	Treatment on cells	Observations	References
<i>Candida albicans</i>	Tapping	Glass substrate, air	Lemon grass oil and its vapor	Variable roughness and height; 3D morphological changes	Tyagi and Malik (2010)
<i>Escherichia coli</i> ; <i>Staphylococcus aureus</i>	Tapping	Glass coverslip, air	EGCG and H <sub>2</sub> O <sub>2</sub>	Perforations or grooves in the cell envelopes; cell lysis; damage to the cell walls	Cui et al. (2012)
<i>E. coli</i> ; <i>Staphylococcus xylosum</i> ; <i>Zygosaccharomyces bailii</i>	Intermittent contact	Cell-TAK-coated coverslip, air	Monocaprylate	Indentations and membrane disruption; rougher surface	Hyldgaard et al. (2012)
<i>E. coli</i>	Contact	Fixation coverslip, air	2,4-dichlorophenoxyacetic acid	Increase in surface roughness and negative charge; loss of envelope integrity	Bhat et al. (2015)
<i>Aspergillus oryzae</i>	Contact	Isopore polycarbonate membrane, liquid	–	Different surface morphology and macromolecular interactions during spore germination	Van der Aa, Asther, and Dufrière (2002)

<i>E. coli</i> ; <i>Pichia pastoris</i> ; <i>Aureobasidium pullulans</i> <i>Lactobacillus crispatus</i>	Tapping	Stainless steel coupon, air	Low concentration neutralized electrolysed water and ultrasound combination	Disordered cellular structure and irregular surface with breaches in the wall	Zhao, Zhang, and Yang (2017)
	Contact	Poly-L-lysine covered glass slide, liquid	–	Variety in surface properties among different strains; elasticity and force maps	Schaer-Zammaretti and Ubbink (2003)
<i>E. coli</i> ; <i>Salmonella typhimurium</i>	Noncontact	Mica sheet, air	Low concentration electrolysed water combined with short-time heat	Cell shrinkage; breakage of flagella and some indentations; visible lesions and impaired membrane structure	Liu, Jin, Feng, Yang, and Fu (2019)
<i>E. coli</i>	Tapping	Stainless steel coupon, air	Electrolysed water, H <sub>2</sub> O <sub>2</sub> and citric acid	Shrunk and fracture; decreased length, width and height	Zhang and Yang (2017)
<i>Rhodococcus ruber</i> ; <i>Rhodococcus opacus</i> ; <i>Micrococcus luteus</i> ; <i>E. coli</i> ; <i>Pseudomonas fluorescens</i>	Tapping	Glass coverslip, air	<i>n</i> -decane, cyclohexane, toluene, butanol and acetonitrile	Changes in size, surface/volume ratio and surface roughness	Kuyukina, Ivshina, Korshunova, and Rubtsova (2014)

(Continued)



**Table 6.2** (Continued)

<b>Food microorganism</b>	<b>Operation mode</b>	<b>Sample carrier and imaging environment</b>	<b>Treatment on cells</b>	<b>Observations</b>	<b>References</b>
<i>Listera innocua</i>	Tapping	Mica sheet, air	Sodium hypochlorite and lactic acid combination	Irregular cell body; lower cell width and height; higher root-mean-square (RMS) roughness	Chen et al. (2019)
<i>E. coli</i>	Tapping	Mica sheet, air	Lactic acid	Increased cell width; decreased height and surface roughness; the morphology of pathogenic strain maintained better than nonpathogenic strain	Chen et al. (2020)
<i>Listera innocua</i>	Tapping	Mica sheet, air	Electrolysed water generated by adding NaHCO <sub>3</sub> before/after electrolysis	Irregular and shrunken cell surface; decreased width and height	He, Zhao, Chen, Zhao, and Yang (2021)

In addition to the big contribution AFM makes to dynamic topographical characterization of microbial surfaces after different treatments, AFM investigation of microbial biofilms is also a vital part in the study of microbial systems, helping to identify the structural details at different stages of biofilm formation and determine the external effects on biofilm adhesiveness (Wright, Shah, Powell, & Armstrong, 2010), which is introduced in the following section.

## 6.3 Microbial biofilm studies

### 6.3.1 Biofilm morphological imaging

AFM is a useful tool to study the formation and adhesion of biofilms. Studies show that microorganisms can form biofilms on different biotic surfaces (food surfaces) as well as abiotic ones (food contact surfaces) as their survival strategy during food processing, and remain in adhesion despite short exposure time, posing a threat to food safety and human health (Papaioannou, Giaouris, Berillis, & Boziaris, 2018). Biofilm can be defined as a community of microbial cells embedded within extracellular polymeric substance (EPS) composed of a mixture of compounds like nucleic acids, polysaccharides, proteins, and lipids (Park et al., 2012). Once the bacteria are attached to the surface and form biofilms, they will exhibit far more tolerance and persistence than their planktonic counterparts against sanitizers, partly due to the complex structure of EPS. Therefore, recognizing the roles EPS materials play in the biofilm structural differentiation is of great importance to facilitate development of appropriate control strategies to biofilms existed on the food or food contact surfaces.

One advantage of AFM in biofilm study is that it can characterize EPS structure and components in the biofilm's natural status without affecting its original formation process. Some researchers used AFM to demonstrate the effect of flow rate on the architecture of *E. coli* O157:H7 biofilms formed on a microfluidic platform under laminar flows, with the aim of better understanding how biofilms respond and adapt to the environmental stress such as flow conditions during their culture period (Lim et al., 2008). More biofilms were produced under flow culture at a rate of 5  $\mu\text{L}/\text{min}$  in 5 days when compared to those under a static culture condition, with increased surface coverage rate observed in fluidic condition. Moreover, the bacteria suffered more stress under fluidic condition, with bumpy surface and increased cell surface roughness due to more EPS produced to adapt the environmental stress. The changes in cellular size and

biofilm height also indicated the stress imposed by the flow conditions, as a smaller cell size and lower biofilm depth were noticed under laminar flow. The study showed direct evidence that bacteria could alter their morphology of biofilms in the face of an environmental stress, and AFM could provide a 3D high-resolution model to help us better understand the dynamic process within biofilms in nanoscale.

### 6.3.2 Biofilm adhesive property study

In addition to the imaging of microbial biofilms, AFM could also be applied to study the elasticity and adhesive properties of biofilms by force measurement. Some researchers pressed the tip into the cells to determine the adhesive forces between the tip and the cell surface biomolecules and obtain the cellular spring constant through a series of force cycles (Volle, Ferguson, Aidala, Spain, & Núñez, 2008b). Based on the AFM images, the different fibrous structures (pili, fimbriae, and flagella) on the cell surfaces of five different bacterial strains (two Gram-positive, three Gram-negative) might adhere to the tip and cause different force curve cycles, which included both the extension and the retraction curves with different force and distance components in different cell types (Fig. 6.2). It was noticed that Gram-positive cells had higher spring constants than -negative strains, indicating they are stiffer when probed, which could be attributed to their thick cell walls of peptidoglycan as well as high cellular turgor pressures. Moreover, the extension and retraction curves showed us that the outside surfaces of all biofilm-colonising cells were coated by a soft layer of EPS, which contributed to different patterns of adhesion among different strains of cells due to its different thickness and stickiness. Larger forces and shorter distances were noted in the Gram-positive cells during adhesion events, whereas the Gram-negative cells were characterized by smaller forces and longer distances, reflecting different strains' different biofilm forming abilities.

Currently, many AFM studies were focused on imaging and force measurements together, providing a more in depth understanding of the adhesion mechanisms of biofilms on the surface and leading to new strategies on how to avoid biofilm formation during food processing. Rodriguez et al. used AFM to study the effects of various probe parameters (e.g., probe contact time, probe loading force, probe loading pressure, and probe material) and the relative humidity on the adhesiveness of *Listeria* biofilms at a cellular level, hoping to gain a deeper insight into the mechanism of bacterial transfer from food equipment surfaces to foods, which often happens in food industry (Rodriguez, Autio, & McLandsborough, 2008). They found that *Listeria*

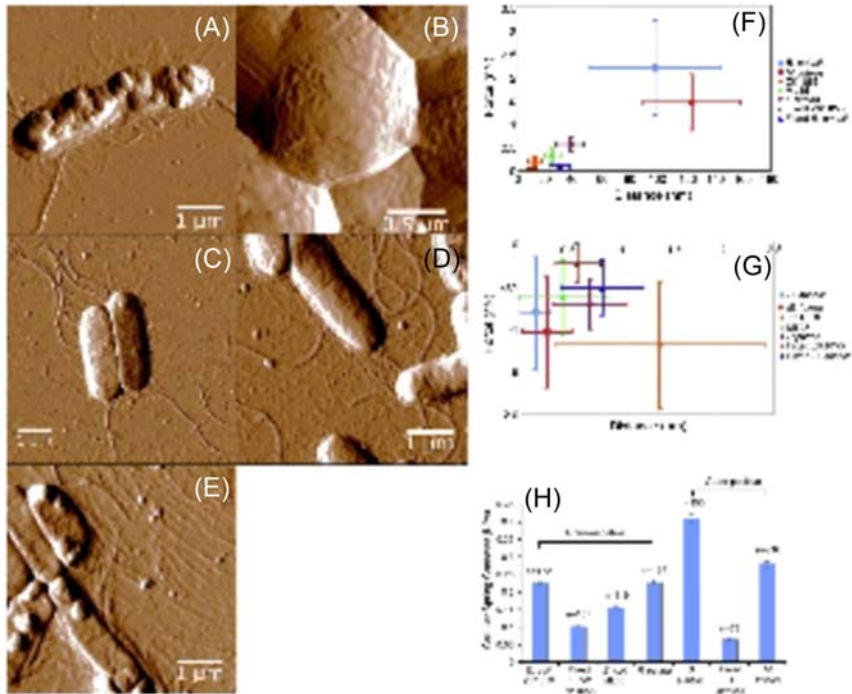


**Figure 6.2** Atomic force microscopy (AFM) imaging of biofilms: (A) *Bacillus subtilis*; (B) *Micrococcus luteus*; (C) *Escherichia coli* ZK 1056; (D) *Pseudomonas putida*; and (E) *E. coli* ML 35. AFM force measurement: the distance and force components of the extension curve (F) and retraction curve (G) and cellular spring constants (H) for biofilms and fixed planktonic cells. All subgraphs are reproduced with permission from Elsevier (From Volle, C. B., Ferguson, M. A., Aidala, K. E., Spain, E. M., & Núñez, M. E. (2008a). Spring constants and adhesive properties of native bacterial biofilm cells measured by atomic force microscopy. *Colloids and Surfaces B: Biointerfaces*, 67(1), 32–40. <https://doi.org/10.1016/j.colsurfb.2008.07.021>).

grew as single cells or in the form of microcolonies on the surface of stainless steel coupons, instead of colonizing the entire surface. After imaging, the force–distance curves were portrayed, which revealed that the biofilms had a more tendency to adhere to hydrophobic surfaces than hydrophilic surfaces based on the pull-off force measurement by using two different colloidal probes, whereas other parameters mentioned above had little effect on biofilm adhesiveness.

### 6.3.3 Biofilm dynamic process study

In addition, the dynamic cellular processes within biofilms can also be imaged and monitored by using AFM. Some researchers investigated the

morphological changes of *E. coli* cells during biofilm formation in dilute and rich media, respectively, showing the dynamic process of cell adherence, cell division and reproduction, and EPS excretion under AFM scanning (Núñez, Martín, Chan, & Spain, 2005). Moreover, the researchers also used *Bdellovibrio*, a predatory bacterium that can invade and attack Gram-negative bacteria, as a tool for eliminating *E. coli* biofilms in this study. AFM results demonstrated the dynamic interactions between the predator and prey, such as the morphological changes of *Bdellovibrio* including the structures of flagella and pili involved in their motility and adhesion and the structural changes of *E. coli* including the transformation of shape (Fig. 6.3). Other researchers further investigated the changes of

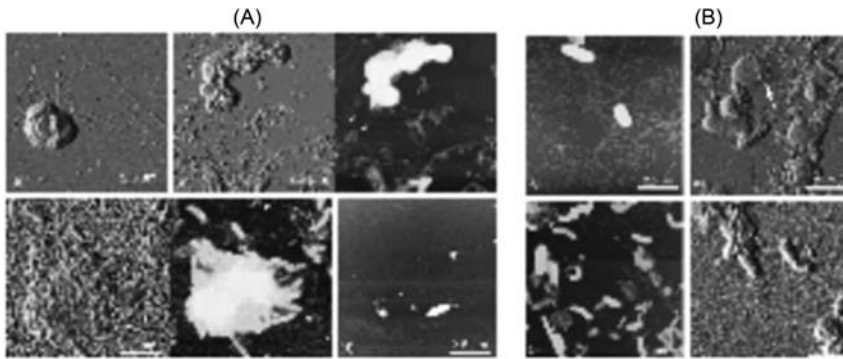


**Figure 6.3** The dynamic processes of *Bdellovibrios* added to *Escherichia coli* biofilm cultured in a dilute medium (A) and rich medium (B), respectively. A: (a) *Bdelloplasts*, prey cells with predatory *Bdellovibrios* growing inside (image taken after biofilm growing and infected by *Bdellovibrio* for 24 h); (b) *Bdelloplasts* and *E. coli* cell debris. Left side is a deflection image and right side is a height image (dark to white means low to high) (image taken after biofilm growing and infected by *Bdellovibrio* for 48 and 24 h, respectively); (c) A frantic feeding in progress. Deflection and height images both show the centered *Bdelloplasts* were surrounded by the well-fed *Bdellovibrios* (imaging time same as (b)); (d) Within 24–48 h, almost all *E. coli* prey cells were infected. Only debris and *Bdellovibrios* can be found (imaging time the same as (a)). B: (a) A lot of abandoned flagella and a few *E. coli* cells after 24 h biofilm initiation; (b) *Bdelloplasts* containing *Bdellovibrios* inside (arrow) after 48 h biofilm initiation; (c) *E. coli* cells were attacked by *Bdellovibrio* predators, most of which were well-fed and healthy, while some of which were narrow and unhealthy after 48 h biofilm initiation; (d) clusters of *E. coli* cells still existed despite not in large communities after 5 days of *Bdellovibrio* attacks. All subgraphs are reproduced with permission from Elsevier (From Núñez, M. E., Martín, M. O., Chan, P. H., & Spain, E. M. (2005). Predation, death, and survival in a biofilm: *Bdellovibrio* investigated by atomic force microscopy. *Colloids and Surfaces B: Biointerfaces*, 42(3–4), 263–271. <https://doi.org/10.1016/j.colsurfb.2005.03.003>).

elasticity and adhesive properties of *E. coli* biofilms after being invaded by *Bdellovibrio*, finding a series of chemical and physical changes, which can be probed by AFM (Volle et al., 2008a). The invaded prey cells were shorter, rounder, and softer than normal cells, with lower spring constants and larger pull-off forces, indicating a decrease in *E. coli* biofilm's elasticity and an increase in adhesiveness after the invasion by *Bdellovibrio* predator. Overall, these studies open up an opportunity of imaging and measuring dynamic events happened within biofilms.

## 6.4 Microbial macromolecule studies

In addition to above studies at the cellular level of whole cells, AFM can also be applied to characterize the biomolecules on the surface of microorganisms at the macromolecular level, unraveling key microbial problems by examining the interactions between AFM tips and single molecules. In the force spectroscopy mode, the nanomechanical properties of surface macromolecules such as proteins, nucleic acids, and polysaccharides can be probed and characterized, and when the tip is coated or immobilized with specific molecules, some specific interactions could be measured due to the molecular recognition (Alsteens et al., 2017).

### 6.4.1 Surface layer protein study

Surface layer (S layer) is a part of the bacterial cell wall and encloses the whole cell surface, which, as the outermost interaction zone, keeps cell safe from the external environment. It consists of monomolecular arrays or double layers of strain-dependent surface layer proteins (Slps) built via self-assembly in vivo, which also possess the natural capability to reassemble into stable crystalline structures in vitro, such as solid surface and the air–water interface, providing a suitable condition for AFM analysis. Some researchers used AFM to explore the structural changes of surface layer protein A (SlpA), which was isolated from *Propionibacterium freudenreichii* and deposited on mica sheet for recrystallization, after being exposed to different environmental conditions. SlpA was found to form a paracrystalline hexagonal lattice on a mica sheet, which was maintained but became softer upon mild heating (Fig. 6.4A). Although its lattice assembly was not modified with increase in temperature, the increasing mobilities of this structure could affect the cell–cell or cell–environment interactions, due to a high proportion of disordered and flexible regions existing in SlpA, which could serve as a brush at the bulk/protein interface. On

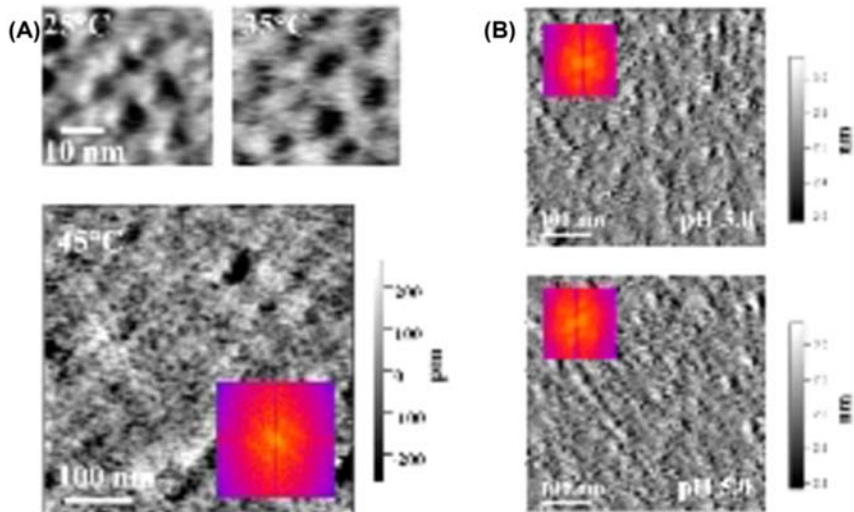


**Figure 6.4** Atomic force microscopy images of the recrystallized SlpA layer from *Propionibacterium freudenreichii* PFCIRM 118 strain at pH 6.7 under different temperatures (A) and at 25°C under different pH (B). The red figures inserted are the Fourier-transformed images. All subgraphs are reproduced with permission from American Chemical Society (From De Sa Peixoto, P., Roiland, C., Thomas, D., Briard-Bion, V., Le Guellec, R., Parayre, S., Deutsch, S. M., Jan, G., & Guyomarc'h, F. (2015). Recrystallized S-layer protein of a probiotic propionibacterium: Structural and nanomechanical changes upon temperature or pH shifts probed by solid-state NMR and AFM. *Langmuir*, 31(1), 199–208. <https://doi.org/10.1021/la503735z>).

the other hand, when the environmental pH decreased below the isoelectric point (pI) of the SlpA ( $\sim 4.71$ ), the protein film experienced significant changes of protein–water internal bonds (Fig. 6.4B), which was also reported in another study (Toca-Herrera, Moreno-Flores, Friedmann, Pum, & Sleytr, 2004), in which researchers used AFM as well and found visible degradation of the protein film when the pH decreased to 3.0. These results again proved that the environmental stresses can result in structural changes of protein regions existed in S layer films, accompanied by elasticity variations quantified by AFM technique. In another study, wild-type S layer glycoprotein isolated from *Geobacillus stearothermophilus* and its nonglycosylated counterpart on gold-covered sensor surfaces was also examined by AFM, comparing the differences of their recrystallization process and the surface properties in the presence or absence of the glycan residues (Schuster & Sleytr, 2015). They found that the water had a tendency to bind or couple to the outermost glycan residues of the wild-type

glycoprotein, causing higher surface nano-roughness due to the water-exposed glycans.

### 6.4.2 Surface molecular interaction study

In addition to probing surface layer proteins, other cell surface macromolecules that can generate intercellular interactions and mediate cell adhesion and aggregation behaviors can also be measured by AFM. Some researchers used biofunctionalized probes to investigate the lectin–carbohydrate interactions happening during the flocculation process of yeast cells, which is an important step in food fermentation industry (Touhami, Hoffmann, Vasella, Denis, & Dufrière, 2003). The adhesion forces between oligoglucose- or lectin-terminated probes and yeast cells under flocculating and nonflocculating conditions were measured, respectively, showing quite different modes of specific interactions between lectins and glucose residues, with around 120 pN adhesion forces recorded under a flocculating condition by using both two functionalized probes, whereas no interaction was observed under a nonflocculating condition. These results provided new insight into the flocculation mechanisms of yeast cells at the molecular level.

Besides lectin and carbohydrate interactions, other molecular recognition, such as enzyme and substrate, ligand and receptor, complementary strands of DNA, antibody and antigen, etc., can also be measured by using biologically modified AFM tip, which plays an important role in detecting foodborne pathogens as part of nanotechnology application in food safety (Hinterdorfer & Dufrière, 2006). AFM-based methods allow imaging of cells' molecular recognition sites on biointerfaces, followed by mapping a series of kinetic and mechanical properties of binding sites. More importantly, when combined with biofunctionalized probes, AFM can provide more specific and sensitive binding to achieve single molecular interaction detection, which is hard to be realized by conventional tips (Wong, Joselevich, Woolley, Cheung, & Lieber, 1998).

Among many AFM applications based on microbial molecules, the development of specific and sensitive biosensors for microorganism identification is one of the fundamental and critical prospects in food industry, and the antibody–antigen adsorption could be one advanced strategy. Some researchers used AFM to evaluate the surface morphology of the protein A and the antibody attachment to protein A, which is a cell wall protein and has natural affinity towards immunoglobulin molecules for



analyte binding (Lee, Pillai, Singh, & Willing, 2008). On combining the tapping and contact modes, the alterations of average step height between the solid gold surface and the protein A layer were increased from  $3.0 \pm 1.0$  nm to  $6.0 \pm 1.0$  nm, an interesting phenomenon observed when the protein A was attached to antibody. These results indicated that the antibodies grew in an “island model” and adsorbed randomly across the protein A layer, providing partial surface coverage and forming single monolayer on the gold quartz crystals. This study could contribute significantly to the development of more sensitive and specific biosensors to detect microbial contamination in food safety control.

## 6.5 Representatively reported atomic force microscopy studies about different types of microorganisms

### 6.5.1 Prokaryotic microorganisms

Prokaryotic cells include bacteria and archaea (Koonin & Wolf, 2008). Although, as mentioned above, a number of bacteria are pathogenic and can cause food poisoning and infectious diseases in humans, most bacteria are harmless, and many are helpful. By characterizing microbial surface properties, AFM can not only provide us with clues for controlling microbial contamination in food industry, but also provide us with the scope for probiotics' characterization, unraveling probiotic properties at the nanometer level, and thus providing more guidance for the application of probiotics in the host's gastro-intestinal tract or in food industrial process.

*Lactobacillus* species are well-known probiotics normally residing in human's digestive, urinary, and genital systems, helping to break down food and relieve general digestion problems (Heeney, Gareau, & Marco, 2018). Surface properties of lactobacilli explored by AFM could provide us detailed information of different microbial adhesion and aggregation abilities among different strains under native conditions. For example, some researchers used AFM to compare *L. crispatus*, *L. helveticus*, and *L. johnsonii*'s surface topography and molecular interactions, and found the surface of the first two species were covered completely by the S layer, leading to the absence of adhesion peaks on force volume images (Schaer-Zammaretti & Ubbink, 2003), whereas *L. johnsonii* strains showed high adhesion forces and soft gel-like behaviors that might be associated with surfaces rich in polysaccharides or peptidoglycans. This study might

be one of the first attempts to use AFM for investigating the surface properties of different lactic acid bacteria around 20 years ago.

On the other hand, it is well believed that pili play an important role in probiotic-host interactions; however, up to now, a limited number of studies related to the characterization of the pili structure and function in a native state have been conducted, as purifying pili is a challenging and costly task (Spacova, O'Neill, & Lebeer, 2020). Fortunately, some researchers used AFM to investigate the pili structure of *Lactocaseibacillus rhamnosus* GG, which is also one probiotic strain with antipathogenic and immunomodulatory properties (Dos Santos Morais et al., 2020). By dripping bacterial suspension directly on mica substrates, the pili structure could be imaged and their length, height, and thickness could all be measured under AFM examination. Moreover, AFM could even recognize different pilin types based on their molecular size, establishing new mechanistic insights into adhesion capacity of probiotic strains (Kant, Palva, von Ossowski, & Krishnan, 2020). As most fermented foods on the market are probiotic foods, imaging the structural and physicochemical properties of probiotics' surfaces with AFM can have wide-ranging implications for selecting optimal probiotics in food processing.

### 6.5.2 Eukaryotic microorganisms

Eukaryotes are an extraordinarily diverse group with more complex external and internal structures than prokaryotes (Medinger et al., 2010). Algae, protozoa, fungi, and helminths are all examples of eukaryotic microorganisms, and since their sizes are generally larger than the bacterial sizes, imaging them via AFM becomes more difficult and time-consuming due to an increased height and broader scanned area. Fortunately, by immobilizing them on silicon surface coated with glutaraldehyde, eukaryotic microorganisms such as *Pichia pastoris* (yeast representative) and *Chlorella vulgaris* (algae representative) could be imaged repeatedly and stably by AFM under physiological conditions, without being removed by the AFM probe tip during repeated and long-time scanning (Günther, Suhr, Raff, & Pollmann, 2014).

In addition, considering many fungal pathogens can bind to abiotic surfaces to form biofilms, using AFM to decipher the underlying molecular interactions in fungal adhesion could provide us more strategies for combating fungal infections. For example, some researchers investigated

the role of cell adhesion proteins of *Candida glabrata* by means of AFM (El-Kirat-Chatel et al., 2015). According to the data of hydrophobic force and interaction force obtained from chemical force microscopy (CFM) and single-cell force spectroscopy (SCFS), respectively, Epa6, a principal adhesin protein belonging to Epa family at the cell surface, was found to be responsible for strong hydrophobic interactions between yeast cells and abiotic surfaces, making *C. glabrata* cells attach firmly to hydrophobic substrates. This study showed that CFM and SCFS, the two AFM-based techniques, could provide a molecular basis for fungal biofilm formation, which was critical for the development of an effective biofilm control measure in food industry.

Fungal spores, like the seeds in the plant world, are units of sexual or asexual reproduction serving a purpose for fungal dispersal and survival (Dijksterhuis, 2019). Direct surface measurements of fungal spores can give us more information about spore physical properties during spore germination and outgrowth. One researcher used chemically functionalized AFM probes (i.e., OH- and CH<sub>3</sub>-terminated probes) to characterize the spore surface properties (morphology and molecular interactions) of *Phanerochaete chrysosporium*, one saprophytic fungus with great degradation capacity to aromatic polymer lignin (Dufrêne, 2000). This study might be one of the first attempts to use AFM to map spore's topography and measure the adhesion forces between the spore surface and functionalized probes. The direct visualization demonstrated that the spores of *P. chrysosporium* were in clubbed patterns with a lateral diameter of around 10 nm, and the absence of adhesive forces indicated that the spore surface was homogeneously hydrophilic, which contributed to fungal spore's protection and dispersion roles (Dufrêne, 2000).

### 6.5.3 Viruses

Viruses are acellular microorganisms, and a wide variety of them can cause foodborne outbreaks due to their adhesive nature on food products or food contact surfaces, such as norovirus and hepatitis A virus (Bosch, Pintó, & Guix, 2016). Therefore, understanding the underlying mechanisms of virus adhesion can offer us clues for developing effective virus control protocols to reduce the disease transmission. AFM-based approach in characterizing virus adhesion is gaining ever-increasing popularity. For example, some researchers used AFM to investigate the adhesion features of three bacteriophages (Ms2, Q $\beta$  and GA) on abiotic surfaces, and found the interfacial properties and the

hydrophobic/hydrophilic balance of both phages and attachment substrates all affected virions adhering behavior and led to different adhesion capacities (Dika, Ly-Chatain, Francius, Duval, & Gantzer, 2013).

Moreover, other researchers evaluated virus adhesion force on different food contact surfaces and found Ms2 exhibited more adhesion force to polyvinyl chloride (PVC) than to glass under AFM examination (Shim et al., 2017); however, this strong adhesion on PVC could be broken off and weakened when surfactant (e.g., sodium dodecyl sulfate) was incorporated during attachment. The attachment and detachment observations shown in this study could help deepen our understanding of the physico-chemical determinants of virus adhesion and potentially enable us to come up with corresponding ways to interrupt virus adhesion to food contact surfaces.

## 6.6 Combined use of atomic force microscopy with other techniques

Although AFM has been proved to be an invaluable tool to obtain information about the surface morphology and physical properties of microorganisms and macromolecular interactions, there are still some limitations of this “powerful” technique, such as slow scanning speed and difficulty in analyzing soft materials (Yang et al., 2007). Therefore, in order to obtain more comprehensive and detailed information of microorganisms, AFM combined with other complementary techniques seems to be a promising way, offering new possibilities to provide a full characterization of samples. And, in turn, this combination could also solve some key problems of other techniques with the help of AFM.

### 6.6.1 Atomic force microscopy and infrared combination

Several studies suggest that AFM combined with infrared (IR) spectroscopy could provide both physical and chemical probing of a single bacterium cell in the nanoscale range, overcoming spatial resolution limitation of conventional IR spectroscopy, whose spatial resolution is restricted to several microns (Deniset-Besseau, Prater, Virolle, & Dazzi, 2014; Roman, Wrobel, Panek, Paluszkiewicz, & Kwiatek, 2019). Considering the size of most bacteria fail to reach that minimum threshold (e.g., the diameter of *S. aureus* is only around 400 nm), IR spectroscopy alone is inapplicable to the analysis at single-cell or intracellular level. Fortunately, the combined AFM–IR approach can improve resolution greatly (about 20 nm

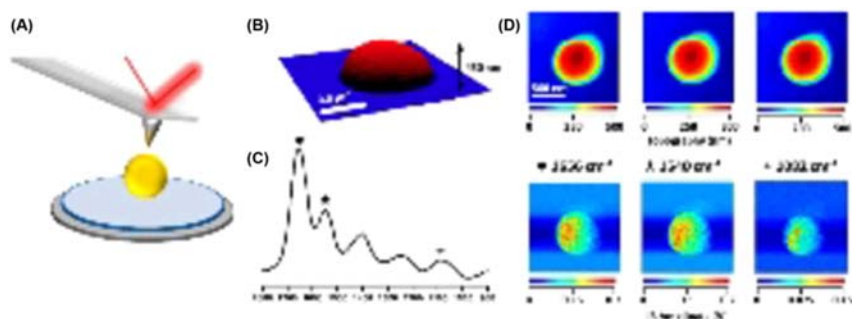


**Figure 6.5** An overview of the atomic force microscopy (AFM)–IR working for single-bacterium studies. (A) Setting diagram of the AFM–IR with the AFM cantilever located on the top of a single bacterial cell for probing; (B) AFM height profile of a single *Staphylococcus aureus* cell; (C) AFM–IR spectrum obtained from the middle part of the cell presented in (B); and (D) AFM–IR image of single *S. aureus* cell. First row: height images recorded at the same time with each IR map; Second row: each IR map, representing the corresponding absorbance intensity of marked band ( $1656$ ,  $1540$ , and  $1082\text{ cm}^{-1}$ ) in (C). All subgraphs are reproduced with permission from the American Chemical Society (From Kochan, K., Nethercott, C., Perez-Guaita, D., Jiang, J. H., Peleg, A. Y., Wood, B. R., & Heraud, P. (2019). Detection of antimicrobial resistance-related changes in biochemical composition of *Staphylococcus aureus* by means of atomic force microscopy-infrared spectroscopy. *Analytical Chemistry*, 91(24), 15397–15403. <https://doi.org/10.1021/acs.analchem.9b01671>).

resolution), providing single-cell images and corresponding absorbance intensity of selected wavenumber values from the same chosen spot (Kochan, Peleg, Heraud, & Wood, 2020).

An overview of the working of AFM–IR is given in Fig. 6.5. In brief, the photothermal expansion response generated by the biological sample after absorbing the tuned pulses of IR radiation is the key step for AFM–IR measurement, which can be detected by AFM cantilever for morphology characterization and then trigger the following AFM–IR spectrum collection and multivariate data analysis for absorbance intensity of selected band. The AFM–IR spectrum showed several bands, indicating different kinds of intracellular biological components based on the different position of their functional groups (Fig. 6.5C). More importantly, no localized biochemical differences were found in all of the tested bacteria, demonstrating that a single spectrum collected from one sample can be an indicator of its composition as a whole. This example shows that the AFM–IR method enables detection of biological components at or below the bacterial surface by obtaining information of specific marker bands, which cannot be achieved by each used alone (Kochan et al., 2019).

### 6.6.2 Atomic force microscopy and Raman spectroscopy combination

The combination of AFM and tip-enhanced Raman spectroscopy (TERS) has received more and more attention recently, as it can provide both morphological and chemical fingerprints simultaneously at the micro- and nanoscale, which is an outstanding advantage in microbiology study (Liu et al., 2012; Rusciano, Zito, Pesce, & Sasso, 2017). Some researchers first used this combined method to investigate *Bacillus subtilis* spores, finding that the TERS-based imaging maps were related to AFM-phase maps, which meant the distribution of biological components in the complicated spore system could be identified and discriminated (Rusciano et al., 2014). Considering *B. subtilis* spores are hard to be inactivated under adverse environmental conditions and several related foodborne outbreaks have been reported (Kramer & Gilbert, 1989), understanding the physicochemical properties of *B. subtilis* spores by using this combined approach could provide important guidance to food decontamination.

### 6.7 Conclusion and future trends

Since its invention in 1986, AFM has provided a major thrust to microbiological research and its applications, such as characterizing the surface properties as well as manipulating molecular interactions of food microorganisms, contribute a lot to food safety. In this chapter, we have discussed recent progress in the application of AFM for the multiparametric and multifunctional characterization of microbiological systems, which can provide deeper insight into the food microbiology.

As the surface analysis tool, AFM allows high-resolution imaging of cell-surface structures under real-time monitoring conditions close to their native state. Examples include the observation of single cell's surface dynamic changes after environmental treatments and structural differentiation during biofilm development. Besides, many surface physical properties could be quantified by force measurements, such as the adhesion and aggregation behaviors, the stiffness of cell walls, and the surface charge and hydrophobicity. More importantly, through tip functionalization with biomolecules, the studies of molecular interactions and recognitions can be implemented, considering AFM as the only force-measuring method that enables functionalized probe to map the spatial distribution of single molecular binding sites on cellular surfaces. Besides characterizing

foodborne pathogens, imaging the structural and physicochemical properties of probiotics' surfaces with AFM is also helpful in deepening our understanding on the probiotic mechanisms, contributing to a better application in food processing.

Future research could focus more on how to improve the scanning rate of AFM, as current time resolution is still a limiting factor (Shibata, Yamashita, Uchihashi, Kandori, & Ando, 2010). Moreover, the combination of AFM with other complementary optical techniques, such as infrared spectroscopy, Raman spectroscopy, or confocal fluorescence microscopy, has been used recently to obtain more comprehensive information about the structure–function relationship of microorganisms. We expect that in future studies, AFM-based method combined with other modern approaches or suitable functionalized tips could have a broader range of utility in the food microbiology area, to address food safety problems and challenges from the perspective of the structure and function of microbial cell surfaces.

## Acknowledgements

This study was funded by Applied Basic Research Project (Agricultural) Suzhou Science and Technology Planning Programme (SNG2020061), Natural Science Foundation of Jiangsu Province (BK20181184), Singapore Ministry of Education Academic Research Fund Tier 1 (A-8000469-00-00), and an industry grant supported by Shenzhen Zhiyun Optoelectronics Co., Ltd. (R-143-000-A24-597).

## Declaration of competing interest

We declare that we do not have any commercial or associative interest that represents a conflict of interest in connection with this manuscript. We have no financial and personal relationships with other people or organizations that can inappropriately influence our work.

## References

- Alsteens, D., Gaub, H. E., Newton, R., Pfreundschuh, M., Gerber, C., & Müller, D. J. (2017). Atomic force microscopy-based characterization and design of biointerfaces. *Nature Reviews Materials*, 2(5). Available from <https://doi.org/10.1038/natrevmats.2017.8>.
- Araújo, G. R. D. S., Viana, N. B., Gómez, F., Pontes, B., & Frases, S. (2019). The mechanical properties of microbial surfaces and biofilms. *Cell Surface*, 5. Available from <https://doi.org/10.1016/j.tcs.2019.100028>.

- Bhat, S. V., Booth, S. C., Vantomme, E. A. N., Afroj, S., Yost, C. K., & Dahms, T. E. S. (2015). Oxidative stress and metabolic perturbations in *Escherichia coli* exposed to sub-lethal levels of 2,4-dichlorophenoxyacetic acid. *Chemosphere*, *135*, 453–461. Available from <https://doi.org/10.1016/j.chemosphere.2014.12.035>.
- Bosch, A., Pintó, R. M., & Guix, S. (2016). Foodborne viruses. *Current Opinion in Food Science*, *8*, 110–119. Available from <https://doi.org/10.1016/j.cofs.2016.04.002>.
- Braga, P. C., & Ricci, D. (2004). Atomic force microscopy: Biomedical methods and applications (Vol. 242).
- Chen, L., Liu, Q., Zhao, X., Zhang, H., Pang, X., & Yang, H. (2022). Inactivation efficacies of lactic acid and mild heat treatments against *Escherichia coli* strains in organic broccoli sprouts. *Food Control*, *133*, 108577. Available from <https://doi.org/10.1016/j.foodcont.2021.108577>.
- Chen, L., Zhang, H., Liu, Q., Pang, X., Zhao, X., & Yang, H. (2019). Sanitising efficacy of lactic acid combined with low-concentration sodium hypochlorite on *Listeria innocua* in organic broccoli sprouts. *International Journal of Food Microbiology*, *295*, 41–48. Available from <https://doi.org/10.1016/j.ijfoodmicro.2019.02.014>.
- Chen, L., Zhao, X., Wu, J., Liu, Q., Pang, X., & Yang, H. (2020). Metabolic characterisation of eight *Escherichia coli* strains including “Big Six” and acidic responses of selected strains revealed by NMR spectroscopy. *Food Microbiology*, *88*. Available from <https://doi.org/10.1016/j.fm.2019.103399>.
- Cui, Y., Oh, Y. J., Lim, J., Youn, M., Lee, I., Pak, H. K., . . . Park, S. (2012). AFM study of the differential inhibitory effects of the green tea polyphenol (-)-epigallocatechin-3-gallate (EGCG) against Gram-positive and Gram-negative bacteria. *Food Microbiology*, *29*(1), 80–87. Available from <https://doi.org/10.1016/j.fm.2011.08.019>.
- De Sa Peixoto, P., Roiland, C., Thomas, D., Briard-Bion, V., Le Guellec, R., Parayre, S., . . . Guyomarç’h, F. (2015). Recrystallized S-layer protein of a probiotic propionibacterium: Structural and nanomechanical changes upon temperature or pH shifts probed by solid-state NMR and AFM. *Langmuir*, *31*(1), 199–208. Available from <https://doi.org/10.1021/la503735z>.
- Deniset-Besseau, A., Prater, C. B., Virolle, M. J., & Dazzi, A. (2014). Monitoring TriAcylGlycerols accumulation by atomic force microscopy based infrared spectroscopy in *Streptomyces* species for biodiesel applications. *Journal of Physical Chemistry Letters*, *5*(4), 654–658. Available from <https://doi.org/10.1021/jz402393a>.
- Dijksterhuis, J. (2019). Fungal spores: Highly variable and stress-resistant vehicles for distribution and spoilage. *Food Microbiology*, *81*, 2–11. Available from <https://doi.org/10.1016/j.fm.2018.11.006>.
- Dika, C., Ly-Chatain, M. H., Francius, G., Duval, J. F. L., & Gantzer, C. (2013). Non-DLVO adhesion of F-specific RNA bacteriophages to abiotic surfaces: Importance of surface roughness, hydrophobic and electrostatic interactions. *Colloids and Surfaces A: Physicochemical and Engineering Aspects*, *435*, 178–187. Available from <https://doi.org/10.1016/j.colsurfa.2013.02.045>.
- Dos Santos Morais, R., El-Kirat-Chatel, S., Burgain, J., Simard, B., Barrau, S., Paris, C., . . . Gaiani, C. (2020). A fast, efficient and easy to implement method to purify bacterial pili from *Lactocaseibacillus rhamnosus* GG based on multimodal chromatography. *Frontiers in Microbiology*, *11*. Available from <https://doi.org/10.3389/fmicb.2020.609880>.
- Dufrène, Y. F. (2000). Direct characterization of the physicochemical properties of fungal spores using functionalized AFM probes. *Biophysical Journal*, *78*(6), 3286–3291. Available from [https://doi.org/10.1016/S0006-3495\(00\)76864-0](https://doi.org/10.1016/S0006-3495(00)76864-0).
- El-Kirat-Chatel, S., Beaussart, A., Derclaye, S., Alsteens, D., Kucharíková, S., Van Dijk, P., & Dufrène, Y. F. (2015). Force nanoscopy of hydrophobic interactions in the fungal pathogen *Candida glabrata*. *ACS Nano*, *9*(2), 1648–1655. Available from <https://doi.org/10.1021/nn506370f>.



- Günther, T. J., Suhr, M., Raff, J., & Pollmann, K. (2014). Immobilization of microorganisms for AFM studies in liquids. *RSC Advances*, 4(93), 51156–51164. Available from <https://doi.org/10.1039/c4ra03874f>.
- He, Y., Zhao, X., Chen, L., Zhao, L., & Yang, H. (2021). Effect of electrolysed water generated by sodium chloride combined with sodium bicarbonate solution against *Listeria innocua* in broth and on shrimp. *Food Control*, 127, 108134. Available from <https://doi.org/10.1016/j.foodcont.2021.108134>.
- Heaton, J. C., & Jones, K. (2008). Microbial contamination of fruit and vegetables and the behaviour of enteropathogens in the phyllosphere: A review. *Journal of Applied Microbiology*, 104(3), 613–626. Available from <https://doi.org/10.1111/j.1365-2672.2007.03587.x>.
- Heeney, D. D., Gareau, M. G., & Marco, M. L. (2018). Intestinal Lactobacillus in health and disease, a driver or just along for the ride? *Current Opinion in Biotechnology*, 49, 140–147. Available from <https://doi.org/10.1016/j.copbio.2017.08.004>.
- Hinterdorfer, P., & Dufrene, Y. F. (2006). Detection and localization of single molecular recognition events using atomic force microscopy. *Nature Methods*, 3(5), 347–355. Available from <https://doi.org/10.1038/nmeth871>.
- Hylgaard, M., Sutherland, D. S., Sundh, M., Mygind, T., & Meyer, R. L. (2012). Antimicrobial mechanism of monocaprylate. *Applied and Environmental Microbiology*, 78(8), 2957–2965. Available from <https://doi.org/10.1128/AEM.07224-11>.
- Kant, A., Palva, A., von Ossowski, I., & Krishnan, V. (2020). Crystal structure of lactobacillar SpaC reveals an atypical five-domain pilus tip adhesin: Exposing its substrate-binding and assembly in SpaCBA pili. *Journal of Structural Biology*, 211(3), 107571. Available from <https://doi.org/10.1016/j.jsb.2020.107571>.
- Kochan, K., Nethercott, C., Perez-Guaita, D., Jiang, J. H., Peleg, A. Y., Wood, B. R., & Heraud, P. (2019). Detection of antimicrobial resistance-related changes in biochemical composition of *Staphylococcus aureus* by means of atomic force microscopy-infrared spectroscopy. *Analytical Chemistry*, 91(24), 15397–15403. Available from <https://doi.org/10.1021/acs.analchem.9b01671>.
- Kochan, K., Peleg, A. Y., Heraud, P., & Wood, B. R. (2020). Atomic force microscopy combined with infrared spectroscopy as a tool to probe single bacterium chemistry. *Journal of Visualized Experiments*, 2020(163), 1–18. Available from <https://doi.org/10.3791/61728>.
- Koonin, E. V., & Wolf, Y. I. (2008). Genomics of bacteria and archaea: The emerging dynamic view of the prokaryotic world. *Nucleic Acids Research*, 36(21), 6688–6719. Available from <https://doi.org/10.1093/nar/gkn668>.
- Kramer, J.M., & Gilbert, R.J. (1989). *Bacillus cereus* and other *Bacillus* species. *Foodborne Bacterial Pathogens* (Vol. 19, pp. 21–70).
- Kuyukina, M. S., Ivshina, I. B., Korshunova, I. O., & Rubtsova, E. V. (2014). Assessment of bacterial resistance to organic solvents using a combined confocal laser scanning and atomic force microscopy (CLSM/AFM). *Journal of Microbiological Methods*, 107, 23–29. Available from <https://doi.org/10.1016/j.mimet.2014.08.020>.
- Lee, K. G., Pillai, S. R., Singh, S. R., & Willing, G. A. (2008). The investigation of protein A and Salmonella antibody adsorption onto biosensor surfaces by atomic force microscopy. *Biotechnology and Bioengineering*, 99(4), 949–959. Available from <https://doi.org/10.1002/bit.21644>.
- Lim, J., Lee, K. M., So, H. K., Nam, S. W., Yoo, J. O., Hyun, S. Y., . . . Park, S. (2008). Nanoscale characterization of *Escherichia coli* biofilm formed under laminar flow using atomic force microscopy (AFM) and scanning electron microscopy (SEM). *Bulletin of the Korean Chemical Society*, 29(11), 2114–2118. Available from <https://doi.org/10.5012/bkcs.2008.29.11.2114>.

- Liu, Q., Jin, X., Feng, X., Yang, H., & Fu, C. (2019). Inactivation kinetics of *Escherichia coli* O157:H7 and *Salmonella typhimurium* on organic carrot (*Daucus carota* L.) treated with low concentration electrolyzed water combined with short-time heat treatment. *Food Control*, *106*, 106702. Available from <https://doi.org/10.1016/j.foodcont.2019.06.028>.
- Liu, Q., Wei, L., Wang, J., Peng, F., Luo, D., Cui, R., . . . Li, Y. (2012). Cell imaging by graphene oxide based on surface enhanced Raman scattering. *Nanoscale*, *4*(22), 7084–7089. Available from <https://doi.org/10.1039/c2nr32525j>.
- Medinger, R., Nolte, V., Pandey, R. V., Jost, S., Ottenwalder, B., Schlotterer, C., & Boenigk, J. (2010). Diversity in a hidden world: Potential and limitation of next-generation sequencing for surveys of molecular diversity of eukaryotic microorganisms. *Molecular Ecology*, *19*(1), 32–40. Available from <https://doi.org/10.1111/j.1365-294X.2009.04478.x>.
- Nunez, M. E., Martin, M. O., Chan, P. H., & Spain, E. M. (2005). Predation, death, and survival in a biofilm: *Bdellovibrio* investigated by atomic force microscopy. *Colloids and Surfaces B: Biointerfaces*, *42*(3–4), 263–271. Available from <https://doi.org/10.1016/j.colsurfb.2005.03.003>.
- Papaioannou, E., Giaouris, E. D., Berillis, P., & Boziaris, I. S. (2018). Dynamics of biofilm formation by *Listeria monocytogenes* on stainless steel under mono-species and mixed-culture simulated fish processing conditions and chemical disinfection challenges. *International Journal of Food Microbiology*, *267*, 9–19. Available from <https://doi.org/10.1016/j.ijfoodmicro.2017.12.020>.
- Park, S. H., Cheon, H. L., Park, K. H., Chung, M. S., Choi, S. H., Ryu, S., & Kang, D. H. (2012). Inactivation of biofilm cells of foodborne pathogen by aerosolized sanitizers. *International Journal of Food Microbiology*, *154*(3), 130–134. Available from <https://doi.org/10.1016/j.ijfoodmicro.2011.12.018>.
- Rodríguez, A., Autio, W. R., & McLandsborough, L. A. (2008). Effects of contact time, pressure, percent relative humidity (%RH), and material type on *Listeria* biofilm adhesive strength at a cellular level using atomic force microscopy (AFM). *Food Biophysics*, *3*(3), 305–311. Available from <https://doi.org/10.1007/s11483-008-9085-4>.
- Roman, M., Wrobel, T. P., Panek, A., Paluszkiwicz, C., & Kwiatek, W. M. (2019). Nanoscale AFM-IR spectroscopic imaging of lipid heterogeneity and effect of irradiation in prostate cancer cells. *Nanotechnology*, *30*(42). Available from <https://doi.org/10.1088/1361-6528/ab31dd>.
- Rusciano, G., Zito, G., Istatico, R., Sirec, T., Ricca, E., Bailo, E., & Sasso, A. (2014). Nanoscale chemical imaging of *Bacillus subtilis* spores by combining tip-enhanced Raman scattering and advanced statistical tools. *ACS Nano*, *8*(12), 12300–12309. Available from <https://doi.org/10.1021/nn504595k>.
- Rusciano, G., Zito, G., Pesce, G., & Sasso, A. (2017). Cell imaging by spontaneous and amplified Raman spectroscopies. *Journal of Spectroscopy*, *2017*. Available from <https://doi.org/10.1155/2017/2193656>.
- Schaer-Zammaretti, P., & Ubbink, J. (2003). Imaging of lactic acid bacteria with AFM—Elasticity and adhesion maps and their relationship to biological and structural data. *Ultramicroscopy*, *97*(1–4), 199–208. Available from [https://doi.org/10.1016/S0304-3991\(03\)00044-5](https://doi.org/10.1016/S0304-3991(03)00044-5).
- Schuster, B., & Sleytr, U. B. (2015). Relevance of glycosylation of S-layer proteins for cell surface properties. *Acta Biomaterialia*, *19*, 149–157. Available from <https://doi.org/10.1016/j.actbio.2015.03.020>.
- Shibata, M., Yamashita, H., Uchihashi, T., Kandori, H., & Ando, T. (2010). High-speed atomic force microscopy shows dynamic molecular processes in photoactivated bacteriorhodopsin. *Nature Nanotechnology*, *5*(3), 208–212. Available from <https://doi.org/10.1038/nnano.2010.7>.

- Shim, J., Stewart, D. S., Nikolov, A. D., Wasan, D. T., Wang, R., Yan, R., & Shieh, Y. C. (2017). Differential MS2 interaction with food contact surfaces determined by atomic force microscopy and virus recovery. *Applied and Environmental Microbiology*, 83(24). Available from <https://doi.org/10.1128/AEM.01881-17>.
- Spacova, I., O'Neill, C., & Lebeer, S. (2020). Lacticaseibacillus rhamnosus GG inhibits infection of human keratinocytes by *Staphylococcus aureus* through mechanisms involving cell surface molecules and pH reduction. *Beneficial Microbes*, 11(7), 703–715. Available from <https://doi.org/10.3920/BM2020.0075>.
- Surveillance for Foodborne Disease Outbreaks. (2019). Centers for Disease Control and Prevention (CDC).
- Toca-Herrera, J. L., Moreno-Flores, S., Friedmann, J., Pum, D., & Sleytr, U. B. (2004). Chemical and thermal denaturation of crystalline bacterial S-layer proteins: An atomic force microscopy study. *Microscopy Research and Technique*, 65(4–5), 226–234. Available from <https://doi.org/10.1002/jemt.20127>.
- Touhami, A., Hoffmann, B., Vasella, A., Denis, F. A., & Dufrière, Y. F. (2003). Aggregation of yeast cells: Direct measurement of discrete lectin-carbohydrate interactions. *Microbiology*, 149(10), 2873–2878. Available from <https://doi.org/10.1099/mic.0.26431-0>.
- Tyagi, A. K., & Malik, A. (2010). In situ SEM, TEM and AFM studies of the antimicrobial activity of lemon grass oil in liquid and vapour phase against *Candida albicans*. *Micron*, 41(7), 797–805. Available from <https://doi.org/10.1016/j.micron.2010.05.007>.
- Van der Aa, B. C., Asther, M., & Dufrière, Y. F. (2002). Surface properties of *Aspergillus oryzae* spores investigated by atomic force microscopy. *Colloids and Surfaces B: Biointerfaces*, 24(3–4), 277–284. Available from [https://doi.org/10.1016/S0927-7765\(01\)00277-6](https://doi.org/10.1016/S0927-7765(01)00277-6).
- Volle, C. B., Ferguson, M. A., Aidala, K. E., Spain, E. M., & Núñez, M. E. (2008a). Quantitative changes in the elasticity and adhesive properties of *Escherichia coli* ZK1056 prey cells during predation by *Bdello vibrio* bacteriovorus 109. *Journal of Langmuir*, 24(15), 8102–8110. Available from <https://doi.org/10.1021/la8009354>.
- Volle, C. B., Ferguson, M. A., Aidala, K. E., Spain, E. M., & Núñez, M. E. (2008b). Spring constants and adhesive properties of native bacterial biofilm cells measured by atomic force microscopy. *Colloids and Surfaces B: Biointerfaces*, 67(1), 32–40. Available from <https://doi.org/10.1016/j.colsurfb.2008.07.021>.
- Wong, S. S., Joselevich, E., Woolley, A. T., Cheung, C. L., & Lieber, C. M. (1998). Covalently functionalized nanotubes as nanometresized probes in chemistry and biology. *Nature*, 394(6688), 52–55. Available from <https://doi.org/10.1038/27873>.
- Wright, C. J., Shah, M. K., Powell, L. C., & Armstrong, I. (2010). Application of AFM from microbial cell to biofilm. *Scanning*, 32(3), 134–149. Available from <https://doi.org/10.1002/sca.20193>.
- Yang, H., Wang, Y., Lai, S., An, H., Li, Y., & Chen, F. (2007). Application of atomic force microscopy as a nanotechnology tool in food science. *Journal of Food Science*, 72(4), R65–R75. Available from <https://doi.org/10.1111/j.1750-3841.2007.00346.x>.
- Zhang, J., & Yang, H. (2017). Effects of potential organic compatible sanitisers on organic and conventional fresh-cut lettuce (*Lactuca sativa* Var. Crispa L). *Food Control*, 72, 20–26. Available from <https://doi.org/10.1016/j.foodcont.2016.07.030>.
- Zhao, L., Zhang, Y., & Yang, H. (2017). Efficacy of low concentration neutralised electrolyzed water and ultrasound combination for inactivating *Escherichia coli* ATCC 25922, *Pichia pastoris* GS115 and *Aureobasidium pullulans* 2012 on stainless steel coupons. *Food Control*, 73, 889–899. Available from <https://doi.org/10.1016/j.foodcont.2016.09.041>.

- Zhao, L., Zhao, M. Y., Phey, C. P., & Yang, H. (2019). Efficacy of low concentration acidic electrolysed water and levulinic acid combination on fresh organic lettuce (*Lactuca sativa* Var. Crispa L.) and its antimicrobial mechanism. *Food Control*, *101*, 241–250. Available from <https://doi.org/10.1016/j.foodcont.2019.02.039>.
- Zhao, X., Chen, L., Zhao, L., He, Y., & Yang, H. (2020). Antimicrobial kinetics of nisin and grape seed extract against inoculated *Listeria monocytogenes* on cooked shrimps: Survival and residual effects. *Food Control*, *115*, 107278. Available from <https://doi.org/10.1016/j.foodcont.2020.107278>.

This page intentionally left blank

## CHAPTER 7

# Application of atomic force microscopy for food foams and emulsions

**Christelle Lopez**

INRAE, BIA, Nantes, France

### 7.1 Introduction

Many food systems consist of at least two immiscible phases, such as oil and water phases for emulsions (e.g., milk, dairy and vegetable creams, mayonnaise) and nanoemulsions in which the oil is dispersed in the aqueous phase as droplets, but also air or other gas and water phases for foams (e.g., whipped cream such as Chantilly, espresso coffee cream, egg white foams) (Fig. 7.1A).

These food systems have a large interfacial area between the immiscible phases which is thermodynamically unfavorable. As a consequence, the lipid droplets in emulsions and the air bubbles in foams are not physically stable without the presence of interface stabilizers. This interfacial area that delimits the dispersed oil droplets in oil-in-water (O/W) emulsions and the dispersed air bubbles in foams is deformable and dynamic. The surface-active molecules that are amphiphilic in nature diffuse, adsorb, and rearrange easily in the interfacial regions to reduce the interfacial tension by which the formation of small, stable, and dispersed droplets and bubbles is facilitated. The food-grade emulsifiers and surfactants are, for example, lecithin, Tween 20 or 80, sodium alginate, whey protein isolate (WPI), sodium caseinate, casein hydrolysates, maltodextrin,  $\kappa$ -carrageenan. In recent years, food-grade Pickering colloidal particles have gained considerable interest because of their ability to form stable particle-stabilized lipid droplets in emulsions and air bubbles in foams (Fig. 7.1A). Pickering stabilizers are solid or soft colloidal particles that partially wet both phases and form a mechanical barrier. They physically stabilize the interface against coalescence and Ostwald ripening. Besides emulsions, which contain lipid

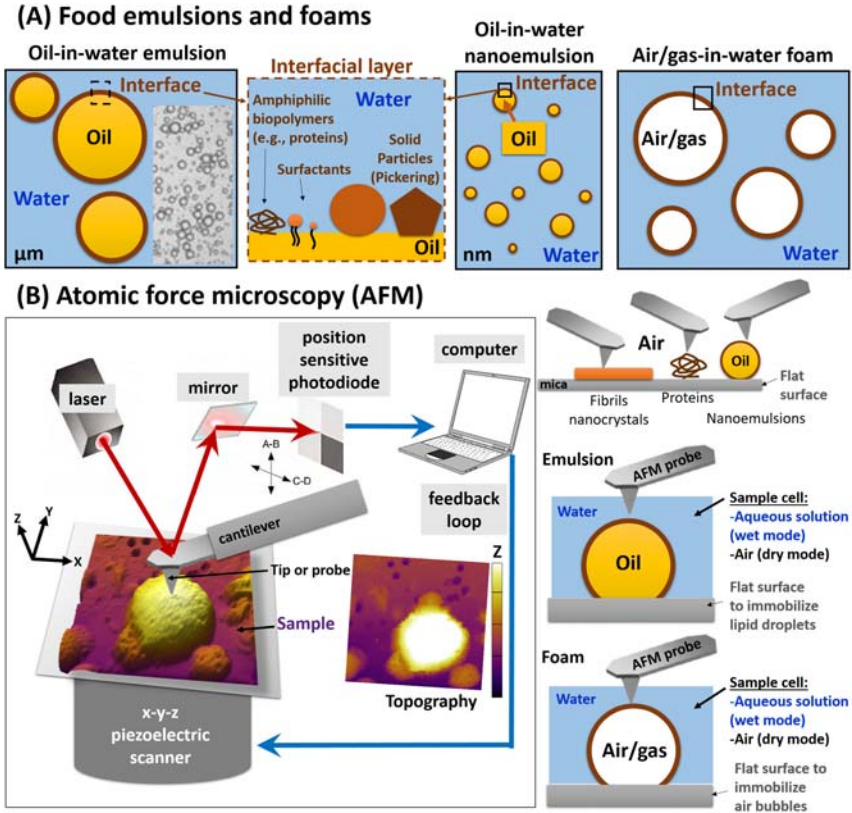


**Figure 7.1** Application of atomic force microscopy (AFM) for food emulsions and foams. (A) Schematic representation of oil-in-water emulsion and nanoemulsion containing lipid droplets with a focus on the interface, and air/gas-in-water foam containing air bubbles. (B) Principle of AFM applied to air-dried interfacial components adsorbed in a flat substrate (e.g., mica) and to spherical lipid droplets and air bubbles in an aqueous environment where temperature, pH, and ionic strength can be changed.

droplets with diameters in the range of micrometers to hundreds of micrometers, nanoemulsions are colloidal O/W dispersions containing nanometer-scaled oil droplets with size ranging from 20 to 500 nm that are widely applied in food industries (Fig. 7.1A). Due to the unique properties of nanoemulsion droplets, such as very small size, very high stability, and extremely large surface area (up to 300 m<sup>2</sup>/g oil), they have become one of several emerging technologies in the design of delivery systems for encapsulating, protecting against oxidation and degradation, controlling the release rate of active core ingredients, and enhancing the bioavailability of many

lipophilic bioactive compounds in food industries (Aswathanarayan & Vittal, 2019). Nanoemulsions of functional compounds are, for example, prepared to encapsulate components such as fish oil, alpha-tocopherol, or beta-carotene.

Besides the processed and engineered O/W emulsions and nanoemulsions, natural emulsions are also of importance in food systems. Natural O/W emulsions consist in lipid assemblies designed by nature, for example, the fat globules in milk, the oil bodies (OBs) in plants and seeds, and the low-density lipoproteins in egg yolk. These natural lipid droplets are covered by layers of phospholipids and membrane-associated proteins. As for processed emulsions, the physical stability and functions of natural O/W emulsions are governed by the surface composition and microstructure as well as by the interfacial properties of the natural lipid droplets.

Increasing the understanding of the O/W emulsions, nanoemulsions, and foams properties as well as their respective interfaces is of interest for food scientists and industries.

The interface composition (molecules adsorbed to the interface), the morphology (i.e., shape and size) of the interface stabilizers, the microstructure of the interfacial layer, the dynamic interaction forces between surface components, between droplets or between droplet and emulsifiers, as well as the interface mechanical properties are involved in the emulsifying properties and physical stability of the dispersed food systems (emulsions, nanoemulsions, and foams), their macroscopic behavior, and the overall quality of food products. The characterization of the droplet and bubble topography and the control of the interfacial region are therefore crucial.

The characterization of the oil/water interface in emulsions and nanoemulsions, and of the air/water interface in foams is often complicated due to the small size of the lipid droplets and air bubbles that may range from the nanometer scale to micrometers or hundreds of micrometers. Such characterization requires the use of combined chemical and biophysical techniques. Among these techniques, atomic force microscopy (AFM) has raised attention in the last three decades since it has opened access to the nanoscale imaging of molecular and colloidal individual structures. Furthermore, AFM force spectroscopy provides information on the mechanical properties of soft matter materials and interfaces. Also, AFM offers the possibility of performing imaging and force measurements in aqueous media and following the dynamics of systems upon environmental changes (e.g., temperature, pH, ionic strength).



Facing the rising interest for AFM to investigate food foams and emulsions, in this chapter I have highlighted new scientific advances and provided examples of application of AFM imaging and force spectroscopy to interfacial components, planar interfaces, as well as air bubbles in food foams and lipid droplets in O/W emulsions and nanoemulsions. Section 7.2 presents the fundamentals of AFM applied to food emulsions and foams including the operating modes of imaging, the determination of force–distance curves, and the preparation of lipid droplets or air bubbles samples for AFM investigations. Section 7.3 presents applications of AFM for food foams. Section 7.4 describes application of AFM for food emulsions and nanoemulsions. Section 7.5 describes the use of AFM imaging and force spectroscopy to probe milk lipid systems including supported membranes, unsupported membranes such as liposomes as well as O/W emulsions containing unprocessed and processed milk fat globules. The last section of this chapter puts spotlight on future opportunities and challenges to overcome to develop AFM combined with other techniques providing complementary information to better understand and control interfaces, food emulsions, and foams.

## **7.2 Atomic force microscopy applied to food foams and emulsions: fundamentals, operating modes, imaging for topography and force–distance curves for nanomechanics**

### **7.2.1 Fundamentals of atomic force microscopy: investigation of surfaces**

Since it was invented by Binnig, Quate, and Gerber (1986), AFM has become one of the most widespread technologies to image the sample surface structure at the nanoscale level and used in investigation of the interfacial properties of many organic and biological materials, including the food emulsions and foams, from micron to nanoscale. With the advances and innovations, AFM is being established as an important technique for interface characterization, due to its unique advantages over traditional imaging (transmission and electron microscopy) and surface force-determining approaches. By employing nanostructured tips also called probes to scan material surfaces at nanoscale resolution, AFM imaging can provide information on the micro/nanostructured surface topography, and AFM force spectroscopy provides information on the mechanical properties by measuring forces at the nanometer scale. By using functionalized probes, AFM can also investigate specific surface interactions at the nanometer scale.

## 7.2.2 Atomic force microscope

A typical AFM equipment consists of a sharp tip (also known as a probe) attached to the end of a flexible cantilever that acts like a spring (Fig. 7.1B). The cantilever, also known as spring system or force sensor, is designed with a very low spring constant so that it is very sensitive to any forces. The cantilever bends in the presence of attractive and repulsive forces and allows to calculate force from its deflection following Hooke's law: Force = (spring constant)  $\times$  (deflection). The configurations of the AFM tips determine the resolution and quality of the images taken. The AFM tips can be classified according to their shape (e.g., square-base pyramid, rectangular-base pyramid, circular symmetric, spike), materials (e.g., silicone, silicon nitride, silicon oxide, high-density carbon), and coating materials (e.g., uncoated, gold-coated, platinum-coated, diamondlike-carbon coated). The AFM tip can have different functionalized or modified groups (e.g.,  $-\text{CO}_2\text{H}$ ,  $-\text{NH}_2$ ,  $-\text{OH}$ ,  $-\text{CF}_3$ ,  $-\text{CH}_3$ ,  $-\text{NHS}$ , etc.), and attached colloidal spheres. A photodiode detects the deflections of the cantilever during scanning over the sample surface via a laser beam focused on and reflected from the rear of the cantilever. A computer that controls the AFM system acquires the electrical signals from the photodiode to generate feedback signals to a piezoelectric scanner and the cantilever to maintain the tip at either a constant force or constant height above the sample and to display surface topographic images as well as force–distance curve measuring the interaction forces between the atoms on the tip and the sample surface. The feedback loop controls the force between the sample and the tip, and the z-sample position.

In AFM, the sample surface topography is constructed from the deflection of the cantilever, which is determined by the sample surface features, as the cantilever tip scans over the region of interest on the sample surface (Fig. 7.1B).

Depending on applications, AFM can be operated under various environmental conditions, for example, in air—“dry mode”, in aqueous environment or under water—“wet mode”, and under vacuum.

## 7.2.3 Operating modes for imaging

The operation of AFM can be classified into three different modes: (1) the contact mode, (2) the noncontact mode, and (3) the tapping mode (from TappingMode, Bruker), depending on the interaction between AFM tip and the sample surface.

1. In the contact mode, the AFM tip directly and physically contacts the sample surface during scanning, and the sample surface profiles

are generated by operating with either constant height (e.g., the AFM tips scan the sample surface laterally without moving in the z-direction) or constant force (e.g., the force between the AFM tip and the sample surface is kept unchanged). Due to frictional forces of the AFM tip applying to the sample surface, the contact mode of AFM can damage the sample surface and possibly distort the features of the images generated. Consequently, the contact mode AFM is not suitable for the characterization of soft material surfaces, such as lipid droplets in emulsions and nanoemulsions and air bubbles in foams.

2. In the noncontact mode, the AFM cantilever tip moves about 50–150 Å above the sample surface and oscillates near or at its natural resonance frequency. As the AFM tip approaches the sample surface, the attractive van der Waals forces acting between the tip and the sample cause shifting of the resonance frequency and subsequently deflection of the cantilever. Unlike the contact mode, the noncontact AFM allows imaging of the soft materials with no contact between the tip and the sample. However, it is very difficult to obtain high-resolution images from the noncontact mode AFM because the true distance between the sample surface and the AFM tip, which is an important parameter for the enhancement of topographical images, cannot be determined. In addition, the noncontact mode AFM is unable to image the true sample surface, because the sample surface is typically contaminated with a fluid layer that leads to large damping effects on the cantilever resonance. Therefore, the noncontact mode AFM is not suitable for the study of biological materials under aqueous conditions, such as aqueous food emulsions, nanoemulsions, and foams, as well as their respective aqueous interfaces and hydrated interfacial components.
3. The tapping mode, or intermittent contact mode, is a combination of contact and noncontact modes in which the AFM tip oscillates near or at its natural resonance frequency over the sample surface and is allowed to slightly ‘tap on’ the sample surface in a minimal amount of time. Therefore, the shear forces applied on the sample surface are negligible, which enabled the tapping mode AFM to become the most widely used technique for high-resolution imaging of soft samples under aqueous conditions, such as emulsions, nanoemulsions, liposomes, membranes, and foams as well as oil/water and gas/water interfaces, and hydrated components.

### 7.2.4 Force—distance curves for determining surface material properties

In addition to imaging the sample surface topography, the determination of the force—distance curve, which can be employed to investigate many surface material properties including surface forces, is another important function of the AFM technique. To perform the force measurement in most commercial AFM equipments, the cantilever deflection signals from the photodiode are monitored as the piezoelectric scanner moves the sample surface up and down (z-direction), by which the cantilever tip approaches, touches on, and retracts from the sample surface to complete a circular movement. A plot of the tip—sample interaction forces vs the tip—sample distance, known as a force—distance curve, provides quantitative information about the interfacial forces acting between the tip and the sample surface. The deflection of the cantilever from its original position is dependent on the distance between the tip and the sample surface. From the force—distance curve, the interaction forces between the tip and the sample can be determined when the spring constants of the cantilever are known. By functionalization and modification of the tip with substrates having different origins and natures, and by attaching colloidal particles/droplets to the tip, the applicability of the AFM for surface force measurement has been enormously expanded from two rigid solid surfaces to two deformable soft droplets, and even between two surfaces that are premodified with the functional groups desired. In addition to surface forces, the surface elasticity of the materials analyzed can be extracted from the force—distance curve.

### 7.2.5 Probing air bubbles, lipid droplets, and interfaces

AFM allows investigation of the morphology of lipid droplets and air bubbles as well as interfaces, that is, air/water interfaces as in foams and oil/water interfaces as in nanoemulsions and emulsions.

To successfully image the lipid (oil) droplets or air bubbles morphology and surface topography, the lipid droplets in nanoemulsions and emulsions or the air bubbles in foams must be firmly attached in their native and intact state to very smooth solid surfaces to resist the lateral forces caused by the AFM scanning tip (Fig. 7.1B). Surfaces commonly used to fix the droplets include mica, glass, and silicon oxide. Among them, mica (a nonconducting layered mineral composed of multiple 1-nm-thick layers) is the most preferred because of its unique properties such as being atomically flat, clean

after cleavage, easy to cut to the desired size, relatively inexpensive, and negatively charged surface that can be modified to make the surface positive. The binding (adhesion) of droplets on the substrate surface is usually accomplished via electrostatic attraction (e.g., adsorption) between the charges on the sample and those on the mica surface. The negatively charged surface of mica can be modified to make the surface positive. In this case, surface coating chemicals such as poly-L-lysine, poly-D-lysine, polyethylenimine, or aminopropyltriethoxy-silane are used to modify the substrate before the droplets are deposited on the substrate surface. A strong binding of the components, for example proteins, to the mica substrate is necessary for successful transfer and AFM imaging.

In addition, the lipid droplets or air bubbles must be well dispersed on the solid surface, which is determined by several factors, including the exposure time and the dilution ratio of the samples, the interfacial free energy and electrostatic energy associated with the droplets or bubbles, the hydrophilic/hydrophobic forces interacting between droplets or bubbles, surface, and solution, and the additives and surfactants present in the dispersed systems. In most of the studies reported in the literature, the sample preparation followed a similar procedure. Most emulsions and nanoemulsions must be diluted into distilled water (or buffer with controlled pH and ionic strength) from 100 to 1000 times to avoid agglomeration and coalescence of the lipid droplets. The diluted dispersion is then deposited on the freshly cleaved mica substrate. In some cases, the deposited droplets were washed with distilled water or buffer before AFM experiments in order to remove the unadsorbed lipid droplets. The deformation of the oil/water and air/water interfaces often complicates direct AFM measurement in many soft matter systems, particularly with lipid droplets and air bubbles, as they are often the most deformable or “softest” materials to study.

The most common AFM operating mode used to characterize the lipid droplets in O/W emulsions is the tapping mode to avoid damaging on the droplet surface, and the imaging is often performed in air under dry conditions. This means that the droplets deposited on flat substrate surfaces were dehydrated and that the AFM was operated under the air mode. However, the dehydration process during sample preparation can result in the flattening of the particles, that is, deformation of the shape of lipid droplets and air bubbles. Although the use of AFM for topography and interfacial characterization has been successful in imaging of micrometer-sized lipid droplets or air bubbles on a solid surface in an aqueous solution, few studies have been performed in these conditions.

### 7.3 Application of atomic force microscopy for food foams

Atomic force microscopy has been successfully applied to image the surface of air bubbles or planar model systems approaching the surface of air bubbles, in order to better understand the surface properties and the mechanisms involved in the physical properties of foams.

The physical instability of foams is mainly due to difficulties in preventing and overcoming the mechanisms of disproportionation. Disproportionation corresponds to the transition of matter from smaller particles that are more soluble to larger particles. To reduce disproportionation a thick, elastic, nondesorbing film is required at the hydrophilic (water)/hydrophobic (air) interface. It has been suggested that a film with a surface elastic modulus above 100 mN/m at the air/water interface could significantly delay air bubble disproportionation. However, this type of film cannot be achieved with typical surface-active agents. For example,  $\beta$ -lactoglobulin, a surface-active protein widely used in food products, provides a more elastic interfacial layer compared to low-molecular-weight surfactants but this layer still only has a dilatational modulus of 30–40 mN/m and shear modulus of about 1 mN/m, meaning it is not sufficient to overcome disproportionation. Foams stabilized with particles or protein aggregates as Pickering stabilizers may considerably increase foam stability compared to foams prepared with native proteins. AFM has been used to image the morphology of interfacial components to better understand air bubble surface microstructure in the context of the reduction of air bubble disproportionation and physical stabilization of foams. Several technical strategies are used by authors: (1) AFM imaging of components involved in the air/water interface deposited onto a solid substrate and imaged in dry condition, (2) AFM imaging of components adsorbed at planar Langmuir films, and (3) AFM imaging of air bubbles (Fig. 7.1).

#### 7.3.1 Components involved in the air/water interface

In most of the studies, the samples are diluted and deposited onto a solid substrate, mainly on freshly cleaved mica, and dehydrated to be imaged by AFM under dry condition.

As an example, AFM was used to examine the morphology of rice proteins, mainly the alkali-soluble glutelin, after various heat treatments to better understand its surface properties in the formation of foams (Zhao, Xiong, Chen, Zhu, & Wang, 2020). Fresh glutelin solution (0.2 mg/mL)

was dripped onto a freshly cleaved mica surface and dried at room temperature for 2 h. Morphological images were collected at the tapping mode using a nanoprobe cantilever tip at a frequency of 50–100 kHz. Images were analyzed using the AFM instrument software.

AFM height images permitted the determination of the morphology and size changes of rice glutelin aggregates both before and after the heat treatment. AFM images showed a wide range of protein aggregates at pH 12 for untreated rice glutelin, while the size of rice glutelin aggregates was observed to be significantly reduced as the heat treatment temperature was increased to 100°C. In the AFM imaging process, glutelin was in an almost anhydrous state and may shrink to some extent, showing a smaller size compared to dynamic light scattering measurements. These results indicated that high-temperature heat treatment can effectively improve the functional properties of rice glutelin and has strong application potential. However, the air/water interface characteristics and foam stabilization mechanism of modified rice glutelin have yet to be further explored.

### 7.3.2 Components adsorbed at planar Langmuir films

In some studies, authors transfer the components of interfacial interest to a solid substrate, by using the Langmuir-Blodgett or the Langmuir-Schaefer techniques. Two examples of AFM studies are given below.

In the first example, AFM was used to examine Chaplin E films formed at the air/water interface under different pH conditions in comparison with two surface-active proteins from milk that are commonly used in the food industry, that is, the  $\beta$ -casein and  $\beta$ -lactoglobulin (Dokouhaki et al., 2020). The AFM experiments were performed in tapping mode with ultrasharp SiN gold-coated cantilevers to study the morphology, thickness, and roughness of Chaplin E,  $\beta$ -lactoglobulin, or  $\beta$ -casein films formed by these surface-active agents at the air/water interface and transferred from the air/water interface onto the solid surface of silicon (Si) wafers using the Langmuir-Blodgett technique and subsequently imaged using AFM. Before AFM experiments, the appropriate amount of sample at pH 3.0, 7.0, or 10.0 was applied to the surface of the water of a Teflon Langmuir trough with a single Delrin barrier at the corresponding pH and left for 20 min to reach equilibrium. The monolayer was compressed at a rate of 50 cm<sup>2</sup>/min to the bending point. The film formed at the air/water interface was transferred to the surface of Si wafers using the Langmuir-Blodgett technique. The transfer was

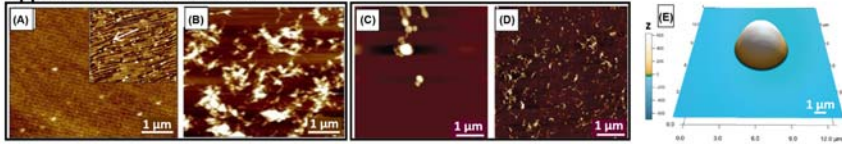
performed using a constant surface pressure by dipping the substrate through the air/water interface and then removing the substrate at a rate of 8 mm/min. The air-dried films were then scanned by AFM within 24 h of transfer. AFM topography height images were recorded for each sample. The film thickness was estimated by scratch analysis (mechanical removal of the film) and by tracing a profile along with the film and the scratched zone.

In this first example, AFM allowed to characterize the morphology of Chaplin E films formed at the planar air/water interface (Fig. 7.2A and B). AFM images revealed distinct differences between the films formed by Chaplin E under different pH conditions. The film formed under acidic conditions was smooth and homogenous. It contained ordered structures that were closely packed and aligned in one direction with 2 nm thickness. In contrast, under basic conditions, Chaplin E formed a heterogeneous film that appeared to contain aggregated clusters of disordered fibrils arranged randomly on the substrate with 17 nm thickness. AFM images showed that at low pH Chaplin E can form films of similar thickness to other surface-active proteins, such as  $\beta$ -casein and  $\beta$ -lactoglobulin while at a higher pH, the Chaplin E films are thicker and more heterogeneous in structure. The author concluded that the results obtained by AFM were in good agreement with the previously reported *in situ* observation of Chaplin E films formed at the air/water interface at pH 3.0 or 10.0 by Brewster angle microscopy.

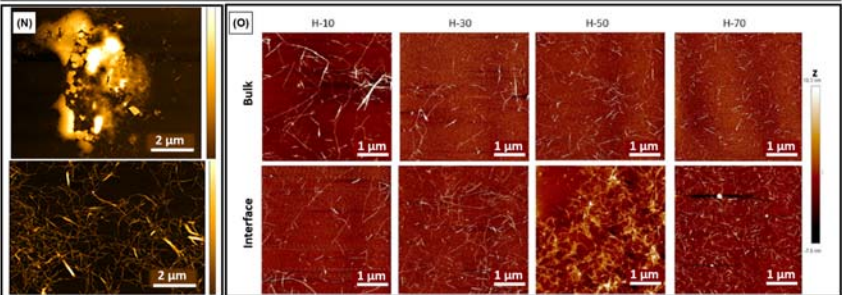
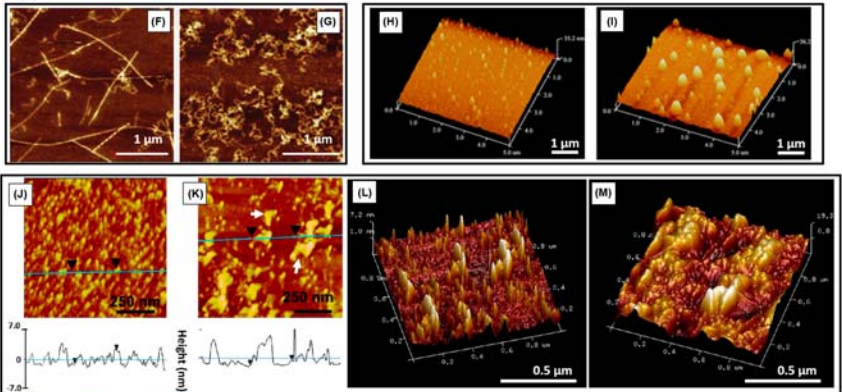
In the second example, AFM was used to observe the morphology of native  $\beta$ -lactoglobulin and its aggregates adsorbed at the air/water interface at different pHs (Hu et al., 2019). AFM imaging was performed using Peak Force Tapping Mode. A silicone cantilever with a driving frequency of 70 kHz and an elastic constant of 0.4 N/m was used for scanning. A modified Langmuir–Schaefer technique was employed to transfer interfacial structures onto a mica substrate. Native  $\beta$ -lactoglobulin and its aggregates (0.1 mg/mL) were adjusted to pH 7.0 and pH 4.0. Then, the samples were placed in a small dish, and let stand for 1 h. A freshly cleaved mica sheet was pinched with small tweezers to touch the air/water interface of the sample solutions and immediately removed again. The mica was then dipped into ethanol for phase exchange and removal of any unabsorbed material before slowly drying in an ambient environment. In order to improve the binding of proteins to the mica substrate, the negatively charged mica was modified by treatment using (3-amino-propyl)-triethoxysilane to carry positive charges when depositing the



**Application of AFM to foams**



**Application of AFM to emulsions**



**Application of AFM to egg yolk low density lipoproteins (LDL)**

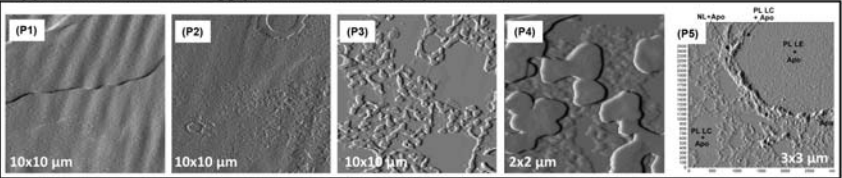


**Figure 7.2** Examples of application of atomic force microscopy (AFM) to food foams (A–E) and food emulsions (F–O), including egg yolk low-density lipoproteins (LDL) (P). (A,B) AFM height mode images of the interfacial film formed by Chaplin E at pH 3.0 (A) or pH 10.0 (B). The film at the air/water interface was transferred onto a Si wafer surface prior to imaging. Images correspond to a sample area of  $5 \times 5 \mu\text{m}$ . The inset in image (A) shows a magnified sample area of  $1 \times 1 \mu\text{m}$ . The arrow in the inset shows the direction of alignment for ordered structures within the Chaplin E film. (C,D) AFM height images of 0.1 mg/mL nanoparticles (C) and fibrils (D) of  $\beta$ -lactoglobulin at pH 4.0. (E) Tapping mode AFM 3D height image of an air bubble

samples at pH 7.0. No surface modification was needed for sample preparation at pH 4.0.

AFM images showed that at both pH 7.0 and pH 4.0, native  $\beta$ -lactoglobulin formed a relatively more homogenous interfacial adsorption film. The interfacial structure formed by fibrils of  $\beta$ -lactoglobulin exhibited a continuous network feature, while that of nanoparticles of  $\beta$ -lactoglobulin was rather dispersed (Fig. 7.2C and D). Comparison between pH 7.0 and pH 4.0 revealed a higher degree of aggregation at pH 4.0, which should be attributed to lower surface charges of the protein samples at pH 4.0, and thus weaker electrostatic repulsion.

### 7.3.3 Air bubbles under the atomic force microscope

Few authors investigated under the AFM microscope 3D air bubbles in an aqueous medium. This is due to strong methodological difficulties encountered to adsorb air bubbles in a solid substrate (without deforming or breaking them) and their physical instability under stimulation by the AFM tip.

- 
- ◀ immobilized on an octadecyltrichlorosilane-modified surface in water. (F,G) AFM height images of nanofibrils derived from whey protein isolate glycosylated with lactose after heating in 10% (F) and 50% v/v (G) aqueous ethanol at 85°C and pH 2 for 24 h. (H,I) 3D-view AFM height images of peanut protein isolate from alkaline extraction (H) and ultrasound-assisted extraction for 50 min (I). (J–M) AFM height images of soy protein isolate in the native state (J) or preheated (K) with the respective height profiles, and 3D-view AFM height images in the absence of NaCl (L) or with 400 mM NaCl (M). (N) AFM height image of untreated microcrystalline cellulose (top) and treated cellulose nanocrystals (bottom). (O) AFM height images of bulk (top) and Langmuir film air/water interfacial layer (bottom) of cellulose nanoparticles with different lengths. (P1–P5) AFM images taken in air (deflection signal) of LDL film formed at the air/water interface and transferred onto mica, at pH 7, at different surface pressures: (P1) 22 mN/m (after neutral lipid collapse); (P2) 30 mN/m (before apoprotein–lipid transition); (P3) 45 mN/m (after apoprotein–lipid transition); (P4) 45 mN/m, AFM image taken in butanol, the composition, and the phase of different structures observed are represented by the letters *PL* *LE*, phospholipids in liquid expanded phase; *PL* *LC*, phospholipids in liquid condensed phase; *Apo*, apoproteins; *NL*, neutral lipids. For (A,B) Adapted from [Dokouhaki et al. \(2020\)](#). (C,D) Adapted from [Hu et al. \(2019\)](#). (E) Adapted from [Uddin, Tan, and Dagastine \(2011\)](#). (F,G) Adapted from [Liu, Li, Qin, and Zhong \(2021\)](#). (H,I) Adapted from [Sun, Zhang, Zhang, Tian, and Chen \(2021\)](#). (J–M) Adapted from [Liu and Tang \(2013\)](#). (N) Adapted from [Dias Meirelles, Rodrigues Costa, and Cunha \(2020\)](#). (O) Adapted from [Ni, Fan, and Sun \(2020\)](#). (P) Adapted from [Dauphas et al. \(2007a\)](#).

Prof. R. Dagastine's group (University of Melbourne, Australia) successfully imaged air bubbles by AFM. Air bubbles generated by an ultrasound transducer and immobilized on an octadecyltrichlorosilane modified surface were imaged in water using tapping mode AFM to visualize their morphology and determine the contact angle (Fig. 7.2E) (Uddin et al., 2011). These authors showed that the needle probe AFM tip can be used to measure the surface tension of an air bubble in an aqueous solution for a range of solution conditions, including anionic, cationic, and nonionic surfactant solutions.

## 7.4 Application of atomic force microscopy for food emulsions and nanoemulsions

In the field of emulsions (Fig. 7.1A), AFM is being established as an important technique for (1) visualizing the morphology of emulsifiers (e.g., pectins, protein/polysaccharide complexes, proteins, nanofibrils, nanoparticles, nanocrystals) used to stabilize O/W interfaces, (2) visualizing the morphology and size of the lipid droplets, (3) probing the interactions between the surface of lipid droplets and components such as proteins, and (4) examining the mechanical properties of O/W interfaces (processed lipid droplets), and lipid membranes as well as the mechanical surface properties of natural emulsion lipid droplets such as oil bodies from plants or seeds, and milk fat globules.

In the field of nanoemulsions (Fig. 7.1A), AFM imaging and measurements of interfacial interaction forces of nanoemulsion lipid droplets are essential to tailor and design intelligent nanoemulsion-based systems. AFM is used to image the lipid droplets. Currently, the use of AFM to characterize nanoemulsions, especially in food science and nutrition sectors, has been limited to the determination of the morphology (shape, sphericity, and structure) and the size of droplets. Nanoemulsions were successfully imaged using AFM, demonstrating a highly potential applicability of AFM to study nanoemulsions in food sciences (Ho, Abik, & Mikkonen, 2021). AFM is therefore of great aid in designing and tailoring nanoemulsion-based delivery systems of bioactive compounds.

The following sections show examples of the use of AFM imaging (1) to determine the morphology of components used to stabilize O/W emulsions, (2) to determine the morphology of components adsorbed at planar Langmuir films prepared to mimick the O/W interface, and (3) to visualize the morphology of lipid droplets and determine the mechanical properties.

### 7.4.1 Morphology of components used to stabilize oil-in-water emulsions

AFM has been used to characterize the morphology of components (e.g., pectin, proteins, cellulose nanocrystals [CNC]) and/or of complexes or nanoparticles formed from various components (e.g., protein–saccharide nanoparticles) that are involved in the emulsifying properties. Some of these components are used as Pickering stabilizers adsorbed at the surface of oil droplets in O/W emulsions (Fig. 7.1A). AFM imaging performed at the nanoscale level is essential since it is well-known that the structure of the components (for example the proteins) adsorbed on the oil/water interface is critical for their emulsifying activity.

Before AFM imaging, the components are deposited on freshly cleaved mica sheets and air-dried. AFM height images are presented as 2D or 3D representations. Height profiles of selected particles in 2D images performed as a function of section length give information about the size dimensions of the components, that is, length, width, and height. Several examples are given below.

#### 7.4.1.1 Example 1: applications of atomic force microscopy to pectins

- Atomic force microscopy was used to image natural or cross-linked sugar beet pectin (Lin, Yu, Ai, Zhang, & Guo, 2020). Pectin samples were dissolved in Milli-Q water, drop-deposited onto a freshly cleaved mica sheet, and air-dried at room temperature for 20 min. The molecular morphologies of sugar beet pectins were imaged by AFM under tapping mode. Individual molecules were clearly imaged. Linear and branched strands were assigned to polysaccharide chains, while tadpole-looking structures were assigned to protein–polysaccharide complexes. The authors also observed large-sized spherical structures attached to multiple divergent stands, resulting in an irregularly shaped aggregate that was interpreted as a possible aggregation of sugar beet pectin molecules during air drying.
- The morphology of nanoparticles composed of genipin-crosslinked sugar beet pectin and bovine serum albumin was imaged by AFM under tapping mode (Lin et al., 2021). Such studies were involved in the context of their potentialities as novel Pickering stabilizers.
- The nanostructure of sweet potato pectin was characterized using AFM in tapping mode (Arachchige, Mu, & Ma, 2020). Sweet potato pectin was dissolved in distilled water (0.1 mg/mL), and 1  $\mu$ L was

placed on the surface of a freshly cleaved mica glued to a magnetic stainless steel disk, air-dried, and then scanned by the tip. In the AFM images, polysaccharide chains were observed as extended linear or branched complex polymer structures, protein appeared as globular structures, and some of the polysaccharide chains were joined together around protein.

#### **7.4.1.2 Example 2: applications of atomic force microscopy to protein/polysaccharide complexes**

Atomic force microscopy was used to investigate the ability of biopolymer protein/polysaccharide complexes to stabilize O/W emulsions. In this context, the ability of cationic lactoferrin (LF)/anionic gum arabic (GA) electrostatic complexes to be used as emulsifiers to form and stabilize high internal phase emulsions (emulsions with dispersed phase volume fractions above about 74%) was studied (Cheng et al., 2021). AFM was utilized to determine the morphology of the LF/GA complexes. Prior to analysis, the complexes were diluted 1000-fold with pH-adjusted water, and then 10  $\mu$ L of this diluted sample was placed on a newly exfoliated mica sheet. The sample was then allowed to air-dry overnight before images were obtained using an AFM instrument operating in tapping mode. AFM images clearly showed that the morphology of the electrostatic complexes formed was influenced by the LF:GA ratio. The measured height of the LF/GA complexes decreased with increasing GA, which supported the visual observations and particle size measurements. At lower GA concentrations, there appeared to be larger particles present and evidence of complex aggregation (4:1 LF:GA). As the GA level was increased, the individual complexes became smaller and there was less aggregation. The morphology of the complexes affected their adsorption to oil drop surfaces.

#### **7.4.1.3 Example 3: applications of atomic force microscopy to protein fibrils**

- Protein nanofibrils have recently shown unique properties in preparing O/W emulsions, with the stability improved after fibrillation of glycosylated proteins. Protein nanofibrils with tunable material properties may be significant for functional food applications. In this context, the morphology of WPI based protein nanofibrils has been examined by AFM (Liu et al., 2021). Dispersions of protein nanofibrils were deposited onto a freshly cleaved mica disk and dried at room temperature for 4 h prior to loading onto the AFM microscope. The samples were

analyzed in the tapping mode. Worm-like nanofibrils of various lengths were imaged by AFM (Fig. 7.2F and G). Section analysis of AFM images permitted the determination of the height of individual nanofibrils.

- The morphology of ovotransferrin fibrils was examined by AFM imaging in tapping mode (Wei, Cheng, & Huang, 2019). In order to facilitate AFM imaging of single fibrils, fibril dispersions were diluted prior to imaging and the absence of dilution effect on fibril appearance was verified. Diluted fibril dispersions were spread onto the surface of a freshly cleaved mica and dried using nitrogen stream. AFM images showed straight and worm-like fibrils. Ovotransferrin fibrils with a contour length range of 150–550 nm occupied 66% of total fibrils. The average contour length of 337 nm measured in this study thanks to AFM imaging met the requirement of eligible Pickering emulsifiers.

#### **7.4.1.4 Example 4: applications of atomic force microscopy to protein nanostructures**

- Vegetable proteins play an important role in the food industry because of their interesting nutritional value and functional properties such as the physical stabilization of O/W emulsions. Some novel nonthermal physical technologies, such as ultrasound, have been applied to improve the functional properties of proteins by changing their structural organisation. In this context, the surface topography and nanostructures of peanut protein isolate (PPI) were visualized by AFM (Sun et al., 2021). The diluted protein suspension (15 µg/mL) was dropped onto a freshly cleaved mica substrate, and the substrate was dried naturally. The images were collected using a Si<sub>3</sub>N<sub>4</sub> cantilevered probe in the noncontact mode. The resonance frequency of the tip was 20–40 kHz, and the scan rate was about 0.5–2 Hz. At least 10 images from each sample were analyzed to obtain statistically meaningful results. The authors found that the average diameter of PPI particles increased from 121 ± 35 to 194 ± 93 nm with increasing ultrasound time, while the control exhibited smaller particle diameters (96 ± 35 nm) (Fig. 7.2H and I).

AFM was also used to visualize the morphology of peanut protein nanoparticles on mica using tapping mode AFM images with different concentrations of sodium (Ning et al., 2020). AFM images showed that the peanut protein nanoparticles were roughly spherical with a size around 160–280 nm, but with the increase in ionic strength from 0 to 500 mM, the nanoparticle size progressively increased.

- Nanoparticle aggregates of soy protein isolate (SPI) developed into a kind of Pickering-like stabilizer for O/W emulsions were examined by AFM in tapping mode (Liu & Tang, 2013). The heated SPI dispersions at varying concentrations (0 – 500 mM) of NaCl were diluted with the distilled water of the same concentrations of NaCl, to a final protein concentration of 2 µg/mL. A 2 µL droplet of the diluted samples was immediately spread on a freshly cleaved mica disk and air-dried for 30 min at ambient temperature. For imaging under ambient conditions, single-beam uncoated silicon cantilevers were used. The drive frequency was set at 300 kHz, and the scan rate was 1.0 Hz. The authors found that the SPI exhibited spherical-shape clusters with heights ranging from about 2.0 to 4.0 nm and widths of approximately 40 – 60 nm while the heating resulted in considerable changes in particle morphology with more irregular and large particles. On increasing ionic strength, the extent of particle clustering progressively increased, and especially when the ionic strength was above 300 mM, most of the particles became associated and clustered, and were even transformed to much larger irregular particles (Fig. 7.2J–M).
- Food-grade soft gel particles consisting of caseins, which are commercially available proteinaceous ingredients produced from milk, can be used to stabilize O/W emulsions. Morphologies of casein particles were determined with AFM (Wang et al., 2018). The dispersions at a concentration of 3% (w/v) were diluted 3000-fold with deionized water. Before AFM determination, a drop of the diluted dispersions was added onto a cleaved mica surface at room temperature (about 25°C) for about 6 h. 2D AFM height images of the casein particles associated with section profiles permitted the determination of morphological parameters of the casein particles, that is, diameter, width, and height relative to the mica surface. The heights of all the casein particles were smaller than the width, indicating the casein gel soft particles can deform on the mica surface.

#### **7.4.1.5 Example 5: applications of atomic force microscopy to cellulose nanocrystals**

Cellulose nanocrystals (CNC) are bio-based solid particles arisen as promising stabilizers for Pickering emulsions in the food, pharmaceutical, and cosmetics industries. The scientists aimed at understanding

the stabilization mechanism of O/W emulsion using CNC as stabilizing particles. AFM has been used to characterize the morphology of the CNC.

- In [Dias Meirelles et al. \(2020\)](#), an aqueous CNC suspension (1.0  $\mu\text{L}$ ) was placed on a grid with a mica surface and dried at room temperature to perform AFM analysis. The images were obtained with an AFM microscope equipped with a camera, under controlled conditions (relative moisture of 10% and temperature of 25°C). AFM images showed that microcrystalline cellulose, without any treatments, formed agglomerates of large sizes, that is, particles with a size higher than 10  $\mu\text{m}$ . However, CNC dispersed in more separate networks were observed after the acid treatment, centrifugation, dialysis, vacuum filtration and an additional step of the ultrasound process, characteristic of CNC ([Fig. 7.2N](#)). The morphology obtained was needle-like showing that the isolation of cellulose microcrystalline to CNC was successfully done. From the analysis of AFM images, the authors determined that the lower dimension of CNC was nanometric, while the length of the nanocrystals was higher than 1  $\mu\text{m}$ .
- The morphology of dispersions composed of CNC mixed with bovine serum albumin was determined by AFM in tapping mode, in the context of Pickering O/W emulsions stabilized by protein-covered CNC ([Liu, Zheng, Huang, Tang, & Ou, 2018](#)). A drop of diluted suspension (0.001 wt.%) was deposited onto a freshly cleaved mica substrate. The samples were left to dry at ambient temperature. The applied drive frequency and scan rate were 150 kHz and 1.0 Hz, respectively.

#### 7.4.2 Morphology of components adsorbed at planar Langmuir films

In order to investigate the organization of components at the oil/water interface in O/W emulsions, interfacial layers can be prepared and visualized by AFM at planar Langmuir films (air/water interface). Comparison with the same components in bulk can be performed in order to determine the impact of adsorption at the interface on the morphology of the particles and structure of the interfacial layer. The planar films are generally imaged by AFM under dried conditions. Several examples illustrating the use of AFM to visualize the microstructure of planar Langmuir films are presented below.



#### **7.4.2.1 Example 1: applications of atomic force microscopy to cellulose nanoparticles adsorbed at planar Langmuir films**

Atomic force microscopy was used to visualize cellulose nanoparticles from ginkgo seed shells adsorbed at planar Langmuir films after using the Langmuir-Schaefer technique (Ni et al., 2020) (Fig. 7.2O). After dilution of the cellulose suspension to 0.001% (w/v), the glass vial was filled with 10 mL sample suspension avoiding the introduction of air bubbles. Subsequently, the vial was carefully placed for 24 h to make cellulose nanoparticles adsorb at the air/water interface. Freshly cleaved micas were treated using 3-amino-propyl-triethoxysilane (0.05% v/v) to convert charge for 60 s, then washed with deionized water, and dried in air. The resulting mica was dipped horizontally on the air/water interface, and then dipped in ethanol (above 99.8% v/v) to exchange phase and remove unadsorbed cellulose nanoparticles.

The authors found that for high concentrations, cellulose nanoparticles were randomly dispersed at the interface and caused high surface coverage. The authors reported that this was consistent with the result reported for curved droplets in O/W emulsions. However, the interfacial layer formed was a discontinuous interfacial layer, probably indicating the weak interfacial layer strength. The interfacial behavior of cellulose nanoparticles demonstrated the occurrence of cellulose entanglements at the interface. The network structure formed was attributed to excluded volume interactions and capillary interactions, and to the strength of capillary interactions depending on the contact angle.

#### **7.4.2.2 Example 2: applications of atomic force microscopy to whey protein-based systems adsorbed at planar Langmuir films**

Atomic force microscopy was used to image Langmuir-Blodgett films of WPI-based systems and to further understand the interfacial microstructure (Yang, Thielen, Berton-Carabin, van der Linden, & Sagis, 2020). Langmuir-Blodgett films of the protein-stabilized interfaces were prepared using a Langmuir film balance. Protein layers were formed by spreading protein solution on the surface and were equilibrated for 30 min. The surface pressure was monitored using a Wilhelmy plate. The layer was compressed reducing the surface area of the trough, with barriers moving at 5 mm/min. After reaching a stable surface pressure, the films were transferred on a freshly cleaved mica substrate with 1 mm/min withdraw speed. The films were dried in a desiccator and stored at room temperature until AFM analysis. AFM images of the Langmuir-Blodgett films

were recorded in tapping mode using ScanAsyst-air model nonconductive pyramidal silicon nitride probes (Bruker) with a normal spring constant of 0.40 N/m. A lateral scan frequency of 0.977 Hz was employed for all topographical images. The lateral resolution was set to  $512 \times 512$  pixels<sup>2</sup> in a scan area of  $2 \times 2 \mu\text{m}^2$  for WPI films and  $10 \times 10 \mu\text{m}^2$  for aggregate and bead films. At least two locations were visualized for each sample to ensure a good representativeness. The AFM images were analyzed using software.

In this study, AFM revealed the topography of the layers made by loading each protein Langmuir-Blodgett film onto a mica substrate at various surface pressures. AFM images of these films made from native WPI-, aggregate-, and bead-stabilized interfaces showed that the native WPI and aggregate films had a highly heterogeneous structure in which the proteins form a dense clustered network. The spherical WPI gel beads produced by cold gelation of WPI heat-denatured aggregates with calcium salt bridges were randomly distributed throughout the film, separated by large areas, where smaller proteinaceous materials were present. WPI beads were present at the interface at a surface pressure of 19 and 23 mN/m. The beads co-existed with aggregates, while thin regions were present between the beads and aggregates, even at the higher compression. AFM images indicated that smaller protein constituents were present in the bead films, which further supported the hypothesis of their contribution to the interfacial properties. The absence of the aggregates at a higher surface pressure than 23 mN/m could suggest the loss of the aggregates at the surface, which does not necessarily suggest the loss of the aggregates from the interface. Aggregates could remain at the interface, but could be pushed down toward the bulk phase upon compression, which causes them to be invisible for AFM topographical measurements.

#### ***7.4.2.3 Example 3: applications of atomic force microscopy to natural lipid droplets surface such as the egg yolk low-density lipoproteins adsorbed at planar Langmuir films***

The natural interfacial layers of lipid droplets such as the egg yolk low-density lipoproteins are difficult to examine at the nanoscale level. Researchers have therefore develop strategies to adsorb the small lipid droplets and spread their interfacial material at air/water planar Langmuir films before AFM imaging in air.

As an example, the pioneer work performed by Dr. M. Anton's group (INRAE, France) successfully permitted the observation by AFM of the

structure of planar Langmuir films made by low density lipoproteins (LDL) from hen egg yolk, which are composed of apoproteins, neutral lipids, and phospholipids and are the most important contributors to egg yolk emulsifying properties (Dauphas et al., 2007a,b). These egg yolk LDL have been deposited, adsorbed and spread at the air/water interface to form a monolayer which has been compressed to measure an isotherm using Langmuir trough. This isotherm presented three transitions. The AFM images revealed that the structures observed in the egg yolk LDL film were different depending on the surface pressure  $\pi$  (Fig. 7.2P). The apoproteins and neutral lipids appeared to be miscible up to the apoprotein–lipid transition, when demixing occurred. The structures observed after the apoprotein–lipid transition should be due to the demixing between apoproteins and neutral lipids. On the other hand, apoproteins and phospholipids seemed miscible despite the surface pressure. Hence, thanks to AFM examination of interfacial films of LDL transferred onto mica at pH 7 and imaged in air, the authors interpreted that the first transition ( $\pi = 19$  mN/m) could be attributed to the free neutral lipid collapse; the second transition ( $\pi = 41$  mN/m) could be attributed to the demixing of apoprotein–neutral lipid complexes; and the last transition ( $\pi = 51$  mN/m) could correspond to phospholipid collapse or to demixing of apoprotein–phospholipid complexes. The interpretations were based on the morphology of the components visualized in the AFM images. Unfortunately, AFM does not bring direct information on the chemical composition of the samples that is necessary to identify the components (apoproteins, neutral lipids, phospholipids).

In the research area of egg yolk, AFM imaging in air was also used to investigate the surface of egg yolk granules after their adsorption at air/water planar Langmuir films (Shen et al., 2020).

### 7.4.3 Nanoemulsions and emulsions: lipid droplets under the atomic force microscopy tip

Nanoemulsions and emulsions that contain lipid droplets, that are three-dimensional lipid assemblies, of nanometer to hundreds of micrometer size range can be imaged by AFM.

Most of the AFM investigations on O/W emulsions and nanoemulsions were performed after deposition of the aqueous system containing the lipid droplets onto a freshly cleaved mica and air-dried. Few authors investigated the morphology and nanomechanical properties of processed lipid droplets, or natural lipid droplets such as the OBs from plants or

seeds and the fat globules from milk in the aqueous medium (see Section 7.5).

Examples illustrating the use of AFM for the characterization of the lipid droplets in nanoemulsions and emulsions are presented below.

#### **7.4.3.1 Example 1: applications of atomic force microscopy imaging to air-dried lipid droplets**

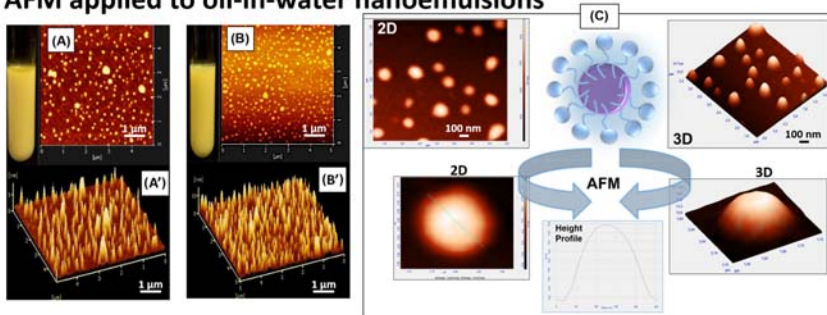
- AFM was used to determine the morphology and size of lipid droplets in O/W nanoemulsions.

For example, O/W nanoemulsions composed of two different carrier oils, that are long-chain triacylglycerols (TAGs) or medium-chain TAGs, stabilized by scallop gonad protein isolates, and encapsulating beta-carotene were imaged by AFM at ambient temperature (Han et al., 2020) (Fig. 7.3A and B). The nanoemulsions were diluted 1000-fold with Milli-Q water, and then 10  $\mu\text{L}$  of a suspension of nanoemulsion was placed, spread, and naturally air-dried at ambient temperature on a freshly cleaved mica substrate. The AFM images of the samples were acquired in tapping mode, adopting microfabricated silicon cantilever tips with scan rate of 1 Hz, spring constant of 0.12 N/m, and cantilevers length of 200  $\mu\text{m}$ .

In another example, lipid droplets in O/W nanoemulsions were allowed to adsorb on a fresh mica surface for 24 h by dipping it in the prepared samples. Then, the surfaces were rinsed in double-distilled water and dried at room temperature for about 2 h. AFM morphology observations were performed with a scanning speed of 0.5 Hz, a low-resonance-frequency pyramidal silicon cantilever resonating at 250–331 kHz at a constant force of 20–80 N/m (Waglewska & Bazylińska, 2021) (Fig. 7.3C). AFM imaging allowed the examination of the lipid droplets with a nanoscale resolution able to determine their size and morphology.

- AFM was used to visualize O/W emulsions containing lipid droplets stabilized by lipophilic soybean proteins and hydroxypropyl methylcellulose at different pH values (Li et al., 2020). The emulsion morphology was examined by AFM in tapping mode. Prior to AFM imaging, each emulsion was diluted to 10  $\mu\text{g}/\text{mL}$  with 20 mM PBS (0.01 M, pH 3, 5, or 7) and then placed on a freshly cleaved mica disk and air-dried for 20 min. The authors examined the microstructure of the emulsions and visualized aggregation of the lipid droplets at acidic pH, which was alleviated in the presence of hydroxypropyl methylcellulose.
- AFM was used to investigate *Pseudosciaena crocea* roe protein-stabilized O/W emulsions under digestive conditions (Tang et al., 2020)

### AFM applied to oil-in-water nanoemulsions



### AFM applied to oil-in-water emulsions during *in vitro* digestion

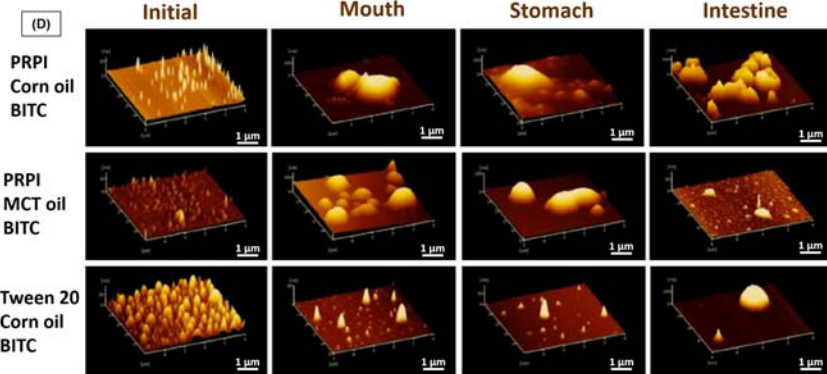


**Figure 7.3** Examples of atomic force microscopy (AFM) imaging applied to oil-in-water nanoemulsions and emulsions. (A,B) AFM phase images (top) and AFM 3D height images (bottom) of nanoemulsions composed of long-chain triacylglycerols (A,A') or medium-chain triacylglycerols (B,B') and encapsulating beta-carotene. (C) AFM images of oil-in-water nanoemulsions with 2D and 3D representations. (D) AFM images of three oil-in-water emulsion systems during the gastrointestinal tract digestion process. The emulsions were composed of corn oil or medium-chain triacylglycerol oil, stabilized by *Pseudosciaena crocea* roe protein isolate or Tween 20, and were encapsulating benzyl isothiocyanate. For (A,B) Adapted from [Han et al. \(2020\)](#). (C) Adapted from [Waglewska and Bazylińska \(2021\)](#). (D) Adapted from [Tang et al. \(2020\)](#).

(Fig. 7.3D). Emulsions were diluted 5000-fold by pH 8 phosphate buffer. Samples (5 μL) were dropped onto the surface of freshly cleaved mica and air-dried until no liquid was visible on the mica surface. Then, the samples were tested in dynamic force microscopy mode, which is a hybrid of the two most fundamental measurement methods, represented by contact mode and true noncontact mode. The cantilever vibrates in free space in the vicinity of the resonant frequency like in noncontact mode, and at the

same time, as the vibrating cantilever gets very close to the sample surface, it taps the surface repeatedly. The tip “contacts” the sample surface as in contact mode. The probe type used in this experiment was SI-DF-40P2. AFM images allowed the visualization of structural changes of the emulsions during the gastrointestinal tract digestion process in the mouth, the stomach, and the intestine. AFM images provided information about the size of the emulsion lipid droplets, their aggregation, and the roughness of the emulsion surface structures.

#### **7.4.3.2 Example 2: application of atomic force microscopy force spectroscopy to plant oil bodies in water**

Natural OBs from plants and seeds are lipid droplets with a mean diameter of 1–3  $\mu\text{m}$ . OBs have a core rich in TAGs enveloped by a monolayer of phospholipids with embedded proteins. Their applications in the industrial food sector are closely related to the hemi-membrane composition and mechanical properties, which remain difficult to determine on a single droplet level.

The nanomechanical properties of natural OBs from soybean, sesame, and peanut were investigated by AFM (Yang, Su et al., 2020). The negatively charged OBs (zeta potential  $-25$  mV at pH 7) were deposited on a glass substrate covered by poly-L-lysine in order to impart positive charges to the substrate and facilitate the immobilization of OBs (Fig. 7.4). Any free OBs were removed by washing with ultrapure water prior to AFM experiments. The glass substrate with immobile OBs was then loaded into the AFM fluid cell. The colloidal probe (a spherical silica particle about 20  $\mu\text{m}$  in diameter) was attached to a tipless AFM probe. The spring constant of the cantilevers was determined using the in-built thermal tuning method (Hutter & Bechhoefer, 1993) before each experiment. The AFM probe was slowly lowered into the fluid cell containing substrate-attached OBs in water (Fig. 7.4). The locations of the center of the probe cantilever and an immobilized OB were determined by an optical microscope installed on the AFM (Fig. 7.4A). The colloidal probe was moved to the top of the center of an immobilized OB and was used to apply force to the OB. Force curves were acquired as the AFM probe vertically compressed the OB and returned. The resulting force ( $F$ )–deformation ( $\delta$ ) curves (Fig. 7.4C) were used to evaluate the mechanical properties of the OBs using different mechanical models. The approach curves increased gradually and smoothly with the increase of deformation after the contact point ( $\delta = 0$ ), indicating that the OBs did not rupture or slip under the

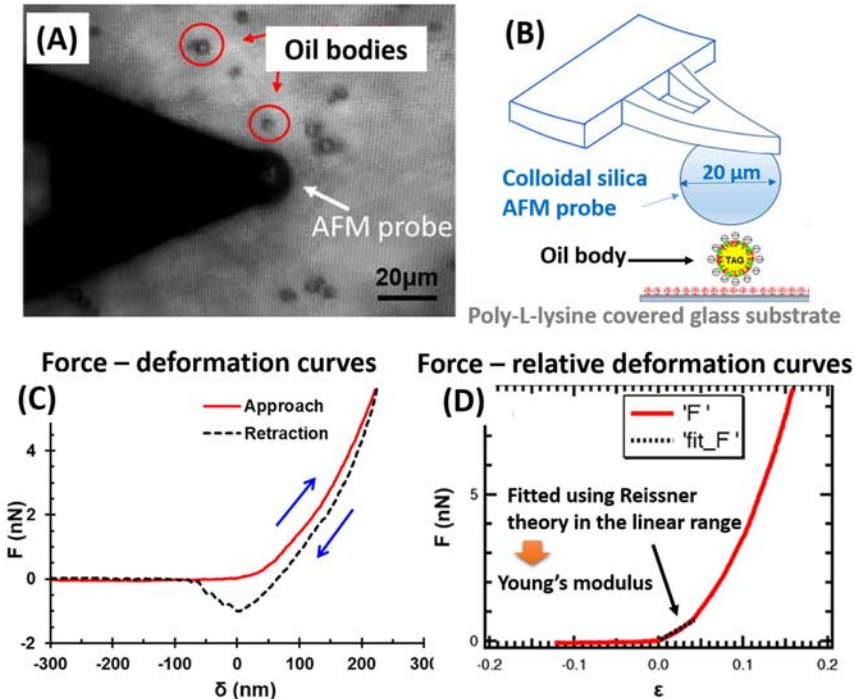


**Figure 7.4** Atomic force microscopy (AFM) is used to investigate the nanomechanical properties of natural plant oil bodies. (A) Optical microscopy image showing the cantilever on the top of the hydrated sample containing oil bodies immobilized on a poly-L-lysine-modified glass substrate. (B) Schematic representation of the colloidal AFM probe and a single negatively charged oil body immobilized on the positively charged substrate. (C) Force–deformation curve during approach (solid line) and retraction (dashed line) of an AFM colloidal probe on a soybean oil body. (D) Force–relative deformation curve recorded for a soybean oil body with 2 μm diameter fitted using the Reissner theory in the linear range. Adapted from Yang et al. (2020b).

force applied in the measurements. In this work, the authors showed that OBs are soft but robust natural lipid droplets that can recover following compressive strains as large as 0.3. They concluded that the elastic membrane theory combined with the effect of interfacial tension is a suitable model used to calculate the Young's modulus of the lipid droplets under large deformation. This pioneer study provided insights into the mechanical properties of OBs and expanded the application of AFM in the field of mechanical measurements on food hydrocolloids.

## 7.5 Application of atomic force microscopy to dairy lipid systems: membranes, liposomes, and emulsions

### 7.5.1 Milk: from natural to processed oil-in-water emulsions

Milk is a natural O/W emulsion in which the lipids are organized as droplets called the milk fat globules with a size ranging from 0.1 to 10  $\mu\text{m}$  and a mean diameter around 4  $\mu\text{m}$ . The milk fat globules are biological lipid assemblies that can be considered as complex soft matter colloidal systems with unique functional properties (Lopez, Cauty, & Guyomarc'h, 2019). They are naturally secreted in milk by the mammary epithelial cells as unique lipid delivery assemblies providing energy, nutrients, and bioactive molecules that contribute to the optimal growth of newborns. Milk fat globules are composed of a core of hydrophobic lipids, the TAG, surrounded by a biological membrane called the milk fat globule membrane (MFGM). The MFGM is organized as a trilayer of polar lipids with a lateral segregation of milk-sphingomyelin (about 30% of polar lipids) and cholesterol in the outer bilayer (Lopez, 2020). The MFGM also contains membrane proteins that form a glycocalyx around fat globules in milk. Milk fat globules and more precisely the MFGM offer complexity at the oil/water interface that could be involved in many biological functions, for example in the gastrointestinal tract, that are not yet fully elucidated.

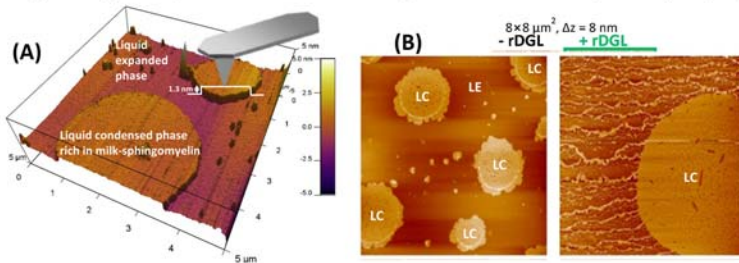
The structure and surface properties of milk fat globules can be altered by technological processes such as the mechanical treatment of homogenization and thermal treatments (pasteurization, ultra high temperature) (Lopez, Cauty, & Guyomarc'h, 2015). Natural and processed milk fat globules can also be submitted to environmental changes upon processing and storage (temperature, pH, ionic strength).

The examination of milk lipid assemblies and dairy emulsions is of special interest to elucidate their functions, for example in dairy products and in the gastrointestinal tract upon digestion.

For the last 10 years, several research groups worldwide used AFM to investigate milk lipid assemblies organized in the form of air-dried planar Langmuir films, hydrated supported lipid bilayers (SLBs) and unsupported lipid bilayers (liposomes), as well as natural or processed milk fat globules. Information on the morphology, topography and on the mechanical properties of lipid assemblies, at the nanoscale and at the individual particle levels, requires experiments by AFM imaging and AFM force spectroscopy (recording of force-distance curves).



**Monolayers of polar lipids from the milk fat globule membrane (MFGM): topography**



**Supported lipid bilayers of MFGM polar lipids : interaction with proteins**

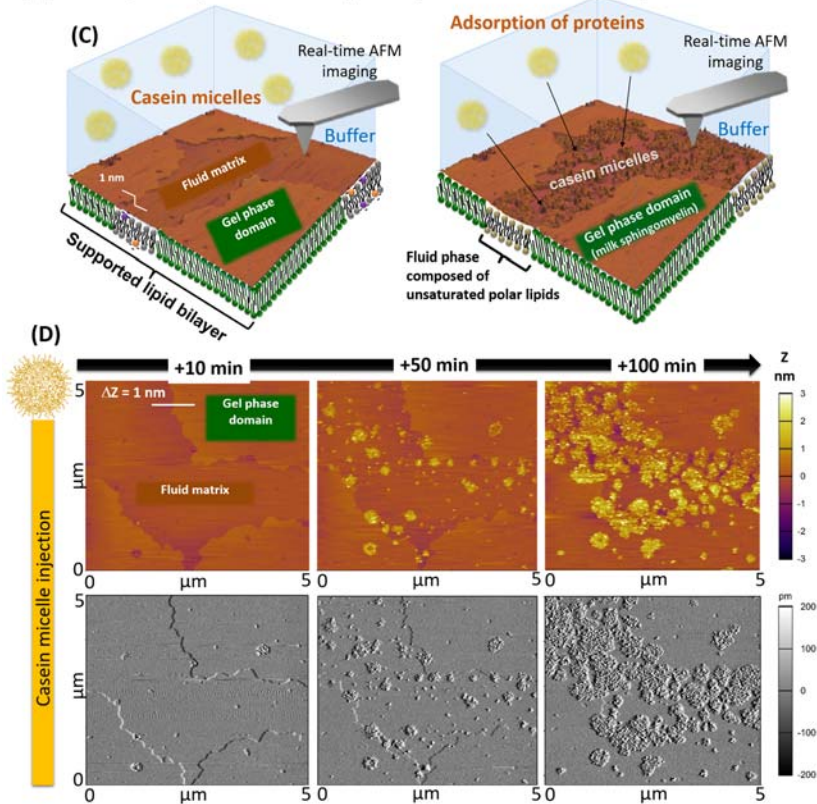


**Figure 7.5** Application of atomic force microscopy (AFM) imaging for lipid monolayers and supported lipid bilayers (SLBs). (A,B) Air-dried planar Langmuir films of polar lipids from the milk fat globule membrane: (A) phase separation between a liquid condensed phase forming spherical domains rich in the saturated milk-sphingomyelin surrounded by a liquid expanded phase composed of unsaturated polar lipids. (B) Insertion of recombinant dog gastric lipase. (C,D) Adsorption of proteins on SLBs in an aqueous environment: (C) AFM images of SLBs showing heterogeneity in their topography with the coexistence of ordered lipid domains rich in the

### 7.5.2 Topography of lipid monolayers and membranes in air

In the pioneer work performed by Prof. R. Jimenez-Flores' group (CalPoly, USA), AFM imaging of a monolayer film prepared by depositing the MFGM components isolated from buttermilk powder onto a mica surface at a film pressure of 40 mN/m showed the formation of a lipid domain (Jiménez-Flores & Brisson, 2008). This AFM study has opened the doors for other investigations of milk lipid systems.

From a methodological point of view, supported lipid monolayers are generally prepared by the Langmuir-Blodgett method at a defined surface pressure, deposited on mica, dried, and observed by AFM in air. AFM imaging of these dried lipid monolayers provides information on their topography and morphology of the interface, including phase separation of lipids and shape of lipid domains. The nanoscale resolution of AFM applied to air-dried supported milk lipid monolayers permitted the measurements of differences in height of 1.3 nm between sphingomyelin-rich domains in the liquid condensed phase (circular shape) and the surrounding matrix composed of unsaturated milk polar lipids in the liquid expanded phase (Fig. 7.5A) (Lopez, 2020). AFM imaging of Langmuir-Blodgett films composed of milk polar lipids was also used to examine the preferential insertion of recombinant dog gastric lipase (Fig. 7.5B) (Bourlieu et al., 2016). These AFM images of lipid monolayers taken in dry conditions do not consider the dynamic processes of lipid domain formation nor the dynamic interactions between the lipid monolayers and proteins.

### 7.5.3 Topography and mechanical properties of hydrated lipid bilayers

Lipid bilayers are well-adapted systems to get information on complex membranes such as the MFGM. Lipid bilayers can be supported (SLBs) or unsupported (liposomes) to avoid the possible effect of the underlying substrate below the membrane. Among surface imaging techniques, in recent years AFM has emerged as a powerful tool to provide information on specific features on the surface of SLBs. AFM imaging can be combined with

- 
- ◀ saturated milk-sphingomyelin and a fluid phase (left); preferential adsorption of casein micelles in the fluid phase of the membrane (right). (D) Kinetics recorded as a function of time showing the progressive adsorption of casein micelles on SLBs imaged by AFM. For (A) Adapted from Lopez (2020). (B) Adapted from Bourlieu et al. (2016). (C,D) Adapted from Obeid, Guyomarc'h, David-Briand et al. (2019).

AFM force spectroscopy to provide both structural and nanomechanical information. AFM can operate as a nanoscale indenter on every pixel of a force map and provide local mechanical information. Indentation by AFM of a lipid bilayer can provide information on the elastic properties such as the Young modulus and on the breakthrough force that is determined when the AFM tip pierces the bilayer.

### **7.5.3.1 Supported lipid bilayers**

Atomic force microscopy has become a well-established technique for imaging SLBs at nanometer resolution but also for investigating their mechanical stability and elastic properties (measurement of the Young modulus). SLBs can be deposited on mica using the Langmuir-Schaffer method. SLBs can also be formed on a mica substrate by the method of vesicle fusion (Mingeot-Leclercq, Deleu, Brasseur, & Dufrene, 2008).

The topography of SLBs formed by the method of vesicle fusion, composed of selective lipids (e.g., milk-sphingomyelin and dioleoylphosphatidylcholine (DOPC)) or the whole lipid composition of the MFGM, was examined by AFM. The SLBs were prepared and imaged by AFM in an aqueous phase that was close to the physiological conditions of milk (buffer pH 6.7). Furthermore, kinetics in temperature were performed between 60°C and 6°C to investigate changes in the topography of the SLBs as a function of the phase state of the milk polar lipids (Murthy, Guyomarc'h, & Lopez, 2016). Above 40°C, corresponding to temperatures at which all the lipids were fluid in the SLBs, the AFM images showed a flat surface of the SLBs. For temperatures below 40°C, the AFM images evidenced phase separation of the saturated high-melting temperature milk-sphingomyelin with the formation of gel-phase domains higher by about 1 nm than the surrounding fluid phase composed of the unsaturated low-melting temperature milk polar lipids (Guyomarc'h, Murthy, & Lopez, 2016; Murthy et al., 2016) (Fig. 7.6). Gel-gel phase separation within milk-sphingomyelin domains was also imaged thanks to the nanoscale resolution of AFM (Guyomarc'h, Chen, Et-Thakafy, Zou, & Lopez, 2017). The two distinct gel phases exhibited a difference in height of 0.5–1.1 nm and were interpreted as interdigitation of individual sphingomyelin molecules with mismatch between the chains. Such gel-gel phase separation evidenced by AFM affects the topography of the membranes and could be involved in specific biological functions, for example, the insertion of proteins such as membrane proteins, the digestive enzymes, or microbial enzymes.

## Supported lipid bilayers of MFGM polar lipids : AFM imaging and force mapping

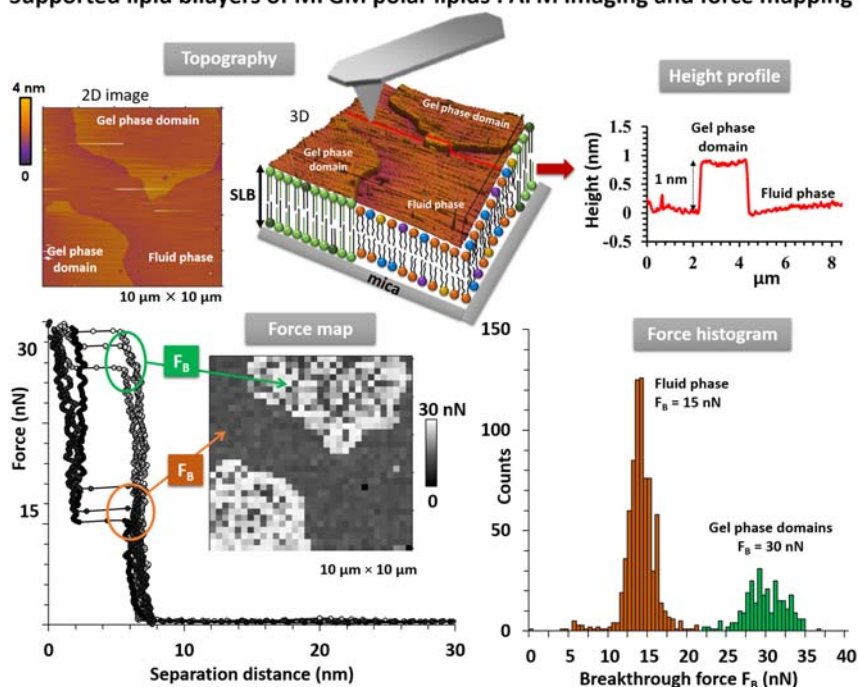


**Figure 7.6** Atomic force microscopy imaging and force spectroscopy of supported lipid bilayers (SLBs) composed of milk polar lipids from the milk fat globule membrane showing phase separation and heterogeneities in the nanomechanical properties. Adapted from *Murthy et al. (2016)*.

A unique feature of AFM in aqueous environments is its ability to monitor dynamic processes, such as the interaction of SLBs with proteins (Fig. 7.5C and D). The casein micelles, which are the main milk protein assemblies (100 nm in diameter), were injected in the aqueous phase above SLBs of selective lipid compositions and revealed their preferential adsorption in the fluid phase of the membrane compared to the ordered phase rich in milk-sphingomyelin (Obeid, Guyomarc'h, David-Briand et al., 2019).

Besides imaging, AFM can be used to investigate the mechanical stability of a membrane with nanoscale lateral resolution. The applied load is increased till a breakthrough event occurs in the force curve, allowing the determination of the breakthrough force ( $F_B$ ). Heterogeneities in the nanomechanical properties of bilayer membranes composed of milk polar lipids have been quantified (Murthy et al., 2016). The domains rich in

milk-sphingomyelin in the gel phase exhibit a higher  $F_B$  than the surrounding fluid matrix composed of the unsaturated polar lipids (30 nN vs 15 nM, respectively) (Fig. 7.6). The nanomechanical properties of SLBs are affected by the temperature with  $F_B$  that increases when the temperature decreases. The nanomechanical properties of SLBs are also affected by the lipid composition of the membrane; for example, the presence of cholesterol lowered the  $F_B$  of the SLBs composed of milk polar lipids (Guyomarc'h et al., 2014; Murthy, Guyomarc'h, Paboeuf, Vié, & Lopez, 2015), while the presence of palmitoyl-ceramide molecules increased the  $F_B$  of SLBs composed of milk-sphingomyelin and of the fluid phospholipid DOPC (Murthy, Guyomarc'h, & Lopez, 2018).

The elastic properties of planar SLBs composed of milk polar lipids from the MFGM and milk-sphingomyelin in the gel, fluid, or liquid-ordered phase were investigated by AFM through the determination of the Young modulus in hydrated conditions (buffer, pH 6.7) at 20°C (below phase transition temperature) and then at 50°C (above phase transition temperature) (Et-Thakafy, Guyomarc'h, & Lopez, 2019). AFM imaging was performed in contact mode with metal-to-ligand charge transfer (MLCT) probes. Force spectroscopy experiments were performed in the same imaged area and using the same probe as for AFM imaging. Force mapping was performed with an applied load of up to 200 pN. The Young modulus was calculated by fitting the force curves using the classical Hertz model. For the SLBs composed of milk polar lipids from the MFGM, at 20°C the Young modulus was 16 MPa for the gel phase domains and 10 MPa for the surrounding fluid phase while at 50°C the Young modulus for 4 MPa for the homogeneous and fluid SLBs. For the SLBs composed of milk-sphingomyelin in the gel phase the Young modulus was 18 MPa while it corresponded to 4 MPa in the fluid phase and to 1 to 2 MPa in the liquid-ordered phase formed in the presence of cholesterol.

These pioneer results obtained by probing hydrated SLBs using AFM increased the knowledge of the mechanical stability and elastic properties of membranes composed of milk polar lipids.

### **7.5.3.2 Unsupported lipid bilayers: liposome membranes**

Atomic force microscopy is a suitable technique to image and probe the mechanical properties of liposome membranes (Et-Thakafy et al., 2017). Indentation measurements on volumetric objects such as small unilamellar vesicles (liposomes) has proven to be a sensitive approach to examine,

using AFM, the elastic properties of membranes by measuring the Young modulus at the nanoscale. Furthermore, indentation measurements on liposomes avoid the possible effect of the rigid support compared to SLBs.

As an example, we develop here the AFM indentation experiments that have been performed on liposomes composed of sphingomyelins differing in their saturation and acyl chain length in comparison with the naturally complex milk-sphingomyelin (Et-Thakafy, Delorme, Guyomarc'h, & Lopez, 2018). In this study, AFM indentation on liposomes with controlled compositions has been performed to determine the impact of the naturally complex heterogeneity of milk-sphingomyelin (composed of individual sphingomyelins with variations in saturation and acyl chain length), on the overall mechanical properties of milk-sphingomyelin membranes (Fig. 7.7). The liposomes were prepared at 65°C by sonication of the selected sphingomyelins (alone or in combination) and the suspension was left to cool and equilibrate at 20°C. The liposomes had a mean diameter of 120 nm. The liposome suspension was deposited onto silicon surface and then left to incubate at 20°C for 30 min. Unadsorbed liposomes were removed. In these AFM experiments, silicon surface has been chosen since it has a lower charge density than freshly cleaved mica, which prevented excessive deformation or fusion of the liposomes. Furthermore, the nanorugosity of

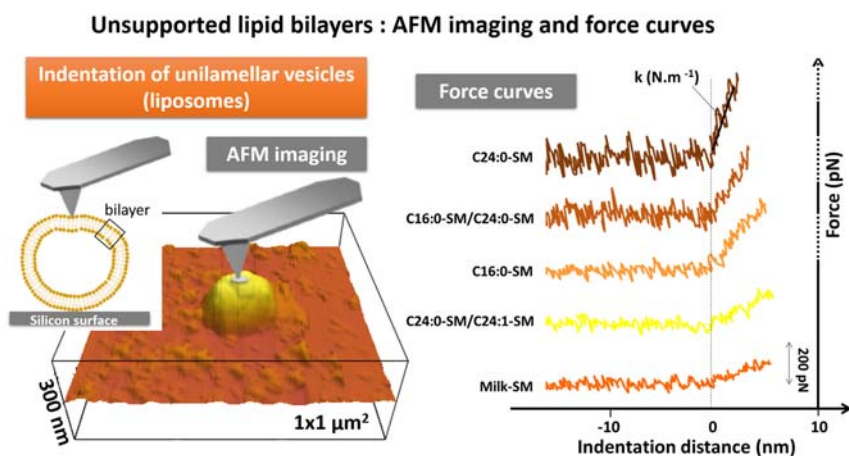


**Figure 7.7** Atomic force microscopy height image of a liposome corresponding to unsupported lipid bilayer and force curves recorded at the top of liposomes of various compositions (acyl chains of sphingomyelin, SM) as indicated in the figure. The recording of these force curves permitted the determination of the Young modulus of the unsupported membranes. Adapted from Et-Thakafy et al. (2018).

silicone surface was thought to help immobilization of the liposomes. The samples of immobilized liposomes were imaged in contact mode with silicon MLCT probes. Contact mode was preferred over tapping mode in order to use soft probes for imaging and keep the same probe for indentation. The Young modulus calculated from the force curves showed high values for individual saturated sphingomyelin (C16:0-SM and C24:0-SM) and their equimolar mixture, and a high decrease in the Young modulus in the presence of unsaturated chains (C24:0-SM vs C24:0-SM/C24:1-SM) (Et-Thakafy *et al.*, 2018). Altogether these AFM nanoindentation experiments applied to milk-sphingomyelin revealed that the natural complexity of the composition in membrane lipids, including various chain lengths and unsaturation of the acyl chains, impacts their mechanical properties.

#### 7.5.4 Surface topography and roughness of milk fat globules

In a pioneer AFM work, Prof. R. Dagastine and collaborators examined the surface morphology and roughness of milk fat globules in their natural state and after processing (homogenisation), with nanometer resolution (Balasuriya, Ong, Gras, & Dagastine, 2012). An important preliminary step was to enhance the adhesion of milk fat globules on a substrate support. The AFM fluid cell was fitted with a circular glass disk coated with poly-L-lysine. Milk fat globules were allowed to attach to the poly-L-lysine glass disk. The cantilevers used were triangular silicon nitride MLCT cantilevers (Veeco, Santa Barbara, USA). AFM imaging was conducted at a room temperature (20°C–25°C) in alternative current or intermittent contact mode at slow scanning speeds because of the delicate nature of the MFGM and to impose the minimum amount of force possible on its surface. AFM images showed changes in the morphology and roughness of milk fat globule surface with processing, with a higher roughness for homogenized samples compared to the non-processed samples (Balasuriya *et al.*, 2012).

AFM imaging provides details on the surface morphology of unprocessed milk fat globules covered by the MFGM rich in phospholipids and of homogenized milk fat globules at the nanoscale (Fig. 7.8). The roughness of the surface is higher for homogenized milk fat globules due to the adsorption of casein micelles (milk protein assemblies of 100 nm in diameter) at the surface of milk fat globules. AFM imaging also provides information on the size of the particles and confirms that the diameter of

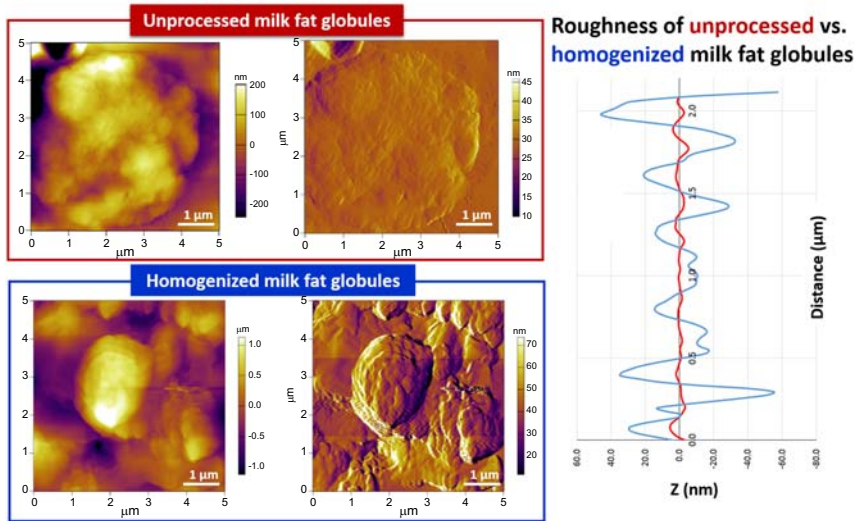


**Figure 7.8** Atomic force microscopy height images and height profiles showing the surface roughness of unprocessed and homogenized milk fat globules. *Results from Dr. C. Lopez and collaborators (INRAE, France).*

milk fat globules is decreased from 4  $\mu\text{m}$  to less than 1  $\mu\text{m}$  after milk homogenization.

These AFM works showed that the surface of complex soft matter colloids such as milk fat globules can be quantitatively characterized using AFM with a nanometer resolution and revealed differences in morphology and roughness due to processing.

### 7.5.5 Probing specific interactions and adhesion forces involved at the surface of milk fat globules

Atomic force microscopy senses interaction forces in the pN to nN range, acting between a tip at the end of a flexible cantilever and a sample surface (Müller, Krieg, Alsteens, & Dufrêne, 2009). In order to probe specific interactions or adhesion forces, the AFM tip is functionalized with the molecule of interest. The objects need to be immobilized on a surface. Interactions between the functionalized probes and the immobilized objects produce a random series of adhesion peaks on the AFM retraction force curves, evidencing multiple intermolecular interactions (Francius et al., 2009; Friedrichs et al., 2013). To date, investigations performed by AFM force spectroscopy to measure interaction and adhesion forces between individual objects involved in food applications were essentially



conducted on bacteria interacting with the milk fat globule membrane (Guerin et al., 2018), and on lipid droplets such as milk fat globules (Obeid, Guyomarc'h, Francius et al., 2019; Obeid et al., 2020) as detailed below.

### 7.5.5.1 Specific interactions: single molecule force spectroscopy

Specific interaction forces, for example between a protein and an antibody, can be investigated by AFM force spectroscopy with grafted tips.

Concerning milk emulsion applications, pioneer experiments have been conducted in Dr. C. Lopez's group (INRAE, France) to detect the presence of a major membrane-specific protein, the butyrophilin, by AFM on the surface of the biological membrane surrounding milk fat globules, the MFGM (Fig. 7.9). The AFM tip was functionalized by grafting anti-butyrophilin monoclonal antibody. Single molecule force spectroscopy performed on immobilized milk fat globules allowed the detection of butyrophilin by specific molecular recognition with butyrophilin/anti-butyrophilin interactions. The targeted butyrophilin was evidenced by the recording of a single rupture peak on the AFM retraction force

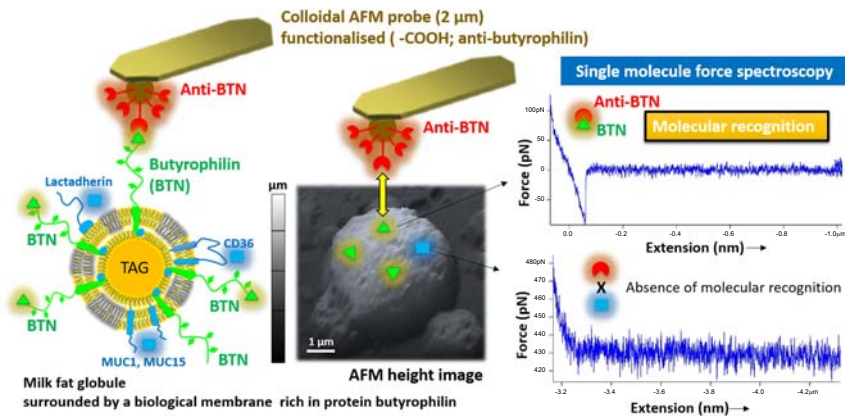


**Figure 7.9** Application of atomic force microscopy (AFM) to detect and localize a major protein, the butyrophilin, in the biological membrane surrounding fat globules in milk, through specific interactions between the antibody anti-butyrophilin and butyrophilin. Left: schematic representations of the AFM set-up using functionalized colloidal probes and of a milk fat globule. Middle: AFM height image of a milk fat globule immobilized on a substrate to perform the specific interaction experiments. Right: interaction curves showing the specific interaction between butyrophilin and the anti-butyrophilin attached to the colloidal AFM probe and the absence of adhesion in other parts of the membrane. *Results from Dr. C. Lopez and collaborators (INRAE, France).*

curve that was due to specific molecular recognition. The areas of the milk fat globule membrane did not exhibit any peaks in the retraction curves where other proteins (e.g., lactadherin, CD36, MUC1, MUC15) than butyrophilin were present. Single molecule force mapping combined with AFM imaging of immobilized milk fat globules revealed the spatial distribution of butyrophilin on the surface of milk fat globules. These AFM experiments were combined with scanning electron microscopy observations of milk fat globules performed in the presence of anti-butyrophilin linked to gold particles.

Another example of specific interactions investigated by single molecule AFM force spectroscopy concerns the grafting of AFM tips with the lysenin toxin for the specific recognition of sphingomyelin-rich domains in milk polar lipid membranes (SLBs) and on the surface of milk fat globules (Dr. C. Lopez's group, INRAE, France). These AFM experiments were combined with confocal laser scanning microscopy experiments with the fluorescently labeled lysenin toxin able to interact with milk-sphingomyelin domains and the fluorescent dye Rhodamine-DOPE able to solubilize in the fluid matrix surrounding sphingomyelin domains.

#### **7.5.5.2 Adhesion forces**

AFM was used to examine the adhesion forces between the main proteins of milk (i.e., the casein micelles) and unprocessed milk fat globules or homogenized milk fat globules at neutral and acidic pH (Obeid, Guyomarc'h, Francius et al., 2019; Obeid et al., 2020).

Milk fat globules were immobilized on isopore polycarbonate track-etched Millipore filters of 0.6- $\mu\text{m}$  pore size (Fig. 7.10). The filter membrane was gently rinsed with buffer in order to remove loosely immobilized milk fat globules, attached inside a Petri dish using a double-sided adhesive tape, and then immersed in a buffer. For AFM imaging, AFM silicon MSNL10 probes (nominal spring constant 0.01–0.03 N/m) were used. For adhesion force measurements, the AFM probes with attached 5  $\mu\text{m}$  borosilicate glass particles coated with gold and modified with  $\text{NH}_3$  groups (Novascan, Ames, USA; nominal spring constant 0.01 N/m) were used. The probes were incubated overnight in a dispersion of casein micelles, and then washed and kept in buffer at pH 6.7 until use. The successful grafting of caseins to the AFM probes was validated by confocal laser scanning microscopy (CLSM) experiments using fluorescent caseins (Fig. 7.10). The cantilever spring constant was determined prior to each AFM force spectroscopy experiment using the thermal noise calibration

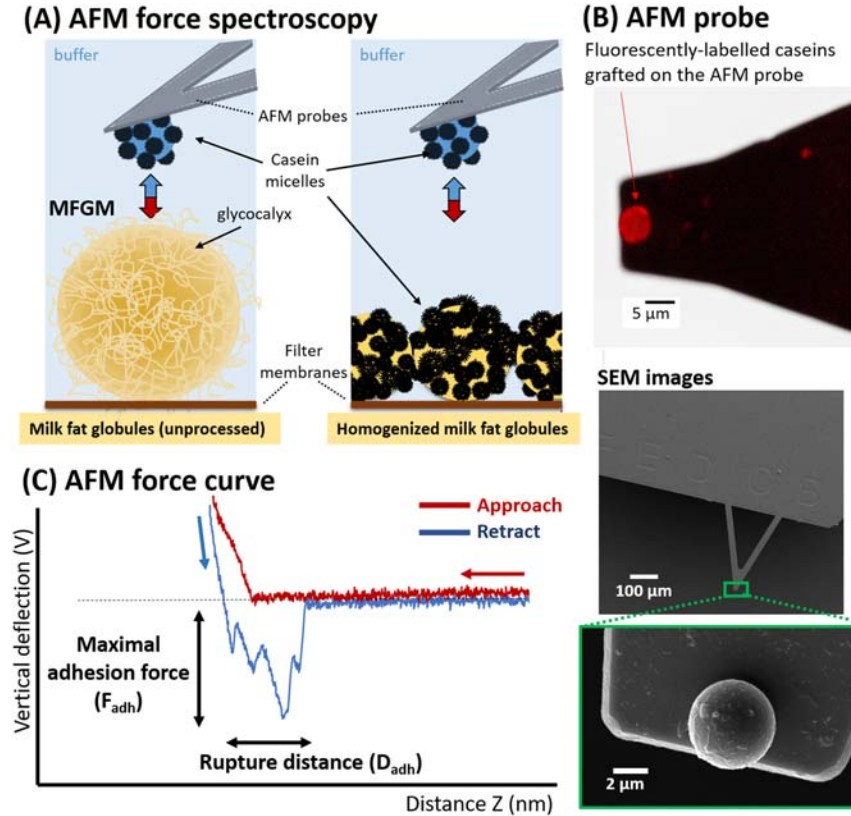


**Figure 7.10** Atomic force microscopy (AFM) experiments are able to probe the interactions between casein micelles and unprocessed or homogenized milk fat globules. (A) AFM force spectroscopy experiments are performed with colloidal probes functionalized with casein micelles. (B) AFM probes are examined by confocal laser scanning microscopy to visualize the caseins adsorbed on the colloidal probe, and by scanning electron microscopy (SEM). (C) AFM force curves are recorded during approach and retraction of the functionalized AFM probe. *Adapted from Obeid et al. (2019).*

method. Force maps exhibiting significant and specific adhesion events in the retraction force curves were recorded between the casein micelles-modified probes and the immobilized milk fat globules. The maximal adhesion forces ( $F_{adh}$ ), the adhesion work (area below the baseline,  $W_{adh}$ ), and the rupture distance ( $D_{adh}$ ) were determined. The worm-like chain (WLC) model fitted the adhesion events visible on the retraction force curves. Although the WLC model describes the mechanical stretching response of single molecules (Marszalek & Dufrene, 2012), it provides

supplementary insights into the integrity and flexibility of molecules during multiple interactions which are likely to occur when using colloidal probes (Guerin et al., 2018).

AFM imaging and adhesion force measurements were performed through the force-mapping mode at pH 6.7 and at pH 4.5 (Fig. 7.11). AFM-based force spectroscopy experiments performed at the particle scale level showed that the adhesion forces between individual milk fat globules

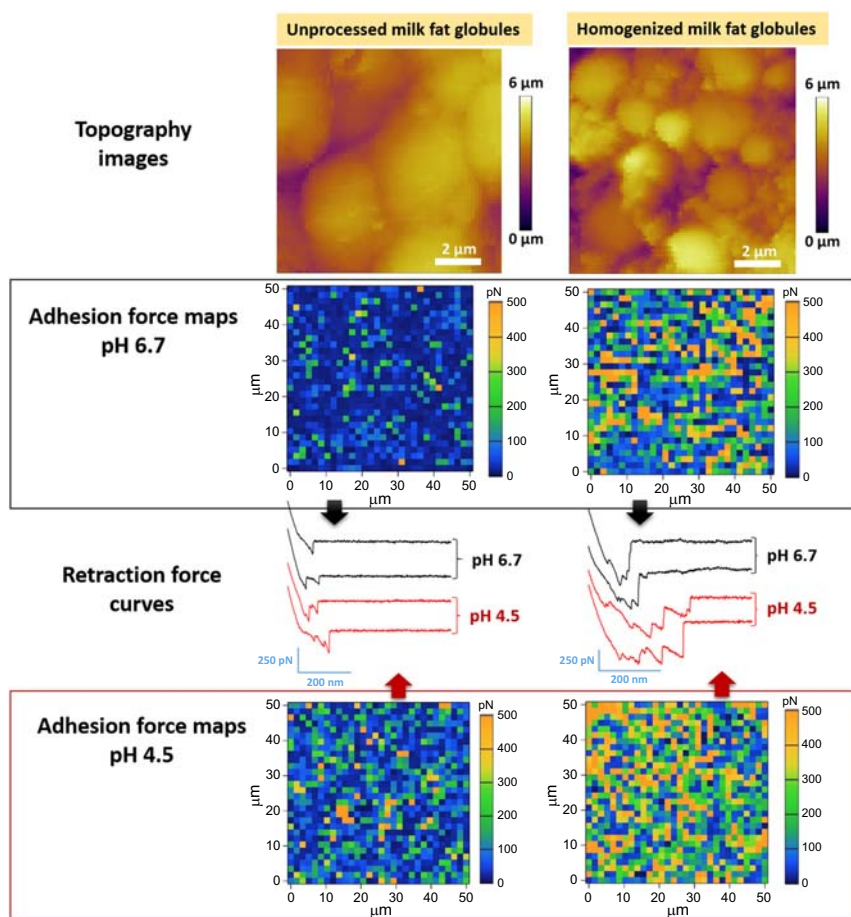


**Figure 7.11** Atomic force microscopy (AFM) experiments are able to probe the interactions between casein micelles and unprocessed or homogenized milk fat globules. AFM height images of unprocessed and homogenized milk fat globules immobilized on a flat substrate, AFM force maps and force curves are recorded at pH 6.7 and pH 4.5. Adapted from *Obeid et al. (2019)*.

and casein micelles are higher after homogenization, especially at acidic pH where the adhesion forces increased from 109 to 201 pN for unprocessed and homogenized fat globules, respectively (Obeid, Guyomarç'h, Francius et al., 2019). Furthermore, the adhesion forces are enhanced by about 1.7-fold at pH 4.5 after ultra-high temperature (UHT) treatment of homogenized milk, from 176 to 296 pN, thanks to highly reactive heat-denatured whey proteins located at the surface of milk fat globules and caseins (Obeid et al., 2020). These findings cast light on the importance of colloidal particle's surface properties and pH on their connectivity with the surrounding matrix which modulates the bulk microstructure and rheological properties with potential functional consequences.

This pioneer work showed that AFM-based force spectroscopy permits quantification of the interactions occurring at the colloidal particle's surface level.

## 7.6 Conclusions

Food foams and emulsions have benefited from technological development of AFM from biology and material physics. AFM has opened access to the nanoscale imaging, in air and aqueous environments, of colloidal structures and of oil/water interfaces in emulsions and air/water interfaces in foams. Furthermore, AFM allows correlation of topography imaging and force-deformation maps obtained in liquid, and their dynamics upon environmental changes such as the temperature and pH. AFM also allows precise topography imaging, determination of surface roughness and indentation of lipid membranes, supported and unsupported such as liposomes, and oil droplets such as the natural OBs and milk fat globules and provides quantitative information about nanomechanical properties with a high spatial resolution. AFM applications have therefore been expanded in the field of mechanical measurements on food colloids. Future opportunities and challenges to overcome exist. The recent development of high-speed imaging will be useful to track dynamic surface rearrangement phenomena at air/water interfaces in foams and oil/water interfaces in emulsions, as well as structural reorganizations due for example to enzymes upon digestion. A major limitation of AFM is that no direct identification of the chemical components is possible. In the future, the coupling of AFM imaging and nanomechanical AFM indentation with high spatial resolution spectroscopy techniques (infrared spectroscopy, Raman spectroscopy) and microscopy techniques such as CLSM,

super-resolution optical microscopy, total internal reflection fluorescence microscopy, and electron microscopy will be useful to further understand the oil/water and air/water interfaces.

## Acknowledgments

All the scientists who have performed worldwide stimulating experiments and contributed to the development of AFM imaging and force spectroscopy are acknowledged. Dr. C. Lopez thanks her collaborators, including the PhD student O. Et-Thakafy and the post-docs A.V.R. Murthy and S. Obeid for their significant contribution to the development of AFM methods to investigate milk lipid membranes and dairy emulsions.

## References

- Arachchige, M. P. M., Mu, T., & Ma, M. (2020). Structural, physicochemical and emulsifying properties of sweet potato pectin treated by high hydrostatic pressure and/or pectinase: A comparative study. *Journal of the Science of Food and Agriculture*, *100*, 4911–4920.
- Aswathanarayan, J. B., & Vittal, R. R. (2019). Nanoemulsions and their potential applications in food industry. *Frontiers in Sustainable Food Systems*, *3*.
- Balauriya, T. S., Ong, L., Gras, S. L., & Dagastine, R. R. (2012). Changes in morphological and nano-mechanical properties of the milk fat globule membrane during processing. *RSC Advances*, *2*, 2384–2394.
- Binnig, G., Quate, C. F., & Gerber, C. (1986). Atomic force microscope. *Physical Review Letters*, *56*, 930–933.
- Bourlieu, C., Paboeuf, G., Chever, S., Pezennec, S., Cavalier, J.-F., Guyomarc'h, F., ... Carrière, F. (2016). Adsorption of gastric lipase onto multicomponent model lipid monolayers with phase separation. *Colloids and Surfaces B: Biointerfaces*, *143*, 97–106.
- Cheng, C., Wu, Z., Wang, Y., Chen, J., Zhong, Y., Liang, R., ... Liu, W. (2021). Tunable high internal phase emulsions (HIPEs) formulated using lactoferrin-gum Arabic complexes. *Food Hydrocolloids*, *113*, 106445.
- Dauphas, S., Beaumal, V., Gunning, P., Mackie, A., Wilde, P., Vié, V., ... Anton, M. (2007a). Structure modification in hen egg yolk low density lipoproteins layers between 30 and 45 mN/m observed by AFM. *Colloids and Surfaces. B, Biointerfaces*, *54*, 241–248.
- Dauphas, S., Beaumal, V., Gunning, P., Mackie, A., Wilde, P., Vié, V., ... Anton, M. (2007b). Structures and rheological properties of hen egg yolk low density lipoprotein layers spread at the air-water interface at pH 3 and 7. *Colloids and Surfaces. B, Biointerfaces*, *57*, 124–133.
- Dias Meirelles, A. A., Rodrigues Costa, A. L., & Cunha, R. L. (2020). Cellulose nanocrystals from ultrasound process stabilizing O/W Pickering emulsion. *International Journal of Biological Macromolecules*, *158*, 75–84.
- Dokouhaki, M., Prime, E. L., Qiao, G. G., Kasapis, S., Day, L., & Gras, S. L. (2020). Structural-rheological characteristics of Chaplin E peptide at the air/water interface; a comparison with beta-lactoglobulin and beta-casein. *International Journal of Biological Macromolecules*, *144*, 742–750.
- Et-Thakafy, O., Delorme, N., Gaillard, C., Mériadeac, C., Artzner, F., Lopez, C., & Guyomarc'h, F. (2017). Mechanical properties of membranes composed of gel-phase

- or fluid-phase phospholipids probed on liposomes by atomic force spectroscopy. *Langmuir: The ACS Journal of Surfaces and Colloids*, *33*, 5117–5126.
- Et-Thakafy, O., Delorme, N., Guyomarc'h, F., & Lopez, C. (2018). Mechanical properties of milk sphingomyelin bilayer membranes in the gel phase: Effects of naturally complex heterogeneity, saturation and acyl chain length investigated on liposomes using AFM. *Chemistry and Physics of Lipids*, *210*, 47–59.
- Et-Thakafy, O., Guyomarc'h, F., & Lopez, C. (2019). Young modulus of supported lipid membranes containing milk sphingomyelin in the gel, fluid or liquid-ordered phase, determined using AFM force spectroscopy. *Biochimica et Biophysica Acta (BBA) - Biomembranes*, *1861*, 1523–1532.
- Francius, G., Alsteens, D., Dupres, V., Lebeer, S., De Keersmaecker, S., Vanderleyden, J., ... Dufrene, Y. F. (2009). Stretching polysaccharides on live cells using single molecule force spectroscopy. *Nature Protocols*, *4*, 939–946.
- Friedrichs, J., Legate, K. R., Schubert, R., Bharadwaj, M., Werner, C., Müller, D. J., & Benoit, M. (2013). A practical guide to quantify cell adhesion using single-cell force spectroscopy. *Methods (San Diego, Calif.)*, *60*, 169–178.
- Guerin, J., Soligot, C., Burgain, J., Huguet, M., Francius, G., El-Kirat-Chatel, S., ... Borges, F. (2018). Adhesive interactions between milk fat globule membrane and *Lactobacillus rhamnosus* GG inhibit bacterial attachment to Caco-2 TC7 intestinal cell. *Colloids and Surfaces B: Biointerfaces*, *167*, 44–53.
- Guyomarc'h, F., Chen, M., Et-Thakafy, O., Zou, S., & Lopez, C. (2017). Gel-gel phase separation within milk sphingomyelin domains revealed at the nanoscale using atomic force microscopy. *Biochimica et Biophysica Acta - Biomembranes*, *1859*, 949–958.
- Guyomarc'h, F., Murthy, A. V. R., & Lopez, C. (2016). Sphingomyelin-rich domains in bilayer models of the milk fat globule membrane: Temperature governs structural and mechanical heterogeneity.
- Guyomarc'h, F., Zou, S., Chen, M., Milhiet, P.-E., Godefroy, C., Vie, V., & Lopez, C. (2014). Milk sphingomyelin domains in biomimetic membranes and the role of cholesterol: Morphology and nanomechanical properties investigated using AFM and force spectroscopy. *Langmuir: The ACS Journal of Surfaces and Colloids*, *30*, 6516–6524.
- Han, J.-R., Shang, W.-H., Yan, J.-N., Du, Y.-N., McClements, D. J., Xiao, H., ... Zhu, B.-W. (2020). Protection of  $\beta$ -carotene from chemical degradation in emulsion-based delivery systems using scallop (*Patinopecten yessoensis*) gonad protein isolates. *Food and Bioprocess Technology*, *13*, 680–692.
- Ho, T. M., Abik, F., & Mikkonen, K. S. (2021). An overview of nanoemulsion characterization via atomic force microscopy. *Critical Reviews in Food Science and Nutrition*.
- Hu, J., Yang, J., Xu, Y., Zhang, K., Nishinari, K., Phillips, G. O., & Fang, Y. (2019). Comparative study on foaming and emulsifying properties of different beta-lactoglobulin aggregates. *Food & Function*, *10*, 5922–5930.
- Hutter, J. L., & Bechhoefer, J. (1993). Calibration of atomic-force microscope tips. *Review of Scientific Instruments*, *64*, 1868–1873.
- Jiménez-Flores, R., & Brisson, G. (2008). The milk fat globule membrane as an ingredient: Why, how, when? *Dairy Science & Technology*, *88*, 5–18.
- Li, Y., Zhong, M., Xie, F., Sun, Y., Zhang, S., & Qi, B. (2020). The effect of pH on the stabilization and digestive characteristics of soybean lipophilic protein oil-in-water emulsions with hypromellose. *Food Chemistry*, *309*, 125579.
- Lin, J., Meng, H., Yu, S., Wang, Z., Ai, C., Zhang, T., & Guo, X. (2021). Genipin-crosslinked sugar beet pectin-bovine serum albumin nanoparticles as novel pickering stabilizer. *Food Hydrocolloids*, *112*, 106306.
- Lin, J., Yu, S., Ai, C., Zhang, T., & Guo, X. (2020). Emulsion stability of sugar beet pectin increased by genipin crosslinking. *Food Hydrocolloids*, *101*, 105459.

- Liu, F., & Tang, C.-H. (2013). Soy protein nanoparticle aggregates as pickering stabilizers for oil-in-water emulsions. *Journal of Agricultural and Food Chemistry*, 61, 8888–8898.
- Liu, F., Zheng, J., Huang, C.-H., Tang, C.-H., & Ou, S.-Y. (2018). Pickering high internal phase emulsions stabilized by protein-covered cellulose nanocrystals. *Food Hydrocolloids*, 82, 96–105.
- Liu, G., Li, W., Qin, X., & Zhong, Q. (2021). Flexible protein nanofibrils fabricated in aqueous ethanol: Physical characteristics and properties of forming emulsions of conjugated linolenic acid. *Food Hydrocolloids*, 114, 106573.
- Lopez, C. (2020). Structure of the milk fat globule membrane: New scientific advances revealing the role of sphingomyelin in topographical and mechanical heterogeneities. *Dairy Fat Products and Functionality*, 41–66.
- Lopez, C., Cauty, C., & Guyomarc'h, F. (2015). Organization of lipids in milks, infant milk formulas and various dairy products: Role of technological processes and potential impacts. *Dairy Science & Technology*, 95, 863–893.
- Lopez, C., Cauty, C., & Guyomarc'h, F. (2019). Unraveling the complexity of milk fat globules to tailor bioinspired emulsions providing health benefits: The key role played by the biological membrane. *European Journal of Lipid Science and Technology*, 121, 1800201.
- Marszalek, P. E., & Dufrêne, Y. F. (2012). Stretching single polysaccharides and proteins using atomic force microscopy. *Chemical Society Reviews*, 41, 3523–3534.
- Mingeot-Leclercq, M.-P., Deleu, M., Brasseur, R., & Dufrêne, Y. F. (2008). Atomic force microscopy of supported lipid bilayers. *Nature Protocols*, 3, 1654–1659.
- Müller, D. J., Krieg, M., Alsteens, D., & Dufrêne, Y. F. (2009). New frontiers in atomic force microscopy: Analyzing interactions from single-molecules to cells. *Current Opinion in Biotechnology*, 20, 4–13.
- Murthy, A. V. R., Guyomarc'h, F., & Lopez, C. (2016). The temperature-dependent physical state of polar lipids and their miscibility impact the topography and mechanical properties of bilayer models of the milk fat globule membrane. *Biochimica et Biophysica Acta - Biomembranes*, 1858, 2181–2190.
- Murthy, A. V. R., Guyomarc'h, F., & Lopez, C. (2018). Palmitoyl ceramide promotes milk sphingomyelin gel phase domains formation and affects the mechanical properties of the fluid phase in milk-SM/DOPC supported membranes. *Biochimica et Biophysica Acta (BBA) - Biomembranes*, 1860, 635–644.
- Murthy, A. V. R., Guyomarc'h, F., Paboef, G., Vié, V., & Lopez, C. (2015). Cholesterol strongly affects the organization of lipid monolayers studied as models of the milk fat globule membrane: Condensing effect and change in the lipid domain morphology. *Biochimica et Biophysica Acta (BBA) - Biomembranes*, 1848, 2308–2316.
- Ni, Y., Fan, L., & Sun, Y. (2020). Interfacial properties of cellulose nanoparticles with different lengths from ginkgo seed shells. *Food Hydrocolloids*, 109, 106121.
- Ning, F., Ge, Z., Qiu, L., Wang, X., Luo, L., Xiong, H., & Huang, Q. (2020). Double-induced se-enriched peanut protein nanoparticles preparation, characterization and stabilized food-grade pickering emulsions. *Food Hydrocolloids*, 99, 105308.
- Obeid, S., Guyomarc'h, F., David-Briand, E., Gaucheron, F., Riaublanc, A., & Lopez, C. (2019). The phase and charge of milk polar lipid membrane bilayers govern their selective interactions with proteins as demonstrated with casein micelles. *Journal of Colloid and Interface Science*, 534, 279–290.
- Obeid, S., Guyomarc'h, F., Francius, G., Guillemain, H., Wu, X., Pezenec, S., ... Lopez, C. (2019). The surface properties of milk fat globules govern their interactions with the caseins: Role of homogenization and pH probed by AFM force spectroscopy. *Colloids and Surfaces B: Biointerfaces*, 182, 110363.
- Obeid, S., Guyomarc'h, F., Tanguy, G., Leconte, N., Rousseau, F., Dolivet, A., ... Jan, G. (2020). The adhesion of homogenized fat globules to proteins is increased by milk heat



- treatment and acidic pH: Quantitative insights provided by AFM force spectroscopy. *Food Research International*, 129, 108847.
- Shen, Y., Chang, C., Shi, M., Su, Y., Gu, L., Li, J., & Yang, Y. (2020). Interactions between lecithin and yolk granule and their influence on the emulsifying properties. *Food Hydrocolloids*, 101, 105510.
- Sun, X., Zhang, W., Zhang, L., Tian, S., & Chen, F. (2021). Effect of ultrasound-assisted extraction on the structure and emulsifying properties of peanut protein isolate. *Journal of the Science of Food and Agriculture*, 101, 1150–1160.
- Tang, Y., Wang, X., Jiang, H., Song, L., Cui, H., Zhang, Z., & Lin, S. (2020). Pseudosciaena crocearoe protein-stabilized emulsions for oral delivery systems: In vitro digestion and in situ intestinal perfusion study. *Journal of Food Science*, 85, 2923–2932.
- Uddin, M. H., Tan, S. Y., & Dagastine, R. R. (2011). Novel characterization of microdrops and microbubbles in emulsions and foams using atomic force microscopy. *Langmuir: The ACS Journal of Surfaces and Colloids*, 27, 2536–2544.
- Waglewska, E., & Bazylińska, U. (2021). Biodegradable amphoteric surfactants in titration-ultrasound formulation of oil-in-water nanoemulsions: Rational design, development, and kinetic stability. *International Journal of Molecular Sciences*, 22, 11776.
- Wang, P., Chen, C., Guo, H., Zhang, H., Yang, Z., & Ren, F. (2018). Casein gel particles as novel soft Pickering stabilizers: The emulsifying property and packing behaviour at the oil-water interface. *Food Hydrocolloids*, 77, 689–698.
- Wei, Z., Cheng, J., & Huang, Q. (2019). Food-grade Pickering emulsions stabilized by ovotransferrin fibrils. *Food Hydrocolloids*, 94, 592–602.
- Yang, J., Thielen, I., Berton-Carabin, C. C., van der Linden, E., & Sagis, L. M. C. (2020a). Nonlinear interfacial rheology and atomic force microscopy of air-water interfaces stabilized by whey protein beads and their constituents. *Food Hydrocolloids*, 101, 105466.
- Yang, N., Su, C., Zhang, Y., Jia, J., Leheny, R. L., Nishinari, K., . . . Phillips, G. O. (2020b). In situ nanomechanical properties of natural oil bodies studied using atomic force microscopy. *Journal of Colloid and Interface Science*, 570, 362–374.
- Zhao, M., Xiong, W., Chen, B., Zhu, J., & Wang, L. (2020). Enhancing the solubility and foam ability of rice glutelin by heat treatment at pH12: Insight into protein structure. *Food Hydrocolloids*, 103, 105626.

## CHAPTER 8

# Application of atomic force microscopy for food powders and contact materials

Regis Badin<sup>1</sup>, Jennifer Burgain<sup>1</sup> and Claire Gaiani<sup>1,2</sup>

<sup>1</sup>LiBio (Laboratoire d'Ingénierie des Biomolécules), Université de Lorraine, Vandoeuvre-lès-Nancy Cedex, France

<sup>2</sup>Ministry of Higher Education, Research and Innovation, IUF (Institut Universitaire de France), Paris, France

### 8.1 Introduction

Many food ingredients are supplied in powdered form, as reducing water content increases shelf life and aids storage, handling, and transport. Food powders are therefore of great importance to the food industry. They include various raw materials and ingredients, such as flours, spices, and processed products like instant coffee or powdered milk. Powders either originate from liquid conversion into powder by various techniques such as spray-drying, freeze-drying, drum-drying, belt-drying, or crystallization, or from size reduction of solid materials induced by grinding, crushing, milling, attrition, or pulverization (Karam, Petit, Zimmer, Baudelaire Djantou, & Scher, 2016) (Fig. 8.1). It should be noted that particle surfaces, in that case, are essentially constituted by broken structures (Bhandari, 2013). Because of these various origins, particle size and shape distributions, chemical and surface composition, as well as physical properties are highly variable. Therefore, more than one analytical technique is often required to obtain a full set of information about a given scientific question.

Atomic force microscopy (AFM) may be a powerful tool by bringing much of this information (Burgain et al., 2017). Indeed, AFM presents many benefits. Its resolution capacity is sensitive at the nanoscale, and it does not require samples pretreatment or vacuum conditions compared to the other types of microscopy techniques, such as scanning electron microscopy (SEM), transmission electron microscopy, confocal laser scanning microscopy or compared to spectroscopy techniques such as time of flight–secondary ion mass spectrometry. AFM is also a useful tool that allows studying nanomechanics and chemical surface properties of food

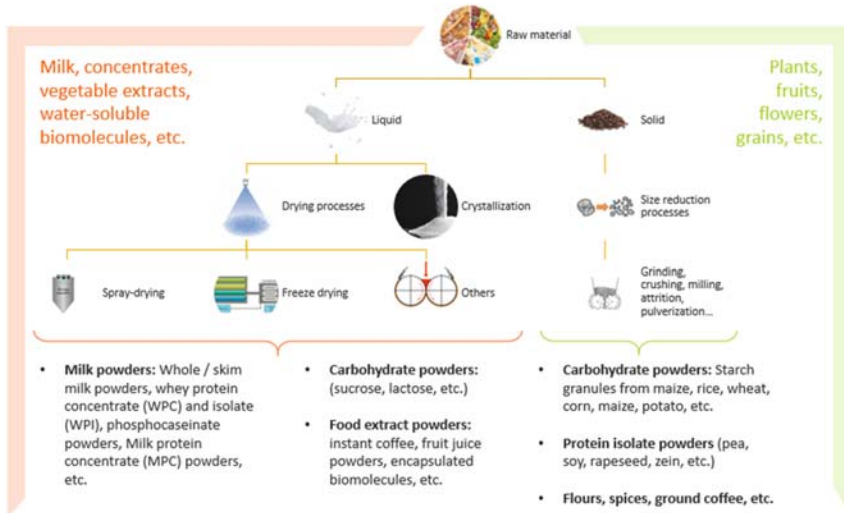


**Figure 8.1** Methods to obtain a large variety of food powders.

powders (Burgain et al., 2017; Gaiani, Burgain, & Scher, 2013; Liu & Cheng, 2011a). However, even if AFM is now a well-developed technique in many scientific fields, its application to food objects, especially food powders, is only emerging.

The first part introduces the use of AFM during the formulation and processing of food powders. Part 2 focuses on AFM as a technique to better investigate scientific questions dealing with powder functionalities. Part 3 highlights contact materials with a focus on food packaging. Finally, promising and innovant AFM applications are detailed in part 4.

## 8.2 Atomic force microscopy: a powerful tool during formulation and processing of food powders

There is a tremendous interest in surface analysis techniques that can evaluate physicochemical characteristics of food and to predict their behavior during formulation and processing. A vast range of ingredients are available for formulating food powders leading to a broad range of possible structure forms. Powder structure is, for example, very important when considering product sensory properties or powder functional properties. Biomacromolecules such as carbohydrates, proteins, and lipids are the main building blocks from which food powders are made (Liu & Cheng, 2011a). Theoretically, almost all of these macromolecules could be

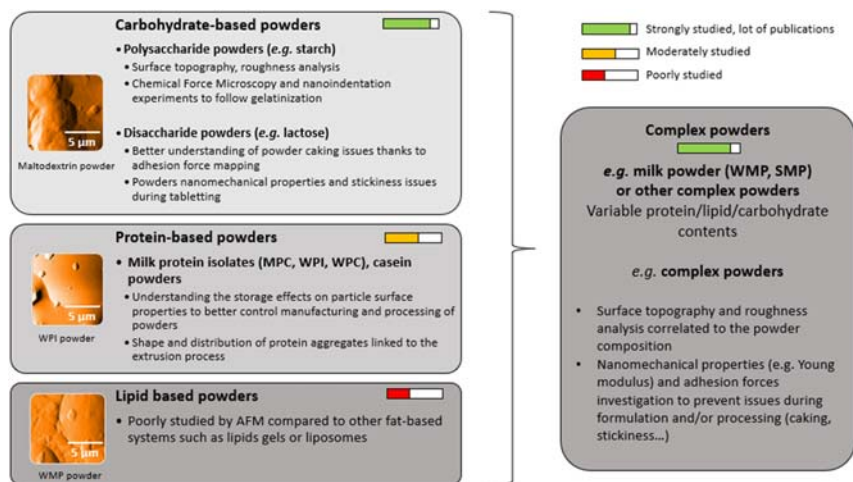


**Figure 8.2** Summary of atomic force microscopy (AFM) studies on food macromolecules powders and examples of surface topographies obtained by AFM. MPC, milk protein concentrate; WPI, whey protein isolate; WPC, whey protein concentrate; WMP, whole milk powder; SMP, skim milk powder.

analyzed by AFM; however, in practical research, most AFM studies on food powders are focused on carbohydrates and proteins (Fig. 8.2). These macromolecules are able to interact between each other or with other organic and inorganic substances, and all of these interactions will determine the exact matrix structure. Knowing that, AFM can be a highly valuable tool to characterize food powders.

## 8.2.1 Carbohydrate-based powders

Carbohydrate powders are mostly studied via AFM for two main reasons. Firstly, AFM can be used to make correlations with physicochemical parameters (such as molecular weight, radius of gyration, etc.) without the necessity of dissolving the samples into aqueous and diluted media (Funami, 2010). Secondly, AFM can also be used to correlate with macroscopic behaviors and observe carbohydrates in their native form without destructive chemical and physical modification.

### 8.2.1.1 Polysaccharide-based powders

Starch is among the most important polysaccharide in the human diet, and starch powders were one of the first food powders to be investigated in depth by AFM since the 1990s. New insights regarding their surface

topography and structure were relevant in order to have a better understanding of their behavior during processing and formulation. Various starch sources were studied by AFM: starches from various botanical sources (Ohtani, Yoshino, Hagiwara, & Maekawa, 2000); starches from rice grains (Dang & Copeland, 2003; Dang, Braet, & Copeland, 2006; Ohtani, Yoshino, Ushiki, Hagiwara, & Maekawa, 2000); pea (Parker, Kirby, & Morris, 2008; Ridout, Gunning, Parker, Wilson, & Morris, 2002; Ridout, Parker, Hedley, Bogracheva, & Morris, 2004); potato (An, Yang, Liu, & Zhang, 2008; Baldwin, Adler, Davies, & Melia, 1998; Baldwin, Davies, & Melia, 1996; Dang et al., 2006; Szymońska & Krok, 2003); corn (An et al., 2008; Baker, Miles, & Helbert, 2001); wheat (Baldwin et al., 1996, 1998); maize (Ridout et al., 2002; Tomoia-Cotisel et al., 2010); tapioca (Wuttisela, Triampo, & Triampo, 2009), and also more recently banana (Peroni-Okita et al., 2015).

#### **8.2.1.1.1 Formulation**

Starch generally contains 20%–25% of amylose and 75%–80% of amylopectin, depending on the botanical source (Liu & Cheng, 2011a). Tomoia-Cotisel et al. (2010) characterized the native structure of maize starch granules at the nanoscale. Thus, they showed the presence of many characteristics protrusions, pores, and pressions. These surface properties were related to the highly branched amylopectin molecules, and it was in agreement with the blocklet model for starch granules. Amylose and amylopectin branched structures were also investigated thanks to the surface analyze of larger starch granules particles. Thanks to surface topographies analysis performed by AFM, it was shown that surface roughness is highly variable on the different starch granules, leading to the existence of much smoother or much rougher areas. All that work brings insights into starch granule structure and molecular organization in order to enhance the food powder formulation parameters.

#### **8.2.1.1.2 Processing**

The main process studied for starch is gelatinization. This endothermic process corresponds to the loss of crystallinity in the starch granules under heat and moist conditions. The disruption of molecular order within the starch granule results in granular swelling, crystallite melting, viscosity development, and solubilization (Kadam, Tiwari, & O'Donnell, 2015). Dang and Copeland (2003) investigated the impact of water and cooking processes on cut rice grains. A partial loss of ordered layered structures was

observed for starches in contact with water. The total loss was noticed for cooked grains as a result of gelatinization. Also, the nanostructure of two starches (potato and corn) and two heating processes (convective and microwave heating) were compared (An et al., 2008). Microwave heating was found to cause incomplete gelatinization of starch by comparison with convective heating. The starch nature was also important as the heating modes influenced potato starch more than corn starch. This information on starch nanostructure and the fine state of starch gelatinization/retrogradation would be highly helpful when selecting powders for food formulation and processing. A general conclusion drawn from these studies was that amylose played a key role in forming molecular networks in retrograded starch. Another process characterized by the help of AFM is starch treatment with enzymes or acid. To be used in the food or pharmaceutical field as a binder excipient, the starch needs to be modified. Acid-modified tapioca starch is one of the major ways to prepare medicinal tablets by direct compression (Wuttisela et al., 2009). With this process, different amylose/amylopectin ratios are produced and studied by surface chemical force microscopy, which illustrates the ability of AFM to characterize powder surfaces chemically. AFM probes were functionalized with hydroxide and methyl groups and revealed modifications of both phosphate domains and carbon backbone depending on the hydrolysis intensity. With hydrolysis, the amylopectin ratio increased and exposed more phosphate pockets, whereas the carbon backbone presented a plate-like structure. With this technique, (Wuttisela et al., 2009) recorded molecular and chemical entities on the surface of starch granule powders. Other studies (Ohtani, Yoshino, Hagiwara, et al., 2000; Ohtani, Yoshino, Ushiki, et al., 2000) used AFM to characterize the structure of starch granules from various botanical sources at the nanometer scale. The technique was useful for studying the effect of physical destruction on starch granules' physical properties. Thus, it was demonstrated that fine particles with a diameter of approximately 30 nm existed in each starch granule. It was also shown that these particles are able to form chain structures, which may correspond to the blocklet or single cluster, which has been proposed as a model for starch structuration. Finally, AFM versatility was also used to investigate the effect of mechanical damages at a microstructural level (Barrera et al., 2013). Thus, it was shown that increasing starch damage degree also increases the surface roughness of starch granules and the presence of surface irregularities. This work was very useful to have a better understanding of how milling processes impact powder surface morphology.

### 8.2.1.2 Disaccharide powders

Lactose is naturally present in milk and formed of one galactose molecule and one glucose molecule. Sucrose is another disaccharide composed of two other monosaccharides (glucose and fructose). These two disaccharide powders are strongly used as ingredients for infant formula, food products, and drugs. For instance, the aim of the lactose crystallization process is to recover the sugar in the most stable and nonhygroscopic  $\alpha$ -lactose monohydrate form and consequently prevent storage defects such as agglomeration and caking (Foster, Bronlund, & Paterson, 2006). Therefore, the investigation of the surface is of particular interest during formulation and after processing. It could be done by scanning electron microscopy, but it is sometimes difficult to identify the amorphous or crystalline state of the powder, and it is also impossible to perform a quantification.

#### 8.2.1.2.1 Formulation

Amorphous sugars are very hygroscopic and can cause caking problems during and after spray drying (Foster et al., 2006). This is particularly true in powders such as whey powders which have a high lactose content (Schuck & Dolivet, 2002). Therefore, lactose crystallization is a particularly studied topic (Perkins et al., 2007; Tejedor et al., 2017). For example, Tejedor et al. (2017) developed an interesting and innovative AFM approach for evaluating particle surface amorphicity using the possibility of characterizing nanomechanical properties of particle surfaces thanks to force spectroscopy. For this purpose, the behavior of three  $\alpha$ -lactose monohydrate powders (crystalline, partially amorphized, and completely amorphous) in response to humidity was compared. Crystalline and amorphous regions vary systematically in nanomechanical data, which were treated to follow the crystallization of amorphous material in response to humidity. They also developed in situ AFM to study the crystallization in real time, and therefore, provides dynamical information. Quantitative AFM measurements were also done by (Hooton, Jones, & Price, 2006) in order to compare the relative forces of interaction of micronized particles and a selection of sugar substrates, including lactose, raffinose, trehalose, and xylitol. A linear correlation was observed between the formulations and the cohesive–adhesive ratios of the AFM force measurements. The observed link may provide critical insight into the formulation of preparations containing these sugars.

### 8.2.1.2.2 Processing

Two size reduction processes (roller and ball mill grinding) were applied to sucrose powder in lipophilic suspensions by [Middendorf, Bindrich, Mischnick, Franke, and Heinz \(2018\)](#). Different surface states depending on the type of grinding were obtained and analyzed by combining AFM and AFM-local thermal analysis. This allows authors to characterize local distributions of different surface states on sucrose particles at the nanoscale. For this purpose, local softening temperatures were measured. The originality of the study is based on links done between the distribution of crystalline and amorphous areas on sucrose particle surfaces and the different flow behaviors despite a similar particle size distribution, which is an important aspect to apprehend during processing. Tableting is a classical process performed in the food and pharmaceutical industries, mostly with lactose as a binder ([Bunker, Zhang, Blanchard, & Roberts, 2011](#); [Masterson & Cao, 2008](#); [Sindel & Zimmermann, 2001](#); [Tejedor et al., 2017](#)). Understanding the mechanical properties of lactose powders (as well as other binders) at the submicron scale can be very important for process development. The hardness of individual sucrose and lactose particles was quantified using AFM nanoindentation ([Masterson & Cao, 2008](#)). The rigidity was higher for sucrose particles than lactose particles. The results were then related to the tableting performance in order to have a better understanding of the solid behavior during the process. It is important to note that the authors also highlighted slight variations of the hardness value dependent on the load applied to the surface during nanoindentation experiments. AFM is also known to allow adhesion force measurements, which are crucial to be taken into consideration to predict issues during the tableting process, especially in order to avoid the stickiness behavior of food powders. Thus, ([Bunker et al., 2011](#)) investigated the adhesive properties of tablet components by measuring adhesive interactions between single lactose particle and coated tablet punch. This was made under various controlled relative humidity values. The surface roughness was also studied, and a predicting model was established in order to correlate values obtained with adhesion on powder's stickiness. With these experiments, they proved that surface roughness plays a major role in lactose-punch adhesion. It was also shown by adhesion forces mapping that poor relative humidity (i.e., between 30% and 60%) conditions could be responsible for a significant increase in adhesion between the two components. In the same way, it was proven in another study that controlling relative humidity conditions is crucial because they are also



responsible of an increase of capillary forces, which cause high stickiness of lactose powders on tablet tools (Tejedor et al., 2017). It is also important to not forget particle-particle interactions during the tableting process, which play an essential role in the tableting efficiency (Sindel & Zimmermann, 2001).

### 8.2.2 Fat-based powders

Fat-based powders are an important part of food ingredients. Nevertheless, they are poorly studied by AFM compared to lipids gel or liposomes (mostly used as drug/bioactive delivery systems), which were strongly investigated (Et-Thakafy et al., 2017; Et-Thakafy, Guyomarc'h, & Lopez, 2019; Ruozzi, Tosi, Leo, & Vandelli, 2007; Spyratou, Mourelatou, Makropoulou, & Demetzos, 2009; Teschke & De Souza, 2002). In such cases, AFM was useful to provide precious information about surface topography and physical properties (such as Young modulus) at the same time. Moreover, AFM may turn out to be easier to use on such ingredients, as lipids gels or liposomes are relatively flat and have small structures. This can make them less difficult to analyze compared to food powders which are mostly micrometer scaled and could present relatively high surface roughness. Indeed, in sinuous powder structures, it may be difficult to analyze the surface, as it is needed for the AFM tip to follow precisely the surface (especially in contact mode) to reproduce sample topography.

However, the study of fat-based powder was done by (Murrieta-Pazos et al., 2011) by comparing skim and whole milk powders, which differ in fat composition. AFM topography revealed that the whole milk powder surface was significantly flatter than the skim milk powder surface. These results were in agreement with images obtained by SEM. Furthermore, average surface roughness analysis also demonstrates high variation between the two types of powder. This was about 306 nm for skim milk powder and 146 nm for whole milk powder for a defined surface area. These results were correlated with X-ray photoelectron spectroscopy (XPS) results, which show a high-fat surface content compared to skim milk powder which exhibits a more protein/carbohydrate-based surface. Emulsifying agents are often added during formulation to improve some functional properties (Middendorf, Juadjur, Bindrich, & Mischnick, 2015). They work as spacers between the sucrose particles and reduce particle-particle interactions so that they decrease the friction between the

particles. Therefore, powder flow can be induced easily while maintaining a low viscosity. Thus, AFM was also used to better understand the mechanism of action of a food emulsifier (polyglycerol polyricinoleate—PGPR) added to a powder and to determine specific interaction in a complex fat-based system composed of an emulsifier, cocoa butter, and sucrose particles. It was shown that, compared to soy lecithin, lower concentrations of PGPR were required.

Solid lipid microparticles (SLM) can be presented as a spray-dried powder able to protect a bioactive molecule. Even if the majority of SLM-related work exploits AFM only to image particle surface topography (i.e., shapes and sizes), the authors tried to measure the viscoelastic properties of SLM surfaces based on the interactions of the particle surface with the probe. In this study, SLM were prepared with two lipids (com-*pitrol* or stearic acid). AFM was used to assess the distribution of the bioactive within the particle. For this purpose, the nanomechanical properties of the SLM surface were investigated. It was possible to differentiate between the SLM with and without the bioactives and to observe surface changes occurring by spray drying (Wolska, Sznitowska, Krzemińska, & Monteiro, 2020). Even if the results were not conclusive, AFM seems to be a promising technique not only for obtaining topographical images but also for analyzing the distribution of the bioactives on the surfaces of lipid microparticles.

### 8.2.3 Proteins powders

Protein powders were also investigated by AFM, mainly in order to have a better understanding of the relationship between powder surface properties and manufacturing conditions. High protein content powders are highly studied because formulation and processing highly impact on particle surface properties which impact themselves functional properties of these powders, such as rehydration ability, which is defined as a prerequisite to every industrial use (Burgain, Scher, Petit, Francius, & Gaiani, 2016). For example, dairy protein powders were studied, especially whey protein isolate (WPI) powders which are commonly used as ingredients in a lot of formulated foods (Burgain, El Zein, et al., 2016; Burgain, Scher, et al., 2016; Fyfe et al., 2011; Qi & Onwulata, 2011).

Thanks to AFM, Qi and Onwulata (2011) gained insights into how the extrusion process changed the shape and distribution of whey protein aggregates under various moisture content. Results were compared to

classical freeze-dried and spray-dried techniques. AFM was a convenient and powerful tool for direct visualization of process impact and eventually discovering new biomaterials by playing on the combined effect of heat and shear during extrusion. Zein is another promising protein powder from maize and is particularly suitable for biodegradable film formulations (Guo, Liu, An, Li, & Hu, 2005). AFM helped investigate the zein globules' structure, height, and diameter distribution in order to better understand the film formation mechanisms. Thus, highly branched structures and rod formation were highlighted, thanks to topography imaging.

It is also important to consider that the storage conditions significantly impact food powder surface, and thus, their functional properties. (Burgain, El Zein, et al., 2016; Burgain, Scher, et al., 2016), demonstrated storage effects on high protein content milk powders. Thus, it was shown that high-temperature conditions (60°C,  $a_w = 0,2$ , one month) modify the particle surface properties. Thanks to chemical force microscopy and the use of a hydrophobic-coated cantilever, an increase in surface hydrophobicity was evidenced, mostly because of the powder browning due to the Maillard reaction. These results were correlated to XPS results which show a decrease of amino acids at the surface (Burgain, El Zein, et al., 2016).

### **8.3 A better understanding and control of powder functional properties with atomic force microscopy**

Atomic force microscopy was identified as an interesting technique to better investigate scientific questions dealing with powder functionalities. It is now generally accepted that particle surface, in its turn, has a strong impact on the functional properties of a powder, such as rehydration, caking, flowability, and stickiness (Fig. 8.3). Thus, using AFM to focus on the particle surface properties is an interesting and judicious choice of application.

#### **8.3.1 Reconstitution ability of food powders**

A complete powder reconstitution is an essential prerequisite to every industrial use. Unfortunately, it is not systematically the case, particularly for powders with high protein content or presenting a surface fat coverage where difficulties to reconstitute are observed even after long reconstitution times. Although it is impossible to give a general rule for the influence of surface properties of powders on the reconstitution (due to the

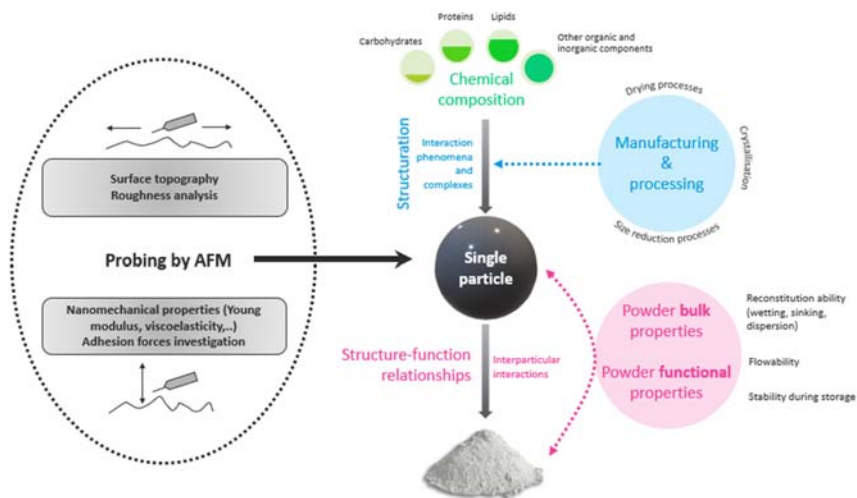


**Figure 8.3** Use of atomic force microscopy to probe single-particle surface properties variability and their impact on food powders' functional properties.

complex link between particle structure and composition dependently on powder manufacturing conditions), it has been evidenced that increasing our knowledge about powder surface properties by using AFM leads to a better view of the reconstitution as described hereafter.

### 8.3.1.1 Powder wetting

When poured at the surface of an aqueous liquid, powder particles in contact with the liquid surface begin to absorb water by capillary diffusion. Water migration into particles often induces particle swelling due to the relaxation of polymer chains, which soften the particle and increase its size, facilitating the further reconstitution steps. Wetting is generally improved for large particles and agglomerates, as well as for more spherical particles (Selomulya & Fang, 2013). However, surface properties are also critical for powder wetting. A high fat or protein surface content often increases surface hydrophobicity, leading to poor wettability (Kim, Chen, & Pearce, 2002; Nijdam & Langrish, 2006; Schuck, Dolivet, & Jeantet, 2012; Sharma, Jana, & Chavan, 2012), whereas carbohydrates (such as lactose or sucrose), minerals, and surfactants, enhancing interactions with water, improve powder wettability (Hammes, Englert, Noreña, & Cardozo, 2015).

Wetting properties are, however, poorly related to surface properties studies by AFM. Recent studies are currently working on enhancing the wetting properties of WPI powders, which are known to be weakly

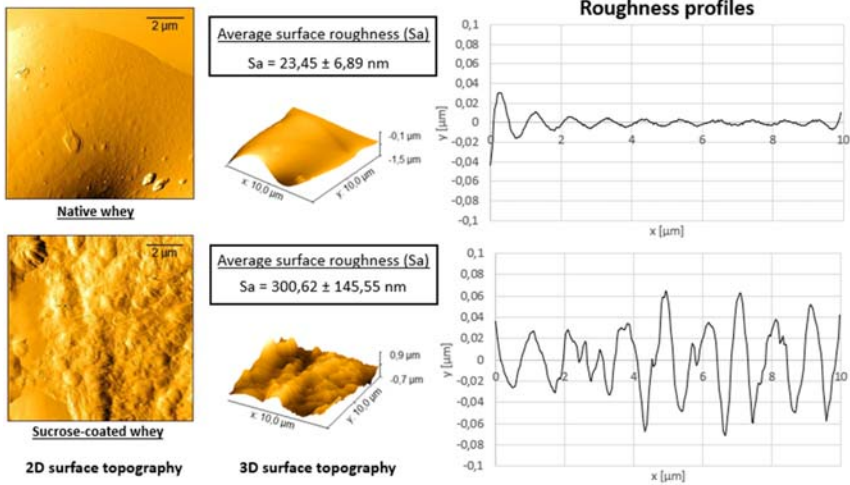


**Figure 8.4** Surface topographies and roughness profiles analysis of native whey powder and sucrose-coated whey powder (60 min).

wettable (Gaiani, Schuck, Scher, Desobry, & Banon, 2007). To enhance this parameter, industrials widely use carbohydrates coating (e.g., sucrose) in order to initiate a better first contact with water. To this end, this recent study investigates the coating impact on particle surface properties as shown in Fig. 8.4.

Thus, it was then evidenced that the coating was nicely done on whey powders. Indeed, sucrose-coated whey powders areas were identified to be significantly rougher than the native areas. AFM was also useful to show the coating by studying particles' nanomechanics properties, such as the Young modulus (E) at the powder surface (Fig. 8.5).

Thanks to elasticity mapping, it was also shown that the coating is effectively done on whey powders. Indeed, more highly variable Young modulus values on the coated areas were recorded compared to native whey protein powders. Thus, sucrose-coated areas on whey protein powders exhibit Young modulus value clusters similar to the elasticity mapping obtained for pure sucrose powder, which surface was too hard ( $> 1 \text{ GPa}$ ) to be characterized with the used cantilever. This result was in agreement with the Young modulus values calculated by AFM nanoindentation by other authors (Masterson & Cao, 2008; Ramos & Bahr, 2007). It is also generally recognized that wetting plays a major role in many processes because of its impact on the emerging adhesives forces. Most of the time, high wetting angles during wetting between a solid and

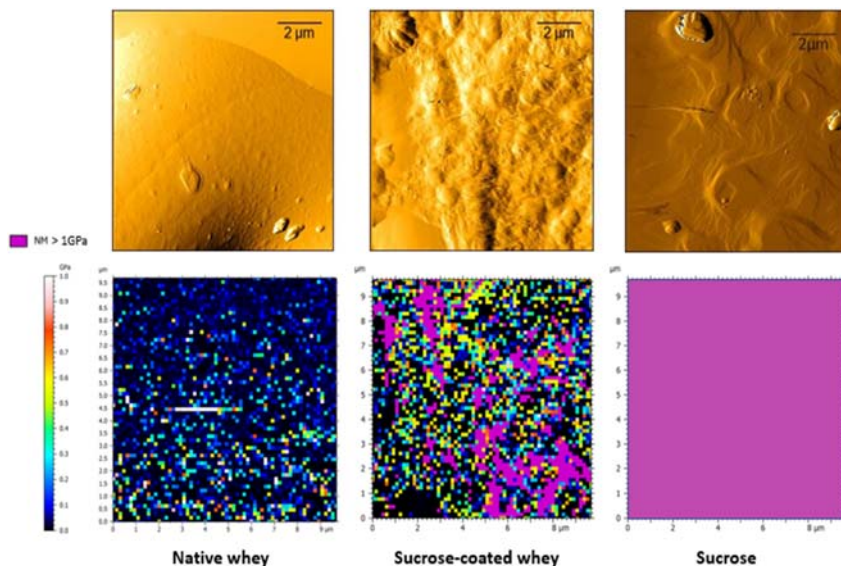


**Figure 8.5** Young modulus mapping of native whey powder (left), sucrose-coated whey powder (middle), and sucrose powder (right) and their topography associated.

a liquid lead to much higher adhesion forces (Fritzsche & Peuker, 2015). Knowing that it is possible to investigate wetting properties by using AFM, Fritzsche and Peuker (2015) used coated nanoparticles with different surface energies in order to obtain different wetting angles and correlate them with adhesion forces. Using AFM, they glued a coated nanoparticle at the end of the cantilever with the aim to evaluate adhesion forces with the wetting substrate. They also worked at distinguish capillary or non-capillary adhesion events on the measured force curves. Thus, they successfully proved that improved wetting led to a decrease of capillary forces but lead to an increase of non-capillary forces and they also related it to surface roughness measurements. These results show how AFM can be a very useful tool for investigating the functional properties of powders, such as rehydration, and more precisely, wetting.

### 8.3.1.2 Powder dispersion

During powder dispersion, both particle size reduction and specific surface area increase occurred, facilitating interactions of the powder with water. Particles of high porosity, low density, and/or low cohesion are known to have better dispersion properties (Goalard, Samimi, Galet, Dodds, & Ghadiri, 2006). Chemical composition is crucial for this last reconstitution

step: particles rich in hydrophobic molecules (such as fatty powders) or cross-linked proteins (like dairy powders with a high casein content) are less soluble (Schuck et al., 2012), whereas hydrophilic components such as sugars and minerals often improve powder solubility (Davenel, Schuck, Mariette, & Brulé, 2002; Schuck & Dolivet, 2002). Recently, the combination of AFM in topography and nanoindentation modes highlighted the presence of surface heterogeneity (hollow zones) and the development of hard regions on the surface of casein powders (Burgain, Scher, et al., 2016). Spatially resolved force/indentation curves evidenced significantly stiffer surface for aged powder (Young modulus of 20 GPa) compared to the fresh one (0.2 GPa). These findings were fully consistent with the formation of a crust at the powder surface. Correlations of these AFM analyses with dispersion properties were able to better understand the behavior of casein-rich powders subjected to long-term storage and/or high temperature. Nanoindentation experiments also permitted to identify harder bumps (corresponding to tightly packed caseins) than hollows. Similar observations were performed by (Fyfe et al., 2011) on milk protein concentrate powders (80% proteins) with a crust formation during storage. In addition, the AFM technique demonstrated an increase in surface hydrophobicity. These two observations resulted in a powder solubility decrease. Advantages and drawbacks of various surface techniques (including AFM) related to the food powder field are in depth presented in (Burgain et al., 2017; Gaiani et al., 2013; Murrieta-Pazos et al., 2012). During storage, changes in physicochemical and functional properties of WPI powders were outlined (Burgain, El Zein, et al., 2016). After short-term storage at 60°C for 1 month, local modifications on particle surface were explored by chemical force microscopy. Links between storage, particle surface hydrophobicity, and Maillard compounds were highlighted. Maillard reaction (due to the presence of lactose) was identified as the main phenomenon responsible for powder alteration during storage.

### 8.3.2 Powder caking

Even if agglomeration is a unit operation in the food industry to improve the properties of fine powders to generate better flowability and easier handling, unwanted agglomeration can easily appear for materials that are sensitive to moisture and temperature. Caking designates the formation of a solid bridge between two particles in contact and induces the alteration of food powder use and handling properties (Foster, 2002), such as the

reconstitution, agglomeration, handling or conveying, packaging, etc. Powder caking is often due to a sintering (i.e., molecular diffusion from amorphous particles to contact zone between particles) but also other mechanisms, including melting/crystallizing lipids, sugars, or minerals. By using a combination of AFM-based techniques, including phase imaging and nanoindentation, some authors (Prime, Leaper, et al., 2011; Prime, Stapley, Rielly, Jones, & Leaper, 2011) demonstrated that the material properties both at the surface and in the particle wall of a model milk powder system are not uniform. In turn, these material properties govern some caking mechanisms. These model powders were composed of various ratio of protein (sodium caseinate), carbohydrate (maltodextrin), and fat (soya oil). Material properties differences at the surface were measured. Nonuniform topography played a crucial role in the caking behavior of the powder. Voids at the particle surface were identified to be oil. Their area was circular, their distribution was uniform, and their consistency was soft. Therefore, these oil patches may act both as a moisture barrier to prevent caking but, due to a softer consistency, could also be more prone to induce caking. Humidity and temperature cycling programs were performed to follow morphology changes and precise onset of caking was measured within a short period time. It appears in multicomponent powders that AFM can bring additional data that can be used to prevent powder caking.

Amorphous hygro-sensitive materials such as maltodextrins may experiment caking as a result of the environmental conditions (temperature and humidity). AFM with the use of glass transition temperature can deliver valuable information about the onset of sintering induced caking. Particles above their glass transition temperature have been investigated (Haider, Niederreiter, Palzer, Hounslow, & Salman, 2018). Thanks to knowledge of how individual amorphous particles behave under these conditions, recommendations can be given for industrial applications. For these amorphous water sensible materials, it was concluded that temperature and humidity are the key parameters determining undesired agglomeration or caking.

Amorphous lactose is particularly prone to moisture uptake during storage. When the temperature exceeds the glass transition temperature, it undergoes from a glassy to a rubbery state. It is generally achieved either when increasing temperature and/or moisture, these latter decreasing the glass transition temperature of the product by the so-called plasticizing effect (Roos & Karel, 1991). Transformation of lactose into a crystalline state has detrimental effects, leading to powder stickiness enhancement (Tejedor et al., 2017). These detrimental processes may also occur in



other food powders, generally sugar-rich food materials, such as fruit juices and honey. It is attributed to low molecular weight sugar powders, such as fructose, glucose, and sucrose, and organic acids, such as citric, malic, and tartaric acids. These compounds being hygroscopic in an amorphous state, AFM is particularly suitable to perform characterization in order to limit stickiness and caking.

### 8.3.3 Powder cohesion and flowability

A challenge for lactose powder is to avoid segregation and inhomogeneity in the final powder formulation. This is particularly true in pharmaceutical industries for mixtures presenting low quantities of powders in formulations. Therefore, the study of single-particle force measurements by AFM may be complementary to the results obtained in shear testing as it allows for identifying the nature of the forces acting between powder particles.

The thickness of adsorbed moisture layer at the surface of  $\alpha$ -lactose monohydrate from different sources was studied thanks to AFM. This value is of great interest as it directly plays on the interactions between two particles and, at another level, the bulk. With the developed approach, (Dey, Cleaver, & Zhdan, 2000) were able to characterize the deformation of the liquid layer (due to attractive van der Waals forces) when two particles enter in contact. (Colbert, Grandbois, & Abatzoglou, 2015) also identify the nature of the forces acting between various forms of lactose particles (i.e., crystalline and semicrystalline). The analysis of the amplitude and the range of interaction of force–distance curves during detachment between two single particles allow the identification of the nature of the inter-particle forces driving the adhesion. They modified the moisture level from 20% to 60% relative humidity and identified capillarity as the dominating adhesion. These results at the nanoscale were linked with powder rheology results and explained how the flow properties of crystalline lactose decrease when the humidity increases. As water is more present in the interstitial space between the particles, the water film formed at the surface of the particles participates to the creation of water bond between them when they enter in contact with each other.

### 8.3.4 Food powders as a vehicle of bioactive molecules

Food powders are highly valuable vectorization matrix components for the encapsulation and delivery of bioactive molecules. A lot of food powders are used as an encapsulant, such as carbohydrates powders

(maltodextrins) or milk powders (WPIs), which are widely studied matrixes. Most of the studies of encapsulation in food powders concern curcumin (Neves, Desobry-Banon, Perrone, Desobry, & Petit, 2019), polyphenols (e.g., flavonoids such as quercetin) (Karadag, Ozcelik, & Huang, 2014), oils (e.g., orange-peel oil) (Ghasemi, Jafari, Assadpour, & Khomeiri, 2017), or probiotic bacteria (e.g., *Lactobacillus*) (Abd El-Salam & El-Shibiny, 2015; Guerin et al., 2016).

Quercetin is a polyphenolic compound able to exhibit antioxidant, anti-inflammatory, and anticancer properties. However, this bioactive molecule presents poor water solubility and oral bioavailability (Karadag et al., 2014). To improve these functional properties, quercetin was encapsulated into particles. Maltodextrin was used as an efficient carrier to deliver quercetin after formulation via high pressure treatments and spray-drying. In order to improve the formulation for antioxidant efficiency and to optimize quercetin delivery, particles were characterized by AFM. The presence of nanosized irregularly shaped quercetin particles was confirmed. Pure quercetin showed a lack of particle size uniformity and relatively larger size, whereas formulated quercetin into maltodextrins exhibited particle size uniformity and lack of larger needle-type crystalline structures.

Orange peel oil is used as a flavoring agent in many formulations (Ghasemi et al., 2017). Due to its volatile properties, protection into pectin/whey carrier complexes is an option for optimal protection. Formulations at low pH (i.e., pH 3) demonstrated higher encapsulation efficiency than formulations performed at pH 6 and 9. In these conditions, more spherical particles were observed, and it was related to better protection of the bioactive molecule.

Probiotics are living microorganisms that, in appropriate concentrations, confer a health benefit on the host. Encapsulation has begun to be a widely used process in dairy products in order to increase the survival rate of probiotic bacteria. (Guerin et al., 2016) used AFM to have a better understanding of the interactions between *Lactobacillus rhamnosus* GG (LGG) and whey proteins coming from a reconstituted WPI powder. Thanks to the use of different mutant strains and the analysis of nanoindentation experiments with their associated force curves, it was proved that the spaCBA pili of the bacteria especially interacts specifically with the  $\beta$ -Lactoglobulin. LGG was also microencapsulated with gelled WPI thanks to an extrusion technique. In other studies, AFM in tapping mode was used to assess the good entrapment of the bacteria in the matrix

(Doherty et al., 2010, 2011). The produced matrix was able to protect the cells during in vitro stomach incubation (Doherty et al., 2011) and also during ex-vivo digestion (Doherty et al., 2012).

Thus, AFM proved to be a very versatile tool again. This technique demonstrated its usefulness in better understanding complex matrixes as the one found in encapsulation processes. In these cases, AFM helped to obtain precious information about surface topographies, and it also helped to have a better understanding of the interaction between the compounds of the matrix.

## 8.4 Contact materials related to food

These last years, emerging tendencies in food packaging have given an enhancement to food processing industries. There is a strong and continuous demand for cleaner packaging by keeping taste, flavor, and quality for healthier ingredients as well as extending their shelf life and ensuring product safety. Therefore, the quality of the packaging is increasingly investigated with advanced techniques such as AFM. This technique is an irreplaceable tool for the topography analysis of plastic and biodegradable materials (Marinello, La Storia, Mauriello, & Passeri, 2019). AFM, as a local probe microscope, allows the analysis of physical and/or mechanical properties of interfaces. This provides relevant information at the nanoscale about different parameters such as dimensions, shapes, evolution, adhesion, or even Young modulus (Fig. 8.6). Packaging materials are therefore particularly suitable for this technique.

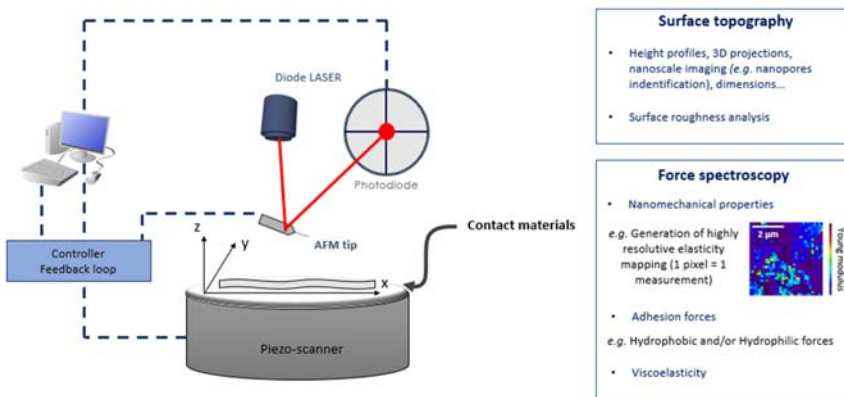


**Figure 8.6** Summary of how atomic force microscopy can be applied to probe food contact material surface properties.

### 8.4.1 Morphological studies of food material surfaces

Morphological and topographical surface studies are the main characterizations performed with AFM in the food packaging field. The technique allows imaging of surfaces with a very fine detail resolution and with minor impact due to a nondestructive sample preparation. Numerous authors characterized film surfaces. (Ghanbarzadeh & Oromiehi, 2008) used AFM in order to compare various formulations (comprising a mix of zein, whey proteins, glycerol, and olive oil) to select those presenting a continuous matrix with low pores and cracks, also with a good structural integrity. Thus, they showed that zein films containing olive oil presented a smoother surface with fewer pores and cracks. They also showed that zein films exhibit a low surface roughness compared to the whey protein films (Fig. 8.7). Liu and Cheng (2011b) compared soluble soybean polysaccharide/gelatin blend edible films. Films were visualized by AFM to check the compatibility of gelatin and soybean polysaccharide blends (Liu & Cheng, 2011a). AFM revealed a continuous and dense structure, indicating good compatibility of the components blends. For packaging exhibiting antimicrobial activity, the presence of nanoparticles was identified and evidenced as a contoured structure (Basu et al., 2017). The formation of protrusions and indentations due to the addition of nanoparticles (i.e., zinc oxide) embedded in the film surface was identified and correlated to an enhancement in its barrier properties (Sadeghi & Shahedi, 2016).

Atomic force microscopy measures are systematically considered with film mechanical properties, such as tensile strength, elongation, or barrier properties. Therefore, AFM analysis is generally performed concurrently with a universal testing machine equipped with load cells (Marinello et al., 2019). For example, the heat sealability, stretchability, and resistance to fracture of films were significantly improved by blending gelatin and soybean polysaccharides. In the particular case of active packaging, AFM measurements can be associated with oxygen or water vapor permeability, sometimes to contact angle analyses as the functional property to reach for a food contact material is often a control of permeability or wettability (Ghanbarzadeh & Oromiehi, 2008).

### 8.4.2 Quantitative studies of food material surfaces

Atomic force microscopy also has the possibility to estimate quantitative information. A common information obtained directly from images is surface roughness. Therefore, surface roughness modifications were associated

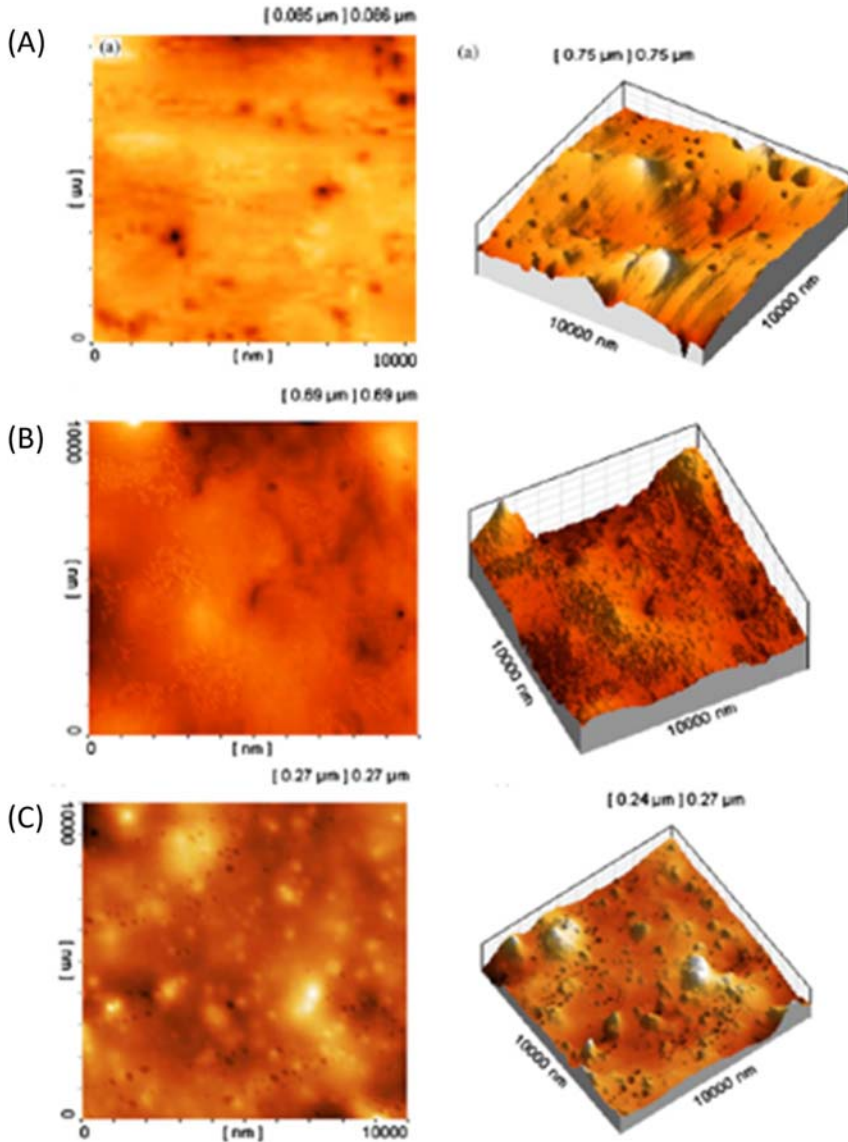


**Figure 8.7** Atomic force microscopy topographies of different films at  $10 \times 10 \mu\text{m}$  scan size and their 3D projection. (A) A whey-glycerol, (B) zein-glycerol, and (C) zein-olive oil + whey-glycerol. Modified from Ghanbarzadeh, B., & Oromiehi, A. R. (2008). *Biodegradable biocomposite films based on whey protein and zein: Barrier, mechanical properties and AFM analysis*. *International Journal of Biological Macromolecules*, 43(2), 209–215. <https://doi.org/10.1016/j.ijbiomac.2008.05.006>.

with changes in materials adhesion properties, wettability, chemical functionality, and sometimes bioactivity (Marinello et al., 2019). Quantification of shape, number, volume, and area of micropores containing active molecules was done. These data were discussed in view of the modulation and release of these active molecules from chitosan coating membranes (Xing et al., 2016). As explained earlier in 8.4.1, (Ghanbarzadeh & Oromiehi, 2008) characterized the surface properties of different film formulations, comprising whey proteins and/or zein mixed with a plasticizer such as glycerol and olive oil. Thus, they quantitatively studied the morphological properties of such films thanks to classical roughness parameters and showed that zein films had a lower surface roughness compared to the whey protein films (Fig. 8.7). Another study investigates a promising application of zein, a protein from maize, as the main source of biodegradable films and plastics for packaging (Guo et al., 2005). The zein globules morphologies, height, and diameter distribution were investigated thanks to surface topographies by AFM. It was shown that the globules' height and diameters are mainly comprised between 150 and 550 nm. They also explored the mechanism of the zein film formation by topography imaging, and showing that zein proteins form highly branched rod structures.

## 8.5 Prospects and advanced atomic force microscopy techniques to characterize food powders

Combining AFM with other techniques can be complementary to obtain more information about the sample. One of the most promising developments in the field concerns AFM-infrared spectroscopy (AFM-IR) as a super-resolution tool combining scanning probe microscopy with infrared spectroscopy. In fact, merging AFM and infrared spectroscopy could be very helpful in chemical mapping of a powder sample at the nanoscale (Liu & Yang, 2019). The AFM-IR technique is based on using an IR transparent prism (e.g., ZnSe) as a sample substrate and a tunable IR laser-focused near the AFM tip (Dazzi et al., 2012). When this IR laser is set to a wavelength value near the absorption wavelength of the sample, the AFM tip can be used to detect the absorbed radiation. Based on the linear relation between the cantilever oscillation and the IR absorption, it is possible to create IR absorption spectra of nanoscale regions of the sample (Dazzi & Prater, 2017). Although AFM-IR is a promising technique to better understand the chemical composition, it was never used on food

powders. AFM-IR was mostly used to study specific polymers, for example, biodegradable polymers (Marcott, Lo, Kjoller, Prater, & Noda, 2011) and polymer blends (Tang, Bao, & Su, 2016; Ye et al., 2012). For example, AFM-IR was used to study the effect of photocatalytic aging on Nano-TiO<sub>2</sub>-coated polypropylene plastics, which are widely used for agricultural or industrial applications, especially for bottle caps regarding food contact material (Luo, Xiang, Li, Zhao, & Pan, 2020). Thus, the authors compared the morphology and the chemical composition of new and photo-aged polypropylene plastics. Thanks to the analysis of nanoscale AFM-IR spectra, a new peak of 3400 cm<sup>-1</sup> was observed and associated with the photocatalytic reaction between nano-TiO<sub>2</sub> and water vapor of the ambient environment. These reactions changed the chemical composition of these plastics, generating new hydroxyl radicals at their surface (Luo, Xiang, Li, Zhao, & Pan, 2021). Similarly, in another study, it was highlighted that aging affects the surface properties of such microplastics by increasing the surface roughness and increasing the global Young modulus. Moreover, they were able to correlate these results to chemical modifications due to photoaging thanks to AFM-IR. Indeed, the detection of a sharp peak at 1706 cm<sup>-1</sup> was associated with an oxidation of C-H bonds. By comparing AFM-IR spectra and surface topographies, they were able to detect nanoscale chemical variation in aged microplastics (Fig. 8.8) (Luo, Xiang, Zhao, Li, & Pan, 2020). This technique was also already used in the pharmaceutical field to study many drugs formulation and especially complex drug-polymer blends (Harrison, Bilgili, Beaudoin, & Taylor, 2013; Li & Taylor, 2016; Van Eerdenbrugh, Lo, Kjoller, Marcott, & Taylor, 2012a; Van Eerdenbrugh, Lo, Kjoller, Marcott, & Taylor, 2012b).

Similarly, the AFM-Raman technique has recently emerged to (1) image the powder topography and roughness at nanoscale with the AFM and (2) determine at the same time the chemical composition and functional groups thanks to Raman spectroscopy. Understanding the physical and chemical properties of blend materials is essential to control the final properties of a product. Finally, these results show how promising it could be to combine AFM with infrared or Raman spectroscopy to obtain precious information about the morphological, mechanical, and chemical properties of food powders or contact materials. The application of these techniques could be very promising for the near future, and it may help formulations converge more efficiently on optimal processing conditions.

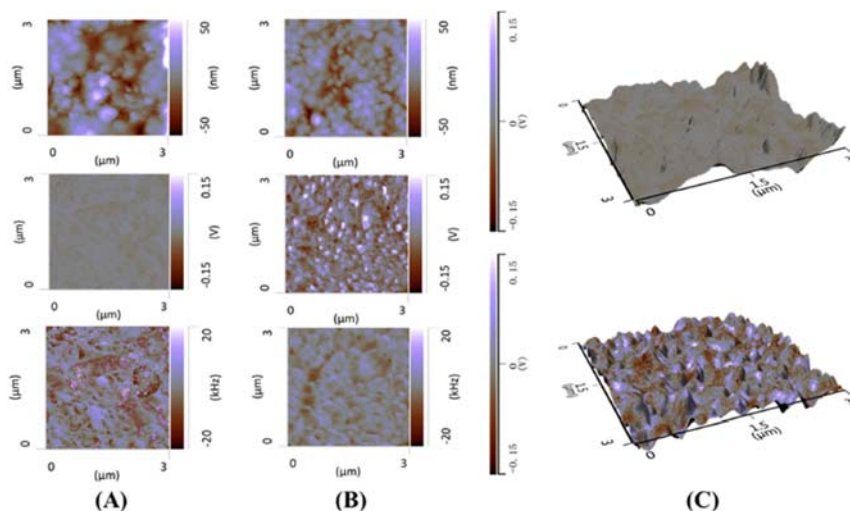


**Figure 8.8** From top to bottom: Atomic force microscopy (AFM) topographies combining AFM-IR images at peak  $1706\text{ cm}^{-1}$  and frequency images of (A) unaged and (B) aged microplastics. (C) 3D projections obtained from topographical and AFM-IR images of unaged (top) and aged (bottom) of microplastics. *Modified from Luo, H., Xiang, Y., Zhao, Y., Li, Y., & Pan, X. (2020). Nanoscale infrared, thermal, and mechanical properties of aged microplastics revealed by an atomic force microscopy coupled with infrared spectroscopy (AFM-IR) technique. Science of the Total Environment, 744. <https://doi.org/10.1016/j.scitotenv.2020.140944>.*

## 8.6 Conclusion

AFM demonstrated significant advantages as it requires a minimal sample powder and is nondestructive. Even if the technique has a relatively long acquisition time, is somewhat arduous, and unlikely to be used as a routine means, it provides unambiguous diagnostic equipment for troubleshooting related to powder surfaces. With all these examples, it was demonstrated that it is useful for:

1. qualitatively analyze the structure of powders (qualitative imaging),
2. performing quantitative structural analysis and establishing links between AFM images and powder functional properties,
3. measuring interaction forces between a functionalized AFM tip (chemically or by fixing a food particle) and the powder sample to establish links between forces and powder functional properties
4. measuring local elastic properties and adhesion forces by nanoindentation.



## References

- Abd El-Salam, M. H., & El-Shibiny, S. (2015). Preparation and properties of milk proteins-based encapsulated probiotics: A review. *Dairy Science and Technology*, 95(4), 393–412. Available from <https://doi.org/10.1007/s13594-015-0223-8>.
- An, H., Yang, H., Liu, Z., & Zhang, Z. (2008). Effects of heating modes and sources on nanostructure of gelatinized starch molecules using atomic force microscopy. *LWT - Food Science and Technology*, 41(8), 1466–1471. Available from <https://doi.org/10.1016/j.lwt.2007.08.026>.
- Baker, A. A., Miles, M. J., & Helbert, W. (2001). Internal structure of the starch granule revealed by AFM. *Carbohydrate Research*, 330(2), 249–256. Available from [https://doi.org/10.1016/S0008-6215\(00\)00275-5](https://doi.org/10.1016/S0008-6215(00)00275-5).
- Baldwin, P. M., Adler, J., Davies, M. C., & Melia, C. D. (1998). High resolution imaging of starch granule surfaces by atomic force microscopy. *Journal of Cereal Science*, 27(3), 255–265. Available from <https://doi.org/10.1006/jcrs.1998.0189>.
- Baldwin, P. M., Davies, M. C., & Melia, C. D. (1996). Starch granule surface imaging using low-voltage scanning electron microscopy and atomic force microscopy. *International Journal of Biological Macromolecules*, 21, 103–107. Available from [https://doi.org/10.1016/s0141-8130\(97\)00048-2](https://doi.org/10.1016/s0141-8130(97)00048-2).
- Barrera, G. N., Calderón-Domínguez, G., Chanona-Pérez, J., Gutiérrez-López, G. F., León, A. E., & Ribotta, P. D. (2013). Evaluation of the mechanical damage on wheat starch granules by SEM, ESEM, AFM and texture image analysis. *Carbohydrate Polymers*, 98(2), 1449–1457. Available from <https://doi.org/10.1016/j.carbpol.2013.07.056>.
- Basu, A., Kundu, S., Sana, S., Halder, A., Abdullah, M. F., Datta, S., & Mukherjee, A. (2017). Edible nano-bio-composite film cargo device for food packaging applications. *Food Packaging and Shelf Life*, 11, 98–105. Available from <https://doi.org/10.1016/j.foodpack.2017.01.011>.
- Bhandari, B. (2013). Introduction to food powders. Handbook of food powders. 1–25. DOI 10.1533/0780857098672.1.
- Bunker, M., Zhang, J., Blanchard, R., & Roberts, C. J. (2011). Characterising the surface adhesive behavior of tablet tooling components by atomic force microscopy. *Drug Development and Industrial Pharmacy*, 37(8), 875–885. Available from <https://doi.org/10.3109/03639045.2010.546402>.
- Burgain, J., El Zein, R., Scher, J., Petit, J., Norwood, E. A., Francius, G., & Gaiani, C. (2016). Local modifications of whey protein isolate powder surface during high temperature storage. *Journal of Food Engineering*, 178, 39–46. Available from <https://doi.org/10.1016/j.jfoodeng.2016.01.005>.
- Burgain, J., Petit, J., Scher, J., Rasch, R., Bhandari, B., & Gaiani, C. (2017). Surface chemistry and microscopy of food powders. *Progress in Surface Science*, 92(4), 409–429. Available from <https://doi.org/10.1016/j.progsurf.2017.07.002>.
- Burgain, J., Scher, J., Petit, J., Francius, G., & Gaiani, C. (2016). Links between particle surface hardening and rehydration impairment during micellar casein powder storage. *Food Hydrocolloids*, 61, 277–285. Available from <https://doi.org/10.1016/j.foodhyd.2016.05.021>.
- Colbert, M. J., Grandbois, M., & Abatzoglou, N. (2015). Identification of inter-particular forces by atomic force microscopy and how they relate to powder rheological properties measured in shearing tests. *Powder Technology*, 284, 396–402. Available from <https://doi.org/10.1016/j.powtec.2015.06.059>.
- Dang, J. M. C., & Copeland, L. (2003). Imaging rice grains using atomic force microscopy. *Journal of Cereal Science*, 37(2), 165–170. Available from <https://doi.org/10.1006/jcrs.2002.0490>.

- Dang, J. M. C., Braet, F., & Copeland, L. (2006). Nanostructural analysis of starch components by atomic force microscopy. *Journal of Microscopy*, 224(2), 181–186. Available from <https://doi.org/10.1111/j.1365-2818.2006.01681.x>.
- Davenel, A., Schuck, P., Mariette, F., & Brulé, G. (2002). NMR relaxometry as a non-invasive tool to characterize milk powders. *Lait*, 82(4), 465–473. Available from <https://doi.org/10.1051/lait:2002024>.
- Dazzi, A., Prater, C. B., Hu, Q., Chase, D. B., Rabolt, J. F., & Marcott, C. (2012). AFM-IR: Combining atomic force microscopy and infrared spectroscopy for nanoscale chemical characterization. *Applied Spectroscopy*, 66(12), 1365–1384. Available from <https://doi.org/10.1366/12-06804>.
- Dazzi, A., & Prater, C. B. (2017). AFM-IR: Technology and applications in nanoscale infrared spectroscopy and chemical imaging. *Chemical Reviews*, 117(7), 5146–5173. Available from <https://doi.org/10.1021/acs.chemrev.6b00448>.
- Dey, F. K., Cleaver, J. A. S., & Zhdan, P. A. (2000). Atomic force microscopy study of adsorbed moisture on lactose particles. *Advanced Powder Technology*, 11(4), 401–413. Available from <https://doi.org/10.1163/156855200750172024>.
- Doherty, S. B., Auty, M. A., Stanton, C., Ross, R. P., Fitzgerald, G. F., & Brodtkorb, A. (2012). Survival of entrapped *Lactobacillus rhamnosus* GG in whey protein micro-beads during simulated ex vivo gastro-intestinal transit. *International Dairy Journal*, 22(1), 31–43. Available from <https://doi.org/10.1016/j.idairyj.2011.06.009>.
- Doherty, S. B., Gee, V. L., Ross, R. P., Stanton, C., Fitzgerald, G. F., & Brodtkorb, A. (2010). Efficacy of whey protein gel networks as potential viability-enhancing scaffolds for cell immobilization of *Lactobacillus rhamnosus* GG. *Journal of Microbiological Methods*, 80(3), 231–241. Available from <https://doi.org/10.1016/j.mimet.2009.12.009>.
- Doherty, S. B., Gee, V. L., Ross, R. P., Stanton, C., Fitzgerald, G. F., & Brodtkorb, A. (2011). Development and characterisation of whey protein micro-beads as potential matrices for probiotic protection. *Food Hydrocolloids*, 25(6), 1604–1617. Available from <https://doi.org/10.1016/j.foodhyd.2010.12.012>.
- Et-Thakafy, O., Delorme, N., Gaillard, C., Mériade, C., Artzner, F., Lopez, C., & Guyomarch, F. (2017). Mechanical properties of membranes composed of gel-phase or fluid-phase phospholipids probed on liposomes by atomic force spectroscopy. *Langmuir*, 33(21), 5117–5126. Available from <https://doi.org/10.1021/acs.langmuir.7b00363>.
- Et-Thakafy, O., Guyomarc'h, F., & Lopez, C. (2019). Young modulus of supported lipid membranes containing milk sphingomyelin in the gel, fluid or liquid-ordered phase, determined using AFM force spectroscopy. *Biochimica et Biophysica Acta - Biomembranes*, 1861(9), 1523–1532. Available from <https://doi.org/10.1016/j.bbamem.2019.07.005>.
- Foster, K.D. (2002). The prediction of sticking in dairy powders.
- Foster, K. D., Bronlund, J. E., & Paterson, A. H. J. (2006). Glass transition related cohesion of amorphous sugar powders. *Journal of Food Engineering*, 77(4), 997–1006. Available from <https://doi.org/10.1016/j.jfoodeng.2005.08.028>.
- Fritzsche, J., & Peuker, U. A. (2015). *Wetting and adhesive forces on rough surfaces—An experimental and theoretical study*, . *Procedia Engineering* (Vol. 102, pp. 45–53). Elsevier Ltd. Available from <https://doi.org/10.1016/j.proeng.2015.01.105>.
- Funami, T. (2010). Atomic force microscopy imaging of food polysaccharides. *Food Science and Technology Research*, 16(1), 1–12. Available from <https://doi.org/10.3136/fstr.16.1>.
- Fyfe, K. N., Kravchuk, O., Le, T., Deeth, H. C., Nguyen, A. V., & Bhandari, B. (2011). Storage induced changes to high protein powders: Influence on surface properties and solubility. *Journal of the Science of Food and Agriculture*, 91(14), 2566–2575. Available from <https://doi.org/10.1002/jsfa.4461>.

- Gaiani, C., Burgain, J., & Scher, J. (2013). Surface composition of food powders. In *Handbook of food powders* (pp. 339–378). <https://doi.org/10.1533/9780857098672.2.339>.
- Gaiani, C., Schuck, P., Scher, J., Desobry, S., & Banon, S. (2007). Dairy powder rehydration: Influence of protein state, incorporation mode, and agglomeration. *Journal of Dairy Science*, *90*(2), 570–581. Available from [https://doi.org/10.3168/jds.S0022-0302\(07\)71540-0](https://doi.org/10.3168/jds.S0022-0302(07)71540-0).
- Ghanbarzadeh, B., & Oromiehi, A. R. (2008). Biodegradable biocomposite films based on whey protein and zein: Barrier, mechanical properties and AFM analysis. *International Journal of Biological Macromolecules*, *43*(2), 209–215. Available from <https://doi.org/10.1016/j.ijbiomac.2008.05.006>.
- Ghasemi, S., Jafari, S. M., Assadpour, E., & Khomeiri, M. (2017). Production of pectin-whey protein nano-complexes as carriers of orange peel oil. *Carbohydrate Polymers*, *177*, 369–377. Available from <https://doi.org/10.1016/j.carbpol.2017.09.009>.
- Goalard, C., Samimi, A., Galet, L., Dodds, J. A., & Ghadiri, M. (2006). Characterization of the dispersion behavior of powders in liquids. *Particle and Particle Systems Characterization*, *23*(2), 154–158. Available from <https://doi.org/10.1002/ppsc.200601024>.
- Guerin, J., Bacharouche, J., Burgain, J., Lebeer, S., Francius, G., Borges, F., . . . Gaiani, C. (2016). Pili of *Lactobacillus rhamnosus* GG mediate interaction with  $\beta$ -lactoglobulin. *Food Hydrocolloids*, *58*, 35–41. Available from <https://doi.org/10.1016/j.foodhyd.2016.02.016>.
- Guo, Y., Liu, Z., An, H., Li, M., & Hu, J. (2005). Nano-structure and properties of maize zein studied by atomic force microscopy. *Journal of Cereal Science*, *41*(3), 277–281. Available from <https://doi.org/10.1016/j.jcs.2004.12.005>.
- Haider, C. I., Niederreiter, G., Palzer, S., Hounslow, M. J., & Salman, A. D. (2018). Unwanted agglomeration of industrial amorphous food powder from a particle perspective. *Chemical Engineering Research and Design*, *132*, 1160–1169. Available from <https://doi.org/10.1016/j.cherd.2018.02.023>.
- Hammes, M. V., Englert, A. H., Noreña, C. P. Z., & Cardozo, N. S. M. (2015). Study of the influence of soy lecithin addition on the wettability of buffalo milk powder obtained by spray drying. *Powder Technology*, *277*, 237–243. Available from <https://doi.org/10.1016/j.powtec.2015.02.047>.
- Harrison, A. J., Bilgili, E. A., Beaudoin, S. P., & Taylor, L. S. (2013). Atomic force microscope infrared spectroscopy of griseofulvin nanocrystals. *Analytical Chemistry*, *85*(23), 11449–11455. Available from <https://doi.org/10.1021/ac4025889>.
- Hooton, J. C., Jones, M. D., & Price, R. (2006). Predicting the behavior of novel sugar carriers for dry powder inhaler formulations via the use of a cohesive-adhesive force balance approach. *Journal of Pharmaceutical Sciences*, *95*(6), 1288–1297. Available from <https://doi.org/10.1002/jps.20618>.
- Kadam, S. U., Tiwari, B. K., & O'Donnell, C. P. (2015). *Improved thermal processing for food texture modification. Modifying food texture: Novel ingredients and processing techniques* (pp. 115–131). Elsevier. Available from <https://doi.org/10.1016/B978-1-78242-333-1.00006-1>.
- Karadag, A., Ozcelik, B., & Huang, Q. (2014). Quercetin nanosuspensions produced by high-pressure homogenization. *Journal of Agricultural and Food Chemistry*, *62*(8), 1852–1859. Available from <https://doi.org/10.1021/jf404065p>.
- Karam, M. C., Petit, J., Zimmer, D., Baudelaire Djantou, E., & Scher, J. (2016). Effects of drying and grinding in production of fruit and vegetable powders: A review. *Journal of Food Engineering*, *188*, 32–49. Available from <https://doi.org/10.1016/j.jfoodeng.2016.05.001>.
- Kim, E. H. J., Chen, X. D., & Pearce, D. (2002). Surface characterization of four industrial spray-dried dairy powders in relation to chemical composition, structure and

- wetting property. *Colloids and Surfaces B: Biointerfaces*, 26(3), 197–212. Available from [https://doi.org/10.1016/S0927-7765\(01\)00334-4](https://doi.org/10.1016/S0927-7765(01)00334-4).
- Li, N., & Taylor, L. S. (2016). Nanoscale infrared, thermal, and mechanical characterization of telaprevir-polymer miscibility in amorphous solid dispersions prepared by solvent evaporation. *Molecular Pharmaceutics*, 13(3), 1123–1136. Available from <https://doi.org/10.1021/acs.molpharmaceut.5b00925>.
- Liu, D., & Cheng, F. (2011a). Advances in research on structural characterisation of agricultural products using atomic force microscopy. *Journal of the Science of Food and Agriculture*, 91(5), 783–788. Available from <https://doi.org/10.1002/jsfa.4284>.
- Liu, D., & Cheng, F. (2011b). Advances in research on structural characterisation of agricultural products using atomic force microscopy. *Journal of the Science of Food and Agriculture*, 91(5), 783–788. Available from <https://doi.org/10.1002/jsfa.4284>.
- Liu, Q., & Yang, H. (2019). Application of atomic force microscopy in food microorganisms. *Trends in Food Science & Technology*, 87, 73–83. Available from <https://doi.org/10.1016/j.tifs.2018.05.010>.
- Luo, H., Xiang, Y., Li, Y., Zhao, Y., & Pan, X. (2020). Weathering alters surface characteristic of TiO<sub>2</sub>-pigmented microplastics and particle size distribution of TiO<sub>2</sub> released into water. *Science of the Total Environment*, 729. Available from <https://doi.org/10.1016/j.scitotenv.2020.139083>.
- Luo, H., Xiang, Y., Li, Y., Zhao, Y., & Pan, X. (2021). Photocatalytic aging process of Nano-TiO<sub>2</sub> coated polypropylene microplastics: Combining atomic force microscopy and infrared spectroscopy (AFM-IR) for nanoscale chemical characterization. *Journal of Hazardous Materials*, 404. Available from <https://doi.org/10.1016/j.jhazmat.2020.124159>.
- Luo, H., Xiang, Y., Zhao, Y., Li, Y., & Pan, X. (2020). Nanoscale infrared, thermal and mechanical properties of aged microplastics revealed by an atomic force microscopy coupled with infrared spectroscopy (AFM-IR) technique. *Science of the Total Environment*, 744. Available from <https://doi.org/10.1016/j.scitotenv.2020.140944>.
- Marcott, C., Lo, M., Kjoller, K., Prater, C., & Noda, I. (2011). Spatial differentiation of sub-micrometer domains in a poly(hydroxyalkanoate) copolymer using instrumentation that combines atomic force microscopy (AFM) and infrared (IR) spectroscopy. *Applied Spectroscopy*, 65(10), 1145–1150. Available from <https://doi.org/10.1366/11-06341>.
- Marinello, F., La Storia, A., Mauriello, G., & Passeri, D. (2019). Atomic Force microscopy techniques to investigate activated food packaging materials. *Trends in Food Science and Technology*, 87, 84–93. Available from <https://doi.org/10.1016/j.tifs.2018.05.028>.
- Masterson, V. M., & Cao, X. (2008). Evaluating particle hardness of pharmaceutical solids using AFM nanoindentation. *International Journal of Pharmaceutics*, 362(1–2), 163–171. Available from <https://doi.org/10.1016/j.ijpharm.2008.06.015>.
- Middendorf, D., Bindrich, U., Mischnick, P., Franke, K., & Heinz, V. (2018). AFM-based local thermal analysis is a suitable tool to characterize the impact of different grinding techniques on sucrose surface properties. *Journal of Food Engineering*, 235, 50–58. Available from <https://doi.org/10.1016/j.jfoodeng.2018.04.021>.
- Middendorf, D., Juadjur, A., Bindrich, U., & Mischnick, P. (2015). AFM approach to study the function of PGPR's emulsifying properties in cocoa butter based suspensions. *Food Structure*, 4, 16–26. Available from <https://doi.org/10.1016/j.foostr.2014.11.003>.
- Murrieta-Pazos, I., Gaiani, C., Galet, L., Calvet, R., Cuq, B., & Scher, J. (2012). Food powders: Surface and form characterization revisited. *Journal of Food Engineering*, 112(1–2), 1–21. Available from <https://doi.org/10.1016/j.jfoodeng.2012.03.002>.
- Murrieta-Pazos, I., Gaiani, C., Galet, L., Cuq, B., Desobry, S., & Scher, J. (2011). Comparative study of particle structure evolution during water sorption: Skim and

- whole milk powders. *Colloids and Surfaces B: Biointerfaces*, 87(1), 1–10. Available from <https://doi.org/10.1016/j.colsurfb.2011.05.001>.
- Neves, M. I. L., Desobry-Banon, S., Perrone, I. T., Desobry, S., & Petit, J. (2019). Encapsulation of curcumin in milk powders by spray-drying: Physicochemistry, rehydration properties, and stability during storage. *Powder Technology*, 345, 601–607. Available from <https://doi.org/10.1016/j.powtec.2019.01.049>.
- Nijdam, J. J., & Langrish, T. A. G. (2006). The effect of surface composition on the functional properties of milk powders. *Journal of Food Engineering*, 77(4), 919–925. Available from <https://doi.org/10.1016/j.jfoodeng.2005.08.020>.
- Ohtani, T., Yoshino, T., Hagiwara, S., & Maekawa, T. (2000). High-resolution imaging of starch granule structure using atomic force microscopy. *Starch/Staerke*, 52(5), 150–153. Available from [https://doi.org/10.1002/1521-379X\(200006\)52:5 < 150::AID-STAR150 > 3.0.CO;2-F](https://doi.org/10.1002/1521-379X(200006)52:5 < 150::AID-STAR150 > 3.0.CO;2-F).
- Ohtani, T., Yoshino, T., Ushiki, T., Hagiwara, S., & Maekawa, T. (2000). Structure of rice starch granules in nanometre scale as revealed by atomic force microscopy. *Journal of Electron Microscopy*, 49(3), 487–489. Available from <https://doi.org/10.1093/oxfordjournals.jmicro.a023833>.
- Parker, M. L., Kirby, A. R., & Morris, V. J. (2008). In situ imaging of pea starch in seeds. *Food Biophysics*, 3(1), 66–76. Available from <https://doi.org/10.1007/s11483-007-9050-7>.
- Perkins, M., Ebbens, S. J., Hayes, S., Roberts, C. J., Madden, C. E., Luk, S. Y., & Patel, N. (2007). Elastic modulus measurements from individual lactose particles using atomic force microscopy. *International Journal of Pharmaceutics*, 332(1–2), 168–175. Available from <https://doi.org/10.1016/j.ijpharm.2006.09.032>.
- Peroni-Okita, F. H. G., Gunning, A. P., Kirby, A., Simão, R. A., Soares, C. A., & Cordenunsi, B. R. (2015). Visualization of internal structure of banana starch granule through AFM. *Carbohydrate Polymers*, 128, 32–40. Available from <https://doi.org/10.1016/j.carbpol.2015.04.019>.
- Prime, D. C., Leaper, M. C., Jones, J. R., Richardson, D. J., Rielly, C. C., & Stapley, A. G. F. (2011). Caking behavior of spray-dried powders—Using scanning probe microscopy to study nanoscale surface properties and material composition. *Chemical Engineering & Technology*, 34. Available from <https://doi.org/10.1002/ceat.201000527>, <https://doi.org/1104-1108>.
- Prime, D. C., Stapley, A. G. F., Rielly, C. D., Jones, J. R., & Leaper, M. C. (2011). Analysis of powder caking in multicomponent powders using atomic force microscopy to examine particle properties. *Chemical Engineering and Technology*, 34(1), 98–102. Available from <https://doi.org/10.1002/ceat.201000211>.
- Qi, P. X., & Onwulata, C. I. (2011). Physical properties, molecular structures, and protein quality of texturized whey protein isolate: Effect of extrusion moisture content. *Journal of Dairy Science*, 94(5), 2231–2244. Available from <https://doi.org/10.3168/jds.2010-3942>.
- Ramos, K. J., & Bahr, D. F. (2007). Mechanical behavior assessment of sucrose using nanoindentation. *Journal of Materials Research*, 22(7), 2037–2045. Available from <https://doi.org/10.1557/JMR.2007.0249>.
- Ridout, M. J., Gunning, A. P., Parker, M. L., Wilson, R. H., & Morris, V. J. (2002). Using AFM to image the internal structure of starch granules. *Carbohydrate Polymers*, 50(2), 123–132. Available from [https://doi.org/10.1016/S0144-8617\(02\)00021-8](https://doi.org/10.1016/S0144-8617(02)00021-8).
- Ridout, M. J., Parker, M. L., Hedley, C. L., Bogracheva, T. Y., & Morris, V. J. (2004). Atomic force microscopy of pea starch: Origins of image contrast. *Biomacromolecules*, 5(4), 1519–1527. Available from <https://doi.org/10.1021/bm0499280>.
- Roos, Y., & Karel, M. (1991). Plasticizing effect of water on thermal behavior and crystallization of amorphous food models. *Journal of Food Science*, 56(1), 38–43. Available from <https://doi.org/10.1111/j.1365-2621.1991.tb07970.x>.

- Ruozzi, B., Tosi, G., Leo, E., & Vandelli, M. A. (2007). Application of atomic force microscopy to characterize liposomes as drug and gene carriers. *Talanta*, 73(1), 12–22. Available from <https://doi.org/10.1016/j.talanta.2007.03.031>.
- Sadeghi, K., & Shahedi, M. (2016). Physical, mechanical, and antimicrobial properties of ethylene vinyl alcohol copolymer/chitosan/nano-ZnO (ECNZn) nanocomposite films incorporating glycerol plasticizer. *Journal of Food Measurement and Characterization*, 10(1), 137–147. Available from <https://doi.org/10.1007/s11694-015-9287-7>.
- Schuck, P., & Dolivet, A. (2002). Lactose crystallization: Determination of  $\alpha$ -lactose monohydrate in spray-dried dairy products. *Lait*, 82(4), 413–421. Available from <https://doi.org/10.1051/lait:2002020>.
- Schuck, P., Dolivet, A., & Jeantet, R. (2012). Analytical methods for food and dairy powders. <https://doi.org/10.1002/97811118307397>
- Selomulya, C., & Fang, Y. (2013). *Food powder rehydration. Handbook of food powders: Processes and properties* (pp. 379–408). Elsevier Inc. Available from <https://doi.org/10.1533/9780857098672.2.379>.
- Sharma, A., Jana, A. H., & Chavan, R. S. (2012). Functionality of milk powders and milk-based powders for end use applications—A review. *Comprehensive Reviews in Food Science and Food Safety*, 11(5), 518–528. Available from <https://doi.org/10.1111/j.1541-4337.2012.00199.x>.
- Sindel, U., & Zimmermann, I. (2001). Measurement of interaction forces between individual powder particles using an atomic force microscope. *Powder Technology*, 117(3), 247–254. Available from [https://doi.org/10.1016/S0032-5910\(00\)00373-9](https://doi.org/10.1016/S0032-5910(00)00373-9).
- Spyratou, E., Mourelatou, E. A., Makropoulou, M., & Demetzos, C. (2009). Atomic force microscopy: A tool to study the structure, dynamics and stability of liposomal drug delivery systems. *Expert Opinion on Drug Delivery*, 6(3), 305–317. Available from <https://doi.org/10.1517/17425240902828312>.
- Szymońska, J., & Krok, F. (2003). Potato starch granule nanostructure studied by high resolution non-contact AFM. *International Journal of Biological Macromolecules*, 33, 1–7. Available from [https://doi.org/10.1016/s0141-8130\(03\)00056-4](https://doi.org/10.1016/s0141-8130(03)00056-4).
- Tang, F., Bao, P., & Su, Z. (2016). Analysis of nanodomain composition in high-impact polypropylene by atomic force microscopy-infrared. *Analytical Chemistry*, 88(9), 4926–4930. Available from <https://doi.org/10.1021/acs.analchem.6b00798>.
- Tejedor, M. B., Nordgren, N., Schuleit, M., Pazesh, S., Alderborn, G., Millqvist-Fureby, A., & Rutland, M. W. (2017). Determination of interfacial amorphicity in functional powders. *Langmuir*, 33(4), 920–926. Available from <https://doi.org/10.1021/acs.langmuir.6b03969>.
- Teschke, O., & De Souza, E. F. (2002). Liposome structure imaging by atomic force microscopy: Verification of improved liposome stability during adsorption of multiple aggregated vesicles. *Langmuir*, 18(17), 6513–6520. Available from <https://doi.org/10.1021/la025689v>.
- Tomoia-Cotisel, M., Coica, N., Cota, C., Racz, C.P., Petean, I., Bobos, L.D., ... Horovitz, O. (2010). Structure of starch granules revealed by atomic force microscopy. *Studia Universitatis Babeş-Bolyai Chemia* (Vol. 2).
- Van Eerdenbrugh, B., Lo, M., Kjoller, K., Marcott, C., & Taylor, L. S. (2012a). Nanoscale mid-infrared evaluation of the miscibility behavior of blends of dextran or maltodextrin with poly(vinylpyrrolidone). *Molecular Pharmaceutics*, 9(5), 1459–1469. Available from <https://doi.org/10.1021/mp300059z>.
- Van Eerdenbrugh, B., Lo, M., Kjoller, K., Marcott, C., & Taylor, L. S. (2012b). Nanoscale mid-infrared imaging of phase separation in a drug-polymer blend. *Journal of Pharmaceutical Sciences*, 101(6), 2066–2073. Available from <https://doi.org/10.1002/jps.23099>.
- Wolska, E., Sznitowska, M., Krzemińska, K., & Monteiro, M. F. (2020). Analytical techniques for the assessment of drug-lipid interactions and the active substance

- distribution in liquid dispersions of solid lipid microparticles (SLM) produced de novo and reconstituted from spray-dried powders. *Pharmaceutics*, 12(7), 1–23. Available from <https://doi.org/10.3390/pharmaceutics12070664>.
- Wuttisela, K., Triampo, W., & Triampo, D. (2009). Chemical force mapping of phosphate and carbon on acid-modified tapioca starch surface. *International Journal of Biological Macromolecules*, 44(1), 86–91. Available from <https://doi.org/10.1016/j.ijbiomac.2008.10.005>.
- Xing, Y., Xu, Q., Yang, S. X., Chen, C., Tang, Y., Sun, S., ... Li, X. (2016). Preservation mechanism of chitosan-based coating with cinnamon oil for fruits storage based on sensor data. *Sensors (Switzerland)*, 16(7). Available from <https://doi.org/10.3390/s16071111>.
- Ye, J., Midorikawa, H., Awatani, T., Marcott, C., Lo, M., Kjoller, K., & Shetty, R. (2012). Nanoscale infrared spectroscopy and AFM imaging of a polycarbonate/acrylonitrile-styrene/butadiene blend. *Microscopy and Analysis*, 26, 24–27. Available from <https://doi.org/10.1088/0957-4484/23/21/215301>.

## CHAPTER 9

# Advances in food material nanomechanics by means of atomic force microscopy

Benjamin Arredondo-Tamayo<sup>1</sup>, Stefany Cárdenas-Pérez<sup>2</sup>,  
Juan V. Méndez-Méndez<sup>3</sup>, Israel Arzate-Vázquez<sup>3</sup>,  
Héctor H. Torres-Ventura<sup>1</sup> and José J. Chanona-Pérez<sup>1</sup>

<sup>1</sup>Departamento de Ingeniería Bioquímica, Escuela Nacional de Ciencias Biológicas, Instituto Politécnico Nacional, Mexico City, Mexico

<sup>2</sup>Geobotany and Landscape Planning, Faculty of Biological and Veterinary Sciences, Nicolaus Copernicus University, Toruń, Poland

<sup>3</sup>Centro de Nanociencias y Micro y Nanotecnologías, Instituto Politécnico Nacional, Mexico City, Mexico

### 9.1 Introduction

Atomic force microscopes are close-field scanning instruments for nano-scale research. Rather than using light or electron beams, as is the case with other microscopes, this particular type utilizes a sharp tip to sense samples. Since the radius of the tip curvature is of nanometric size, in the best conditions atomic force microscopy (AFM) can reach subnanometric spatial resolution (Binnig, Quate, & Gerber, 1986). The versatility of AFM techniques allows for topographic and mechanical property information of biological samples to be obtained, with the latter made possible by the capability of contacting samples at the nanoscale level. This technique can estimate the nanomechanical properties of biological samples, as well as evaluate certain phenomena that occur during the interaction between the tip and the sample (Müller & Dufrene, 2010; Tseng, 2011; Yan, Geng, & Hu, 2015).

Determining the mechanical properties at a nanometric scale in food samples through AFM has been recently considered an innovative method. This technique applies small loads on the surface of food materials, which is based on the use of microcantilevers attached with nanometric tips (Cárdenas-Pérez et al., 2016; Korayem, Noroozi, & Daeinabi, 2012; Zdunek & Kurenda, 2013). Food samples can be analyzed in a vacuum, air, and liquid, including viable cells near their natural growth



environment, while its flexibility can provide nanomechanics measurements along with true 3D topographic images of sample surfaces.

Over the past few decades, the analytical capabilities of AFM have been successfully applied in material science, as well as micro and nanofabrication technologies, but only recently has it emerged as a tool for the evaluation of nanomechanical properties in food research (Cárdenas-Pérez et al., 2019; Wen, Xu, Liu, Corke, & Sui, 2020). Some properties can be assessed using the nanoindentation technique with AFM, such as Young's modulus, adhesion, elasticity, stiffness, and strength of the interaction between sample-tip, among other nanomechanical properties. Nanoindentation utilizing AFM has been used to evaluate mechanical properties at a nanometric scale in different food materials, such as animal and plant cells, beneficial and pathogenic microorganisms, packing biopolymers, proteins, and carbohydrates (Khan, Patel, Mahiuddin, & Karim, 2020; Shi, He, Ding, Wang, & Zhong, 2019; Yang et al., 2007). Previously, all these elements were difficult to study at the nanoscale due to the resolution limits of other measuring conventional instruments, such as texture analyzers and microindenter that can only evaluate the mechanical properties at macro and microscopic levels. The importance of assessing nanomechanical properties in food lies in the ability to evaluate the structure–functionality relationships and the changes, occurring in the biopolymers of surface cell wall. For instance, it is possible to determine the changes that occur in perishable food due to the external environment, as raw or processed food constantly changes over time due to its chemical composition, the addition of ingredients, reactions of microorganisms, as well as interference from the environment such as humidity, temperature, pressure, etc. (Lu, 2013).

AFM has become an important analytical tool for evaluating nanomechanical properties in food science and technology, but their uses and applications have not been widely known in food research until now. For this reason, this contribution aims to provide a brief guide for nonexperts in the principles of assessing nanomechanical properties by means of AFM in biological materials, specifically in food materials, as well as providing some of the most relevant works carried out in this research field.

## 9.2 Operation modes in atomic force microscopy

The principle of surface probing in AFM comes from Hooke's law, which stipulates that the probe is a cantilever with a sharp tip at its end which moves to the proximity of the sample surface and forces itself between the

cantilever tip and sample surface, leading to deflections of the cantilever. This technique determines material properties, such as surface morphology, magnetic force gradient, electric field gradient, electrical carrier concentration, thermal surface, and mechanical properties. The tip is selected according to size, geometry, stiffness composition, the type of interaction with a surface, and the interaction zone (Butt, Cappella, & Kapp, 2005; Dufrière, 2008; Morris, Kirby, & Gunning, 1999).

The tip with a moveable cantilever (or the sample on some AFM models) is fixed on a 3D piezoelectric scanner drive which can move precisely along x, y, and z axes. During this operation, a laser diode emits a beam onto the back of the cantilever over the tip. As the cantilever deflects under the load, the angular deflection of the reflected laser beam is detected by a position-sensitive photodiode (Fig. 9.1). The magnitude of the beam deflection changes in response to the interaction force between the tip and the sample. The AFM system senses these changes in position and can map surface topography or monitor the interaction force tip sample. As there is a risk that the tip can crash into the surface if it is

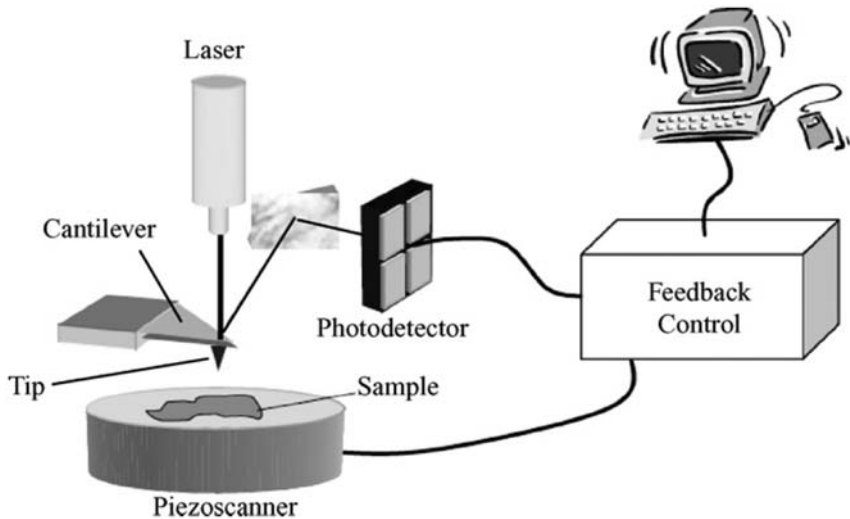


**Figure 9.1** Diagram of the principle of operation of an atomic force microscope. The laser is reflected from the tip to the photodetector that follows the fluctuations of the tip in the three axes when scanning the sample surface. The scanner-controller-computer system directs the scan and obtains the topographic image by a computer. From Gaboriaud, F. & Dufrière, Y. F. (2007). *Atomic force microscopy of microbial cells: application to nanomechanical properties, surface forces, and molecular recognition forces*. *Colloids and Surfaces B: Biointerfaces*, 54(1), 10–19; Copyright 2007 Elsevier.

scanned at a constant height, a feedback mechanism is employed in most of the first AFM instruments to adjust the tip-to-sample distance to maintain a constant force during the operation (Cappella & Dietler, 1999). Current devices use optimized modes and algorithms to control sample distance and force during sample scanning.

The most important AFM applications in the study of nanoscale food structures can be classified into two major fields: imaging to visualize sample topography and force spectroscopy. At the same time, imaging mode is divided into two categories: contact mode and dynamic mode, which in turn includes intermittent and noncontact modes. In addition, other AFM imaging techniques have been implemented that map properties such as conductance and friction on a surface. However, the contact and intermittent modes have been predominantly used for analyzing biological materials (Emam-Djomeh, Pure, & Pure, 2020).

Contact mode is the basis for all AFM techniques and is the most widely used AFM imaging mode for scientific materials, in which the tip and the sample surface essentially maintain contact during the scan. This process involves the tip moving (raster scans) over the sample's surface while cantilever deflections are monitored with the photodiode detector (Jalili & Laxminarayana, 2004). A feedback loop scans the cantilever deflections along the x-y axis as input and distance, and along the z-axis between the probe and support as output. Sample height and cantilever deflection are scanned and recorded as AFM signals on a computer and plotted as an image, in which each x-y position on the sample is presented as a pixel (Fig. 9.1), while the recorded signals can be shown in the user's preferred color. The resolution of the images depends on the applied force, as well as the elasticity constant of the beam used. Low stiffness cantilevers are typically used to boost the deflection signal. However, the continuous direct contact between the tip and sample causes significant lateral force, which can distort soft samples or even peel off samples that are not firmly absorbed on the substrate (Liu & Wang, 2010).

The dynamic mode includes intermittent (also known as tapping mode, adaptable to air or liquid environments) and noncontact modes. In both techniques, the attached AFM tip oscillates near to or slightly above its resonance frequency during the scan (Garcia & Perez, 2002; Kim & Chelikowsky, 2014). The oscillation's amplitude is normally 100–200 nm, with the tip intermittently contacting the sample's surface during the scan. Consequently, this significantly reduces the force exerted by the tip on the sample surfaces compared to the contact mode. Furthermore, the driving

frequency of the cantilever is usually around 10 kHz in a liquid environment, while in an intermittent mode in liquid and air environments, the usual range is 100–400 kHz (Mendoza-Madrigal et al., 2013). In noncontact mode, the cantilever vibrates slightly above its resonance frequency with a normal amplitude of several nanometers (less than 10 nm) (Andreas, Placidi, & Rega, 2013; Putman, Van der Werf, De Grooth, Van Hulst, & Greve, 1994). The tip never actually contacts the sample surface during the scan, but van der Waals forces and other long-range interactions extending above the surface influence the motion of the tip and provide information about the sample's surface. The contact mode could normally provide higher resolution, but recent advances in noncontact techniques have led to spatial resolution up to an atomic level in the air and liquid environments (Ellner, Pou, & Pérez, 2019; Fukuma, Kobayashi, Matsushige, & Yamada, 2005; Gross et al., 2012). Therefore, the use of the dynamic mode is preferred for soft samples such as biological materials, including food samples (Arzate-Vázquez et al., 2012).

On the other hand, phase-contrast images are considered a secondary mode of AFM, where the offset of the cantilever oscillation in relation to the signal sent to the piezo controller is used as the basis for obtaining images (Türe, Blomfeldt, Gällstedt, & Hedenqvist, 2012). These phase images can be obtained due to changes in material properties such as viscoelasticity, adhesion, and friction, all of which may cause the phase offset. In addition, these images can be generated simultaneously as the microscope is operating in any of the cantilever vibration modes, such as tapping mode. Variations in phase offset also show modifications in the sample surface, particularly in its mechanical properties. The system's feedback loop operates, as usual, considering the variations in cantilever deflections or vibration amplitudes to measure the topography of the samples. The phase offset is monitored at the same time as the topographic image is captured so that topography images and material properties are obtained simultaneously. This alternate and useful imaging technique has several applications, such as determining contaminants, differentiating regions of high or low adhesion and even surface hardness, mapping various elements in the composite materials, as well as electrical and magnetic properties. Overall, the phase imaging mode is useful for characterizing the distribution and differences in the composition of the surface of different materials (Shi et al., 2019). Despite the benefits that phase imaging offers for the qualitative characterization of material composition, it has been scarcely used for biological materials because they are comprised of

light elements that do not show significant differences in their molecular weights.

The force spectroscopy technique measures interaction force and nanomechanical properties of samples by generating force curves (Geng, Chyasnavichyus, Meyers, & Wu, 2019; Rief, Oesterhelt, Heymann, & Gaub, 1997). In this operation mode, the cantilever deflection (force signal) is recorded as a function of its vertical displacement (distance signal) as the tip approaches towards and retracts from the sample to obtain a force-distance curve. A force curve diagram describes the events that occurred during the tip-cantilever approach to a rough surface and the different mechanical properties that can be estimated, such as Young's modulus, plasticity index, adhesion and peak force, dissipation work, and deformation distance (Fig. 9.2). Moreover, spatial resolution can be achieved by generating a force-volume image by acquiring force-distance curves over a grid of points on the sample surface. For example, it can be used for measuring the strength of cell adhesion at the single-molecule level in biological materials, including specific and nonspecific forces

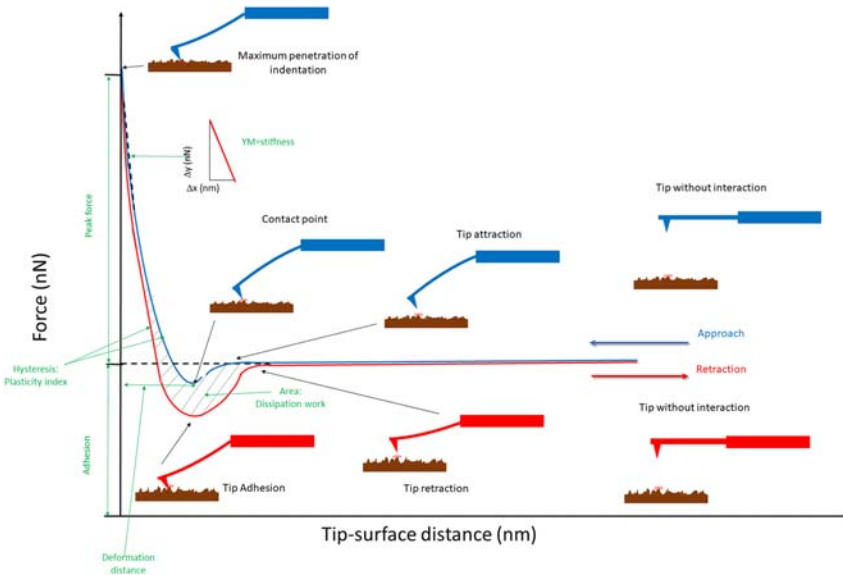


**Figure 9.2** Force curve (tip-surface distance vs force) during AFM nanoindentation. Approach (blue) and retraction (red) curves. Figure shows the cantilever approaching and retracting process. Green represents certain nanomechanical properties that can be obtained from a force curve. *From J. J. Chanona-Pérez. (2020). Force curve during AFM nanoindentation. Instituto Politecnico Nacional.*

involved between cell surfaces and different nanomechanical properties (Gaboriaud & Dufrière, 2007).

It is important to understand that the forces generated during the interaction between the tip and the sample surface act as a function of the separation distance between them. In order to describe these interactions, the Lennard-Jones potential model can be used (Jalili & Laxminarayana, 2004) which represents a generic model of tip–sample interaction. This model, which depicts the van der Waals force versus sample–point distance axes, perceives an attraction force as the tip approaches, which in turn changes to repulsion as the tip continues its movement toward the surface (Fig. 9.3).

The force between the AFM tip and the sample surface is always repulsive and approximately  $10^{-9}$  to  $10^{-6}$  N. Moreover, the curve's slope is very steep in the repulsive region, while the cantilever deflection ( $\Delta z$ ) is proportional to the force ( $F$ ) applied on the tip ( $F = -k\Delta z$ , where  $k$  is the spring constant of the cantilever). In noncontact mode, the tip–sample force is attractive as the cantilever oscillates (amplitude  $< 10$  nm, resonant

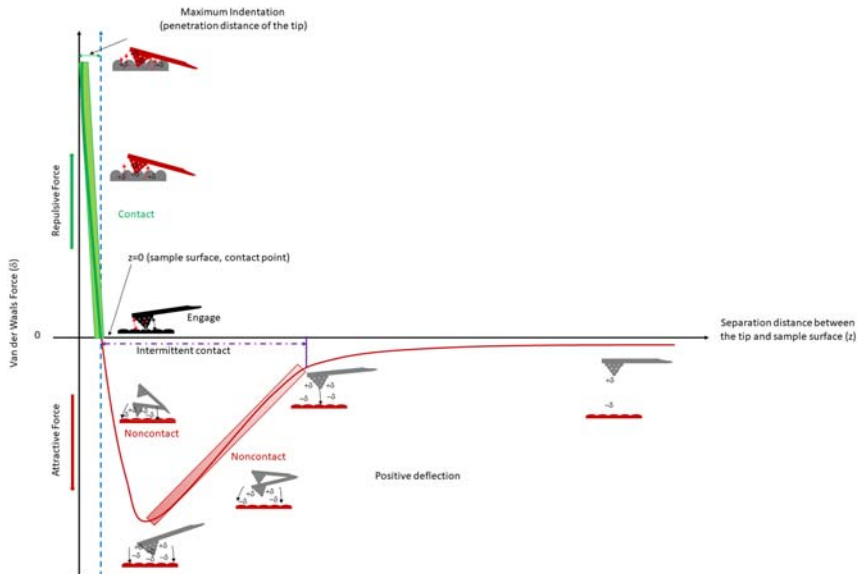


**Figure 9.3** Diagram of the van der Waals forces ( $\delta$ ) versus tip-to-sample distance as the tip approaches and makes an indentation on the sample surface as well as the illustrative position of cantilever deflections. From J. J. Chanona-Pérez. (2020). *Diagram of the van der Waals forces vs tip-to-sample distance. Instituto Politecnico Nacional.*

frequency of 100–400 kHz) above the sample (1–10 nm), with the tip–sample force in this mode around  $10^{-12}$  N. Furthermore, in intermittent mode, the cantilever oscillates (amplitude  $>20$  nm) close to its resonance frequency and the oscillation amplitude is monitored (Binnig et al., 1986). The tip experiences both attractive and repulsive forces, while the feedback control system ensures that the oscillation amplitude is constant, thereby guaranteeing a constant tip–sample interaction force (San Paulo & García, 2001; Zhong & Wang, 2019).

Another relatively new operation mode is PeakForce Tapping (PFT), a patented and enhanced operating mode introduced around 10 years ago. This technique uses force as a feedback variable to reduce peak–sample interaction forces while maintaining the scanning speeds used in tapping mode (Lam & Ikeda, 2017). PFT and tapping mode have similar operating principles as both avoid lateral forces and intermittent contact with the sample. However, PFT works differently than a nonresonance mode, as it is an oscillating technique with the advantages of contact and tapping imaging modes, mainly in direct force control and prevention of lateral force damage. The difference between the conventional force curve and the force–volume imaging is that the  $z$  position is modulated by a sine wave, which avoids unwanted resonances at the tipping points while the topography trace is improved (Fig. 9.4A and B).

In addition, it is possible to obtain continuous force curves at frequencies ranging between 1 and 10 kHz, which also allows image speeds in the tapping mode range which is lower than the standard tapping mode frequency in fluids. Furthermore, the parameter that remains continuous in the feedback cycle in the PFT is the maximum peak load force, but not the amplitude of the cantilever oscillations. PFT enables the researcher to precisely control probe–sample interaction enabling the lowest available imaging forces. This superior force control results in the most consistent, highest resolution AFM imaging (Fig. 9.4B) for the widest range of sample types, from the softest biological samples to very hard materials (Obeid & Guyomarc’h, 2020). It is an ideal mode for materials research and biological samples due to its unprecedented low imaging forces and simple operation with no cantilever tuning necessary. A comparative diagram between the operation principles of traditional tapping versus PFT modes is shown in Fig. 9.4. Moreover, PFT mode can provide nanomechanical property maps of surface samples using PeakForce Quantitative Nanomechanics (QNM) option, where image and force curves are acquired quickly and simultaneously during sample scanning (Fig. 9.4B).

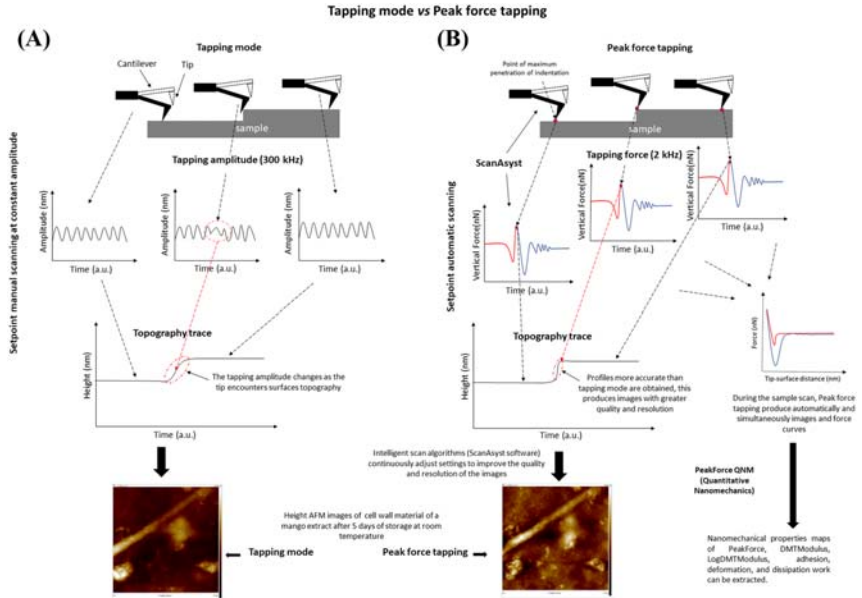


**Figure 9.4** Comparative diagram between the operation principles of tapping (A) versus PeakForce Tapping (B) modes. In red, approach curves, and in blue, retract curves. AFM, atomic force microscopy. From J. J. Chanona-Pérez. (2020). Comparative diagram between the operation principles of tapping vs PeakForce Tapping modes. Instituto Politecnico Nacional.

ScanAsyst is patented software that optimizes the capture of AFM imaging, and instinctively adjusts scanning parameters such as setpoints, feedback gains, and scanning speed. The algorithm continuously inspects the image quality status to set the appropriate parameter settings. This makes it straightforward to obtain images by simply selecting the region and scanning area in either air or fluid operation and using the same mechanism as PFT to adjust all of the image’s critical parameters automatically. As peak force feedback directly controls the interaction force, there is no difference in the peak force of the soft or hard areas of the sample (Dawidowicz, Nowakowski, Typek, & Dybowski, 2019; Syahida, Ismail-Fitry, Ainun, & Hanani, 2020). The direct interaction force control allows delivering an evenly optimized feedback loop for all areas of the heterogeneous sample. A real-time feedback loop continuously inspects and adjusts the gain to keep the data within a predefined noise level. This contrasts with manual gain adjustment, where a gain is commonly used for a full image in conventional tapping mode. ScanAsyst improves the gain



according to the current state of the sample in different sections. The program also improves the setpoint to the minimal force needed to scan the sample (surface), controls the scanning speed, and, if necessary, automatically reduces the z limit. As a result, high-quality images (Fig. 9.4B) are displayed without the need to adjust external or user image parameters, reducing acquisition time and standardizing AFM images.

A reliable method widely used for biomechanical analysis is force-volume imaging, which links force indentation and surface topography by simultaneously collecting a set of information containing topographic data and force-distance curves (Gaboriaud, Parcha, Gee, Holden, & Strugnell, 2008). The method is known as force-volume, where each force curve is measured and selected manually in a single or several positions in the scanning zone (x, y). Moreover, the force and distance curves represent an additional axis or another dimension from different local nanomechanical properties that can be manually calculated by force curve analysis (Fig. 9.5A). Therefore, the force-volume data set resembles a stack of horizontal cuts, each representing the force data matrix at a certain height. A single force-volume image represents one of these cuts, showing the distribution (x, y) of the selected force data over the scanning zone at that height.

In the time it takes for the AFM to develop, certain microscope models can measure several force curves as a matrix of points. This indentation method is known as point and shoot, whereby an abundant collection of force curves can be obtained semiautomatically as a matrix or a force data canvas and allows the acquisition of several high-precision force measurements that can be accurately targeted (Gavara, 2016). These data can be represented in the form of a histogram of nanomechanical properties, for example, % frequency versus Young's modulus (Fig. 9.5B). An example of nanoindentation with the point and shoot method is illustrated in Fig. 9.6, where a V-shape cantilever is indenting apple tissue surface, and a force curve is shown.

An optimized mode called PeakForce QNM that works with PFT has a similar operation principle to force-volume. Nevertheless, the production of topography images and several nanomechanical properties is simultaneously and automatically estimated. This technique can also determine how the molecules or cells respond to mechanical stimuli or external forces. This would mean that topography images and individual force curves at any local points, region of interest, or whole maps could be obtained (Fig. 9.5C). QNM technology facilitates the production of

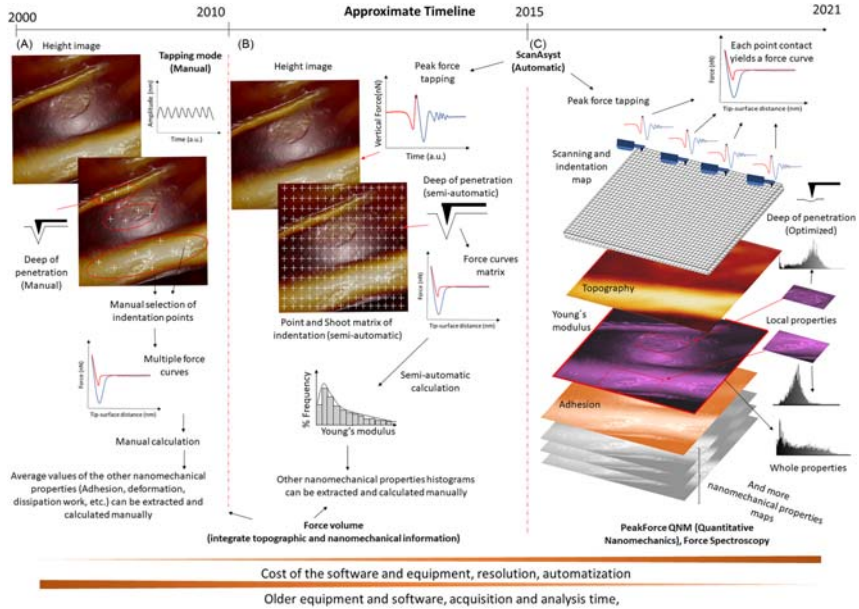


**Figure 9.5** Descriptive diagram on the evolution of the time for nanomechanical properties evaluation using different AFM operation modes, (A) tapping mode and manual indentation, (B) PeakForce Tapping and point and shoot method, (C) PeakForce Quantitative Nanomechanics mode. *From J. J. Chanona-Pérez. (2020). Descriptive diagram on the evolution of the time for nanomechanical properties evaluation using different AFM operation modes. Instituto Politecnico Nacional.*

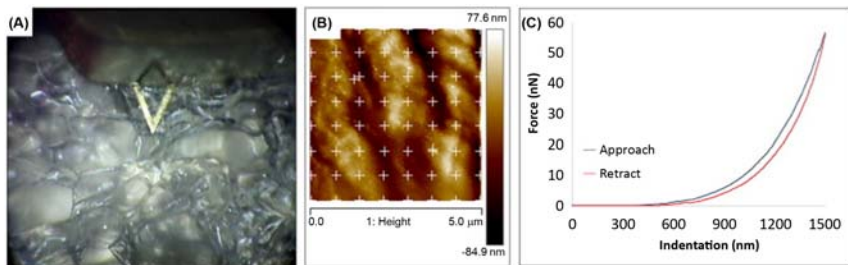


**Figure 9.6** Example of nanoindentation: (A) selected image of the cantilever during the nanoindentation of apple tissue, (B) height image of tissue in the region of indentation. White crosses represent the matrix of points of the mechanical measurements ( $8 \times 8$ ) in an area of  $5 \times 5 \mu\text{m}$ , (C) Typical force curve obtained from the nanoindentation points. *From Cárdenas-Pérez, S., Chanona-Pérez, J., Méndez-Méndez, J., Calderón-Domínguez, G., López-Santiago, R., & Arzate-Vázquez, I. (2016). Nanoindentation study on apple tissue and isolated cells by atomic force microscopy image and fractal analysis. Innovative Food Science & Emerging Technologies, 34, 234–242 Copyright 2016 Elsevier.*

nanomechanical maps that include modulus, adhesion, dissipation, and deformation, among others, while simultaneously imaging sample topography at nanometric scale resolution is also collected. As PFT and ScanAsyst can directly control the peak normal force and minimize the lateral force on the probe, it is nondestructive to both the tip and sample as the penetration is automatically controlled in contrast with the aforementioned modes of the indentation. The force–distance data is therefore analyzed directly, meaning that there is no ambiguity regarding the source of image contrast as often occurs with other techniques. The quantitative data produced can help identify components and their mixing at interfaces, as well as map mechanical properties at previously unattainable resolutions (Ortega-Toro, Contreras, Talens, & Chiralt, 2015). Furthermore, PeakForce QNM provides the highest and quickest resolution mapping of nanomechanical properties, the most quantitative nanomechanical mapping, as well as the widest operating range for samples from extremely soft materials ( $\sim 1$  kPa) to hard metals (100 GPa). Overall, new AFM technology for producing nanomechanical properties in food science improves resolution, automatization, acquisition speed, and analysis time. However, investment costs in software and equipment increase over time. However, due to the simplicity of atomic force microscopes, a lot of old equipment still operates in various research laboratories, and it is possible to use the previous modes of operation to obtain nanomechanical properties in biological samples with similar results to those obtained with current systems.

### 9.3 Proteins stretching

Multifrequency AFM is a series of techniques in which the cantilever is excited by (at least) two signals at two different frequencies that are linked as a result of nonlinear sample–point interaction to evaluate a sample's nanomechanical properties. Another technique that can perform nanoscratching and undertake tests to examine adhesion and durability is known as nanoscratch–mode, a flexible tool for analyzing both thin films and bulk materials. The nanoscratch technique provides the potential to investigate deformation and fracture modes that are not possible with standard indentation techniques. A nanoscratch test is performed by applying a normal load in a controlled manner while measuring the required force by moving the tip laterally across the sample. In choosing the appropriate normal load profile and lateral displacement pattern, many different types

of tests can be performed (Chichti, George, Delemen, Radjai, & Lullien-Pellerin, 2013).

Another application that can obtain nanomechanical properties in AFM through the mechanical manipulation of immobilized single polymer chains on solid substrates is the stretching of molecules tied between the tip of the cantilever and the sample as they are extended and stretched between the tip of the cantilever and the surface of the substrate. This method has become important in the field of biology due to the study of phenomena such as protein unfolding, which is complicated or impossible to carry out with other techniques. Specifically, immobilization of the protein chain on a solid surface allows a single protein molecule to be pulled or pushed in specific directions. When pulled, the internal structure of the protein molecule is mechanically opened, and when pushed, it is deformed into a compressed form until it is flattened (Hugel & Seitz, 2001; Scholl, Li, Josephs, Apostolidou, & Marszalek, 2019).

The tip contacts the surface, the substrate molecules interact with the tip (approach), and the overhang is then retracted. As the cantilever moves away from the surface, the protein unfolds until it reaches a force that partially breaks the boundaries of the tip and the proteins, or the chains attached to the protein may fail with the pulling forces. Finally, the tip is released and returns to its initial position. The deflection reflects the forces between the tip and the surface. If a single molecule remains between the tip and the surface, then the cantilever deflection gives a measure of the force applied to the molecule. The adhesive interaction between the tip and the molecule usually occurs in the repulsive contact part of the force curve, but the valuable characteristics for molecular stretching are found in the retraction curve (Ikai, Afrin, & Sekiguchi, 2007). A detailed explanation of the stretching process of a protein can be found in Fig. 9.7, where the approach phase can be seen (points 1–3, blue line), as well as the cantilever deviation, which is set to zero because the tip has not yet reached the sample (point 1). After the point-to-sample contact (point 2), the cantilever is bent upwards due to a repulsive force that increases linearly with the approach (point 3). The retraction phase of the tip surface (point 4–5, red line) initially leads to a relaxation of the cantilever deflection until the repulsive force drops to zero. In the subsequent retraction, the junction between the tip and the sample on the surface exerts a force that bends the overhang downwards (point 4). The downward bending of the retracting cantilever continues to increase until the tip–sample is finally separated when a certain critical force breaks or unbinds.

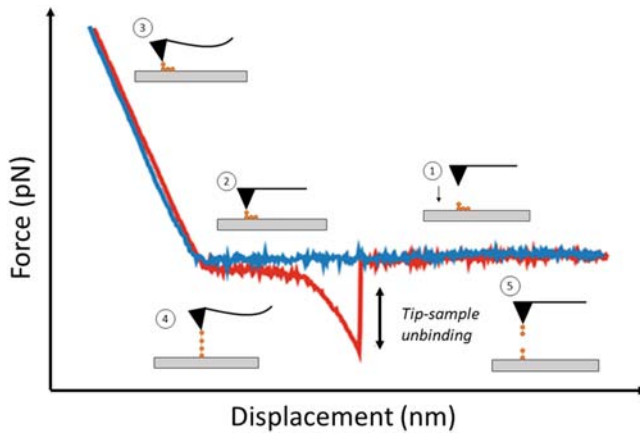


**Figure 9.7** Simplified scheme of force-distance curves during stretching process of a protein. From J. J. Chanona-Pérez. (2020). *scheme of force-distance curves during stretching process of a protein. Instituto Politecnico Nacional.*

Tip-sample unbinding is indicated by a sharp spike in the retraction curve that reflects an abrupt drop of the cantilever to its position of rest (point 5).

According to several studies, the information provided by this technique is the size of the protein's polymeric chains, the mechanical rigidity of the folded structure of a protein molecule, the force needed to break certain molecular bonds, and whether a mechanical structural element is deployed which results in a sudden increase in the polymer's length and a drop in the force (Kurland, Drira, & Yadavalli, 2012; Marszalek, Li, Oberhauser, & Fernandez, 2002; Mateu, 2012).

## 9.4 Suppliers, sample preparation, fixation, and tip selection

At the beginning of AFM, few suppliers were selling the specialized microscopes, although companies manufacturing the required equipment and a subsequent market have emerged. All the above makes the AMF a multifaceted characterization microscopy technique, which has led several companies to develop analytical instruments to create different patented techniques, algorithms, and operation modes. A significant quantity of published scientific articles involving AFM have been published, and more than 500 patents have been issued related to various types of microscopy, such as scanning probe microscopes (SPM) and atomic force

microscopes. The market for AFM was valued at the US \$441 million in 2019 and is projected to increase to the US \$586 million by 2024. Moreover, several governments around the world have provided substantial backing to advance research and development in nanotechnology and nanoscience. There are currently 14 companies that distribute atomic force microscopes, mainly concentrated in the USA and Germany. In alphabetic order, the companies that market atomic force microscopes are Bruker (USA), Hitachi (Japan), Horiba (Japan), NanoMagnetics Instruments (UK), Nanonics Imaging (Israel), Nanosurf (Switzerland), NT-MDT (Russia), Oxford Instruments (UK), Park Systems (South Korea), WITec (Germany). When acquiring atomic force microscopes, it is very important to evaluate all the available options in the market and the applications for selecting the most suitable equipment for industrial and research requirements. The following link shows the major and local suppliers of atomic force microscopes: [https://www.photonics.com/Buyers\\_Guide/Atomic\\_Force\\_Microscopes/ca45525](https://www.photonics.com/Buyers_Guide/Atomic_Force_Microscopes/ca45525).

Overall, the different configurations and operating modes of the atomic force microscopes depend on the manufacturer. However, it can be said that AFM has a generic way of working, but sample preparation, fixation, and tip selection are important issues for successfully purchasing nanomechanical equipment. Various recommendations are highlighted below, and it is suggested that new users consult the procedures provided by each manufacturer to operate the microscopes successfully. Some examples of microindenter and AFM systems from our facilities are shown in Fig. 9.8. In the case of the microindenter tester (Fig. 9.8A), the tip size and load force can evaluate a sample's mechanical properties at the microscale, while with typical AFM systems (Fig. 9.8B and C), images in tapping mode and manual indentation assays can be produced. In the case of the BioAFM, topographic and fluorescence images, PFT, point and shoot, and QNM mode are available (Fig. 9.8D).

While sample preparation for AFM analysis is relatively simple, it is still one of the most important steps for correctly carrying out AFM. In fact, it is a key factor in obtaining high-quality, reproducible, and safe AFM results. The most important aspect is keeping the sample surface clean in atmospheric or empty environments and the sample surface and solution clean in liquid environments (Morris et al., 1999). Depending on the condition of the sample, there may be different strategies for sample preparation, for example:

For solid samples, AFM can be directly applied to visualize the samples in an atmospheric, vacuum, or cryogenic environments. In order to observe



**Figure 9.8** Examples of instruments for obtaining micro and nanomechanical properties used in food science, (A) microindenter (TTX-NHT, CSM Instruments, Switzerland), with a diamond Berkovich tip (pyramidal geometric), (B) basic atomic force microscope (Dilnova, Veeco, USA), (C) classic model of an atomic force microscope (Multimode, Veeco, USA), (D) BioAFM (Bioscope Catalyst, Bruker, USA).

the samples in a liquid environment, the appropriate liquid should be added to the sample before the AFM operation (the samples should not be solubilized in the liquid). For samples that are deposited on liquid substrates, the AFM can be directly applied to view the samples in liquid environments. To observe these samples in atmosphere, vacuum, or cryogenic environments, the liquid is removed before the AFM operation. During this process, a change in the shape of the samples may occur, so it is crucial to ensure that no change in shape is evident. For samples that are dispersed in solution, the solution is poured onto flat substrates (freshly cut mica, glass, silica, etc.) for AFM operation in the atmosphere, vacuum, or cryogenic environments. Moreover, if the samples are required to undergo analysis in a liquid environment, the samples must be deposited on flat substrates by electrostatic attraction between the charges on the sample surface and the charges on the substrate (Tamayo, Humphris, Owen, & Miles, 2001).

For biological samples, mica, glass, and silica are excellent substrates, of which mica is the most frequently used. Generally, tapes or syringe needles are used to peel the clean mica surface to obtain freshly cleaved, flat, and nonconductive mica flakes as substrates. The mica surface is negatively charged, but it can be modified to make the surface positive. If the water layer on the mica surface is too thick under ambient conditions, the capillary force between the tip and the water layer and the viscous force between the tip and the sample will reduce the resolution of the AFM. Therefore, it is important to remove the excess moisture (retaining appropriate moisture to maintain the physiological structure of biological samples) on the mica and sample surfaces as much as possible prior to AFM imaging. However, live-cell or bacteria immobilization on substrates is still challenging when undertaking AFM. Until now, some methods have been developed and can be classified into physical and chemical methods. Physical methods include substrate surface physical modification by adhesive proteins such as collagens and novel soft substrate development such as agar gel surface. Chemical methods include substrate surface chemical modification by crosslinking agents such as glutaraldehyde and polycations (El Kirat, Burton, Dupres, & Dufrene, 2005).

In order to obtain images and nanomechanical properties in liquid media, fluid cells are required of different types depending on the supplier of the microscope. The main parts of a fluid cell are shown in Fig. 9.9, where a cantilever holder is provided with an O-ring to seal the cell and contain the liquids as indicated (Fig. 9.9A). This system maintains the samples in similar conditions to their original biological environment, meaning that cell turgidity, osmotic pressure, and temperature can be controlled during nanoindentation assays, as shown in Fig. 9.9B.

Nanomechanical-AFM techniques for cells and plant tissues have been of particular interest as they can provide a plethora of information about the plant cells when they are subjected to natural or external modifications. However, there are still many concerns regarding sample preparation and fixation. Table 9.1 provides a summary of studies that deal with nanomechanics in plants and their respective fixation methods as well as the equipment used.

A diagrammatic example of fixation of isolated cell and plant tissue is shown in Fig. 9.10, where single cells are attached under a glass slide functionalized with histological gelatin for its nanoindentation in studies of cell mechanics (Fig. 9.10A and B), while Fig. 9.10C and D show a strategy for the fixation of a small sample of plant tissue.



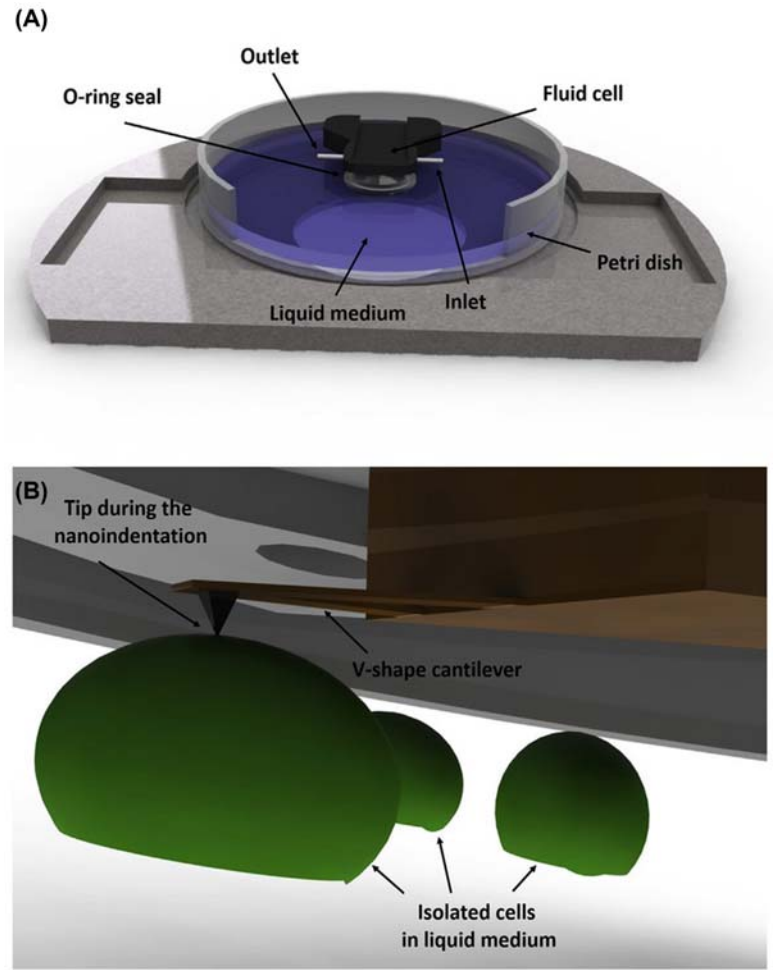


**Figure 9.9** (A) Liquid cell with cantilever holder and O-ring seal, (B) cell nanoindentation with a tip inside a fluid cell. From Cárdenas-Pérez, S., Chanona-Pérez, J. J., Méndez-Méndez, J. V., Arzate-Vázquez, I., Hernández-Varela, J. D., & Vera, N. G. (2019). *Recent advances in AFM for assessing the nanomechanical properties of food materials. Trends in Food Science & Technology*, 87, 59–72; Copyright 2019 Elsevier.

AFM has been proven to play an important role in understanding complex structure modifications in the tissue cells of plant crops due to polymeric rearrangement to cope with environmental factors or to natural morphogenesis processes. This type of analysis has faced issues related to a proper sample fixation, but various publications have proposed different techniques to overcome this obstacle. It is important to note that studying mechanical properties

**Table 9.1** Sample fixation techniques for nanoindentation in plant tissues.

Aim of the analysis	Sample	Equipment	Sample preparation and fixation	Results	References
Identify the response to UV stress in grapevine	Grapevine cells	Multimode AFM (Nanoscope IIIa; Veeco Co., CA)	Coverslips treated with 0.1% (w/v) poly-L-lysine (Sigma, USA) to immobilize cells on the glass surface	Cell walls strengthened by UV stress	Lesniewska et al. (2004)
Nanoindentation of crop stalks cell walls	Cotton stalk, soybean stalk, cassava stalk, rice straw, and wheat straw	XE-100, PSIA Corp., Korea	Air-dried stalks were cut into small slices and then embedded in epoxy resin. They were then mounted onto an ultramicrotome and cross-sectioned. The smoothed specimens were conditioned at 21°C and 60% RH in the nanoindentation test room	The elastic modulus of wheat straw was found to be 20.8 GPa, which was higher than that of the other four crops	Wu et al. (2010)
Nanoindentation in fruit cells and tissue	Apple tissue and cells	Bruker, Bioscope Catalyst ScanAsyst, USA	Tissue was cut by a shaving blade and held between two slides (the upper glass slide has a small window). For the isolated cells, a glass slide was covered with a thin film of histological fixator gelatin solution 40%. A drop of the single-cellsolution was deposited on the glass. This procedure improved the adhesion and firmly immobilized the isolated cells	The immobilization methods for apple tissue and isolated cells worked successfully. The Young modulus obtained for the cells in tissue was greater than that for single isolated cells	Cárdenas-Pérez et al. (2016)

*(Continued)*

**Table 9.1** (Continued)

Aim of the analysis	Sample	Equipment	Sample preparation and fixation	Results	References
Overcoming the main issues in the measurement of mechanical properties of plant tissues	Flower bud	N/A	The closed flower bud is placed on double-sided tape (biocompatible glue can also be used). Then, quickly add a drop of water and cover the sample (this avoids dehydration and reduces adhesion of the tip to the sample)	AFM can be used to study the cell wall softening, as well as the change between organs, tissues, or developmental stages	<a href="#">Bovio et al. (2019)</a>

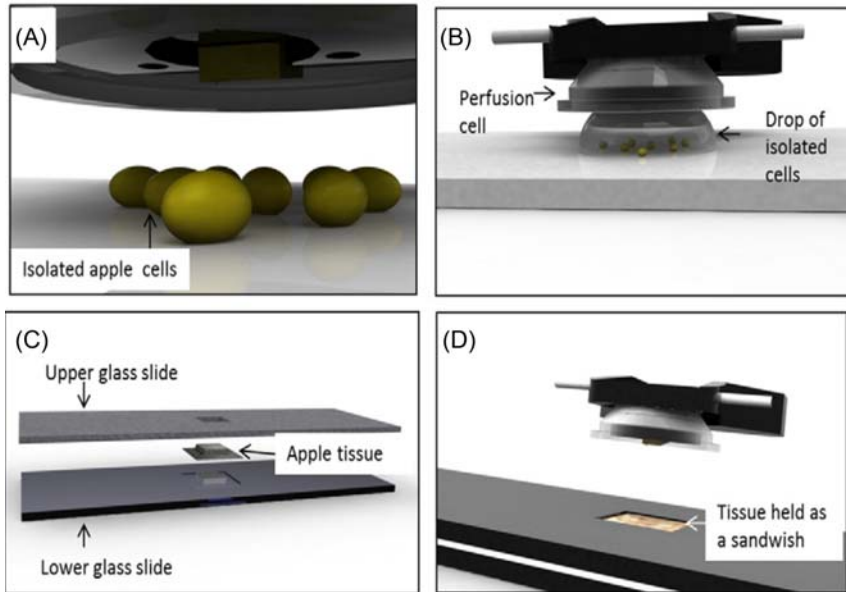


**Figure 9.10** Schematic diagram of the fixation of single cells and apple tissue: (A) isolated apple cells fixed with gelatin to the slide, (B) perfusion cell above the drop of isolated cells, (C) the two glass slides that hold the apple tissue, (D) perfusion cell above the tissue held between two slides as a sandwich piece. From Cárdenas-Pérez, S., Chanona-Pérez, J., Méndez-Méndez, J., Calderón-Domínguez, G., López-Santiago, R., & Arzate-Vázquez, I. (2016). Nanoindentation study on apple tissue and isolated cells by atomic force microscopy image and fractal analysis. *Innovative Food Science & Emerging Technologies*, 34, 234–242; Copyright 2016 Elsevier.

in plant cells and their alterations due to different modifications can provide the solution to many food, agricultural, and industrial problems that are related to the mechanical properties of the plant cell walls. Plant nanomechanics provides a greater understanding of the contribution of individual compounds to the overall mechanical properties of the cell wall, which is important for optimizing cell wall composition for more resistant crops.

## 9.5 Probe selection

AFM probes are made of silicon and silicon nitride as well as a reflective layer normally made of gold or antimony bonded by an adhesive using photolithographic micromachining techniques. Tips may range in size from 2 nm to tens of microns in height, with a radius of curvature as small as 2 nm. Cantilevers are usually 100–200  $\mu\text{m}$  long and 0.5–2  $\mu\text{m}$  thick,

while their spring constants range from 0.01 to hundreds of nN per nm. A wide range of AFM tips with different shapes, spring constants, and resonant frequencies are now commercially available. For atomic resolution, the front atom of the tip should ideally be the only atom that interacts strongly with the sample. In order to reduce the forces caused by the shaft of the tip, the tip radius should be as small as possible. Furthermore, it has recently been recognized that the coordination of the front atom is of critical importance, as well as the sharpness of a tip. The tip and sample can be viewed as two giant molecules (Calabri, Pugno, Menozzi, & Valeri, 2008).

Therefore, choosing an appropriate tip performs a crucial role, as it will play an important role in successfully producing an image of the target sample and obtaining high-resolution results or an exact surface topography. Sample particularity, AFM test mode, and test medium will all intervene in the tip selection. In addition, soft cantilevers are generally good for contact mode because they deflect without deforming the surface of the sample. Moreover, stiff cantilevers are good for dynamic modes because they have high resonant frequencies to provide optimal results. During intermittent contact mode imaging, the tip will easily stick onto the sample if its constant force is not large enough. Generally, the shapes of the cantilever (rectangle or triangle) do not directly influence the images. The tip geometry is also an important factor because it determines the mathematical model (see Fig. 9.11A–C) that will be applied to adjust and interpret the indentation curve. The tips with spherical geometry follow Hertz's mathematical model, while those with conical geometry follow Sneddon's model. Based on Hertz's model, Bilodeau built a model for the case of a pyramidal tip with a square silicon nitride base. The Hertz model describes the indentation of an infinitely hard, spherical indenter (the probe tip) on an elastic cylinder (the sample). This model is appropriate when the indentation depth is significantly less than the probe's radius of curvature. This theory suggests an elastic contact of two spherical bodies and requires several assumptions for its validity: frictionless and nonconforming contact, small contact area relative to overall body dimensions, and small deformations on contact. One of the most important approaches is the absence of adhesion or surface forces. When the depth of the indentation is close to or exceeds the tip's radius of curvature, the Sneddon model of contact between an infinitely hard conical indenter and an elastic cylinder is more appropriate and commonly used for biological samples. In a conventional nanoindentation test (not using AFM), forces of more than 1 mN are common, leading to large deformations in the order of 1  $\mu\text{m}$  (Cárdenas-Pérez et al., 2019). Different

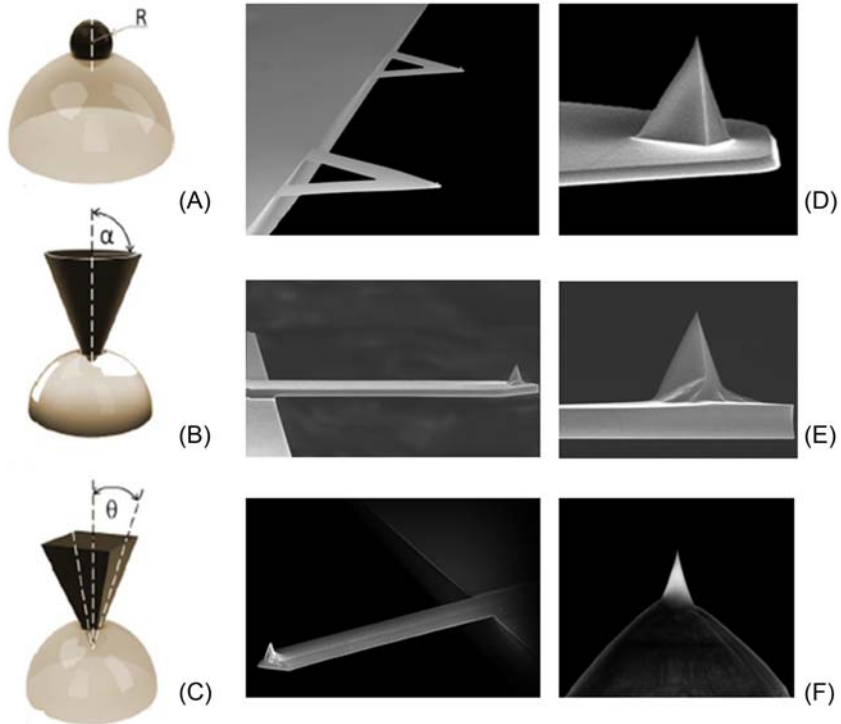


**Figure 9.11** Different mathematical models are used in atomic force microscopy (AFM) nanoindentation according to the indenter geometry: (A) Hertz model, (B) Sneddon model, and (C) model for a pyramidal indenter. Example of commercial tips and cantilevers for AFM (Bruker brand): (D) SNL-10, (E) RTESPA-300, and (F) AD-40-AS. From Cárdenas-Pérez, S., Chanona-Pérez, J. J., Méndez-Méndez, J. V., Arzate-Vázquez, I., Hernández-Varela, J. D., & Vera, N. G. (2019). Recent advances in AFM for assessing the nanomechanical properties of food materials. *Trends in Food Science & Technology*, 87, 59–72; Copyright 2019 Elsevier.

tip suppliers provide statistics and probing recommendations, such as cantilever force constants, which allow the operator to select the cantilever according to the character of the sample (Fig. 9.11D–F).

## 9.6 Approaches in food science research with atomic force microscopy

The application of AFM in food science research has been varied due to its advantages for studying the structure and nanomechanical properties of food materials and related processes. Overall, it is possible to consider a

classification according to the different needs or requirements that exist in food science using AFM. Table 9.2 provides a brief description and some references associated with the highlighted applications.

Considering these approaches, over the past few years, the acquisition of nanomechanical properties through AFM has been of particular interest in food science research. Thus, recent advances in this area are summarized in the following section.

## 9.7 Recent research on nanomechanical properties of food materials

AFM has been successfully applied to the study of a broad range of food samples from the smallest biomolecules (proteins, carbohydrates, lipids, etc.), microorganisms (virus, bacteria, yeast), animal and plant cells, and up to food packaging materials. In this section, the main focus is on recent progress in applying AFM in order to obtain mechanical properties in different food samples. The early studies that introduced the development of food material research were conducted on plants, particularly the outer tissues of *Arabidopsis* and onion. For example, Milani et al. (2011) designed an AFM approach to investigate the elastic modulus of the outer cell wall in living apical meristems in *Arabidopsis*. Three levels of complexity were identified on the meristem surface, with significant heterogeneity in stiffness at the regional, cellular, and even subcellular levels. It was also established that the outer cell wall was much stiffer at the tip of the meristem (covering the stem cell pool) than at the meristem flanks. Therefore, the results showed the existence of a multiscale spatialization of the mechanical properties of the meristem surface. In another study, Peaucelle (2014) measured the apparent Young's modulus of cell walls at subcellular resolutions across regions of up to  $100 \times 100 \mu\text{m}$  in floral meristems, hypocotyls, and roots. Beuzamy et al. (2015) developed a method applied to epidermal onion shells that combines topography quantification, nanoindentation force measurements, and interpretation using a mechanical model for point loading of thin elastic layers, using AFM to estimate cell wall elastic properties and turgor pressure from a single force-depth curve. Current studies of interest include Seifert et al. (2020), who used dynamic AFM methods to visualize the overall linear viscoelastic behavior and cell relaxation times of multicellular organisms in vivo with nanoscale resolution. This work obtained images of cells on the surface of living *Arabidopsis* hypocotyls to obtain topographic maps of their

**Table 9.2** Classification of approaches in food science research with atomic force microscopy.

Applications	Description	References
Qualitative imaging for structural analysis of food biomolecules	To understand the structures and morphology of food biomolecules, it will be useful to analyze their function.	Baselt et al. (1993), Gunning et al. (2003), Iwasaki et al. (2005), Doherty et al. (2011)
Molecular interaction: interaction between food biomolecules and other substances	The interaction between food biomolecules and other substances or cell growth is involved in many biological processes, such as the formation of in vivo food biomolecules and the treatment of in vitro food biomolecules.	Gad, Itoh, and Ikai (1997), Tay et al. (2006), Zhang et al. (2016)
Topographic characterization of food biomaterials	AFM can be applied to characterize the surface topography of food biomaterials. In addition, surface roughness and particle size distribution could be analyzed for biomaterial films.	Wang et al. (2003), Yang et al. (2005), Rousseau (2006), Oymaci and Altinkaya (2016), Shi et al. (2019)
Fine or quantitative structural analysis: effects of processing and storage of food components	Analyzing the effects of different processing and preservation conditions of food ingredients is important for developing and applying new technologies.	Yang et al. (2005), Iwasaki et al. (2005), Liu and Zhong (2013), Pieczywek et al. (2020)
Food molecular manipulation	Many food macromolecules have a tangled structure. Manipulation of molecules offers us an	Nakao et al. (2002), Yang, An, and Li (2006), Wang et al. (2020)

(Continued)



**Table 9.2** (Continued)

Applications	Description	References
Nanomechanical properties	<p>opportunity to observe the reactions between food macromolecules directly.</p> <p>A probe can be used as an indenter to measure or predict the mechanical properties of food materials at the nanoscale for a better understanding of their behavior.</p>	<p>Cárdenas-Pérez et al. (2019), Nicolás-Álvarez, Andraca-Adame, and Chanona-Pérez (2019), Rongkaumpan et al. (2019), Pieczywek et al. (2020), Rojas-Candelas et al. (2021)</p>

storage and loss, as well as relaxation times of their cell walls. In addition, it was demonstrated that the cell walls, despite their complex molecular composition, show a continuity of simple and linear viscoelastic behavior across the scales following the standard linear solid model almost perfectly with characteristic nanoscale patterns of relaxation times, elasticity, and viscosity, whose values correlate linearly with the macroscopic growth rate. Therefore, the time scales tested by AFM dynamic experiments (milliseconds) are key to understanding macroscopic scale dynamics (e.g., growth) as predicted by the physics of polymer dynamics.

As for food materials, such as fruits and vegetables, there are also studies on the analysis of their nanomechanical properties as well as their textures. One such study was conducted by [Chichti et al. \(2015\)](#), which aimed to use AFM to study nanomechanical properties of starch and gluten powders. The results showed that gluten had low mechanical properties, similar to soft materials such as talc, while starch had higher hardness and shear strength (close to calcite) compared to gluten. This work proved that AFM could be useful for analyzing and comparing the nanomechanical properties of food samples. In another study, [Zdunek et al. \(2016\)](#) determined the mechanical properties of pear cell walls. The study found that Young's modulus of the pear's primary cell walls decreases linearly

during ripening on the tree before harvest and increases during storage after harvest, thereby showing little evidence of a direct relationship between Young's modulus of the primary cell walls and fruit firmness. Furthermore, [Cárdenas-Pérez et al. \(2017\)](#) studied the microstructural and physicochemical changes during the ripening process of apples and established a link with the nanomechanical properties evaluated on the surface of the tissues. A mathematical model was proposed to predict the nanomechanical properties using only the firmness and texture parameters of the fruit image. The resulting model for evaluating Young's module correlates well with the evaluated parameters. Therefore, it is suggested that the nanomechanical properties could be useful for guiding the design and creation of biological structures by synthetic biology. More recently, [Rongkaumpan et al. \(2019\)](#) studied the molecular mechanism that supports the differences in texture between banana and mango. The properties of the fruit's cell surface and the potential contribution of the cells and cell wall components to oral processing and texture perception were analyzed. Smooth surfaces were detected by AFM, indicating traces of medium lamellae in banana cells, while mango cells had cleaner and smoother surfaces, suggesting an absence of medium lamellae and more advanced cell wall removal. Bulk rheology experiments showed that both fruits had similar apparent viscosity. The results indicate that cell wall surface properties contribute to the lubricating behavior associated with texture perception in the oral phase.

The nanoindentation AFM technique in plants has become increasingly important for understanding cell wall structure modifications during cell growth or when they are subjected to different stress environments. This technique has already been reported in plant samples with different purposes. Most of these studies aim to deepen the understanding of the plant cell walls' complex structure and their correlation with their mechanical properties. It is widely known that the cell walls of the plants have to confer mechanical support as well as having important functions with regard to cell size. For instance, during the plant's growth, the primary cell walls are developed in a matrix containing three main components: cellulose, hemicelluloses, and pectin. This primary cell wall provides the cell's mechanical support allowing them to expand ([Cosgrove, 1998](#); [Xi, Kim, & Tittmann, 2015](#)). AFM nanoindentation techniques can be applied in thin, small, and heterogeneous crop plant samples such as cells, as well as stem, leaf, and root tissue. The nanoindentation with an AFM is suitable for testing plant samples as it preserves

them in their natural conditions. Some studies have used AFM to test nanomechanical properties of plant tissue with different targets. [Vogler et al. \(2017\)](#) reported some important reasons for testing nanomechanical properties in plant tissue. For instance, many industrial problems are related to the mechanical properties of the plant cell wall, for example, the impact of the plant mechanics due to the removal of lignin, which is a costly process in paper production. Another highlighted example is the pollen tubes that suffer alterations in the biochemical composition of their cell walls due to external environmental stress affecting the mechanical properties of the tubes, reflected in the pollen vitality and germination of plants. Moreover, modern agriculture has to deal with a worldwide problem related to the loss of cell wall rigidity due to its polymeric composition, and this is reflected in high harvest losses. Therefore, the knowledge acquired on the correlation between mechanical stability and the biochemical composition of the cell walls could help to produce more resistant crops.

For instance, in an early work of nanoindentation on food materials, [Lesniewska et al. \(2004\)](#) used AFM to test the stress modifications that occur when grapevine cells are affected by an external factor such as UV light. It was observed that the UV-affected cells displayed extra expansions around the cell wall that correspond to pectin chains, while this expansion was not observed in control cells. AFM was used to test the cell wall elastic modulus that accounts for the cell wall's mechanical properties ([Fig. 9.12](#)), and it was concluded that the UV-treated cell wall strengthens as a plant defense strategy compared with the control.

[Wu et al. \(2010\)](#) evaluated the elastic modulus of crop cell walls by nanoindentation, aiming to understand the strength properties of the individual crop fibers at the microscopic level. In this study, soybean (*Glycine max*) stalk, cotton (*Gossypium herbaceum*) stalk, cassava (*Manihot esculent*) stalk, rice (*Oryza sativa* L.) straw, and wheat (*Triticum aestivum* L.) straw were investigated by means of nanoindenter equipped with a three-sided pyramid diamond indenter tip (Berkovich type). However, AFM was not used as these materials are very hard. The study reported that wheat straw has the highest elastic modulus of 20.8 GPa among the five crops, followed by the rice straw and cassava stalk with 19.4 and 19.0 GPa, respectively. It was concluded that the different cell wall structure components and microfibril angle are key contributors to this difference. For instance, the cellulose and lignin content of wheat straw were 5.5% higher than that of rice straw ([Liu & Yu, 2002](#)).

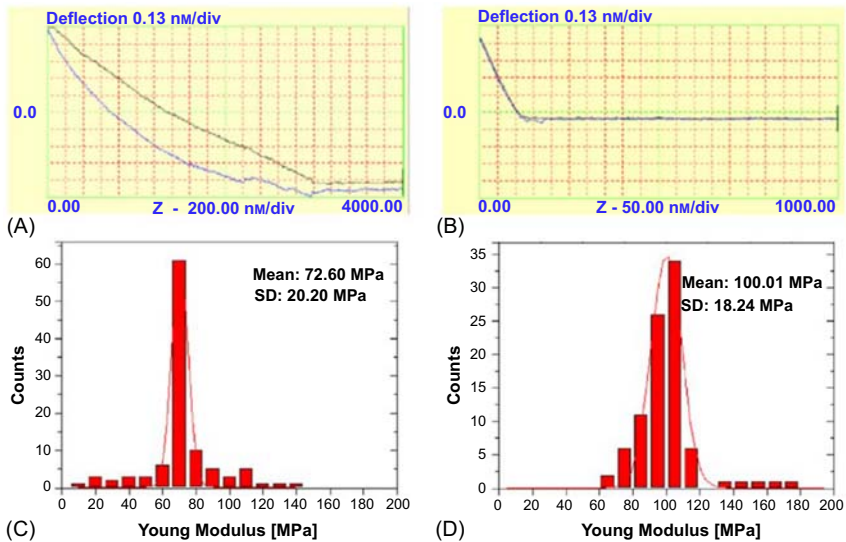


**Figure 9.12** Cell wall mechanical properties. (A) Typical deflection curve on untreated cell showing long-range repulsive force. (B) Typical deflection curve on UV-treated cell taken 3.5 h after elicitation showing short-range repulsive force. The corresponding measured elastic moduli on grapevine, (C) in average 72 MPa for untreated cell walls, and (D) 100 MPa for UV-treated cell walls. From Lesniewska, E., Adrian, M., Klingner, A., & Pugin, A. (2004). Cell wall modification in grapevine cells in response to UV stress investigated by atomic force microscopy. *Ultramicroscopy*, 100 (3–4), 171–178; Copyright 2004 Elsevier.

In another study conducted by Barrera, Méndez-Méndez, Arzate-Vázquez, Calderón-Domínguez, and Ribotta (2019), Young's modulus was evaluated and compared using different instrumental techniques (texturometer, microindenter, and AFM nanoindentation with diamond tip), at different multiscale compression levels (macro, micro, and nanometric), and in different regions (bran, endosperm, and germ) in the wheat kernel (Fig. 9.13). In this study, the Young's Modulus was estimated, and results were influenced by the technique used, indentation depth, studied region, tip geometry scale, and the sensitivity of the analytical instruments. Moreover, complexity cellular structure surface affected the dispersion of data obtained using different techniques. Thus, the variation of the mechanical properties of wheat kernel could be evaluated at different scales. The importance of this study was to illustrate that the mechanical properties of food materials are correlated when multiscale devices are used to evaluate nanomechanical properties. This concept has been shown

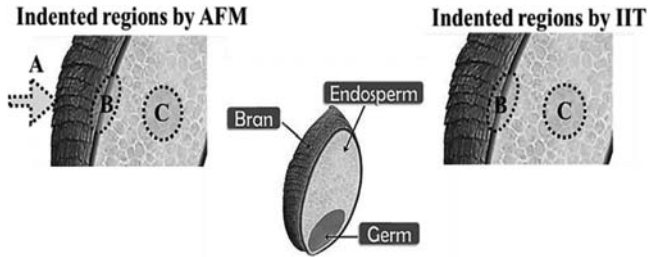


**Figure 9.13** Schematic representation of the indented regions by atomic force microscopy and nanoindenter. (A) Central region of the surface of whole grain; (B) central region of the bran layer (grain longitudinal section); (C) central region of the endosperm (grain longitudinal section). From Barrera, G. N., Méndez-Méndez, J., Arzate-Vázquez, I., Calderón-Domínguez, G., & Ribotta, P. D. (2019). Nano and micromechanical properties of wheat grain by atomic force microscopy (AFM) and nanoindentation (IIT) and their relationship with the mechanical properties evaluated by uniaxial compression test. *Journal of Cereal Science*, 90, 102830; Copyright 2019 Elsevier.

in previous studies on different food materials, where macro, micro, and nanomechanical properties are influenced by the type of indented tissue, as well as study region, complexity of surface microstructure, indentation level in soft and hard materials at different growth stages (Cárdenas-Pérez et al., 2016, 2017; Cárdenas-Pérez, Chanona-Pérez, Güemes-Vera, Cybulska, & Szymanska-Chargot, 2018; Marin-Bustamante, Chanona-Pérez, Guemes-Vera, Arzate-Vázquez, & Perea-Flores, 2018; Nicolás-Álvarez et al., 2019).

Kozlova et al. (2019) reported the nanomechanical properties of primary cell walls in the inner tissues of growing plant organs. They aim to promote an understanding of individual tissue roles in the plant growth processes. It was interesting to note that their procedure does not include fixation, resin-embedding, or drying plant material, which facilitates more accurate measurements. The sample was embedded in 3% (w/w) of low melting point agarose, and the transverse and longitudinal sections of maize root were investigated by being placed in a plastic Petri dish for AFM (Fig. 9.14). A local decrease in maize cell wall elasticity was found due to higher Young's modulus of the meristematic apex while elongating epidermal cells were found to have lower Young's modulus.

In another study, Nicolás-Álvarez et al. (2019) used AFM to evaluate nanomechanical properties on the surface of tomato root tissues over two different growth timelines. The researchers tested a taproot system that was divided into four zones: (1) root cap, (2) dividing cells, (3) elongating

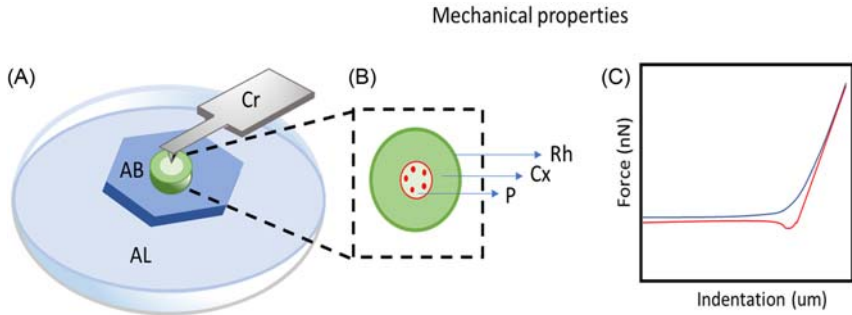


**Figure 9.14** Representation of plant sample preparation for testing nanomechanics. (A) Transverse section of maize root placed in a plastic Petri dish with agarose layer and agarose block. (B) Three regions of maize root that can be analyzed by atomic force microscopy cantilever (Cr): pith (P), cortex (Cx), and rhizodermis (Rh). (C) Force-indentation curve to calculate Young's modulus. *Modified from Kozlova, L., Petrova, A., Ananchenko, B., & Gorshkova, T. (2019). Assessment of Primary Cell Wall Nanomechanical Properties in Internal Cells of Non-Fixed Maize Roots. Plants, 8(6), 172.*

cells, and (4) absorption zone (Fig. 9.15A). Structurally, the taproot is formed by three layers of cells for each region, and cells were nanoindented with an AFM tip in the absorption zone, while obtained force curves were analyzed to determine stiffness (Fig. 9.15B and C).

The researchers established that the mechanical parameters depend on the indented region, tissue type, and growth time, meaning that stiffness increases in the epidermal cells along with the growth time while the parenchyma cells' stiffness decreases. Results also show the differences in Young's modulus between three regions, where the epidermis and vascular bundles have the highest YM values compared to parenchyma cells. Moreover, the mechanical properties can help to determine the viscoelasticity behavior of each region by calculating the plasticity index ( $\eta$ ). In this case, the viscoelastic behavior values of the vascular bundles increased over time, which can be linked to the vascular tissue that tends to be stiffer for the supporting functions.

Regarding the nanomechanical properties of animal cells, there are research studies that use AFM to analyze the morphology and mechanical properties of different foods of animal origin. For example, [Soltanizadeh and Kadivar \(2014\)](#) produced a compilation-base of related research on the nanomechanical characteristics of meat and its components postmortem, stating that the nanomechanical properties of muscle cells and connective tissues, particularly when the muscle undergoes different changes,

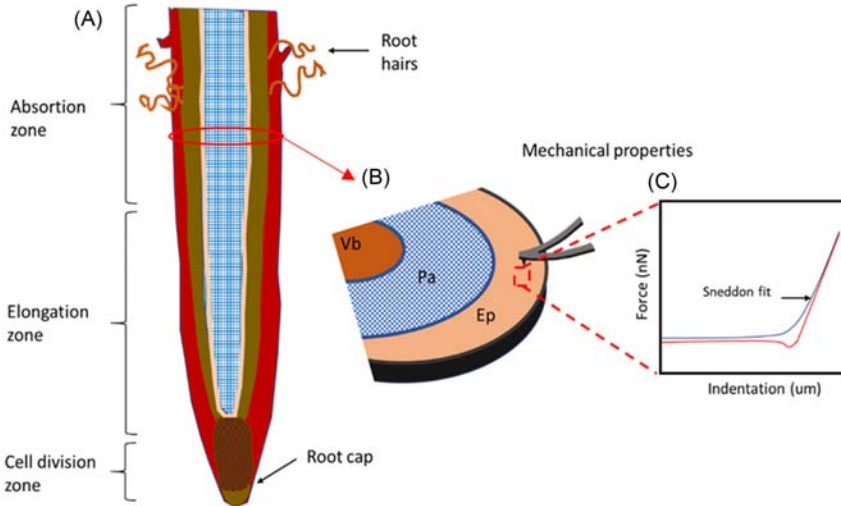


**Figure 9.15** (A) Schematic showing the taproot of the tomato representing the absorption zone with radicular hairs and the region in which root cross-sectioning was performed; (B) indentation scheme of the tomato root cross-section with atomic force microscopy; (C) nanoindentation force curve of the tomato root in absorption zone. Ep: epidermis, Pa: parenchyma, and Vb: vascular bundles. *Modified from Nicolás-Álvarez, D. E., Andraca-Adame, J. A., Chanona-Pérez, J. J., & et al. (2019). Evaluation of nanomechanical properties of tomato root by atomic force microscopy. Microscopy and Microanalysis, 25(4), 989–997.*

are useful in justifying many characteristics of postmortem meat. They concluded that the nanomechanical properties of muscle cells and connective tissues provided explanations for the changes in the rigidity of meat during storage. In a further study, [Matsumoto et al. \(2015\)](#) used AFM to examine the fibril formation processes of tilapia and porcine collagen. Through analyzing the results of human mesenchymal stem cell adhesion to tilapia collagen, this work showed that the degree of fibril formation of tilapia collagen was essential for osteoblastic differentiation from human mesenchymal stem cells.

In a different study, [Murthy et al. \(2016\)](#) used the AFM to study the temperature-dependent physical state of polar lipids and their miscibility impact on the topography and mechanical properties of bilayer models of the milk fat cell membrane. The AFM results showed that the milk fat cell membranes are dynamic systems, while their heterogeneity in nanostructure and mechanical properties were temperature-dependent. This work showed that AFM could be applied when analyzing the processing

of milk fat globules. In addition, there are also studies in which research is carried out with proteins of both animal and plant origin, including that of Zhang et al. (2016), where the effect of time and power density on the surface topography of wheat gluten was investigated. With increasing incubation time and power, the cross-linked structure of raw wheat gluten changed to irregular agglomerates, with the surface roughness increasing at first and then decreasing. The AFM results indicated that the cross-linked structure of wheat gluten composed of glutenin and gliadin bound by disulfide bonds was broken down by ultrasound, which caused the growth of agglomerates. In order to clarify the development of this research, Shi et al. (2019) conducted a review on the use of AFM applied to several types of proteins.

There are also other relevant studies, such as those that focus on the mechanical properties of harder materials, for example, the shells of some foods. For instance, Arzate-Vázquez, Flores-Johnson, Nicolás-Bermúdez, & Chanona-Pérez, (2019) investigated the porosity of the layers of calcified chicken eggshell using AFM and image processing. AFM topographic images were obtained from different locations for each layer and roughness parameters, surface area values, pore size and shape, surface porosity, area occupied by pores along with pore density. In general, the pores located in all layers had a circular shape and similar sizes. Additionally, the calcified eggshell had a sandwich-like structure where porosity may influence gas exchange and mechanical properties.

Finally, it is important to study the surface nanostructural and nanomechanical properties of food microorganisms (foodborne pathogens, spoilage microorganisms, and beneficial bacteria) to understand their behavior in various food processes as well as to clarify bactericidal mechanisms and cellular responses under adverse environments. As shown by Francois et al. (2013), the analysis of the biomechanical and biochemical properties of the yeast cell wall was carried out using AFM with the aim of understanding the effects caused by environmental stresses, temperature changes, osmotic pressure, shear stress, and antifungal agents on the surface of living yeast cells. Zeng et al. (2015) analyzed the effect of the amyloid function on the stiffness and robustness of the amyloid generator *Pseudomonas*. It was found that wild-type cells and fap mutant amyloid cells showed a compromised surface morphology after air drying, while amyloid fibrils that overexpressed pFap cells did not collapse and were able to maintain rod-shaped forms, suggesting that the amyloid made the cells more resistant to drying. To understand the pattern of adhesion forces on the



**Table 9.3** Summary of different studies on the nanomechanical properties of some food materials.

Food sample	Operation mode	Equipment and probe	Comments	References
<b>Plant materials</b>				
Arabidopsis	PeakForce QNM mode	Nanoscope IIIa Probe: oxides silicon nitride (NP-S)	Elastic modulus of the outer cell wall in living apical meristems	Milani et al. (2011)
Arabidopsis	Force-volume imaging mode	Bioscope I (Bruker), Probe: standard silicon nitride triangular	At the beginning and end of cell growth, rigidity was low, while during the exponential growth stage, rigidity increased	Radotić et al. (2012)
Onion epidermal peels	Contact mode liquid, point, and shoot	Catalyst model AFM (Bruker) Probe: (SD-Sphere-NCH-S-10)	Estimation of cell wall elastic properties and turgor pressure from a single force-depth curve	Beauzamy, Derr, and Boudaoud (2015)
Tomato root	Point and shoot	Bioscope Catalyst ScanAsyst, Bruker Probe: NP-10	Tissue surfaces were characterized on different days of growth through Young's modulus and plasticity	Nicolás-Álvarez et al. (2019)
Wheat and potato starch granules	Tapping mode in air and contact mode	MFP-3D (Asylum Research, USA) Probe: CSG10, NSG10 (NT-MDT)	Fine morphological structures such as growth rings and blocking domains	Salerno et al. (2014)
Apple tissue	Point and shoot	Catalyst, Bruker. Probe: ScanAsyst Fluid	Young's modulus values of the apple tissue showed a wide distribution during ripening. Food quality parameters can be predicted	Cárdenas-Pérez et al. (2017)

Mango	High-speed tapping mode	Multimode 8 (Bruker) Probe: ScanAsyst-HR	Evaluation of softening during the maturation process, in which the elastic module of the primary cell wall was evaluated. This parameter decreased and could be attributed to the softening of the fruit	Cárdenas-Pérez et al. (2018)
Apricot	Tapping mode	Park XE15, Park Systems, USA	Nanostructures of pectin polysaccharides were characterized, indicating that pectin depolymerization occurred during ripening	Deng et al. (2019)
Banana and mango	PeakForce QNM	Multimode AFM with J scanner (Bruker)	Properties of the fruit cell surface and the potential contribution of the cells and cell wall components to oral processing and texture perception	Rongkaumpan et al. (2019)
Animal tissues Bovine meat	Contact mode	Scanning Probe Microscope (Veeco)	Elastic module for the fiber bundles was obtained, showing that they have negligible viscous properties	Yoo, Reed, Shin, and Demer (2014)
Rainbow smelt	Contact mode	MFP-3D (Asylum Research) Probe: HQ: CSC37/Cr-Au, Mikromasch	Young's modulus of the eye sections of the rainbow smelt to understand hyperosmotic	Stewart (2016)

(Continued)

**Table 9.3** (Continued)

Food sample	Operation mode	Equipment and probe	Comments	References
<b>Proteins</b>				
Casein	Contact mode liquid	MFP-3D (Asylum Research) Probe: Silicon nitride MLCT	Young's modulus of small objects such as the milk casein micelles evaluation	Bahri et al. (2018)
Wheat gluten	PeakForce QNM	Nanoscope V (Bruker) Probe: standard peak force-mode silicon	The nanomechanical properties were studied and height, Young's modulus and adhesion maps were obtained.	Zhang et al. (2015)
Whey protein	Contact mode liquid	MFP-3D (Asylum Research) Probe: Silicon nitride MLCT	Particle topography and mechanical properties were investigated	Bahri et al. (2019)
Microorganisms and bacteria				
<i>Pseudomonas</i>	Tapping mode	JPK Instruments, Germany Probe: OMCL-AC160TS (Olympus)	The effect of the amyloid function on the stiffness and robustness of the amyloid generator <i>Pseudomonas</i> was analyzed	Zeng et al. (2015)
<i>Escherichia coli</i>	Tapping mode	MFP-3D Bio (Asylum Research) Probe: silicon nitride probe (DNP, Veeco Instruments Inc.)	Quantify the adhesion forces between the bacterial surface and the AFM tip after treatment with blueberry fractions	Gupta et al. (2016)

surface of *Pseudomonas*, a colloidal AFM probe was used after UV oxidation or silanization to modify its hydrolytic properties. A further report by Gupta et al. (2016) used AFM to quantify the adhesion forces between the bacterial surface and the AFM tip after treatment with blueberry fractions. The measured adhesion forces depended on both the bacterial strains and the blueberry fractions. This study shows that AFM can be used efficiently to measure the adhesion forces between bacterial surfaces as well as the tip after antibacterial treatments and that it can be useful to analyze the surface properties of bacteria after treatments. Table 9.3 summarizes different studies on the nanomechanical properties of food materials, condensing some of the important characteristics of the evaluations made, such as the material examined, the equipment and the cantilever model used, and the scanning mode employed, as well as comments about the results obtained.

A brief overview of Young's module values compiled from different food materials is shown in Fig. 9.16 (Cárdenas-Pérez et al., 2019). Overall, the stiffness range of animal and plant tissues varies widely from kPa to MPa, but hard biological materials such as purified nanocrystals cellulose (Lahiji et al., 2010) and seed shells (Barrera et al., 2019) can reach stiffness values of GPa. However, a wider compilation of the micro and nanomechanical properties of biological materials, including food, is

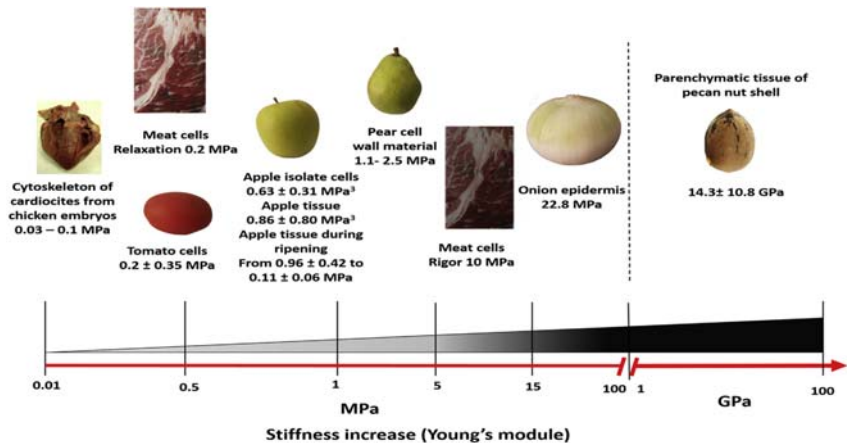


**Figure 9.16** Overview of stiffness in food materials obtained from different nanoindentation techniques. Adapted with permission from Cárdenas-Pérez, S., Chanona-Pérez, J. J., Méndez-Méndez, J. V., Arzate-Vázquez, I., Hernández-Varela, J. D., & Vera, N. G. (2019). Recent advances in AFM for assessing the nanomechanical properties of food materials. *Trends in Food Science & Technology*, 87, 59–72; Copyright 2019 Elsevier.

required to obtain a comprehensive database that incorporates the micro and nanoindentation methods, as well as the operating conditions used. Furthermore, these methods will need to be properly standardized in the future to reduce discrepancies in the data reported in the literature. Finally, evaluating nanomechanical properties by AFM is an important approach for research in the field of food and the design of new nanomaterials with superior properties and wide-ranging applications.

## 9.8 Conclusion

AFM has made it possible to associate structural and mechanical properties at nanoscale in biological and food materials. The advances in the AFM technique have provided a better understanding of molecular food components, which can be applied to improve processes and food properties. The study of the mechanical properties in different cell types is of great interest for understanding how tissue and cells change through their growth or when they are processed. Furthermore, it has been demonstrated that macro and microstructure are related to nanomechanical properties. Therefore, in the future, AFM will continue to play an important role in food research, and the analytical techniques mentioned will be applied in other fields. With further improvements to equipment, it will be possible to investigate a wider range of samples in different media. In addition, combinations with other complementary analytical techniques may provide more comprehensive information for future investigations. Moreover, AFM will provide opportunities for food researchers to discover more realistic perspectives at the nanoscale. The focused application of nanoimaging and force spectroscopy was, and continues to be, a significant aid for research into discovering and understanding the nature of matter and its interactions. The key advantage of AFM compared to other nanoscale imaging methods is the ability to observe substances at the nanoscale in their natural state and environment. Its application in the food sector is emerging as a tool to reveal the hidden sides of our knowledge towards nanoscale food substances, as in recent years, AFM has played an important role in developing our understanding of food structures and molecular networks.

## References

- Andreaus, U., Placidi, L., & Rega, G. (2013). Microcantilever dynamics in tapping mode atomic force microscopy via higher eigenmodes analysis. *Journal of Applied Physics*, 113 (22), 224–302.

- Arzate-Vázquez, I., Chanona-Pérez, J. J., Calderón-Domínguez, G., Terres-Rojas, E., Garibay-Febles, V., Martínez-Rivas, A., & Gutiérrez-López, G. F. (2012). Microstructural characterization of chitosan and alginate films by microscopy techniques and texture image analysis. *Carbohydrate Polymers*, *87*(1), 289–299.
- Arzate-Vázquez, J. V., Méndez-Méndez, E. A., Flores-Johnson, J., Nicolás-Bermúdez, J. J., Chanona-Pérez, & Santiago-Cortés E. (2019). Study of the porosity of calcified chicken eggshell using atomic force microscopy and image processing. *Micron*, 50–57.
- Bahri, A., Chevalier-Lucia, D., Marchesseau, S., Schmitt, C., Gergely, C., & Martin, M. (2019). Effect of pH change on size and nanomechanical behavior of whey protein microgels. *Journal of Colloid and Interface Science*, *555*, 558–568.
- Bahri, A., Martin, M., Gergely, C., Marchesseau, S., & Chevalier-Lucia, D. (2018). Topographical and nanomechanical characterization of casein nanogel particles using atomic force microscopy. *Food Hydrocolloids*, *83*, 53–60.
- Barrera, G. N., Méndez-Méndez, J., Arzate-Vázquez, I., Calderón-Domínguez, G., & Ribotta, P. D. (2019). Nano- and micro-mechanical properties of wheat grain by atomic force microscopy (AFM) and nano-indentation (IIT) and their relationship with the mechanical properties evaluated by uniaxial compression test. *Journal of Cereal Science*, *90*, 102830.
- Baselt, D., Revel, J., & Baldeschwieler, J. (1993). Subfibrillar structure of type I collagen observed by atomic force microscopy. *Biophysical Journal*, *65*(6), 2644.
- Beauzamy, L., Derr, L., & Boudaoud, A. (2015). Quantifying hydrostatic pressure in plant cells by using indentation with an atomic force microscope. *Biophysics Journal*, *208*, 2448–2456.
- Binnig, G., Quate, C. F., & Gerber. (1986). Atomic force microscope. *Physical Review Letters*, *56*(9), 930.
- Bovio, S., Long, Y., & Monéger, F. (2019). Use of atomic force microscopy to measure mechanical properties and turgor pressure of plant cells and plant tissues. *Journal of Visualized Experiments*, 149.
- Butt, H. J., Cappella, B., & Kappl, M. (2005). Force measurements with the atomic force microscope: Technique, interpretation and applications. *Surface Science Reports*, *59* (1–6), 1–152.
- Calabri, C. L., Pugno, N., Menozzi, C., & Valeri, S. (2008). AFM nanoindentation: Tip shape and tip radius of curvature effect on the hardness measurement. *Journal of Physics: Condensed Matter*, *20*(47).
- Cappella, B., & Dietler, G. (1999). Force-distance curves by atomic force microscopy. *Surface Science Reports*, *34*(1–3), 1–104.
- Cárdenas-Pérez, S., Chanona-Pérez, J., Güemes-Vera, N., Cybulska, J., Szymanska-Chargot, M., et al. (2018). Structural, mechanical and enzymatic study of pectin and cellulose during mango ripening. *Carbohydrate Polymers*, *196*, 313–321.
- Cárdenas-Pérez, S., Chanona-Pérez, J., Méndez-Méndez, J., Calderón-Domínguez, G., López-Santiago, R., & Arzate-Vázquez, I. (2016). Nanoindentation study on apple tissue and isolated cells by atomic force microscopy image and fractal analysis. *Innovative Food Science & Emerging Technologies*, *34*, 234–242.
- Cárdenas-Pérez, S., Chanona-Pérez, J. J., Méndez-Méndez, J. V., Arzate-Vázquez, I., Hernández-Varela, J. D., & Vera, N. G. (2019). Recent advances in AFM for assessing the nanomechanical properties of food materials. *Trends in Food Science & Technology*, *87*, 59–72.
- Cárdenas-Pérez, S., Méndez-Méndez, J. V., Chanona-Pérez, J. J., Zdunek, A., Güemes-Vera, N., Calderón-Domínguez, G., & Rodríguez-González, F. (2017). Prediction of the nanomechanical properties of apple tissue during its ripening process from its firmness, color and microstructural parameters. *Innovative Food Science & Emerging Technologies*, *39*, 79–87.

- Chichti, E., George, M., Delenne, J. Y., Radjai, F., & Lullien-Pellerin, V. (2013). Nano-mechanical properties of starch and gluten biopolymers from atomic force microscopy. *European Polymer Journal*, *49*(12), 3788–3795.
- Chichti, E., George, M., Delenne, J., et al. (2015). Changes in the starch protein interface depending on common wheat grain hardness revealed using atomic force microscopy. *Plant Science*, *239*, 1–8.
- Cosgrove, D. J. (1998). Cell wall loosening by expansins. *Plant Physiology*, *118*(2), 333–339.
- Dawidowicz, A. L., Nowakowski, P., Typek, R., & Dybowski, M. P. (2019). Effect of food packaging material on some physicochemical properties of polyacrylate varnish layers. *Food Packaging and Shelf Life* (Chicago, Ill.: 1978), *21*, 100–370.
- Deng, L., Pan, Z., Zhang, Q., Liu, Z., et al. (2019). Effects of ripening stage on physico-chemical properties, drying kinetics, pectin polysaccharides contents and nanostructure of apricots. *Carbohydrate Polymers*, *222*, 114980.
- Doherty, S., Gee, V., Ross, R., Stanton, C., & Fitzgerald, G. (2011). Development and characterisation of whey protein micro-beads as potential matrices for probiotic protection. *Food Hydrocolloids*, *25*(6), 1604–1617.
- Dufrène, Y. F. (2008). AFM for nanoscale microbe analysis. *Analyst*, *133*(3), 297–301.
- El Kirat, K., Burton, I., Dupres, V., & Dufrene, Y. F. (2005). Sample preparation procedures for biological atomic force microscopy. *Journal of Microscopy*, *218*(3), 199–207.
- Ellner, M., Pou, P., & Pérez, R. (2019). Molecular identification, bond order discrimination, and apparent intermolecular features in atomic force microscopy studied with a charge density-based method. *ACS Nano*, *13*(1), 786–795.
- Emam-Djomeh, Z., Pure, A. E., & Pure, M. E. (2020). *Atomic force microscopy (AFM) of nanoencapsulated food ingredients. Characterization of nanoencapsulated food ingredients* (pp. 159–188). Academic Press.
- Francois, J., Formosa, C., Schiavone, M., Pillet, F., et al. (2013). Use of atomic force microscopy (AFM) to explore cell wall properties and response to stress in the yeast *Saccharomyces cerevisiae*. *Current Genetics*, *59*(4), 187–190.
- Fukuma, T., Kobayashi, K., Matsushige, K., & Yamada, H. (2005). True molecular resolution in liquid by frequency-modulation atomic force microscopy. *Applied Physics Letters*, *86*(19), 193108.
- Gaboriaud, F., & Dufrène, Y. F. (2007). Atomic force microscopy of microbial cells: Application to nanomechanical properties, surface forces and molecular recognition forces. *Colloids and Surfaces B: Biointerfaces*, *54*(1), 10–19.
- Gaboriaud, F., Parcha, B. S., Gee, M. L., Holden, J. A., & Strugnell, R. A. (2008). Spatially resolved force spectroscopy of bacterial surfaces using force–volume imaging. *Colloids and Surfaces B: Biointerfaces*, *62*(2), 206–213.
- Gad, M., Itoh, A., & Ikai, A. (1997). Mapping cell wall polysaccharides of living microbial cells using atomic force microscopy. *Cell Biology International*, *21*(11), 697–706.
- García, R., & Perez, R. (2002). Dynamic atomic force microscopy methods. *Surface Science Reports*, *47*(6–8), 197–301.
- Gavara, N. (2016). Combined strategies for optimal detection of the contact point in AFM force-indentation curves obtained on thin samples and adherent cells. *Scientific Reports*, *6*(1), 1–13.
- Geng, X., Chyasnachyus, M., Meyers, G., & Wu, D. (2019). Surface elastic modulus of latex films studied with atomic force microscopy (AFM) and its correlation with dirt pick-up resistance (DPUR) performance. *Progress in Organic Coatings*, *126*, 168–177.
- Gross, L., Mohn, F., Moll, N., Schuler, B., Criado, A., Guitián, E., & Meyer, G. (2012). Bond-order discrimination by atomic force microscopy. *Science (New York, N.Y.)*, *337* (6100), 1326–1329.

- Gunning, A., Giardina, T., Faulds, C., Juge, N., Ring, S., Williamson, G., & Morris, V. (2003). Surfactant-mediated solubilisation of amylose and visualisation by atomic force microscopy. *Carbohydrate Polymers*, *51*(2), 177–182.
- Gupta, P., Song, B., Neto, C., & Camesano, T. (2016). Atomic force microscopy-guided fractionation reveals the influence of cranberry phytochemicals on adhesion of *Escherichia coli*. *Food & Function*, *7*(6), 2655–2666.
- Hugel, T., & Seitz, M. (2001). The study of molecular interactions by AFM force spectroscopy. *Macromolecular Rapid Communications*, *22*(13), 989–1016.
- Ikai, A., Afrin, R., & Sekiguchi, H. (2007). Pulling and pushing protein molecules by AFM. *Current Nanoscience*, *3*(1), 17–29.
- Iwasaki, T., Washio, M., & Yamamoto, K. (2005). Atomic force microscopy of thermally treated myosin filaments. *Journal of Agricultural and Food Chemistry*, *53*(11), 4589–4592.
- Jalili, N., & Laxminarayana, K. (2004). A review of atomic force microscopy imaging systems: Application to molecular metrology and biological sciences. *Mechatronics*, *14*(8), 907–945.
- Khan, M. I. H., Patel, N., Mahiuddin, M., & Karim, M. A. (2020). Characterisation of mechanical properties of food materials during drying using nanoindentation. *Journal of Food Engineering*, *291*, 110306.
- Kim, M., & Chelikowsky, J. R. (2014). Simulated non-contact atomic force microscopy for GaAs surfaces based on real-space pseudopotentials. *Applied Surface Science*, *303*, 163–167.
- Korayem, M. H., Noroozi, M., & Daeinabi, K. (2012). Control of an atomic force microscopy probe during nano-manipulation via the sliding mode method. *Scientia Iranica*, *19*(5), 1346–1353.
- Kozlova, L., Petrova, A., Ananchenko, B., & Gorshkova, T. (2019). Assessment of primary cell wall nanomechanical properties in internal cells of non-fixed maize roots. *Plants*, *8*(6), 172.
- Kurland, N. E., Drira, Z., & Yadavalli, V. K. (2012). Measurement of nanomechanical properties of biomolecules using atomic force microscopy. *Micron (Oxford, England: 1993)*, *43*(2–3), 116–128.
- Lahiji, R. R., Xu, X., Reifenberger, R., Raman, A., Rudie, A., & Moon, R. J. (2010). Atomic force microscopy characterization of cellulose nanocrystals. *Langmuir: The ACS Journal of Surfaces and Colloids*, *26*(6), 4480–4488.
- Lam, C. W. Y., & Ikeda, S. (2017). The Young's modulus, fracture stress, and fracture strain of gellan hydrogels filled with whey protein microparticles. *Journal of Food Science*, *82*(5), 1157–1162.
- Lesniewska, E., Adrian, M., Klinguer, A., & Pugin, A. (2004). Cell wall modification in grapevine cells in response to UV stress investigated by atomic force microscopy. *Ultramicroscopy*, *100*(3–4), 171–178.
- Liu, H. F., & Yu, Z. H. (2002). Properties of straw fiber. *Journal of Dong Hua University*, *28*(2), 123–128.
- Liu, S., & Wang, Y. (2010). Application of AFM in microbiology: A review. *Scanning*, *32*(2), 61–73.
- Liu, G., & Zhong, Q. (2013). Thermal aggregation properties of whey protein glycosylated with various saccharides. *Food Hydrocolloids*, *32*(1), 87–96.
- Lu, R. (2013). *Principles of solid food texture analysis* (pp. 103–128). Woodhead Publishing.
- Marin-Bustamante, M. Q., Chanona-Pérez, J. J., Guemes-Vera, N., Arzate-Vázquez, I., Perea-Flores, M. J., et al. (2018). Evaluation of physical, chemical, microstructural and micromechanical properties of nopal spines (*Opuntia ficus-indica*). *Industrial Crops and Products*, *123*, 707–718.
- Marszalek, P. E., Li, H., Oberhauser, A. F., & Fernandez, J. M. (2002). Chair-boat transitions in single polysaccharide molecules observed with force-ramp AFM. *Proceedings of the National Academy of Sciences*, *99*(7), 4278–4283.



- Mateu, M. G. (2012). Mechanical properties of viruses analyzed by atomic force microscopy: A virological perspective. *Virus Research*, 168(1–2), 1–22.
- Matsumoto, R., et al. (2015). Rapid oriented fibril formation of fish scale collagen facilitates early osteoblastic differentiation of human mesenchymal stem cells. *Journal of Biomedical Materials Research Part A*, 103(8), 2531–2539.
- Mendoza-Madrigal, A. G., Chanona-Pérez, J. J., Méndez-Méndez, J. V., Palacios-González, E., Calderón-Domínguez, G., & Hernández-Sánchez, H. (2013). Detection of *Lactobacillus plantarum* 299V using microcantilever-based biosensor with dynamic force microscopy. *Revista Mexicana de Ingeniería Química*, 379–389.
- Milani, P., Gholamirad, M., Traas, J., Arnéodo, A., Boudaoud, A., Argoul, F., & Hamant, O. (2011). In vivo analysis of local wall stiffness at the shoot apical meristem in *Arabidopsis* using atomic force microscopy. *The Plant Journal*, 27(6), 1116–1123.
- Morris, V. J., Kirby, A. R., & Gunning, A. P. (1999). *Atomic force microscopy for biologists* (Vol. 57). Imperial College Press.
- Müller, D., & Dufrene, Y. F. (2010). Atomic force microscopy as a multifunctional molecular toolbox in nanobiotechnology. In *Nanoscience and Technology: A Collection of Reviews from Nature Journals*, 269–277.
- Murthy, A., et al. (2016). The temperature-dependent physical state of polar lipids and their miscibility impact the topography and mechanical properties of bilayer models of the milk fat globule membrane. *Biochimica et Biophysica*, 1858(9), 2181–2190.
- Nakao, H., Hayashi, H., Yoshino, T., Sugiyama, S., & Otake, K. (2002). Development of novel polymer-coated substrates for straightening and fixing DNA. *Nano Letters*, 25(5), 475–479.
- Nicolás-Álvarez, D. E., Andraca-Adame, J. A., Chanona-Pérez, J. J., et al. (2019). Evaluation of nanomechanical properties of tomato root by atomic force microscopy. *Microscopy and Microanalysis*, 25(4), 989–997.
- Obeid, S., & Guyomarc'h, F. (2020). Atomic force microscopy of food assembly: Structural and mechanical insights at the nanoscale and potential opportunities from other fields. *Food Bioscience*, 100654, 100–654.
- Ortega-Toro, R., Contreras, J., Talens, P., & Chiralt, A. (2015). Physical and structural properties and thermal behaviour of starch-poly ( $\epsilon$ -caprolactone) blend films for food packaging. *Food Packaging and Shelf Life*, 5, 10–20.
- Oymaci, P., & Altinkaya, S. (2016). Improvement of barrier and mechanical properties of whey protein isolate based food packaging films by incorporation of zein nanoparticles as a novel bionanocomposite. *Food Hydrocolloids*, 56, 1–9.
- Peaucelle, A. (2014). AFM-based mapping of the elastic properties of cell walls: at tissue, cellular, and subcellular resolutions. *Journal of Visualized Experiments*, 89, 51317.
- Pieczywek, P., Koziol, A., Płaziński, W., Cybulska, J., & Zdunek, A. (2020). Resolving the nanostructure of sodium carbonate extracted pectins (DASP) from apple cell walls with atomic force microscopy and molecular dynamics. *Food Hydrocolloids*, 104, 105726.
- Putman, C., Van der Werf, K., De Grooth, B., Van Hulst, N., & Greve, J. (1994). Tapping mode atomic force microscopy in liquid. *Applied Physics Letters*, 64(18), 2454–2456.
- Radotić, K., et al. (2012). Atomic force microscopy stiffness tomography on living *Arabidopsis thaliana* cells reveals the mechanical properties of surface and deep cell-wall layers during growth. *Biophysical journal*, 10(3), 386–394.
- Rief, M., Oesterhelt, F., Heymann, B., & Gaub, H. (1997). Single molecule force spectroscopy on polysaccharides by atomic force microscopy. *Science (New York, N.Y.)*, 275(5304), 1295–1297.
- Rojas-Candelas, L., Chanona-Pérez, J., Méndez, J., Perea-Flores, M., Cervantes-Sodi, H., Hernández-Hernández, H., & Marin-Bustamante, M. (2021). Physicochemical,

- structural and nanomechanical study elucidating the differences in firmness among four apple cultivars. *Postharvest Biology and Technology*, 171, 111342.
- Rongkaumpan, G., Amsbury, S., Andablo-Reyes, E., Linford, H., Connell, S., Knox, J., & Orfila, C. (2019). Cell wall polymer composition and spatial distribution in ripe banana and mango fruit: implications for cell adhesion and texture perception. *Frontiers in Plant Science*, 10.
- Rousseau, D. (2006). On the porous mesostructure of milk chocolate viewed with atomic force microscopy. *LWT-Food Science and Technology*, 39(8), 852–860.
- Salerno, M., Żukowska, A., Thorat, S., Ruffilli, R., Stasiak, M., et al. (2014). High resolution imaging of native wheat and potato starch granules based on local mechanical contrast. *Journal of Food Engineering*, 96–102.
- San Paulo, A., & García, R. (2001). Tip-surface forces, amplitude, and energy dissipation in amplitude-modulation (tapping mode) force microscopy. *Physical Review B*, 64(19), 193411.
- Seifert, J., Kirchhelle, C., Moore, I., & Contera, S. (2020). Mapping cellular nanoscale viscoelasticity and relaxation times relevant to growth of living *Arabidopsis thaliana* plants using multifrequency AFM. *bioRxiv*.
- Scholl, Z. N., Li, Q., Josephs, E., Apostolidou, D., & Marszalek, P. E. (2019). Force spectroscopy of single protein molecules using an atomic force microscope. *Journal of Visualized Experiments*, 144.
- Shi, C., He, Y., Ding, M., Wang, Y., & Zhong, J. (2019). Nanoimaging of food proteins by atomic force microscopy. Part I: Components, imaging modes, observation ways, and research types. *Trends in Food Science & Technology*, 87, 3–13.
- Soltanizadeh, N., & Kadivar, M. (2014). Nanomechanical characteristics of meat and its constituents postmortem: a review. *Critical Reviews in Food Science and Nutrition*, 54(9), 1117–1139.
- Stewart, L.D. (2016). Determining the mechanical properties of Rainbow Smelt (*Osmerus mordax*) eye tissue using atomic force microscopy (AFM) (Doctoral dissertation, Memorial University of Newfoundland).
- Syahida, S. N., Ismail-Fitry, M. R., Ainun, Z. M. A. A., & Hanani, Z. A. N. (2020). Effects of palm wax on the physical, mechanical and water barrier properties of fish gelatin films for food packaging application. *Food Packaging and Shelf. Life (Chicago, Ill.: 1978)*, 23, 100–437.
- Tamayo, J., Humphris, A., Owen, R., & Miles, M. (2001). High-Q dynamic force microscopy in liquid and its application to living cells. *Biophysical Journal*, 81(1), 526–537.
- Tay, S., Kasapis, S., Perera, C., & Barlow, P. (2006). Functional and structural properties of 2S soy protein in relation to other molecular protein fractions. *Journal of Agricultural and Food Chemistry*, 54(16), 6046–6053.
- Tseng, A. (2011). Advancements and challenges in development of atomic force microscopy for nanofabrication. *Nano Today*, 6(5), 493–509.
- Türe, H., Blomfeldt, T. O. J., Gällstedt, M., & Hedenqvist, M. S. (2012). Properties of wheat-gluten/montmorillonite nanocomposite films obtained by a solvent-free extrusion process. *Journal of Polymers and the Environment*, 20(4), 1038–1045.
- Vogler, H., Shamsudhin, N., Nelson, B., & Grossniklaus, U. (2017). *Measuring cytomechanical forces on growing pollen tubes. In Pollen Tip Growth* (pp. 65–85). Cham: Springer.
- Wang, H., Fei, S., Wang, Y., Zan, L., & Zhu, J. (2020). Comparative study on the self-assembly of pectin and alginate molecules regulated by calcium ions investigated by atomic force microscopy. *Carbohydrate Polymer*, 231, 115673.
- Wang, Q., Crofts, A., & Padua, G. (2003). Protein-lipid interactions in zein films investigated by surface plasmon resonance. *Journal of Agricultural and Food Chemistry*, 51(25), 7439–7444.

- Wen, Y., Xu, Z., Liu, Y., Corke, H., & Sui, Z. (2020). Investigation of food microstructure and texture using atomic force microscopy: A review. *Comprehensive Reviews in Food Science and Food Safety*, 19(5), 2357–2379.
- Wu, Y., Wang, S., Zhou, D., Xing, C., Zhang, Y., & Cai, Z. (2010). Evaluation of elastic modulus and hardness of crop stalks cell walls by nano-indentation. *Bioresource Technology*, 101(8), 2867–2871.
- Xi, X., Kim, S. H., & Tittmann, B. (2015). Atomic force microscopy based nanoindentation study of onion abaxial epidermis walls in aqueous environment. *Journal of Applied Physics*, 117(2), 024703.
- Yang, H., An, H., Feng, G., Li, Y., & Lai, S. (2005). Atomic force microscopy of the water-soluble pectin of peaches during storage. *European Food Research and Technology*, 220(5–6), 587–591.
- Yang, H., An, H., Feng, G., & Li, Y. (2005). Visualization and quantitative roughness analysis of peach skin by atomic force microscopy under storage. *LWT-Food Science and Technology*, 38(6), 571–577.
- Yang, H. S., Feng, G. P., An, H. J., & Li, Y. F. (2006). Microstructure changes of sodium carbonate-soluble pectin of peach by AFM during controlled atmosphere storage. *Food Chemistry*, 94(2), 179–192.
- Yan, Y., Geng, Y., & Hu, Z. (2015). Recent advances in AFM tip-based nanomechanical machining. *International Journal of Machine Tools and Manufacture*, 99, 1–18.
- Yang, H., Wang, Y., Lai, S., An, H., Li, Y., & Chen, F. (2007). Application of atomic force microscopy as a nanotechnology tool in food science. *Journal of Food Science*, 72(4), 65–75.
- Yoo, L., Reed, J., Shin, A., & Demer, J. (2014). Atomic force microscopy determination of Young's modulus of bovine extra-ocular tendon fiber bundle. *Journal of Biomechanics*, 47(8), 1899–1903.
- Zdunek, A., & Kurenda, A. (2013). Determination of the elastic properties of tomato fruit cells with an atomic force microscope. *Sensors*, 13(9), 12175–12191.
- Zdunek, A., Koziol, A., Cybulska, J., Lekka, M., & Pieczywek, P. (2016). The stiffening of the cell walls observed during physiological softening of pears. *Planta*, 243(2), 519–529.
- Zeng, G., et al. (2015). Functional bacterial amyloid increases *Pseudomonas* biofilm hydrophobicity and stiffness. *Frontiers in Microbiology*, 9, 1099.
- Zhang, Y., Ma, H., Wang, B., Qu, W., Li, Y., He, R., & Wali, A. (2015). Effects of ultrasound pretreatment on the enzymolysis and structural characterization of wheat gluten. *Food Biophysics*, 10(4), 385–395.
- Zhang, M., Ding, C., Yang, J., Lin, S., Chen, L., & Huang, L. (2016). Study of interaction between water-soluble collagen and carboxymethyl cellulose in neutral aqueous solution. *Carbohydrate Polymers*, 137, 410–417.
- Zhong, J., & Wang, X. (2019). *Evaluation technologies for food quality*. Woodhead Publishing.

## CHAPTER 10

# Current and potential combination of atomic force microscopy with other techniques for food science

**Xin Wang, Yang Liu, Xin Guo, Yaolun Liu and Hao Sun**

Bruker (Beijing) Scientific Technology Co., Ltd., Beijing, P. R. China

### 10.1 Introduction

Since the invention of the atomic force microscopy (AFM) in 1986 (Binnig, Quate, & Gerber, 1986), it has become a more and more important tool for understanding the nanoworld. The uniqueness of AFM is the capabilities of getting 3D sample surface information in real-time and nanoscale with related simpler sample preparation. The flexibilities of working conditions such as in air, liquid, and vacuum also make AFM a powerful tool for studying extensive ranges of samples. In the past 30 years, a lot of efforts have been taken to improve the performance and capabilities of AFM; now, it has been extending the applications beyond surface topography imaging to physical properties mapping and manipulation at the nanoscale.

All these advantages of AFM attract researchers in food science to utilize this tool to understand more details at even molecular scales to reveal clear mechanisms of food production, packaging, transportation, and storage processes. Several good review papers have been published to introduce advances in AFM applications in food science (Finglas, 2019). These chapters focus on advanced applications of AFM techniques for food protein, toxins, polysaccharides, cells, microorganisms, and activated food packing materials, which are very helpful to the food scientist.

Recently, AFM has been further developed to combine its capabilities of nanoscale imaging and manipulation with other different techniques, including IR spectroscopy, Raman, MS, OM, X-ray techniques, and so on, which dramatically expand its application again to chemical properties mapping and spectra study to understand chemical information and dynamics. In this

chapter, we will review current and potential combinations of AFM with other techniques for food science. This chapter will discuss AFM-IR, AFM-Raman, AFM-MS, AFM-OM, AFM-X-Ray, AFM-nDMA, AFM-NMR, AFM-Force Loading Stage, AFM-FluidFM, and AFM-OT combined techniques. For each combined technique, the principle, apparatus, current, and potential applications in food science will be reviewed.

## 10.2 Atomic force microscopy combined with infrared technique for food science

Infrared spectroscopy is a common, reliable analysis tool, widely used in measuring absorption spectrum, a unique fingerprint for researchers to acquire the composition information of materials. IR spectroscopy has been widely used in composition analysis in food industries (Cozzolino, 2015; Nunes, 2014; Rodriguez-Saona & Allendorf, 2011). Due to absorptions of the ester carbonyl groups in lipids ( $1742\text{ cm}^{-1}$ ), the amide groups in protein ( $1545\text{ cm}^{-1}$ ), and the hydroxyl groups in lactose ( $1045\text{ cm}^{-1}$ ), infrared milk analyzers can determine the fat, protein, and lactose contents of milk simultaneously (Luis Rodriguez-Saona & Huseyin Ayvaz, 2017). By determining *cis* and *trans* contents, the source of olive oils can be identified (Gurdeniz, Tokatli, & Ozen, 2007; van de Voort, Ismail, & Sedman, 1995). By coupling Fourier transform infrared spectrometers (FTIR) with an IR microscope, researchers can routinely obtain not only IR spectra from a tiny sample area but also the chemical images with high resolution. However, the spatial resolution of the chemical image is limited by Abbe diffraction limit of infrared light. For typical light of IR spectroscopy with the wavelength from 2.5 to 30  $\mu\text{m}$ , the best spatial resolution is estimated to be from 2.5 to 75  $\mu\text{m}$  (Dazzi & Prater, 2017), which is difficult to demonstrate the chemical details under sub-100 nm spatial scales, such as fine structures on a single cell or even single protein. To break through the diffraction limitation, the foregoers combined AFM with an IR laser system and achieved the chemical spatial resolution at a sub-100 nm scale. According to some specific reports, the resolution of the infrared-chemical image can be 10~20 nm (Gong et al., 2017; Katzenmeyer, Holland, Kjoller, & Centrone, 2015; Lu, Jin, & Belkin, 2014; Richards, Zayats, Keilmann, & Hillenbrand, 2004). In the recent Bruker Dimension IconIR system, <5 nm IR image resolution of PS-b-PMMA block copolymer on Si substrate can be achieved, as shown in Fig. 10.1. Besides the high chemical spatial resolution, the AFM-IR combined system just needs minimum contents of sample. These benefits of the AFM-IR combined system make it a powerful tool for understanding

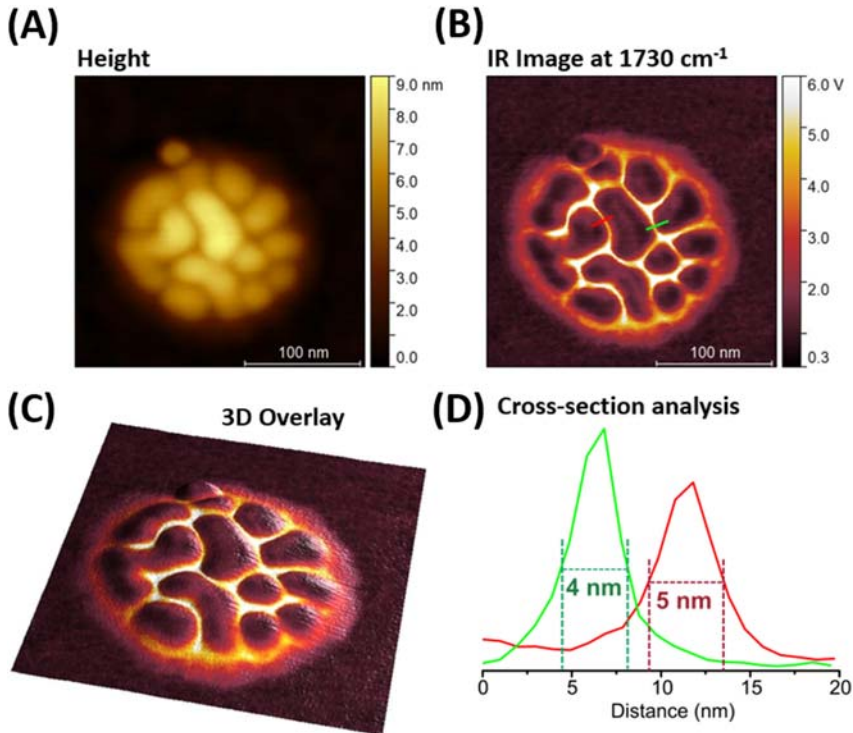


**Figure 10.1** Polystyrene-block-polymethyl methacrylate block copolymer on Si substrate measured by Bruker Dimension IconIR system. The image size is  $250 \times 250$  nm, the laser source is daylight quantum cascade laser, imaging mode is Tapping atomic force microscopy-infrared. (A) Topography image, (B) IR image at  $1730 \text{ cm}^{-1}$ , (C) 3D overlay image of height and IR channels, (D) cross-section analysis of the marked positions in (B), shows  $\sim 5$  nm resolution of IR image.

chemical information at sub-100 nm scale. The spectra from different sample areas can quantitatively uncover the compositions in multiphase polymer materials. With the help of the AFM-IR combined system, the compositions of food packaging materials, for example, coating of cans and antibacterial materials, can be designed and determined at sub-100 nm scales to further understand the relationship between microstructures and properties. Moreover, higher IR resolution makes it possible to acquire the components distribution differences in a single cell (Deniset-Besseau, Prater, Virolle, & Dazzi, 2014; Policar et al., 2011) or a single organelle (Lipiec et al., 2019), or even a single chromosome (Lipiec et al., 2019). It will open a new horizon for understanding the chemical changes in a plant cell, animal cell, or microbial cell during food manufacture, storage, transportation, and consumption.

## 10.2.1 Principle and apparatus

AFM-IR combined systems have been improved for over 10 years, and widely applied in research fields of polymer (Berweger et al., 2013; Felts, Kjoller, Lo, Prater, & King, 2012; Tang, Bao, & Su, 2016; Xu & Raschke, 2013), biology (Deniset-Besseau et al., 2014; Hofweber et al., 2018; Kennedy, Al-Majmaie, Al-Rubeai, Zerulla, & Rice, 2013; Lipiec et al., 2019; Policar et al., 2011; Ruggeri et al., 2015), drug (Harrison, Bilgili, Beaudoin, & Taylor, 2013; Van Eerdenbrugh, Lo, Kjoller, Marcott, & Taylor, 2012), low-dimension materials (Dai et al., 2014; Fei et al., 2012; Xu et al., 2014; Yang, Mayyas, et al., 2020), and paintings (Ma et al., 2019).

This combined system is based on photothermal induced resonance (PTIR) technique, which was developed by Dazzi et al. (Dazzi et al., 2012; Dazzi, Prazeres, Glotin, & Ortega, 2005, 2006). Typical PTIR setups are illustrated in Fig. 10.2. A tunable pulsed laser is employed to illuminate the sample below the AFM tip. When the wavenumber of IR light just matches the sample vibration energy level, the sample absorbs the light and thermally expands. The expansion of the sample illustrates the IR absorption under the

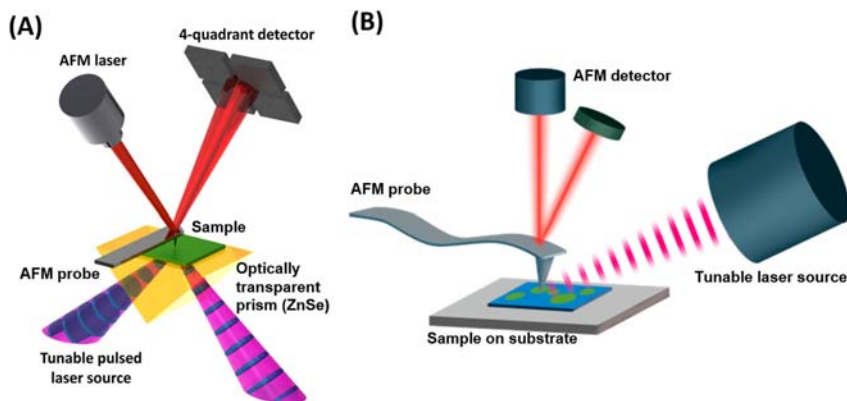


**Figure 10.2** (A) A typical scheme of the photothermal induced resonance technique. A sample is mounted on an optically transparent prism (i.e., ZnSe). A tunable pulsed laser passes through a prism and occurs total reflection. The evanescent wave will excite the thermal expansion which atomic force microscopy detects. (B) Tunable pulsed laser illuminates on a sample from the side (Katzenmeyer, Aksyuk, & Centrone, 2013; Dazzi, & Prater, 2017). (A) and (B) are adapted with permission from Katzenmeyer, A. M., Aksyuk, V., & Centrone, A. (2013). *Nanoscale infrared spectroscopy: Improving the spectral range of the photothermal induced resonance technique. Analytical Chemistry*, 85(4), 1972–1979 and Dazzi, A., & Prater, C. B. (2017). *AFM-IR: Technology and applications in nanoscale infrared spectroscopy and chemical imaging. Chemical Reviews*, 117(7), 5146–5173; Copyright American Chemical Society.

current wavenumber. The AFM cantilever with high sensitivity records the extremely small expansion of the sample at picometer scale. The amplitude of cantilever vibration is proportional to absorption coefficient of IR light, so it can be used to measure the IR absorption under the current wavenumber (Dazzi & Prater, 2017; Kurouski, Dazzi, Zenobi, & Centrone, 2020). The vibration amplitude can be measured with sweeping wavenumber, and IR absorption spectra can be obtained. Although the size of the IR laser spot is large (typically larger than 30  $\mu\text{m}$ ), AFM-IR combined technology can improve lateral spatial resolution to sub-100 nm scale because the gold-coated AFM probe detects the thermal vibration and enhances IR absorption due to the “lightning rod” effect only at tip-sample contact area.

Signal-to-noise ratio (SNR) and sample adaptability were improved in recent years. In Dazzi’s setup, relatively low pulse repetition rate IR laser was used. Lu et al. (2014) developed resonance-enhanced PTIR (RE-PTIR) technique. A quantum cascade laser (QCL) source with a much higher pulse repetition rate can be tuned to match the tip-sample contact resonance frequency. In this way, the cantilever vibration amplitude is maximized, and the SNR of the thermal expansion is strongly enhanced. With RE-PTIR technique, Lu et al. (2014) acquired IR absorption spectra of molecules in the single assembly membrane layer. Traditionally, AFM-IR is based on contact mode, which is difficult to achieve high spatial resolution because the large lateral force may damage the soft and fragile biomaterials, like protein, DNA, and lipid membrane. Tapping mode (Kurouski et al., 2020; Mathurin et al., 2018) was introduced to AFM-IR, which can realize 10 nm spatial resolution of chemical information with a nondestructive measurement (Mathurin et al., 2018).

Different optical path designs also influence the IR spectra measurement. As shown in Fig. 10.2A, an IR laser passes through an optical transparent prism (such as ZnS/ZnSe) and occurs in total reflection. The evanescent wave will pass through the prism-sample interface to excite thermal expansion. This design limits the thickness of the sample to hundreds of nanometers, otherwise the probe cannot “feel” the vibration caused by thermal expansion. Illuminating the sample from the side can break through the thickness limitation, as shown in Fig. 10.2B.

In general, AFM-IR measures the sample vibration caused by thermal expansion when the sample absorbs specific IR light, which is closer to the physical nature of IR absorption spectra of materials. The consistency between the spectra from AFM-IR and those from bulk FTIR has been confirmed by previous researchers (Felts et al., 2012; Tang et al., 2016).



## 10.2.2 Current atomic force microscopy-infrared applications in food science

Atomic force microscopy-infrared combined system has shown irreplaceable peculiarity in polymer analysis at the nanoscale. Most researchers in food science focus on food package materials, which contain conventional polymer, multiphase polymer, and other nanomaterials. Tibolla et al. (Tibolla et al., 2019; Tibolla, Czaikoski, Pelissari, Menegalli, & Cunha, 2020) developed a kind of banana starch-based nanocomposite films with good mechanical property, water-proof ability, and ultraviolet-proof ability, which is strengthened by cellulose nanofibers. The IR spectra at the nanoscale reveal the possible mechanism of strengthening.  $1630\text{ cm}^{-1}$  absorption indicates a new hydrogen-bonding interaction between cellulose and starch molecules. Meanwhile, the AFM-IR spectra found the peaks of residual materials, like protein and lignin, which could help analyze imperfection in the films.

Epoxy is a widely used resin material that is used for internal protective coatings of food containers and beverage cans. The design and control of chemical and physical properties are very important for coatings because some poisonous substance may infiltrate into food and lead to healthy problems. Morsch, Liu, Greensmith, Lyon, and Gibbon (2017) studied the chemical heterogeneity of epoxy-phenolic resin. With additional 4-benzylphenol, the degree of cross-linking decreases. The IR absorption image at  $1112\text{ cm}^{-1}$  shows that only highly cross-linked resin has chemical heterogeneities; in contrast, lightly cross-linked resin is homogeneous. The results are shown in Fig. 10.3.

Morsch, Lyon, and Gibbon (2017) also studied the degradation mechanism of an epoxy-phenolic can coating. Bulk FTIR shows that the resin does not hydrate when immersed in deuterated water ( $\text{D}_2\text{O}$ ). But AFM images obtained by AFM-IR show that the resin experienced network disruption, plasticization, and swelling processes after the  $\text{D}_2\text{O}$  immersion. AFM-IR firstly discovered that  $\text{D}_2\text{O}$  would enrich nanohole regions. The results are shown in Fig. 10.4.

Another application is to study the composition of plastic bag with multilayers. Kelchtermans, Lo, Dillon, Kjoller, and Marcott (2016) studied a cling film with seven layers. The composition of each layer was confirmed by the AFM-IR spectra. As shown in Fig. 10.5A, IR spectra from Layer A and F are consistent with polyethylene (PE), and IR spectra from Layer C, E, and G are consistent with polyamide (PA). The IR spectra of Layer D are consistent with polyethylene-co-(vinyl alcohol)

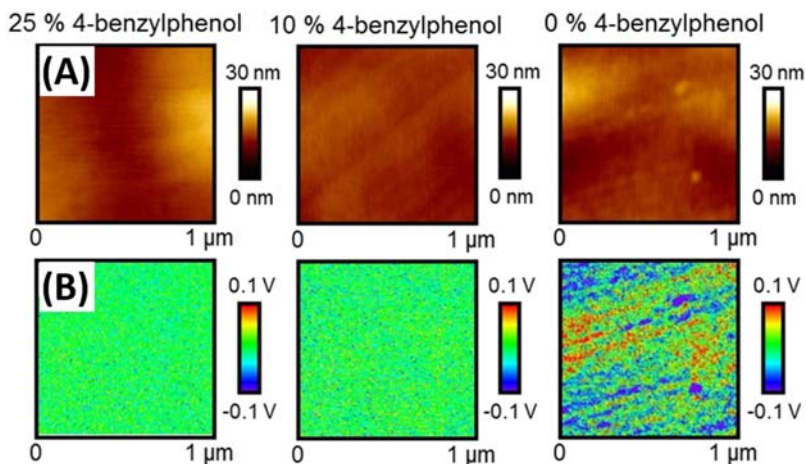


**Figure 10.3** Topography images (A) and infrared (IR) absorption images (B) at  $1112\text{ cm}^{-1}$  with different proportions of 4-benzylphenol. The IR absorption is attributed to secondary hydroxyl groups. Only highly cross-linked resin without 4-benzylphenol shows obviously heterogeneous (Morsch, Liu, Greensmith, Lyon, & Gibbon, 2017). (A) and (B) are adapted with permission from Morsch, S., Liu, Y., Greensmith, P., Lyon, S. B., & Gibbon, S. R. (2017). *Molecularly controlled epoxy network nanostructures. Polymer, 108, 146–153; Copyright (2016) Elsevier.*

(EVOH). This group also studied whether the thin tie-layer exists as glue between two layers. As shown in Fig. 10.5B, within 200 nm of the boundary at Layer B consistent with PE, peak width of the  $\text{CH}_2$ -stretching band is sharper than those away from the boundary, as well as peak position of the  $\text{CH}_2$ -antisymmetric stretching band shifts to a higher wavenumber. These results indicate a thin branched PE-based tie-layer to tie the PE layer to the PA layer. In contrast, tie-layer does not exist between Layer C and D, consistent with that the widths of peaks at  $3296\text{ cm}^{-1}$  broaden gradually across the interface of two layers, as shown in Fig. 10.5C.

One important problem in the food and beverage manufacturing industry is biofilms formed by contaminations and accumulation of microorganisms. The biofilms can cause the performance degradation of food production equipment and the failure of hygienic control (Huang, Chakraborty, & Liang, 2020). Therefore, the characterization of biofilm and the design of new antibacterial materials are critical. Dazzi et al. (2012) confirmed that the AFM-IR spectra collected from a single *Escherichia coli* cell are consistent with biofilm acquired from bulk FTIR. Barlow et al. (Barlow et al., 2016) reported the good performance of the AFM-IR system, which can distinguish 200 nm thick *Pseudomonas protegens* Pf-5 (Pf) bacteria monolayer biofilm from a 300 nm thick

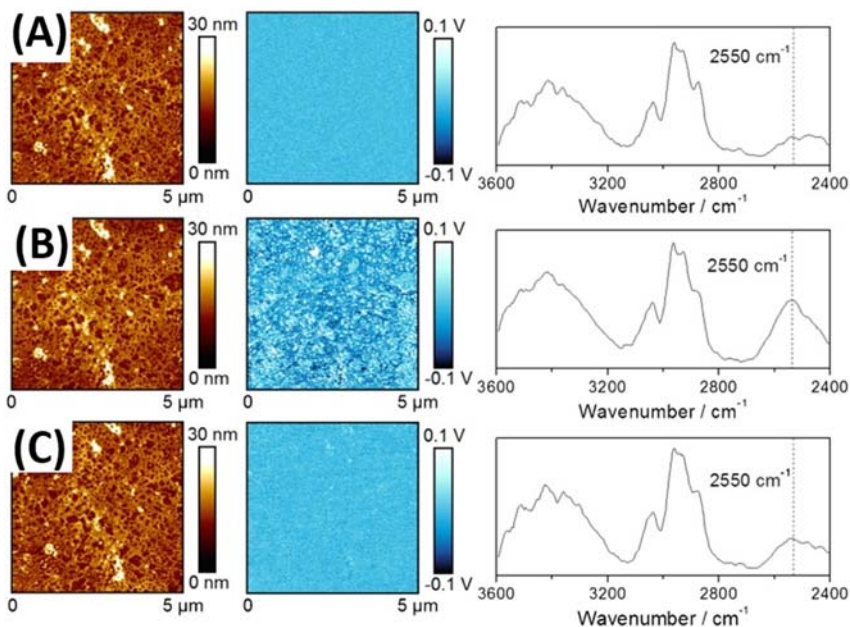


**Figure 10.4** Topography, infrared (IR) absorption at  $2550\text{ cm}^{-1}$  image, and typical IR spectra illustrate the  $\text{D}_2\text{O}$  absorbed in the nanoholes. (A) Resin before contacting with  $\text{D}_2\text{O}$  vapor, 30% relative humidity (RH). (B) Resin after exposure to  $\text{D}_2\text{O}$  vapor, 50% RH. (C) Resin after drying for 48 h, 20% RH. (A) and (B) are adapted with permission from Morsch, S., Lyon, S., & Gibbon, S. R. (2017). *The degradation mechanism of an epoxy-phenolic can coating*. *Progress in Organic Coatings*, 102, 37–43; Copyright (2017) Elsevier.

polyether–polyurethane (PU) clearly. As shown in Fig. 10.6A and B,  $2792$  and  $1732\text{ cm}^{-1}$  absorption peaks are attributed to PU, and  $1658\text{ cm}^{-1}$  absorption is attributed to Pf. However, the absorptions obtained from the Pf-PU area are higher than the bare PU area due to the overlap of  $1732\text{ cm}^{-1}$  peak from PU and  $1658\text{ cm}^{-1}$  peak from Pf, which strengthens the intensity of  $1732\text{ cm}^{-1}$  peak, as shown in Fig. 10.6B and C. By using the absorption at  $1658\text{ cm}^{-1}$  to normalize the absorption at  $1732\text{ cm}^{-1}$ , a clear contrast is shown in Fig. 10.6D. The nearly uniform contrast of  $1732/2792\text{ cm}^{-1}$  in Fig. 10.6E is totally attributed to PU. This frontier work indicates that biofilm can be identified, characterized, and tracked during its formation.

Designing and characterizing antibacterial materials could also involve AFM-IR to reveal the antibacterial mechanism. Nguyen-Tri, Nguyen, & Nguyen (2019) developed a new antibacterial high-density polyethylene (HDPE) containing dumbbell-like  $\text{Fe}_3\text{O}_4\text{-Ag}$  hybrid nanoparticles.

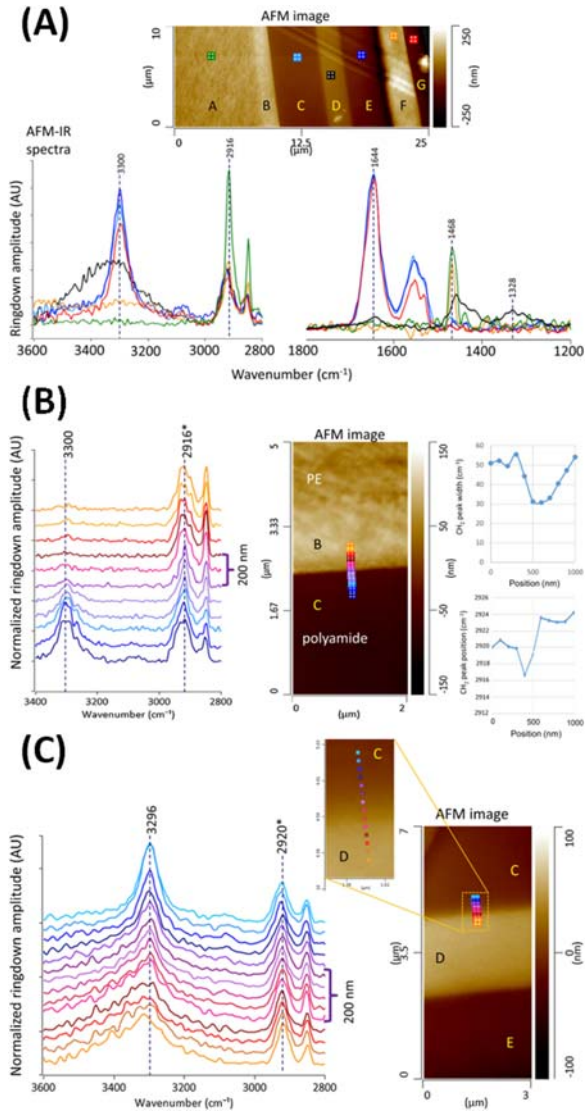


**Figure 10.5** (A) Topography of the seven-layer cling film and infrared spectra acquired from Layer A, C, D, E, F, and G. (B) Spectra acquisition across the interface between Layer B (PE) and Layer C (PA). As approaching the interface from PE side, the shifted peak position and broadened peak width indicate the existence of thin tie-layer. (C) Spectra acquisition across the interface between Layer C (PA) and Layer D (EVOH). Gradually broadening the width of the peak at  $3296\text{ cm}^{-1}$  indicates that there is no tie-layer (Kelchtermans, Lo, Dillon, Kjoller, & Marcott, 2016). (A) to (C) are adapted with permission from Kelchtermans, M., Lo, M., Dillon, E., Kjoller, K., & Marcott, C. (2016). Characterization of a polyethylene–polyamide multilayer film using nanoscale infrared spectroscopy and imaging. *Vibrational Spectroscopy*, 82, 10-15, Copyright (2015) Elsevier.

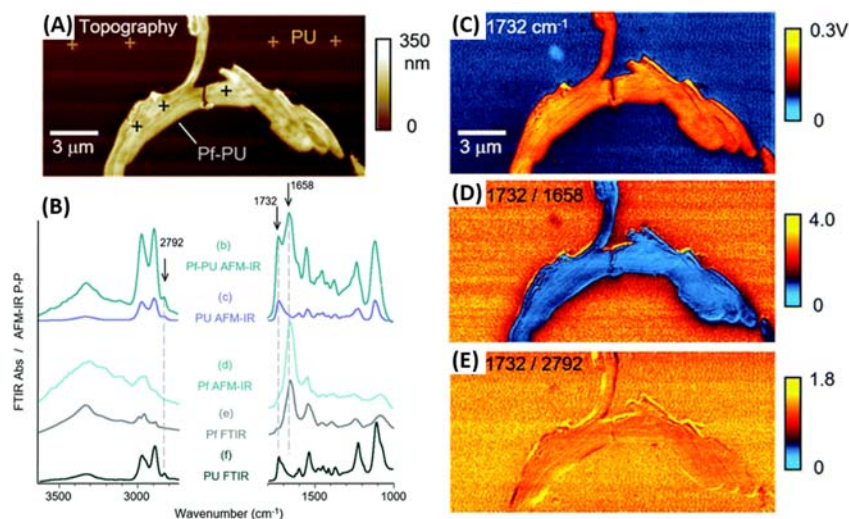


**Figure 10.6** (A) Topography of Pf-5 bacteria on PU. (B) Spectra of Pf-PU, Pf, and PU acquired from atomic force microscopy-infrared (IR) and bulk FTIR. (C)–(E) IR absorption contrast related to 1732, 1732/1658  $\text{cm}^{-1}$ , and 1732/2792  $\text{cm}^{-1}$ , respectively. (A)–(E) are adapted with permission from Barlow, D. E., Biffinger, J. C., Cockrell-Zugell, A. L., Lo, M., Kjoller, K., Cook, D., ... Russell, J. N. (2016). The importance of correcting for variable probe–sample interactions in AFM-IR spectroscopy: AFM-IR of dried bacteria on a polyurethane film. *Analyst*, 141(16), 4848–4854; Copyright (2016) The Royal Society of Chemistry.

AFM-IR technique was used to highlight the distribution of nanoparticles in the HDPE and confirmed existing of the lamellae structure in the spherulite of FeOAg-NPs/HDPE, which should be critical for antibacterial mechanism. Ferreira et al. (2019) developed an antibacterial package material; Ag nanoparticles coated with modified cellulose nanocrystals (MCNC) dispersed in poly(butylene adipate-co-terephthalate), which showed good antimicrobial properties. AFM-IR confirmed the core-shell structure of MCNC modified by adipic acid.

Understanding the structure and composition of food at nanoscale become increasingly important. The mouthfeel, the high-temperature cooking, the low-temperature storage, the accumulation of harmful substances, and microorganism breeding probably are related to phase separation at sub-micrometer scale, which AFM-IR can be a new characterization method. Zhang et al. (2019) studied the structural changes in the complicated artificial meat production line. AFM-IR technique helps to understand the changing of peanut protein during production. Protein

and lipids changing along the production line are shown in Fig. 10.7. The protein and lipid are in phase-separation states at the mixing zone. Then at the melting zone, the aggregation degree of the protein phase rises, and lipids still do not enter the protein phase. After passing the cooling zone, the lipids totally enter the protein phase, and the phase separation disappears. With full knowledge of this process, several artificial protein products, such as artificial meat, tofu, and sausage, have been developed. Ji et al. (2019) used AFM-IR to detect the single particle of toxins in the food industry. AFM-IR spectra from toxins were used to build a database for toxin analysis. With the help of principal component analysis, AFM-IR can identify each toxin in the toxin mixture.

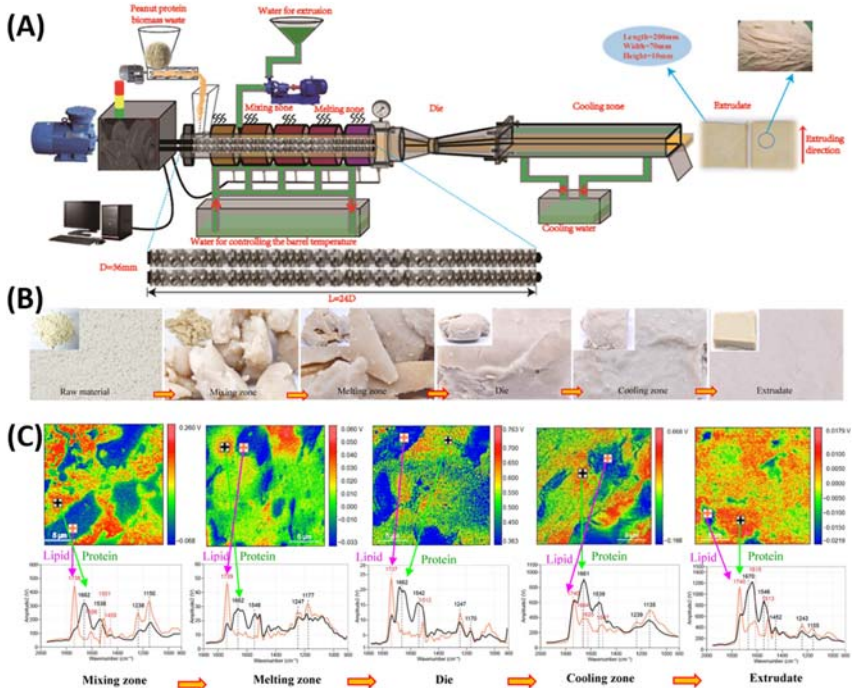


**Figure 10.7** (A) Scheme of high-moisture extrusion process. (B) Photos of peanut proteins in different zones. (C) atomic force microscopy-infrared (IR) absorption images at  $1660\text{ cm}^{-1}$  and AFM-IR spectra of protein and lipids in different zones. The peak at  $1660\text{ cm}^{-1}$  is attributed to protein and  $1740\text{ cm}^{-1}$  to lipid. (A) to (C) are adapted with permission from Zhang, J., Liu, L., Jiang, Y., Faisal, S., Wei, L., Cao, C., ... Wang, Q. (2019). Converting peanut protein biomass waste into “double green” meat substitutes using a high-moisture extrusion process: A multiscale method to explore a process for forming a meat-like fibrous structure. *Journal of Agricultural and Food Chemistry*, 67(38), 10713–10725; Copyright (2019) American Chemical Society.

### 10.2.3 Prospect of atomic force microscopy-infrared applications in food science

Nanotechnology is popular for food science research (Rossi et al., 2014). However, the AFM-IR technique is emerging for researchers to develop various applications in the food industry.

Bulk FTIR technique has been widely used to study protein properties in the food industry. By analysis of the amide-I band around  $1650\text{ cm}^{-1}$ , protein structure can be identified, including  $\alpha$ -helix, antiparallel or parallel  $\beta$ -sheet,  $\beta$ -turn, random coil loop, and intermolecular hydrogen bond (Barth, 2007; López-Lorente & Mizaikoff, 2016; Yang, Yang, Kong, Dong, & Yu, 2015). However, tiny amount of sample detection and high resolution are still challenging for bulk FTIR. The introduction of AFM-IR is a good way to overcome these drawbacks. Amount of protein structure study have proven the reliability of AFM-IR (Qamar et al., 2018; Rizevsky & Kurouski, 2020; Ruggeri et al., 2016). Ruggeri et al. (2015) used AFM-IR to monitor the conformation changing of amyloid protein during the self-assembly and accumulation of peptides. It implies the potential application of AFM-IR to analyze the protein microstructures inside the food.

Due to the high spatial resolution, AFM-IR can help acquire the chemical distribution at the single-cell level. Lipiec et al. (2019) and Wang et al. (2018) uncovered the anti-cancer drug distribution in the cell. Deniset-Besseau et al. (2014) tracked the triacylglycerols accumulation in *Streptomyces* to produce biofuel. Kochan et al. (2018) even studied the IR spectra of septum during the division of live *Staphylococcus aureus*. These works remind us that by applying AFM-IR to the food industry, we can study the chemical composition changing in food during manufacturing progress, the physiological activities of microorganisms in fermentation engineering, and the bacteria multiplication during putrefaction.

Recently, with Fig. 10.2A setup, the AFM-IR technique was used to acquire the IR spectra measurement in water. The IR evanescent wave can only be absorbed by a sample just a few micrometers above the substrate; therefore, little IR light can be absorbed by water, and AFM cantilever mainly detects thermal expansion of the sample. Ramer, Ruggeri, Levin, Knowles, & Centrone (2018) used AFM-IR to acquire the high-quality spectra of self-assembly peptide in water quantitatively. Live cells in water can also be measured by AFM-IR (Kochan et al., 2018; Mayet et al., 2008). It shows the potential food science application of AFM-IR in liquid environment, which cannot be achieved by bulk FTIR.

Katzenmeyer et al. (2015) expanded the light source of the AFM-IR system from infrared to visible range with a spatial resolution 17 nm. It expands the system's capability to obtain spectra information in a much wider range, which means the visible spectroscopy for food science applications can be done at the nanoscale.

Xiaoji Xu's group developed PeakForce-IR (PFIR) (Wang et al., 2020; Wang, Huang, Chan, Li, & Xu, 2017; Wang, Wang, et al., 2017) based imaging mode by combining AFM-IR with PeakForce Tapping mode invented by Bruker, which can directly control imaging force between tip and sample. It was further combined with PFIR and Kelvin probe force microscopy (KPFM), called PFIR-KPFM (Jakob et al., 2020). With this mode, the topography, IR absorption at specified wavenumber, Young's modulus, adhesion force, and surface potential of sample can be acquired just in one-pass scanning, as shown in Fig. 10.8. It makes PFIR based technique a powerful tool in food science to obtain abundant physical and chemical information simultaneously.

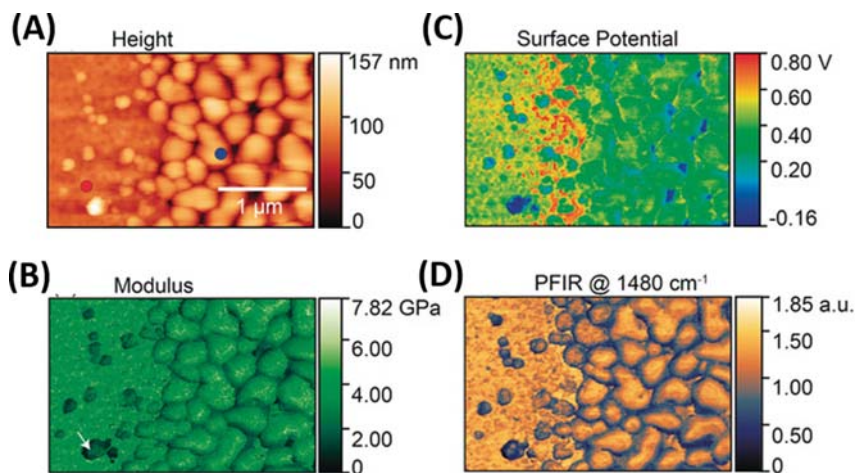


**Figure 10.8** Correlative topography (A), mechanical property (B), surface potential (C), infrared absorption (D) at  $1480\text{ cm}^{-1}$  imaging on  $\text{MAPbBr}_3$  crystal surface. All images were obtained on a modified MultiMode 8 (Bruker, United States). Absorption at  $1480\text{ cm}^{-1}$  is attributed to  $\text{CH}_3\text{NH}_3^+$  ion ( $\text{MA}^+$  ion), which can be used to identify  $\text{MAPbBr}_3$ . (A)–(D) are adapted with permission from Jakob, D. S., Wang, H., Zeng, G., Otzen, D. E., Yan, Y., & Xu, X. G. (2020). Peak force infrared–kelvin probe force microscopy. *Angewandte Chemie International Edition*; Copyright (2020) Wiley-VCH Verlag GmbH & Co. KGaA, Weinheim.



### 10.3 Atomic force microscopy combined with Raman technique for food science

Raman effect or Raman scattering is the inelastic scattering of photons by matters, which means a change of energy and incident direction (Ferrari et al., 2006; Nie & Emery, 1997; Pettinger, Ren, Picardi, Schuster, & Ertl, 2004). Such scattering involves vibrational states change of molecules and causes the frequency shift of scattered light relative to incident light. Unlike elastic scattering, that is Rayleigh scattering, the energy shift scattering, called Stokes or anti-Stokes scattering, provides insight into molecular structural information of materials. Since discovered by C. V. Raman in 1928 (Landsberg & Mandelshtam, 1928; Raman & Krishnan, 1928), it has been widely exploited by chemists and physicists to gain information about materials for a variety of purposes.

In 1974, Fleischmann et al. observed a strong Raman effect from pyridine, which was adsorbed onto a roughened silver electrode surface from an aqueous solution (Fleischmann, Hendra, & McQuillan, 1974). Jeanmaire and Van Duyne (1977) and Albrecht and Creighton (1977) independently recognized that the large intensities observed on the silver surface could not be accounted for simply by the increase in the number of scatterers present. Instead, they proposed an enhancement mechanism for the scattered intensity that occurred in the adsorbed state. Since then, the field of surface-enhanced Raman spectroscopy (SERS) has grown greatly, demonstrating its potential as a high-sensitive and high-selective analytical tool. Now SERS has been widely applied in fields of chemistry, physics, materials science, surface science, nanoscience, and food sciences.

#### 10.3.1 Principle and apparatus

As shown in Fig. 10.9, there are two main instrumental approaches employed to obtain SERS results. Fig. 10.9A shows a schematic diagram of macro-Raman configuration, in which the incident laser is focused on the SERS substrate through a focusing lens at a glancing angle, while the Raman light path is controlled using a large collection lens. Then, the light is focused through the entrance slit of a spectrometer and finally detected by a liquid-nitrogen-cooled charged-coupled device. Such setup is typically used for high raw SERS intensity, although spatial resolution is relatively low.

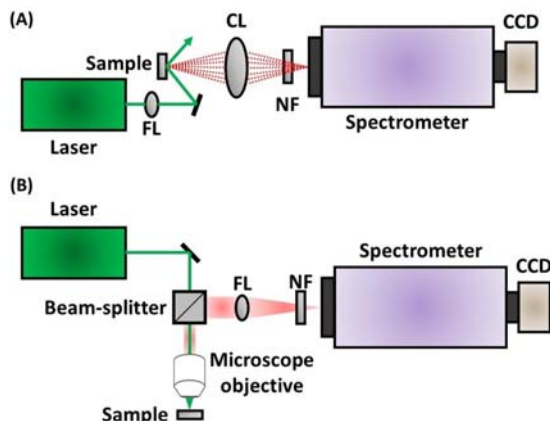


**Figure 10.9** Schematic diagram of surface-enhanced Raman spectroscopy setups for (A) macro-Raman and (B) micro-Raman. Abbreviations: CCD, charge-coupled device; CL, collection lens; FL, focusing lens; NF, notch filter.

When a high spatial resolution is required, micro-Raman configuration, as detailed in Fig. 10.9B, is utilized. In this approach, one high numerical-aperture objective is utilized to focus and collect the laser. The scattered light passes through a notch filter to remove Rayleigh-scattered light, followed by focusing and directing to a spectrometer. This setup is widely used for experiments with scanning SERS over varying wavelengths.

### 10.3.2 Current atomic force microscopy-Raman applications in food science

Thanks to its high detection sensitivity and high specificity, SERS has been widely applied in food science, especially in the field of chemical analysis of various food-related samples, like pollutants, toxins, etc. (Campion & Kambhampati, 1998; Cialla et al., 2012; Huang et al., 2020; Marin et al., 2015; Mishra, Ha, Verma, & Tiwari, 2018; Naumenko, Snitka, Serviene, Bruzaite, & Snopok, 2013; Ramirez-Aldaba et al., 2018; Rusciano et al., 2014). However, its practical applications are often limited because the preparation of the SERS substrates is usually uncontrollable at macron scales. By combining AFM and SERS, researchers could well understand the substrate at the micronanometer scale and use it for SERS analysis to obtain precise chemical information.

A good example is investigating pesticide remnants using SERS on a monolayer photonic crystal (PC), which has been well characterized by AFM (Zhang, Xu, & Chen, 2020). Chen et al. prepared the self-assembled-

monolayer PC substrates by depositing silica particles with space-tunable silver nano-bulges ( $\text{SiO}_2@\text{nAg}$ ). AFM was utilized to reveal that the on-water surface assembly of particles was an easy way to pack them tightly, giving a hexagonal close lattice of  $\text{SiO}_2@\text{nAg}$  particles, shown in Fig. 10.10A and B. As indicated, the PC substrates could avoid the irreproducible SERS on the “same” substrates, which can be further validated by the Raman peak measured at  $1078\text{ cm}^{-1}$ : the relative standard deviation (RSD) was below 3.8% shown in Fig. 10.10C and D. This preparation was facile and reproducible, and the resulting monolayer PC substrates made it possible to collect stable Raman scattering signals, which enabled the quantification of trace thiol substances (the test sample used in this research was p-aminothiophenol). The

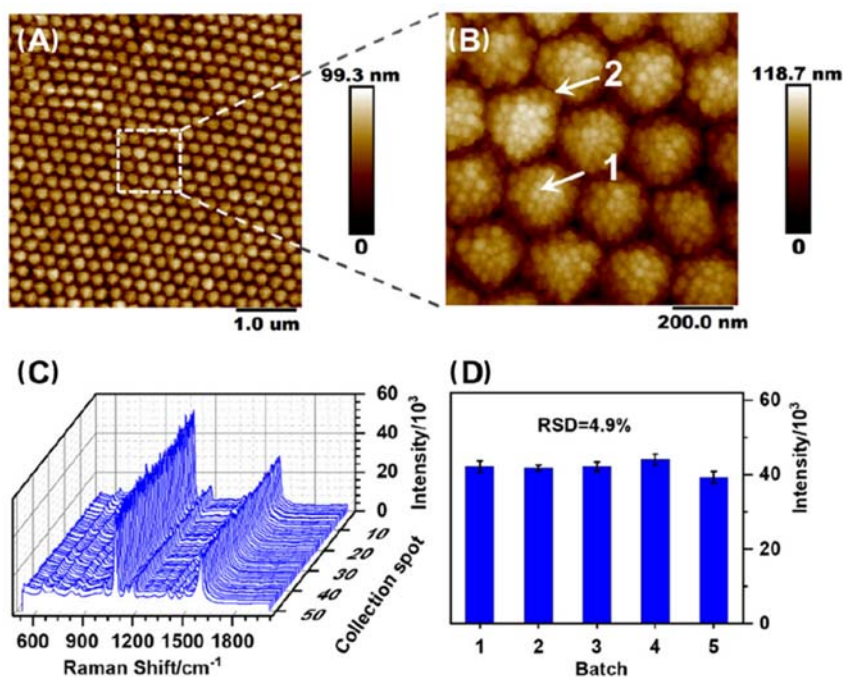


**Figure 10.10** (A) and (B) Atomic force microscopy images of a  $\text{SiO}_2@\text{nAg}$ -assembled monolayer photonic crystal (PC) substrate on a silicon slide, (C) surface-enhanced Raman spectroscopy (SERS) spectra collected from different locations on the same PC substrate, and (D) the statistical deviation of SERS intensities of p-aminothiophenol at  $1087\text{ cm}^{-1}$  acquired from five different PC substrates assembled in five batches. (A)–(D) are adapted with permission from Zhang, C., Xu, J., & Chen, Y. (2020). Preparation of monolayer photonic crystals from Ag nanobulge-deposited  $\text{SiO}_2$  particles as substrates for reproducible SERS assay of trace thiol pesticide. *Nanomaterials*, 10(6); Copyright (2020) MDPI.

PC-based assay was able to enhance the detection sensitivity  $2.2 \times 10^7$ -fold, with the RSD  $< 5\%$ . This PC-based SERS assay was validated to be applicable to the determination of trace thiram pesticide in apple juice samples, pushing the limit of detection down to 34.7 ppb.

SERS greatly enhances Raman signal compared with traditional Raman spectroscopy; as such, the overall sensitivity of SERS is no more the question. However, the main obstacle when using SERS for the practical investigation of interfaces is the inhomogeneity of the SERS substrate across the sample at the nanoscale, which makes it impossible to achieve spatially resolved quantitative analysis of interfaces, especially for applications of detection of toxins and contaminations in food science (Bailo & Deckert, 2008; Campion & Kambhampati, 1998; Cialla et al., 2012; Dieringer et al., 2006; Nie & Emery, 1997; Stiles, Dieringer, Shah, & Van Duyne, 2008). Wessel (1985) proposed a scheme to ensure a constant field enhancement using just one single metal nanoparticle for the investigation of a surface, which, for the first time, demonstrated the potential of quantitative SERS surface analysis at nanoscale. In this design, a sharp metal tip, which acted as an exclusive active site, replaced the rough metal film. The AFM tip was then scanned over the sample surface. Such a setup is now famous as tip-enhanced Raman scattering (TERS). The later experimental verification of this approach proved that, in addition to the field enhancement, the lateral resolution of the method was also improved down to 10 nm, due to the small end radius of the probe (Anderson, 2000; Hartschuh, Sánchez, Xie, & Novotny, 2003; Hayazawa, Inouye, Sekkat, & Kawata, 2000; Pettinger, Picardi, Schuster, & Ertl, 2002; Stöckle, Suh, Deckert, & Zenobi, 2000). The reason of large enhancement and high spatial resolution of Raman signal in TERS setup can be attributed to two mechanisms: the electromagnetic effect and the chemical or charge transfer effect, which apply only to the first layer of adsorbates (Bailo & Deckert, 2008; Stiles et al., 2008). A typical setup of TERS is shown in Fig. 10.11.

Since the first experimental realization of TERS, several research groups have been working in different directions to improve the technique further and expand its applications. Its high lateral resolution and high chemical specification make TERS a potent technique for analyzing and detecting food-involved chemical and biological molecules. A good example is the application of TERS in the study formation of biofilms formed by contaminations of bacteria and organisms, which are one of the key problems in the food and beverage manufacturing industry. Budich et al. utilized TERS to detect membrane components of

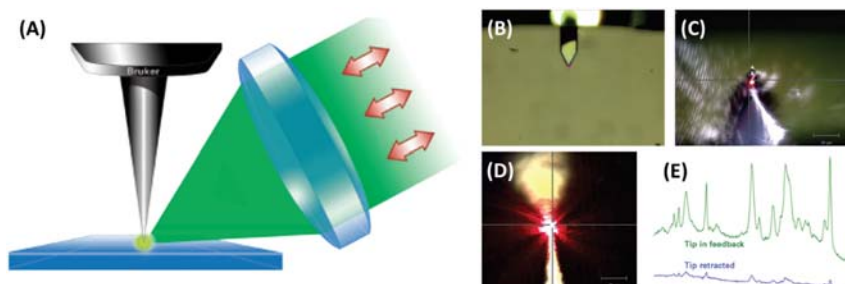


**Figure 10.11** (A) Schematic diagram of tip-enhanced Raman scattering (TERS) setup. (B) Top view of atomic force microscopy (AFM) probe for TERS. (C) Zoom-in view of AFM tip under optical objective. (D) Optical view of TERS tip in contact with sample surface. (E) TERS results of malachite green on gold, acquired with Innova-IRIS system (Bruker, United States) combined with Renishaw inVia Raman Spectroscopy (Renishaw, Britain).

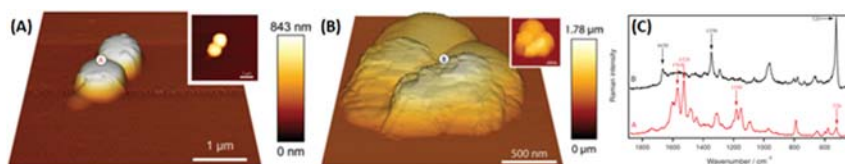


**Figure 10.12** 3D view of atomic force microscopy images of (A) two and (B) at least four *Staphylococcus epidermidis* cells placed on a clean glass cover slide. (C) tip-enhanced Raman scattering results at marked spots in (A) and (B). (A)–(C) are adapted with permission from Budich, C., Neugebauer, U., Popp, J., & Deckert, V. (2008). Cell wall investigations utilizing tip-enhanced Raman scattering. *Journal of Microscopy*, 229(3), 533–539; Copyright (2008) The Royal Microscopical Society.

agglomerated *S. epidermidis*, as shown in Fig. 10.12 (Budich, Neugebauer, Popp, & Deckert, 2008). They detected Raman signals of peptide/protein on cells, shown in Fig. 10.12A; or signals of lipids and saccharides/peptides mixtures on cells, shown in Fig. 10.12B. The spectra on different cells demonstrated differences, as shown in Fig. 10.12C; nevertheless, both suggested traces of Gram-negative bacteria. In summary, this work showed capability of TERS in investigation of surface structure of cell walls with high chemical specificity.

Rusciano et al. observed an external glycoprotein layer on the spore surface of *Bacillus subtilis* using a 14-nm gold nanoparticle coated AFM probe and correlated the TERS signal to the AFM phase mapping (Rusciano et al., 2014). Naumenko et al. used TERS to highlight the glucose dehydrogenase (GDH) protein spectrum analysis with electrochemical etching gold wire (Naumenko et al., 2013). Such results revealed great

potential application of TERS in biofilm research. The operation in TERS is based on AFM and therefore provides easy and natural sample preparation, preserving clues of biofilm formation.

Another good example is that Neugebauer et al. used TERS to observe single *S. epidermidis*. They reported DNA, RNA, and sugar on membrane surface of using silver-coated probe (Neugebauer et al., 2006; Neugebauer et al., 2007). The cell surface of *S. epidermidis* is mainly composed of a peptidoglycan layer with pervaded polysaccharides and a variety of surface proteins, which is a typical composition of the cytoplasm membrane in all Gram-positive bacteria. It is also likely to find teichoic acid or polysaccharide intercellular adhesion, depending on the growth conditions. Fig. 10.13 shows the topographic image of *S. epidermidis* obtained in tapping mode AFM using an ultrasharp silver-coated tip. The first TERS spectra (as shown in

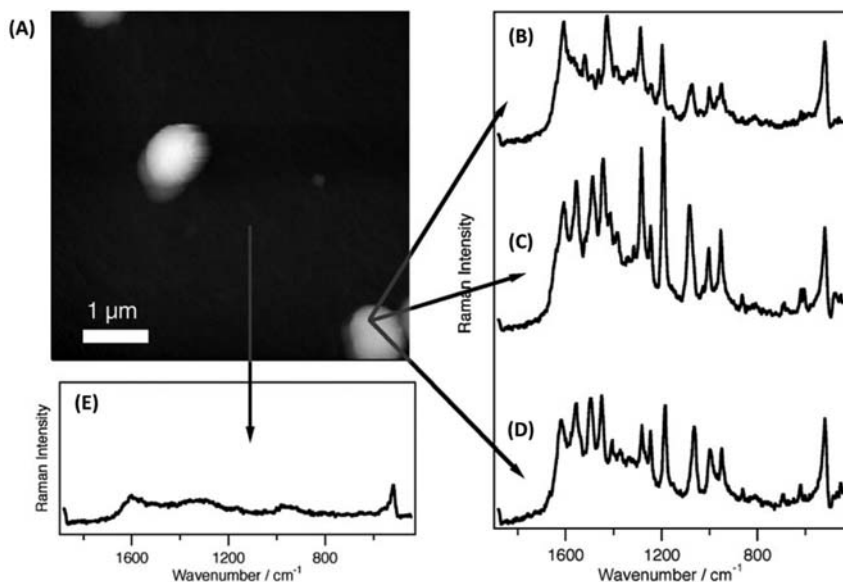


**Figure 10.13** (A) Topographic image of *Staphylococcus epidermidis* with marked locations of the corresponding tip-enhanced Raman scattering (TERS) measurements. (B)–(D) denote TERS spectra measured with a silver-coated atomic force microscopy tip on top of a bacterium, whereas (E) corresponds to a reference TERS measurement on the glass surface. The band around  $520\text{ cm}^{-1}$  is attributed to Raman scattering of the silicon tip. (A)–(E) are adapted with permission from Neugebauer, U., Rösch, P., Schmitt, M., Popp, J., Julien, C., Rasmussen, A., ... Deckert, V. (2006). On the way to nanometer-sized information of the bacterial surface by tip-enhanced Raman spectroscopy. *Chemphyschem: A European Journal of Chemical Physics and Physical Chemistry*, 7(7), 1428–1430; Copyright (2006) WILEY-VCH Verlag GmbH & Co. KGaA, Weinheim.

Fig. 10.13B–D) were from the cell surface, and the second spectrum (recorded in Fig. 10.13E) corresponded to a background reference of the glass surface. The enhancement factor was calculated to be around  $10^4$ – $10^5$ . The majority of TERS peaks on the bacteria surface could be assigned to peptides, lipids, and carbohydrates abundant on the cell surface of bacteria (Neugebauer et al., 2007). As demonstrated in this work that TERS could be performed even on complex organisms, intriguing possibilities arise, and the work implies wide applications ranging from a simple reduction in background signals due to the high lateral resolution, to the study of diffusion dynamics of single proteins on the cell surface (Neugebauer et al., 2006).

### 10.3.3 Prospect of atomic force microscopy-Raman applications in food science

The TERS enabled real synergy of AFM and Raman techniques and enlarged application of SERS and achieved high spatial resolution structural investigation. With TERS, one can study samples over different sample conditions, such as in liquid and in vivo, which is critical in food analysis and detection. Presently, TERS has demonstrated its capability in detection of trace amounts of inorganic materials (like carbon nanotubes, silicon, etc.) (Hayazawa et al., 2000; Ramirez-Aldaba et al., 2018; Stöckle et al., 2000), organic compounds (such as benzenethiol, rhodamine, etc.) (Ivanova & Spiteller, 2014; Sharma, Jaiswal, Duffy, & Jaiswal, 2019; Wessel, 1985), biomacromolecules (including DNA, RNA, peptides, etc.) (de sa Peixoto et al., 2015; Huang et al., 2020; Ramirez-Aldaba et al., 2018; Sarabia-Sainz et al., 2017). These results have proven that TERS would be an ideal approach for detecting toxins and microbes in food industry.

The most prominent feature of TERS is its high chemical specificity which allows detection at extremely low sample concentrations. It provides a molecular view of small ensembles of molecules, even at the single-molecule level. This feature suggests the potent capability of TERS in the investigation of interaction at the molecular level. One, but may not the only one ultimate goal of TERS in terms of application is label-free identification of sequency structure of biomacromolecules, including DNA/RNA, proteins, polysaccharides, and so on. Nowadays, the main challenge lies in reproducible mass preparation of TERS tips. One thing is that the enhancement factor could not be controlled accurately with high repeatability. Another limit is that the tip would pick up material easily or even damage during imaging. Many researchers and groups are working to standardize TERS probe fabrication and prepare robust probes. Once this obstacle is removed, the commercially available

TERS probes would greatly expand TERS' applications in practical food science. The potent AFM imaging would provide various information, including morphologies and mechanical properties, of test samples *in vivo* or *in vitro*. At the same time, TERS would reveal its chemical components, and what's more, such analysis would be routine and fast, which is required in toxin detection, study of microbe's contamination of food package materials, and so on. Such fast and quantitative analysis could be used to review dynamic processes at molecular scale, such as food production, transportation, cooking, and spoilage.

## 10.4 Other atomic force microscopy-combined techniques and their potential applications in food science

### 10.4.1 Atomic force microscopy combined with mass spectrometry

The utilization of mass spectrometry (MS) has grown rapidly in food analysis and food safety, including capillary electrophoresis-MS (Ibáñez, Simó, García-Cañas, Cifuentes, & Castro-Puyana, 2013), liquid chromatography-MS (Di Stefano et al., 2012; Malik, Blasco, & Picó, 2010), matrix-assisted laser desorption ionization coupled to time-of-flight MS (MALDI-TOF-MS), and ambient ionization MS (electrospray ionization [ESI] or atmospheric pressure chemical ionization) (Wang, Wang, & Cai, 2013). Among them, ESI and MALDI have been the most used methods for food analysis (Pernemalm & Lehtio, 2014; Zhong, Zhang, Jiang, & Li, 2014). They are suitable for large molecules analysis such as protein (Calvano, De Ceglie, & Zambonin, 2014; Usbeck, Kern, Vogel, & Behr, 2013), lipid (Shen et al., 2013), polymer (Romão et al., 2010), DNA (Pattemore, Rice, Marshall, Waugh, & Henry, 2010), even for the detection of food adulteration, protein structural modification after processing (Kawasaki, Shimomae, Watanabe, & Arakawa, 2009; Kern, Usbeck, Vogel, & Behr, 2013; Law, 2010; Marchetti-Deschmann et al., 2012; Marcos et al., 2013). The topography features from AFM and chemical information from MS can be obtained in real time (Liang et al., 2016). Since 2000, several AFM-MS combined systems have been reported (Lee et al., 2004; Wetzal et al., 2005).

Ovchinnikova et al. studied thin-film caffeine surfaces by a combined AFM-MS system. A nanothermal analysis (nano-TA) probe with ESI-MS obtained the coregister local nanomechanical measurements and topography using AFM with MS-based chemical profiling of specific surface features, as shown in Fig. 10.14 (Ovchinnikova, Nikiforov, Bradshaw, Jesse, & Van Berkel, 2011; Price, Reading, Hammiche, & Pollock, 1999). The nano-TA



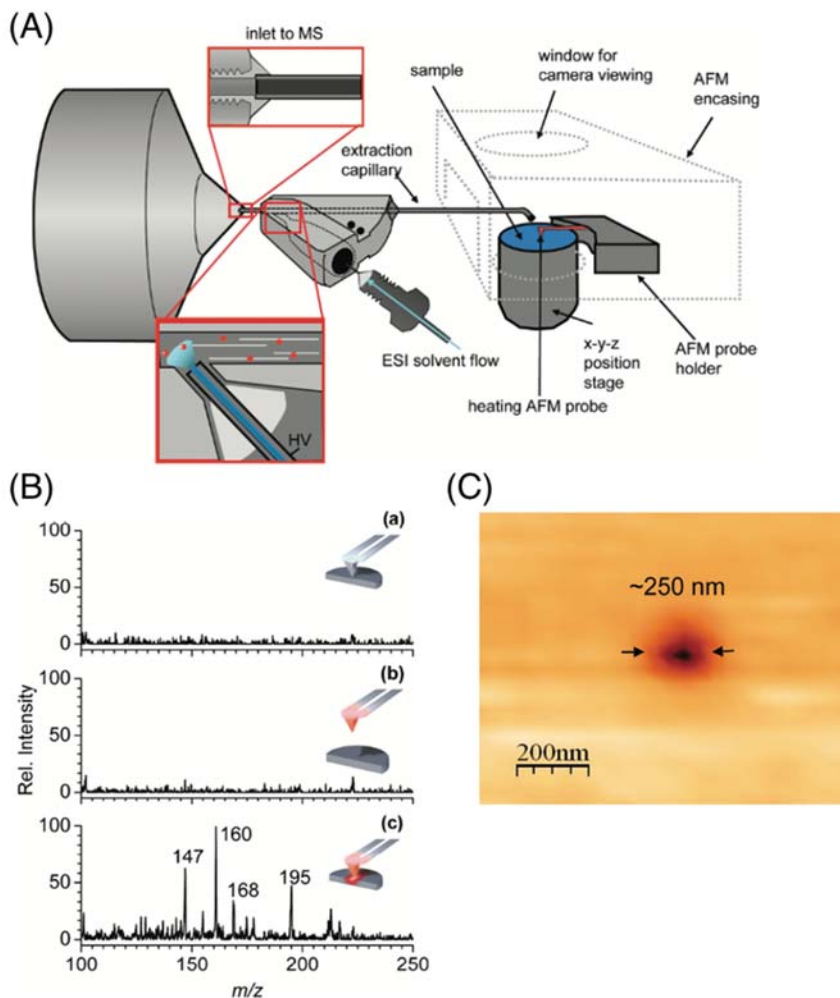


**Figure 10.14** (A) Molecules under the heated tip can be absorbed into extraction capillary. (B) The mass spectra of thin film caffeine surface, while (a) tip was on the surface but not heated, (b) tip was retracted from surface and heated, (c) tip was on the surface and heated. (C) The crater which was heated by tip. (A) to (C) are adapted with permission from Ovchinnikova, O. S., Nikiforov, M. P., Bradshaw, J. A., Jesse, S., & Van Berkel, G. J. (2011). Combined atomic force microscope-based topographical imaging and nanometer-scale resolved proximal probe thermal desorption/electrospray ionization—mass spectrometry. *ACS Nano*, 5(7), 5526-5531, Copyright (2011) American Chemical Society.

probe with 30 nm tip was heated to 350°C. By 30-s sampling time, it made a 250 nm diameter and 100 nm deep conical desorption craters on caffeine surface. Desorbed intact caffeine molecules from surface can be ionized by an AP secondary ionization source. Similar setup was also reported by Owens et al. (Owens, Berenbeim, Patterson, Dillon, & de Vries, 2014).

In 2015, Ovchinnikova et al. developed a hybrid AFM-MS instrument. Compared to previous methods which MS information can only be obtained from an individual spot or a series of a few spot samples, this hybrid AFM-MS can obtain coregistered topographical and mass spectral imaging (Ovchinnikova et al., 2015). Poly(2-vinylpyridine) (P2VP) was used in nanotech gels to monitor food freshness. In the experiment, shown in Fig. 10.15, a nano-TA probe was used for thermal desorption/secondary ionization MS. Coregistered topography and mass spectral imaging were obtained by comparing the MS sampling time and nano-TA probe position. P2VP islands can be distinguished from block copolymer polystyrene-block-poly(2-vinylpyridine) (PS-*b*-P2VP) using coregistered topography, elastic modulus, and MS chemical image.

### 10.4.2 Atomic force microscopy combined with optical microscopy

Optical microscopy (OM) is the most appropriate and standard technique for food structure evaluation (Kaláb, Allan-Wojtas, & Miller, 1995). The resolution of modern OM is about 200–300 nm in  $x$  and  $y$  directions and 500 nm in  $z$  direction. With the development of new microscopy imaging techniques, such as epifluorescence microscopy, confocal microscopy, and super-resolution microscopy, they have tremendously improved the resolution and range of OM applications in food science (Auty, 2013; Bonilla & Clausen, 2022; Ferrando & Spiess, 2000; Hohlbein, 2021; Zhu, Zhou, & Sun, 2019). Combined AFM with OM techniques could obtain 3D topography, mechanical properties, chemical maps, optical, fluorescence, and super-resolution images simultaneously (Dufrêne et al., 2017; Muller et al., 2021).

Unsaturated fatty acid has important nutritional value. Hohlbein et al. (Yang, Verhoeff, Merckx, van Duynhoven, & Hohlbein, 2020) used confocal laser scanning microscopy to investigate the lipid anti-oxidant mechanics of ascorbic acid in mayonnaise. Ascorbic acid can prevent lipids oxidant with the help of lipid-soluble antioxidant by converting tocopherol radicals to tocopherol. On the contrary, it will

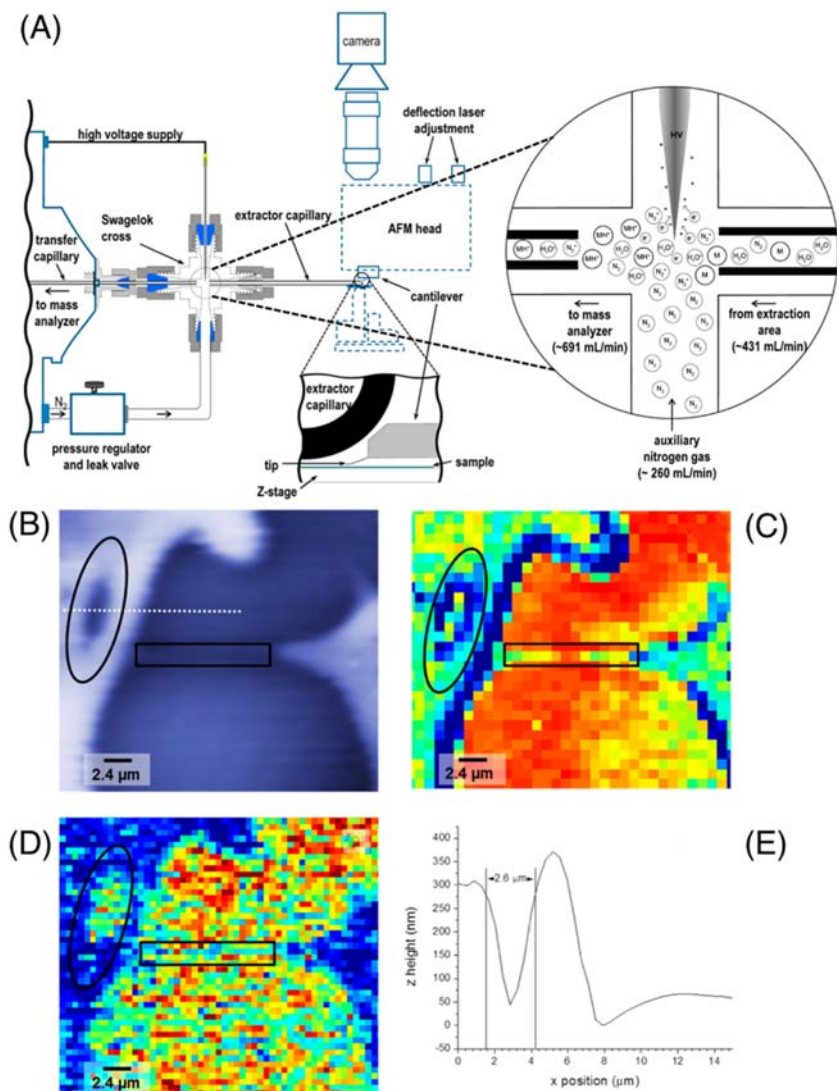


**Figure 10.15** (A) Schematic diagram of hybrid atomic force microscopy (AFM)-MS setup. (B) AFM topography image of polystyrene-block-b-poly(2-vinylpyridine) (PS-b-P2VP). (C) Elastic modulus of PS-b-P2VP. (D) MS chemical image for  $m/z$  (mass charge ratio) 106. (E) White dot cross-section line in (B) of circular area. Both the elastic modulus and mass spectrometry chemical image indicate this is a P2VP island. (A)–(E) are adapted with permission from Ovchinnikova, O. S., Tai, T., Bocharova, V., Okatan, M. B., Belianinov, A., Kertesz, V., . . . Van Berkel, G. J. (2015). Co-registered topographical, band excitation nanomechanical, and mass spectral imaging using a combined atomic force microscopy/mass spectrometry platform. *ACS Nano*, 9(4), 4260-4269; Copyright (2015) American Chemical Society.

be prooxidant if lipids drops are stripped at the interface and water phase. If combined with single molecular modified AFM tips, the components and mechanics of antioxidant species may be better understood.

Casein micelles (CMs) are important components of milk. The destabilization of CMs in lower pH is essential for producing dairy foods such as cheese and yogurt. Voets et al. (Foroutanparsa, Brüls, Tas, Elizabeth P. Maljaars, & Voets, 2021) used direct stochastic optical reconstruction microscopy (dSTORM) to probe individual CMs at their hydrated state at each given pH before gel network formation. dSTORM is a kind of single-molecule localization microscopy (SMLM) which has super-resolution at about 10 nm. If combined with AFM, fluorescently labeled fine structures, and AFM topography of CMs can be obtained simultaneously at single molecular level.

Recently, Odermatt et al. (2015) combined two kinds of SMLM and AFM to investigate biological samples, as shown in Fig. 10.16. F-actin was chosen as a test sample to compare and validate the resolution of dSTORM and AFM topography. Fixed bacterial and mammalian cells were chosen as test samples to obtain 3D morphology structure from AFM and 2D projection of spatial distribution of fusion protein simultaneously. The combination of SMLM and AFM can

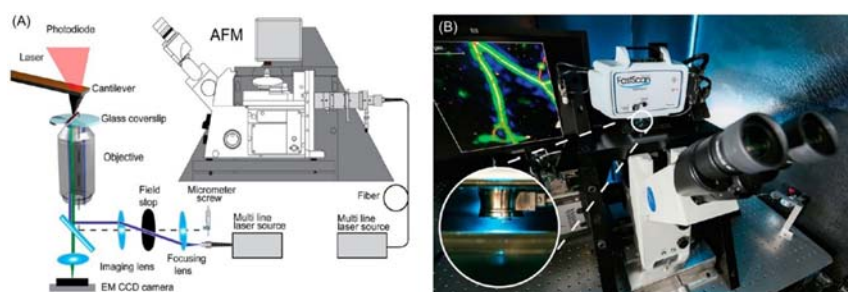


**Figure 10.16** Atomic force microscopy (AFM)-single-molecule localization microscopy instrument setup. (A) Schema of optical path with cantilever. (B) Inverted optical microscope is mounted on an  $x/y$  translation stage. A FastScan AFM head is mounted on mechanical support without contacting the optical microscopy body. (A) and (B) are adapted with permission from Odermatt, P. D., Shivanandan, A., Deschout, H., Jankele, R., Nievergelt, A. P., Feletti, L., . . . Fantner, G. E. (2015). High-resolution correlative microscopy: Bridging the gap between single molecule localization microscopy and atomic force microscopy. *Nano Letters*, 15(8), 4896-4904; Copyright (2015) American Chemical Society.

provide complementary information about different aspects of the biological samples.

### 10.4.3 Atomic force microscopy combined with X-ray techniques

X-ray techniques, including X-ray photoelectron spectroscopy (XPS), X-ray diffraction (XRD), and so on, are powerful tools that can identify the elements and their chemical state on the sample surface, as well as determine the atomic and molecular structure of crystalline materials. In food science, these techniques are extensively used for food composition (Esmaili et al., 2018; Fyfe et al., 2011; Gaiani et al., 2006, 2009; Jafari, Assadpoor, Bhandari, & He, 2008; Li et al., 2017; Porras-Saavedra et al., 2015; Wojtczak et al., 2018; Zhao, Ao, Du, Zhu, & Liu, 2010), quality (Oliveira, Barros, Rosell, & Steel, 2017; Purohit & Rao, 2017; Wang et al., 2007; Zhou et al., 2015), contamination (Araujo-Díaz, Leyva-Porras, Aguirre-Bañuelos, Álvarez-Salas, & Saavedra-Leos, 2017; Athmaselvi, Kumar, Balasubramanian, & Roy, 2014; Calligaris, Arrighetti, Barba, & Nicoli, 2008; Chiavaro, 2013; Miyagawa, Shintani, Katsuki, Nakagawa, & Adachi, 2017; Stevenson, Doorenbos, Jane, J-I, & Inglett, 2006), process (Bugeat et al., 2015; Dharmaraj, Parameswara, Somashekar, & Malleshi, 2014; Lopez, Lesieur, Bourgaux, Keller, & Ollivon, 2001; Lopez, Lesieur, Keller, & Ollivon, 2000; Lopez, Mathers, Ezzati, Jamison, & Murray, 2006; Ramel & Marangoni, 2017), and package (Atapour et al., 2019; Biswas, Tiimob, Abdela, Jeelani, & Rangari, 2019; Chen, Zhou, Zou, & Gao, 2019) analysis. Combined AFM with X-ray techniques, local X-ray absorption or diffraction information, and surface topography on the nanoscale can be obtained simultaneously.

Rodrigues et al. designed an optics-free AFM which can be installed on most of the synchrotron radiation end-stations for AFM and X-ray combined experiments. By using the tuning fork tips, spectroscopy and diffraction data can reach about 100 times better lateral resolution compared to conventional instrument (Rodrigues et al., 2008; Scheler et al., 2014). In Fig. 10.17, surface topography was obtained by the tuning fork AFM, and an X-ray beam whose intensity can be modulated by a chopper was aligned under tip. The photoemitted electrons from sample or tip were induced on the tip and transferred to current which was synchronously detected. Several different AFM-X-ray combined systems have been designed in recent years, including AFM combined with XRD, grazing incidence X-ray scattering, grazing incidence diffraction

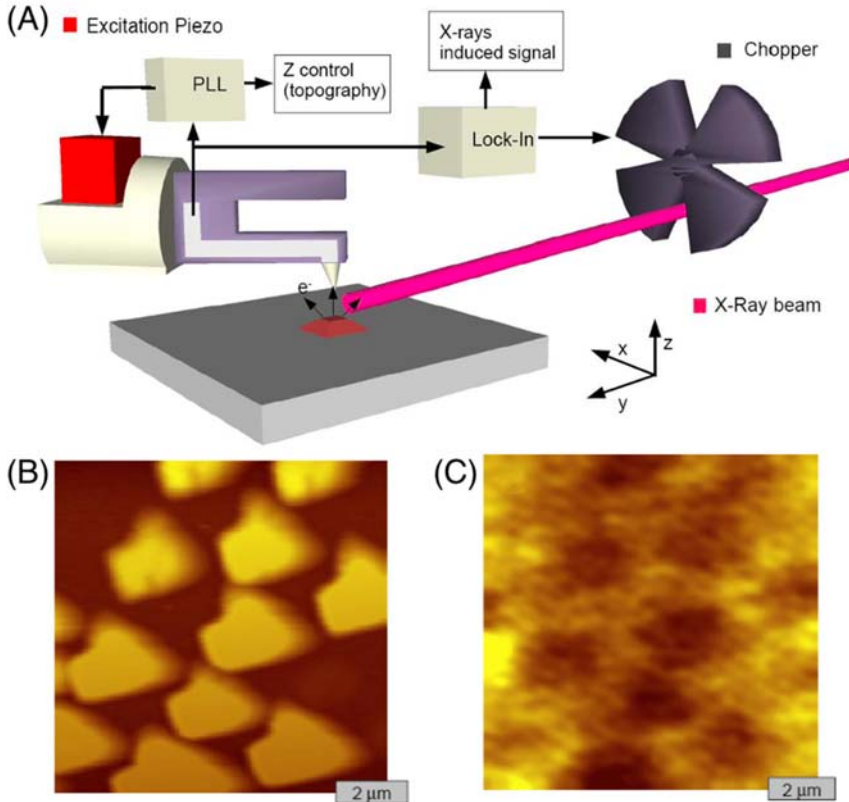


**Figure 10.17** (A) Schematic diagram of combined tuning fork atomic force microscopy (AFM) and X-ray. The X-ray absorption signal was reflected by the current induced on the tip. (B) AFM topography image of sample with SiGe island (86% Si, 14% Ge). (C) Current image of sample with SiGe. Darker areas correspond to SiGe islands. (A) to (C) are adapted with permission from Rodrigues, M. S, Dhez, O., Denmat, S. L., Chevrier, J., Felici, R., & Comin, F. (2008). Local detection of X-ray spectroscopies with an in-situ atomic force microscope. *Journal of Instrumentation*, 3(12); Copyright (2008) Institute of Physics.

(Slobodskyy et al., 2015; Vitorino et al., 2016), and X-ray transmission microscope (Schmid et al., 2010).

Biaxial-oriented polypropylene film is a kind of food package material that has a high barrier against permeation of gases, moisture, and flavor. The relation between its roughness and oxygen content was analyzed by AFM and XPS (Moosheimer & Bichler, 1999). Poly (lactic acid) is good material for food packaging due to its environment friendly properties, such as biodegradability and biocompatibility. However, it needs

modification to overcome its high permeability of gases. Using both AFM with XRD, topography and crystallinity information can be obtained (Kaczmarek, Nowicki, Vuković-Kwiatkowska, & Nowakowska, 2013). AFM can show the surface topography and mechanical properties, well X-ray data can reveal the ordered crystalline phase in deeper layers of polymer films. The combined technique can help understand, design, and review modification process.

#### 10.4.4 Atomic force microscopy combined with nanodynamic mechanical analysis

Mechanical properties of many materials express strong time dependence, which is well known as viscoelasticity. Viscoelastic behavior reflects the combined viscous and elastic responses, under mechanical stress of materials (Ferry, 1980). Dynamic mechanical analysis (DMA) is one of the most appropriate methods to investigate viscoelastic properties. DMA works by applying an oscillating force to the material, and the resultant displacement of the sample is measured.

AFM can combine with DMA to measure viscoelastic behavior at nanoscales. In the AFM-nDMA setup, AFM probe is utilized as a stylus to periodically compress on sample. Driven by a sine wave with desired frequency, the probe applies oscillating force on the sample while the force is analyzed by a cantilever deflection signal. In the meantime, scanner movement is captured, shown in Fig. 10.18. Sample deformation could be deduced by subtracting cantilever deflection from scanner movement. From records of cantilever deflection and sample deformation, one could calculate sample's stiffness as a function of driving frequency. Next, contact mechanism is taken into consideration to obtain moduli information from stiffness results.

AFM-nDMA technique has been employed to study viscoelastic properties at nanoscale in various materials, especially polymer, which is widely used in the food packing industry. Epitaxial lamellar of advanced polymers are key in packing industry, and the structural-property relationship of the synthesized polymer guides researchers in designing and improving novel packing materials. AFM imaging has been widely utilized to study the orientation and microphase-separation behavior of packing polymers in epitaxial lamellar (Varghese et al., 2020; Wang et al., 2005; Wu et al., 2018; Magonov, 2006). Bulk DMA technique is nearly a routine approach for studying viscoelastic properties and glass-transition temperature of packing polymers (Marin et al., 2015; Mishra, Ha, Verma, & Tiwari, 2018;

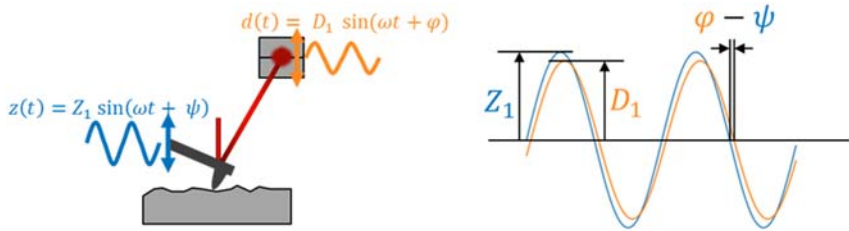


**Figure 10.18** Principle of AFM-nDMA. (A) An oscillating force with a drive frequency  $\omega$  is applied to AFM probe, and the force is measured by deflection signal,  $d(t)$ , while scanner movement is also recorded as  $z(t)$ . (B)  $d(t)$  and  $z(t)$  are recorded and analyzed, while the phase difference  $\varphi - \psi$  is calculated for further viscoelastic characterization.

Ning et al., 2012; Varghese et al., 2020; Wang et al., 2005; Wu et al., 2018; Yang & White, 2012; Carr, 2013; Magonov, 2006). However, previous work mingled average behavior obtained from DMA with local structural information imaged under AFM. Now, equipped with AFM-nDMA combination technique, one could utilize the AFM probe as a stylus for DMA. After capturing morphology, orientation, and chemical information of interested regions, the AFM probe is then compressed such region under desired driving frequency, and finally, the local viscoelastic property is revealed with spatial resolution down to tens of nanometers. Since the interface behavior at nanoscale determines macroscale properties (Cheng et al., 2016; Nguyen, Liang, Ito, & Nakajima, 2018; Qu et al., 2011; Ueda, Liang, Ito, & Nakajima, 2019; Wang et al., 2010), AFM-nDMA would reveal more details of epitaxial lamellae at interface, enabling researchers to design advanced packing polymers.

### 10.4.5 Atomic force microscopy combined with nuclear magnetic resonance

NMR spectroscopy is one of the most accepted methods for determining the structural properties of macromolecular such as proteins, polysaccharides, and nucleotides. This method can analyze the composition and measure the physicochemical properties and functionality of food in its natural status. Its popularity increased rapidly among food scientists (Hatzakis, 2019). The applications of NMR in food science include authentication and classification (Dais & Hatzakis, 2013; Marcone et al., 2013; Spyros & Dais, 2012), quality control (Marcone et al., 2013), sensory evaluation (Malmendal et al., 2011), structural and compositional



analysis (Bertocchi & Paci, 2008; Cheng & Neiss, 2012; Vlahov, 1999), molecular mechanism in food components (Fernandes, Brás, Mateus, & Freitas, 2015; Leydet et al., 2012; Tiziani, Schwartz, & Vodovotz, 2008), as well as relation between nutrition and health (Ramakrishnan & Luthria, 2017). The chemical information from NMR as well as structural and mechanical information from AFM can be obtained simultaneously if we can combine AFM and NMR (de sa Peixoto et al., 2015; Rainey & Goh, 2002; Zhang, Dai, Deng, & Zhao, 2015).

Mousoulis et al. fabricated radio frequency (RF) planar micro coils on top of commercial AFM cantilevers. Operating in 500 MHz high-frequency NMR magnets, this AFM/NMR probe can obtain physical features (e.g., mechanical stiffness) in nanoscale resolution of AFM and spectroscopic information of NMR in real-time, as shown in Fig. 10.19 (Mousoulis, Maleki, Ziaie, & Neu, 2013).

A few works used both AFM and NMR, but applications in food science using real combined systems werenot reported. By using both solid-state

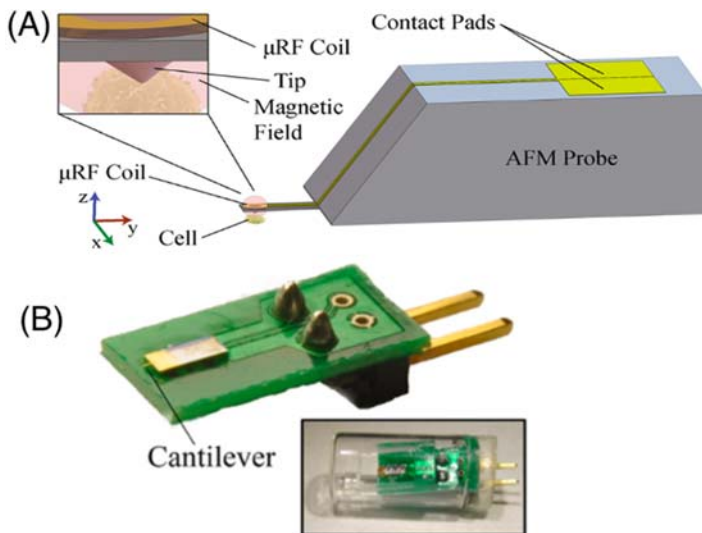


**Figure 10.19** (A) A radio frequency (RF) coil was fabricated on the backside of a commercial atomic force microscopy cantilever by focused ion beam, which Parylene-C works as insulator. The gold coil was both transmitter and receiver of the RF pulse. (B) The cantilever was adhesive to a custom-designed printed circuit board. (A) and (B) are adapted with permission from Mousoulis, C., Maleki, T., Ziaie, B., & Neu, C. P. (2013). Atomic force microscopy-coupled microcoils for cellular-scale nuclear magnetic resonance spectroscopy. *Applied Physics Letters*, 102(14), 143702; Copyright (2013) American Institute of Physics.

NMR and AFM, it is possible to get high-resolution information on bacterial surface layers (S-layers) at nanoscale, even angstrom scale, which is difficult to be reached by crystallography and electron microscopy in S-layer proteins research (de sa Peixoto et al., 2015). High hydrostatic pressure treatment of squid tropomyosin Tod p1 (a water-soluble 38 kDa protein, TMTp1) changed the surface topography, characteristic domain, and allergenicity. Their connections can be investigated by combining NMR characteristic regions and AFM topography images (Zhang et al., 2015).

#### 10.4.6 Atomic force microscopy combined with force-loading stage

The tensile, anti-fatigue, and wearproof performance of package materials are very important in food industry. Food and food packages would undergo extruding, stretching, or shearing process during their manufacture and transportation. Monitoring the changing of topography and mechanical properties in situ when applying loading force is very helpful for researchers to understand the food process and develop food package materials with higher mechanical performance.

It is not complicated to combine a force-loading stage with a tip-scanning AFM, which has enough room for the stage under AFM probe for AFM measurement. Homemade and commercial solutions have already been widely used in materials research fields. The easiest method is just to keep one state of sample with a certain loading force and do AFM measurement. As shown in Fig. 10.20A, Bagrov et al. fixed pre-stretched film to the circular frame for AFM measurement (Bagrov et al., 2014). Zhang et al. used a frame with a steel rod shown in Fig. 10.20B to lock the pre-stretched rubber for in situ measurement (Zhang, Sun, et al., 2020). However, the condition of sample cannot be changed during measurement. Homemade force-loading stage, with motors and force sensors to control the position and loading force, as shown in Fig. 10.20C, can be placed on the sample stage of AFM. Therefore, AFM can scan the same area of sample under different loading forces to monitor the changes of topography and mechanical properties. With this setup, Seshadri et al. acquired the changes in topography of human hair under a series of strains to study the affection of physical and chemical damage on hair, shown in Fig. 10.20C and D (Seshadri & Bhushan, 2008). Similar force-loading stage designs have been widely used to stretch polymer film (Bokobza, Bresson, Garnaud, & Zhang, 2012; Tambe & Bhushan, 2004; Thomas, Ferreiro, Coulon, & Seguela, 2007), and even cell wall of onion

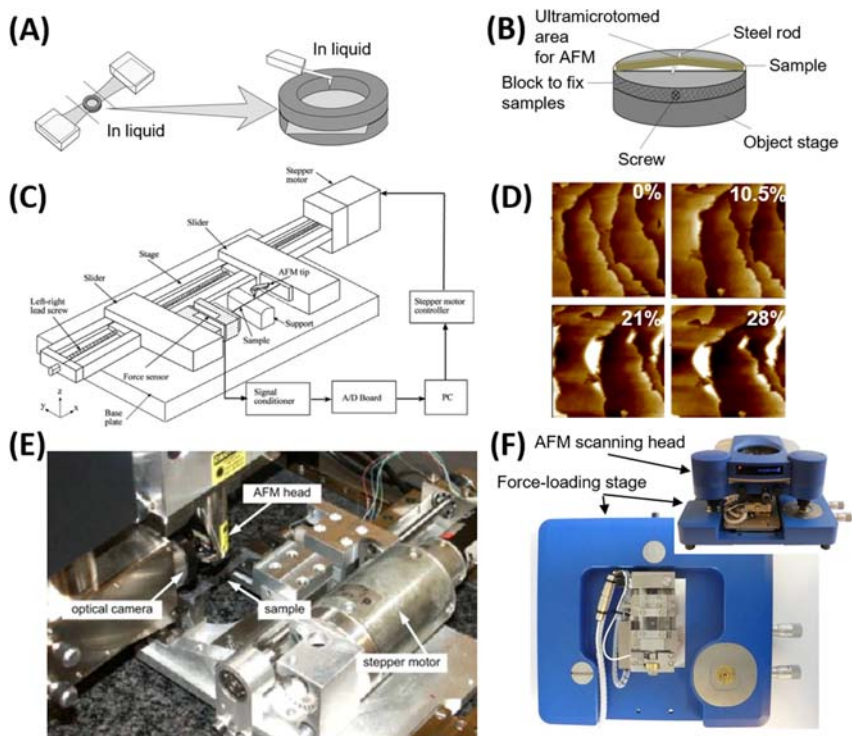


**Figure 10.20** (A) and (B) Two methods to hold the prestretched film for atomic force microscopy (AFM) measurement. (C) Scheme of a home-built force-loading stage. (D) AFM topography of human hair under the strain of 0%, 10.5%, 21%, and 28%. (E) AFM is used to study the properties changes of polymer film in situ with a homemade force-loading stage. (F) A kind of commercial AFM and force-loading stage combination system from Bruker. (A) is adapted with permission from *Bagrov et al. (2014)*; Copyright (2013) Royal Microscopical Society. (B) is adapted with permission from *Zhang, Sun, et al. (2020)*; Copyright (2020) American Chemical Society. (C) and (D) are adapted with permission from *Seshadri and Bhushan (2008)*; Copyright (2007) Elsevier Ltd. (E) is adapted with permission from *Thomas et al. (2007)*; Copyright (2007) Elsevier Ltd.

(Zhang, Vavylonis, Durachko, & Cosgrove, 2017). Zhang et al. studied the orientation changing and movement of cellulose microfibrils in the onion cell walls during the elastic and plastic stretching progress (Zhang et al., 2017). Commercial solutions are also available. Fig. 10.20F shows one commercial force-loading stage from Bruker.

Besides stretching samples, shearing testing is used to study the cracks inside samples. George et al. studied the shear yielding property of poly-methyl methacrylate (PMMA) by measuring the cracks growth on its surface with double cleavage drilled compression (DCDC) method

(George et al., 2018). As shown in Fig. 10.21A and B, a hole was punched on a cuboid of PMMA, and stress was applied along x direction to press the sample by force-loading stage. The cracks grew slowly along x direction, which was recorded by AFM, marked in Fig. 10.21C. Preiß et al. evaluated the fracture toughness of ultrathin gold film by monitoring the crack growth on the film by bending the film with gas pressure, as shown in Fig. 10.21D (Preiß, Merle, & Göken, 2017).

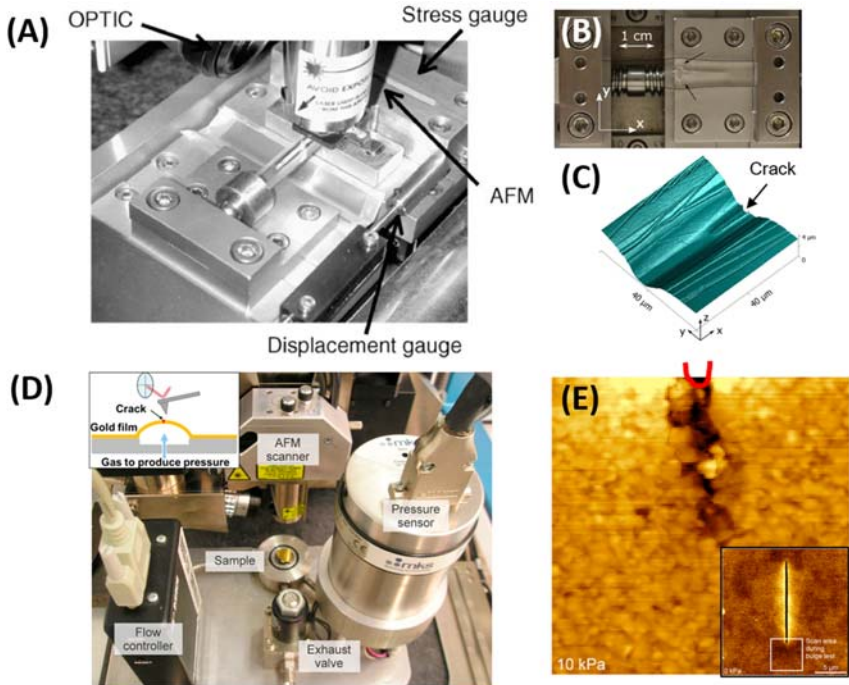


**Figure 10.21** (A) Setup for a combination of atomic force microscopy (AFM) with force-loading stage. (B) Setup of force-loading stage for DCDC method. (C) AFM topography, the crack was marked by an arrow. (D) Setup for fracture toughness measurement of ultrathin gold film. Inset: gold film is supported by the frame and bent by gas pressure. (E) AFM image shows the front of crack growth under gas pressure of 10 kPa. Red line refers to the end of the through-thickness linear notch. Inset: AFM image of the notch under zero loading force. White square marks the scanning region of (E). (A) to (C) are adapted with permission from George, M., Nziakou, Y., Goerke, S., Genix, A. C., Bresson, B., Roux, S., . . . Ciccotti, M. (2018). *In situ* AFM investigation of slow crack propagation mechanisms in a glassy polymer. *Journal of the Mechanics and Physics of Solids*, 112, 109–125; Copyright (2017) Elsevier Ltd. (D) and (E) are adapted with permission from Preiß, E. I., Merle, B., & Göken, M. (2017). *Understanding the extremely low fracture toughness of freestanding gold thin films by in-situ bulge testing in an AFM. Materials Science and Engineering: A*, 691, 218–225; Copyright (2017) Elsevier Ltd.

A through-thickness linear notch was introduced onto the film, and the crack can grow along the line, shown in Fig. 10.21E.

### 10.4.7 Atomic force microscopy combined with fluidic force microscopy

Fluidic force microscopy, also known as FluidFM, becomes more and more popular in biological research field. Meister et al. developed FluidFM technique to execute single-cell injection and nanoprinting with AFM system (Meister, Gabi, et al., 2009; Meister, Polesel-Maris, et al., 2009). Now it has a commercial solution from Cytosurge AG, Switzerland. The core technology of FluidFM is the microchanneled probe. As shown in Fig. 10.22A, compared with a typical AFM probe, FluidFM probe has a channel buried inside the cantilever and a hole connecting to the channel at the tip. On the other side of the channel, a high-precision pressure-control pump is connected to produce suction or jet force at the tip of probe. The pump controls the volume with superhigh resolution of 0.1 pL during suction or injection (Guillaume-Gentil et al., 2016). There are three kinds of FluidFM probes, micropipette, nanopipette, and nanosyringe, as shown in Fig. 10.22C–E. Micropipette probe does

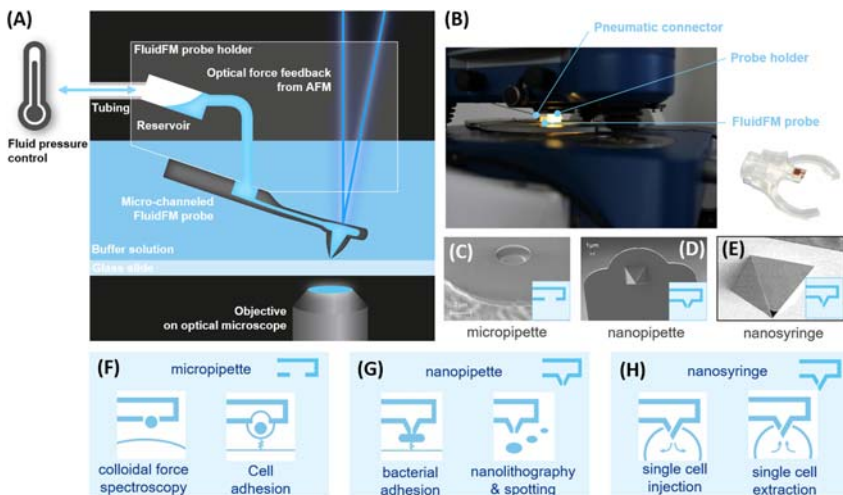


**Figure 10.22** (A) Scheme of FluidFM combined with atomic force microscopy (AFM). (B) Photo to illustrate the probe mounting on the head of AFM. (C)–(E) The SEM image of different kinds of FluidFM probes, including micropipette, nanopipette, and nanosyringe. (F)–(H) Typical applications of FluidFM probes.

not have tip, and the hole is just open on the front of cantilever. This kind of probe can be used to catch, manipulate, and release cells or colloid spheres for isolation of cells (Guillaume-Gentil, Zambelli, & Vorholt, 2014) and adhesion measurement (Helfricht, Mark, Dorwling-Carter, Zambelli, & Papastavrou, 2017; Potthoff et al., 2012). Nanopipette probe has a hole with flattened edge at the tip, which can manipulate cells like bacteria (Hofherr, Müller-Renno, & Ziegler, 2020), release inks for nanoprinting (Hirt et al., 2015) or 3D printing (Hirt et al., 2016). The front of nanosyringe probe has a hole with sharp end, which can stab through the membrane of cells like a knife, so that the probe can touch inside of cells and inject or suck contents (Guillaume-Gentil et al., 2016, 2017; Meister, Gabi, et al., 2009). The nanopipette or nanosyringe probes can perform AFM imaging as traditional AFM probes (Meister, Gabi, et al., 2009).

With a micropipette probe, cells strongly adhering to the surface can be isolated and manipulated for further AFM measurement and be possibly assembled to form artificial 3D structures and then confirmed by AFM, which have potential application in culturing artificial meat in laboratory. Nanopipette probe can catch bacteria on the surface of biomaterials to measure the adhesion force by AFM force spectroscopy and can be used to study the bacterial growth on the surface of food or food packages by monitoring topography and mechanical changing. Nanopipette probe can also transfer the contents in microchannel to substrate. It has been confirmed that FluidFM can construct complicated structures like a hollow vase or a triple helix (Hirt et al., 2016). It might be a potential reference for 3D printing food additives to study their effect on mouthfeel of food by mechanical measurement of AFM. Nanosyringe probe has been used to extract cytoplasmic or nucleus contents for further analysis, such as MS analysis (Guillaume-Gentil et al., 2017) for components analysis, fluorescent microscopy (Guillaume-Gentil et al., 2016) for enzymatic activity analysis, and quantitative polymerase chain reaction (Guillaume-Gentil et al., 2016) for gene transcription, etc., as shown in Fig. 10.23A–E, which should be useful in studying the physical and chemical properties changes in food process. This kind of probe can also perform injection experiments. Guillaume-Gentil et al. used it to study cellular transfection (Guillaume-Gentil et al., 2013). The vector of pmaxGFP was injected into nuclear region of HeLa cell with nanosyringe probe. The cell emitted green fluorescence of pmaxGFP after culture, as shown in Fig. 10.23F–I. With this special transfection technique, new heterozygous tissues can be designed, which can help promote new food materials development.

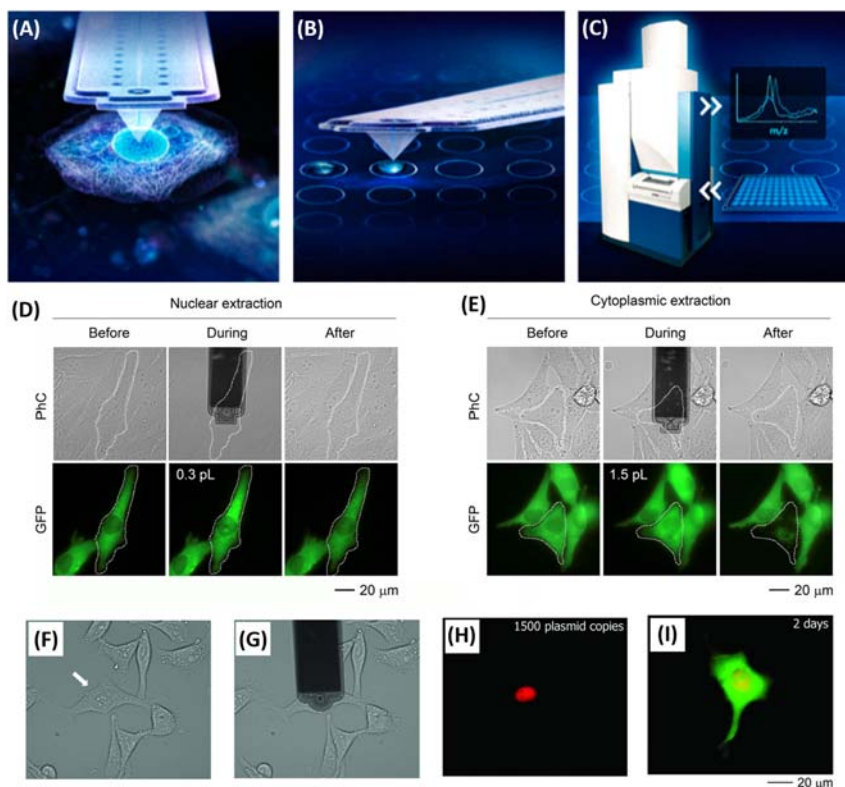


**Figure 10.23** (A) Using nanosyringe probe to extract metabolites from cytoplasm of live cell. (B) Nanosyringe probe releases the cytoplasmic extract onto sample plate of MS. (C) MS analysis on cytoplasmic extract. (D) Nuclear extract using nanosyringe probe. (E) Cytoplasmic extract using nanosyringe probe. (F–I) Transfection of a HeLa cell with pmaxGFP. Before (F) and during (G) injection into nucleus of HeLa cell. (H) The dextran-tetramethylrhodamine (red dye) is coinjected with vector of pmaxGFP into nucleus as a positioning indicator. (I) Two days after the injection, cell emitted green fluorescence. (A)–(C) are adapted with permission from [Guillaume-Gentil et al. \(2017\)](#); Copyright (2017) American Chemical Society. (D) and (E) are adapted with permission from [Guillaume-Gentil et al. \(2016\)](#), Copyright (2016) Elsevier Inc. (F)–(I) are adapted with permission from [Guillaume-Gentil et al. \(2013\)](#), Copyright (2013) WILEY-VCH Verlag GmbH & Co. KGaA.

### 10.4.8 Atomic force microscopy combined with optical tweezer

In 1970, Ashkin published the ground-breaking work on optical traps and optical forces ([Ashkin, 1970](#)). Then he developed the first system with a single-beam optical trap to catch silica beads with microns size in 1986

(Ashkin, Dziedzic, Bjorkholm, & Chu, 1986). Besides silica beads, he also tried to trap viruses and bacteria with optical traps, opening the door to biological applications on optical tweezer (OT) (Ashkin & Dziedzic, 1987). Now, OT is widely used in single-molecule force measurement (Kellermayer, Smith, Granzier, & Bustamante, 1997; Neuman & Nagy, 2008; Schnitzer & Block, 1997) and biological manipulations (Bolognesi et al., 2018; Diekmann et al., 2016; Johansen, Fenaroli, Evensen, Griffiths, & Koster, 2016; Reiner et al., 2010; Sparkes, Ketelaar, De Ruijter, & Hawes, 2009; Takahashi et al., 2018; Yamazaki et al., 2019). Due to the distinguishing contribution to the development and applications of OT, Ashkin shared the Nobel prize in Physics in 2018.

OT is possible to combine with AFM. Typically, an infrared laser is used to form an optical trap, which can catch the sphere-like samples with a larger refractive index than environment. The infrared laser can be led to the position near the AFM probe by optical fibers. A typical optical fiber trap setup (Hu, Wang, & Liang, 2004) is shown in Fig. 10.24A. Optical fiber is fixed on 3D control arm. The end of the fiber is immersed in liquid and the fiber-led laser forms an optical trap for sample capture and release. Three-dimensional control arm can move the optical trap for sample manipulation. When the sample is caught by an optical trap, there is still enough free space above the sample, allowing the AFM probe to approach sample surface for further AFM measurement.

Another way to execute AFM-OT is to take advantage of the light path in an inverted optical microscope (IOM) combined with bio-AFM, as shown in Fig. 10.24B. The infrared laser is led into the IOM and then reflected by the reflective mirror inside the microscope. Laser passes through the water immersion objective and is focused. The focused laser can trap samples in the focus point. This setup does not need additional devices above the trapped sample, and the room above the sample allows AFM combination. Compared with the fiber-based optical traps, whose number of traps is limited by the number of fibers, the microscope-based setup can generate more than one trap with one laser path. One commercial solution of AFM-OT is called Bruker OT-AFM Combi-System, shown in Fig. 10.24C. It combines AFM, OT, and IOM together, which can execute sample manipulation, AFM measurement, and advanced optical imaging (like laser scanning confocal microscopy) on one platform.

OT has shown wide applications in manipulation (capture, move, and release) and immobilization of beads (Johansen et al., 2016; Kirkham et al., 2015, 2020), cells (Auka et al., 2019; Johansen et al., 2016;



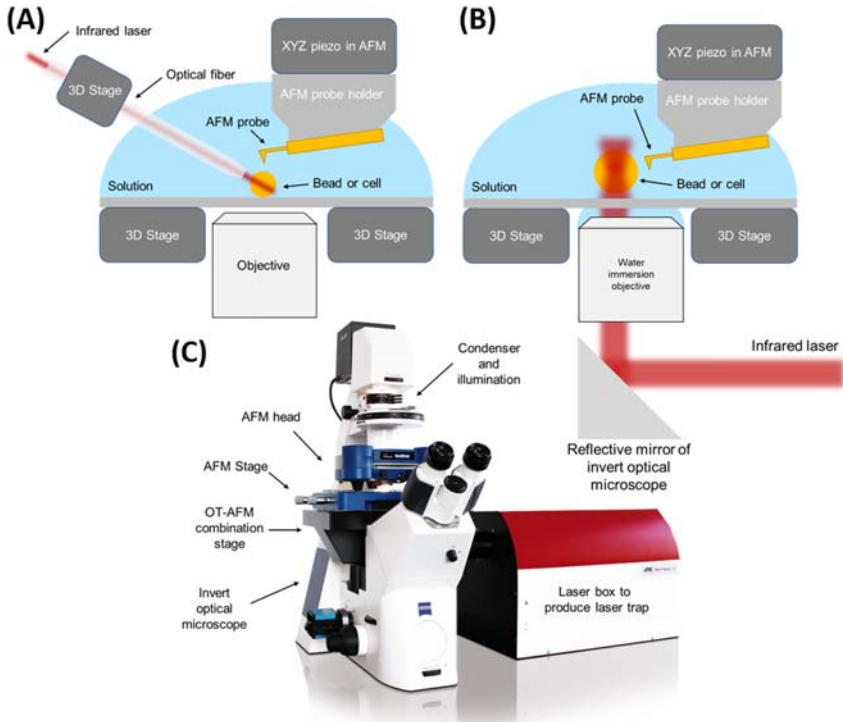


**Figure 10.24** (A) atomic force microscopy (AFM) combined with the fiber-based optical trap. (B) AFM combined with OT based on IOM. (C) Illustration of a commercial solution that combines AFM and OT.

Wang et al., 2011; Yamazaki et al., 2019; Zhu, Avsievich, Bykov, Popov, & Meglinski, 2019), bacteria (Diekmann et al., 2016), vesicles (Bolognesi et al., 2018), and organelles (Reiner et al., 2010; Sparkes et al., 2009; Takahashi et al., 2018). Zhu et al. used OT to trap red blood cells (Zhu, Avsievich, et al., 2019). Auka et al. isolated spermatozoa from mixed forensic samples (Auka et al., 2019). Wang et al. used a microscope to auto-recognize cells and separate them by optical trap (Wang et al., 2011). Organelles in a specific cell, like mitochondria (Reiner et al., 2010) or chromosomes (Takahashi et al., 2018) can be obtained by breaking a specific cell and manipulated by OT. Using more than one optical trap, different kinds of cells can be assembled together (Yamazaki et al., 2019), and cells can be put into specific positions in biological framework (Kirkham et al., 2015). The AFM-OT system can use OT to catch a specific cell from a flowing solution, then move and fix the cell under an AFM probe for further AFM measurements.

AFM-OT system takes advantage of both AFM and OT, making it possible to design new food ingredients at single-cell scale and measure the properties of newly produced food materials in situ. For instance, by OT manipulation, cells can be assembled into heterozygous cell clusters or be planted into bioframework for further culture. AFM can measure the mechanical properties of the tissue-like materials to help design new food materials with good taste.

OT can trap colloid beads containing signal molecules (Kirkham et al., 2015, 2020) and assemble colloid beads into specific patterns at a specific position around cells or food samples. Beads with signal molecules can help study how the anisotropic molecule gradient affects the cell growth. Beads with condiments around food samples can help understand the pickling process of food. AFM is a good monitor to measure the topography and mechanical properties to illustrate the sample surface changing in such an anisotropic environment.

## 10.5 Summary

In this chapter, we reviewed several AFM-based combined techniques as well as their current and potential applications in food science and hope to provide a new angle from an equipment perspective for further study by food scientists. Some techniques have been already used in food science, like AFM-IR, AFM-Raman, AFM-MS, AFM-OM, AFM-Force Loading Stage, and AFM-FluidFM, to analyze chemical information and mechanical properties of food samples and food package materials; and some techniques are useful and important in food science, but the AFM combined studies have just been started, like AFM-X-Ray techniques, AFM-NMR, AFM-nDMA, and AFM-OT, which could extend AFM analysis to new areas. Experimental setup of every combined technique is also reviewed to help food scientists understand operation principles. With these AFM-based combined techniques, the relationship between structure and function in food samples and food package materials can be studied with nanoscale resolution, and new insight into processes in the food industry will be provided to food scientists.

## References

- Albrecht, M. G., & Creighton, J. A. (1977). Anomalously intense Raman spectra of pyridine at a silver electrode. *Journal of the American Chemical Society*, 99(15), 5215–5217. Available from <https://doi.org/10.1021/ja00457a071>.

- Anderson, M. S. (2000). Locally enhanced Raman spectroscopy with an atomic force microscope. *Applied Physics Letters*, 76(21), 3130–3132. Available from <https://doi.org/10.1063/1.126546>.
- Araujo-Díaz, S. B., Leyva-Porras, C., Aguirre-Bañuelos, P., Álvarez-Salas, C., & Saavedra-Leos, Z. (2017). Evaluation of the physical properties and conservation of the antioxidants content, employing inulin and maltodextrin in the spray drying of blueberry juice. *Carbohydrate Polymers*, 167, 317–325. Available from <https://doi.org/10.1016/j.carbpol.2017.03.065>.
- Ashkin, A. (1970). Acceleration and trapping of particles by radiation pressure. *Physical Review Letters*, 24(4), 156–159. Available from <https://doi.org/10.1103/PhysRevLett.24.156>.
- Ashkin, A., & Dziedzic, J. M. (1987). Optical trapping and manipulation of viruses and bacteria. *Science (New York, N.Y.)*, 235(4795), 1517. Available from <https://doi.org/10.1126/science.3547653>.
- Ashkin, A., Dziedzic, J. M., Bjorkholm, J. E., & Chu, S. (1986). Observation of a single-beam gradient force optical trap for dielectric particles. *Optics Letters*, 11(5), 288–290. Available from <https://doi.org/10.1364/OL.11.000288>.
- Atapour, M., Wei, Z., Chaudhary, H., Lendel, C., Odnevall Wallinder, I., & Hedberg, Y. (2019). Metal release from stainless steel 316L in whey protein—And simulated milk solutions under static and stirring conditions. *Food Control*, 101, 163–172. Available from <https://doi.org/10.1016/j.foodcont.2019.02.031>.
- Athmaselvi, K. A., Kumar, C., Balasubramanian, M., & Roy, I. (2014). Thermal, structural, and physical properties of freeze dried tropical fruit powder. *Journal of Food Processing*, 2014, 524705. Available from <https://doi.org/10.1155/2014/524705>.
- Auka, N., Valle, M., Cox, B. D., Wilkerson, P. D., Dawson Cruz, T., Reiner, J. E., & Seashols-Williams, S. J. (2019). Optical tweezers as an effective tool for spermatozoa isolation from mixed forensic samples. *PLoS One*, 14(2), e0211810. Available from <https://doi.org/10.1371/journal.pone.0211810>.
- Auty, M. A. E. (2013). *Confocal microscopy: principles and applications to food microstructures* (pp. 96–P98). Elsevier.
- Bagrov, D. V., Yarysheva, A. Y., Rukhlya, E. G., Yarysheva, L. M., Volynskii, A. L., & Bakeev, N. F. (2014). Atomic force microscopic study of the structure of high-density polyethylene deformed in liquid medium by crazing mechanism. *Journal of Microscopy*, 253(2), 151–160. Available from <https://doi.org/10.1111/jmi.12104>.
- Bailo, E., & Deckert, V. (2008). Tip-enhanced Raman scattering. *Chemical Society Reviews*, 37(5), 921–930. Available from <https://doi.org/10.1039/b705967c>.
- Barlow, D. E., Biffinger, J. C., Cockrell-Zugell, A. L., Lo, M., Kjoller, K., Cook, D., ... Russell, J. N. (2016). The importance of correcting for variable probe–sample interactions in AFM-IR spectroscopy: AFM-IR of dried bacteria on a polyurethane film. *Analyst*, 141(16), 4848–4854. Available from <https://doi.org/10.1039/C6AN00940A>.
- Barth, A. (2007). Infrared spectroscopy of proteins. *Biochimica et Biophysica Acta (BBA) - Bioenergetics*, 1767(9), 1073–1101. Available from <https://doi.org/10.1016/j.bbabi.2007.06.004>.
- Bertocchi, F., & Paci, M. (2008). Applications of high-resolution solid-state NMR spectroscopy in food science. *Journal of Agricultural and Food Chemistry*, 56(20), 9317–9327. Available from <https://doi.org/10.1021/jf8019776>.
- Berweger, S., Nguyen, D. M., Muller, E. A., Bechtel, H. A., Perkins, T. T., & Raschke, M. B. (2013). Nano-chemical infrared imaging of membrane proteins in lipid bilayers. *Journal of the American Chemical Society*, 135(49), 18292–18295. Available from <https://doi.org/10.1021/ja409815g>.
- Binnig, G., Quate, C. F., & Gerber, C. (1986). Atomic force microscope. *Physical Review Letters*, 56(9), 930–933.

- Biswas, M. C., Tiimob, B. J., Abdela, W., Jeelani, S., & Rangari, V. K. (2019). Nano silica-carbon-silver ternary hybrid induced antimicrobial composite films for food packaging application. *Food Packaging and Shelf Life*, 19, 104–113. Available from <https://doi.org/10.1016/j.foodres.2018.12.003>.
- Bokobza, L., Bresson, B., Garnaud, G., & Zhang, J. (2012). Mechanical and AFM investigations of elastomers filled with multiwall carbon nanotubes. *Composite Interfaces*, 19(5), 285–295. Available from <https://doi.org/10.1080/15685543.2012.712486>.
- Bolognesi, G., Friddin, M. S., Salehi-Reyhani, A., Barlow, N. E., Brooks, N. J., Ces, O., & Elani, Y. (2018). Sculpting and fusing biomimetic vesicle networks using optical tweezers. *Nature Communications*, 9(1), 1882. Available from <https://doi.org/10.1038/s41467-018-04282-w>.
- Bonilla, J. C., & Clausen, M. P. (2022). Super-resolution microscopy to visualize and quantify protein microstructural organization in food materials and its relation to rheology: Egg white proteins. *Food Hydrocolloids*, 124, 107281. Available from <https://doi.org/10.1016/j.foodhyd.2021.107281>.
- Budich, C., Neugebauer, U., Popp, J., & Deckert, V. (2008). Cell wall investigations utilizing tip-enhanced Raman scattering. *Journal of Microscopy*, 229(3), 533–539. Available from <https://doi.org/10.1111/j.1365-2818.2008.01939.x>.
- Bugeat, S., Perez, J., Briard-Bion, V., Pradel, P., Ferlay, A., Bourgaux, C., & Lopez, C. (2015). Unsaturated fatty acid enriched vs. control milk triacylglycerols: Solid and liquid TAG phases examined by synchrotron radiation X-ray diffraction coupled with DSC. *Food Research International*, 67, 91–101. Available from <https://doi.org/10.1016/j.foodres.2014.10.029>.
- Calligaris, S., Arrighetti, G., Barba, L., & Nicoli, M. C. (2008). Phase transition of sunflower oil as affected by the oxidation level. *Journal of the American Oil Chemists' Society*, 85(7), 591–598. Available from <https://doi.org/10.1007/s11746-008-1241-y>.
- Calvano, C. D., De Ceglie, C., & Zambonin, C. G. (2014). Proteomic analysis of complex protein samples by MALDI-TOF mass spectrometry. In E. L. Nikolaos (Ed.), *Protein downstream processing* (Vol. 1129, pp. 365–380). Totowa, NJ: Humana Press.
- Campion, A., & Kambhampati, P. (1998). Surface-enhanced Raman scattering. *Chemical Society Reviews*, 27(4), 241–250. Available from <https://doi.org/10.1039/a827241z>.
- Carr, J. M. (2013). Confined layered polymeric systems for packaging and capacitor applications. Case Western Reserve University School of Graduate Studies. Retrieved from [http://rave.ohiolink.edu/etdc/view?acc\\_num=case1363104386](http://rave.ohiolink.edu/etdc/view?acc_num=case1363104386)
- Chen, Q.-J., Zhou, L.-L., Zou, J.-Q., & Gao, X. (2019). The preparation and characterization of nanocomposite film reinforced by modified cellulose nanocrystals. *International Journal of Biological Macromolecules*, 132, 1155–1162. Available from <https://doi.org/10.1016/j.ijbiomac.2019.04.063>.
- Cheng, H. N., & Neiss, T. G. (2012). Solution NMR spectroscopy of food polysaccharides. *Polymer Reviews*, 52(2), 81–114. Available from <https://doi.org/10.1080/15583724.2012.668154>.
- Cheng, S., Bocharova, V., Belianinov, A., Xiong, S., Kisliuk, A., Somnath, S., ... Sokolov, A. P. (2016). Unraveling the mechanism of nanoscale mechanical reinforcement in glassy polymer nanocomposites. *Nano Letters*, 16(6), 3630–3637. Available from <https://doi.org/10.1021/acs.nanolett.6b00766>.
- Chiavaro, E. (2013). Crystal polymorph structure determined for extra virgin olive oil. *European Journal of Lipid Science and Technology*, 115(3), 267–269. Available from <https://doi.org/10.1002/ejlt.201200415>.
- Cialla, D., Marz, A., Bohme, R., Theil, F., Weber, K., Schmitt, M., & Popp, J. (2012). Surface-enhanced Raman spectroscopy (SERS): Progress and trends. *Analytical and Bioanalytical Chemistry*, 403(1), 27–54. Available from <https://doi.org/10.1007/s00216-011-5631-x>.

- Cozzolino, D. (2015). The role of vibrational spectroscopy as a tool to assess economically motivated fraud and counterfeit issues in agricultural products and foods. *Analytical Methods*, 7(22), 9390–9400. Available from <https://doi.org/10.1039/C5AY01792K>.
- Dai, S., Fei, Z., Ma, Q., Rodin, A. S., Wagner, M., McLeod, A. S., . . . Basov, D. N. (2014). Tunable phonon polaritons in atomically thin van der Waals crystals of boron nitride. *Science (New York, N.Y.)*, 343(6175), 1125. Available from <https://doi.org/10.1126/science.1246833>.
- Dais, P., & Hatzakis, E. (2013). Quality assessment and authentication of virgin olive oil by NMR spectroscopy: A critical review. *Analytica Chimica Acta*, 765, 1–27. Available from <https://doi.org/10.1016/j.aca.2012.12.003>.
- Dazzi, A., & Prater, C. B. (2017). AFM-IR: Technology and applications in nanoscale infrared spectroscopy and chemical imaging. *Chemical Reviews*, 117(7), 5146–5173. Available from <https://doi.org/10.1021/acs.chemrev.6b00448>.
- Dazzi, A., Prater, C. B., Hu, Q., Chase, D. B., Rabolt, J. F., & Marcott, C. (2012). AFM-IR: Combining atomic force microscopy and infrared spectroscopy for nanoscale chemical characterization. *Applied Spectroscopy*, 66(12), 1365–1384. Available from <https://doi.org/10.1366/12-06804>.
- Dazzi, A., Prazeres, R., Glotin, F., & Ortega, J. M. (2005). Local infrared microspectroscopy with subwavelength spatial resolution with an atomic force microscope tip used as a photothermal sensor. *Optics Letters*, 30(18), 2388–2390. Available from <https://doi.org/10.1364/OL.30.002388>.
- Dazzi, A., Prazeres, R., Glotin, F., & Ortega, J. M. (2006). Subwavelength infrared microspectroscopy using an AFM as a local absorption sensor. *Infrared Physics & Technology*, 49(1), 113–121. Available from <https://doi.org/10.1016/j.infrared.2006.01.009>.
- de sa Peixoto, P., Roiland, C., Thomas, D., Briard-Bion, V., Le Guellec, R., Parayre, S., . . . Guyomarc'h, F. (2015). Recrystallized S-layer protein of a probiotic propionibacterium: Structural and nanomechanical changes upon temperature or pH shifts probed by solid-state NMR and AFM. *Langmuir: The ACS Journal of Surfaces and Colloids*, 31(1), 199–208. Available from <https://doi.org/10.1021/la503735z>.
- Deniset-Besseau, A., Prater, C. B., Virolle, M.-J., & Dazzi, A. (2014). Monitoring TriAcylGlycerols accumulation by atomic force microscopy based infrared spectroscopy in streptomyces species for biodiesel applications. *The Journal of Physical Chemistry Letters*, 5(4), 654–658. Available from <https://doi.org/10.1021/jz402393a>.
- Dharmaraj, U., Parameswara, P., Somashekar, R., & Malleshi, N. G. (2014). Effect of processing on the microstructure of finger millet by X-ray diffraction and scanning electron microscopy. *Journal of Food Science and Technology*, 51(3), 494–502. Available from <https://doi.org/10.1007/s13197-011-0536-4>.
- Di Stefano, V., Avellone, G., Bongiorno, D., Cunsolo, V., Muccilli, V., Sforza, S., . . . Vékey, K. (2012). Applications of liquid chromatography–mass spectrometry for food analysis. *Journal of Chromatography. A*, 1259, 74–85. Available from <https://doi.org/10.1016/j.chroma.2012.04.023>.
- Diekmann, R., Wolfson, D. L., Spahn, C., Heilemann, M., Schüttelz, M., & Huser, T. (2016). Nanoscopy of bacterial cells immobilized by holographic optical tweezers. *Nature Communications*, 7(1), 13711. Available from <https://doi.org/10.1038/ncomms13711>.
- Dieringer, J. A., McFarland, A. D., Shah, N. C., Stuart, D. A., Whitney, A. V., Yonzon, C. R., . . . Van Duyne, R. P. (2006). Surface enhanced Raman spectroscopy: New materials, concepts, characterization tools, and applications. *Faraday Discussions*, 132, 9–26. Available from <https://doi.org/10.1039/b513431p>.
- Dufrière, Y. F., Ando, T., Garcia, R., Alsteens, D., Martinez-Martin, D., Engel, A., . . . Müller, D. J. (2017). Imaging modes of atomic force microscopy for application in molecular and cell biology. *Nature Nanotechnology*, 12(4), 295–307. Available from <https://doi.org/10.1038/nnano.2017.45>.

- Esmaili, Z., Bayrami, S., Dorkoosh, F. A., Akbari Javar, H., Seyedjafari, E., Zargarian, S. S., & Haddadi-Asl, V. (2018). Development and characterization of electrospayed nanoparticles for encapsulation of Curcumin: Development and characterization of electrospayed nanoparticles. *Journal of Biomedical Materials Research. Part A*, 106(1), 285–292. Available from <https://doi.org/10.1002/jbm.a.36233>.
- Fei, Z., Rodin, A. S., Andreev, G. O., Bao, W., McLeod, A. S., Wagner, M., . . . Basov, D. N. (2012). Gate-tuning of graphene plasmons revealed by infrared nano-imaging. *Nature*, 487(7405), 82–85. Available from <https://doi.org/10.1038/nature11253>.
- Felts, J. R., Kjoller, K., Lo, M., Prater, C. B., & King, W. P. (2012). Nanometer-scale infrared spectroscopy of heterogeneous polymer nanostructures fabricated by tip-based nanofabrication. *ACS Nano*, 6(9), 8015–8021. Available from <https://doi.org/10.1021/nn302620f>.
- Fernandes, A., Brás, N. F., Mateus, N., & Freitas, V. d (2015). A study of anthocyanin self-association by NMR spectroscopy. *New Journal of Chemistry*, 39(4), 2602–2611. Available from <https://doi.org/10.1039/C4NJ02339K>.
- Ferrando, M., & Spiess, W. E. L. (2000). Review: Confocal scanning laser microscopy. A powerful tool in food science Revision: Microscopía láser confocal de barrido. Una potente herramienta en la ciencia de los alimentos. *Food Science and Technology International*, 6(4), 267–284. Available from <https://doi.org/10.1177/108201320000600402>.
- Ferrari, A. C., Meyer, J. C., Scardaci, V., Casiraghi, C., Lazzeri, M., Mauri, F., . . . Geim, A. K. (2006). Raman spectrum of graphene and graphene layers. *Physical Review Letters*, 97(18). Available from <https://doi.org/10.1103/PhysRevLett.97.187401>.
- Ferreira, F. V., Mariano, M., Pinheiro, I. F., Cazalini, E. M., Souza, D. H. S., Lepesqueur, L. S. S., . . . Lona, L. M. F. (2019). Cellulose nanocrystal-based poly(butylene adipate-co-terephthalate) nanocomposites covered with antimicrobial silver thin films. *Polymer Engineering & Science*, 59(s2), E356–E365. Available from <https://doi.org/10.1002/pen.25066>.
- Ferry, J. D. (1980). Viscoelastic properties of polymer. *Journal of Research*, 41, 53–61. Available from <https://doi.org/10.6028/jres.041.008>.
- Finglas, P. (2019). Trends in food science & technology, 87, 1–2.
- Fleischmann, M., Hendra, P. J., & McQuillan, A. J. (1974). Raman spectra of pyridine adsorbed at a silver electrode. *Chemical Physics Letters*, 26(2), 163–166. Available from [https://doi.org/10.1016/0009-2614\(74\)85388-1](https://doi.org/10.1016/0009-2614(74)85388-1).
- Foroutanparsa, S., Bröls, M., Tas, R. P., Elizabeth P. Maljaars, C., & Voets, I. K. (2021). Super resolution microscopy imaging of pH induced changes in the microstructure of casein micelles. *Food Structure*, 100231. Available from <https://doi.org/10.1016/j.foostr.2021.100231>.
- Fyfe, K. N., Kravchuk, O., Le, T., Deeth, H. C., Nguyen, A. V., & Bhandari, B. (2011). Storage induced changes to high protein powders: Influence on surface properties and solubility. *Journal of the Science of Food and Agriculture*, 91(14), 2566–2575. Available from <https://doi.org/10.1002/jsfa.4461>.
- Gaiani, C., Ehrhardt, J. J., Scher, J., Hardy, J., Desobry, S., & Banon, S. (2006). Surface composition of dairy powders observed by X-ray photoelectron spectroscopy and effects on their rehydration properties. *Colloids and Surfaces B: Biointerfaces*, 49(1), 71–78. Available from <https://doi.org/10.1016/j.colsurfb.2006.02.015>.
- Gaiani, C., Schuck, P., Scher, J., Ehrhardt, J. J., Arab-Tehrany, E., Jacquot, M., & Banon, S. (2009). Native phosphocaseinate powder during storage: Lipids released onto the surface. *Journal of Food Engineering*, 94(2), 130–134. Available from <https://doi.org/10.1016/j.jfoodeng.2009.01.038>.
- George, M., Nziakou, Y., Goerke, S., Genix, A. C., Bresson, B., Roux, S., . . . Ciccotti, M. (2018). In situ AFM investigation of slow crack propagation mechanisms in a glassy polymer. *Journal of the Mechanics and Physics of Solids*, 112, 109–125. Available from <https://doi.org/10.1016/j.jmps.2017.11.019>.

- Gong, L., Chase, D. B., Noda, I., Marcott, C. A., Liu, J., Martin, D. C., . . . Rabolt, J. F. (2017). Polymorphic distribution in individual electrospun poly[(R)-3-hydroxybutyrate-co-(R)-3-hydroxyhexanoate] (PHBHx) nanofibers. *Macromolecules*, *50*(14), 5510–5517. Available from <https://doi.org/10.1021/acs.macromol.7b01086>.
- Guillaume-Gentil, O., Grindberg, R. V., Kooger, R., Dorwling-Carter, L., Martinez, V., Ossola, D., . . . Vorholt, J. A. (2016). Tunable single-cell extraction for molecular analyses. *Cell*, *166*(2), 506–516. Available from <https://doi.org/10.1016/j.cell.2016.06.025>.
- Guillaume-Gentil, O., Potthoff, E., Ossola, D., Dörig, P., Zambelli, T., & Vorholt, J. A. (2013). Force-controlled fluidic injection into single cell nuclei. *Small (Weinheim an der Bergstrasse, Germany)*, *9*(11), 1904–1907. Available from <https://doi.org/10.1002/sml.201202276>.
- Guillaume-Gentil, O., Rey, T., Kiefer, P., Ibáñez, A. J., Steinhoff, R., Brönnimann, R., . . . Vorholt, J. A. (2017). Single-cell mass spectrometry of metabolites extracted from live cells by fluidic force microscopy. *Analytical Chemistry*, *89*(9), 5017–5023. Available from <https://doi.org/10.1021/acs.analchem.7b00367>.
- Guillaume-Gentil, O., Zambelli, T., & Vorholt, J. A. (2014). Isolation of single mammalian cells from adherent cultures by fluidic force microscopy. *Lab on a Chip*, *14*(2), 402–414. Available from <https://doi.org/10.1039/C3LC51174J>.
- Gurdeniz, G., Tokatli, F., & Ozen, B. (2007). Differentiation of mixtures of monovarietal olive oils by mid-infrared spectroscopy and chemometrics. *European Journal of Lipid Science and Technology*, *109*(12), 1194–1202. Available from <https://doi.org/10.1002/ejlt.200700087>.
- Harrison, A. J., Bilgili, E. A., Beaudoin, S. P., & Taylor, L. S. (2013). Atomic force microscope infrared spectroscopy of griseofulvin nanocrystals. *Analytical Chemistry*, *85*(23), 11449–11455. Available from <https://doi.org/10.1021/ac4025889>.
- Hartschuh, A., Sánchez, E. J., Xie, X. S., & Novotny, L. (2003). High-resolution near-field raman microscopy of single-walled carbon nanotubes. *Physical Review Letters*, *90*(9), 095503. Available from <https://doi.org/10.1103/PhysRevLett.90.095503>.
- Hatzakis, E. (2019). Nuclear magnetic resonance (NMR) spectroscopy in food science: A comprehensive review: NMR spectroscopy in food science. . . *Comprehensive Reviews in Food Science and Food Safety*, *18*(1), 189–220. Available from <https://doi.org/10.1111/1541-4337.12408>.
- Hayazawa, N., Inouye, Y., Sekkat, Z., & Kawata, S. (2000). Metallized tip amplification of near-field Raman scattering. *Optics Communications*, *183*(1), 333–336. Available from [https://doi.org/10.1016/S0030-4018\(00\)00894-4](https://doi.org/10.1016/S0030-4018(00)00894-4).
- Helfricht, N., Mark, A., Dorwling-Carter, L., Zambelli, T., & Papastavrou, G. (2017). Extending the limits of direct force measurements: Colloidal probes from sub-micron particles. *Nanoscale*, *9*(27), 9491–9501. Available from <https://doi.org/10.1039/C7NR02226C>.
- Hirt, L., Grüter, R. R., Berthelot, T., Cornut, R., Vörös, J., & Zambelli, T. (2015). Local surface modification via confined electrochemical deposition with FluidFM. *RSC Advances*, *5*(103), 84517–84522. Available from <https://doi.org/10.1039/C5RA07239E>.
- Hirt, L., Ihle, S., Pan, Z., Dorwling-Carter, L., Reiser, A., Wheeler, J. M., . . . Zambelli, T. (2016). Template-free 3D microprinting of metals using a force-controlled nanopipette for layer-by-layer electrodeposition. *Advanced Materials*, *28*(12), 2311–2315. Available from <https://doi.org/10.1002/adma.201504967>.
- Hofherr, L., Müller-Renno, C., & Ziegler, C. (2020). FluidFM as a tool to study adhesion forces of bacteria—Optimization of parameters and comparison to conventional bacterial probe scanning force spectroscopy. *PLoS One*, *15*(7), e0227395. Available from <https://doi.org/10.1371/journal.pone.0227395>.
- Hofweber, M., Hutten, S., Bourgeois, B., Spreitzer, E., Niedner-Boblenz, A., Schifferer, M., . . . Dormann, D. (2018). Phase separation of FUS is suppressed by its nuclear import

- receptor and arginine methylation. *Cell*, 173(3). Available from <https://doi.org/10.1016/j.cell.2018.03.004>, 706–719.e713.
- Hohlbein, J. (2021). Single-molecule localization microscopy as an emerging tool to probe multiscale food structures. *Food Structure*, 30, 100236. Available from <https://doi.org/10.1016/j.foosr.2021.100236>.
- Hu, Z., Wang, J., & Liang, J. (2004). Manipulation and arrangement of biological and dielectric particles by a lensed fiber probe. *Optics Express*, 12(17), 4123–4128. Available from <https://doi.org/10.1364/opex.12.004123>.
- Huang, Y., Chakraborty, S., & Liang, H. (2020). Methods to probe the formation of biofilms: Applications in foods and related surfaces. *Analytical Methods*, 12(4), 416–432. Available from <https://doi.org/10.1039/C9AY02214G>.
- Ibáñez, C., Simó, C., García-Cañas, V., Cifuentes, A., & Castro-Puyana, M. (2013). Metabolomics, peptidomics and proteomics applications of capillary electrophoresis-mass spectrometry in foodomics: A review. *Analytica Chimica Acta*, 802, 1–13. Available from <https://doi.org/10.1016/j.aca.2013.07.042>.
- Ivanova, B., & Spiteller, M. (2014). Raman spectroscopic and mass spectrometric determination of aflatoxins. *Food Analytical Methods*, 7(1), 242–256. Available from <https://doi.org/10.1007/s12161-013-9701-x>.
- Jafari, S. M., Assadpoor, E., Bhandari, B., & He, Y. (2008). Nano-particle encapsulation of fish oil by spray drying. *Food Research International*, 41(2), 172–183. Available from <https://doi.org/10.1016/j.foodres.2007.11.002>.
- Jakob, D. S., Wang, H., Zeng, G., Otzen, D. E., Yan, Y., & Xu, X. G. (2020). Peak force infrared–kelvin probe force microscopy. *Angewandte Chemie International Edition*. Available from <https://doi.org/10.1002/anie.202004211>, n/a(n/a).
- Jeanmaire, D. L., & Van Duyne, R. P. (1977). Surface raman spectroelectrochemistry: Part I. Heterocyclic, aromatic, and aliphatic amines adsorbed on the anodized silver electrode. *Journal of Electroanalytical Chemistry and Interfacial Electrochemistry*, 84(1), 1–20. Available from [https://doi.org/10.1016/S0022-0728\(77\)80224-6](https://doi.org/10.1016/S0022-0728(77)80224-6).
- Ji, B., Kenaan, A., Gao, S., Cheng, J., Cui, D., Yang, H., . . . Song, J. (2019). Label-free detection of biotoxins via a photo-induced force infrared spectrum at the single-molecular level. *Analyst*, 144(20), 6108–6117. Available from <https://doi.org/10.1039/C9AN01338E>.
- Johansen, P. L., Fenaroli, F., Evensen, L., Griffiths, G., & Koster, G. (2016). Optical micromanipulation of nanoparticles and cells inside living zebrafish. *Nature Communications*, 7(1), 10974. Available from <https://doi.org/10.1038/ncomms10974>.
- Kaczmarek, H., Nowicki, M., Vuković-Kwiatkowska, I., & Nowakowska, S. (2013). Crosslinked blends of poly(lactic acid) and polyacrylates: AFM, DSC and XRD studies. *Journal of Polymer Research*, 20(3), 91. Available from <https://doi.org/10.1007/s10965-013-0091-y>.
- Kaláb, M., Allan-Wojtas, P., & Miller, S. S. (1995). Microscopy and other imaging techniques in food structure analysis. *Trends in Food Science & Technology*, 6(6), 177–186. Available from [https://doi.org/10.1016/S0924-2244\(00\)89052-4](https://doi.org/10.1016/S0924-2244(00)89052-4).
- Katzenmeyer, A. M., Aksyuk, V., & Centrone, A. (2013). Nanoscale infrared spectroscopy: Improving the spectral range of the photothermal induced resonance technique. *Analytical Chemistry*, 85(4), 1972–1979. Available from <https://doi.org/10.1021/ac303620y>.
- Katzenmeyer, A. M., Holland, G., Kjoller, K., & Centrone, A. (2015). Absorption spectroscopy and imaging from the visible through mid-infrared with 20 nm resolution. *Analytical Chemistry*, 87(6), 3154–3159. Available from <https://doi.org/10.1021/ac504672t>.
- Kawasaki, H., Shimomae, Y., Watanabe, T., & Arakawa, R. (2009). Desorption/ionization on porous silicon mass spectrometry (DIOS-MS) of perfluorooctane sulfonate (PFOS). *Colloids and Surfaces A: Physicochemical and Engineering Aspects*, 347(1–3), 220–224. Available from <https://doi.org/10.1016/j.colsurfa.2009.04.035>.



- Kelchtermans, M., Lo, M., Dillon, E., Kjoller, K., & Marcott, C. (2016). Characterization of a polyethylene–polyamide multilayer film using nanoscale infrared spectroscopy and imaging. *Vibrational Spectroscopy*, *82*, 10–15. Available from <https://doi.org/10.1016/j.vibspec.2015.11.004>.
- Kellermayer, M. S. Z., Smith, S. B., Granzier, H. L., & Bustamante, C. (1997). Folding–unfolding transitions in single titin molecules characterized with laser tweezers. *Science (New York, N.Y.)*, *276*(5315), 1112. Available from <https://doi.org/10.1126/science.276.5315.1112>.
- Kennedy, E., Al-Majmaie, R., Al-Rubeai, M., Zerulla, D., & Rice, J. H. (2013). Nanoscale infrared absorption imaging permits non–destructive intracellular photosensitizer localization for subcellular uptake analysis. *RSC Advances*, *3*(33), 13789–13795. Available from <https://doi.org/10.1039/C3RA42185F>.
- Kern, C. C., Usbeck, J. C., Vogel, R. F., & Behr, J. (2013). Optimization of matrix–assisted–laser–desorption–ionization–time–of–flight mass spectrometry for the identification of bacterial contaminants in beverages. *Journal of Microbiological Methods*, *93*(3), 185–191. Available from <https://doi.org/10.1016/j.mimet.2013.03.012>.
- Kirkham, G. R., Britchford, E., Upton, T., Ware, J., Gibson, G. M., Devaud, Y., . . . Shakesheff, K. (2015). Precision assembly of complex cellular microenvironments using holographic optical tweezers. *Scientific Reports*, *5*(1), 8577. Available from <https://doi.org/10.1038/srep08577>.
- Kirkham, G. R., Ware, J., Upton, T., Allen, S., Shakesheff, K. M., & Buttery, L. D. K. (2020). Localized induction of gene expression in embryonic stem cell aggregates using holographic optical tweezers to create biochemical gradients. *Regenerative Engineering and Translational Medicine*, *6*(3), 251–261. Available from <https://doi.org/10.1007/s40883-019-00114-5>.
- Kochan, K., Perez–Guaita, D., Pissang, J., Jiang, J.–H., Peleg, A. Y., McNaughton, D., . . . Wood, B. R. (2018). In vivo atomic force microscopy–infrared spectroscopy of bacteria. *Journal of The Royal Society Interface*, *15*(140), 20180115. Available from <https://doi.org/10.1098/rsif.2018.0115>.
- Kurouski, D., Dazzi, A., Zenobi, R., & Centrone, A. (2020). Infrared and Raman chemical imaging and spectroscopy at the nanoscale. *Chemical Society Reviews*, *49*(11), 3315–3347. Available from <https://doi.org/10.1039/C8CS00916C>.
- Landsberg, G. S., & Mandelsham, L. I. (1928). Eine neue Erscheinung bei der Lichtzerstreuung in Krystallen. *Die Naturwissenschaften*, *16*(28), 557–558. Available from <https://doi.org/10.1007/BF01506807>.
- Law, K. P. (2010). Laser desorption/ionization mass spectrometry on nanostructured semiconductor substrates: DIOS™ and QuickMass™. *International Journal of Mass Spectrometry*, *290*(2–3), 72–84. Available from <https://doi.org/10.1016/j.ijms.2009.12.006>.
- Lee, D. W., Wetzel, A., Bennewitz, R., Meyer, E., Despont, M., Vettiger, P., & Gerber, C. (2004). Switchable cantilever for a time–of–flight scanning force microscope. *Applied Physics Letters*, *84*(9), 1558–1560. Available from <https://doi.org/10.1063/1.1651641>.
- Leydet, Y., Gavara, R., Petrov, V., Diniz, A. M., Jorge Parola, A., Lima, J. C., & Pina, F. (2012). The effect of self–aggregation on the determination of the kinetic and thermodynamic constants of the network of chemical reactions in 3–glucoside anthocyanins. *Phytochemistry*, *83*, 125–135. Available from <https://doi.org/10.1016/j.phytochem.2012.06.022>.
- Li, X., Tu, H., Huang, M., Chen, J., Shi, X., Deng, H., . . . Du, Y. (2017). Incorporation of lysozyme–rectorite composites into chitosan films for antibacterial properties enhancement. *International Journal of Biological Macromolecules*, *102*, 789–795. Available from <https://doi.org/10.1016/j.ijbiomac.2017.04.076>.
- Liang, Z., Yin, Z., Yang, H., Xiao, Y., Hang, W., & Li, J. (2016). Nanoscale surface analysis that combines scanning probe microscopy and mass spectrometry: A critical

- review. *TrAC Trends in Analytical Chemistry*, 75, 24–34. Available from <https://doi.org/10.1016/j.trac.2015.07.009>.
- Lipiec, E., Ruggeri, F. S., Benadiba, C., Borkowska, A. M., Kobierski, J. D., Miszczyk, J., . . . Kwiatek, W. M. (2019). Infrared nanospectroscopic mapping of a single metaphase chromosome. *Nucleic Acids Research*, 47(18). Available from <https://doi.org/10.1093/nar/gkz630>, e108–e108.
- Lopez, A. D., Mathers, C. D., Ezzati, M., Jamison, D. T., & Murray, C. J. L. (2006). Global and regional burden of disease and risk factors, 2001: Systematic analysis of population health data. *The Lancet*, 367(9524), 1747–1757. Available from [https://doi.org/10.1016/S0140-6736\(06\)68770-9](https://doi.org/10.1016/S0140-6736(06)68770-9).
- Lopez, C., Lesieur, P., Bourgaux, C., Keller, G., & Ollivon, M. (2001). Thermal and structural behavior of milk fat. *Journal of Colloid and Interface Science*, 240(1), 150–161. Available from <https://doi.org/10.1006/jcis.2001.7664>.
- Lopez, C., Lesieur, P., Keller, G., & Ollivon, M. (2000). Thermal and structural behavior of milk fat. *Journal of Colloid and Interface Science*, 229(1), 62–71. Available from <https://doi.org/10.1006/jcis.2000.6988>.
- López-Lorente, Á. I., & Mizaikoff, B. (2016). Mid-infrared spectroscopy for protein analysis: Potential and challenges. *Analytical and Bioanalytical Chemistry*, 408(11), 2875–2889. Available from <https://doi.org/10.1007/s00216-016-9375-5>.
- Lu, F., Jin, M., & Belkin, M. A. (2014). Tip-enhanced infrared nanospectroscopy via molecular expansion force detection. *Nature Photonics*, 8(4), 307–312. Available from <https://doi.org/10.1038/nphoton.2013.373>.
- Luis Rodriguez-Saona, & Huseyin Ayzaz, R. L. W. (2017). Infrared and Raman spectroscopy. In S. Suzanne Nielsen (Ed.), *Food analysis* (5th ed., pp. 107–127). Cham, Switzerland: Springer.
- Ma, X., Beltran, V., Ramer, G., Pavlidis, G., Parkinson, D. Y., Thoury, M., . . . Berrie, B. H. (2019). Revealing the distribution of metal carboxylates in oil paint from the micro- to nanoscale. *Angewandte Chemie International Edition*, 58(34), 11652–11656. Available from <https://doi.org/10.1002/anie.201903553>.
- Magonov, S. N. (2006). Atomic force microscopy in analysis of polymers. In: Meyers, R.A., & Provder, T. (Eds.), *Encyclopedia of Analytical Chemistry*. Available from <https://doi.org/10.1002/9780470027318.a2003>.
- Malik, A. K., Blasco, C., & Picó, Y. (2010). Liquid chromatography–mass spectrometry in food safety. *Journal of Chromatography. A*, 1217(25), 4018–4040. Available from <https://doi.org/10.1016/j.chroma.2010.03.015>.
- Malmendal, A., Amoresano, C., Trotta, R., Lauri, I., De Tito, S., Novellino, E., & Randazzo, A. (2011). NMR spectrometers as “magnetic tongues”: Prediction of sensory descriptors in canned tomatoes. *Journal of Agricultural and Food Chemistry*, 59(20), 10831–10838. Available from <https://doi.org/10.1021/jf203803q>.
- Marchetti-Deschmann, M., Winkler, W., Dong, H., Lohninger, H., Kubicek, C. P., & Allmaier, G. (2012). Using spores for *Fusarium* spp. classification by MALDI-based intact cell/spore mass spectrometry. *Food Technology and Biotechnology*, 50, 334–342.
- Marcone, M. F., Wang, S., Albabish, W., Nie, S., Somnarain, D., & Hill, A. (2013). Diverse food-based applications of nuclear magnetic resonance (NMR) technology. *Food Research International*, 51(2), 729–747. Available from <https://doi.org/10.1016/j.foodres.2012.12.046>.
- Marcos, B., Gou, P., Guàrdia, M. D., Hortós, M., Colleo, M., Mach, N., . . . Arnau, J. (2013). Surface-enhanced laser desorption/ionisation time-of-flight mass spectrometry: A tool to predict pork quality. *Meat Science*, 95(3), 688–693. Available from <https://doi.org/10.1016/j.meatsci.2012.10.014>.
- Marin, L., Ailincăi, D., Mares, M., Paslaru, E., Cristea, M., Nica, V., & Simionescu, B. C. (2015). Imino-chitosan biopolymeric films. Obtaining, self-assembling, surface and

- antimicrobial properties. *Carbohydrate Polymers*, 117, 762–770. Available from <https://doi.org/10.1016/j.carbpol.2014.10.050>.
- Mathurin, J., Pancani, E., Deniset-Besseau, A., Kjoller, K., Prater, C. B., Gref, R., & Dazzi, A. (2018). How to unravel the chemical structure and component localization of individual drug-loaded polymeric nanoparticles by using tapping AFM-IR. *Analyst*, 143(24), 5940–5949. Available from <https://doi.org/10.1039/C8AN01239C>.
- Mayet, C., Dazzi, A., Prazeres, R., Allot, F., Glotin, F., & Ortega, J. M. (2008). Sub-100 nm IR spectromicroscopy of living cells. *Optics Letters*, 33(14), 1611–1613. Available from <https://doi.org/10.1364/OL.33.001611>.
- Meister, A., Gabi, M., Behr, P., Studer, P., Vörös, J., Niedermann, P., ... Zambelli, T. (2009). FluidFM: Combining atomic force microscopy and nanofluidics in a universal liquid delivery system for single cell applications and beyond. *Nano Letters*, 9(6), 2501–2507. Available from <https://doi.org/10.1021/nl901384x>.
- Meister, A., Polesel-Maris, J., Niedermann, P., Przybylska, J., Studer, P., Gabi, M., ... Heinzlmann, H. (2009). Nanoscale dispensing in liquid environment of streptavidin on a biotin-functionalized surface using hollow atomic force microscopy probes. *Microelectronic Engineering*, 86(4), 1481–1484. Available from <https://doi.org/10.1016/j.mee.2008.10.025>.
- Mishra, R. K., Ha, S. K., Verma, K., & Tiwari, S. K. (2018). Recent progress in selected bio-nanomaterials and their engineering applications: An overview. *Journal of Science: Advanced Materials and Devices*, 3(3), 263–288. Available from <https://doi.org/10.1016/j.jsamd.2018.05.003>.
- Miyagawa, Y., Shintani, K., Katsuki, K., Nakagawa, K., & Adachi, S. (2017). Thermal and structural changes of rapeseed oil during isothermal storage at low temperature. *Food Structure*, 11, 8–15. Available from <https://doi.org/10.1016/j.foostr.2016.12.004>.
- Moosheimer, U., & Bichler, C. (1999). Plasma pretreatment of polymer films as a key issue for high barrier food packagings. *Surface and Coatings Technology*, 116–119, 812–819. Available from [https://doi.org/10.1016/S0257-8972\(99\)00137-1](https://doi.org/10.1016/S0257-8972(99)00137-1).
- Morsch, S., Liu, Y., Greensmith, P., Lyon, S. B., & Gibbon, S. R. (2017). Molecularly controlled epoxy network nanostructures. *Polymer*, 108, 146–153. Available from <https://doi.org/10.1016/j.polymer.2016.11.050>.
- Morsch, S., Lyon, S., & Gibbon, S. R. (2017). The degradation mechanism of an epoxy-phenolic can coating. *Progress in Organic Coatings*, 102, 37–43. Available from <https://doi.org/10.1016/j.porgcoat.2016.03.019>.
- Mousoulis, C., Maleki, T., Ziaie, B., & Neu, C. P. (2013). Atomic force microscopy-coupled microcoils for cellular-scale nuclear magnetic resonance spectroscopy. *Applied Physics Letters*, 102(14), 143702. Available from <https://doi.org/10.1063/1.4801318>.
- Muller, D. J., Dumitru, A. C., Lo Giudice, C., Gaub, H. E., Hinterdorfer, P., Hummer, G., ... Alsteens, D. (2021). Atomic force microscopy-based force spectroscopy and multiparametric imaging of biomolecular and cellular systems. *Chemical Reviews*, 121(19), 11701–11725. Available from <https://doi.org/10.1021/acs.chemrev.0c00617>.
- Naumenko, D., Snitka, V., Serviene, E., Bruzaite, I., & Snopok, B. (2013). In vivo characterization of protein uptake by yeast cell envelope: Single cell AFM imaging and  $\mu$ -tip-enhanced Raman scattering study. *Analyst*, 138(18), 5371–5383. Available from <https://doi.org/10.1039/C3AN00362K>.
- Neugebauer, U., Rösch, P., Schmitt, M., Popp, J., Julien, C., Rasmussen, A., ... Deckert, V. (2006). On the way to nanometer-sized information of the bacterial surface by tip-enhanced Raman spectroscopy. *Chemphyschem: A European Journal of Chemical Physics and Physical Chemistry*, 7(7), 1428–1430. Available from <https://doi.org/10.1002/cphc.200600173>.
- Neugebauer, U., Schmid, U., Baumann, K., Ziebuhr, W., Kozitskaya, S., Deckert, V., ... Popp, J. (2007). Towards a detailed understanding of bacterial metabolism—

- Spectroscopic characterization of staphylococcus epidermidis. *ChemPhysChem*, 8(1), 124–137. Available from <https://doi.org/10.1002/cphc.200600507>.
- Neuman, K. C., & Nagy, A. (2008). Single-molecule force spectroscopy: Optical tweezers, magnetic tweezers and atomic force microscopy. *Nature Methods*, 5(6), 491–505. Available from <https://doi.org/10.1038/nmeth.1218>.
- Nguyen, H. K., Liang, X., Ito, M., & Nakajima, K. (2018). Direct mapping of nanoscale viscoelastic dynamics at nanofiller/polymer interfaces. *Macromolecules*, 51(15), 6085–6091. Available from <https://doi.org/10.1021/acs.macromol.8b01185>.
- Nguyen-Tri, P., Nguyen, V., & Nguyen, T. A. (2019). Biological activity and nanostructure of Fe<sub>3</sub>O<sub>4</sub>-Ag/high density polyethylene nanocomposite. *Journal of Composites Science*, 3(2). Available from <https://doi.org/10.3390/jcs3020034>.
- Nie, S. M., & Emery, S. R. (1997). Probing single molecules and single nanoparticles by surface-enhanced Raman scattering. *Science (New York, N.Y.)*, 275(5303), 1102–1106. Available from <https://doi.org/10.1126/science.275.5303.1102>.
- Ning, N., Fu, S., Zhang, W., Chen, F., Wang, K., Deng, H., ... Fu, Q. (2012). Realizing the enhancement of interfacial interaction in semicrystalline polymer/filler composites via interfacial crystallization. *Progress in Polymer Science*, 37(10), 1425–1455. Available from <https://doi.org/10.1016/j.progpolymsci.2011.12.005>.
- Nunes, C. A. (2014). Vibrational spectroscopy and chemometrics to assess authenticity, adulteration and intrinsic quality parameters of edible oils and fats. *Food Research International*, 60, 255–261. Available from <https://doi.org/10.1016/j.foodres.2013.08.041>.
- Odermatt, P. D., Shivanandan, A., Deschout, H., Jankele, R., Nievergelt, A. P., Feletti, L., ... Fantner, G. E. (2015). High-resolution correlative microscopy: Bridging the gap between single molecule localization microscopy and atomic force microscopy. *Nano Letters*, 15(8), 4896–4904. Available from <https://doi.org/10.1021/acs.nanolett.5b00572>.
- Oliveira, L. C., Barros, J. H. T., Rosell, C. M., & Steel, C. J. (2017). Physical and thermal properties and X-ray diffraction of corn flour systems as affected by whole grain wheat flour and extrusion conditions: Starch study in wholegrain extrudates. *Starch - Stärke*, 69(9-10), 1600299. Available from <https://doi.org/10.1002/star.201600299>.
- Ovchinnikova, O. S., Nikiforov, M. P., Bradshaw, J. A., Jesse, S., & Van Berkel, G. J. (2011). Combined atomic force microscope-based topographical imaging and nanometer-scale resolved proximal probe thermal desorption/electrospray ionization-mass spectrometry. *ACS Nano*, 5(7), 5526–5531. Available from <https://doi.org/10.1021/nn200939e>.
- Ovchinnikova, O. S., Tai, T., Bocharova, V., Okatan, M. B., Belianinov, A., Kertesz, V., ... Van Berkel, G. J. (2015). Co-registered topographical, band excitation nanomechanical, and mass spectral imaging using a combined atomic force microscopy/mass spectrometry platform. *ACS Nano*, 9(4), 4260–4269. Available from <https://doi.org/10.1021/acsnano.5b00659>.
- Owens, S. C., Berenbeim, J. A., Patterson, C. S., Dillon, E. P., & de Vries, M. S. (2014). Sub-micron proximal probe thermal desorption and laser mass spectrometry on painting cross-sections. *Anal. Methods*, 6(22), 8940–8945. Available from <https://doi.org/10.1039/C4AY00919C>.
- Pattemore, J. A., Rice, N., Marshall, D. F., Waugh, R., & Henry, R. J. (2010). Cereal variety identification using MALDI-TOF mass spectrometry SNP genotyping. *Journal of Cereal Science*, 52(3), 356–361. Available from <https://doi.org/10.1016/j.jcs.2010.06.004>.
- Pernemalm, M., & Lehtiö, J. (2014). Mass spectrometry-based plasma proteomics: State of the art and future outlook. *Expert Review of Proteomics*, 11(4), 431–448. Available from <https://doi.org/10.1586/14789450.2014.901157>.
- Pettinger, B., Picardi, G., Schuster, R., & Ertl, G. (2002). Surface-enhanced and STM-tip-enhanced Raman spectroscopy at metal surfaces. *Single Molecules*, 3(5–6), 285–294. [10.1002/1438-5171\(200211\)3:5/6 <285::AID-SIMO285 >3.0.CO;2-X](https://doi.org/10.1002/1438-5171(200211)3:5/6 <285::AID-SIMO285 >3.0.CO;2-X).

- Pettinger, B., Ren, B., Picardi, G., Schuster, R., & Ertl, G. (2004). Nanoscale probing of adsorbed species by tip-enhanced Raman spectroscopy. *Physical Review Letters*, *92*(9). Available from <https://doi.org/10.1103/PhysRevLett.92.096101>.
- Policar, C., Waern, J. B., Plamont, M.-A., Clède, S., Mayet, C., Prazeres, R., ... Dazzi, A. (2011). Subcellular IR Imaging of a metal–carbonyl moiety using photothermally induced resonance. *Angewandte Chemie International Edition*, *50*(4), 860–864. Available from <https://doi.org/10.1002/anie.201003161>.
- Porras-Saavedra, J., Palacios-González, E., Lartundo-Rojas, L., Garibay-Febles, V., Yáñez-Fernández, J., Hernández-Sánchez, H., ... Alamilla-Beltrán, L. (2015). Microstructural properties and distribution of components in microparticles obtained by spray-drying. *Journal of Food Engineering*, *152*, 105–112. Available from <https://doi.org/10.1016/j.jfoodeng.2014.11.014>.
- Potthoff, E., Guillaume-Gentil, O., Ossola, D., Polesel-Maris, J., LeibundGut-Landmann, S., Zambelli, T., & Vorholt, J. A. (2012). Rapid and serial quantification of adhesion forces of yeast and mammalian cells. *PLoS One*, *7*(12), e52712. Available from <https://doi.org/10.1371/journal.pone.0052712>.
- Preiß, E. I., Merle, B., & Göken, M. (2017). Understanding the extremely low fracture toughness of freestanding gold thin films by in-situ bulge testing in an AFM. *Materials Science and Engineering: A*, *691*, 218–225. Available from <https://doi.org/10.1016/j.msea.2017.03.037>.
- Price, D. M., Reading, M., Hammiche, A., & Pollock, H. M. (1999). Micro-thermal analysis: Scanning thermal microscopy and localised thermal analysis. *International Journal of Pharmaceutics*, *192*(1), 85–96. Available from [https://doi.org/10.1016/S0378-5173\(99\)00275-6](https://doi.org/10.1016/S0378-5173(99)00275-6).
- Purohit, S. R., & Rao, P. S. (2017). Water absorption and gelatinization kinetics of non-issuable rice and its characterization. *Journal of Food Measurement and Characterization*, *11*(4), 2110–2118. Available from <https://doi.org/10.1007/s11694-017-9595-1>.
- Qamar, S., Wang, G., Randle, S. J., Ruggeri, F. S., Varela, J. A., Lin, J. Q., ... George-Hyslop, P., St (2018). FUS phase separation is modulated by a molecular chaperone and methylation of arginine cation- $\pi$  interactions. *Cell*, *173*(3). Available from <https://doi.org/10.1016/j.cell.2018.03.056>, 720-734.e715.
- Qu, M., Deng, F., Kalkhoran, S. M., Gouldstone, A., Robisson, A., & Van Vliet, K. J. (2011). Nanoscale visualization and multiscale mechanical implications of bound rubber interphases in rubber–carbon black nanocomposites. *Soft Matter*, *7*(3), 1066–1077. Available from <https://doi.org/10.1039/C0SM00645A>.
- Rainey, J. K., & Goh, M. C. (2002). Parallel atomic force microscopy and NMR spectroscopy to investigate self-assembled protein–nucleotide aggregates. *The Journal of Physical Chemistry. B*, *106*(21), 5553–5560. Available from <https://doi.org/10.1021/jp015593u>.
- Ramakrishnan, V., & Luthria, D. L. (2017). Recent applications of NMR in food and dietary studies: Recent applications of NMR in food and dietary studies. *Journal of the Science of Food and Agriculture*, *97*(1), 33–42. Available from <https://doi.org/10.1002/jsfa.7917>.
- Raman, C. V., & Krishnan, K. S. (1928). A new type of secondary radiation. *Nature*, *121*(3048), 501–502. Available from <https://doi.org/10.1038/121501c0>.
- Ramel, P. R., & Marangoni, A. G. (2017). Characterization of the polymorphism of milk fat within processed cheese products. *Food Structure*, *12*, 15–25. Available from <https://doi.org/10.1016/j.foostr.2017.03.001>.
- Ramer, G., Ruggeri, F. S., Levin, A., Knowles, T. P. J., & Centrone, A. (2018). Determination of polypeptide conformation with nanoscale resolution in water. *ACS Nano*, *12*(7), 6612–6619. Available from <https://doi.org/10.1021/acsnano.8b01425>.
- Ramirez-Aldaba, H., Vazquez-Arenas, J., Sosa-Rodríguez, F. S., Valdez-Perez, D., Ruiz-Baca, E., Trejo-Cordoba, G., ... Lara, R. H. (2018). Changes in biooxidation mechanism and transient biofilm characteristics by As(V) during arsenopyrite colonization

- with *Acidithiobacillus thiooxidans*. *Journal of Industrial Microbiology & Biotechnology*, 45(8), 669–680. Available from <https://doi.org/10.1007/s10295-018-2051-3>.
- Reimer, J. E., Kishore, R. B., Levin, B. C., Albanetti, T., Boire, N., Knipe, A., ... Deckman, K. H. (2010). Detection of heteroplasmic mitochondrial DNA in single mitochondria. *PLoS One*, 5(12), e14359. Available from <https://doi.org/10.1371/journal.pone.0014359>.
- Richards, D., Zayats, A., Keilmann, F., & Hillenbrand, R. (2004). Near-field microscopy by elastic light scattering from a tip. *Philosophical Transactions of the Royal Society of London. Series A: Mathematical, Physical and Engineering Sciences*, 362(1817), 787–805. Available from <https://doi.org/10.1098/rsta.2003.1347>.
- Rizevsky, S., & Kurouski, D. (2020). Nanoscale structural organization of insulin fibril polymorphs revealed by atomic force microscopy–infrared spectroscopy (AFM-IR). *Chembiochem: A European Journal of Chemical Biology*, 21(4), 481–485. Available from <https://doi.org/10.1002/cbic.201900394>.
- Rodrigues, M. S., Dhez, O., Denmat, S. L., Chevrier, J., Felici, R., & Comin, F. (2008). Local detection of X-ray spectroscopies with an in-situ atomic force microscope. *Journal of Instrumentation*, 3(12). Available from <https://doi.org/10.1088/1748-0221/3/12/P12004>, P12004–P12004.
- Rodriguez-Saona, L. E., & Allendorf, M. E. (2011). Use of FTIR for rapid authentication and detection of adulteration of food. *Annual Review of Food Science and Technology*, 2(1), 467–483. Available from <https://doi.org/10.1146/annurev-food-022510-133750>.
- Romão, W., Franco, M. F., Iglesias, A. H., Sanvido, G. B., Maretto, D. A., Gozzo, F. C., ... De Paoli, M.-A. (2010). Fingerprinting of bottle-grade poly(ethylene terephthalate) via matrix-assisted laser desorption/ionization mass spectrometry. *Polymer Degradation and Stability*, 95(4), 666–671. Available from <https://doi.org/10.1016/j.polyimdegradstab.2009.11.046>.
- Rossi, M., Cubadda, F., Dini, L., Terranova, M. L., Aureli, F., Sorbo, A., & Passeri, D. (2014). Scientific basis of nanotechnology, implications for the food sector and future trends. *Trends in Food Science & Technology*, 40(2), 127–148. Available from <https://doi.org/10.1016/j.tifs.2014.09.004>.
- Ruggeri, F. S., Longo, G., Faggiano, S., Lipiec, E., Pastore, A., & Dietler, G. (2015). Infrared nanospectroscopy characterization of oligomeric and fibrillar aggregates during amyloid formation. *Nature Communications*, 6(1), 7831. Available from <https://doi.org/10.1038/ncomms8831>.
- Ruggeri, F. S., Vieweg, S., Cendrowska, U., Longo, G., Chiki, A., Lashuel, H. A., & Dietler, G. (2016). Nanoscale studies link amyloid maturity with polyglutamine diseases onset. *Scientific Reports*, 6(1), 31155. Available from <https://doi.org/10.1038/srep31155>.
- Rusciano, G., Zito, G., Isticato, R., Sirec, T., Ricca, E., Bailo, E., & Sasso, A. (2014). Nanoscale chemical imaging of *Bacillus subtilis* spores by combining tip-enhanced Raman scattering and advanced statistical tools. *ACS Nano*, 8(12), 12300–12309. Available from <https://doi.org/10.1021/nm504595k>.
- Sarabia-Sainz, H. M., Torres-Arreola, W., Marquez-Rios, E., Santacruz-Ortega, H. C., Rouzaud-Sandez, O., Valenzuela-Soto, E. M., ... Marina Ezquerra-Brauer, J. (2017). Interrelation of collagen chemical structure and nanostructure with firmness of three body regions of jumbo squid (*Dosidicus gigas*). *Food Biophysics*, 12(4), 491–499. Available from <https://doi.org/10.1007/s11483-017-9505-4>.
- Scheler, T., Rodrigues, M., Cornelius, T. W., Mocuta, C., Malachias, A., Magalhães-Paniago, R., ... Metzger, T. H. (2014). Probing the elastic properties of individual nanostructures by combining in situ atomic force microscopy and micro-x-ray diffraction. *Applied Physics Letters*, 4.
- Schmid, I., Raabe, J., Sarafimov, B., Quitmann, C., Vranjkovic, S., Pellmont, Y., & Hug, H. J. (2010). Coaxial arrangement of a scanning probe and an X-ray microscope as a

- novel tool for nanoscience. *Ultramicroscopy*, 110(10), 1267–1272. Available from <https://doi.org/10.1016/j.ultramic.2010.05.002>.
- Schnitzer, M. J., & Block, S. M. (1997). Kinesin hydrolyses one ATP per 8-nm step. *Nature*, 388(6640), 386–390. Available from <https://doi.org/10.1038/41111>.
- Seshadri, I. P., & Bhushan, B. (2008). In situ tensile deformation characterization of human hair with atomic force microscopy. *Acta Materialia*, 56(4), 774–781. Available from <https://doi.org/10.1016/j.actamat.2007.10.033>.
- Sharma, S., Jaiswal, S., Duffy, B., & Jaiswal, A. K. (2019). Nanostructured materials for food applications: Spectroscopy, microscopy and physical properties. *Bioengineering-Basel*, 6(1). Available from <https://doi.org/10.3390/bioengineering6010026>, 26-Article No.: 26.
- Shen, Q., Dong, W., Yang, M., Baibado, J. T., Wang, Y., Alqouqa, I., & Cheung, H.-Y. (2013). Lipidomic study of olive fruit and oil using TiO<sub>2</sub> nanoparticle based matrix solid-phase dispersion and MALDI-TOF/MS. *Food Research International*, 54(2), 2054–2061. Available from <https://doi.org/10.1016/j.foodres.2013.10.001>.
- Slobodskyy, T., Zozulya, A. V., Tholapi, R., Liefeth, L., Fester, M., Sprung, M., & Hansen, W. (2015). Versatile atomic force microscopy setup combined with micro-focused X-ray beam. *Review of Scientific Instruments*, 86(6), 065104. Available from <https://doi.org/10.1063/1.4922605>.
- Sparkes, I. A., Ketelaar, T., De Ruijter, N. C. A., & Hawes, C. (2009). Grab a golgi: Laser trapping of golgi bodies reveals in vivo interactions with the endoplasmic reticulum. *Traffic (Copenhagen, Denmark)*, 10(5), 567–571. Available from <https://doi.org/10.1111/j.1600-0854.2009.00891.x>.
- Spyros, A., & Dais, P. (2012). *NMR spectroscopy in food analysis*. Royal Society of Chemistry.
- Stevenson, D. G., Doorenbos, R. K., Jane, J.-I., & Inglett, G. E. (2006). Structures and functional properties of starch from seeds of three soybean (*Glycine max* (L.) Merr.) varieties\*. *Starch - Stärke*, 58(10), 509–519. Available from <https://doi.org/10.1002/star.200600534>.
- Stiles, P. L., Dieringer, J. A., Shah, N. C., & Van Duyne, R. R. (2008). Surface-enhanced Raman spectroscopy. *Annual Review of Analytical Chemistry*, 1, 601–626. Available from <https://doi.org/10.1146/annurev.anchem.1.031207.112814>.
- Stöckle, R. M., Suh, Y. D., Deckert, V., & Zenobi, R. (2000). Nanoscale chemical analysis by tip-enhanced Raman spectroscopy. *Chemical Physics Letters*, 318(1), 131–136. Available from [https://doi.org/10.1016/S0009-2614\(99\)01451-7](https://doi.org/10.1016/S0009-2614(99)01451-7).
- Takahashi, T., Okeyo, K. O., Ueda, J., Yamagata, K., Washizu, M., & Oana, H. (2018). A microfluidic device for isolating intact chromosomes from single mammalian cells and probing their folding stability by controlling solution conditions. *Scientific Reports*, 8(1), 13684. Available from <https://doi.org/10.1038/s41598-018-31975-5>.
- Tambe, N. S., & Bhushan, B. (2004). In situ study of nano-cracking in multilayered magnetic tapes under monotonic and fatigue loading using an AFM. *Ultramicroscopy*, 100(3), 359–373. Available from <https://doi.org/10.1016/j.ultramic.2003.10.006>.
- Tang, F., Bao, P., & Su, Z. (2016). Analysis of nanodomain composition in high-impact polypropylene by atomic force microscopy-infrared. *Analytical Chemistry*, 88(9), 4926–4930. Available from <https://doi.org/10.1021/acs.analchem.6b00798>.
- Thomas, C., Ferreiro, V., Coulon, G., & Seguela, R. (2007). In situ AFM investigation of crazing in polybutene spherulites under tensile drawing. *Polymer*, 48(20), 6041–6048. Available from <https://doi.org/10.1016/j.polymer.2007.07.062>.
- Tibolla, H., Czaikoski, A., Pelissari, F. M., Menegalli, F. C., & Cunha, R. L. (2020). Starch-based nanocomposites with cellulose nanofibers obtained from chemical and mechanical treatments. *International Journal of Biological Macromolecules*, 161, 132–146. Available from <https://doi.org/10.1016/j.ijbiomac.2020.05.194>.

- Tibolla, H., Pelissari, F. M., Martins, J. T., Lanzoni, E. M., Vicente, A. A., Menegalli, F. C., & Cunha, R. L. (2019). Banana starch nanocomposite with cellulose nanofibers isolated from banana peel by enzymatic treatment: In vitro cytotoxicity assessment. *Carbohydrate Polymers*, 207, 169–179. Available from <https://doi.org/10.1016/j.carbpol.2018.11.079>.
- Tiziani, S., Schwartz, S. J., & Vodovotz, Y. (2008). Intermolecular interactions in phytochemical model systems studied by NMR diffusion measurements. *Food Chemistry*, 107(2), 962–969. Available from <https://doi.org/10.1016/j.foodchem.2007.08.089>.
- Ueda, E., Liang, X., Ito, M., & Nakajima, K. (2019). Dynamic moduli mapping of silica-filled styrene–butadiene rubber vulcanizate by nanorheological atomic force microscopy. *Macromolecules*, 52(1), 311–319. Available from <https://doi.org/10.1021/acs.macromol.8b02258>.
- Usbeck, J. C., Kern, C. C., Vogel, R. F., & Behr, J. (2013). Optimization of experimental and modelling parameters for the differentiation of beverage spoiling yeasts by matrix-assisted-laser-desorption/ionization–time-of-flight mass spectrometry (MALDI–TOF MS) in response to varying growth conditions. *Food Microbiology*, 36(2), 379–387. Available from <https://doi.org/10.1016/j.fm.2013.07.004>.
- van de Voort, F. R., Ismail, A. A., & Sedman, J. (1995). A rapid, automated method for the determination of cis and trans content of fats and oils by fourier transform infrared spectroscopy. *Journal of the American Oil Chemists' Society*, 72(8), 873–880. Available from <https://doi.org/10.1007/BF02542063>.
- Van Eerdenbrugh, B., Lo, M., Kjoller, K., Marcott, C., & Taylor, L. S. (2012). Nanoscale mid-infrared imaging of phase separation in a drug–polymer blend. *Journal of Pharmaceutical Sciences*, 101(6), 2066–2073. Available from <https://doi.org/10.1002/jps.23099>.
- Varghese, S., Fredrich, S., Vantomme, G., Prabhu, S. R., Teyssandier, J., De Feyter, S., ... Schenning, A. P. H. J. (2020). Epitaxial growth of light-responsive azobenzene molecular crystal actuators on oriented polyethylene films. *Journal of Materials Chemistry C*, 8(2), 694–699. Available from <https://doi.org/10.1039/C9TC05407C>.
- Vitorino, M. V., Fuchs, Y., Dane, T., Rodrigues, M. S., Rosenthal, M., Panzarella, A., ... Costa, L. (2016). An in situ atomic force microscope for normal-incidence nanofocus X-ray experiments. *Journal of Synchrotron Radiation*, 23(5), 1110–1117. Available from <https://doi.org/10.1107/S1600577516011437>.
- Vlahov, G. (1999). Application of NMR to the study of olive oils. *Progress in Nuclear Magnetic Resonance Spectroscopy*, 35(4), 341–357.
- Wang, B., Wei, L., Yao, L., Li, L. J., Yang, Y., & Chen, Y. (2007). Pressure-induced single-walled carbon nanotube (n,m) selectivity on Co–Mo catalysts. *Journal of Physical Chemistry C*, 111(40), 14612–14616.
- Wang, D., Fujinami, S., Nakajima, K., Inukai, S., Ueki, H., Magario, A., ... Nishi, T. (2010). Visualization of nanomechanical mapping on polymer nanocomposites by AFM force measurement. *Polymer*, 51(12), 2455–2459. Available from <https://doi.org/10.1016/j.polymer.2010.03.052>.
- Wang, L., Huang, D., Chan, C. K., Li, Y. J., & Xu, X. G. (2017). Nanoscale spectroscopic and mechanical characterization of individual aerosol particles using peak force infrared microscopy. *Chemical Communications*, 53(53), 7397–7400. Available from <https://doi.org/10.1039/C7CC02301D>.
- Wang, L., Wagner, M., Wang, H., Pau-Sanchez, S., Li, J., Edgar, J. H., & Xu, X. G. (2020). Revealing phonon polaritons in hexagonal boron nitride by multipulse peak force infrared microscopy. *Advanced Optical Materials*, 8(5), 1901084. Available from <https://doi.org/10.1002/adom.201901084>.
- Wang, L., Wang, H., Wagner, M., Yan, Y., Jakob, D. S., & Xu, X. G. (2017). Nanoscale simultaneous chemical and mechanical imaging via peak force infrared microscopy. *Science Advances*, 3(6), e1700255. Available from <https://doi.org/10.1126/sciadv.1700255>.



- Wang, X., Chen, S., Kong, M., Wang, Z., Costa, K. D., Li, R. A., & Sun, D. (2011). Enhanced cell sorting and manipulation with combined optical tweezer and microfluidic chip technologies. *Lab on a Chip*, *11*(21), 3656–3662. Available from <https://doi.org/10.1039/C1LC20653B>.
- Wang, X., Wang, S., & Cai, Z. (2013). The latest developments and applications of mass spectrometry in food-safety and quality analysis. *TrAC Trends in Analytical Chemistry*, *52*, 170–185. Available from <https://doi.org/10.1016/j.trac.2013.08.005>.
- Wang, Y., Heinemann, F., Top, S., Dazzi, A., Policar, C., Henry, L., ... Vessieres, A. (2018). Ferrocens labelled with an infrared rhenium tricarbonyl tag: Synthesis, antiproliferative activity, quantification and nano IR mapping in cancer cells. *Dalton Transactions*, *47*(29), 9824–9833. Available from <https://doi.org/10.1039/C8DT01582A>.
- Wang, Y., Na, B., Zhang, Q., Tan, H., Xiao, Y., Li, L., ... Men, Y. (2005). Lamellar orientation in the blends of linear low density polyethylene and isotactic polypropylene induced by dynamic packing injection molding. *Journal of Materials Science*, *40*(24), 6409–6415. Available from <https://doi.org/10.1007/s10853-005-1746-9>.
- Wessel, J. (1985). Surface-enhanced optical microscopy. *Journal of the Optical Society of America B*, *2*(9), 1538–1541. Available from <https://doi.org/10.1364/JOSAB.2.001538>.
- Wetzel, A., Socoliuc, A., Meyer, E., Bennewitz, R., Gnecco, E., & Gerber, C. (2005). A versatile instrument for in situ combination of scanning probe microscopy and time-of-flight mass spectrometry. *Review of Scientific Instruments*, *76*(10), 103701. Available from <https://doi.org/10.1063/1.2082004>.
- Wojtczak, E., Gadzinowski, M., Makowski, T., Maresz, K., Kubisa, P., Bednarek, M., & Pluta, M. (2018). Encapsulation of hydrophobic vitamins by polylactide stereocomplexation and their release study: Encapsulation of hydrophobic vitamins by polylactide stereocomplexation and their release study. *Polymer International*, *67*(11), 1523–1534. Available from <https://doi.org/10.1002/pi.5674>.
- Wu, Y., Emdadi, L., Schulman, E., Shu, Y., Tran, D. T., Wang, X., & Liu, D. (2018). Overgrowth of lamellar silicalite-1 on MFI and BEA zeolites and its consequences on non-oxidative methane aromatization reaction. *Microporous and Mesoporous Materials*, *263*, 1–10. Available from <https://doi.org/10.1016/j.micromeso.2017.11.040>.
- Xu, X. G., Ghamsari, B. G., Jiang, J.-H., Gilburd, L., Andreev, G. O., Zhi, C., ... Walker, G. C. (2014). One-dimensional surface phonon polaritons in boron nitride nanotubes. *Nature Communications*, *5*(1), 4782. Available from <https://doi.org/10.1038/ncomms5782>.
- Xu, X. G., & Raschke, M. B. (2013). Near-field infrared vibrational dynamics and tip-enhanced decoherence. *Nano Letters*, *13*(4), 1588–1595. Available from <https://doi.org/10.1021/nl304804p>.
- Yamazaki, T., Kishimoto, T., Leszczyński, P., Sadakane, K., Kenmotsu, T., Watanabe, H., ... Taniguchi, H. (2019). Construction of 3D cellular composites with stem cells derived from adipose tissue and endothelial cells by use of optical tweezers in a natural polymer solution. *Materials (Basel)*, *12*(11). Available from <https://doi.org/10.3390/ma12111759>.
- Yang, H., Yang, S., Kong, J., Dong, A., & Yu, S. (2015). Obtaining information about protein secondary structures in aqueous solution using Fourier transform IR spectroscopy. *Nature Protocols*, *10*, 382–396. Available from <https://doi.org/10.1038/nprot.2015.024>.
- Yang, J., Mayyas, M., Tang, J., Ghasemian, M. B., Yang, H., Watanabe, K., ... Kalantar-Zadeh, K. (2020). Boundary-induced auxiliary features in scattering-type near-field fourier transform infrared spectroscopy. *ACS Nano*, *14*(1), 1123–1132. Available from <https://doi.org/10.1021/acsnano.9b08895>.
- Yang, J., & White, J. L. (2012). Crystallization behavior of polypropylene/ethylene butene copolymer blends. *Journal of Applied Polymer Science*, *126*(6), 2049–2058. Available from <https://doi.org/10.1002/app.35184>.

- Yang, S., Verhoeff, A. A., Merckx, D. W. H., van Duynhoven, J. P. M., & Hohlbein, J. (2020). Quantitative spatiotemporal mapping of lipid and protein oxidation in mayonnaise. *Antioxidants*, 9(12), 1278. Available from <https://doi.org/10.3390/antiox9121278>.
- Zhang, C., Xu, J., & Chen, Y. (2020). Preparation of monolayer photonic crystals from Ag nanobulge-deposited SiO<sub>2</sub> particles as substrates for reproducible SERS assay of trace thiol pesticide. *Nanomaterials*, 10(6). Available from <https://doi.org/10.3390/nano10061205>.
- Zhang, J., Liu, L., Jiang, Y., Faisal, S., Wei, L., Cao, C., . . . Wang, Q. (2019). Converting peanut protein biomass waste into “double green” meat substitutes using a high-moisture extrusion process: A multiscale method to explore a process for forming a meat-like fibrous structure. *Journal of Agricultural and Food Chemistry*, 67(38), 10713–10725. Available from <https://doi.org/10.1021/acs.jafc.9b02711>.
- Zhang, T., Vavylonis, D., Durachko, D. M., & Cosgrove, D. J. (2017). Nanoscale movements of cellulose microfibrils in primary cell walls. *Nature Plants*, 3(5), 17056. Available from <https://doi.org/10.1038/nplants.2017.56>.
- Zhang, X., Sun, S., Ning, N., Yan, S., Wu, X., Lu, Y., & Zhang, L. (2020). Visualization and quantification of the microstructure evolution of isoprene rubber during uniaxial stretching using AFM nanomechanical mapping. *Macromolecules*, 53(8), 3082–3089. Available from <https://doi.org/10.1021/acs.macromol.9b02656>.
- Zhang, Y., Dai, B., Deng, Y., & Zhao, Y. (2015). AFM and NMR imaging of squid tropomyosin Tod p1 subjected to high hydrostatic pressure: Evidence for relationships among topography, characteristic domain and allergenicity. *RSC Advances*, 5(89), 73207–73216. Available from <https://doi.org/10.1039/C5RA13655E>.
- Zhao, X., Ao, Q., Du, F., Zhu, J., & Liu, J. (2010). Surface characterization of ginger powder examined by X-ray photoelectron spectroscopy and scanning electron microscopy. *Colloids and Surfaces B: Biointerfaces*, 79(2), 494–500. Available from <https://doi.org/10.1016/j.colsurfb.2010.05.019>.
- Zhong, X., Zhang, Z., Jiang, S., & Li, L. (2014). Recent advances in coupling capillary electrophoresis-based separation techniques to ESI and MALDI-MS: Liquid Phase Separations. *Electrophoresis*, 35(9), 1214–1225. Available from <https://doi.org/10.1002/elps.201300451>.
- Zhou, Z., Ren, X., Wang, F., Li, J., Si, X., Cao, R., . . . Blanchard, C. (2015). High pressure processing manipulated buckwheat antioxidant activity, anti-adipogenic properties and starch digestibility. *Journal of Cereal Science*, 66, 31–36. Available from <https://doi.org/10.1016/j.jcs.2015.09.002>.
- Zhu, R., Avsievich, T., Bykov, A., Popov, A., & Meglinski, I. (2019). Influence of pulsed He-Ne laser irradiation on the red blood cell interaction studied by optical tweezers. *Micromachines (Basel)*, 10(12). Available from <https://doi.org/10.3390/mi10120853>.
- Zhu, Z., Zhou, Q., & Sun, D.-W. (2019). Measuring and controlling ice crystallization in frozen foods: A review of recent developments. *Trends in Food Science & Technology*, 90, 13–25. Available from <https://doi.org/10.1016/j.tifs.2019.05.012>.

This page intentionally left blank

# Index

*Note:* Page numbers followed by “*f*” and “*t*” refer to figures and tables, respectively.

## A

- Amplitude modulation mode, 46
- Application of atomic force microscopy
  - to dairy lipid systems
    - natural oil-in-water emulsion, 215–228
    - surface of milk fat globules, 222–223
  - for food emulsions
    - nanoemulsions and emulsions, 209–210
  - for food foams
    - air bubbles, 201–202
    - air/water interface, 197–198
    - at planar Langmuir films, 198–201
  - in food microorganism research
    - advantages and disadvantages, 163*t*
    - microbial biofilm study, 169–173
    - microbial macromolecule study, 173–176
    - with other techniques, 179–181
    - single microbial cell study, 162–169
    - types of microorganisms, 176–179
  - for food polysaccharides
    - measurement of molecule interactions, 147–148
    - plant polysaccharide, 122–146
  - nanoemulsions and emulsions
    - to air-dried lipid droplets, 210–214
    - to oil bodies, 211–213
  - at planar Langmuir films, 207–210
  - applications of, 208
  - whey protein-based systems, 208–209
  - to stabilized oil-in-water emulsions, 203–207
    - cellulose nanocrystals, 206–207
    - pectins, 203–204
    - protein fibrils, 204–205
    - protein nanostructures, 205–206
    - protein/polysaccharide complexes, 204
  - surface of milk fat globules
    - adhesion forces, 224–225
    - specific interaction forces, 223–228
    - surface topography and roughness of milk fat globules, 220–222
    - topography and mechanical properties of hydrated lipid bilayers, 217
    - supported, 217–222
    - unsupported, 218–220
    - topography of lipid monolayers and membranes in air, 215–216
- Atomic force microscopy (AFM)
  - advantages for food research, 4–5
  - applied to food foams and emulsions
    - application to foams and emulsions, 195–196
    - atomic force microscope, 193
    - force–distance curves, 195
    - investigation of surfaces, 192
    - operating modes for imaging, 193–194
  - basic principles of, 16–23, 18*f*
  - combined techniques
    - AFM combined with fluidic force microscopy, 340–341
    - AFM combined with force-loading stage, 337–340, 339*f*
    - AFM combined with mass spectrometry, 327–329
    - AFM combined with nanodynamic mechanical analysis, 334–335
    - AFM combined with nuclear magnetic resonance, 335–337
    - AFM combined with optical microscopy, 329–332
    - AFM combined with optical tweezer, 342–345
    - AFM combined with X-ray techniques, 332–334
  - disadvantages for food research, 5–6
  - for food and biological samples, 45–46
    - cantilever selection, 53–57

## Atomic force microscopy (AFM)

*(Continued)*

- data analysis, 69–75
- data optimization, 67–69
- force measurement procedure by, 62–66
- imaging procedure by AFM, 57–62
- nanomanipulation procedure by AFM, 66
- sample preparation for food samples, 50–53
- substrates, 46–50
- for food foams and emulsions, 192–214
- for food powder sand contact materials
  - contact materials related to food, 250–253
  - functional properties with, 242–250
  - powerful tool during formulation and processing of, 234–242
  - prospects and advanced, 253–254
- for food proteins
  - bean proteins, 92–95
  - collagen and gelatin, 106–110
  - egg, 110–112
  - grain, 88–92
  - meat, 97–99
  - milk, 96–101
  - peanut, 95–96
  - seafood, 104–106
- history of, 15–16
- and infrared combination, 179–180
- integration with other instruments, 30
- measurement items, 29–30
- new imaging modes, 27–29
- with other techniques for food science
  - correlative topography, 319*f*
  - high-moisture extrusion process, 317*f*
  - infrared (IR) absorption images, 313*f*
  - microscopy-infrared applications in, 312–319
  - photothermal induced resonance technique, 310*f*
  - polystyrene-block-polymethyl methacrylate block copolymer, 309*f*
  - principle and apparatus, 310–311
  - seven-layer cling film and infrared spectra, 315*f*

- topography of Pf-5 bacteria on PU, 316*f*
  - and Raman spectroscopy combination, 181
  - research ways and applications, 30–36
  - studies about different types of
    - microorganisms
      - eukaryotic, 177–178
      - prokaryotic, 176–177
      - viruses, 178–179
- Atomic force microscopy requirements for food samples
- functions and characteristics of, 47*t*

**B**

- Basic principles of atomic force microscopy
- basic components, 17–20
    - geometry and representative schemes of, 20*f*
    - and principles, 18*f*
  - food science and technology research, 17
  - working conditions, basic functions, and theory, 20–23
    - atomic force microscopy operation modes, 22*f*
- Bean proteins
- pea proteins, 93–95
  - soy proteins, 92–93

**C**

- Cantilever selection
- resonance frequency and quality factor, 56
  - spring constant, 54–55
  - tip functionalization, 56–57
  - tip geometry, 55–56
- Collagen, 106–108

**D**

- Data analysis
- artifacts cause
    - by electronic noise, 74–75
    - by friction, 74
    - by high-frequency operation, 73–74
    - by inappropriate imaging parameters, 74
    - by optical interference, 73, 73*f*

- by scanner, 71–73
- by tip-sample convolution, 69–71, 71*f*
- by vibration, 75
- image analysis, 75
  - bearing function, 75
  - roughness, 75
  - section function, 75
- by scanner
  - edge overshoots caused by the scanner, 72*f*
  - typical image artifacts, 69–75, 70*t*
  - UHV conditions, 71*f*
- Data optimization
  - offline, 68–69
    - erase scan line, 69
    - flatten, 68
    - plane fit, 68
  - real-time, 67–68
    - integral gain, 67–68
    - proportional gain, 68
    - scan rate, 67
    - scan size, 67
    - setpoint, 67
- Dynamic mode, 21
- E**
- Egg proteins, 110–112
- F**
- Fixation of single cells and apple tissue, 283*f*
- Fluidic force microscopy, 340–341
- Food protein extraction, 85–86
- Food science research with atomic force microscopy
  - approaches in, 285–286
  - classification of, 287*t*
- Force–distance curve, 193
- Force-loading stage, 337–340, 339*f*
- Food material nanomechanics, advances in
  - food science research with AFM, 285–286
  - nanomechanical properties of food materials, 286–300
  - operation modes in AFM, 264–274
  - probe selection, 283–285
  - proteins stretching, 274–276
  - suppliers, sample preparation, fixation, and tip selection, 276–283
- Force measurements
  - approach and retraction force–distance curves, 26*f*
  - calculate spring constant
    - Sader method, 65–66
    - thermal tune method, 64–65
  - force measurement, 66
  - measure deflection sensitivity, 63–64
  - and nanomanipulation, 23–27
  - panorama of forces measurable with atomic force microscopy, 25*f*
  - procedure by atomic force microscopy, 62*f*
    - calculate spring constant, 64–66
- Frequency modulation mode, 46
- Functional properties with atomic force microscopy
  - caking, 246–248
  - cohesion and flow ability, 248
  - contact materials related to food, 250–253
  - control of powder, 242–250
  - food powders as a vehicle of bioactive molecules, 248–250
  - morphological studies of food material surfaces, 251
  - quantitative studies of food material surfaces, 251–253
  - reconstitution ability of, 242–246
  - dispersion, 245–246
  - wetting, 243–245
- G**
- Gelatin, 109–110
- Grain proteins
  - maize proteins, 91
  - protamex-hydrolyzed rice bran, 89*f*
  - rice proteins, 88–89
  - sorghum proteins, 91–92
  - wheat proteins, 89–90
- I**
- Imaging procedure by atomic force microscopy, 58*f*

Imaging procedure by atomic force microscopy (*Continued*)  
 acquire and save the image, 61  
 adjust photodiode signal, 60  
 align laser, 59  
   front end of the cantilever, 59  
   maximize the laser SUM signal, 59  
 cantilever tune, 60  
 clean workspace, 62  
 enable software, 59  
 engage atomic force microscopy probe, 60–61  
   automatically engage, 61  
   manually engage, 60  
 mount probe, 59  
   holder, 59  
 mount sample, 57–59  
   load, 58–59  
   prepare, 57–58  
 optimize scan parameters, 61  
 power on system, 57  
 set initial scan parameters, 60  
 shutdown system, 61  
 unmount probe and sample, 61  
 withdraw, 61  
 Intermittent contact mode, 46

## L

Lennard-Jones potential, 23–24

## M

Maize proteins, 91  
 Mass spectrometry, 327–329  
 Measurement items, technical  
   configuration, 29*f*  
 Measurement of molecule interactions of  
   polysaccharides  
   and food components, 147–148  
   polysaccharides–polysaccharides,  
     147–148  
   polysaccharides–protein, 148  
 Microbial biofilm study  
   biofilm adhesive property study,  
     170–171  
   biofilm dynamic process study, 171–173  
   biofilm morphological imaging,  
     169–170

dynamic processes of *Bdellovibrios*, 172*f*  
 imaging of biofilms, 171*f*  
 Microbial macromolecule studies  
   surface layer protein study, 173–175  
   surface molecular interaction study,  
     175–176  
 Milk fat globule membrane (MFGM), 210  
 Milk proteins  
   caseins, 97–99  
   *Lactobacillus rhammosus* GG, 101*f*  
   pale, soft, and exudative-like meat, 103*f*  
   whey proteins, 99–101  
 Mycoproteins, 83–84

## N

Nanodynamic mechanical analysis,  
   334–335  
 Nanomanipulation procedure by atomic  
   force microscopy, 66  
 Nanomechanical properties of food  
   materials  
   atomic force microscopy and  
     nanoindenter, 292*f*  
   cell wall mechanical properties, 291*f*  
   plant sample preparation for testing  
     nanomechanics, 293*f*  
   research on, 286–300  
   of some food materials, 296*t*  
 New imaging modes, 27–29  
 Nuclear magnetic resonance, 335–337

## O

Operation modes in atomic force  
   microscopy, 264–274  
   example of nanoindentation, 273*f*  
   force curve during nanoindentation, 268*f*  
   for nanomechanical properties  
     evaluation, 273*f*  
   *versus* PeakForce Tapping, 271*f*  
   principle of operation of AFM, 265*f*  
   van der Waals forces, 269*f*  
 Optical microscopy, 329–332  
 Optical tweezer, 342–345

## P

Paper method, 59  
 PeakForce QNM, 27–28, 272–274

- PeakForce Tapping, 27–28, 28*f*
- Peanut proteins
  - ultrasonication-assisted extraction time
    - on arachin and conarachin, 96*f*
- Plant polysaccharide, 143–146
  - atomic force microscopy images of
    - different extracts, 144*f*
  - cellulose, 142–143
  - data of nanostructural characters of
    - polysaccharides, 145*t*
  - pectin, 126–141
    - atmosphere storage by, 140*f*
    - degradation during cell wall
      - disassembly, 127–139
    - nanostructural analysis of, 139–141
    - quality, quantity, and morphology
      - features of, 129*t*
    - sodium carbonate-soluble pectin
      - chains, 133*f*
    - water-soluble, 134*f*, 136*f*
  - starch, 122–126
    - atomic force microscopy study of
      - starch films, 124–126
    - morphology and structure properties
      - of, 122–124
    - native starch films, 125*f*
    - surface of fractionated potato starch
      - granules, 123*f*
- Plasticizing effect, 247–248
- Probe selection, mathematical models, 285*f*
- Processing of food powders
  - carbohydrate-based powders, 235–240
    - disaccharide, 238–240
    - formulation, 236
    - polysaccharide-based, 235–237
    - processing, 236–237
  - fat-based, 240–241
  - powerful tool during formulation and,
    - 234–242
  - proteins, 241–242
  - study on macromolecules, 235*f*
- Proteins stretching, 274–276
- R**
- Raman technique, AFM combined with,
  - 320–327
  - applications in food science, 321–326
  - principle and apparatus, 320–321
  - prospect of, in food science, 326–327
  - surface-enhanced Raman spectroscopy
    - setups, 321*f*
  - tip-enhanced Raman scattering (TERS)
    - setup, 324*f*
- Research ways and applications
  - in food sciences, 34–36
  - research type, 30–33, 32*t*
- Rice proteins, 88–89
- S**
- Sample preparation, 87–88
- Sample preparation for food samples
  - artificially supported lipid layers, 51–52
  - bulk solid sample, 53
  - cells, 52–53
  - food powder, 53
  - individual biomolecules, 51
- ScanAsyst, 27–28
- Seafood proteins
  - myofibrils extracted from fish balls, 105*f*
- Single microbial cell studies
  - antimicrobial mechanism evaluation,
    - 165–169
  - for different food microorganisms, 166*t*
  - Escherichia coli* (A–D), 164*f*
  - morphological change evaluation,
    - 162–165
- Sorghum proteins, 91–92
- Spring constant, 64
- Static mode, 21
- Substrates
  - glass, 49–50
  - graphite, 50
  - mica, 49
- T**
- Tapping mode, 266–267
- Techniques for nanoindentation in plant
  - tissues, 281*t*
- W**
- Wheat proteins, 89–90
- X**
- X-ray techniques, 332–334



# FUNDAMENTALS AND APPLICATION OF ATOMIC FORCE MICROSCOPY FOR FOOD RESEARCH

Edited by

**Jian Zhong**

Xinhua Hospital, Shanghai Institute of Pediatric Research, Shanghai Key Laboratory of Pediatric Gastroenterology and Nutrition, Shanghai Jiao Tong University, Shanghai, China

**Hongshun Yang**

Department of Food Science & Technology, National University of Singapore, Singapore, Singapore

**Claire Gaiani**

Laboratoire d'Ingénierie des Biomolécules, University of Lorraine, Nancy, France

*Provides instruction on the basics and applications of atomic force microscopy in food research*

Many scientists in the field of food science and engineering need to evaluate their developed foods and food contact surfaces at nanoscale, which involves a steep learning curve. ***Fundamentals and Application of Atomic Force Microscopy for Food Research*** systematically describes how to obtain reliable atomic force microscopy (AFM) data, as well as how to apply AFM to different food substances. Divided into two parts, Part I: Introduction of AFM for food research and Part II: Application of AFM for different types of food substances, this book reduces the difficulty of AFM application and shortens the learning time for new hands.

This book is an essential reference for scientists in the fields of food science and engineering, graduate students, and young scientists who want to learn about AFM's capabilities and how it can support their food research and food industry professionals.

## Key Features

- Describes the application of AFM for food research
- Covers applications of AFM for different types of food substances
- Addresses future uses and perspectives of the AFM for the development of food nanotechnology



**ACADEMIC PRESS**

An imprint of Elsevier

[elsevier.com/books-and-journals](http://elsevier.com/books-and-journals)

ISBN 978-0-12-823985-8



9 780128 239858